frontiers | Research Topics

Beneficial and detrimental host cellular responses against Mycobacterium tuberculosis infection

Edited by
Veronica Edith Garcia, Maria Isabel Colombo and Joaquin Pellegrini

Coordinated by
Maria Paula Morelli

Published in
Frontiers in Cellular and Infection Microbiology

ISSN 1664-8714
ISBN 978-2-8325-4097-8
DOI 10.3389/978-2-8325-4097-8

About Frontiers

Frontiers is more than just an open access publisher of scholarly articles: it is a pioneering approach to the world of academia, radically improving the way scholarly research is managed. The grand vision of Frontiers is a world where all people have an equal opportunity to seek, share and generate knowledge. Frontiers provides immediate and permanent online open access to all its publications, but this alone is not enough to realize our grand goals.

Frontiers journal series

The Frontiers journal series is a multi-tier and interdisciplinary set of open-access, online journals, promising a paradigm shift from the current review, selection and dissemination processes in academic publishing. All Frontiers journals are driven by researchers for researchers; therefore, they constitute a service to the scholarly community. At the same time, the *Frontiers journal series* operates on a revolutionary invention, the tiered publishing system, initially addressing specific communities of scholars, and gradually climbing up to broader public understanding, thus serving the interests of the lay society, too.

Dedication to quality

Each Frontiers article is a landmark of the highest quality, thanks to genuinely collaborative interactions between authors and review editors, who include some of the world's best academicians. Research must be certified by peers before entering a stream of knowledge that may eventually reach the public - and shape society; therefore, Frontiers only applies the most rigorous and unbiased reviews. Frontiers revolutionizes research publishing by freely delivering the most outstanding research, evaluated with no bias from both the academic and social point of view. By applying the most advanced information technologies, Frontiers is catapulting scholarly publishing into a new generation.

What are Frontiers Research Topics?

Frontiers Research Topics are very popular trademarks of the *Frontiers journals series*: they are collections of at least ten articles, all centered on a particular subject. With their unique mix of varied contributions from Original Research to Review Articles, Frontiers Research Topics unify the most influential researchers, the latest key findings and historical advances in a hot research area.

Find out more on how to host your own Frontiers Research Topic or contribute to one as an author by contacting the Frontiers editorial office: frontiersin.org/about/contact

Beneficial and detrimental host cellular responses against Mycobacterium tuberculosis infection

Topic editors

Veronica Edith Garcia — UNIVERSIDAD DE BUENOS AIRES, Argentina
Maria Isabel Colombo — Universidad Nacional de Cuyo, Argentina
Joaquin Pellegrini — INSERM U1104 Centre d'immunologie de Marseille-Luminy (CIML), France

Topic coordinator

Maria Paula Morelli – University of Buenos Aires, Argentina

Citation

Garcia, V. E., Colombo, M. I., Pellegrini, J., Morelli, M. P., eds. (2023). *Beneficial and detrimental host cellular responses against Mycobacterium tuberculosis infection*. Lausanne: Frontiers Media SA. doi: 10.3389/978-2-8325-4097-8

Table of contents

frontiers | Frontiers in Cellular and Infection Microbiology

TYPE Editorial
PUBLISHED 27 November 2023
DOI 10.3389/fcimb.2023.1332084

OPEN ACCESS

EDITED AND REVIEWED BY
Thomas Rudel,
Julius Maximilian University of Würzburg, Germany

*CORRESPONDENCE
Verónica Edith García
vgarcia@qb.fcen.uba.ar

RECEIVED 02 November 2023
ACCEPTED 15 November 2023
PUBLISHED 27 November 2023

CITATION
Pellegrini JM, Morelli MP, Colombo MI and García VE (2023) Editorial: Beneficial and detrimental host cellular responses against *Mycobacterium tuberculosis* infection. *Front. Cell. Infect. Microbiol.* 13:1332084. doi: 10.3389/fcimb.2023.1332084

Editorial: Beneficial and detrimental host cellular responses against *Mycobacterium tuberculosis* infection

Joaquin Miguel Pellegrini[1], María Paula Morelli[2,3], María Isabel Colombo[4] and Verónica Edith García[2,3]*

[1]Centre d'Immunologie de Marseille Luminy, INSERM, Centre national de la recherche scientifique (CNRS), Aix-Marseille Université, Parc Scientifique et Technologique de Luminy, Case 906, Marseille, France, [2]Departamento de Química Biológica, Facultad de Ciencias Exactas y Naturales, Universidad de Buenos Aires, Ciudad Autónoma de Buenos Aires, Argentina, [3]Instituto de Química Biológica de la Facultad de Ciencias Exactas y Naturales (IQUIBICEN), Facultad de Ciencias Exactas y Naturales, Universidad de Buenos Aires, Consejo Nacional de Investigaciones Científicas y Técnicas (CONICET), Ciudad Autónoma de Buenos Aires, Argentina, [4]Instituto de Histología y Embriología de Mendoza, Facultad de Ciencias Médicas, Universidad Nacional de Cuyo-CONICET, Mendoza, Argentina

KEYWORDS

tuberculosis, host-pathogen interactions, *Mycobacterium tuberculosis*, immune response, immunometabolism, genetic

Editorial on the Research Topic
Beneficial and detrimental host cellular responses against *Mycobacterium tuberculosis* infection

Tuberculosis (TB) is a contagious infectious disease caused by *Mycobacterium tuberculosis* (*Mtb*), an exceptionally successful pathogen. In fact, it is estimated that *Mtb* has killed nearly 1000 million people since the XIX century. The most updated mortality data indicate that in 2021, 1.4 million people died of TB (World Health Organization, 2022), converting this pathogenic bacteria into the second leading infectious cause of death globally after COVID-19. *Mtb*, a microorganism that has produced suffering and death since it was identified almost 150 years ago, urgently requires a better vaccine to prevent TB-dependent morbidity and mortality (Rahlwes et al., 2023). The immune response against *Mtb* is highly complex. *Mtb* invades humans by air and establishes infection in the lung by using a large number of different virulence factors. After infection, *Mtb* interacts with different cells of the innate and adaptive immune compartments. These cells play an important role in the modulation and development of the pathology. *Mtb*-infected alveolar macrophages and dendritic cells are both reservoirs of infection and function to activate an adaptive immune response. *Mtb*-infected cells migrate from the lung to draining lymph nodes to prime and activate T and B cells to limit progression of infection (Urdahl et al., 2011; Shaler et al., 2012; Carpenter and Lu, 2022). Infected macrophages, along with non-infected phagocytes, (macrophages, monocytes and neutrophils), and T cells recruited by the inflammation and tissue damage will in turn form the characteristic TB granuloma

(Cohen et al., 2022; Cronan, 2022). A well-formed granuloma prevents the progression of infection, limiting tissue damage to a small region, which is beneficial for the host. Most *Mtb*-infected people will contain TB infection at this step and be asymptomatic (latent TB). In the case of the bacteria, the granuloma maintains the pathogen in a state of dormancy avoiding clearance by the immune system (Park et al., 2003). An efficient host protection against *Mtb* infection is associated with the induction, activation and proliferation of T helper 1 (Th1) cells (Cooper et al., 1993; Newport et al., 1996; Salgame, 2005). However, IFN-γ alone is not sufficient for the complete eradication of the bacteria, suggesting that other cytokines might be required for pathogen removal. Accordingly, cellular responses to *Mtb* induce IL-17 production, contributing to granuloma formation and control of bacterial growth (Cooper, 2010). However, excessive IL-17 levels exacerbate inflammation, increasing neutrophil recruitment and tissue damage (Lázár-Molnár et al., 2010). Despite the great steps made in the characterization of the acquired cellular response in TB patients, it remains to be elucidated what exactly constitutes a protective response or leads to disease pathology. Furthermore, how *Mtb* is able to evade host immune surveillance and persist is not fully clarified yet.

Our Research Topic was launched on May 18th 2022 with a planned close on November 11th 2022, but it was extended until October 25th 2023 due to the flow of submissions.

We are pleased to present a comprehensive Research Topic that delves into the intricate web of host-pathogen interactions during TB. Our Research Topic encompasses articles within a diverse range of disciplines, including cellular biology, endocrinology, host and bacterial genetics, epigenetics, immune regulation, immunometabolism, neuroimmunology, and aging. Through these multidisciplinary contributions, we aim to unravel the multifaceted dynamics underlying TB infection, shedding light on the disease's diverse facets and offering valuable insights for researchers and healthcare professionals. We invite readers to explore the ever-evolving landscape of TB research and foster a deeper understanding of this global health challenge.

Outline of contributions

In a very complete review, Wang et al. summarized the latest research progress on related signal transduction molecules in the interaction between *Mtb* and the host. In particular, Wang et al. focus on the special *Mtb* cell structure and the research progress of the interaction between this pathogen and host cell surface pattern recognition receptors (such as CLRs, NLRs, and TLRs), as well as macrophage effector molecules and autophagy. The authors reviewed many papers about the fight of the immune system against *Mtb* and the bacteria immune evasion. They even introduced the structure of *Mtb* by describing the particular cell wall of this bacteria, which is mainly composed of peptidoglycan, arabino galactose, trehalose-6,6'-dimycolate, mycolic acid and muramyl dipeptide. In addition they also describe the interaction of *Mtb* effector proteins and the host, and the molecular mechanism of *Mtb* escape from host membrane surface pattern receptors. This study may provide research ideas to find new anti-tuberculosis drugs and the development of host-directed treatment strategies.

There is still much to know about how *Mtb* evades the immune system. Margenat et al., explored the interaction and activity of the *Mtb* virulence factor PtpA, a tyrosine phosphatase released into the macrophage during infection (Bach et al., 2008; Mascarello et al., 2010), on the alpha subunit of the human trifunctional protein enzyme (*h*TFP), a PtpA substrate. During *Mtb* infection, PtpA interacts with several eukaryotic proteins in the macrophage cytosol, modulating phagosome maturation, innate immune response, apoptosis, and potentially host-lipid metabolism. Interestingly, it has been shown that the alpha subunit of *h*TFP is no longer detected in mitochondria during macrophage infection with the virulent *Mtb* H37Rv. Therefore, here, Margenat et al. investigated if PtpA could be the bacterial factor responsible for this effect by analysing the PtpA activity and interaction with $hTFP_{\alpha}$. The authors were able to demonstrate that PtpA in fact promotes the survival of mycobacteria in infected cells, affecting not only the innate immunity response (Wang et al., 2017; Bach et al., 2008; Wang et al., 2015; Wang et al., 2020) and apoptosis (Poirier et al., 2014), but also macrophage pathways involved in lipid metabolism.

Ma et al. reported that heme oxygenase-1 (HMOX1) is an essential regulator of *Mtb*-induced ferroptosis. The outcome of the host-pathogen interaction between macrophages and *Mtb* is critical for the development of TB (Xu et al., 2014). Therefore, intracellular *Mtb* either can be eradicated through macrophage apoptosis (Lee et al., 2009) and autophagy (Alam et al., 2017), or can persistently survive and grow in macrophages. Indeed, *Mtb* can induce macrophage necrosis leading to the spread of infection to other cells by evolving an immune escape mechanism (Liu et al., 2017; Pajuelo et al., 2018; Zhai et al., 2019). Therefore, understanding the molecular mechanism of *Mtb*-induced macrophage deaths, particularly macrophage necrosis, may lead to uncover novel targets for host-directed therapy (HDT) of TB. Interestingly, ferroptosis is another form of programmed cell death (PCD) that is a type of necrosis dependent on iron (Dixon et al., 2012; Amaral et al., 2016). This PCD is induced by massive lipid peroxidation and has been demonstrated to be one of the mechanisms used by *Mtb* to spread after host infection. In the present study, Ma et al. investigated the role of HMOX1 in macrophage ferroptosis in response to mycobacterial infection by using transcriptome analysis of peripheral blood from TB patients. Moreover, the authors analysed HMOX1 mechanism in ferroptosis by employing mice and RAW264.7 cells infected with Bacillus Calmette-Guérin (BCG). Their results demonstrated that HO-1 is a negative regulator of murine macrophage ferroptosis during BCG infection, in part through a mechanism by which HO-1 inhibits intracellular ROS production and iron accumulation altering the death of *Mtb* in infected macrophages.

Yuan et al. studied the regulation of murine miR-25-3p, a miRNA that was upregulated on exosomes of macrophages after 72-h BCG infection. Initially, they determined by bioinformatics analysis that the target gene of miR-25-3p is *DUSP10* (dual-specificity protein phosphatase 10). Previously, Nomura et al. (2012) demonstrated the suppressive activity of DUSP10 on ERK (Nomura et al., 2012). Using a mimic and an inhibitor of mmu-

miR-25-3p, a siRNA of DUSP10, and PD98059 (ERK Inhibitor) Yuan et al. evaluated the autophagy flux and the ability to eliminate BCG in murine macrophages. Thus, they demonstrated that mmu-miR-25-3 was able to inhibit DUSP10, promoting ERK1/2 phosphorylation and thereby increasing autophagy induced by BCG. Furthermore, they observed that upregulation of mmu-miR-25-3p also promotes autophagy and it was able to reduce BCG survival in Raw264.7 cells and facilitate the clearance of residual mycobacteria. Thus, miR-25-3p could be used for the construction of a novel anti-tuberculosis drug delivery system using exosomes as vectors loaded with antibiotics and specific miRNAs that have anti-TB and immunoregulatory functions.

Many biological and immunological aspects of TB are not completely elucidated, such as the complex process of immunoregulation mediated by regulatory T cells (Treg cells) and the enzymes indoleamine 2,3-dioxygenase (IDO) and heme oxygenase 1 (HO-1). In this study, Lozano-Ordaz et al. compared the contribution of these immunoregulatory factors in mice infected with *Mtb* strains with different levels of virulence: the mild virulence reference strain H37Rv or a highly virulent clinical isolate (strain 5186). The authors concluded that Treg cells, IDO and HO-1 activities are detrimental during late pulmonary TB induced by the mild virulence *Mtb*, probably because these factors decrease immune protection mediated by the Th1 response. In contrast, Treg cells, IDO and HO-1 are beneficial when the infection is produced by a highly virulent strain, possibly by regulation the excessive inflammation.

Osei-Wusu et al. used mycobacteria isolates including L4 (worldwide distributed) and L5 (West Africa-restricted and highly infectious) *Mtb* strains to study the association between bacterial and human genetics, particularly the inherent variation in the immune response of macrophages from Ghanaian Ewe and Akan self-reported ethnic groups. Data from *ex vivo* infections of monocytes-derived macrophages (MDMs) showed that Ewe MDMs exhibited a greater tendency to phagocyte L4 strains in comparison to Akan MDMs, while the latter displayed a higher replication rate for L4 *Mtb* strains. Conversely, Akan MDMs demonstrated increased uptake of L5, despite Ewe MDMs having a substantially higher replication rate for L5 strains. Moreover, the influence of self-reported ethnicity vanished when cells derived from the blood of cured TB cases were used. These observations corroborate findings from epidemiological studies where L5 infections were associated with the Ewe ethnic group (Asante-Poku et al., 2015). Thus, these findings suggest that host ethnicity (implying host genetic diversity), *Mtb* genetic diversity, and prior *Mtb* exposure collectively influence macrophage responses.

Another article in this Research Topic also explored the influence of host genetics and epigenetics on the susceptibility to *Mtb* infection, by affecting adaptive immune responses of TB patients. As it is well known, IFN-γ plays a key role in immune protection against *Mtb*. Single nucleotide polymorphisms in several candidate genes, especially polymorphisms in cytokine genes are known to modulate cytokine levels, which may influence susceptibility to tuberculosis infection and disease. Álvarez et al. propose of the +874 A/T (rs2430561) gene polymorphism, a genomic variant at a single nucleotide in the IFN-γ gene, as a possible genetic biomarker of susceptibility to TB. Specifically, demonstrated that AA genotype of the rs2430561 single nucleotide polymorphism was overrepresented in patients with active disease. They found that the A allele and AA genotype at rs2430561 are overrepresented in TB patients with active disease, and the presence of the T allele reduces IFN-γ production in *Mtb*-stimulated PBMCs in TB patients as compared to healthy donors. Furthermore, they observed increased DNA methylation levels in the IFN-γ promoter (in CpG island at position -53) in TB patients compared to individuals with latent TB. Therefore, methylation of this site could be used as a predictor of TB reactivation. is a genomic variant at a single base position in the DNA.

Immunometabolism has become a growing area of research with great impact on autoimmunity, cancer and infectious diseases. The metabolism of immune cells correlates with their microanatomical localization, activation, proliferation or function (O'Sullivan et al., 2019). By studying human CD1c+ myeloid dendritic cells from blood, Triglia et al. analysed glucose dependency of these cells when exposed to BCG, the only vaccine licensed to prevent TB disease. They showed that the challenge with BCG boosts the glycolytic function of CD1c+ mDCs, which has an impact in cytokine secretion and expression of CD40 and CCR7 but not in phagocytosis. Interestingly, this work showed that the maturation and migration of these cells in response to BCG are not exclusively dependent on the glycolytic pathway, and significant differences arise in this term between BCG-infected versus uninfected bystander DCs. These data highlight the complexity of the host response and provide evidence on the differences that can be found in immune responses to vaccines consisting of whole bacteria versus those composed of bacterial-derived antigens.

Exacerbation of the immune response is detrimental to host tissues and analysis of particular factors that counteract inflammation, such as corticosteroids and peroxisome proliferator-activated receptors (PPARs), is crucial. Accordingly, Diaz et al. investigated the contribution of PPAR Gamma to tuberculosis physiopathology. PPARs, which belong to the nuclear receptor superfamily, are a family of 3 ligand-activated transcription factors: PPARα (NR1C1), PPARβ/δ NR1C2), and PPARγ (NR1C3). These three subtypes of PPARs are encoded by different genes but show similar structural features. Diaz et al. showed that an increased expression of PPARsϒ in peripheral blood mononuclear cells (PBMCs) from patients was associated with TB severity. Moreover, by using THP-1 cells, the authors observed that radiation-killed *Mtb* modulated PPARsϒ expression and agonists decreased pro- and anti-inflammatory cytokines. As expected, cortisol treatment together with a PPARϒ agonist lowered the levels of this proinflammatory cytokine in stimulated cultures.

It has been described that people over 65 years old, face a notably elevated susceptibility and mortality to TB. This underscores that the elderly population constitutes a substantial reservoir for *Mtb* infection. In this Research Topic, Lafuse et al. analysed the effect of social disruption stress (SDR) on the lungs of young and old mice and their response to TB infection. This report shows that SDR induces the accumulation of CD11b+ myeloid cells in an age-independent manner but causes an immunosuppressive environment in the lung of aged mice characterized by reduced pro-

inflammatory cytokine production (IL-1β, TNF and CXCL2) and augmented levels of norepinephrine. Interestingly, when challenged with *Mtb*, psychological stress in old mice negatively affects the control of the infection by increasing differentiation of IL-10-secreting T cells. Thus, this work demonstrates psycho-neuroimmune mechanisms that operate after psychological stress and might undermine disease susceptibility. Its relevance is manifested by considering that anxiety and depression are two common symptoms experienced by patients with TB (Wang et al., 2018; Duko et al., 2020), directly related with decreased treatment efficacy, physical skills, and reduced quality of life (Dos Santos et al., 2017; Ruiz-Grosso et al., 2020).

We acknowledge with gratitude the participation of reviewers and authors in this Research Topic, which allowed to achieve a collection of original and high impact articles that introduce new concepts in this field of research. TB remains a relentless threat, claiming the lives of thousands each year, with the most socially and economically disadvantaged populations paying the heaviest price. Continuous investment and research into pathogen interactions, host immune responses and variations in endotypes found in the population, will pave the way for better treatments, diagnostics and vaccines.

Author contributions

JP: Conceptualization, Project administration, Writing – original draft, Writing – review & editing. MM: Project administration, Writing – original draft, Writing – review & editing. MC: Supervision, Writing – original draft, Writing – review & editing. VG: Conceptualization, Funding acquisition, Project administration, Supervision, Writing – original draft, Writing – review & editing.

Funding

The author(s) declare that no financial support was received for the research, authorship, and/or publication of this article.

Conflict of interest

The authors declare that the research was conducted in the absence of any commercial or financial relationships that could be construed as a potential conflict of interest.

The author(s) declared that they were an editorial board member of Frontiers, at the time of submission. This had no impact on the peer review process and the final decision.

Publisher's note

References

Alam, M. Z., Devalaraja, S., and Haldar, M. (2017). The heme connection: linking erythrocytes and macrophage biology. *Front. Immunol.* 8. doi: 10.3389/fimmu.2017.00033

Amaral, E. P., Conceição, E. L., Costa, D. L., Rocha, M. S., Marinho, J. M., Cordeiro-Santos, M., et al. (2016). N-acetyl-cysteine exhibits potent anti-mycobacterial activity in addition to its known anti-oxidative functions. *BMC Microbiol.* 16, 251. doi: 10.1186/s12866-016-0872-7

Asante-Poku, A., Yeboah-Manu, D., Otchere, I. D., Aboagye, S. Y., Stucki, D., Hattendorf, J., et al. (2015). Mycobacterium africanum is associated with patient ethnicity in Ghana. *PLoS Negl. Trop. Dis.* 9, e3370. doi: 10.1371/journal.pntd.0003370

Bach, H., Papavinasasundaram, K. G., Wong, D., Hmama, Z., and Av-Gay, Y. (2008). Mycobacterium tuberculosis virulence is mediated by PtpA dephosphorylation of human vacuolar protein sorting 33B. *Cell Host Microbe* 3, 316–322. doi: 10.1016/j.chom.2008.03.008

Carpenter, S. M., and Lu, L. L. (2022). Leveraging antibody, B cell and Fc receptor interactions to understand heterogeneous immune responses in tuberculosis. *Front. Immunol.* 13. doi: 10.3389/fimmu.2022.830482

Cohen, S. B., Gern, B. H., and Urdahl, K. B. (2022). The tuberculous granuloma and preexisting immunity. *Annu. Rev. Immunol.* 40, 589–614. doi: 10.1146/annurev-immunol-093019-125148

Cooper, A. M. (2010). Editorial: Be careful what you ask for: is the presence of IL-17 indicative of immunity? *J. Leukoc. Biol.* 88 (2), 221–3 doi: 10.1189/jlb.0310146

Cooper, A. M., Dalton, D. K., Stewart, T. A., Griffin, J. P., Russell, D. G., and Orme, I. M. (1993). Disseminated tuberculosis in interferon gamma gene-disrupted mice. *J. Exp. Med.* 178, 2243–2247. doi: 10.1084/jem.178.6.2243

Cronan, M. R. (2022). In the thick of it: formation of the tuberculous granuloma and its effects on host and therapeutic responses. *Front. Immunol.* 13. doi: 10.3389/fimmu.2022.820134

Dixon, S. J., Lemberg, K. M., Lamprecht, M. R., Skouta, R., Zaitsev, E. M., Gleason, C. E., et al. (2012). Ferroptosis: an iron-dependent form of nonapoptotic cell death. *Cell* 149, 1060–1072. doi: 10.1016/j.cell.2012.03.042

Dos Santos, A. P. C., Lazzari, T. K., and Silva, D. R. (2017). Health-related quality of life, depression and anxiety in hospitalized patients with tuberculosis. *Tuberc. Respir. Dis.* 80, 69–76. doi: 10.4046/trd.2017.80.1.69

Duko, B., Bedaso, A., and Ayano, G. (2020). The prevalence of depression among patients with tuberculosis: a systematic review and meta-analysis. *Ann. Gen. Psychiatry* 19, 30. doi: 10.1186/s12991-020-00281-8

Lázár-Molnár, E., Chen, B., Sweeney, K. A., Wang, E. J., Liu, W., Lin, J., et al. (2010). Programmed death-1 (PD-1)–deficient mice are extraordinarily sensitive to tuberculosis. *Proc. Natl. Acad. Sci.* 107, 13402–13407. doi: 10.1073/pnas.1007394107

Lee, J., Hartman, M., and Kornfeld, H. (2009). Macrophage apoptosis in tuberculosis. *Yonsei Med. J.* 50, 1–11. doi: 10.3349/ymj.2009.50.1.1

Liu, C. H., Liu, H., and Ge, B. (2017). Innate immunity in tuberculosis: host defense vs pathogen evasion. *Cell. Mol. Immunol.* 14, 963–975. doi: 10.1038/cmi.2017.88

Mascarello, A., Chiaradia, L. D., Vernal, J., Villarino, A., Guido, R. V. C., Perizzolo, P., et al. (2010). Inhibition of Mycobacterium tuberculosis tyrosine phosphatase PtpA by synthetic chalcones: kinetics, molecular modeling, toxicity and effect on growth. *Bioorg. Med. Chem.* 18, 3783–3789. doi: 10.1016/j.bmc.2010.04.051

Newport, M. J., Huxley, C. M., Huston, S., Hawrylowicz, C. M., Oostra, B. A., Williamson, R., et al. (1996). A mutation in the interferon-gamma-receptor gene and susceptibility to mycobacterial infection. *N Engl. J. Med.* 335, 1941–1949. doi: 10.1056/NEJM199612263352602

Nomura, M., Shiiba, K.-I., Katagiri, C., Kasugai, I., Masuda, K., Sato, I., et al. (2012). Novel function of MKP-5/DUSP10, a phosphatase of stress-activated kinases, on ERK-dependent gene expression, and upregulation of its gene expression in colon carcinomas. *Oncol. Rep.* 28, 931–936. doi: 10.3892/or.2012.1862

O'Sullivan, M., Triglia Van Nierop, D., Gogan, K., and Keane, J. (2019). Immunometabolism directs human CD1c-positive myeloid dendritic cell responses to BCG infection. *Am. J. Respir. Crit. Care Med.* 199, A4237–A4237. doi: 10.1164/ajrccm-conference.2019.199.1_MeetingAbstracts.A4237

Pajuelo, D., Gonzalez-Juarbe, N., Tak, U., Sun, J., Orihuela, C. J., and Niederweis, M. (2018). NAD+ Depletion triggers macrophage necroptosis, a cell death pathway exploited by mycobacterium tuberculosis. *Cell Rep.* 24, 429–440. doi: 10.1016/j.celrep.2018.06.042

Park, H.-D., Guinn, K. M., Harrell, M. I., Liao, R., Voskuil, M. I., Tompa, M., et al. (2003). Rv3133c/dosR is a transcription factor that mediates the hypoxic response of Mycobacterium tuberculosis. *Mol. Microbiol.* 48, 833–843. doi: 10.1046/j.1365-2958.2003.03474.x

Poirier, V., Bach, H., and Av-Gay, Y. (2014). Mycobacterium tuberculosis promotes anti-apoptotic activity of the macrophage by PtpA protein-dependent dephosphorylation of host GSK3α. *J. Biol. Chem.* 289, 29376–29385. doi: 10.1074/jbc.M114.582502

Rahlwes, K. C., Dias, B. R. S., Campos, P. C., Alvarez-Arguedas, S., and Shiloh, M. U. (2023). Pathogenicity and virulence of Mycobacterium tuberculosis. *Virulence* 14, 2150449. doi: 10.1080/21505594.2022.2150449

Ruiz-Grosso, P., Cachay, R., de la Flor, A., Schwalb, A., and Ugarte-Gil, C. (2020). Association between tuberculosis and depression on negative outcomes of tuberculosis treatment: A systematic review and meta-analysis. *PLoS One* 15, e0227472. doi: 10.1371/journal.pone.0227472

Salgame, P. (2005). Host innate and Th1 responses and the bacterial factors that control Mycobacterium tuberculosis infection. *Curr. Opin. Immunol.* 17, 374–380. doi: 10.1016/j.coi.2005.06.006

Shaler, C. R., Horvath, C., Lai, R., and Xing, Z. (2012). Understanding delayed T-cell priming, lung recruitment, and airway luminal T-cell responses in host defense against pulmonary tuberculosis. *Clin. Dev. Immunol.* 2012, 628293. doi: 10.1155/2012/628293

Urdahl, K. B., Shafiani, S., and Ernst, J. D. (2011). Initiation and regulation of T-cell responses in tuberculosis. *Mucosal Immunol.* 4, 288–293. doi: 10.1038/mi.2011.10

Wang, J., Ge, P., Qiang, L., Tian, F., Zhao, D., Chai, Q., et al. (2017). The mycobacterial phosphatase PtpA regulates the expression of host genes and promotes cell proliferation. *Nat. Commun.* 8 (1). doi: 10.1038/s41467-017-00279-z

Wang, J., Li, B.-X., Ge, P.-P., Li, J., Wang, Q., Gao, G. F., et al. (2015). Mycobacterium tuberculosis suppresses innate immunity by coopting the host ubiquitin system. *Nat. Immunol.* 16, 237–245. doi: 10.1038/ni.3096

Wang, X., Li, X., Zhang, Q., Zhang, J., Chen, H., Xu, W., et al. (2018). A survey of anxiety and depressive symptoms in pulmonary tuberculosis patients with and without tracheobronchial tuberculosis. *Front. Psychiatry* 9. doi: 10.3389/fpsyt.2018.00308

Wang, Y, Shi, Q, Chen, Q., Zhou, X, Yuan, H, Jia, X, et al. (2022). Emerging advances in identifying signal transmission molecules involved in the interaction between *Mycobacterium* tuberculosis and the host. *Front. Cell. Infect. Microbiol.* 12, 956311. doi: 10.3389/fcimb.2022.956311

Wang, L., Wu, J., Li, J., Yang, H., Tang, T., Liang, H., et al. (2020). Host-mediated ubiquitination of a mycobacterial protein suppresses immunity. *Nature* 577, 682–688. doi: 10.1038/s41586-019-1915-7

World Health Organization. (2022). *Global tuberculosis report 2022* (Geneva: World Health Organization). Available at: https://www.who.int/teams/global-tuberculosis-programme/tb-reports/global-tuberculosis-report-2022.

Xu, G., Wang, J., Gao, G. F., and Liu, C. H. (2014). Insights into battles between Mycobacterium tuberculosis and macrophages. *Protein Cell* 5, 728–736. doi: 10.1007/s13238-014-0077-5

Zhai, W., Wu, F., Zhang, Y., Fu, Y., and Liu, Z. (2019). The immune escape mechanisms of mycobacterium tuberculosis. *Int. J. Mol. Sci.* 20, 340. doi: 10.3390/ijms20020340

frontiers | Frontiers in Cellular and Infection Microbiology

TYPE Review
PUBLISHED 25 July 2022
DOI 10.3389/fcimb.2022.956311

OPEN ACCESS

EDITED BY
Veronica Edith Garcia,
University of Buenos Aires, Argentina

REVIEWED BY
Azger Dusthackeer,
National Institute of Research in Tuberculosis (ICMR), India
Silvia De La Barrera,
Consejo Nacional de Investigaciones Científicas y Técnicas (CONICET), Argentina
Jianping Xie,
Southwest University, China

*CORRESPONDENCE
Qin Li
2020000301@hmc.edu.cn
Lijun Ge
gelijun@zcmu.edu.cn

†These authors have contributed equally to this work

SPECIALTY SECTION
This article was submitted to Bacteria and Host, a section of the journal Frontiers in Cellular and Infection Microbiology

RECEIVED 30 May 2022
ACCEPTED 30 June 2022
PUBLISHED 25 July 2022

CITATION
Wang Y, Shi Q, Chen Q, Zhou X, Yuan H, Jia X, Liu S, Li Q and Ge L (2022) Emerging advances in identifying signal transmission molecules involved in the interaction between *Mycobacterium tuberculosis* and the host.
Front. Cell. Infect. Microbiol. 12:956311.
doi: 10.3389/fcimb.2022.956311

Emerging advances in identifying signal transmission molecules involved in the interaction between *Mycobacterium tuberculosis* and the host

Yue Wang[1†], Qiyuan Shi[2†], Qi Chen[1], Xuebin Zhou[2], Huiling Yuan[1], Xiwen Jia[1], Shuyuan Liu[1], Qin Li[2*] and Lijun Ge[1*]

[1]College of Life Science, Zhejiang Chinese Medical University, Hangzhou, China, [2]School of Pharmacy, Hangzhou Medical College, Hangzhou, China

Tuberculosis caused by *Mycobacterium tuberculosis* (MTB) is an ancient chronic infectious disease and is still the leading cause of death worldwide due to a single infectious disease. MTB can achieve immune escape by interacting with host cells through its special cell structure and secreting a variety of effector proteins. Innate immunity-related pattern recognition receptors (PPR receptors) play a key role in the regulation of signaling pathways.

In this review, we focus on the latest research progress on related signal transduction molecules in the interaction between MTB and the host. In addition, we provide new research ideas for the development of new anti-tuberculosis drug targets and lead compounds and provide an overview of information useful for approaching future tuberculosis host-oriented treatment research approaches and strategies, which has crucial scientific guiding significance and research value.

KEYWORDS

***Mycobacterium tuberculosis*, innate immunity, signaling pathway, immune escape, chronic infectious disease**

Introduction

Mycobacterium tuberculosis (MTB), discovered in 1882 by the German bacteriologist Robert Koch, was proven to be the causative agent of human tuberculosis, which seriously endangers human health and public safety (Abrahams et al., 2018). After centuries of struggle, the disease has been gradually brought under control, but in recent

years, it has become increasingly serious due to various factors. It is now one of the top ten causes of death worldwide and is the leading cause of death from infectious diseases. For example, according to the World Health Organization (WHO) 2020 World Tuberculosis Report, there were approximately 10 million new tuberculosis cases in 2019, of which approximately 3.3% of new tuberculosis cases and 17.7% of previously treated patients were MDR/RR-TB (multidrug-resistant tuberculosis/rifampicin-resistant tuberculosis). Three countries accounted for the largest proportion of drug-resistant tuberculosis, namely, India (27%), China (14%) and Russia (8%), with approximately 1.5 million deaths (Global tuberculosis report, 2020). Thus, the current situation of tuberculosis prevention and treatment remains very severe.

MTB is an intracellular bacterium, and the results of MTB infection largely depend on the host's response to the invading pathogen and how the pathogen escapes from the host's immune response. For this reason, elucidating the interaction between MTB and the host helps to explain the molecular mechanism involved in the infection of specific mycobacterium proteins (Brennan et al., 2007). The primary host cell targets of MTB are alveolar macrophages, which are the main effector cells for clearing MTB. After the MTB pattern recognition receptor expressed on the surface of macrophages binds to specific MTB surface-related molecules, macrophages can enact a variety of immune responses to eliminate MTB. Meanwhile, MTB utilizes a variety of mechanisms to escape the body's immune killing to survive in its cells. As a typical intracellular bacterium, MTB has evolved a variety of immune escape strategies for long-term coexistence with the host (Barreteau et al., 2008). This review is followed by an introduction of the molecular mechanisms triggered by signal transmission molecules in the interaction between Mycobacterium and the host to provide new ideas for the study of tuberculosis infection and pathogenicity.

Structural features of mycobacterium tuberculosis

MTB is an obligate, aerobic, slender, slightly curved bacillus, with a size of 1-4×0.4 μm, without flagellum, with fimbriae and microcapsules but without forming spores. The structural characteristics of MTB cells are summarized in Figure 1. MTB grows slowly mainly because the lipid content accounts for approximately 60% of the dry weight of the cell wall, which affects the absorption of nutrients (Marrakchi et al., 2014).

The unique cell wall components of MTB play a crucial role in immune escape and are also an important target of many anti-tuberculosis drugs (Kalscheuer et al., 2019). Compared with other pathogenic bacteria, the bacterial wall of MTB has neither lipoteichoic acid, teichoic acid (major wall components of most Gram-positive bacteria) nor lipopolysaccharide (major wall components of most Gram-negative bacteria) (Figure 2) (Table 1).

The cell wall of MTB is mainly composed of Peptidoglycan (PG), Arabino galactose (AG), Trehalose-6,6'-dimycolate (TDM), Mycolic acid (MA) and Muramyl dipeptide(MDP). The MTB cell membrane has a PG layer similar to that of gram-positive bacteria, which plays a key role in cell growth, communication, and stimulation of the host's immune response (Kanji et al., 2019). The outer layer is the arabinan chain formed by highly branched AG, and the nonreducing end of the glycan chain is connected to the MA (Canezin et al., 2018) in the outer layer, which affects the permeability of dyes into MTB cells (Kleinnijenhuis et al., 2011). Thus, the outer layer of MTB,

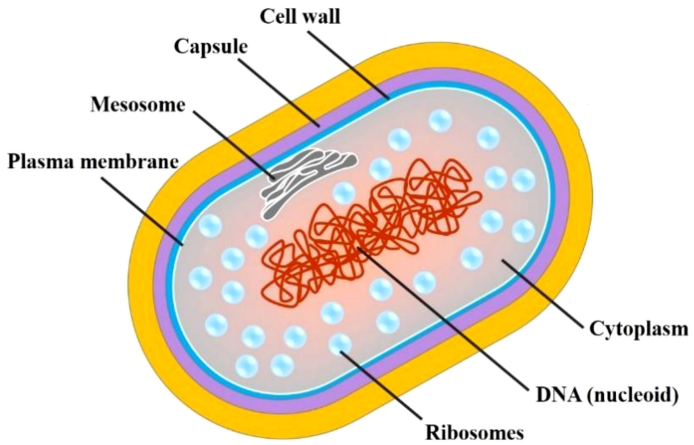

FIGURE 1
Cell structure of MTB.

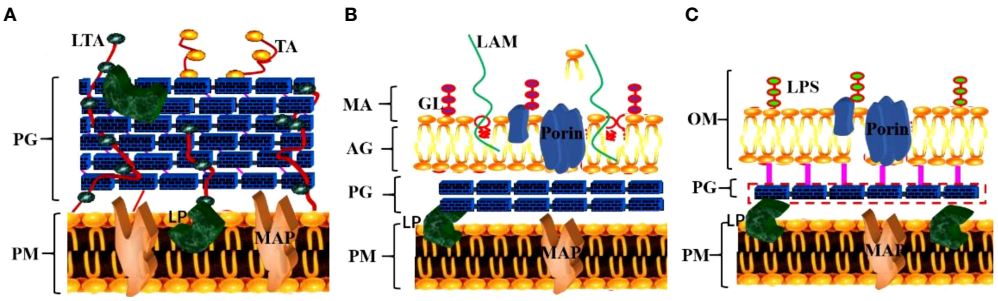

FIGURE 2
Specific structural components of the MTB cell wall. **(A)** The cell wall structure of gram-positive bacteria; **(B)** The cell wall structure of MTB; **(C)** The cell wall structure of gram-negative bacteria. (TA, teichoic acid; LTA, lipoteichoic acid; PG, peptidoglycan; PM, plasma membrane; LP, lipoprotein; MAP, membrane-associated protein; GL, glycolipid; LAM, lipoarabinomannan; MA, mycolic acid; AG, arabinogalactan; LPS, lipopolysaccharide; OM, outer membrane).

comprising predominantly lipids and carbohydrates, plays a crucial role in MTB survival and infection (Arcos et al., 2011).

In addition, many researchers have found that MTB can reduce the concentration of bacterial drugs through the efflux pump system, alleviate damage to itself, and induce drug resistance, which is another key mechanism of MTB immune escape (Richa et al., 2019). The efflux pump system of MTB is achieved by transporters located on the plasma membrane. There are currently five known MTB related transporter families, namely, ATP-binding cassette (ABC), Major Facilitator Superfamily (MFS), Resistance Nodulation Division (RND), Small Multidrug Resistance (SMR) and Multidrug and Toxic-Compound Extrusion (MATE) (Kallenius et al., 2016). Recent work indicated that THP-1 cells infected with MTB H37Rv and subsequently exposed to rifampicin for 72 hours expressed 10 efflux pump-related genes. Four genes in the ABC family and 1 gene in the MFS family were significantly increased at 0.0015 mg/L rifampicin (Benjawan et al., 2015). Therefore, the MTB surface proteoglycan and its unique Mycoplasma acid of its cell wall and the efflux pump on the plasma membrane are important mechanisms used to protect itself from injury and to promote immune escape.

Mechanisms of interaction between MTB effector proteins and the host

The mechanism of MTB immune escape is related to its special cell wall structure as well immune damage caused by the toxicity of metabolites produced by MTB proliferation in host cells (Ji-Hae et al., 2021). MTB is an intracellular pathogen that secretes a variety of effector proteins into host cells, which in turn interfere with cell signaling pathways and biological functions and ultimately promote the survival of pathogens in host cells and lead to host cell lesions. For example, lipopolysaccharide (LPS) and lipoarabinomannan (LAM) in the cell wall of MTB can be recognized by TLR2/TLR1 or TLR2/TLR6 heterodimers on the membrane of host immune cells, which in turn activate the expression of NF-κB and cytokines, further leading to host cell injury (Wong, 2017).

TABLE 1 Some immune escape molecules of MTB interacting with host cells.

Host cell PPR signal	MTB-related cell components and effector molecules			Target of host cell
	Cell wall Special components	The efflux pump system	Effector proteins	
TLRs	PG	ABC	PTPA	TRM27、GADD45A
NLRs	AG	MFS	MCE2E	eEFIA、MAPK
CLRs	MA	RND		ERK、JNK
CRs	TDM	SMR	MCE3E	ERK
MRs	MDP	MATE	ESAT-6	NLRP3

TLRs, Toll-like receptors; NLRs, Nod-like receptors; CLRs, C-type lectin receptors; CRs, Complement receptors; MRs, Mannose receptors;PG, Peptidoglycan; AG, Arabino galactan; MA, Mycolic acid; TDM, Trehalose-6,6'-dimycolate; MDP, Muramyl dipeptide; ABC, ATP-binding cassette; MFS, Major Facilitator Superfamily; RND, Resistance Nodulation Division; SMR, Small Multidrug Resistance; MATE, Multidrug and Toxic-Compound Extrusion; PtpA, Protein tyrosine phosphatase; MCE2E, MCE family proteins 2E; MCE3E, MCE family proteins 3E; ESAT-6, Early secretory antigentic target-6 protein; TRM27,Tripartite motif 27; GADD45A, Growth arrest and DNA damage inducible gene Gadd45; eEFIA, Eukaryotic translation elongation factor 1A; MAPK, Mitogen-activated protein kinase; ERK, Extracellular regulated protein kinases; JNK, c-Jun N-terminal kinase; NLRP3, NOD-like receptor thermal protein domain associated protein 3.

At present, recent studies have revealed the dynamic process and molecular mechanism of the interaction between MTB effector proteins, such as protein tyrosine phosphatase (PtpA), MCE family proteins (Mce2E and Mce3E) and the host cell. PtpA can be secreted into host cells to bind ubiquitin molecules and be activated by the latter, which in turn dephosphorylates host p-JNK and p-p38 and inhibits the activation of the JNK/p38 signaling pathway. For example, PtpA can antagonize the host interaction protein TRIM27 (a ubiquitin ligase) mediated JNK/p38 signal pathway by binding to the ring domain of TRIM27 protein (Jing et al., 2016). In addition, PtpA can also inhibit the activation of the NF-κB signaling pathway in a phosphatase activity-independent manner (Valérie et al., 2014; Mohd et al., 2021). Similar research results have shown that PtpA can regulate innate immune signaling pathways in the host cytoplasm as well as enter the host nucleus to regulate potential target genes, and PtpA can directly bind to the promoter region of the GADD45A gene and inhibit its transcription (Wang et al., 2017). The MTB genome contains four MCE (Mammaian cell entry) operons (Mce1-4), and the proteins encoded by them constitute a large class of MCE family. Previous studies have suggested that MCE family proteins play an important role in the entry, intracellular survival and pathogenesis of MTB, but its host regulatory function and mechanism are far from clear (Foot Perkowski et al., 2016; Singh et al., 2016). Recent studies have found that the Mce3E protein of MTB can specifically target the ERK signaling pathway of the host through its DEF motif (a MAPK binding motif), and ultimately promote the intracellular survival of mycobacteria. And MTB Mce2E operon contained a D motif (another MAPK binding motif) by further bioinformatics analysis. And the results showed that in macrophages, Mce3E specifically inhibited ERK signaling pathway through its DEF motif, while Mce2E simultaneously inhibited ERK and JNK signaling pathway through its D motif (Li et al., 2015). It is worth mentioning that Mce2E can also inhibit the K48 ubiquitination of the host cell proliferation promoting protein eEF1A1 in epithelial cells and increase its protein stability, thereby promoting the proliferation of human non-small cell lung cancer A549 cells derived from epithelial cells, while Mce3E does not have this function (Wei et al., 2019) (Figure 3). Therefore, these studies suggest that MTB can secrete a variety of effector proteins to co regulate some host signal pathways and functions, but the specificity and intensity of different effector proteins may be different. And the breakthrough of this research result will provide new ideas and specific targets for the future development of anti-MTB drugs from the perspective of the interaction between MTB effector proteins and host cells (Augenstreich and Briken, 2020).

In addition, it has been demonstrated that, when MTB enters the host lung tissue, the hydrolytic enzymes in alveolar lining fluid (ALF) can hydrolyze mannose and glucose of the MTB cell

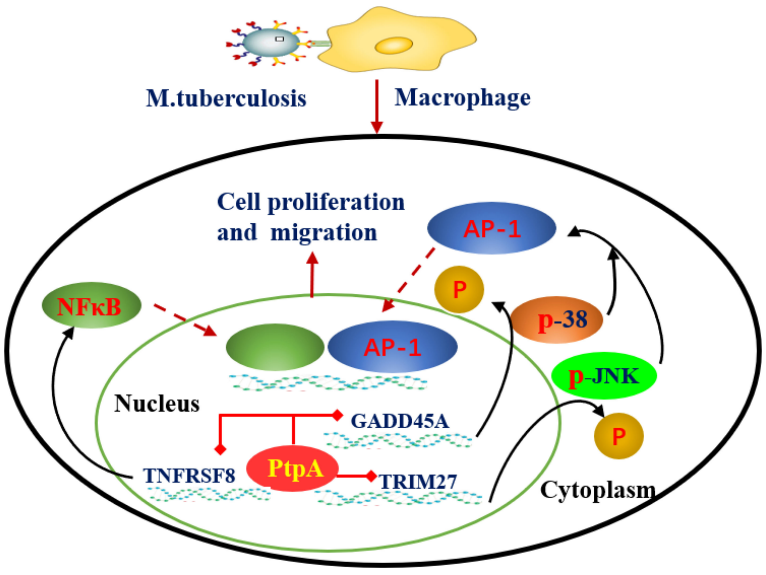

FIGURE 3
Mechanism by which MTB-PtpA enters the host cell nucleus to inhibit natural immune function. MTB PtpA is secreted into the host cell to bind ubiquitin molecules and is activated, and activated PtpA can inhibit the transcription of TNFRSF8 in the host nucleus, thus inhibiting the NF-κB signaling pathway. PtpA can also bind directly to the promoter region of the GADD45A or RNF187 gene and inhibit its transcription, dephosphorylating p-JNK and p-p38 to inhibit the activation of the JNK/p38 signaling pathway. (TNFRSF8, a member of the TNF-receptor superfamily; Trim27, belonging to E3 ubiquitin ligase family, can activate JNK/p38 signal pathway of host cells in a ubiquitin ligase activity dependent manner; GADD45A, a regulator of p38 MAPKs by inhibiting p38 phosphorylation and activity).

envelope molecules, thereby disrupting the structure of the MTB cell wall (Mika et al., 2013). In recent years, many researchers have suggested that this change significantly reduces the virulence factors mannose-capped lipoarabinomannan (Man-LAM) and trehalose-6,6'-dimycolate (TDM) on the surface of MTB (Tuladhar and Kanneganti, 2020). For example, MTB-secreted ESAT-6 protein can improve the permeability of phagosomes in host phagocytes and activate NLRP3 (Jain et al., 2020). Thus, after thousands of years of development, MTB has coevolved with humans. Its unique cell structure and metabolic effector proteins, in addition to the acquired drug resistance caused by gene mutations coexisting with the host under the action of drugs, have become primary reasons for the escape mechanism of MTB. MTB has become one of the most successful pathogens by changing its morphology, colonies, virulence, immunogenicity and drug resistance.

Molecular mechanism of MTB escape from host PPR signal transduction

In recent years, the interaction between MTB and its host has become increasingly understood. However, at present, the molecular mechanism of the interaction between the secreted proteins of MTB and the proteins of the host cell is not completely clear, especially how MTB escapes from host pattern recognition receptor signaling (Allue-Guardia et al., 2021). Studies have demonstrated that MTB can change the immune function of host cells by secreting different effector proteins at different stages of infection. These results suggest that the immune escape of MTB is closely related to the host cell membrane surface pattern receptor (PPR) (Pathak and Das, 2020). For example, after entering the host, the cell wall components of MTB, such as phosphatidylinositol mannose (PIM), lipoarabinomannan (LAM), and some other outer membrane molecules, are recognized by macrophages through membrane surface pattern receptors. These receptors include Toll-like receptors (TLRs), Nod-like receptors (NLRs), C-type lectin receptors (CLRs) and complement receptors (CRs), mannose receptors (MRs), and Fc receptors of immunoglobulin (FcRs) (Cervantes et al., 2017). Most recognition and activation of the host immune system requires the above receptors to further activate downstream related signaling pathways and trigger host immune defense, including programmed cell death of different types, such as cell apoptosis and autophagy. Therefore, understanding the different innate recognition pathways of the host can help to reveal the pathogenic mechanisms of MTB and develop new control measures (Krakauer et al., 2019). Next, we will focus on the interaction between MTB effector proteins and host surface pattern receptors (PPRs), such as CLRs, NLRs, and TLRs, and the latest research on how MTB evades these receptors (Table 1).

Molecular mechanism by which MTB escapes host TLR receptor signaling

Toll-like receptors (TLRs) are intrinsic pattern recognition receptors. The acquired immune response can be induced by the recognition of pathogen-associated molecular patterns (PAMPs) on the surface of specific microorganisms to promote the synthesis and release of cytokines and the maturation of antigen-presenting cells (Kawai et al., 2011). TLRs are a family of single membrane-spanning receptors that can be divided into three parts: the extracellular domain, cytoplasmic domain and transmembrane domain (Takeuchi et al., 2010). The extracellular domain of TLRs contains three extracellular domain proteins, namely, MD-1, MD-2 and RP105, which are used to recognize receptors and form receptor complexes with other coreceptors. The cytoplasmic domain of TLRs is highly homologous to that of IL-1R family members and is called the Toll-IL-1 receptor domain (TIR domain). There are 11 members of the TLR family. According to TLR protein localization and recognition substrates, they can be divided into two categories: plasma membrane-anchored TLRs and endosomal TLRs (Kumar et al., 2018). These are distinct molecular structures on microbes, and different sets of TLRs have been associated with the recognition of pathogens, such as the recognition of viruses by TLR3, TLR7, TLR8 and TLR9 (Kay et al., 2013; Liu et al., 2013; Hossain et al., 2013). TLRs mainly function through two signal transduction pathways, the myeloid differentiation factor 88 (MyD88)-dependent signaling pathway and the MyD88-independent signaling pathway, which induce the production of both proinflammatory cytokines and type I IFNs (Nguyen et al., 2020). These two distinct responses are mediated *via* the selective use of adaptor molecules recruited to the Toll/IL-1 receptor (TIR) domains of TLRs after ligand binding (Kawai et al., 2006). Thus, when TLRs are activated, they activate their downstream IL-1R-associated kinase (IRAK), tumor necrosis factor receptor (TNFR), and TNFR-associated factor 6 (TRAF-6), which further activate NF-κB and lead to immune and inflammatory responses (Liu et al., 2007). Many studies have confirmed that TLRs play a crucial role in TB infection (Doyle et al., 2006). For instance, among the TLR family, TLR2 can recognize lipoprotein, LPS, and CpG DNA at the cell wall of MTB and secreted membrane vesicles (Liu et al., 2018). In addition, it can activate the downstream NF-κB signaling pathway and stimulate the secretion of TNF-α to activate macrophages (Fiske et al., 2019). Meanwhile, it can stimulate the expression of vitamin D receptor and vitamin D-1-hydroxylase gene to induce the release of cathelicidins (Liu et al., 2021). Another study found that TLR2 could recognize the MTB LPQH (19 kDa lipoprotein) and lysosomal inhibiting LPRI and activate macrophages, which initiate innate immunity and activate T lymphocytes to participate in the clearance of MTB (Picard et al., 2003). TLR2 can form heterodimers with both

TLR1 and TLR6. These heterodimers have been implicated in the recognition of mycobacterial cell wall glycolipids, including LAM, lipomannan (LM), mycobacterial glycoproteins (MGs), phosphatidylinositol mannitol (PIM), triacylated (TLR2/TLR1) and diacylated (TLR2/TLR6) lipoproteins (Bulut et al., 2005; Singh et al., 2019).

To date, studies agree that LAM, as a cell wall component of nonpathogenic mycobacterium, is a TLR2 activator with strong immunogenicity. LAM from pathogenic mycobacteria lacks immunogenicity (Drage et al., 2009). TLR2 is believed to be important in the initiation of the innate host defense against MTB (Kleinnijenhuis et al., 2009). In addition, IL-1β production is dependent upon TLR2 and TLR6 stimulation but not TLR4 or TLR9 (Yang et al., 2019). TLR2 polymorphisms affect host susceptibility to MTB. TLR2 ligands of MTB can change the host cell environment, which is conducive to bacterial retention (Konowich et al., 2017). MTB can affect the fate of infected cells by regulating the TLR signaling pathway. For example, LRP of MTB can inhibit the PI3K/Akt signaling pathway activated by TLR2 and inhibit the production of anti-inflammatory factors and macrophage antigen presentation. PtpA and Mce3E of MTB regulate the MAPK and NF-κB signaling pathways. Interestingly, it has been reported that GRP160 can also regulate the entry of MTB into macrophages through the MAPK/ERK signaling pathway, indicating that the GPCR and TLR signaling pathways may play a synergistic role (Mercedes Romero et al., 2014; Mehta et al., 2021). The interaction between TLRs and MTB infection is shown in Figure 4.

In addition, TLR4 is an important pattern recognition receptor that is expressed in mononuclear macrophages, dendritic cells and alveolar II-type epithelial cells and plays a crucial role in resistance to MTB infection. In the TLR family, TLR4 is a type I transmembrane protein. However, unlike the TLR2 signal transduction pathway, TLR4 can activate the MyD88-dependent pathway, induce the release of inflammatory cytokines and costimulators, and also activate the MyD88-independent pathway to produce type I interferon (IFN) (Niu et al., 2018). After TLR4 is stimulated by ligands, TLR4 activates transcriptional regulatory factors by connecting and transmitting TLR4 downstream signals through transduction molecules, such as NF-κB, inducing infected cells to secrete inflammatory factors and type I IFN, which ultimately initiates innate and acquired

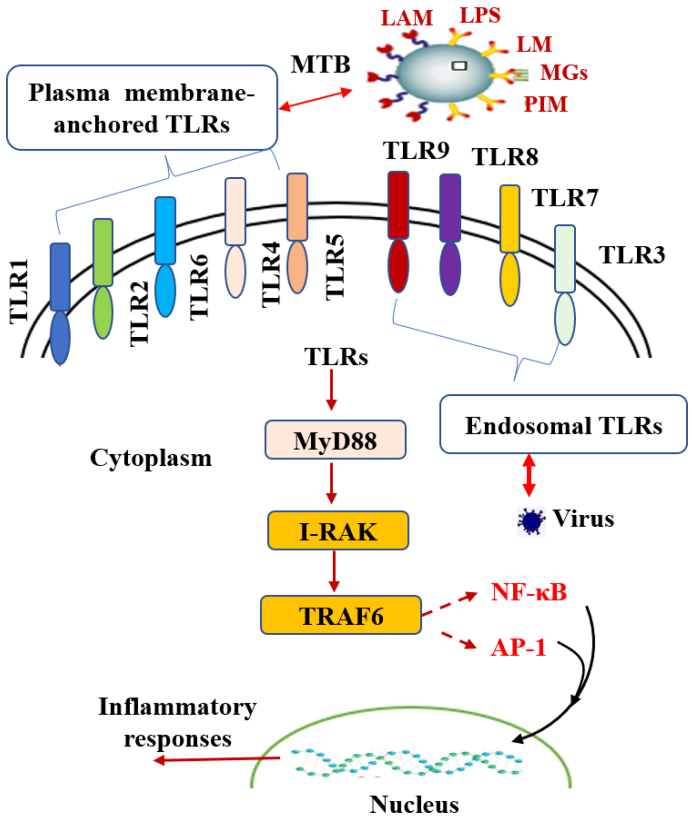

FIGURE 4
The interaction between TLRs and MTB infection. TLRs play a vital role in TB infection. Toll-like receptors are divided into plasma membrane-anchored TLRs and endosomal TLRs according to the localization of TLR proteins. As TLRs are activated, they activate downstream IRAK, TNFR and TRAF-6 through the MyD88-dependent signaling pathway, further activating NF-kB and AP-1 and producing a series of inflammatory reactions.

immune responses (Thada et al., 2021). TLR4 was found to be involved in LPS-induced activation of alveolar II-type epithelial cells (AEC II), leading to the large-scale release of TNF-α and IL-6, while single immunoglobin IL-1 receptor-related protein (SIGIRR) overexpression inhibited TLR4 signal transduction in LPS-triggered AEC II, alleviating the inflammatory response (Alemnew et al., 2021). Recent studies have found that AEC II cells infected with strong MTB strains demonstrate an inhibition trend on TLR2 and TLR4 signaling pathways, and the inflammatory response of cells is significantly stronger than that of weak MTB strains, indicating that AEC II also differ in the immune regulation mechanism of MTB infection with different virulence levels (Krutzik et al., 2003). Overexpression of TLR2 and TLR4 in human cell lines is directly related to MTB infection (Kang et al., 2002). Furthermore, polymorphisms in both TLR2 and TLR4 are possibly associated with increased susceptibility to MTB infection (Lorenz et al., 2000; Rook et al., 2005).

At present, an increasing number of clinical diagnostic studies have confirmed that the gene expression levels of the TLR family are closely related to MTB patients. For example, the TLR distribution in MTB granuloma lesions indicates that TLR1, TLR2, and TLR4 are expressed in both immune cells and nonimmune cells; however, TLR9 is only detectable in immune cells (Martinez-Perez et al., 2020). Interestingly, similar results were found in which the relative mRNA expression levels of TLR2, TLR4, and TLR8 in tuberculosis patients were significantly increased (Davila et al., 2008). Furthermore, in an animal model of TB, TLR8-deficient mice succumb more rapidly to MTB infection, despite efficiently controlling the number of viable bacilli in different organs. Thus, in this model of MTB infection, TLR8 plays a key role in dampening inflammation and tissue damage (Najmi et al., 2010).

Other studies have also confirmed that the expression and activation of TLRs can be used as auxiliary indicators for the diagnosis and differential diagnosis of tuberculosis. For instance, mice lacking the TLR ligand protein MyD88 are more sensitive to MTB infection, and the same phenomenon was found following TLR2 gene deletion. However, whether the TLR signaling pathway resists MTB infection is controversial; for instance, it has been reported that MyD88 rather than TLRs plays a key role in the activation of the macrophage response, and the release of cytokines does not depend on TLRs (Kramnik and Beamer, 2016).

Molecular mechanism of MTB escaping the host NLR receptor signal

Recently, the role of the cytoplasmic receptor NLR in microbial infection has attracted much attention. The nucleotide oligomerization domain (NOD)-like receptor (NLR) is a kind of innate immune intracellular recognition receptor in the cell cytoplasm that plays a key role in the regulation of innate immunity (Nargis et al., 2016; Alvarez-Jiménez et al., 2018). The interaction between monocyte-derived dendritic cells and MTB was observed under an electron microscope. It was found that MTB could escape from the phagocyte to the cytoplasm depending on early secretory antigen target (ESXA). ESXA is also a cell wall-binding protein with periodic replication from phagocytosed lysosomes to the cytoplasm (Tan et al., 2020). Thus, cytoplasmic pattern recognition receptors are also involved in host innate and acquired immunity against MTB.

The NLR acts as a scaffold protein in the cytoplasm, assembling signaling platforms that trigger the NF-κB and mitogen-activated protein kinase (MAPK) signaling pathways and control inflammatory caspase activation. Muramyl dipeptide (MDP) of MTB recognized by NOD2 can stimulate the release of host inflammatory factors and nitrogen oxides (NO) to play a bactericidal role, and activated NOD2 induces autophagy (Cubillos-Angulo et al., 2021). The MTB MDP is unique in that it has an N-glycolyl modification rather than the N-acetylated modification found in other bacteria (Donovan et al., 2017). Studies have demonstrated that MDP in MTB can promote macrophages through the receptor-interacting protein kinase 2 (PIP2) and interferon regulatory factor 5 (IRF5) pathways, producing type I IFN signaling, such as IFN-α/β, which counteracts the role of the host protective IL-1β and IFN-γ signaling pathways (Sabir et al., 2017). Mice with type I IFN receptor deficiency did not have altered MTB burdens in the lungs, possibly even promoting the reproduction of extrapulmonary bacteria (Wan et al., 2018). Furthermore, the cytoplasmic receptor NLR plays a role in pyroptosis in host cells. Studies have demonstrated that, after MTB activates host cells, NLR is recruited to the inflammasomes of the macromolecular complex, causing host cells to secrete IL-1β, IL-18, and IL-33 and leading to pyroptosis (Qu et al., 2020). In addition, the inflammation caused by MTB infection of host cells is mainly related to NLRP3 in the NLR family (Beckwith et al., 2020). Recent studies have demonstrated that, in human macrophages, MTB relies on ESAT-6 to activate the inflammatory response and release IL-1β, leading to pyroptosis, while in mouse dendritic cells, IL-1β secretion is independent of NLRP3, and no evidence of pyroptosis has been found (Wilson et al., 2015).

Molecular mechanism of MTB evasion of host CLR receptor signaling

C-type lectin receptors (CLRs) are a superfamily of proteins containing carbon hydrate recognition domains (CRDs). According to subcellular localization, it can be divided into two categories, soluble and membrane-type C-type lectins, and it is a crucial pattern recognition receptor (PRR) in the innate immune system (Zhao et al., 2014). Mycobacterium cord factor

TDM (trehalose-6,6'-dimycolate) is a glycosolipid of mycoacid and trehalose that exists in the outer layer of bacterial cells. Studies have confirmed that TDM can bind to macrophage C-type lectin receptor (CLR) to induce changes in downstream pathways (Barkan et al., 2010).

Interestingly, researchers have found that TDM-induced acellular granulomas are very similar to *Mycobacterium tuberculosis*-infected granulomas when TDM-emulsified oil droplets are injected into mice (Behr et al., 2015). The genes responsible for TDM synthesis in MTB include cyclopropane synthase PcaA and CmaA2. If these genes are deleted, the structure of Cladophyll acid changes, and the host's immune response changes accordingly. Recently, it was found that mutant strains of MTB-PcaA lacking cyclopropane synthase induced a reduced ability of wild-type mouse macrophages to produce proinflammatory cytokines and to form new granulomas (Hayley et al., 2017).

Studies have confirmed that, after the binding of TDMS receptors to CLRs, macrophages are activated through the SYK/CARD9/BCL10 pathway to produce cytokines (Mohlopheni et al., 2010). Further studies have shown that CARD9-deficient mice can initiate an effective adaptive immune response, but the growth of MTB in host cells is not restricted (Matthew Wagener et al., 2018). These findings suggested that MTB can produce an inflammatory level sufficient to promote granulomatous development without stimulating host cell death by fine-tuning mycoacid synthesis, allowing MTB to slowly persist or proliferate, thereby evading the host immune response.

Molecular mechanism of MTB escaping the host macrophage effect

After being engulfed by macrophages, MTB can block the fusion of phagocytes and lysosomes, thus avoiding lysosomal attack. The phagosome of *Mycobacteri*a cannot be incorporated into the vesicular ATP enzyme; thus, the transmembrane transport of the intimal system cannot be controlled by the energy produced by hydrolyzing ATP (Yu et al., 2018). The specific molecular mechanism by which MTB inhibits phagosome-lysosome fusion is not yet known and needs further study. At present, it is believed that the serine/threonine protein kinases (STPKs) of MTB are effective molecules for inhibiting phagosome-lysosome fusion (Shukla et al., 2014). A recent study showed that MTB containing STPKs could inhibit phagosome-lysosomal fusion, while MTB without STPKs could not locate the lysosome-like structure of host cells (Lee et al., 2018). It is suggested that the mechanism may be related to the regulation of the tricarboxylic acid cycle and the perception of amino acid content by effector molecules containing Ser/Thr kinase through the phosphorylated substrate GarA (Alber, 2009; Pahari et al., 2020).

Molecular mechanism of MTB escaping host autophagy

Autophagy is a process in which the host is responsible for cell homeostasis and can be induced, which can remove damaged organelles or unnecessary subcellular structures. Autophagy first forms autophagic vesicles with a double-membrane structure. When the inclusion bodies in the cytoplasm fuse with lysosomes, the substances swallowed by autophagy vesicles are digested.

Research has found that MTB can be located in autophagy vesicles in host cells, and lysosomes obtained from phagocytes containing MTB can cause autophagy in host cells by acidification, thus eliminating MTB. After lipopolysaccharide treatment of host cells, the number of MTB in autophagy vesicles increases sharply, which suggests that TLR4 mediates autophagy induction (Mohd et al., 2021; Romagnoli et al., 2018). A further study found that MTB activates macrophage autophagy mainly by intracellular vitamin D receptor and IL-1R (Degiacomi et al., 2017; Strong et al., 2020).

The antigenic target protein ESX-1 of MTB is a multibasement membrane complex that forms a channel on the membrane (Niu et al., 2011). Recent research found that ESX-1 can increase the permeability of phagocytes and activate NLRP3 receptors. When the ESX-1 content decreases, the virulence of MTB also decreases. In addition, MTB can use the host miRNA pathway to coordinate autophagy and reprogram host lipid metabolism to ensure its intracellular survival and retention (Martinez et al., 2016; Mirzaei et al., 2021).

Summary and prospects

In this review, we focus on the special cell structure of MTB and the research progress of the interaction between MTB and host cell surface pattern recognition receptors (such as CLRs, NLRs, and TLRs), as well as macrophage effector molecules and autophagy. At present, through the study of these signaling pathways, researchers have a certain understanding of the mechanism by which MTB resides in the host but a very limited understanding of the molecular mechanism of escape from host pattern recognition receptor signal transduction. MTB can change host cell immune function through a variety of molecular mechanisms (Bussi and Gutierrez, 2019). In this paper, we reviewed a large number of papers about how the immune system senses and fights MTB and how MTB escapes the immune system. We also introduced the structure of MTB, the interaction of MTB effector proteins and the host and the

molecular mechanism of MTB escape from host membrane surface pattern receptors. This study may provide research ideas for the discovery of new anti-tuberculosis drugs and the development of host-oriented treatment strategies.

In the future, we should continue exploring the effector components of MTB interacting with host cells through various effective screening techniques, such as transposon mutation libraries (López-Agudelo et al., 2020) and Crispr-Cas9 mutation libraries (Qiyao et al., 2020). In addition, the protein–protein interactions between MTB and host cells usually involve bacterial pathogenicity and persistence, and these proteins play a potential role in the pathogenesis of tuberculosis. Therefore, further understanding of the MTB-host molecular interaction network will be helpful to understand the molecular mechanisms by which MTB escape the host's immune response. These studies will help identify new methods and strategies for the prevention and treatment of tuberculosis and lay a foundation for the early eradication of tuberculosis.

Author contributions

All authors listed have made a substantial, direct, and intellectual contribution to the work and approved it for publication. Conceptualization, QL and LG; validation, QL and LG; formal analysis, YW and QS; investigation, YW and QS; data curation, QC, XZ and HY; writing—original draft preparation, QL and LG; writing—review and editing, LG; SL and YW; supervision, QL and LG; project administration, LG; funding acquisition, QL and LG.

Conflict of interest

The authors declare that the research was conducted in the absence of any commercial or financial relationships that could be construed as a potential conflict of interest.

Funding

This research was supported by the National Natural Science Foundation of China (No. 81673639) and the Natural Science Foundation of Zhejiang Province (LY20H280002).and Zhejiang Chinese Medical University (No. 2022TS001).

Publisher's note

References

Abrahams, K. A., and Besra, G. S. (2018). Mycobacterial cell wall biosynthesis: A multifaceted antibiotic target. *Parasitology* 145, 116–133. doi: 10.1017/S0031182016002377

Alber, T. (2009). Signaling mechanisms of the mycobacterium tuberculosis receptor Ser/Thr protein kinases. *Curr. Opin. Struct. Biol.* 19 (6), 650–657. doi: 10.1016/j.sbi.2009.10.017

Alemnew, B., Hoff, S. T., Abebe, T., Abebe, M., Aseffa, A., Howe, R., et al. (2021). *Ex vivo* mRNA expression of toll-like receptors during latent tuberculosis infection. *BMC Immunol.* 22 (9). doi: 10.1186/s12865-021-00400-4

Allue-Guardia, A., Garcia, J. I., and Torrelles, J. B. (2021). Evolution of drug-resistant mycobacterium tuberculosis strains and their adaptation to the human lung environment. *Front. Microbiol.* 12, 612675. doi: 10.3389/fmicb.2021.612675

Alvarez-Jiménez, V. D., Leyva-Paredes, K., García-Martínez, M., Vázquez-Flores, L., García-Paredes, V. G., Campillo-Navarro, M., et al. (2018). Extracellular vesicles released from mycobacterium tuberculosis-infected neutrophils promote macrophage autophagy and decrease intracellular mycobacterial survival. *Front. Immunol.* 9, 272. doi: 10.3389/fimmu.2018.00272

Arcos, J., Sasindran, S. J., Fujiwara, N., Turner, J., Schlesinger, L. S., and Torrelles, J. B. (2011). Human lung hydrolases delineate mycobacterium tuberculosis-macrophage interactions and the capacity to control infection. *J. Immunol.* 187, 372–381. doi: 10.4049/jimmunol.1100823

Augenstreich, J., and Briken, V. (2020). Host cell targets of released lipid and secreted protein effectors of mycobacterium tuberculosis. *Front. Cell Infect. Microbiol.* 10, 595029. doi: 10.3389/fcimb.2020.595029

Chakaya, J, Khan, M, Ntoumi, F, Aklillu, E, Fatima, R, Mwaba, P, et al. (2020). *Global tuberculosis report 2020* (Geneva: World Health Organization). Licence: CC BY-NC-SA 3.0 IGO.

Barkan, D., Rao, V., George, D., Sukenick, G. D., and Glickman, M. S.. (2010). Redundant function of cmaA2 and mmaA2 in mycobacterium tuberculosis cis cyclopropanation of oxygenated mycolates. *J. Bacteriol.* 192 (14), 3661–3668. doi: 10.1128/JB.00312-10

Barreteau, H., Kovac, A., Boniface, A., Sova, M., Gobec, S., and Blanot, D. (2008) Cytoplasmic steps of peptidoglycan biosynthesis. *FEMS Microbiol. Rev.* 32, 168–207. doi: 10.1111/j.1574-6976.2008.00104.x

Beckwith, K. S., Beckwith, M. S., Ullmann, S., Sætra, R. S., Kim, H., Marstad, A., et al. (2020). Plasma membrane damage causes NLRP3 activation and pyroptosis during mycobacterium tuberculosis infection. *Nat. Commun.* 11, 2270. doi: 10.1038/s41467-020-16143-6

Behr, M. A., and Divangahi, M. (2015). Freund's adjuvant, NOD2 and mycobacteria. *Curr. Opin. Microbiol.* 23, 126–132. doi: 10.1016/j.mib.2014.11.015

Benjawan, K., Vivek, N., Sittiruk, R., Namwat, W, Paemanee, A, Lulitanond, V., et al. (2015). Comparative proteomics of activated THP-1 cells infected with mycobacterium tuberculosis identifies putative clearance biomarkers for tuberculosis treatment. *PloS One* 10 (7), e0134168. doi: 10.1371/journal.pon

Brennan, P. J., and Crick, D. C. (2007). The cell-wall core of mycobacterium tuberculosis in the context of drug discovery. *Curr. Top. Med. Chem.* 7, 475–488. doi: 10.2174/156802607780059763

Bulut, Y., Michelsen, K. S., Hayrapetian, L., Naiki, Y., Spallek, R., Singh, M., et al. (2005). Mycobacterium tuberculosis heat shock proteins use diverse toll-like receptor pathways to activate pro-inflammatory signals. *J. Biol. Chem.* 280 (22), 20961–20967. doi: 10.1074/jbc.M411379200

Bussi, C., and Gutierrez, M. G. (2019). Mycobacterium tuberculosis infection of host cells in space and time 43, 4, 341–361. doi: 10.1093/femsre/fuz006

Canezin, P. H., Caleffi-Ferracioli, K. R., Scodro, R. B. L., Dias Siqueira, V. L., Pavan, F. R., Esteves Barros, I. L., et al. (2018). Intramacrophage mycobacterium tuberculosis efflux pump gene regulation after rifampicin and verapamil exposure. *J. Antimicrob. Chemother.* 73, 1770–1776. doi: 10.1093/jac/dky091

Cervantes, J. L. (2017). MyD88 in mycobacterium tuberculosis infection. *Med. Microbiol. Immunol.* 206, 187–193. doi: 10.1007/s00430-017-0495-0

Cubillos-Angulo, J. M., Fernandes, C. D., Araújo, D. N., Carmo, C. A., Arriaga, M, , B., and and Andrade, B. B. (2021). The influence of single nucleotide polymorphisms of NOD2 or CD14 on the risk of mycobacterium tuberculosis diseases: A systematic review. *Syst. Rev.* 10, 174. doi: 10.1186/s13643-021-01729-y

Davila, S., Hibberd, M. L., HariDass, R., Wong, H. E.E., Sahiratmadja, E., Bonnard, C., et al. (2008). Genetic association and expression studies indicate a role of toll-like receptor 8 in pulmonary tuberculosis. *PloS Genet.* 4, e1000218. doi: 10.1371/journal.pgen.1000218

Degiacomi, G., Benjak, A., Madacki, J., Boldrin, F., Provvedi, R., Palù, G., et al. (2017). Essentiality of mmpL3 and impact of its silencing on mycobacterium tuberculosis gene expression. *Sci. Rep.* 7, 43495. doi: 10.1038/srep43495

Donovan, M. L., Schultz, T. E., Duke, T. J., and Blumenthal, A. (2017). Type I interferons in the pathogenesis of tuberculosis: Molecular drivers and immunological consequences. *Front. Immunol.* 8, 1633. doi: 10.3389/fimmu.2017.01633

Doyle, S. L., and O'Neill, L. A. (2006). Toll-like receptors: from the discovery of NFkappaB to new insights into transcriptional regulations in innate immunity. *Biochem. Pharmacol.* 72, 1102–1113. doi: 10.1016/j.bcp.2006.07.010

Drage, M. G., Pecora, N. D., Hise, A. G., Febbraio, M., Silverstein, R. L., Golenbock, D. T., et al. (2009). TLR2 and its coreceptors determine responses of macrophagesand dendritic cells to lipoproteins of mycobacterium tuberculosis. *Cell Immunol.* 258, 29–37. doi: 10.1016/j.cellimm.2009.03.008

Fiske, C. T., Blackman, A., Maruri, F., Rebeiro, P. F., Huaman, M., Kator, J., et al. (2019). Increased vitamin d receptor expression from macrophages after stimulation with m. tuberculosis among persons who have recovered from extrapulmonary tuberculosis. *BMC Infect. Dis.* 19, 366. doi: 10.1186/s12879-019-3958-7

Foot Perkowski, E., Miller, B. K., McCann, J. R., Sullivan, J. T., Malik, S., Coy Allen, I., et al. (2016). An orphaned mce-associated membrane protein of mycobacterium tuberculosis is a virulence factor that stabilizes mce transporters. *Mol. Microbiol.* 100 (1), 90–107. doi: 10.1111/mmi.13303

Hayley, C. W., DiFazio, R. M., Linderman, J. J., Flynn, J. L., and Kirschner, D. E. (2017). Identifying mechanisms driving formation of granuloma-associated fibrosis during mycobacterium tuberculosis infection. *J. Theor. Biol.* , 429: 1–429:17. doi: 10.1016/j.jtbi.2017.06.017

Hossain, M. M., and Norazmi, M. N. (2013). Pattern recognition receptors and cytokines in mycobacterium tuberculosis infection-the doubleedged sword. *BioMed. Res. Int.* 2013, 179174. doi: 10.1155/2013/179174

Jain, N., Kalam, H., Singh, L., Sharma, V., Kedia, S., Das, P., et al. (2020). Mesenchymal stem cells offer a drug-tolerant and immune-privileged niche to mycobacterium tuberculosis. *Nat. Commun.* 11, 3062. doi: 10.1038/s41467-020-16877-3

Ji-Hae, P., Dahee, S., Keu Eun San, K., Lee, W., and Shin, S. J. (2021). Understanding metabolic regulation between host and pathogens: New opportunities for the development of improved therapeutic strategies against mycobacterium infection. *Front. Cell Infect. Microbiol.* 11, 635335. doi: 10.3389/fcimb.2021.635335

Jing, W., Teng, J. L. L., Zhao, D., Ge, P., Li, B., Woo, P. C. Y., et al (2016). The ubiquitin ligase TRIM27 functions as a host restriction factor antagonized by mycobacterium tuberculosis PtpA during mycobacterial infection. *Sci. Rep.* 6, 34827. doi: 10.1038/srep34827

Kallenius, G., Correia, M., Buteme, H., Hamasur, B., and Svenson, S. B. (2016). Lipoarabinomannan, and its related glycolipids, induce divergent and opposing immune responses to mycobacterium tuberculosis depending on structural diversity and experimental variations. *Tuberculosis (Edinb)* 96, 120–130. doi: 10.1016/j.tube.2015.09.005

Kalscheuer, R., Palacios, A., Anso, I., Cifuente, J., Anguita, J., Jacobs, W. R.Jr, et al. (2019). The mycobacterium tuberculosis capsule: A cell structure with key implications in pathogenesis. *Biochem. J.* 476, 1995–2016. doi: 10.1042/BCJ20190324

Kang, T. J., Lee, S. B., and Chae, G. T. (2002). A polymorphism in the toll-like receptor 2 is associated with IL-12 production from monocyte in lepromatous leprosy. *Cytokine* 20, 56–62. doi: 10.1006/cyto.2002.1982

Kanji, A., Hasan, R., and Hasan, Z. (2019). Efflux pump as alternate mechanism for drug resistance in mycobacterium tuberculosis. *Indian J. Tuberc* 66, 20–25. doi: 10.1016/j.ijtb.2018.07.008

Kawai, T., and Akira, S. (2006). TLR signaling. *Cell Death Differ.* 13, 816–25. doi: 10.1038/sj.cdd.4401850

Kawai, T., and Akira, S. (2011). Toll-like receptors and their crosstalk with other innate receptors in infection and immunity. *Immun* 34, 637–50. 36. doi: 10.1016/j.immuni.2011.05.006

Kay, E., Scotland, R. S., and Whiteford, J. R. (2013). Toll-like receptors: role in inflammation and therapeutic potential. *Biofactors* 40 (3), 284–94. doi: 10.1002/biof.1156

Kleinnijenhuis, J., Joosten, L. A., van de Veerdonk, F. L., Savage, N., van Crevel, R., Jan Kullberg, B., et al. (2009). Transcriptional and inflammasome mediated pathways for the induction of IL-1beta production by mycobacterium tuberculosis. *Eur. J. Immunol.* 39 (7), 1914–1922. doi: 10.1002/eji.200839115

Kleinnijenhuis, J., Oosting, M., Joosten, L. A., Netea, M. G., and Van Crevel, R. (2011). Innate immune recognition of mycobacter-ium tuberculosis. *Clin. Dev. Immunol.* 405310, 2011. doi: 10.1155/2011/405310

Konowich, J., Gopalakrishnan, A., Dietzold,, Verma, S., Bhatt, K., Rafi, W., et al. (2017). Divergent functions of toll-like receptor 2 on hematopoietic and non-hematopoietic cells during chronic mycobacterium tuberculosis infection. *J. Immunol.* 198 (2), 741–748. doi: 10.4049/jimmunol.1601651

Krakauer, T.. (2019). Inflammasomes, autophagy, and cell death: The trinity of innate host defense against intracellular bacteria. *Mediators Inflammation* 2471215, 2019. doi: 10.1155/2019/2471215

Kramnik, I., and Beamer, G. (2016). Mouse models of human TB pathology: roles in the analysis of necrosis and the development of host-directed therapies. *Semin. Immunopathol.* 38, 221–237. doi: 10.1007/s00281-015-0538-9

Krutzik, S. R., Ochoa, M. T., Sieling, P. A., Uematsu, S., Ng, Y. W., Legaspi, A., et al. (2003). Activation and regulation of toll-like receptors 2 and 1 in human leprosy. *Nat. Med.* 9, 525–532. doi: 10.1038/nm864

Kumar, V. (2018). Toll-like receptors in immunity and inflammatory diseases: Past, present, and future. *Int. Immunopharmacol* 59, 391–412. doi: 10.1016/j.intimp.2018.03.002

Lee, H.-J., Ko, H.-J., Song, D.-K., and Jung, Y.J. (2018). Lysophosphatidylcholine promotes phagosome maturation and regulates inflammatory mediator production through the protein kinase a–phosphatidylinositol 3 Kinase–p38 mitogen-activated protein kinase signaling pathway during mycobacterium tuberculosis infection in mouse macrophages. *Front. Immunol.* 9, 920. doi: 10.3389/fimmu.2018.00920

Li, J., Chai, Q.-Y., Zhang, Y., Li, B.-X., Wang, J., Qiu, X.-B., et al. (2015). Mycobacterium tuberculosis Mce3E suppresses host innate immune responses by targeting ERK1/2 signaling. *J. Immunol.* 194 (8), 3756–3767. doi: 10.4049/jimmunol.1402679

Liu, S., Jia, H., Hou, T. X., Guo, X., and Zhang, G. (2018). Recombinant Mtb9.8 of mycobacterium bovis stimulates TNF-α and IL-1β secretion by RAW264.7 macrophages through activation of NF-κB pathway *via* TLR2. *Sci. Rep.* 8 (1), 1928. doi: 10.1038/s41598-018-20433-x.

Liu, P. T., Krutzik, S. R., and Modlin, R. L. (2007). Therapeutic implications of the TLR and VDR partnership. *Trends Mol. Med.* 13, 117–124. doi: 10.1016/j.molmed.2007.01.006

Liu, Y., Yin, H., Zhao, M., and Lu, Q.. (2013). TLR2 and TLR4 in autoimmune diseases: a comprehensive review. *Clin. Rev. Allergy Immunol.* 47 (2), 136–47. 46. doi: 10.1007/s12016-013-8402-y.

Liu, L., Zhai, K., Chen, Y., Chen, X., Wang, G., Wu, L., et al. (2021). Effect and mechanism of mycobacterium tuberculosis lipoprotein LpqH in NLRP3 inflammasome activation in mouse ana-1 macrophage. *BioMed. Res. Int.* 2021, 8239135. doi: 10.1155/2021/8239135

López-Agudelo, V. A., Tom, A., Laing, E., Wu, H., Baena, A., Barrera, L. F., et al. (2020). A systematic evaluation of mycobacterium tuberculosis genome-scale metabolic networks. *PloS Comput. Biol.* 16 (6), e1007533. doi: 10.1371/journal.pcbi.1007533

Lorenz, E., Mira, J. P., Cornish, K. L., Arbour, N. C., and Schwartz, D. A. (2000). A novel polymorphism in the toll-like receptor 2 gene and its potential association with staphylococcal infection. *Infect. Immun.* 68, 6398–6401. doi: 10.1128/IAI.68.11.6398-6401.2000

Marrakchi, H., Laneelle, M. A., and Daffe, M. (2014). Mycolic acids: structures, biosynthesis, and beyond. *Chem. Biol.* 21, 67–85. doi: 10.1016/j.chembiol.2013.11.011

Martinez, N., Ketheesan, N., West, K., Vallerskog, T., and Kornfeld, H.. (2016). Impaired recognition of mycobacterium tuberculosis by alveolar macrophages from diabetic mice. *J. Infect. Dis.* 214, 1629–1637. doi: 10.1093/infdis/jiw436

Martinez-Perez, A., Igea, A., Estevez,, Ferreira, C. M., Torrado, E., Gil Castro, A., et al. (2020). Changes in the immune phenotype and gene expression profile driven by a novel tuberculosis nanovaccine: Short and long-term post-immunization. *Front. Immunol.* 11, 589863. doi: 10.3389/fimmu.2020.589863

Matthew Wagener, J., Hoving, C., Ndlovu, H., and Marakalala, M. J.. (2018). Dectin-1-Syk-CARD9 signaling pathway in TB immunity. *Front. Immunol.* 9, 225. doi: 10.3389/fimmu.2018.00225

Mehta, P., Ray, A., and Mazumder, S. (2021). TLRs in mycobacterial pathogenesis: Black and white or shades of Gray. *Curr. Microbiol* 78 (6), 2183–2193. doi: 10.1007/s00284-021-02488-8

Mercedes Romero, M., Ignacio Basile, J., López, B., Ritacco, V., Barrera, L., del Carmen Sasiain, M., et al. (2014). Outbreaks of mycobacterium tuberculosis MDR strains differentially induce neutrophil respiratory burst involving lipid rafts, p38 MAPK and syk. *BMC Infect. Dis.* 14, 262. doi: 10.1186/1471-2334-14-262

Mika, J., Zychowska, M., Popiolek-Barczyk, K., Rojewska, E., and Przewlocka, B. (2013). Importance of glial activation in neuropathic pain. *Eur. J. Pharmacol.* 716, 106–119. doi: 10.1016/j.ejphar.2013.01.072

Mirzaei, R., Babakhani, S., Ajorloo, P., Heidari Ahmadi, R., Hosseini-Fard, S. R., Keyvani, H., et al. (2021). The emerging role of exosomal miRNAs as a diagnostic and therapeutic biomarker in mycobacterium tuberculosis infection. *Mol. Med.* 27, 34. doi: 10.1186/s10020-021-00296-1

Mohd, S., Neha, Q., Javaid Ahmad, S., Kumar Singh, A., Bishai, W. R., Ehtesham, N. Z., et al. (2021). Post translational modifications in tuberculosis: ubiquitination paradox. *Autophagy* 17 (3), 814–817. doi: 10.1080/15548627.2020.1850009

Mohd, S., Neha, Q., Neha, S., Singh, J., Sheikh, J. A., Khubaib, M., et al. (,2021). Mycobacterium tuberculosis RipA dampens TLR4-mediated host protective response using a multi-pronged approach involving autophagy, apoptosis, metabolic repurposing, and immune modulation. *Front. Immunol.* 12, 636644. doi: 10.3389/fimmu.2021.636644

Mohlopheni, J. M., Graham, L. M., and Brown, G. D. (2010). The role of Syk/CARD9-coupled c-type lectin receptors in immunity to mycobacterium tuberculosis infections. *Clin. Dev. Immunol.* 2010, 567571. doi: 10.1155/2010/567571

Najmi, N., Kaur, G., Sharma, S. K., and Mehra, N. K. (2010). Human toll-like receptor 4 polymorphisms TLR4 Asp299Gly and Thr399Ile influence susceptibility and severity of pulmonary tuberculosis in the Asian Indian population. *Tissue Antigens* 76, 102–109. doi: 10.1111/j.1399-0039.2010.01481.x

Nargis, K., Pahari, S., Vidyarthi, A., Aqdas, M., and Agrewala, J. N.. (2016). NOD-2 and TLR-4 signaling reinforces the efficacy of dendritic cells and reduces the dose of TB drugs against mycobacterium tuberculosis. *J. Innate Immun.* 8 (3), 228–242. doi: 10.1159/000439591

Nguyen, H., Gazy, N., and Venketaraman, V. (2020). A role of intracellular toll-like receptors (3, 7, and 9) in response to mycobacterium tuberculosis and Co-infection with HIV. *Int. J. Mol. Sci.* 21 (17), 6148. doi: 10.3390/ijms21176148

Niu, H., Hu, L., Li, Q., Da, Z., Wang, B., Tang, K., et al. (2011). Construction and evaluation of a multistage mycobacterium tuberculosis subunit vaccine candidate Mtb10.4-HspX. *Vaccine* 29, 9451–9458. doi: 10.1016/j.vaccine.2011.10.032

Niu, W., Sun, B., Li, M., Cui, J., Huang, J., Zhang, L., et al. (2018). TLR-4/microRNA-125a/NF-κB signaling modulates the immune response to mycobacterium tuberculosis infection. *Cell Cycle* 17 (15), 1931–1945. doi: 10.1080/15384101.2018.1509636

Pahari, S., Negi, S., Aqdas, M., Arnett, E., Schlesinger, L. S., Agrewala, J. N., et al. (2020). Induction of autophagy through CLEC4E in combination with TLR4: an innovative strategy to restrict the survival of mycobacterium tuberculosis. *Autophagy* 16 (6), 1021–1043. doi: 10.1080/15548627.2019.1658436

Pathak, L., and Das, B. (2020). Initiation of post-primary tuberculosis of the lungs: Exploring the secret role of bone marrow derived stem cells. *Front. Immunol.* 11, 594572. doi: 10.3389/fimmu.2020.594572

Picard, C., Puel, A., Bonnet, M., Ku, C.L., Bustamante, J., Yang, K., et al. (2003). Pyogenic bacterial infections in humans with IRAK-4 deficiency. *Science* 299 (5615), 2076–2079. doi: 10.1126/science.1081902

Qiyao, C., Lin, W., Cui Hua, L., and Ge, B.. (2020). New insights into the evasion of host innate immunity by mycobacterium tuberculosis. *Cell Mol. Immunol.* 17 (9), 901–913. doi: 10.1038/s41423-020-0502-z

Qu, Z., Zhou, J., Zhou, Y., Xie, Y., Jiang, Y., Wu, J., et al. (2020). Mycobacterial EST12 activates a RACK1–NLRP3–gasdermin d pyroptosis–IL-1β immune pathway. *Sci. Adv.* 6 (43), eaba4733. doi: 10.1126/sciadv.aba4733

Richa, M., Sakshi, K., Nitish, M., Bandyopadhyay, P., Mehta, M., Munshi, M., et al. (2019). Targeting redox heterogeneity to counteract drug tolerance in replicating mycobacterium tuberculosis. *Sci. Transl. Med.* 11 (518), eaaw6635. doi: 10.1126/scitranslmed.aaw6635

Romagnoli, A., Petruccioli, E., Palucci, I., Camassa, S., Carata, E., Petrone, L., et al. (2018). Clinical isolates of the modern mycobacterium tuberculosis lineage 4 evade host defense in human macrophages through eluding IL-1β-induced autophagy. *Cell Death Dis.* 9 (6), 624. doi: 10.1038/s41419-018-0640-8

Rook, G. A., Dheda, K., and Zumla, A. (2005). Opinion: immune responses to tuberculosisin developing countries: Implications for new vaccines. *Nat. Rev. Immunol.* 5, 661–667. doi: 10.1038/nri1666

Sabir, N., Hussain, T., Shah, S. Z. A., Zhao, D., Zhou, X., et al. (2017). IFN-beta: A contentious player in host-pathogen interaction in tuberculosis. *Int. J. Mol. Sci.* 18 (12), 2725. doi: 10.3390/ijms18122725.

Shukla, S., Richardson, E. T., Athman, J. J., Shi, L., Wearsch, P. A., McDonald, D., et al. (2014). Mycobacterium tuberculosis lipoprotein LprG binds lipoarabinomannan and determines its cell envelope localization to control phagolysosomal fusion. *PloS Pathog.* 10 (10), e1004471. doi: 10.1371/journal.ppat.1004471

Singh, P., Katoch, V. M., Mohanty, K. K., and Chauhan, D. S.. (2016). Analysis of expression profile of mce operon genes (mce1, mce2, mce3 operon) in different mycobacterium tuberculosis isolates at different growth phases. *Indian J. Med. Res.* 143 (4), 487–494. doi: 10.4103/0971-5916.184305

Singh, B., Saqib, M., Chakraborty, A., and Bhaskarl, S.. (2019). Lipoarabinomannan from mycobacterium indicus pranii shows immunostimulatory activity and induces autophagy in macrophages. *PloS One* 14 (10), e0224239. doi: 10.1371/journal.pone.0224239

Strong, E. J., Jurcic Smith, K. L., Saini, N. K., Ng, T. W., Porcelli, S. A., Lee, S., et al. (2020). Identification of autophagy-inhibiting factors of mycobacterium tuberculosis by high-throughput loss-of-Function screening. *Infect. Immun.* 88 (12), e00269–e00220. doi: 10.1128/IAI.00269-20

Takeuchi, O., and Akira, S.. (2010). Pattern recognition receptors and inflammation. *Cell* 140, 805–820. doi: 10.1016/j.cell.2010.01.022

Tan, H. K., Fan, S. J., Xu, Y. C., Zhou, J. J., Chen, Y. Z., Xie, T. A., et al. (2020). The clinical diagnostic value of xpert MTB/RIF for the detection of mycobacterium tuberculosis in gastric aspirates. *Biosci. Rep.* 40. doi: 10.1042/BSR20200138

Thada, S., Horvath, G. L., Muller, M. M., Dittrich, N., Conrad, M. L., Sur, S., et al. (2021). Interaction of TLR4 and TLR8 in the innate immune response against mycobacterium tuberculosis. *Int. J. Mol. Sci.* 22 (4), 1560. doi: 10.3390/ijms22041560

Tuladhar, S., and Kanneganti, T. D. (2020). NLRP12 in innate immunity and inflammation. *Mol. Aspects Med.* 76, 100887. doi: 10.1016/j.mam.2020.100887

Valérie, P., Bach, H., and Av-Gay, Y. (2014). Mycobacterium tuberculosis promotes anti-apoptotic activity of the macrophage by PtpA protein-dependent dephosphorylation of host GSK3α. *J. Biol. Chem.* 289 (42), 29376–29385. doi: 10.1074/jbc.M114.582502

Wang, J., Ge, P., Qiang, L., Tian, F., Zhao, D., Chai, Q., et al. (2017). The mycobacterial phosphatase PtpA regulates the expression of host genes and promotes cell proliferation. *Nat. Commun.* 8 (1), 244. doi: 10.1038/s41467-017-00279-z

Wan, M., Zhou, Y., and Zhu, Y. (2018). Subversion of macrophage functions by bacterial protein toxins and effectors. *Curr. Issues Mol. Biol.* 25, 61–80. doi: 10.21775/cimb.025.061

Wei, S., Wang, D., Li, H., Bi, L., Deng, J., Zhu, G., et al. (2019). Fatty acylCoA synthetase FadD13 regulates proinflammatory cytokine secretion dependent on the NF-κB signalling pathway by binding to eEF1A1. *Cell Microbiol.* 21 (12), e13090. doi: 10.1111/cmi.13090

Wilson, G. J., Marakalala, M. J., Hoving, J. C., van Laarhoven, A., Drummond, R. A., Kerscher, B., et al. (2015). The c-type lectin receptor Clecsf8/Clec4D is a key component of anti-mycobacterial immunity. *Cell Host Microbe* 17 (2), 252–259. doi: 10.1016/j.chom.2015.01.004

Wong, K. W. (2017). The role of ESX-1 in mycobacterium tuberculosis. *Pathogenesis Microbiol. Spectr.* 5 (3). doi: 10.1128/microbiolspec.TBTB2-0001-2015.

Yang, Q., Liao, M., Wang, W., Zhang, M., Chen, Q., Guo, J., et al. (2019). CD157 confers host resistance to mycobacterium tuberculosis *via* TLR2-CD157-PKCzeta-Induced reactive oxygen species production. *mBio* 10 (4), e01949–e01919. doi: 10.1128/mBio.01949-19

Yu, H., Lupoli, T. J., Kovach, A., Meng, X, Zhao, G., Nathan, C. F., et al. (2018). ATP hydrolysis-coupled peptide translocation mechanism of mycobacterium tuberculosis ClpB. *Proc. Natl. Acad. Sci. U S A* 115 (41), E9560–E9569. doi: 10.1073/pnas.1810648115

Zhao, X.-Q., Zhu, L.-L., Chang, Q., Jiang, C., You, Y., Luo, T., et al. (2014). C-type lectin receptor dectin-3 mediates trehalose 6,6′-dimycolate (TDM)-induced mincle expression through CARD9/Bcl10/MALT1-dependent NF-κB activation. *J. Biol. Chem.* 289 (43), 30052–30062. doi: 10.1074/jbc.M114.588574

frontiers | Frontiers in Cellular and Infection Microbiology

TYPE Original Research
PUBLISHED 16 September 2022
DOI 10.3389/fcimb.2022.990402

OPEN ACCESS

EDITED BY
Joaquin Pellegrini,
INSERM U1104 Centre d'immunologie de Marseille-Luminy (CIML), France

REVIEWED BY
Rogelio Hernandez Pando,
Instituto Nacional de Ciencias Médicas y Nutrición Salvador Zubirán (INCMNSZ), Mexico
Helioswilton Sales-Campos,
Universidade Federal de Goiás, Brazil

*CORRESPONDENCE
William P. Lafuse
lafuse.1@osu.edu
Murugesan V. S. Rajaram
rajaram.3@osu.edu

SPECIALTY SECTION
This article was submitted to Bacteria and Host, a section of the journal Frontiers in Cellular and Infection Microbiology

RECEIVED 09 July 2022
ACCEPTED 26 August 2022
PUBLISHED 16 September 2022

CITATION
Lafuse WP, Wu Q, Kumar N, Saljoughian N, Sunkum S, Ahumada OS, Turner J and Rajaram MVS (2022) Psychological stress creates an immune suppressive environment in the lung that increases susceptibility of aged mice to *Mycobacterium tuberculosis* infection. *Front. Cell. Infect. Microbiol.* 12:990402. doi: 10.3389/fcimb.2022.990402

Psychological stress creates an immune suppressive environment in the lung that increases susceptibility of aged mice to *Mycobacterium tuberculosis* infection

William P. Lafuse[1]*, Qian Wu[1], Naresh Kumar[1], Noushin Saljoughian[1], Shrayes Sunkum[1], Omar Santiagonunez Ahumada[1], Joanne Turner[2] and Murugesan V. S. Rajaram[1]*

[1]Department of Microbial Infection and Immunity, The Ohio State University, Columbus, OH, United States, [2]Host Pathogen Interactions Program, Texas Biomedical Research Institute, San Antonio, TX, United States

Age is a major risk factor for chronic infections, including tuberculosis (TB). Elderly TB patients also suffer from elevated levels of psychological stress. It is not clear how psychological stress impacts immune response to *Mycobacterium tuberculosis* (*M.tb*). In this study, we used social disruption stress (SDR) to investigate effects of psychological stress in young and old mice. Unexpectedly, we found that SDR suppresses lung inflammation in old mice as evidenced by lower pro-inflammatory cytokine levels in bronchial lavage fluid and decreased cytokine mRNA expression by alveolar macrophages. To investigate effects of stress on *M.tb* infection, mice were subjected to SDR and then infected with *M.tb*. As previously reported, old mice were better at controlling infection at 30 days than young mice. This control was transient as CFUs at 60 days were higher in old control mice compared to young mice. Consistently, SDR significantly increased *M.tb* growth at 60 days in old mice compared to young mice. In addition, SDR in old mice resulted in accumulation of IL-10 mRNA and decreased IFN-γ mRNA at 60 days. Also, confocal microscopy of lung sections from old SDR mice showed increased number of CD4 T cells which express LAG3 and CD49b, markers of IL-10 secreting regulatory T cells. Further, we also demonstrated that CD4 T cells from old SDR mice express IL-10. Thus, we conclude that psychological stress in old mice prior to infection, increases differentiation of IL-10 secreting T cells, which over time results in loss of control of the infection.

KEYWORDS
social stress, aging, *Mycobacterium tuberculosis*, inflammaging, granuloma, IL10

Key Points

1. Social Disruption Stress suppresses lung inflammation in old mice
2. SDR prior to infection increases *M.tb* burden at 60 day post-infection in old mice.
3. SDR in old infected mice induces expression of LAG3, CD45b, and IL-10 in CD4 T cells.

Introduction

The global population of people over age 65 is forecast to increase 3-fold by 2050 (to 1.5 billion), a growth rate that will place extraordinary demands on our health care systems (United Nations, D. o. E. a. S. A., Population Division, 2017). Although increased life expectancy is a major achievement of modern medicine, an equally important concern is quality of life for our elderly. In this regard, aging impacts nearly all organ systems, including the immune system, which exhibits a dramatic functional decline over our life span. In turn, waning or altered immunity renders our elderly populations more susceptible to infections, such as influenza, pneumococcal pneumonia, tuberculosis (TB) and more recently COVID19 (Zevallos and Justman, 2003; Krone et al., 2014; Bahadoran et al., 2016; Mehta and Dutt, 2016; Nikolich-Zugich et al., 2020). A second compounding factor for disease susceptibility and outcomes is psychological stress, which is particularly acute in older individuals, who may suffer from chronic illnesses, and/or have limited financial means, emotional support networks, or mobility. An individual's response to such unfortunate circumstances ranges from an acute to a sustained chronic stress response, the latter of which results in anxiety, depression, and increased susceptibility to diseases, including infections (Cohen et al., 2007). The mechanisms by which psychological stress compounds age-related pathologies in response to infections are poorly understood. Thus, this study examined the effect of stress on *Mycobacterium tuberculosis* (*M.tb*) infection the causative agent of TB, and a continuing threat to global health.

Individuals who are 50 years of age or older account for over 50% of all TB deaths (Negin et al., 2015). While many elderly TB cases occur after reactivation of a latent infection, older individuals are also more susceptible to developing active TB after a primary infection (Rajagopalan, 2001). These age-associated vulnerabilities primarily stem from senescence of the adaptive immune system, in particular T cell function (Weiskopf et al., 2009; Ferrando-Martinez et al., 2011; Larbi et al., 2011), and elevation of chronic low-grade inflammation (termed inflammaging) (Franceschi et al., 2000). A primary role for inflammaging in age-dependent decline in immune response is provided by studies with mice. Upon *M.tb* infection older C57BL/6 mice (18 months) are able to control the infection better than young mice (3 months), but over time gradually lose control of the infection compared to young mice (Orme, 1995; Turner et al., 2002; Vesosky and Turner, 2005), a phenomenon that has been attributed to inflammaging (Piergallini and Turner, 2018). Recently, we characterized the impact of aging on the phenotype of mouse alveolar macrophages (AMs) and their immune response to *M.tb* (Lafuse et al., 2019). We reported that AMs from old mice expressed higher mRNA levels of pro-inflammatory cytokines and contained higher cytokine levels in the bronchial fluid compared to young mice, which is indicative of inflammaging occurring in the lung. Also, we identified two distinct AM subpopulations, a major $CD11c^+$ $CD11b^-$ population and a minor $CD11c^+$ $CD11b^+$ population that is increased 4-fold in old mice. We showed that this minor population expressed a unique inflammatory mRNA signature and enhanced *M.tb* phagocytosis and survival compared to the major population, which expressed a more immune regulatory mRNA signature.

To examine the effects of psychological stress on the immune system we have utilized social disruption stress (SDR), a mouse social stressor model that involves repeated defeat in subordinate mice (Allen et al., 2012a; Allen et al., 2012b; Lafuse et al., 2017). Exposure to SDR increases serum levels of pro-inflammatory cytokines IL-1β and IL-6 (Stark et al., 2002; Engler et al., 2008; Kinsey et al., 2008) and increases spleen mass due to accumulation of $CD11b^+$ myeloid cells, which are primed for increased cytokine and microbicidal activity (Stark et al., 2002; Kinsey et al., 2007; Engler et al., 2008; Allen et al., 2012a; Allen et al., 2012b). Other studies have shown that SDR induces

Abbreviations: AMs, alveolar macrophages; *M.tb*, *Mycobacterium tuberculosis*; BAL, bronchoalveolar lavage; SDR, social disruption stress; qRT-PCR, quantitative RT-PCR; NE, norepinephrine; TR1 cells, regulatory type 1 cells; TLR2, Toll Receptor 2.

translocation of primed monocytes from the spleen into peripheral tissues and enhances inflammation (Curry et al., 2010; McKim et al., 2016; McKim et al., 2018). However, the impact of SDR in response to *M.tb* infection in the context of aging has not been not studied.

The current study examined the effect of SDR on the lungs of young and old mice and the response to infection with *M.tb*. In striking contrast to previous studies, we report that SDR does not enhance inflammation in the lung but induces an immune suppressive environment with decreased pro-inflammatory cytokine levels in the BAL fluid and decreased cytokine mRNA levels in AMs. The greatest effect was observed in stressed old mice. AMs from old mice were not primed and instead produced decreased pro-inflammatory cytokine mRNA when stimulated with a TLR2 ligand. SDR prior to infection in old mice substantially increased the *M.tb* burden at 60 days post infection, indicating that SDR exacerbates the loss of control of *M.tb* that occurs with aging. Analysis of lung mRNA from infected mice indicates at 60 days, SDR inhibited the expression of IFN-γ mRNA and increased expression of the immunosuppressive cytokine IL-10. mRNA levels of JAK3, which is most commonly expressed in T cells, were also increased in the lungs of old SDR mice, suggesting increased numbers of T cells. Confocal microscopic analysis of lung sections from old SDR mice showed increased numbers of CD4 T cells that express LAG3 and CD49b, markers of regulatory T cells (Gagliani et al., 2013). Further, we observed that CD4 T cells in old SDR mice express IL-10. Thus, our study suggests that stress in old mice regulate the differentiation of CD4 T cells from host protective Th1 cells to IL-10 secreting regulatory T cells, which would favor *M.tb* growth and loss of control of the infection at day 60. Also, this study indicates that psychological stress prior to infection can have long-term effects on the immune response to infection in the elderly. This is not only relevant to TB but is likely relevant to other lung infections including SARS-CoV2.

Materials and methods

Mice

Male C57BL/6 mice were purchased from Charles River Laboratories (Wilmington, MA) at an age of 3 months (young) or 18 months (old) obtained through a contract to Charles River Laboratories from the National Institute of Aging. Mice were housed in microisolator cages at 3 mice/cage and acclimated to the facility for 1 week prior to use. Male retired CD1 breeder mice were purchased from Charles River Laboratories and housed at 1 mouse/cage. Mice were maintained on a 12 h light/dark schedule and food and water available *ad libitum*. All procedures were approved by The Ohio State University Institutional Laboratory Animal Care and Use Committee.

Social disruption

The SDR stressor was performed as previously described (Lafuse et al., 2017). SDR involves repeated social defeat from interactions between an aggressive intruder male mouse and resident male mice for six consecutive nights. The C57BL/6 mice were randomly divided into SDR or home cage control mice. A retired CD1 breeder mouse was placed in a cage of three C57BL/6 mice, starting at 3 PM. If the intruder mouse did not initiate an attack within 10 min and defeat all three resident mice, the mouse was removed and replaced with a new intruder mouse. After 2 h, the intruder mouse was removed, and resident mice left undisturbed until the following day when the SDR protocol was repeated. The morning after the sixth cycle of SDR, the mice were sacrificed or transferred to the BSL3 vivarium for infection with *M. tb*. Mice with wounds penetrating the cutaneous layer were not used in the study. Home cage control mice were left undisturbed throughout the experiment.

Isolation of AMs and bronchial fluid

Young and old SDR and Home Cage control mice were euthanized by CO_2 following a protocol approved the Ohio State University Institutional Laboratory Animal Care and Use Committee. AMs and bronchial lavage fluid (BAL fluid) were obtained by bronchoalveolar lavage of mice by washing the lungs 10 times with 0.50 ml of sterile endotoxin-free saline (0.90% NaCl). AMs were collected by centrifugation at 300 X g for 10 min. In each experiment, AMs were pooled from 3 SDR or Home Cage mice (~1 million pooled cells). Aliquots of the pooled AMs (each ~50,000 cells) were pelleted, and RNA was isolated using TRIzol reagent (Invitrogen) for basal RNA measurements by quantitative RT-PCR (qRT-PCR). The remaining AMs were used for flow cytometry and TLR2 stimulation experiments. The supernatant fraction containing BAL fluid from individual mice was quickly frozen and stored at -80°C until use.

Isolation of splenocytes

Spleens were removed and a single-cell suspension was obtained by dicing each spleen into 1-2 mm pieces and gently pressing through a 70 μm cell strainer. Erythrocytes were lysed with Gey's lysis buffer (8 mM NH_4Cl, $5KHCO_3$) and splenocytes suspended in PBS.

Flow cytometry

AMs (1 X 10^5) and splenocytes (6 X 10^5) were aliquoted into FACS tubes and centrifuged at 300 X g for 10 min. Cell pellets were resuspended in 100 ul of FACs buffer (PBS with 2% BSA and.10% sodium azide) and incubated with 1 ul Seroblock FcR (BioRAD) for 10 min. Cells were then stained with Abs for 30 min in the dark. Cells were washed twice FACS buffer and analyzed on a LSR II cytometer using FlowJo software (Tree Star). Abs (purchased from Biolegend) used were: BV421 anti-CD11b (clone M1/70), BV785 anti-CD11c (clone N418), BV605 anti-Ly6C (clone HK1-4), allophycocyanin anti-Ly6G (clone 1A8), Alexa 488 anti NK1.1 (clone P136), Alexa 488 anti-CD45R (B220) (clone RA3-6B2), Alexa 488 anti-CD4 (clone GK1.5), and Alexa 488 anti-CD8α (clone 53-6.7). Isotype controls were BV421 rat IgG2b, BV785 hamster IgG, BV605 rat IgG2a, and allophycocyanin hamster IgG. The numbers of each myeloid population/spleen were calculated from the percentage of the population determined by flow cytometry and total spleen counts.

ELISA

Cytokine levels of BAL fluid were determined by ELISA, according to manufacturer's instructions. Aliquots of BAL fluid were added to individual ELISA plate wells (Nunc MaxiSorp plates; Thermal Fisher Scientific). Turbo-TMB-ELISA Substrate (Thermal Fisher Scientific was used for detection. ELISA kits were purchased from R&D Systems (CCL2 [DY439], IL-1β [DY421], TNF-α [DY410], IL-12p70 [DY419], GM-CSF [DY415], M-CSF [DY416], IFN-γ [DY485], IL-17 [DY421] or IL-10 (MABTECH 3432). ELISA kit for norepinephrine was obtained from G-Biosciences. Corticosterone ELISA kit was obtained from ENZO. Protein concentrations of BAL fluid were determined by Bradford assay (BioRAD).

TLR2 stimulation of AMs

AMs were plated in 48-well plates at 50,000 AMs per well in RPMI 1640 media containing 2mM glutamine, 1% pencillin/streptomycin, and 10% heat-inactivated FBS. After 2 h, nonadherent cells were removed by washing and the AMs incubated with 100 ng/ml Pam_3 CSK4 (InVivogen). After 6 h incubation, RNA was isolated using TRIzol reagent.

M. tb infection

Young and old SDR and Home Cage mice were infected with *M.tb* $H_{37}R_v$ (100-200 CFU/mouse) using an Inhalation Exposure System (Glas-col, Terre Haute, IN). After 30 and 60 days of infection, mice were euthanized by CO_2 and lung lobes removed. The *M.tb* burden was determined by plating serial dilutions of tissue homogenates of the left lung lobe onto OADC-supplemented 7H11 agar. *M.tb* CFUs were counted after 3 weeks at 37°C. Right lung lobes from each mouse were homogenized in TRIzol for RNA analysis and PBS for cytokine analysis by ELISA. Right lung lobes were also fixed in 10% formalin and embedded in paraffin. The lung lobes were sectioned and stained with hematoxylin and eosin by the OSU Comparative Pathology and Mouse Phenotyping Shared Resource for Confocal Microscopy.

RNA isolation and qRT-PCR

RNA from AM TRIzol lysates was extracted with chloroform and precipitated with isopropanol. The RNA pellet was washed once with 75% ethanol and RNA reconstituted with DNase/RNase-free water. To isolate RNA from *M.tb* infected lung tissues, TRIzol lysates were extracted with chloroform and purified by Qiagen RNAeasy mini columns with on-column DNA digestion. RNA was reverse transcribed using random primers by the Promega Reverse Transcription System (Thermal Fisher Scientific). Expression of mRNA was determined by qRT-PCR of duplicate samples using IQ SYBR Green Supermix (BioRad). The amplification conditions were 95°C for 2 min, followed by 45 cycles of 95° C for 15s, 60°C for 30s, and 72°C for 30s. Validated mouse primers listed on PrimerBank (Wang et al., 2012) were used and sequences listed in Supplemental Table 1. Expression of mRNA was calculated by the Δ threshold cycle method using β-actin as the normalizer (Livak and Schmittgen, 2001). Levels of mRNA in AMs and mRNA in lung tissue from *M. tuberculosis* infected mice were expressed relative to the level of β-actin.

Confocal microscopy of lung sections

Lung sections from *M.tb* infected mice were subjected to deparaffinization and antigen retrieval prior to blocking for 1 h with 10% goat serum and 1% FBS in a humidified chamber (Wu et al., 2019). The sections were incubated at 4°C with primary antibodies against CD4 (rabbit mAb D7D2Z, Cell Signaling), LAG3 (rat mAb C9BZW, BioLegend), CD49b (biotin labeled rat mAb DX5, BioLegend), and IL-10 (rat Mab MT60, MABTECH). After washing PBS were incubated for 1 h with secondary antibodies Alexa 488 labeled donkey $F(ab')_2$ anti-rabbit IgG and Alexa 647 labeled donkey $F(ab')_2$ anti-rat IgG (Abcam) and Alexa-647 labeled streptavidin (BioLegend). Nuclei were stained with DAPI. All fluorescence images were captured using an Olympus FV 1000 Spectral Confocal system. Mean fluorescence intensity of cells was determined using Image J (version 2.0.0).

Statistical analysis

All data were expressed as mean± SEM. Statistical analysis was performed using GraphPad Prism software. Comparisons were done using one-way ANOVA with Tukey multiple-comparisons *post hoc* test. Differences were considered statistically significant when p values were $p < 0.05$.

Results

Effect of SDR on myeloid populations in the spleen and AM populations in the lung

Our previous studies have shown that SDR in young mice results in the accumulation of $CD11b^+$ myeloid cells in the spleen that express higher levels of IL-1β mRNA than Home Cage control mice (Lafuse et al., 2017). SDR in old mice also induced accumulation of $CD11b^+$ myeloid cells as evidenced by increased spleen weight (Supplemental Figure 1A) and increased numbers of $CD11b^+$ $Ly6C^+$ monocytes and $CD11b^+$ $Ly6G^+$ neutrophils in old mice (Supplemental Figures 1B–D). This indicates that the response of old mice to SDR in the spleen is identical to the response of SDR in young mice.

Studies have shown that SDR induces migration of primed monocytes from the spleen into various organs including the lung (Curry et al., 2010; McKim et al., 2016; McKim et al., 2018). Thus, we next examined the effect of SDR on the AM populations in the lung alveolar space. We have identified two AM populations, a major $CD11c^+$ $CD11b^-$ population with a regulatory phenotype and a minor $CD11c^+$ $CD11b^+$ inflammatory population that is increased 4-fold in old mice (Lafuse et al., 2019). AMs from old mice expressed CD64 (FcγR1), which is absent in dendritic cells (Immunological Genome Consortium, 2012), suggesting that these cells are not dendritic cells. Sorted $CD11c^+$ $CD11b^+$ AMs from old mice expressed higher mRNA levels of CCL2, IL-1β, and IL-6, whereas $CD11c^+$ $CD11b^-$ AMs expressed higher levels of immune-regulatory IFN-β, and IL-10. The $CD11c^+$ $CD11b^+$ population also showed enhanced *M.tb* phagocytosis and survival compared to the $CD11c^+$ $CD11b^-$ population. Thus, this study identified a major AM population with immune-regulatory function and a minor AM population with an inflammatory signature and is more permissive for *M.tb.* In the current study, we determined whether SDR altered these AM populations in the lung. AMs were isolated from the BAL fluid of young and old mice and the two AM populations analyzed by flow cytometry. The dot plots shown in Figures 1A, B is the gating strategy of BAL cells with different macrophage markers (CD11b and CD11c). As we previously reported there were more $CD11c^+$ $CD11b^+$ AMs in the old mice (Figure 1C). However, SDR did not affect the numbers of the two AM populations (Figures 1C, D). We noted the presence of cells that were $CD11c^-$ $CD11b^+$, which are $Ly6G^+$ neutrophils and $Ly6C^+$ monocytes. The numbers of neutrophils and monocytes present in the BAL fluid were not significantly different in young and old mice and was not altered by SDR (Figures 1E, F). A previous study (Curry et al., 2010) reported that $CD11b^+$ myeloid cells migrate into the lung in response to SDR. However, our studies of BAL fluid myeloid cells suggest that $CD11b^+$ myeloid cells that migrate into the lung in response to SDR do not accumulate in the alveolar space and are likely retained in the lung interstitium.

SDR induces an immune suppressive environment in the lung of aged mice

All previous studies have indicated that SDR enhances inflammation in tissues. Thus, to test whether this also holds true for the lung of aged mice, we measured cytokine levels in BAL fluid and cytokine mRNA levels in AMs. Surprisingly, SDR induced lower basal levels of pro-inflammatory cytokines IL-β and TNFα and the CXCL2 chemokine in BAL fluid of old and young mice, with the greatest effect in old mice (Figures 2A–C). Particularly noteworthy was that SDR in old mice greatly attenuated the production of IL-1β and TNFα, as well as the chemokine CXCL2. We also assayed for IL-12p40, CCL2, and IL-6. However, the levels of these cytokines were at or below the detection level. We also determined total protein levels in BAL fluid and found no significant differences in protein levels with age or SDR (Figure 2D).

To determine the effect of SDR on mRNA expression levels of various cytokines and chemokines in the AMs of young and old mice, we isolated RNA from AMs without culture and the mRNA levels of different cytokines and chemokines were determined by qRT-PCR. Our data indicate that cytokine and chemokine mRNA levels paralleled the cytokine levels in the BAL fluid with decreased levels of IL-1β, TNFα, and CXCL2 mRNA in old SDR mice (Figures 2E–G). SDR in young mice had no effect on cytokine mRNA levels. We have previously shown that inflammaging significantly enhances the expression of pro-inflammatory cytokines (Lafuse et al., 2019). Consistent with the previous study, mRNA levels of IL-1β, TNFα, and CXCL2 were significantly higher in old Home Cage mice compared to young Home Cage mice (Figures 2E–G). However, we report that SDR stress significantly mitigated the inflammaging mediated upregulation of cytokines and chemokines. Together, these studies indicate that SDR in aged mice alters the environment of the lung to one that is more immunosuppressive or to one that more closely resembles the environment in young mice.

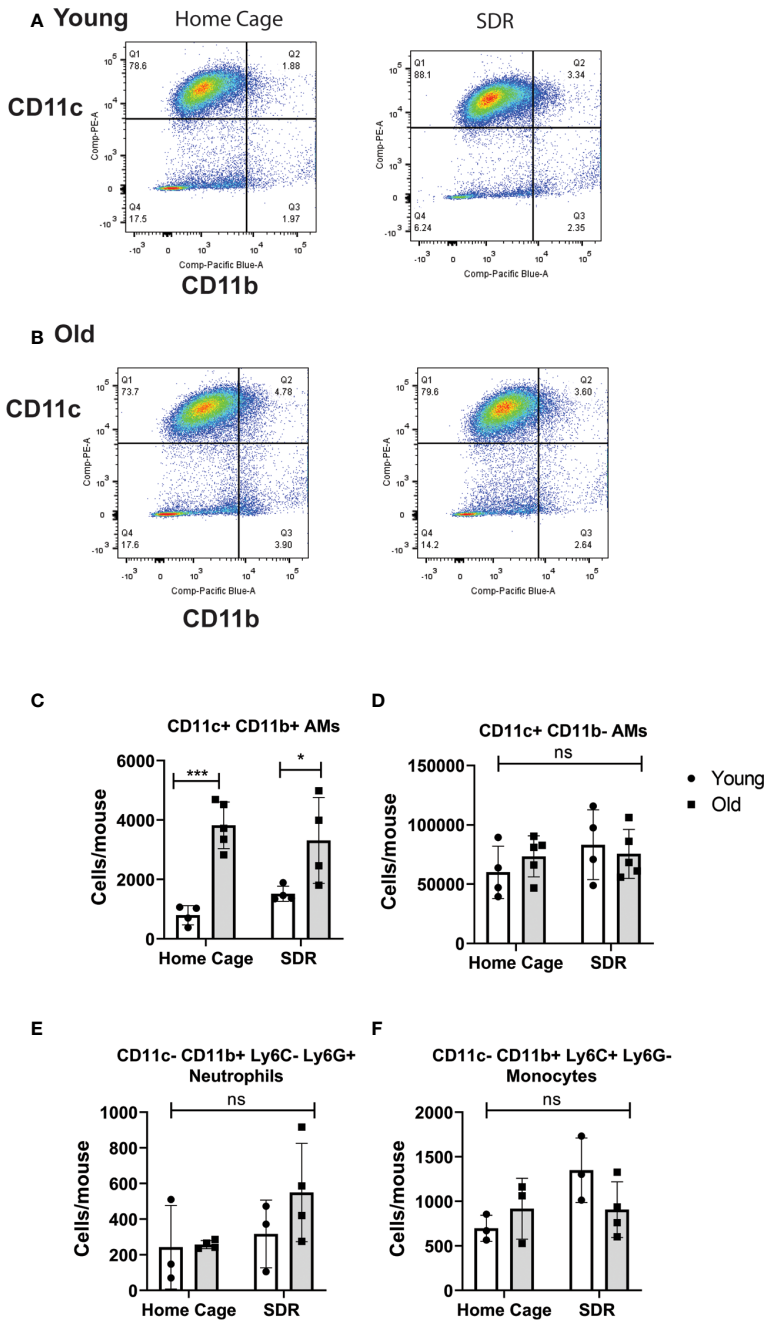

FIGURE 1
Flow cytometry analysis of myeloid cells in BAL fluid from Home Cage and SDR mice. CD11c/CD11b flow plots of BAL cells from young **(A)** and old **(B)** mice. $CD11c^+$ $CD11b^-$ AMs are in quadrant 1. $CD11c^+$ $CD11b^+$ AMs are in quadrant 2. Monocytes and neutrophils present in the $CD11c^-$ $CD11b^+$ cells (quadrant 4) were detected using antibodies to Ly6G and Ly6C. Cell numbers of each population present in BAL fluid were determined. **(C)** $CD11c^+$ $CD11b^-$ AM population **(D)** $CD11c^+$ $CD11b^+$ AM population **(E)** Neutrophils **(F)** Monocytes. Each symbol represents cells present in individual mice. Statistical analysis was performed by one-way ANOVA with Tukey multiple-comparisons *post hoc* test. N=4-5 mice/group. Data are shown as mean ± SE. $*p < 0.05$, $***p < 0.001$. ns, non significant.

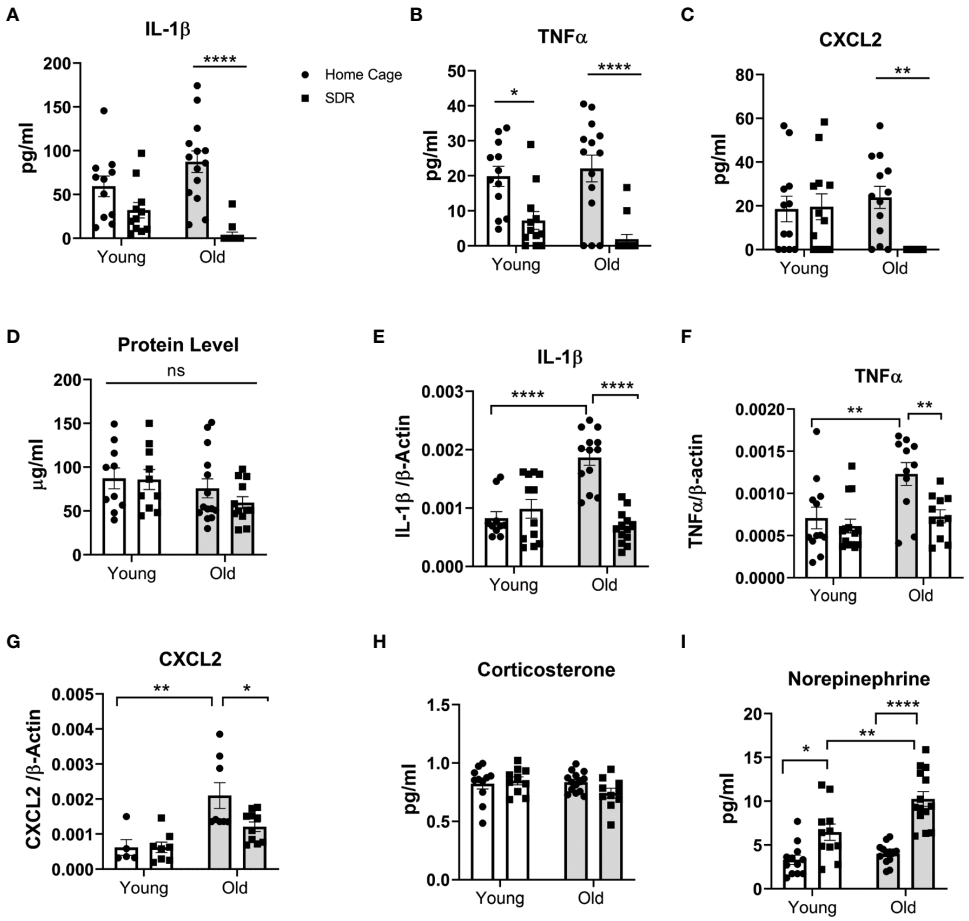

FIGURE 2
SDR in old mice suppresses cytokine levels in BAL fluid and basal mRNA levels in alveolar macrophages. BAL fluid and alveolar macrophages were isolated from individual young (3 months) and old (18 months) Home Cage mice and mice subjected to 6 cycles of SDR. **(A–C)** Cytokine levels in BAL fluid determined by ELISA. Protein levels in BAL fluid were determined by Bio-RAD protein assay **(D)**. **(E–G)** Basal cytokine mRNA expression in AMs. RNA was isolated from individual mice without culture and mRNA levels determined by qRT-PCR. Expression levels were normalized to β-actin mRNA. Protein levels in BAL fluid were determined by Bio-RAD protein assay. **(H, I)** Corticosterone and Norepinephrine levels in BAL fluid determined by ELISA. Each symbol represents individual mice. N=9-15 mice/group. Data are shown as mean ± SE. Statistical analysis was performed by one-way ANOVA with Tukey multiple-comparisons *post hoc* test. ns, non significant. $*p < 0.05$, $**p < 0.01$, $****p < 0.0001$.

SDR increases levels of norepinephrine in BAL fluid

Previous reports indicate that SDR stress increases corticosterone and norepinephrine (NE) in the blood (Avitsur et al., 2001; Hanke et al., 2012). As such, we determined if SDR also increases corticosterone and norepinephrine in the BAL fluid. As shown in Figure 2H, we found no significant differences in corticosterone levels in BAL fluid from young and old mice exposed to SDR. However, SDR increased NE levels in both and young mice with higher levels in old mice (Figure 2I). This suggests that the accumulation of locally produced NE in the alveolar space of the lung may contribute to the immune-suppressive environment induced in the lung by SDR.

AMs from old mice are not primed but immune suppressed in response to TLR2 stimulation

In our previous studies (Allen et al., 2012a; Allen et al., 2012b; Lafuse et al., 2017) we demonstrated that SDR primes monocytes to respond with increased production of pro-inflammatory cytokines when stimulated with a TLR agonist. To determine whether SDR stress alters the TLR mediated immune response of AMs from old mice, we harvested AMs from old Home Cage control mice and SDR mice and then stimulated with the TLR2 agonist Pam_3 CSK4. RNA was isolated after 6 h and the mRNA expression levels of various cytokines determined by qRT-PCR. Instead of being primed, the mRNA levels of pro-inflammatory cytokines IL-1β, TNFα, IL-12p40,

IL-6 were suppressed by SDR stress (Figures 3A–D). This indicates that the immune suppressive environment induced by SDR in old mice inhibits the ability of AMs to respond to TLR2 with a pro-inflammatory cytokine response.

SDR stress exacerbates M.tb growth in the lungs of old mice and reduces the formation of pneumonia

Since we found that SDR stress inhibits the inflammatory response in AMs, we next initiated studies to investigate the effects of SDR on *M.tb* infection. Young and old mice were subjected to 6 cycles of SDR and infected with *M.tb* for 30 and 60 days (30 days is early in the adaptive immune response and 60 days is later in the response). At each time point, mice were euthanized, and lungs were harvested. The left lung lobes were used for CFU assay. Right lung lobes were used for RNA isolation and lung sections for confocal microscopy. Previous studies have shown old mice exhibit early control of *M.tb* that is sustained through 21 days and then gradually wanes (Cooper et al., 1995; Turner and Orme, 2004; Vesosky and Turner, 2005; Vesosky et al., 2006; Rottinghaus et al., 2009; Vesosky et al., 2009). Consistent with these studies, old Home Cage mice at 30 days post-infection controlled the infection better than young Home Cage mice (Figure 4A). SDR had no effect in old mice at 30 days post infection, but interestingly, SDR in young mice decreased *M.tb* burden. However, the early control in old mice is transient (Orme, 1995; Turner et al., 2002; Vesosky and Turner, 2005). Thus, at 60 days of infection, there were more *M.tb* growth in the lungs of old Home Cage compared to young Home Cage mice (Figure 4B). Furthermore, SDR in old mice significantly increased the *M.tb* burden, while not affecting the *M.tb* burden in young mice. In contrast, at 60 days of infection in young mice there was only a slight increase in CFUs compared to CFUs at 30 days, which suggests the infection in young mice has reached a plateau level by 60 days. In a repeat experiment (Supplemental Figure 2), *M.tb* infection in young mice also reached a plateau level of infection by 60 days, while the *M.tb* burden in old mice increased at 60 days post infection and the highest level of infection was in the old SDR mice. Together, the two experiments indicate that old mice have reduced ability to control the infection long-term and exposure to SDR prior to infection in old mice exacerbates the loss of control that occurs with aging.

Lung sections from the infected mice were stained with hematoxylin and eosin. Representative images are shown in Supplemental Figure 3. In young and old home cage and SDR mice infected with *M.tb*, the images shows areas of pneumonia at day 30 and 60 post infection. However, in old SDR mice the areas of pneumonia are smaller at 30 and 60 days compared to old home cage mice. There are also more lymphocytes

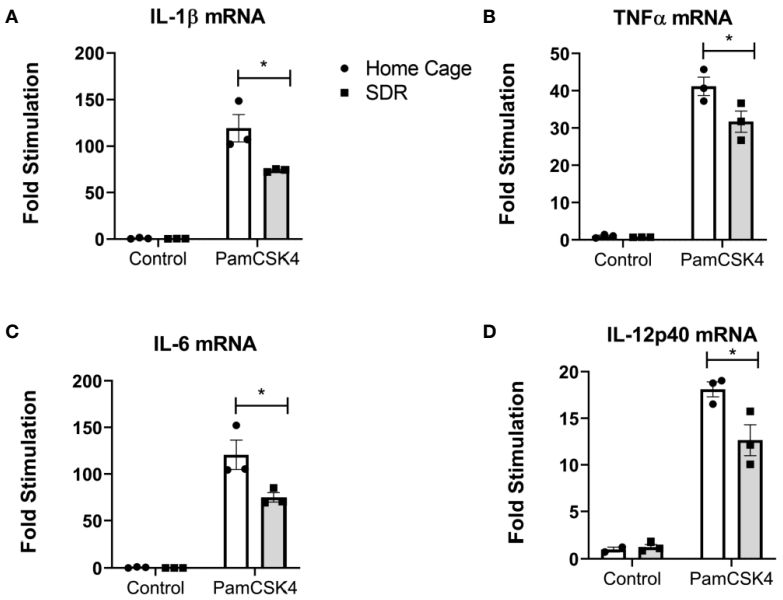

FIGURE 3
SDR suppresses TLR2 induced pro-inflammatory cytokine mRNA levels in AMs from old mice. AMs were pooled from six old Home Cage and six SDR mice were cultured at 37° for 2 hrs. Nonadherent cells were removed by washing and adherent cells stimulated with TLR2 ligand Pam_3CSK_4 (100 ng/ml) for 6 hrs. RNA was isolated and cytokine mRNA levels determined by qRT-PCR. **(A-D)** RNA levels are expressed relative to β-actin mRNA levels. Results are representative of two independent experiments with 3 wells/treatment. Data are shown as mean ± SE. Statistical analysis was performed by one-way ANOVA with Tukey multiple-comparisons *post hoc* test. *$p < 0.05$.

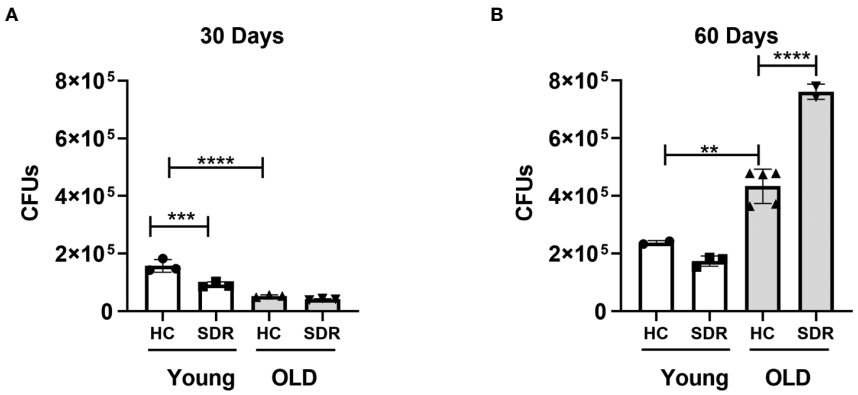

FIGURE 4
Old mice initially control *M.tb* infection better than young mice but eventually lose control of *M.tb* infection, which is further exacerbated by SDR. Young and old Home Cage mice subjected to six cycles of SDR were infected with low dose aerosol of *M. tuberculosis*. At 30 days **(A)** and 60 days **(B)**, the left lung lobes were homogenized and *M. tuberculosis* CFUs enumerated by plating on 7H11 duplicate plates. Results are representative of two independent experiments with 3 mice/group per time point. Data are shown as mean ± SE. Statistical analysis was performed by one-way ANOVA with Tukey multiple-comparisons *post hoc* test. $^{**}p < 0.01$, $^{***}p < 0.001$, $^{****}p < 0.0001$.

surrounding the blood vessels. This suggests that while lymphocytes are able to enter the infected lung of old SDR mice, but they are not able to form pneumonia.

Old SDR mice express decreased mRNA levels of IFN-γ and increased mRNA levels of IL-10

We next examined the mRNA levels of cytokines in the lungs of *M.tb* infected mice. At 30 days post-infection, there were no significant differences in the expression of IFN-γ mRNA (Figure 5A). However, at 60 days post infection, old mice had significantly less IFN-γ mRNA, and the lowest levels were observed in the stressed old mice. The stressed old mice also expressed significantly higher levels of IL-10 mRNA (Figure 5B). mRNA expression of TGF-β1 did not vary with age or stress (Figure 5C). mRNA expression of TGF1-β3 was comparable to the levels of TGF-β1 and also did vary with age or stress (data not shown). We also measured the levels of IL-27, a member of the IL-12 family involved in induction of IL-10-producing T cells (Tait Wojno et al., 2019). IL-27 mRNA was expressed at low levels at 30 days post-infection and at significantly higher levels at 60 days (Figure 5D). However, aging or stress had no effect on the levels of IL-27 mRNA. The increase in IL-27 mRNA at day 60 is of interest, since although IL-27 *in vitro* augments differentiation of naïve T cells toward a IFN-γ-producing phenotype (Takeda et al., 2003; Kamiya et al., 2004; Owaki et al., 2006), expression of IL-27 *in vivo* during various infections, including *M.tb*, has been shown to have a detrimental effect on the control of infections and reduces the amount of IFN-γ produced by CD4 T cells (Abdalla et al., 2015; Wang and Liu, 2016). There were no significant differences in the IFN-γ inducing cytokines IL-12p40 (Figure 5F) and IL-12p35 (data not shown) mRNA levels between home cage and SDR and also between 30 and 60 days. This suggests that lack of IL-12 at 60 days post infection is not a factor in the decreased IFN-γ mRNA. There were also no significant differences in the mRNA levels of T cell cytokines IL-21 (Figure 5E) and IL-17 (Figure 5G). The pro-inflammatory cytokines IL-1β (Figure 5H) and TNFα (Figure 5I) were expressed at high levels, but there was no effect of aging and stress on the mRNA levels. Interestingly, IL-1β mRNA levels were significantly lower at 60 days post infection compared to 30 days post infection. Together, these data show that SDR in old mice increased expression of IL-10 mRNA and decreased expression of IFN-γ mRNA at 60 days post infection, which is consistent with the loss of control of the *M.tb* infection in these mice.

Old SDR mice express higher mRNA levels of JAK3 but the mRNA levels of transcription factors that define T cell subsets are not altered by age or stress

Granuloma formation in *M.tb* infections involves the migration of macrophages and T cells into the infected lung. Therefore, we determined whether aging and SDR stress influenced mRNA levels of constitutively expressed macrophage and T cell markers in the lungs of *M.tb* infected mice at 30 and 60 days. A widely used marker of macrophages is F4/80, which is coded by the *Adgre1* gene (Waddell et al., 2018). Thus, we investigated the effects of aging and SDR stress on

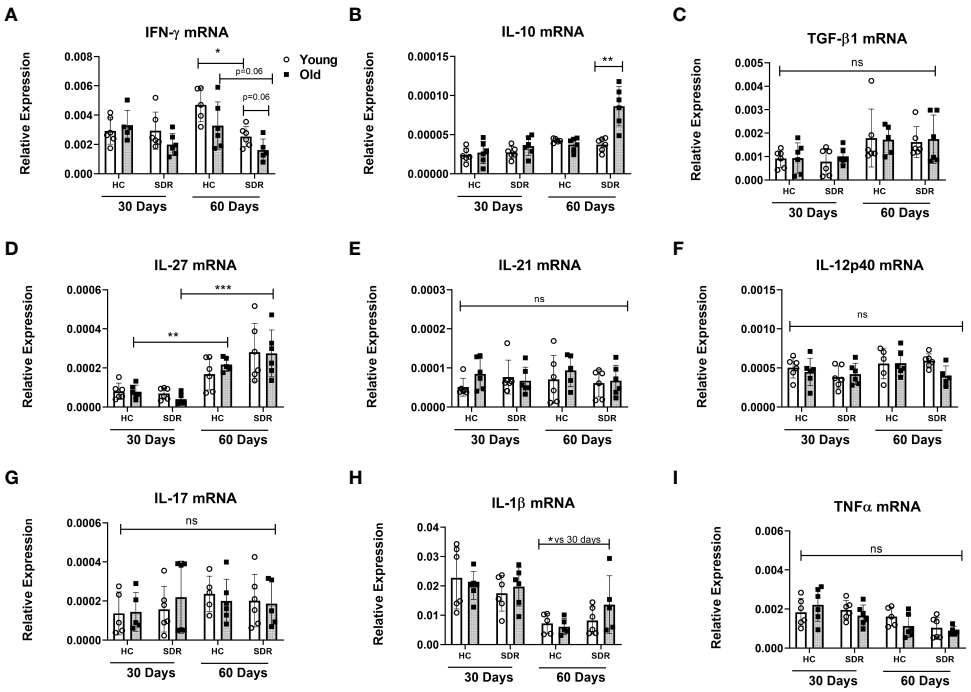

FIGURE 5
mRNA levels of cytokines genes in the lungs of mice infected with *M.tb*. Young and old Home Cage mice and mice subjected to six cycles of SDR were infected with low dose aerosol of *M. tuberculosis* for 30 and 60 days. RNA was isolated from a right lung lobe and mRNA levels determined by qRT-PCR **(A-I)**. RNA levels are expressed relative to β-actin. Results are pooled from two independent experiments. Each symbol represents individual mice. Data are shown as mean ± SE. Statistical analysis was performed by one-way ANOVA with Tukey multiple-comparisons *post hoc* test. *$p < 0.05$, **$p < 0.01$, ***$p < 0.001$. ns, non significant.

Adgre1 mRNA expression. Analysis of Adgre1 mRNA expression showed that aging or stress did not affect expression of this gene (Figure 6A). Interestingly, expression was lower at day 60 compared to day 30. Establishment of protective immunity to *M.tb* infection is dependent on the presence of IFN- γ secreting $CD4^+$ T cells (Green et al., 2013). Thus, we determined the effect of aging and SDR stress on $CD4^+$ T cells in the lungs of *M.tb* infected mice, we measured the mRNA levels of genes involved in T cell differentiation in young and old mice with and without SDR stress. We first determined the expression of JAK3, which is primarily expressed by T cells and NK cells. At 30 days post- infection, old Home Cage mice expressed significantly higher levels of JAK3 mRNA compared to young Home Cage mice (Figure 6B). The expression of JAK3mRNA was not altered by SDR stress in mice at 30 days post infection. However, expression of JAK3mRNA was higher at day 60 compared to day 30 and SDR stress significantly enhanced levels in old mice at 60 days (Figure 6B.). This suggests that there are more T cells present at 60 days post infection than 30 days. However, this increase in T cells did not translate into increased IFN-γ mRNA levels at 60 days (Figure 5A). Nor was there any difference with aging or stress in the mRNA expression of the Th1 transcription factor T-bet at 60 days post infection (Figure 6C). In fact, the levels of T-bet mRNA in the lungs were very low, suggesting that T cells present at 60 days post-infection are not Th1 cells. In contrast, at 30 days post infection T-bet mRNA levels were higher, which is consistent with the role of IFN-γ producing Th1 in the early control of infection in old mice (Turner and Orme, 2004; Vesosky et al., 2006; Rottinghaus et al., 2009; Vesosky et al., 2009). Interestingly, SDR stress in young mice had somewhat higher expression than young home cage mice (p= 0.07), which is consistent with the lower *M.tb* infection in these mice (Figure 4A). We also measured the mRNA levels of the Th2 transcription factor GATA3 and the Th17 transcription factor RORγt. Aging and SDR had no significant effect on GATA3 mRNA expression, which was expressed at low levels at both 30 and 60 days (Figure 6D). RORγt expression was low at both 30 and 60 days, but at 60 days there was significantly higher levels in old SDR mice (Figure 6E). Expression of the mRNA levels of the Treg transcription factor FOXP3 in the lungs of infected mice was also low and not affected by age or stress (Figure 6F). While increased expression of JAK3 suggests increased T cells at day 60, the data indicates that the increased T cells were not Th Cells or Tregs.

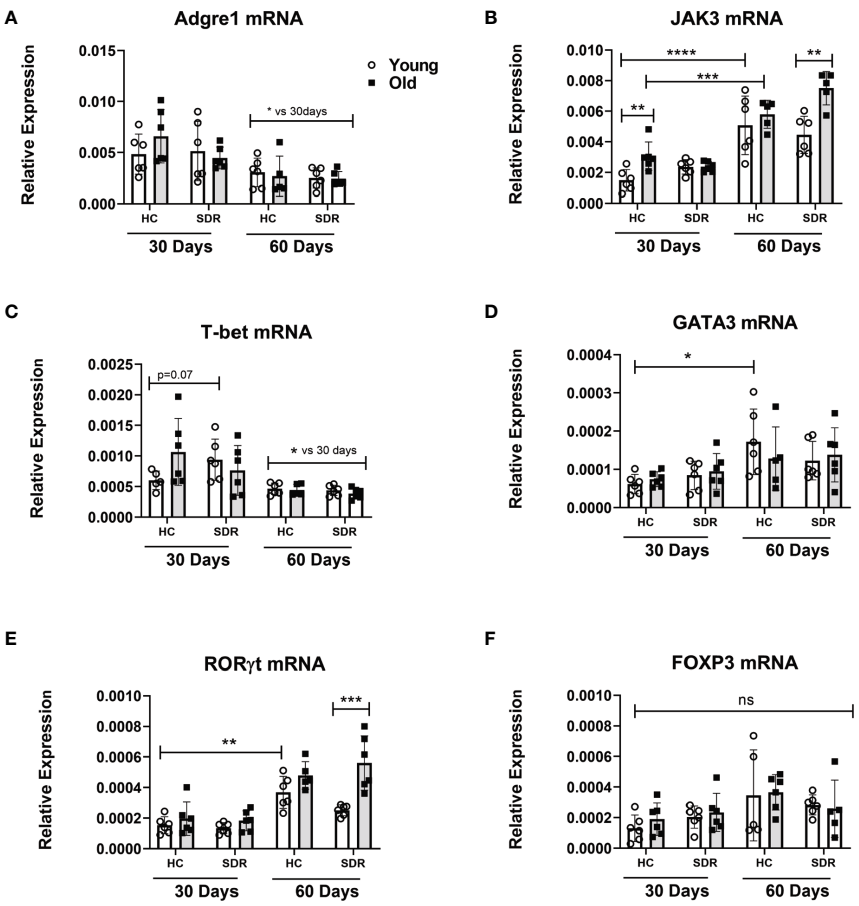

FIGURE 6
mRNA levels of macrophage and T cell genes in the lungs of mice infected with *M.tb*. Young and old Home Cage mice and mice subjected to six cycles of SDR were infected with low dose aerosol of *M. tuberculosis* for 30 and 60 days. RNA was isolated from a right lung lobe and mRNA levels **(A–F)** determined by qRT-PCR. RNA levels are expressed relative to β-actin. Each symbol represents individual mice. Data are shown as mean ± SE. Statistical analysis was performed by one-way ANOVA with Tukey multiple-comparisons *post hoc* test. Results represent 3 mice/group per time point. Data are shown as mean ± SE. *$p < 0.05$, **$p < 0.01$, ***$p < 0.001$, ****$p < 0.0001$. ns, non significant.

Expression of LAG3 and CD49b in CD4$^+$T cells is upregulated by SDR in old mice

Since our data indicates at 60 days post-infection in old SDR mice there is increased IL-10 mRNA levels in the lungs, we next examined whether CD4$^+$ T cells in the lungs of these mice have the phenotype of IL-10 producing regulatory T cells. We examined the CD4$^+$ T cell expression of LAG3 and CD49b by confocal microscopy of tissue sections from mice infected with *M.tb* for 60 days. Co-expression of LAG3 and CD49b identifies FOXP3$^-$ Type 1 regulatory T cells that produce large amounts of IL-10 (Gagliani et al., 2013). We first determined the numbers of CD4$^+$ T cells in the regions of granulomas lung tissue. The numbers of CD4$^+$ T cells were significantly increased in old SDR mice (Figure 7C), confirming the increased expression of JAK3 RNA in old SDR mice (Figure 6). The majority of CD4$^+$ T cells in the lungs of old SDR mice expressed both LAG3 (Figure 7A) and CD49b (Figure 7B). The mean fluorescence intensity of LAG3 expression in CD4$^+$ T cells was highly increased by SDR in old mice (Figure 7D). LAG3 expression was also increased by SDR in young mice, but the intensity was much less compared to the old mice. The mean fluorescence intensity of CD49b was also highly increased by SDR in old mice (Figure 7E), but SDR in young mice had no effect on the expression of CD49b. Thus, the confocal microscopy indicates that SDR prior to infection of old mice results in the presence of CD4 T cells in the lung at 60 days expressing markers of IL-10 secreting regulatory cells.

CD4$^+$T cells in M.tb infected Old SDR mice are producing IL-10

To answer the question whether CD4 T cells in old SDR mice infected with *M.tb* for 60 days are producing IL-10, we

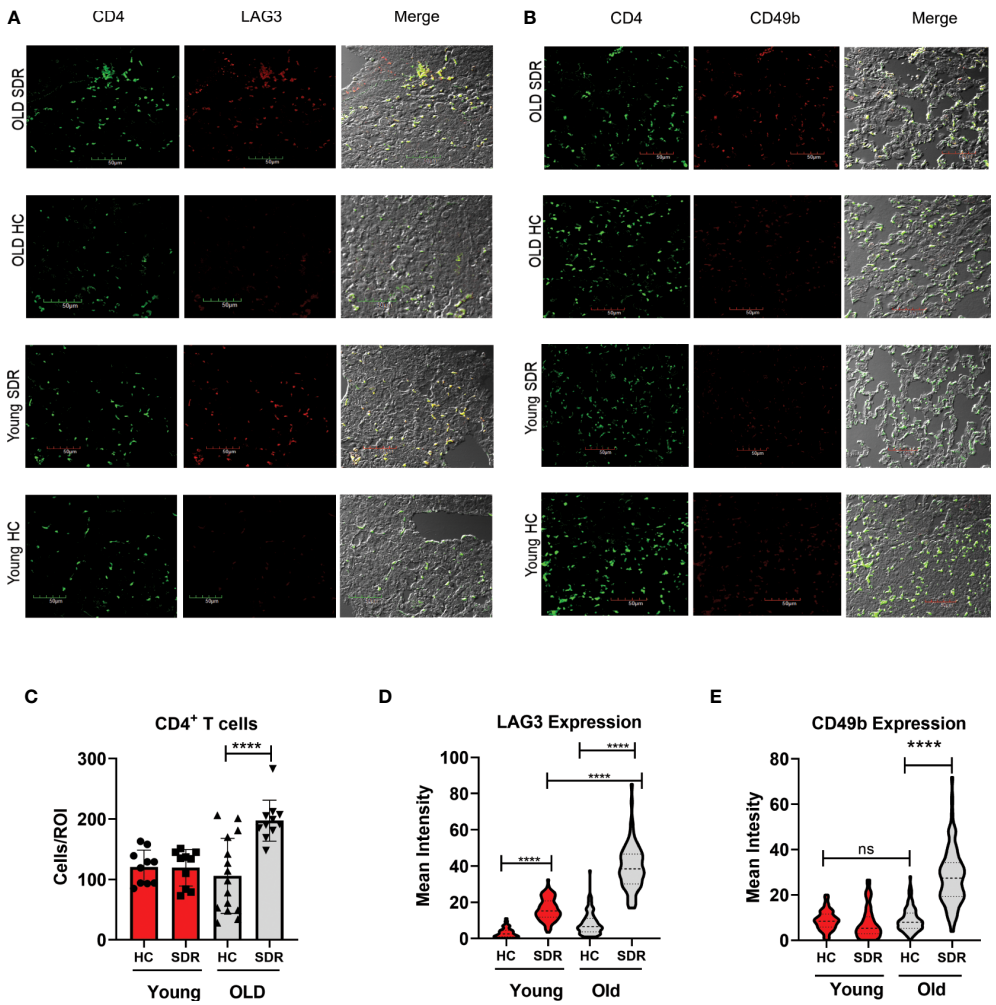

FIGURE 7
SDR in old mice up-regulate expression of LAG3 and CD49b in CD4$^+$T cells **(A)** Representative images of LAG3 expression in CD4$^+$ T cells present in regions of pneumonia **(B)** Representative images of CD49b in CD4$^+$ T cells. **(C)** Granulomatous tissue in old SDR mice contain more CD4 T cells. CD4 T cells were counted in regions of granulomatous tissue. Each symbol represents a region of granulomatous tissue. N=15 regions/group. Mean fluorescence intensity of LAG3 **(D)** and CD49b **(E)** expression in CD4 T cells was determined using Image **(J)** N= 90 cells/group. Statistical analysis was performed by one-way ANOVA with Tukey multiple-comparisons *post hoc* test. ****$p < 0.0001$. ns, non significant.

performed confocal microscopy of the 60 day lung sections with a monoclonal antibody against mouse IL-10 (Figure 8A). Only old SDR mice had significant production of IL-10 (Figure 8B) as there was little IL-10 production in old home cage mice or in the young home cage. The mean fluorescence intensity was slightly elevated in young SDR mice, but not to the level of significance. Also, in the old SDR mice the IL-10 producing cells were almost entirely CD4$^+$ T cells.

Discussion

Social disruption stress is a mouse social stressor that has been widely used to study the effects of psychological stress on immune function and behavior. SDR involves both a physical and a psychological component that includes anxiety behavior. This anxiety behavior in the SDR mouse model is similar to anxiety-like behavior that occurs in humans during stressful periods, which is often associated with an enhanced immune responses (Dhabhar, 2014). SDR in mice is also associated with enhanced immune responses. For example, SDR in young adult mice increases the number of splenic CD11b$^+$ myeloid cells including monocytes and neutrophils (Kinsey et al., 2007; Allen et al., 2012a; Allen et al., 2012b; Lafuse et al., 2017) by a sympathetic nervous system-induced β-adrenergic signaling pathway initiated by release of catecholamines (Hanke et al., 2012). We showed that the splenic CD11b$^+$ myeloid cells are primed by SDR stress induced translocation of gut microbiota to

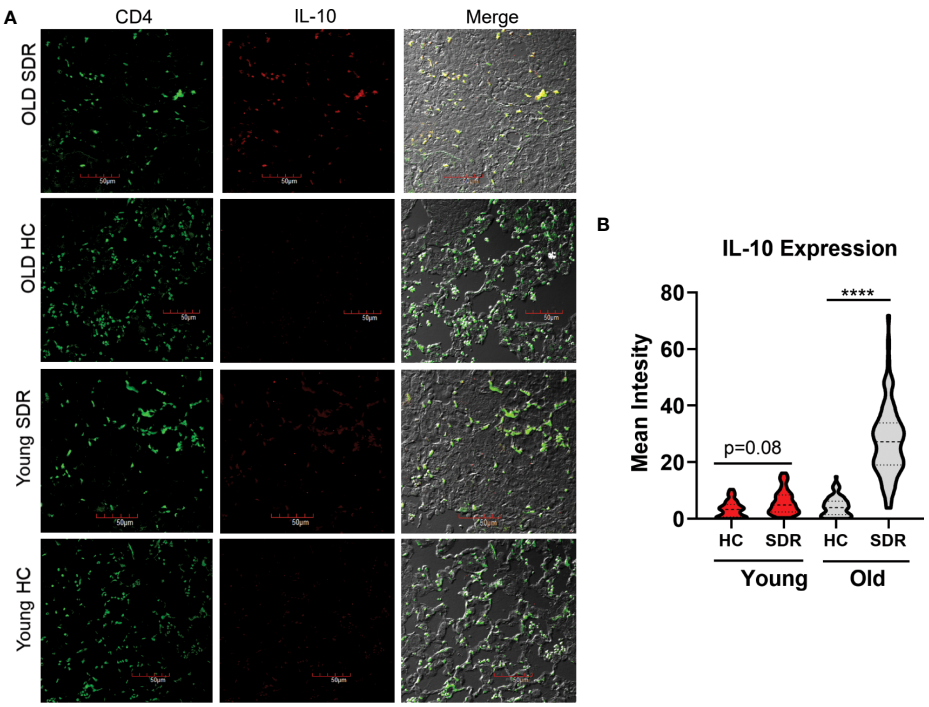

FIGURE 8
SDR in old mice results in production of IL-10 by $CD4^+$ T cells in the lungs of *M.tb* infected mice. Lung tissues sections from mice infected with *M.tb* for 60 days were examined by confocal immunofluorescence microscopy for expression of IL-10 (red fluorescence) in $CD4^+$ T cells (green fluorescence) present in areas of pneumonia. **(A)** Representative images of IL-10 expression in $CD4^+$ T cells. **(B)** Mean fluorescence of IL-10 expression in CD4 T cells was determined using Image (J) N= 90 cells/group. Statistical analysis was performed by one-way ANOVA with Tukey multiple-comparisons *post hoc* test. ****$p < 0.0001$.

the spleen (Allen et al., 2012a; Lafuse et al., 2017). In the current study, we subjected young and old mice to SDR stress. We first confirmed that SDR stress in old mice also induced splenomegaly and increased numbers of spleen monocytes and neutrophils. This suggests that like young mice, SDR stress in old mice activates the sympathetic nervous system (SNS), resulting in increased spleen monocytes. SDR activation of the SNS has also been shown to enhance inflammation by inducing the translocation of primed monocytes from the spleen into peripheral tissues, including the lung (Curry et al., 2010). However, our study found that SDR stress in young and old mice did not increase $CD11c^-$ $CD11b^+$ monocytes and neutrophils in the BAL fluid. This indicates that monocytes migrating to lung in response to SDR stress have not migrated into the alveolar space and most likely localize in the lung interstitium. Since SDR stress in young mice at day 30 has lower *M.tb* burden, translocation of primed macrophages induced by SDR may contribute to *M.tb* resistance in young mice. Another possible explanation is that $CD4^+$ T cells express the β2-adrenergic receptor and are able to response to norepinephrine (Kohm and Sanders, 2001). *In vitro* studies have shown that binding of norepinephrine to naïve $CD4^+$ T cells to secrete 2-4 fold more IFN-γ (Swanson et al., 2001). Further, blocking the release of norepinephrine with the terminal adrenergic toxin 6-0H dopamine at time of *M.tb* infection in mice resulted in significant increase in bacterial load in the lungs, while treatment of mice with a β2-agonist decreased bacteria load (Barrios-Payan J. et al., 2016). Thus, SDR in young mice may increase protection against *M.tb* by two possible mechanisms, first, increasing migration of primed macrophages that resist *M,tb* growth and secondly increasing the production of IFN-γ by $CD4^+$ T cells *via* norepinephrine. These possible explanations will be explored in future research.

In this study we show that instead of creating an inflammatory environment in the lung alveolar space, SDR stress induces an immuno-suppressive environment with markedly decreased cytokine and chemokine levels in old mice. AMs from old SDR mice also contained less cytokine and chemokine mRNA levels than old Home Cage control mice and produced less cytokine mRNA when stimulated with a TLR2 ligand. We found that SDR stress increased norepinephrine in BAL fluid in both young and old mice, but the levels were higher in old SDR mice. SDR stress in young mice has previously been shown to increase norepinephrine in the blood (Avitsur et al., 2001; Hanke et al., 2012), which represent spill-over from SNS activation in tissues. Thus, the increased levels of norepinephrine

in the BAL fluid indicates that SDR stress induces SNS activation in the lung, which results in production of norepinephrine, some of which is retained in the alveolar fluid. Norepinephrine, acting through the β2-adrenergic receptor, suppresses the production of pro-inflammatory cytokines IL-1β, TNFα, IL-6, and IL-12p40 by macrophages and dendritic cells induced by LPS (Koff et al., 1986; Hu et al., 2012; Grailer et al., 2014; Agac et al., 2018). Thus, we conclude that SDR stress induced norepinephrine is contributing factor to the immune-suppressive environment in old mice.

In this study we also examined the effects of psychological stress on *M.tb* infection. Young and old mice were subjected to 6 cycles of SDR prior to infection with *M.tb* for 30 and 60 days. Prior studies have shown that early in the infection old mice control *M.tb* better than young mice but as the infection progresses the old mice lose control of the infection (Orme, 1995; Turner et al., 2002; Vesosky and Turner, 2005). Our studies confirm these previous studies in that we found that at 30 post infection that the lungs of old Home Cage control mice contained fewer *M.tb* CFUs than young Home Cage mice. By 60 days post infection the CFUs were higher in old Home Cage mice than in young Home Cage mice. SDR stress did not have an appreciable effect at 30 days, but at 60 days CFUs were significantly higher in old SDR mice compared to old Home Cage mice. Thus, psychological stress exacerbates the loss of control that occurs with aging.

We also found mRNA levels of IFN-γ were decreased in old SDR mice, while the expression of IL-10 was increased. The expression of the T cell gene Jak3 was also substantially higher at 60 days post infection in old SDR mice compared to old Home Cage mice, suggesting accumulation of T cells in the lungs of old SDR mice. This did not translate into increased IFN-γand T-bet mRNA, suggesting that the accumulated T lymphocytes in the lungs of old SDR mice are not IFN-γ secreting Th1 cells. Our confocal microscopy confirmed increased numbers of CD4 T cells and showed that the expression of LAG3 and CD49b are upregulated in these cells. Further we found that the CD4 T cells in old SDR mice express IL-10. While IL-10 can be produced by both macrophages and T cells, IL-10 production by macrophages during *M.tb* infection occurs early in the infection, but later production of IL-10 by T cells predominates (Moreira-Teixeira et al., 2017). Our studies show that the predominant cells producing IL-10 in lungs of old SDR is CD4 T cells that express LAG3 and CD49b.

IL-10 suppresses both the innate and adaptive immune responses (Rutz and Ouyang, 2016). IL10 acts on macrophages to inhibit release of pro-inflammatory cytokines including TNF-α, IL-1β, and IL-6 (de Waal Malefyt et al., 1991; Fiorentino et al., 1991). IL-10 inhibits antigen presentation by down-regulating expression of MHC II and co-stimulator CD86 on antigen presenting cells and inhibits production of IL-12 required for CD4 Th1 differentiation (de Waal Malefyt et al., 1991; D'Andrea et al., 1993; Willems et al., 1994; Creery et al., 1996). IL-10 can also act on T cells to inhibit proliferation and cytokine production (de Waal Malefyt et al., 1993; Groux et al., 1996; Rojas et al., 1999). Previous reports have indicated that IL-10 plays an inhibitory role in controlling *M.tb* infections in mice (Turner et al., 2002; Beamer et al., 2008; Cyktor et al., 2013). Interestingly, similar to our study, transgenic C57BL/6 mice producing IL-10 under the control of the IL-2 promoter are able to control *M.tb* infection during the early stage, but during the chronic stage there was a significant increase in bacterial load in the lung (Turner et al., 2002). Disease progression in *M.tb* susceptible strain CBA/J also correlates with high levels of IL-10 in the lung (Turner et al., 2002). Blocking IL-10 in CBA/J mice during the chronic stage of infection improved control of bacterial load and improved survival (Beamer et al., 2008). Further, CBA/J mice deficient in IL-10 were able to contain the *M.tb* infection and formed mature, fibrotic granulomas (Cyktor et al., 2013).

IL-10 is produced by $CD4^+$ $FOXP3^-$ T regulatory type I (Tr1) cells and $CD4^+$ $CD25^+$ $FOXP3^+$ Treg cells (Roncarolo et al., 2006; Wei et al., 2017; Roncarolo et al., 2018). Co-expression of LAG3 and CD49b identifies T regulatory Tr1 cells (Gagliani et al., 2013), whereas LAG3 and CD49b are absent on Treg cells. Our confocal microscopy indicates that the IL-10 producing CD4 T cells have the phenotype of Tr1 cells. It has been shown earlier that IL-10 is also secreted by $CD8^+$ T cells during *M.tb* infection (Cyktor et al., 2013; Moreira-Teixeira et al., 2017) and CD8 cells with a Tr1 have been described (Steinbrink et al., 1999; Gilliet and Liu, 2002). Thus, it is possible that there are also IL-10 producing $CD8^+$ Tr1 cells in the lungs of old stressed mice. However, it is likely these $CD8^+$ T cells are few in number, as we found only a few IL-10 producing cells that were not $CD4^+$ T cells. Tr1 cells are antigen specific $CD4^+$ T cells with regulatory activity that secrete large amounts of IL-10 and TGF-β and do not express FOXP3 (Roncarolo et al., 2006; Roncarolo et al., 2018). Differentiation of antigen-specific Tr1 cells has been shown to be dependent on antigen presentation by a subset of IL-10-producing dendritic cells (Wakkach et al., 2003; Gregori et al., 2010). In addition to IL-10, IL-27 promotes the differentiation of Tr1 cells (Pot et al., 2009; Pot et al., 2011). In our study, IL-27 mRNA levels in the lung were higher at 60 days post infection than at 30 days in both stressed and non-stressed mice. Thus, our data suggest that while IL-27 is present in the lungs at 60 days of infections, differences in IL-27 production are not responsible for differences in CD4 T cell and IL-10 expression between young and old stressed mice. While our study points to a role for IL-10 secreting T cells in the loss of control in old stressed mice, more definitive single cell RNAseq analysis of T cell populations in the lungs of old stressed mice will be needed to define the transcriptome of these IL-10 producing T cells and to confirm these T cells have the phenotype of Tr1 cells.

Another question that needs to be addressed is how SDR stress prior to infection alters T cell immunity at the later stage of infection. The effects of SDR on spleen weight, plasma IL-6, release of monocytes into the circulation, and anxiety behavior last at least 8 days after the last SDR cycle but are diminished by

day 24 (Wohleb et al., 2014). This suggests effects of SDR activation of the SNS in the lung and draining lymph nodes will persist during early period in which the adaptive immune system is activated. The first 21 days after *M.tb* is the critical period for the differentiation of *M.tb* antigen specific CD4 T cells. The presence of IL-10 during the first 21 days of *M.tb* infection has a long-term effect on the control of the infection. This was shown by treatment of CBA/J mice during the first 21 days with anti-IL-10R antibody to block effects of IL-10 (Cyktor et al., 2013). This early treatment with anti-IL10R antibody resulted in increased numbers of $CD4^+$ and $CD8^+$ T cells in the draining lymph node and significantly increased IFN-γ mRNA in the lung at day 21. Thus, IL-10 has a significant impact on the differentiation of T cells during the early stage of infection. The anti-IL-10R antibody treatment was halted at day 21, and the long-term effect on *M.tb* infection was examined 100 day later. The early anti-IL-10R treatment significantly decreased *M.tb* burden in the lung and led to formation of mature granulomas with fibrotic capsule.

During the first days of an *M.tb* infection, IL-10 production occurs primarily in myeloid cells, including monocytes, macrophages, and dendritic cells (Moreira-Teixeira et al., 2017). We propose that SDR activation of the SNS in the draining lymph nodes of old mice triggers the production of IL-10 by antigen presenting cells, resulting in differentiation of T cells into IL-10 secreting Tr1 cells, which then migrate to the lung. In this regard, studies have shown that norepinephrine signaling through the β2-adrenergic receptor increases rapid IL-10 production by macrophages and dendritic cells (Agac et al., 2018). IL-10 secreting human Tr1 cells are also induced by a combination of glucocorticoids and β2-agonists (Peek et al., 2005). Our analysis of *M.tb* infection at 60 days post infection, suggests that IL-10 production by T cells and production of IL-27 by macrophages will further expand differentiation of Tr1 cells, which eventually leads to decreased ability of stressed old mice to control the infection. Exactly how aging impacts the stress response remains elusive. One possible explanation is that SDR induces greater activation of the SNS in old mice, resulting in the increased levels of norepinephrine being produced. Aging may also increase the number of APCs that induce differentiation of IL-10 secreting T cells. Our previous study (Lafuse et al., 2019) showed that old mice have higher numbers of a $CD11c^+$ $CD11b^+$ AM subpopulation that phagocytosed more *M.tb* than the major $CD11c^+$ $CD11b^+$ AM population. We found that $CD11c^+$ $CD11b^+$ AM population preferentially express CCR7, which is required for migration to lymph nodes (Forster et al., 1999). This population also expresses high levels of β2-adrenergic receptor mRNA. Thus, we posit that this AM population is involved in trafficking of *M.tb* to the draining lymph node and the higher numbers of this AM population in old mice will lead to increased numbers of IL-10 secreting T cells in old SDR mice compared to young SDR mice.

A limitation to this study is that it does not contain a human component examining effects of psychological stress during tuberculosis in the elderly. Social disruption stress is a chronic stressor that creates anxiety behavior similar to chronic stress in humans (Kinsey et al., 2007). Chronic psychological stress in humans contributes to chronic inflammation that occurs with aging, leading to disease susceptibility. In the elderly, age-related neuroendocrine dysregulation can exacerbate the inflammatory response to the stress (Heffner, 2011). Chronic stress in humans has been shown to be associated with altered T cell cytokine response with decreased production of IFN-γ and increased production of IL-10 (Rink et al., 1998; Glaser R. et al., 2001). Human type-1 regulatory T cells capable of producing high levels of IL-10 have been described (Levings and Roncarolo, 2005). Further, $CD4^+$ $CD25^{hi}$ T regulatory cells are present in the lungs and blood of TB patients (Ribeiro-Rodrigues et al., 2006). Also, an *in vitro* studies demonstrated that human type-1 regulatory T cells that secrete IL-10, suppresses the T cell responses to *Mycobacterium bovis* BCG (Truscott et al., 2010). Although we do not have direct evidence for chronic stress induced type-1 regulatory T cells during human tuberculosis, these studies are supportive of their involvement.

In conclusion, we demonstrate that psychological stress in old mice creates an immune-suppressive environment in the lung, which has long-term effects on ability of the immune system to control an *M.tb* infection. Although our studies indicate that psychological stress in old mice increases the loss of control of the infection by increasing differentiation of IL-10 secreting T cells, further studies are needed to elucidate the mechanisms by which psychological stress alters T cell differentiation. Our studies are applicable to the understanding immune-based mechanisms that contribute to a broad range of lung diseases, for which aging and psychological stress commonly contribute to outcomes.

Data availability statement

The original contributions presented in the study are included in the article/Supplementary Material. Further inquiries can be directed to the corresponding authors.

Ethics statement

The animal study was reviewed and approved by The Ohio State University Institutional Animal care and Use Committee.

Authors contributions

WPL, QW, NK, NS, SS, OA, and MVSR preformed the experiments, analyzed data, and generated figures. Experiments were supervised by WPL and MVSR. WPL and MVSR wrote an initial manuscript draft that was critically edited by JT and

approved by all authors. All authors contributed to the article and approved the submitted version.

Funding

This work was supported by a diversity supplement to National Institutes of Health grants P01-AG051428 (to JT and WPL), AI146252, AI146690 and AG 073720 (to MVSR), and P30-CA016068.

Conflict of interest

The authors declare that the research was conducted in the absence of any commercial or financial relationships that could be construed as a potential conflict of interest.

Publisher's note

Supplementary material

The Supplementary Material for this article can be found online at: https://www.frontiersin.org/articles/10.3389/fcimb.2022.990402/full#supplementary-material

References

Abdalla, A. E., Li, Q., Xie, L., and Xie, J. (2015). Biology of IL-27 and its role in the host immunity against mycobacterium tuberculosis. *Int. J. Biol. Sci.* 11, 168–175. doi: 10.7150/ijbs.10464

Agac, D., Estrada, L. D., Maples, R., Hooper, L. V., and Farrar, J. D. (2018). The beta2-adrenergic receptor controls inflammation by driving rapid IL-10 secretion. *Brain Behavior Immun.* 74, 176–185. doi: 10.1016/j.bbi.2018.09.004

Allen, R. G., Lafuse, W. P., Galley, J. D., Ali, M. M., Ahmer, B. M., and Bailey, M. T. (2012). The intestinal microbiota are necessary for stressor-induced enhancement of splenic macrophage microbicidal activity. *Brain Behavior Immun.* 26, 371–382. doi: 10.1016/j.bbi.2011.11.002

Allen, R. G., Lafuse, W. P., Powell, N. D., Webster Marketon, J. I., Stiner-Jones, L. M., Sheridan, J. F., et al. (2012). Stressor-induced increase in microbicidal activity of splenic macrophages is dependent upon peroxynitrite production. *Infection Immun.* 80, 3429–3437. doi: 10.1128/IAI.00714-12

Avitsur, R., Stark, J. L., and Sheridan, J. F. (2001). Social stress induces glucocorticoid resistance in subordinate animals. *Hormones Behav.* 39, 247–257. doi: 10.1006/hbeh.2001.1653

Bahadoran, A., Lee, S. H., Wang, S. M., Manikam, R., Rajarajeswaran, J., Raju, C. S., et al. (2016). Immune responses to influenza virus and its correlation to age and inherited factors. *Front. Microbiol.* 7, 1841. doi: 10.3389/fmicb.2016.01841

Barrios-Payan J., A., Mata-Espinosa, D., Marquina-Castillo, B., Villanueva, E. B., Gutierrez, M. E. H., Perez-Sanchez, G., et al. (2016). The contribution of the sympathetic nervous system to the immunopathology of experimental pulmonary tuberculosis. *J. Immunol.* 298, 98–105. doi: 10.1016/j.jneuroim.2016.07.012

Beamer, G. L., Flaherty, D. K., Assogba, B. D., Stromberg, P., Gonzalez-Juarrero, M., de Waal Malefyt, R., et al. (2008). Interleukin-10 promotes mycobacterium tuberculosis disease progression in CBA/J mice. *J. Immunol. (Baltimore Md.: 1950)* 181, 5545–5550. doi: 10.4049/jimmunol.181.8.5545

Cohen, S., Janicki-Deverts, D., and Miller, G. E. (2007). Psychological stress and disease. *JAMA* 298, 1685–1687. doi: 10.1001/jama.298.14.1685

Cooper, A. M., Callahan, J. E., Griffin, J. P., Roberts, A. D., and Orme, I. M. (1995). Old mice are able to control low-dose aerogenic infections with mycobacterium tuberculosis. *Infection Immun.* 63, 3259–3265. doi: 10.1128/iai.63.9.3259-3265.1995

Creery, W. D., Diaz-Mitoma, F., Filion, L., and Kumar, A. (1996). Differential modulation of B7-1 and B7-2 isoform expression on human monocytes by cytokines which influence the development of T helper cell phenotype. *Eur. J. Immunol.* 26, 1273–1277. doi: 10.1002/eji.1830260614

Curry, J. M., Hanke, M. L., Piper, M. G., Bailey, M. T., Bringardner, B. D., Sheridan, J. F., et al. (2010). Social disruption induces lung inflammation. *Brain Behavior Immun.* 24, 394–402. doi: 10.1016/j.bbi.2009.10.019

Cyktor, J. C., Carruthers, B., Beamer, G. L., and Turner, J. (2013). Clonal expansions of CD8+ T cells with IL-10 secreting capacity occur during chronic mycobacterium tuberculosis infection. *PLoS One* 8, e58612. doi: 10.1371/journal.pone.0058612

Cyktor, J. C., Carruthers, B., Kominsky, R. A., Beamer, G. L., Stromberg, P., and Turner, J. (2013). IL-10 inhibits mature fibrotic granuloma formation during mycobacterium tuberculosis infection. *J. Immunol. (Baltimore Md.: 1950)* 190, 2778–2790. doi: 10.4049/jimmunol.1202722

D'Andrea, A., Aste-Amezaga, M., Valiante, N. M., Ma, X., Kubin, M., and Trinchieri, G. (1993). Interleukin 10 (IL-10) inhibits human lymphocyte interferon gamma-production by suppressing natural killer cell stimulatory factor/IL-12 synthesis in accessory cells. *J. Exp. Med.* 178, 1041–1048. doi: 10.1084/jem.178.3.1041

de Waal Malefyt, R., Abrams, J., Bennett, B., Figdor, C. G., and de Vries, J. E. (1991). Interleukin 10(IL-10) inhibits cytokine synthesis by human monocytes: an autoregulatory role of IL-10 produced by monocytes. *J. Exp. Med.* 174, 1209–1220. doi: 10.1084/jem.174.5.1209

de Waal Malefyt, R., Haanen, J., Spits, H., Roncarolo, M. G., te Velde, A., Figdor, C., et al. (1991). Interleukin 10 (IL-10) and viral IL-10 strongly reduce antigen-specific human T cell proliferation by diminishing the antigen-presenting capacity of monocytes *via* downregulation of class II major histocompatibility complex expression. *J. Exp. Med.* 174, 915–924. doi: 10.1084/jem.174.4.915

de Waal Malefyt, R., Yssel, H., and de Vries, J. E. (1993). Direct effects of IL-10 on subsets of human CD4+ T cell clones and resting T cells. specific inhibition of IL-2 production and proliferation. *J. Immunol. (Baltimore Md.: 1950)* 150, 4754–4765.

Dhabhar, F. S. (2014). Effects of stress on immune function: the good, the bad, and the beautiful. *Immunologic Res.* 58, 193–210. doi: 10.1007/s12026-014-8517-0

Engler, H., Bailey, M. T., Engler, A., Stiner-Jones, L. M., Quan, N., and Sheridan, J. F. (2008). Interleukin-1 receptor type 1-deficient mice fail to develop social stress-associated glucocorticoid resistance in the spleen. *Psychoneuroendocrinology* 33, 108–117. doi: 10.1016/j.psyneuen.2007.10.007

Ferrando-Martinez, S., Ruiz-Mateos, E., Hernandez, A., Gutierrez, E., Rodriguez-Mendez Mdel, M., Ordonez, A., et al. (2011). Age-related deregulation of naive T cell homeostasis in elderly humans. *Age (Dordrecht Netherlands)* 33, 197–207. doi: 10.1007/s11357-010-9170-8

Fiorentino, D. F., Zlotnik, A., Mosmann, T. R., Howard, M., and O'Garra, A. (1991). IL-10 inhibits cytokine production by activated macrophages. *J. Immunol. (Baltimore Md.: 1950)* 147, 3815–3822.

Forster, R., Schubel, A., Breitfeld, D., Kremmer, E., Renner-Muller, I., Wolf, E., et al. (1999). CCR7 coordinates the primary immune response by establishing functional microenvironments in secondary lymphoid organs. *Cell* 99, 23–23. doi: 10.1016/S0092-8674(00)80059-8

Franceschi, C., Bonafe, M., Valensin, S., Olivieri, F., De Luca, M., Ottaviani, E., et al. (2000). Inflamm-aging. an evolutionary perspective on immunosenescence. *Ann. New York Acad. Sci.* 908, 244–254. doi: 10.1111/j.1749-6632.2000.tb06651.x

Gagliani, N., Magnani, C. F., Huber, S., Gianolini, M. E., Pala, M., Licona-Limon, P., et al. (2013). Coexpression of CD49b and LAG-3 identifies human and mouse T regulatory type 1 cells. *Nat. Med.* 19, 739–748. doi: 10:1038/nm.319

Gilliet, M., and Liu, Y. J. (2002). Generation of human CD8 T regulatory cells by CD40 ligand-activated plasmacytoid dendritic cells. *J. Exp. Med.* 195, 695–704. doi: 10.1084/jem.20011603

Glaser R., R. C., Laskowski, B. F., Malarkey, W. B., Sheridan, J. F., and Kiecolt-Glaser, J. K. (2001). Evidence for a shift in the Th-1 to Th-2 cytokine response associated with chronic stress and aging. *J. Gerontol: Med. Sci.* 56A, M477–M482. doi: 10.1093/gerona/56.8.m477

Grailer, J. J., Haggadone, M. D., Sarma, J. V., Zetoune, F. S., and Ward, P. A. (2014). Induction of M2 regulatory macrophages through the beta2-adrenergic receptor with protection during endotoxemia and acute lung injury. *J. innate Immun.* 6, 607–618. doi: 10.1159/000358524

Green, A. M., DiFazio, R., and Flynn, J. L. (2013). IFN-γ from CD4 T cells is essential for host survival and enhances CD8 T cell function during *Mycobacterium tuberculosis* infection. *J. Immunol. (Baltimore Md.: 1950)* 190, 270–277. doi: 10.4049/jimmunol.1200061

Gregori, S., Tomasoni, D., Pacciani, V., Scripoli, M., Battaglia, M., Magnani, C. F., et al. (2010). Differentiation of type 1 regulatory cells (Tr1) by tolerogenic DC-10 requires the IL-10 depedendent ILT4/HLA-G pathway. *Blood* 116, 935–944. doi: 10.1182/blood-2009-07-234872

Groux, H., Bigler, M., de Vries, J. E., and Roncarolo, M. G. (1996). Interleukin-10 induces a long-term antigen-specific anergic state in human CD4+ T cells. *J. Exp. Med.* 184, 19–29. doi: 10.1084/jem.184.1.19

Hanke, M. L., Powell, N. D., Stiner, L. M., Bailey, M. T., and Sheridan, J. F. (2012). Beta adrenergic blockade decreases the immunomodulatory effects of social disruption stress. *Brain Behavior Immun.* 26, 1150–1159. doi: 10.1016/j.bbi.2012.07.011

Heffner, K. L. (2011). Neuroendocrine effects of stress on immunity in the elderly: Implications for inflammatory disease. *Immunol. Alergy Clin. N. Am.* 31, 05–108. doi: 10.1016/j.iac.2010.09.005

Hu, Z., Chen, R., Cai, Z., Yu, L., Fei, Y., Weng, L., et al. (2012). Salmeterol attenuates the inflammatory response in asthma and decreases the pro-inflammatory cytokine secretion of dendritic cells. *Cell. Mol. Immunol.* 9, 267–275. doi: 10.1038/cmi.2011.56

Immunological Genome Consortium (2012). Gene-expression profiles and transcriptional regulatory pathways that underlie the identity and diversity of mouse tissue macrophages. *Nat. Immunol.* 13, 1118–1128. doi: 10.1038/ni.2419

Kamiya, S., Owaki, T., Morishima, N., Fukai, F., Mizuguchi, J., and Yoshimoto, T. (2004). An indispensable role for STAT1 in IL-27-induced T-bet expression but not proliferation of naive CD4+ T cells. *J. Immunol. (Baltimore Md.: 1950)* 173, 3871–3877. doi: 10.4049/jimmunol.173.6.3871

Kinsey, S. G., Bailey, M. T., Sheridan, J. F., and Padgett, D. A. (2008). The inflammatory response to social defeat is increased in older mice. *Physiol. Behav.* 93, 628–636. doi: 10.1016/j.physbeh.2007.11.003

Kinsey, S. G., Bailey, M. T., Sheridan, J. F., Padgett, D. A., and Avitsur, R. (2007). Repeated social defeat causes increased anxiety-like behavior and alters splenocyte function in C57BL/6 and CD-1 mice. *Brain Behavior Immun.* 21, 458–466. doi: 10.1016/j.bbi.2006.11.001

Koff, W. C., Fann, A. V., Dunegan, M. A., and Lachman, L. B. (1986). Catecholamine-induced suppression of interleukin-1 production. *Lymphokine Res.* 5, 239–247.

Kohm, A. P., and Sanders, V. M. (2001). Norepinhrine and β2-adrenergic receptor stimulation regulate $CD4^+$ T and b lymphocyte function *in vitro* and *in vivo*. *Pharmacol.Rev* 53, 487–525.

Krone, C. L., van de Groep, K., Trzcinski, K., Sanders, E. A., and Bogaert., D. (2014). Immunosenescence and pneumococcal disease: an imbalance in host-pathogen interactions. *Lancet Respir. Med.* 2, 141–153. doi: 10.1016/S2213-2600(13)70165-6

Lafuse, W. P., Gearinger, R., Fisher, S., Nealer, C., Mackos, A. R., and Bailey, M. T. (2017). Exposure to a social stressor induces translocation of commensal lactobacilli to the spleen and priming of the innate immune system. *J. Immunol. (Baltimore Md.: 1950)* 198, 2383–2393. doi: 10.4049/jimmunol.1601269

Lafuse, W. P., Rajaram, M. V. S., Wu, Q., Moliva, J. I., Torrelles, J. B., Turner, J., et al. (2019). Identification of an increased alveolar macrophage subpopulation in old mice that displays unique inflammatory characteristics and is permissive to mycobacterium tuberculosis infection. *J. Immunol. (Baltimore Md.: 1950)* 203, 2252–2264. doi: 10.4049/jimmunol.1900495

Larbi, A., Pawelec, G., Wong, S. C., Goldeck, D., Tai, J. J., and Fulop, T. (2011). Impact of age on T cell signaling: a general defect or specific alterations? *Ageing Res. Rev.* 10, 370–378. doi: 10.1016/j.arr.2010.09.008

Levings, M. K., and Roncarolo, M. G. (2005). Phenotypic and functional differences between human $CD4^+$ $CD25^+$ and type 1 regulatory T cells. *CTMI* 293, 203–326. doi: 10.1007/3-540-27702-1_14

Livak, K. J., and Schmittgen, T. D. (2001). Analysis of relative gene expression data using real-time quantitative PCR and the 2(-delta delta C(T)) method. *Methods (San Diego Calif.)* 25, 402–408. doi: 10.1006/meth.2001.1262

McKim, D. B., Patterson, J. M., Wohleb, E. S., Jarrett, B. L., Reader, B. F., Godbout, J. P., et al. (2016). Sympathetic release of splenic monocytes promotes recurring anxiety following repeated social defeat. *Biol. Psychiatry* 79, 803–813. doi: 10.1016/j.biopsych.2015.07.010

McKim, D. B., Weber, M. D., Niraula, A., Sawicki, C. M., Liu, X., Jarrett, B. L., et al. (2018). Microglial recruitment of IL-1beta-producing monocytes to brain endothelium causes stress-induced anxiety. *Mol. Psychiatry* 23, 1421–1431. doi: 10.1038/mp.2017.64

Mehta, J. B., and Dutt, A. K. (2016). Epidemiology and host factors. *Microbiol. Spectr.* 4. doi: 10.1128/microbiolspec.TNMI7-0018-2016

Moreira-Teixeira, L., Redford, P. S., Stavropoulos, E., Ghilardi, N., Maynard, C. L., Weaver, C. T., et al. (2017). T Cell-derived IL-10 impairs host resistance to mycobacterium tuberculosis infection. *J. Immunol. (Baltimore Md.: 1950)* 199, 613–623. doi: 10.4049/jimmunol.1601340

Negin, J., Abimbola, S., and Marais, B. J. (2015). Tuberculosis among older adults–time to take notice. *Int. J. Infect. Dis.* 32, 135–137. doi: 10.1016/j.ijid.2014.11.018

Nikolich-Zugich, J., Knox, K. S., Rios, C. T., Natt, B., Bhattacharya, D., and Fain, M. J. (2020). SARS-CoV-2 and COVID-19 in older adults: what we may expect regarding pathogenesis, immune responses, and outcomes. *GeroScience* 42, 505–514. doi: 10.1007/s11357-020-00186-0

Orme, I. (1995). Mechanisms underlying the increased susceptibility of aged mice to tuberculosis. *Nutr. Rev.* 53, S35–38; discussion S38-40. doi: 10.1111/j.1753-4887.1995.tb01514.x

Owaki, T., Asakawa, M., Fukai, F., Mizuguchi, J., and Yoshimoto, T. (2006). IL-27 induces Th1 differentiation *via* p38 MAPK/T-bet- and intercellular adhesion molecule-1/LFA-1/ERK1/2-dependent pathways. *J. Immunol. (Baltimore Md.: 1950)* 177, 7579–7587. doi: 10.4049/jimmunol.177.11.7579

Peek, E. J., Richards, D. F., Faith, A., Lavender, P., Lee, T. H., Corrigan, C. J., et al. (2005). Interleukin-10-secreting "regulatory" T cells induced by glucocorticoids and beta2-agonists. *Am. J. Respir. Cell Mol. Biol.* 33, 105–111. doi: 10.1165/rcmb.2005-0100OC

Piergallini, T. J., and Turner, J. (2018). Tuberculosis in the elderly: Why inflammation matters. *Exp. Gerontol* 105, 32–39. doi: 10.1016/j.exger.2017.12.021

Pot, C., Apetoh, L., Awasthi, A., and Kuchroo, V. K. (2011). Induction of regulatory Tr1 cells and inhibition of T_H17 cells by IL-27. *Semin. Immunol.* 23, 438–445. doi: 10.1016/j.smim.2011.08.003

Pot, C., Jin, H., Awasthi, A., Liu, S. M., Lai, C. Y., Madan, R., et al. (2009). Cutting edge: IL-27 induces the transcription factor c-maf, cytokine IL-21, and the costimulatory receptor ICOS that coordinately act together to promote differentiation of IL-10-producing Tr1 cells. *J. Immunol. (Baltimore Md.: 1950)* 183, 797–801. doi: 10.4049/jimmunol.0901233

Rajagopalan, S. (2001). Tuberculosis and aging: a global health problem. *Clin. Infect. Dis.* 33, 1034–1039. doi: 10.1086/322671

Ribeiro-Rodrigues, R., Resende Co, T., Rojas, R., Toossi, Z., Dietze, R., Boom, W.H., et al. (2006). A role for $CD4^+$ $CD25^+$ T cells in regulation of the immune response during human tuberculosis. *Clin. Exp. Immunol.* 144, 25–34. doi: 10.1111/j.1365-2249.2006.03027.x

Rink, L., Cakman, I., and Kirchner, H. (1998). Altered cytokine production in the elderly. *Mech. Ageing Dev.* 102, 199–209. doi: 10.1016/s0047-6374(97)00153-x

Rojas, R. E., Balaji, K. N., Subramanian, A., and Boom, W. H. (1999). Regulation of human CD4(+) alphabeta T-cell-receptor-positive (TCR(+)) and gammadelta TCR(+) T-cell responses to mycobacterium tuberculosis by interleukin-10 and transforming growth factor beta. *Infection Immun.* 67, 6461–6472. doi: 10.1128/IAI.67.12.6461-6472.1999

Roncarolo, M. G., Gregori, S., Bacchetta, R., Battaglia, M., and Gagliani, N. (2018). The biology of T regulatory type 1 cells and their therapeutic application in immune-mediated diseases. *Immunity* 49, 1004–1019. doi: 10.1016/j.immuni.2018.12.001

Roncarolo, M. G., Gregori, S., Battaglia, M., Bacchetta, R., Fleischhauer, K., and Levings, M. K. (2006). Interleukin-10-secreting type 1 regulatory T cells in rodents and humans. *Immunol. Rev.* 212, 28–50. doi: 10.1111/j.0105-2896.2006.00420.x

Rottinghaus, E. K., Vesosky, B., and Turner, J. (2009). Interleukin-12 is sufficient to promote antigen-independent interferon-gamma production by CD8 T cells in old mice. *Immunology* 128, e679–e690. doi: 10.1111/j.1365-2567.2009.03061.x

Rutz, S., and Ouyang, W. (2016). Regulation of interleukin-10 expression. *Adv. Exp. Med. Biol.* 941, 89–116. doi: 10.1007/978-94-024-0921-5_5

Stark, J. L., Avitsur, R., Hunzeker, J., Padgett, D. A., and Sheridan, J. F. (2002). Interleukin-6 and the development of social disruption-induced

glucocorticoid resistance. *J. Neuroimmunol* 124, 9–15. doi: 10.1016/S0165-5728(02)00004-8

Steinbrink, K., Jonuleit, H., Müller, G., Schuler, G., Knop, J., and Enk, A. H. (1999). Interleukin-10-treated human dendritic cells induce a melanoma-antigen-specific anergy in CD8(+) T cells resulting in a failure to lyse tumor cells. *Blood* 93, 1634–1642. doi: 10.1182/blood.V93.5.1634

Swanson, M. A., Lee, W. T., and Sanders, V. M. (2001). IFN-γ production by Th1 cells generated from naïve $CD4^+$ T cells exposed to norepinephrine. *J. Immunol. (Baltimore Md.: 1950)* 166, 232–240. doi: 10.4049/jimmunol.166.1.232

Tait Wojno, E. D., Hunter, C. A., and Stumhofer, J. S. (2019). The immunobiology of the interleukin-12 family: Room for discovery. *Immunity* 50, 851–870. doi: 10.1016/j.immuni.2019.03.011

Takeda, A., Hamano, S., Yamanaka, A., Hanada, T., Ishibashi, T., Mak, T. W., et al. (2003). Cutting edge: role of IL-27/WSX-1 signaling for induction of T-bet through activation of STAT1 during initial Th1 commitment. *J. Immunol. (Baltimore Md.: 1950)* 170, 4886–4890. doi: 10.4049/jimmunol.170.10.4886

Truscott, S. M., Abate, G., Price, J. D., Kemper, C., Atkinson, J. P., and Hoft, D. F. (2010). CD46 engagement on human $CD4^+$ T cells produce T regulatory type1-like regulation of antimycobacterial T cell responses. *Infection and Immunity* 78, 5295–5306. doi: 10.1128/IAI.00513-10

Turner, J., Frank, A. A., and Orme, I. M. (2002). Old mice express a transient early resistance to pulmonary tuberculosis that is mediated by CD8 T cells. *Infection Immun.* 70, 4628–4637. doi: 10.1128/IAI.70.8.4628-4637.2002

Turner, J., Gonzalez-Juarrero, M., Ellis, D. L., Basaraba, R. J., Kipnis, A., Orme, I. M., et al. (2002). *In vivo* IL-10 production reactivates chronic pulmonary tuberculosis in C57BL/6 mice. *J. Immunol. (Baltimore Md.: 1950)* 169, 6343–6351. doi: 10.4049/jimmunol.169.11.6343

Turner, J., and Orme, I. M. (2004). The expression of early resistance to an infection with mycobacterium tuberculosis by old mice is dependent on IFN type II (IFN-gamma) but not IFN type I. *Mech. Ageing Dev.* 125, 1–9. doi: 10.1016/j.mad.2003.09.002

United Nations, D. o. E. a. S. A., Population Division (2017). *World populations ageing-hightlights*, ST/ESA/SER.A 397. (New York, USA).

Vesosky, B., Flaherty, D. K., Rottinghaus, E. K., Beamer, G. L., and Turner, J. (2006). Age dependent increase in early resistance of mice to mycobacterium tuberculosis is associated with an increase in CD8 T cells that are capable of antigen independent IFN-gamma production. *Exp. Gerontol* 41, 1185–1194. doi: 10.1016/j.exger.2006.08.006

Vesosky, B., Rottinghaus, E. K., Davis, C., and Turner, J. (2009). CD8 T cells in old mice contribute to the innate immune response to mycobacterium tuberculosis *via* interleukin-12p70-dependent and antigen-independent production of gamma interferon. *Infection Immun.* 77, 3355–3363. doi: 10.1128/IAI.00295-09

Vesosky, B., and Turner, J. (2005). The influence of age on immunity to infection with mycobacterium tuberculosis. *Immunol. Rev.* 205, 229–243. doi: 10.1111/j.0105-2896.2005.00257.x

Waddell, L. A., Lefevre, L., Bush, S. J., Raper, A., Young, R., Lisowski, Z. M., et al. (2018). ADGRE1 (EMR1, F4/80) is a rapidly-evolving gene expressed in mammalian monocyte-macrophages. *Front. Immunol.* 9 2246. doi: 10.3389/fimmu.2018.02246

Wakkach, A., Fournier, N., Brun, V., Briettmayer, J. P., Cottrez, F., and Groux, H. (2003). Characterization of dendritic cells that induce tolerance and T regulatory 1 cell differentiation in vivo. *Immunity* 18, 605–617. doi: 10.1016/S1074-7613(03)00113-4

Wang, Q., and Liu, J. (2016). Regulation and immune function of IL-27. *Adv. Exp. Med. Biol.* 941, 191–211. doi: 10.1007/978-94-024-0921-5_9

Wang, X., Spandidos, A., Wang, H., and Seed, B. (2012). PrimerBank: a PCR primer database for quantitative gene expression analysis, 2012 update. *Nucleic Acids Res.* 40, D1144–D1149. doi: 10.1093/nar/gkr1013

Weiskopf, D., Weinberger, B., and Grubeck-Loebenstein, B. (2009). The aging of the immune system. *Transplant. Int.* 22, 1041–1050. doi: 10.1111/j.1432-2277.2009.00927.x

Wei, X., Zhang, J., Gu, Q., Huang, M., Zhang, W., Guo, J., et al. (2017). Reciprocal expression of IL-35 and IL-10 defines two distinct effector treg subsets that are required for maintenance of immune tolerance. *Cell Rep.* 21, 1853–1869. doi: 10.1016/j.celrep.2017.10.090

Willems, F., Marchant, A., Delville, J. P., Gérard, C., Delvaux, A., Velu, T., et al. (1994). Interleukin-10 inhibits B7 and intercellular adhesion molecule-1 expression on human monocytes. *Eur. J. Immunol.* 24, 1007–1009. doi: 10.1002/eji.1830240435

Wohleb, E. S., McKim, D. B., Shea, D. T., Powell, N. D., Tarr, A. J., Sheridan, J. F., et al. (2014). Re-establishment of anxiety in stress-sensitized mice is caused by monocyte trafficking from the spleen to the brain. *Biol. Psychiatry* 75, 970–981. doi: 10.1016/j.biopsych.2013.11.029

Wu, Q., Hossfeld, A., Gerberick, A., Saljoughian, N., Tiwari, C., Mehra, S., et al. (2019). Effects of mycobacterium tuberculosis enhancement of macrophage p-glycoprotein expression and activity on intracellular survival during antituberculosis drug treatment. *J. Infect. Dis.* 220, 1989–1998. doi: 10.1093/infdis/jiz405

Zevallos, M., and Justman, J. E. (2003). Tuberculosis in the elderly. *Clinics Geriatric Med.* 19, 121–138. doi: 10.1016/S0749-0690(02)00057-5

frontiers | Frontiers in Cellular and Infection Microbiology

TYPE Original Research
PUBLISHED 23 September 2022
DOI 10.3389/fcimb.2022.1004148

OPEN ACCESS

EDITED BY
Veronica Edith Garcia,
University of Buenos Aires, Argentina

REVIEWED BY
Elba Vazquez,
University of Buenos Aires, Argentina
Alejandro Curino,
Consejo Nacional de Investigaciones Científicas y Técnicas (CONICET), Argentina

*CORRESPONDENCE
Xiaoming Liu,
xiaoming-liu@uiowa.edu
Guangcun Deng
dgc@nxu.edu.cn

SPECIALTY SECTION
This article was submitted to Bacteria and Host, a section of the journal Frontiers in Cellular and Infection Microbiology

RECEIVED 26 July 2022
ACCEPTED 30 August 2022
PUBLISHED 23 September 2022

CITATION
Ma C, Wu X, Zhang X, Liu X and Deng G (2022) Heme oxygenase-1 modulates ferroptosis by fine-tuning levels of intracellular iron and reactive oxygen species of macrophages in response to *Bacillus Calmette-Guerin* infection. *Front. Cell. Infect. Microbiol.* 12:1004148.
doi: 10.3389/fcimb.2022.1004148

Heme oxygenase-1 modulates ferroptosis by fine-tuning levels of intracellular iron and reactive oxygen species of macrophages in response to *Bacillus Calmette-Guerin* infection

Chenjie Ma[1,2], Xiaoling Wu[1,2], Xu Zhang[3], Xiaoming Liu[1,2,4]* and Guangcun Deng[1,2,5]*

[1]Key Laboratory of Ministry of Education for Conservation and Utilization of Special Biological Resources in the Western China, Ningxia University, Yinchuan, China, [2]School of Life Science, Ningxia University, Yinchuan, China, [3]Department of Beijing National Biochip Research Center sub-center in Ningxia, General Hospital of Ningxia Medical University, Yinchuan, China, [4]Department of Anatomy and Cell Biology, University of Iowa, Carver College of Medicine, Iowa City, IA, United States, [5]Analysis and Testing Center, Ningxia University, Yinchuan, China

Macrophages are the host cells and the frontline defense against *Mycobacterium tuberculosis* (Mtb) infection, and the form of death of infected macrophages plays a pivotal role in the outcome of Mtb infections. Ferroptosis, a programmed necrotic cell death induced by overwhelming lipid peroxidation, was confirmed as one of the mechanisms of Mtb spread following infection and the pathogenesis of tuberculosis (TB). However, the mechanism underlying the macrophage ferroptosis induced by Mtb infection has not yet been fully understood. In the present study, transcriptome analysis revealed the upregulation of heme oxygenase-1 (*HMOX1*) and pro-ferroptosis cytokines, but downregulation of glutathione peroxidase 4 (*GPX4*) and other key anti-lipid peroxidation factors in the peripheral blood of both patients with extra-pulmonary tuberculosis (EPTB) and pulmonary tuberculosis (PTB). This finding was further corroborated in mice and RAW264.7 murine macrophage-like cells infected with *Bacillus Calmette-Guerin* (BCG). A mechanistic study further demonstrated that heme oxygenase-1 protein (HO-1) regulated the production of reactive oxygen species (ROS) and iron metabolism, and ferroptosis in BCG-infected murine macrophages. The knockdown of *Hmox1* by siRNA resulted in a significant increase of intracellular ROS, Fe^{2+}, and iron autophagy-mediated factor Ncoa4, along with the reduction of antioxidant factors Gpx4 and Fsp1 in macrophages infected with BCG. The siRNA-mediated knockdown of *Hmox1* also reduced cell survival rate and increased the release of intracellular bacteria in BCG-infected macrophages. By contrast, scavenging ROS by N-acetyl cysteine led to the reduction of intracellular ROS, Fe^{2+}, and Hmox1 concentrations, and subsequently inhibited ferroptosis and the release of intracellular BCG in RAW264.7 cells infected with BCG. These

findings suggest that HO-1 is an essential regulator of Mtb-induced ferroptosis, which regulates ROS production and iron accretion to alter macrophage death against Mtb infections.

KEYWORDS

Heme oxygenase-1, ferroptosis, macrophage, *Mycobacterium tuberculosis*, Bacillus Calmat and Guerin

1 Introduction

Tuberculosis (TB) is a chronic disease caused by the infection of *Mycobacterium tuberculosis* (Mtb), which remains a major public health burden in many developing countries, with approximately 2 billion latent infections and 9.87 million new cases in 2020 (WHO). A recent study confirmed that a co-infection of COVID with Mtb could worsen the COVID-19 infection (Visca et al., 2021). Although considerable efforts have been made in combating Mtb infections and TB disease, the elusive pathogenesis in the development of TB leads to the difficulty and challenges in the prevention and treatment of this ancient disease (Sheedy and Divangahi, 2021). There is not an effective TB vaccine currently available for adults, and clinical treatments for TB are largely dependent on antibiotics such as rifampin. It is therefore a necessity to better understand the pathogenesis of TB disease.

Macrophages are the host cells and the frontline defense of Mtb infections (Korb et al., 2016). The outcome of the host–pathogen interaction between macrophages and Mtb is certainly critical for the development of TB (Xu et al., 2014). In this context, intracellular Mtb either can be eradicated through macrophage apoptosis (Lee et al., 2009) and autophagy (Alam et al., 2017), or can persistently survive and grow in macrophages, and induce macrophage necrosis and spread infection to other cells by evolving an immune escape mechanism (Liu et al., 2017; Pajuelo et al., 2018; Zhai et al., 2019). Therefore, understanding the molecular mechanism of Mtb-induced macrophage deaths, particularly macrophage necrosis, may enable us to uncover novel targets for host-directed therapy (HDT) of TB by altering macrophage death in response to Mtb infections.

In addition to necroptosis and pyroptosis, the two most studied forms of Mtb-induced macrophage necrosis, ferroptosis is another form of programmed cell death (PCD) that is a type of necrosis dependent on iron (Dixon et al., 2012; Amaral et al., 2019). Interestingly, macrophage necrosis induced by Mtb infection shared the typical characteristics of ferroptosis (Shastri et al., 2018; Amaral et al., 2021; Baatjies et al., 2021). In this regard, an external stress such as Mtb infection could elevate intracellular levels of Fe^{2+} and reactive oxygen species (ROS) to trigger the Fenton reaction, and result in the production of large amounts of hydroxyl radicals, sequentially impair glutathione peroxidase 4 (GPX4) activity and anti-lipid peroxidation capacity, and ultimately lead to overwhelming lipid peroxidation of intracellular membrane phospholipids and cell disintegration and death (Dixon et al., 2012; Li et al., 2020). Indeed, the ferroptosis inhibitor could effectively reduce Mtb-induced macrophage necrosis and bacterial load in a mouse infection model (Amaral et al., 2019). These findings suggest that intracellular ROS and lipid peroxidation are essential for ferroptosis in response to Mtb infections, implying that oxidation-related ferrous ion imbalance is involved in cell ferroptosis death; however, the molecular mechanism underpinning the ferrous ion production in Mtb-induced macrophage ferroptosis has not been completely elucidated.

Heme oxygenase 1 protein (HO-1) is encoded by *HMOX1* gene, which is an important stress-responsive enzyme highly expressed in lungs, which catalyzes to degrade heme to Fe^{2+}, carbon monoxide (CO), biliverdin, and bilirubin, and is essential in the balance of intracellular Fe^{2+} and ROS (Araujo et al., 2012). Moreover, HO-1 is also considered as one of the biomarkers for the diagnosis of TB in clinical settings (Rockwood et al., 2017; Yong et al., 2019; Uwimaana et al., 2021; Yang et al., 2022); whether it plays a role in the regulation of Mtb-induced ferroptosis in macrophages, however, has yet been investigated.

In the present study, the involvement of *HMOX1* in macrophage ferroptosis in response to a mycobacterial infection was interrogated by transcriptome analysis of peripheral blood in TB patients, and its mechanism in ferroptosis was further investigated in mice and macrophage-like RAW264.7 cells by infection of *Bacillus Calmette-Guerin* (BCG). Our results demonstrate that HO-1 is a negative regulator of murine macrophage ferroptosis in response to BCG infections, in part through a mechanism by which HO-1 inhibits the intracellular ROS production and iron accretion, but induces Gpx4 expression in murine macrophages infected by BCG.

2 Materials and methods

2.1 Mice

C57BL/6 mice were purchased from Gempharmatech Co., Ltd (Jiang Su, China). Experiments using mice were approved by the

Laboratory Animal Welfare Ethics Review Committee of Ningxia University (NXU-2018-011). Sixteen mice were randomly divided into two groups, PBS control and BCG infection. Mice were housed in specific pathogen-free conditions in a 12-h light/dark cycle with *ad libitum* access to food and water. All animal studies were conducted at the Laboratory Animal Center of Ningxia University (Yinchuan, China).

2.2 Bacteria and infection

Mycobacterium tuberculosis attenuated strain BCG was purchased from Chengdu Institute of Biological Products Ltd (Chengdu, China). The lyophilized bacteria preparation was dissolved and washed with PBS, and subsequently gently sonicated to disrupt bacterial clumps for single-cell suspension in DMEM or PBS. The bacterial suspension was aliquoted and stored at −20°C, and was used within 2 weeks after the preparation. For bacterial infection in mice, mouse was infected with BCG in 100 μl at a dose of 5×10^6 colony-forming units (CFU)/mouse *via* tail vein injection. The lung tissues were harvested for analysis at 30 days post-infection.

2.3 Chemicals and small interfering RNA

GPX4 inhibitor RAS-selective lethal 3 (RSL3) (#HY-100218A) and ROS scavenger N-acetylcysteine (NAC) (#HY-134495) were purchased from MedChemExpress (Shanghai, China), and were dissolved in DMSO. H_2O_2 (#7722-84-1) was from MERCK (Germany). Three small interfering RNAs (siRNAs) to murine *Hmox1* mRNA sequence (Gene ID: NM_010442.2), si-*Hmox1*-27 5'-GTTTCCGCATACAACCAGTGA-3', si-*Hmox1*-193 5'-UUG GAUGUGUACCUCCUUGTT-3', and si-*Hmox1*-672 5'-GCU CUAUCGUGCUCGAAUGAA-3', were designed using *In vivo*Gen-siRNA Wizard Software 3.1 (https://www.invivogen.com/sirnawizard/design_advanced.php, *In vivo*Gen, California, USA). Control siRNA 5'-UUCUCCGAACGUGUCACGUTT-3' served as the scramble siRNA. The siRNAs were synthesized by GenePharma (Shanghai, China).

2.4 Cell culture, *in vitro* BCG infection, and siRNA transfection

RAW264.7 murine monocyte/macrophage-like cells were cultured in DMEM containing 10% calf serum at 37°C in 5% CO_2 atmosphere. For bacterial infection, RAW264.7 cells were seeded in a six-well plate at a density of 2×10^5/well and cultured for 16 h. Cells were then pretreated with NAC for 1 h or transfected with siRNA for 12 h prior to be infected with bacteria at a multiplicity of infection (MOI) of 1, 5, or 10. The cells were harvested for analysis at 24 h post-infection. siRNA was transfected with Lipofectamine RNAiMAX per manufacturer's instructions (ThermoFisher Scientific, Waltham, MA, USA). To test the efficiency of siRNA-mediated knockdown of protein of interest, total proteins of transfected cells were extracted at 24 h post-transfection and were analyzed by Western blotting assay.

2.5 Western blotting

Total proteins of cells were lysed with RAPI buffer containing protease inhibitor (#P0033, Beyotime, Shanghai, China). The protein concentration of soluble fraction of cell lysates was determined using the Pierce™ BCA agents (#23225, ThermoFisher). The protein samples were separated by SDS-PAGE prior to being transferred to PVDF membranes. The PVDF membrane was then blocked with 5% fat-free milk for 1 h at room temperature (RT), before it was incubated with primary antibodies to protein of interest for overnight at 4°C with shaking (45 rpm). The membrane was then washed 3 × 10 min in TBST solution containing 0.2% Tween-20 prior to being incubated in appropriate horseradish peroxidase (HRP)-conjugated secondary antibody for 1 h at RT. The specific binding of protein was developed in Western Lightning® Plus-ECL (#NEL105001EA, PerkinElmer) and visualized in Amersham Imager 600 (Cytiva, USA). The abundance of protein was semi-quantified with ImageJ 1.52a as described elsewhere (Pillai-Kastoori et al., 2020). Beta-actin or tubulin served as internal loading control; GraphPad was used to calculate "Mean ± SD" and statistical analysis. The antibodies used in this study are listed in Supplementary Table S1.

2.6 Measurement of apoptosis and necroptosis

Cells were treated with the Annexin V/PI Apoptosis Detection kit (KGA108-1, keygen Biotech, Nan Jing, China). Cells were washed with PBS, followed by being centrifuged at 2,000 rpm for 5 min, and the medium supernatant was discarded. The resulting cell pellet was washed twice with PBS by centrifugation. A total of $1–5 \times 10^5$ cells were suspended in 500 μl of binding buffer before 5 μl of Annexin V-FITC and 5 μl of propidium iodide were added consecutively. The cell suspension was incubated for 5 min at room temperature in the dark. The above samples were detected using a flow cytometer. The processed samples were detected by flow cytometry.

2.7 Measurement of cell death

Cell viability was measured by Trypan Blue staining assay. 0.4% Trypan Blue solution was added to a single-cell suspension at a ratio of 1:9 in volume. Live/dead cells were read using Invitrogen Countess 3 (ThermoFisher) and the percentage of live cells was calculated.

2.8 Bacterial colony-forming unit count

RAW264.7 macrophages were preincubated in medium containing 2.0 mM NAC for 1 h, or transfected with siRNA-*Hmox1* for 24 h, followed by incubating with BCG at an MOI of 5 for 1 h. The cells were then rinsed with medium to remove unattached bacteria and cultured with fresh medium for an additional 24 h. The culture medium was then collected for accessing the release of intracellular bacteria due to cell necrotic death including ferroptosis by spreading series diluted medium in 7H10 agar plates and incubated at 37°C for 21 days. The number of colonies on the plates was counted as CFU numbers. The final bacterial CFU number was calculated by multiplying the dilution factor and the count on plates.

2.9 Intracellular iron measurement

The content of intracellular ferrous iron (Fe^{2+}) was measured using the Iron Assay kit (#ab83366, Abcam). Only ferrous (Fe^{2+}) can bind to the iron probe to form a stable-colored complex that can be accessed by reading an absorption peak at a wavelength of 539 nm. Solutions of standard curve and reaction were prepared in accordance with the manufacturer's instructions.

2.10 Intracellular ROS detection

Intracellular ROS detection was measured with the CellROX™ Deep Red kit (#C10491, ThermoFisher). CellROX™ Red is a fluorescent probe for measuring ROS in living cells. CellROX™ Red emits a stable bright red fluorescence upon an oxidation by ROS. The maximum absorption/emission wavelength is approximately 485/520 nm.

2.11 Mitochondrial fluorescent staining

Live cell mitochondria were stained with CellLight™ Mitochondria-GFP BacMam 2.0 (#C10508, ThermoFisher). CellLight™ Mitochondria-GFP was added to the cell cultures, and cells were continuously incubated for an additional 16 h at 37℃. The mitochondrial fluorescence was then observed in a laser confocal microscope (SP5, Leica, Germany).

2.12 Lipid peroxidation assay

An Image-iT® Lipid Peroxidation Kit (#C10445, ThermoFisher) was used to assay cellular lipid peroxidation. The BODIPY® 581/591 C11 probe binds to polyunsaturated fatty acids in the cell membrane. Due to the oxidation of fatty acids, the absorption peak of the probe shifts from 590 nm (red) to 510 nm (green); the change in value of the absorption peaks at different wavelengths was calculated using the arithmetic mean. For immunofluorescence assays, live cells were incubated with the BODIPY® 581/591 C11 reagent for 30 min. Cell membrane lipid peroxidation was then respectively observed under excitation (581/488 nm)/emission (591/510 nm) conditions. The staining was observed and imaged under a laser scanning confocal microscope (SP5, Leica, Germany).

2.13 Immunocytofluorescence staining

RAW264.7 cells were seeded on collagen pre-coated sterile cover slides. Cells were fixed in 4% paraformaldehyde for 30 min, washed in PBS for 3× 5 min, and penetrated with 0.1% Triton X-100 (PBST) for 15 min at RT. Cells on slides were then blocked with 5% BSA for 1 h at RT, followed by incubating in primary antibody overnight at 4°C. Slides were then washed 3× 5 min in PBST before they were incubated with appropriate fluorescent secondary antibody with light proof for 1 h at RT. Cell nuclei were counterstained with DAPI. Images were acquired under a laser scanning confocal microscope (SP5, Leica, Germany).

2.14 Immunohistochemistry staining

The lung tissues were fixed in 4% paraformaldehyde and embedded in paraffin. Four-micrometer-thick sections were cut with a Leica RM2135 Microtome (Germany). After xylene deparaffination, rehydration, and antigen retrieval, the sections were blocked in 10% donkey serum blocking buffer. Slides were then incubated in primary antibodies overnight at 4°C, followed by being incubated with HRP-conjugated secondary antibody for 1 h at RT. The antigen–antibody binding was detected with DAB substrate solution. The sections were counterstained with hematoxylin for nuclei. The staining was observed and imaged under the microscope (BA400Digital, Motic, USA). Immunohistochemical (IHC) images were analyzed using ImageJ-IHC profiler for semi-quantification as described elsewhere (Crowe and Yue, 2019). GraphPad 8.0.1 was used for statistical analysis.

2.15 Transmission electron microscopy test

Cell pellets were resuspended in 0.5% glutaraldehyde fixative and incubated for 10 min at 4°C. Cells were re-pelleted and treated with 1% osmium tetroxide. The cell samples were then

dehydrated with a low to high concentration of acetone prior to be embedded in epoxy resin. Fifty-nanometer-thick sections were prepared using Ultramicrotome EM UC7 (Leica, Germany). Samples were stained with uranyl acetate and lead citrate. Transmission electron microscopy was used to observe cell morphology.

2.16 GEO data analysis

The GSE83456 dataset is sourced from the Gene Expression Omnibus (GEO) database. The Ethic Committee of Human Research at General Hospital of Ningxia Medical University approved the protocol of human study. The dataset includes peripheral blood transcriptome sequencing information for three groups, namely, 30 healthy control subjects (Control), 30 individuals with extra-pulmonary tuberculosis (EPTB), and 30 patients with pulmonary tuberculosis (PTB). The demographics of TB patients whose blood samples were collected and used in this study are listed in Supplementary Table S2. The dataset was normalized by Log2 transformation in R software 3.4.1. Subsequently, the gene IDs were converted to gene names. The significance of the three groups of datasets was analyzed in GraphPad 8.0.1 using one-way ANOVA followed by Tukey's multiple comparisons test.

2.17 ELISA testing of clinical samples

The Human Heme Oxygenase 1 (HO-1) ELISA Kit (#ab207621, Abcam) was used to detect HO-1 protein levels in the peripheral blood of clinical TB patients (n = 59) and healthy individuals (n = 26). The Hemin Assay Kit (#ab65332, Abcam) was employed for determining the concentration of H in the serum of TB patients (n = 57) and healthy individuals (n = 26). The measurement was performed per the manufacturer's instructions. The collection and processing of human peripheral blood samples passed the approval of the Medical Research Ethics Review Committee at General Hospital of Ningxia Medical University General Hospital (NO. 2020-410).

2.18 Statistics

All graphical data are expressed as mean ± SD. Graphical data and statistical analyses were processed with GraphPad Prism 8.0.1. Comparisons between the two groups were carried out using an unpaired two-tailed t-test and triple comparisons were statistically analyzed using one-way ANOVA. Charts and legends provide the number of independent experiments and the results of a representative experiment.

3 Results

3.1 Transcriptome analysis of peripheral blood revealed differential expression of ferroptosis-related genes in patients with tuberculosis

To investigate whether ferroptosis is involved in the pathogenesis of TB development in clinic, peripheral blood of healthy individuals (Control, N = 30), patients with PTB (N = 30), and patients with EPTB (N = 30) was collected for transcriptome analysis, and compared with the publicly available GEO database (GSE83456). Collated datasets were processed using log2 normalization, and the ID_REF was converted to gene symbols. The transcriptome analysis demonstrated that anti-lipid peroxidation factor *GPX4*, a major scavenger of phospholipid hydroperoxides, and the key regulator of ferroptosis, was significantly downregulated (Figure 1A), but anti-oxidative stress factor *HMOX1* was upregulated (Figure 1B) in both PTB and EPTB patients, compared to healthy control cohorts. Moreover, the increased level of *HMOX1* transcript was in line with the more abundant HO-1 protein in peripheral blood from TB patients (6.333 ng/ml, N = 57) compared to healthy individuals (2.58 ng/ml, N = 26), as determined by ELISA (Figure 1C). Heme B is a substrate for the enzymatic reaction of HO-1, and forms a chlorine-containing porphyrin, namely, Hemin in blood. Hemin is a potent inducer of HO-1 and plays a certain extent of anti-infective roles in the body (Kim et al., 2021). Hemin content in peripheral blood was significantly higher in TB patients (0.85 ± 0.44 ng/ml, N = 57) than healthy individuals (0.29 ± 0.26 ng/ml, N = 26) (Figure 1D). This result was in line with the concentration of HO-1 protein in peripheral blood TB patients.

In order to reveal a correlation between *HMOX1*, an oxidative stress signature, and ferroptosis regulators, a CorrPlot map was constructed using Spearman rank correlation (Figure 1D). The CorrPlot map showed that the *HMOX1* expression was negatively associated with the level of circulating *GPX4*, suggesting that HO-1 might play a regulatory role in the ferroptosis in TB pathogenesis. In addition, transcriptome analysis also unraveled the differential expression of other ferroptosis genes in peripheral blood of TB patients (Supplementary Figure S1). Among them, the transcripts of *ACSL4*, *LPCAT3*, *ALOX5*, *COQ10A*, *VDAC2*, *NOX4*, *xCT*, and *FTH1* genes were increased in peripheral blood of both patients with PTB and EPTB (Supplementary Figures S1A, D, E, G, I, J, N), while *LPCAT3* and *COQ10B* transcripts were only increased in PTB but not EPTB patients (Supplementary Figures S1B, F), as compared with the healthy individuals. There was no statistical significance in differential expression of transcripts *ALOX15*, *VDAC3*, *SLC3A2*, *NCOA4*, and *LRP8* genes (Supplementary Figures S1D, K, L, M). These

10.3389/fcimb.2022.1004148

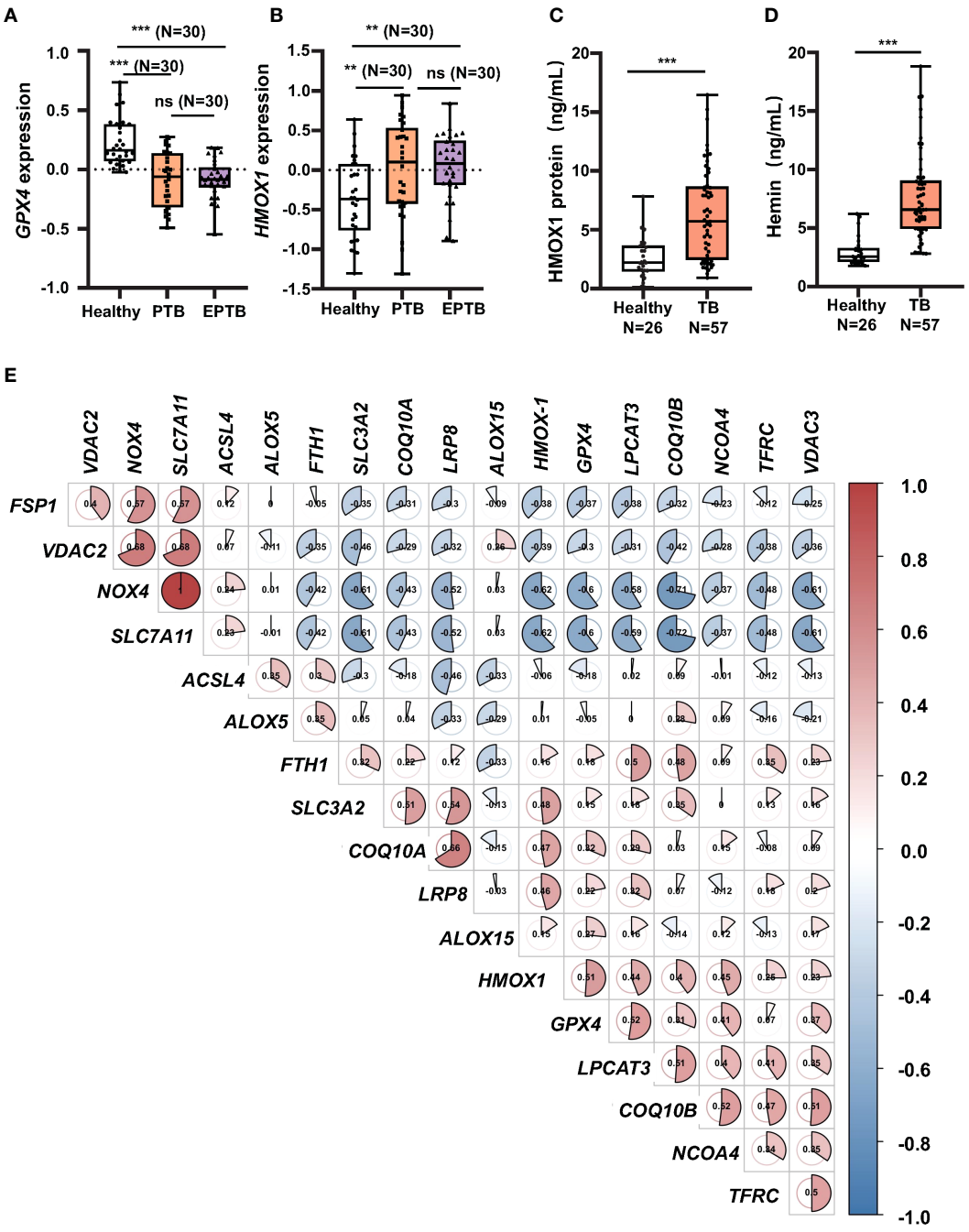

FIGURE 1
Increase of *HMOX1* and decrease of *GPX-4* in peripheral blood of TB patients. Peripheral blood from healthy individuals (*N* = 30), patients with pulmonary TB (PTB, *N* = 30), and patients with extra-pulmonary TB (EPTB, *N* = 30) was collected for transcriptome analysis using GEO database GSE83456 (a transcriptome sequencing dataset of peripheral blood from TB patients). **(A, B)** The differential expression of transcript of the anti-lipid peroxidation factor *GPX4* and **(B)** the oxidative stress regulator *HMOX1* in the peripheral blood of TB patients. **(C)** More abundant circulating HO-1 protein in blood of patients with TB in comparison with healthy subjects as determined by ELISA. **(D)** Hemin content in peripheral blood of patients with TB in comparison with healthy subjects as determined by the Hemin Assay Kit. **(E)** Plotting CorrPlot map in Hiplot (https://hiplot-academic.com/) showed the correlation of *HMOX1* transcript with transcripts of ferroptosis markers in patients with PTB analyzed by Spearman. The color in the CorrPlot map represents the correlation coefficient, darker color represents stronger correlations. Red represents positive correlation while blue represents negative correlation. Cluster analysis using the ward.D2 method in Hiplot. Data were processed using GraphPad Prism 8.0.1 software and ImageJ 1.52.a. Unpaired *t*-test was used to analyze the differential changes of two groups. One-way ANOVA and Tukey's multiple comparisons test was used to analyze the differential changes of multiple groups. Data represented mean ± SD; significant differences were indicated with asterisks (**$p < 0.01$; ***$p < 0.001$). ns, no statistical difference.

data clearly evidence that ferroptosis is involved in the TB pathogenesis.

3.2 BCG induced ferroptosis in macrophages

To test whether the infection of Mycobacteria could induce ferroptosis *in vivo*, 8-week ICR mice were infected with the Mtb-attenuated strain BCG at a dose of 5×10^6 CFU/mouse in 100 μl volume *via* tail vein injection, and the ferroptosis was assessed by the expression of Gpx4 and HO-1 proteins in lungs at 30 days post-infection (Figure 2A). IHC staining assay showed a reduced Gpx4 protein, the signature of cell ferroptosis, and an increased HO-1 protein abundance in lungs of BCG-infected mice compared to the control group (Figures 2B, C), which was in accordance with the transcriptomic findings in peripheral blood of TB patients (Figure 1 and Supplementary Figure S1).

Given the Mtb-infected macrophage death in TB pathogenesis, we next investigated whether the BCG infection could induce ferroptosis in RAW264.7 murine macrophage-like cells. Immunoblotting assay demonstrated a dose-dependent induction of Gpx4 and HO-1 in this type of cells, except for an inhibition of Gpx4 expression in cells infected with a low dose of BCG at an MOI of 5 (Figures 2C–F). Interestingly, the inhibition of Gpx4 and induction of Hmox1 was in a time-dependent manner, when cells were infected with BCG at an MOI of 5 for the 24-h time period (Figures 2G, H, I). Annexin V/PI flow cytometry revealed a dose-dependent reduction of cell necrosis but an increase of apoptosis in RAW264.7 cells at 24 h post-infection of BCG at an MOI range of 5 to 15 (Figure 2J and Supplementary Figure S2A). As expected, the infection of BCG significantly reduced cell viability (Figure 2K) and increased the production of intracellular ROS (Figure 2L; Supplementary Figure S2B) and the intracellular level of Fe^{2+} (Figure 2M). Importantly, the infection of BCG increased the fraction of cells with lipid peroxidation as determined by BODIPY 581/591 C11 assays (Figures 2N and 3A; Supplementary Figure S2C). The ratio of lipid peroxidation cell (Green)/normal cell (Red) was 17.22% in the BCG-infected cells, while it was 3.52% in uninfected cells (Figure 2K). Transmission electron microscope (TEM) observation of BCG-infected RAW264.7 macrophages showed increased mitochondrial membrane ridge breaks compared to uninfected cells (Figure 3B). Mechanistic study by immunocytochemistry (ICC) (Figure 3C) and Western blotting (Figures 3D–F) demonstrated a decrease of anti-ferroptosis regulators Gpx4 and Fsp1, along with the decrease of cell mitochondria staining (Figure 3C), but an increase of pro-ferroptosis marker HO-1 in BCG-infected cells compared with uninfected cells. These observations were further corroborated by a molecular study using Western blotting assay (Figures 3D–F). In addition, the expression of anti-ferroptosis molecules Alox5 (Supplementary Figure S3B), Vdca2 (Supplementary Figure S3C), and Ncoa4 (Supplementary Figure S3D) was also inhibited, while pro-ferroptosis factor xCT (Supplementary Figure S3E) was increased in cells infected with BCG, relative to the uninfected controls. These results indicated that the infection of BCG could induce ferroptosis of RAW264.7 cells, and the increase of intracellular ROS production and the alteration of HO-1 were part of the underlying mechanism of BCG-induced ferroptosis.

3.3 Intracellular ROS contributes to BCG-induced ferroptosis in RAW264.7 macrophages

Next, we sought whether the intracellular ROS contributed to ferroptosis in RAW264.7 cells in response to BCG infections. In order to investigate the effect of ROS in ferroptosis, H_2O_2, a major ROS source, and RSL3, one of the most common inhibitors of GPX4 and inducer of ferroptosis, separately served as positive controls. Optimization experiments showed that the highest inhibition of the ferroptosis regulator Gpx4 was found in RAW264.7 cells exposed to H_2O_2 and RSL3 at concentrations of 0.2 mM and 2 mM, respectively (Supplementary Figures S4A, B). These optimized concentrations were therefore used in further experiments of this report. Indeed, similar to treatments of H_2O_2 and RSL3, the infection of BCG also displayed effects of inhibition of cell viability (Figure 4A), inductions of intracellular Fe^{2+} (Figure 4B) and ROS production (Figure 4C and Supplementary Figure S4C), and increase of lipid peroxidation (Figures 4D, E and Supplementary Figure S4D) in RAW264.7 macrophages at an MOI of 5. As a consequence, these treatments induced mitochondrial membrane ridge breaks (arrows) in RAW264.7 macrophages as determined by electron microscope observation (Figure 4F). Molecular analysis further demonstrated that the infection of BCG significantly inhibited the expression of Gpx4 and Fsp1 proteins, but increased HO-1 expression (Figure 4G). Of note, the treatments of H_2O_2 or RSL3 failed to increased HO-1 protein, although these treatments inhibited Gpx4 and Fsp1 in RAW264.7 cell as seen in BCG-infected cells (Figure 4G). The infection of BCG is comparable to intracellular ROS production and cell peroxidation, and to the inhibition of the expression of Gpx4 and Fsp1 with that of 0.2 mM of H_2O_2, although the effect was to a lesser extent compared to that of 2.0 mM RSL in RAW264.7 cells. These results suggest that HO-1-mediated ROS production may play a major role in the regulation of ferroptosis in macrophages against Mtb infections.

3.4 ROS scavenger NAC reduces BCG-induced macrophage ferroptosis

NAC is a potent antioxidant and ROS scavenger. It is able to reduce the excessive lipid peroxidation induced by BCG infection in macrophages through the scavenging of ROS. To

10.3389/fcimb.2022.1004148

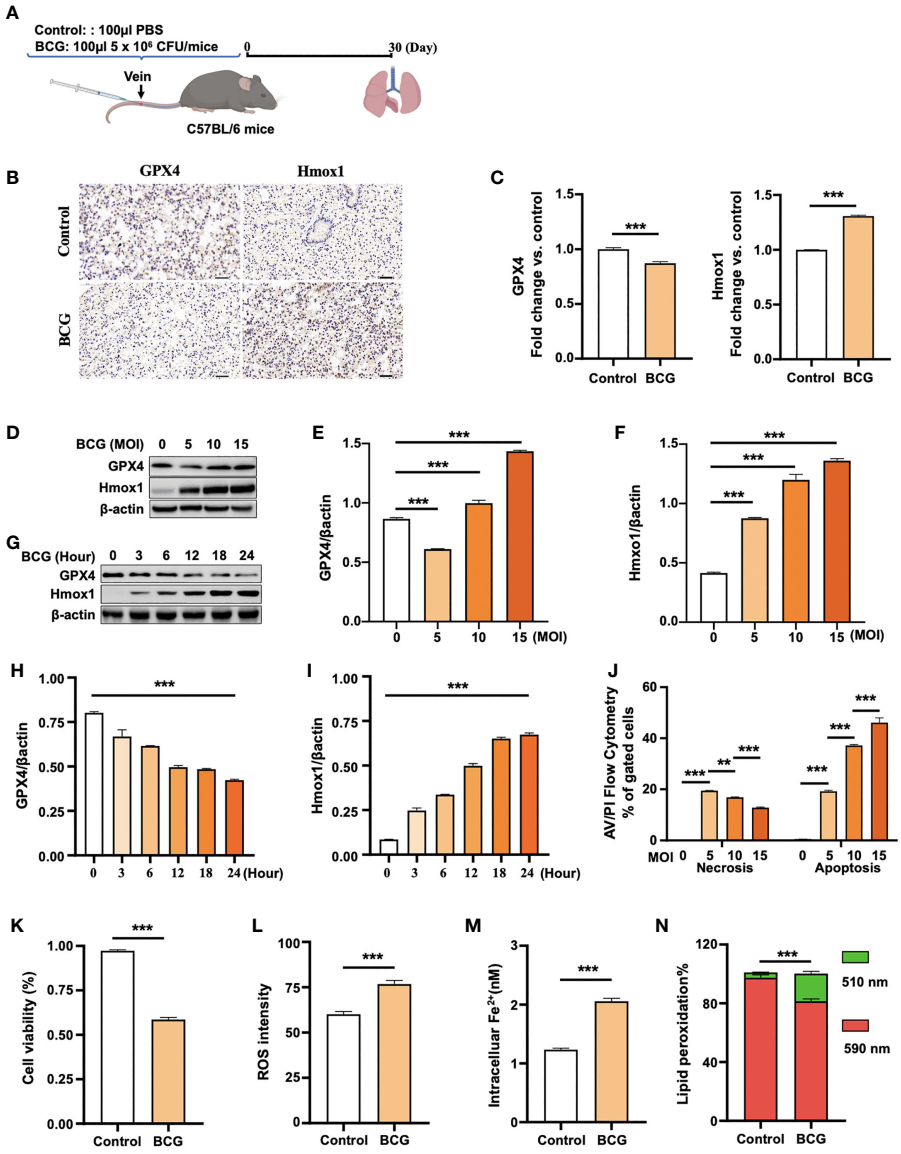

FIGURE 2
BCG induces ferroptosis in macrophages. **(A)** Schematic diagram shows the infection of mice with BCG *via* tail vein injection. The infected mice are analyzed at 30 days post-infection (DPI). **(B, C)** C57BL/6 mice were injected with 5 × 10^6 CFU BCG in 100 μl *via* the tail vein and the lungs were harvested for evaluating the expression of Gpx4 and HO-1 proteins at 30 DPI by immunohistochemical (IHC) assay **(B)** and semi-quantified by ImageJ-IHC Profiler **(C)**. Lungs of mice infected with BCG showed less and more abundant Gpx4 and HO-1 proteins compared to the uninfected controls, respectively. Bar represents 500 μm in **(B)(D-F)** RAW264.7 murine macrophage-like cells were infected with BCG at indicated MOI for 24 h, and the abundance of Gpx4 and HO-1 proteins was examined by Western blotting assay. The representative blots **(D)** and semi-quantification of Gpx4 **(E)** and HO-1 **(F)** showed a dose-dependent induction of Gpx4 and HO-1 in this type of cells, except an inhibition of Gpx4 expression in cells infected with a low dose of BCG at an MOI of 5. **(G–I)** The representative blots **(D)** and semi-quantification of Gpx4 **(H)** and HO-1 **(I)** demonstrated a time-dependent inhibition of Gpx4 and induction of HO-1 in RAW264.7 infected with BCG at an MOI of 5 for a 24-h time period. **(J)** Induction of cell necrosis and apoptosis in RAW264.7 cells at 24 h post-infection of BCG at the indicated MOI determined by using Annexin V/PI in flow cytometry. **(K)** Cell viability assay showed that the infection of BCG decreased the viability of RAW264.7 cells at an MOI of 5 for 24 has detected by Trypan Blue assay. **(L)** The infection of BCG induced the production of intracellular ROS in RAW264.7 cells at an MOI of 5 for 24 has detected by flow cytometry assay. **(M)** The infection of BCG increased the concentration of intracellular Fe^{2+} in RAW264.7 cells at an MOI of 5 for 24 has detected using iron ion probes. **(N)** The infection of BCG induced lipid peroxidation in RAW264.7 cells at an MOI of 5 for 24 h as determined by BODIPY 581/591 C11 assays. Upon oxidation, its excitation of Red/590 nm shifts to 510 nm (Green). The ratio of Green/Red cells in the BCG-infected cells was 17.22%, while the uninfected cells was 3.52%. Data obtained from three independent experiments were processed using GraphPad Prism 8.0.1 software and ImageJ 1.52.a. Unpaired *t*-test was used to analyze the differential changes of the two groups. One-way ANOVA and Tukey's multiple comparisons test was used to analyze the differential changes of multiple groups. Data represented mean ± SD from three independent experiments; significant differences are indicated with asterisks (**$p < 0.01$; ***$p < 0.001$).

10.3389/fcimb.2022.1004148

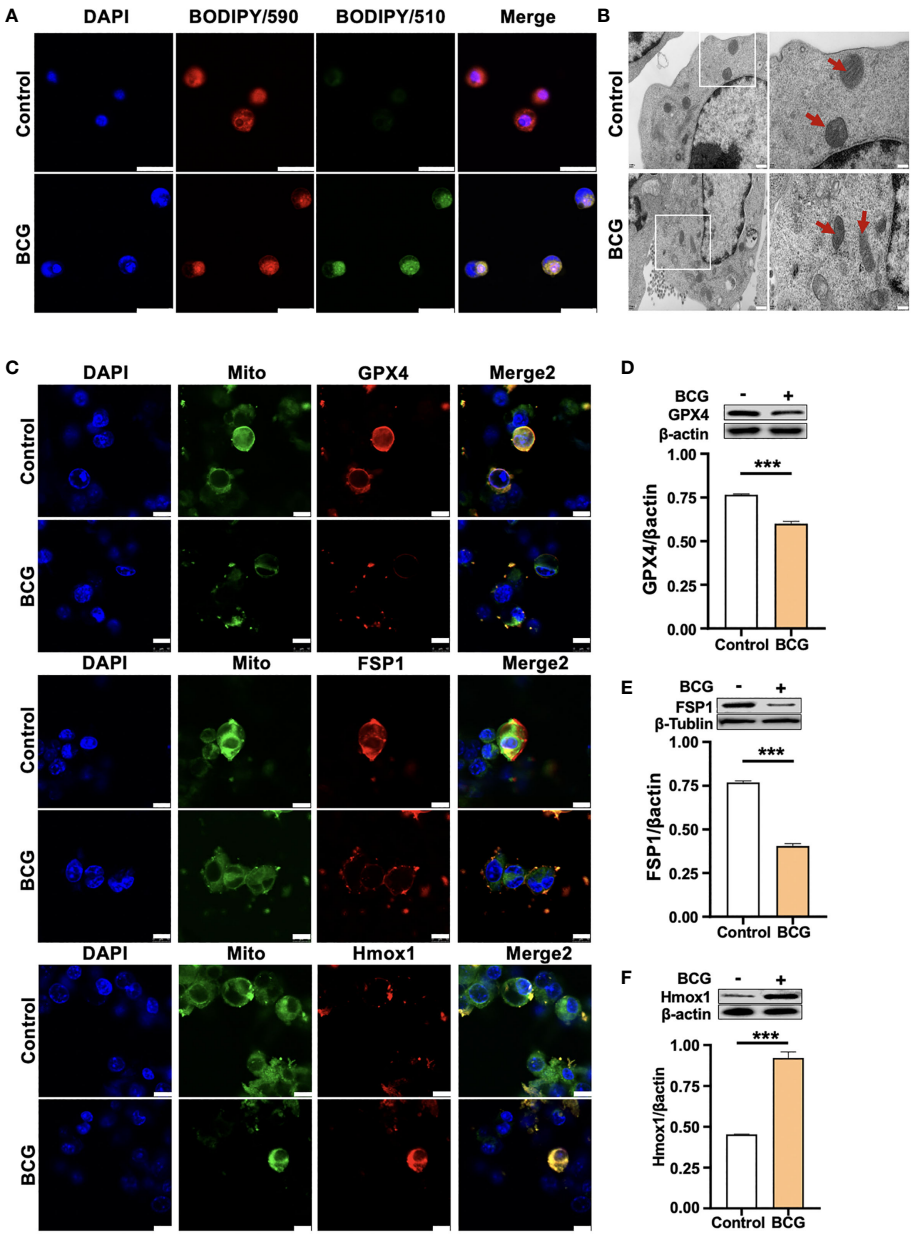

FIGURE 3
HO-1 is involved in the BCG-induced macrophage ferroptosis. **(A)** Representative images of BODIPY 581/591 C11-labeled lipoxidation of polyunsaturated fatty acids. BCG-infected RAW264.7 cells showed a strong positive lipid peroxidation (Green/510 nm) compared to the uninfected cells. **(B)** Representative images of transmission electron microscopy showed mitochondrial membrane ridge breaks (arrows) in RAW264.7 macrophages infected by BCG; the right panel shows the enlarged image of the boxed area in its corresponding image in the left panel. **(C)** Representative immunofluorescence images of Gpx4 (top panels), Fsp1 (middle panels), and HO-1 (bottom panels) showed the decrease of anti-ferroptotic markers Gpx4 and Fsp1, but increased pro-ferroptotic marker HO-1 in BCG-infected cells. Cell mitochondria were labeled with CellLight™ Mitochondria-GFP (green), which were reduced in macrophages following the BCG infection. **(D–F)** Representative blots and semi-quantitative analysis of Gpx4, Fsp1, and HO-1 proteins of RAW264.7 cells. Statistical analysis of data performed using GraphPad Prism 8.0.1 software and ImageJ 1.52.a. Cell nuclei were counterstained with DAPI. Data obtained from three independent experiments were processed using GraphPad Prism 8.0.1 software and ImageJ 1.52.a. Unpaired *t*-test was used to analyze the differential changes of two groups. Data are presented as mean ± SD from three independent experiments (***$p < 0.001$; $n = 3$). Bars, 500 nm in the right panel and 200 nm in the left panel of A, 25 μm in B, and 10 μm in C.

10.3389/fcimb.2022.1004148

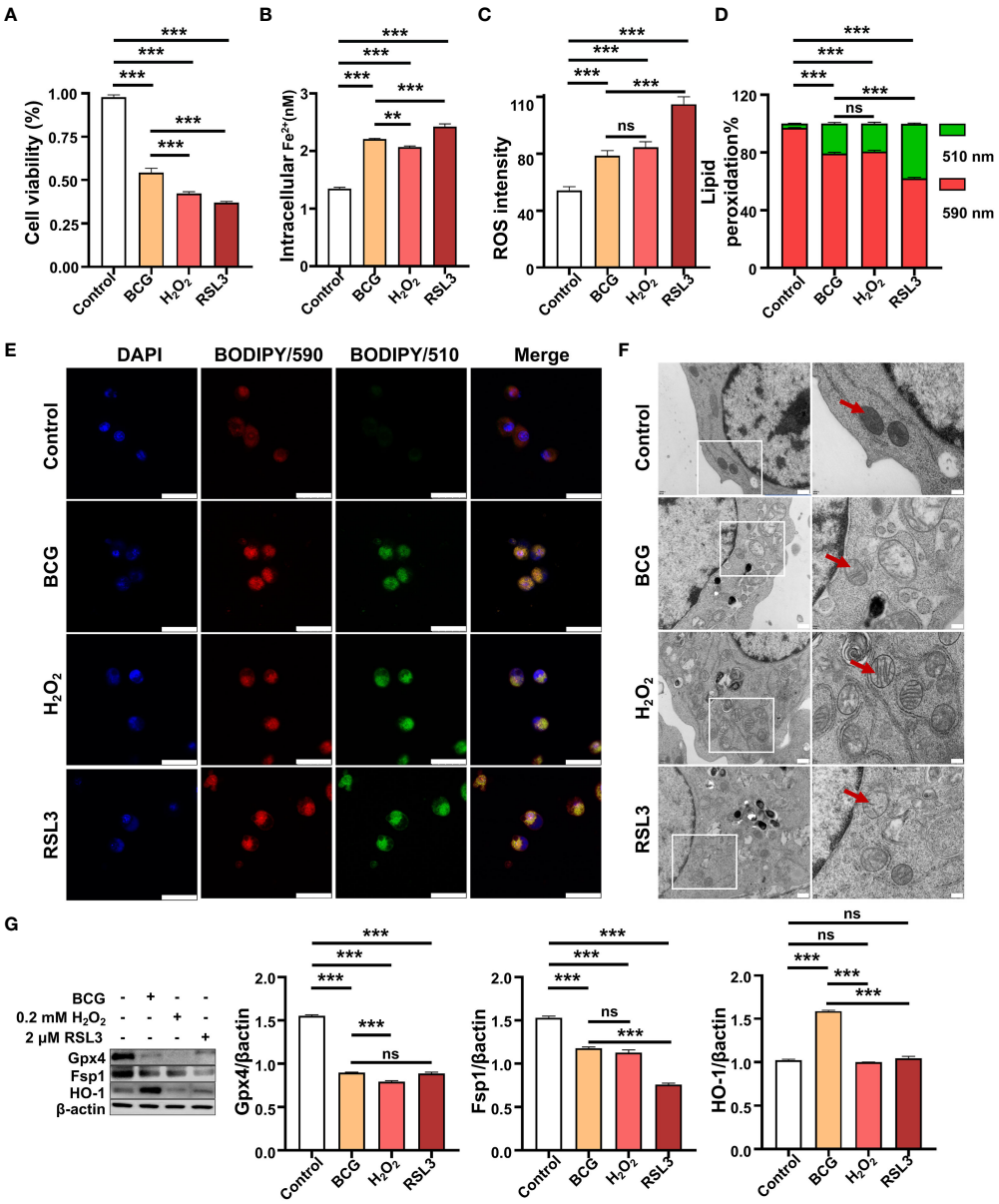

FIGURE 4
BCG induces intracellular ROS production and ferroptosis in RAW264.7 macrophages. **(A–D)** The viability **(A)**, intracellular Fe^{2+} **(B)**, intracellular ROS **(C)**, and lipid peroxidation **(D)** of RAW264.7 macrophages in response to BCG infection (MOI 5), ferroptosis agonist RSL3 (2.0 μM), and H_2O_2 (0.2 mM), major participants of the Fenton response at 24 h post-treatments, as determined by Trypan Blue assay, iron ion probes, flow cytometry, and BODIPY 581/591 C11 assays, respectively. **(E)** Representative fluorescence images of BODIPY 581/591 C11-labeled lipoxidation of polyunsaturated fatty acids in RAW264.7 macrophages infected with BCG (the second panel from top), treated with H_2O_2 (the second panel from bottom), and RSL3 (bottom panel). Cell nuclei were counterstained with DAPI. **(F)** Representative images of transmission electron microscopy showed mitochondrial membrane ridge breaks (arrows) in RAW264.7 macrophages infected with BCG (the second panel from top), treated with H_2O_2 (the second panel from bottom) and RSL3 (bottom panel). The right panel shows the enlarged image of the boxed area in its corresponding image in the left panel. **(G)** Representative blots and semi-quantitative analysis of Gpx4, Fsp1, and HO-1 proteins of RAW264.7 cells treated with the indicated conditions. The infection of BCG increased intracellular Fe^{2+} level and induced ROS (H_2O_2) production and lipid peroxidation and ferroptosis in macrophages, by inhibiting Gpx4 and Fsp1 but inducing HO-1 expression. Data obtained from three independent experiments were processed using GraphPad Prism 8.0.1 software and ImageJ 1.52.a. One-way ANOVA was used to analyze the differences between groups. All values are presented as mean ± SD (**$p < 0.01$, and ***$p < 0.001$; $n = 3$). Bars, 500 nm in the right panel and 200 nm in the left panel of E, 25 μm in F. ns, no statistical difference.

test the effect of NAC on BCG-induced macrophage ferroptosis, RAW264.7 cells were preincubated in medium containing 2.0 mM of NAC for 1 h prior to being infected with BCG. As expected, the treatment of NAC significantly increased anti-lipid peroxidation factor Gpx4 in BCG-infected cells in a dose-dependent manner (Supplementary Figure S5A). The NAC treatment alone significantly increased the cell viability (Figure 5A) and reduced intracellular Fe^{2+} concentration (Figure 5B), intracellular ROS production (Figure 5C, Supplementary Figure S5C), and lipid peroxidation (Figures 5D, E and Supplementary Figure S5C) of RAW264.7 cells in response to the BCG infection. Molecular analysis further demonstrated that the pretreatment of NAC increased the expression of Gpx4 and Fsp1, but decreased Hmox1 proteins in BCG-infected cells (Figure 5F). These data support the notion that intracellular ROS plays a key role in ferroptosis of macrophages in response to Mtb infection (Kuang et al., 2020), and a modulation of *Hmox1* gene may alter ROS production and ferroptosis.

3.5 Knockdown *Hmox1* increases macrophage ferroptosis in response to BCG infections

HO-1 is a key enzyme against oxidative stress by inhibiting ROS production and reducing ROS cytotoxicity (Seiwert et al., 2020); therefore, an inhibition of Hmox1 may impact the ROS

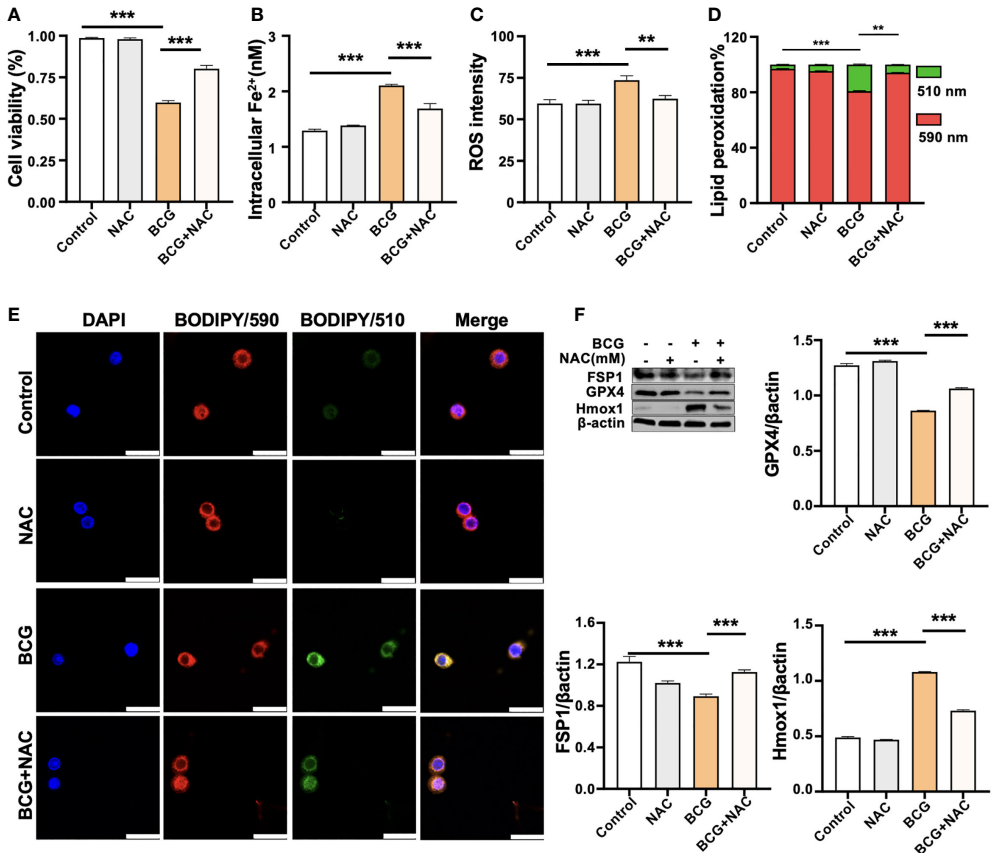

FIGURE 5
ROS scavenger NAC reduces BCG-induced macrophage ferroptosis. RAW264.7 macrophages were preincubated in medium containing 2.0 mM NAC for 1 h prior to being infected with BCG at an MOI of 5 for 24 h, before they were harvested for analysis. **(A–D)** The viability **(A)**, intracellular Fe^{2+} **(B)**, intracellular ROS **(C)**, and lipid peroxidation **(D)** of RAW264.7 macrophages treated with the indicated conditions, as determined by Trypan Blue assay, iron ion probes, flow cytometry, and BODIPY 581/591 C11 assays, respectively. **(E)** Representative fluorescence images of BODIPY 581/591 C11-labeled lipoxidation of polyunsaturated fatty acids in RAW264.7 macrophages of the indicated conditions showed the reduction of BCG-induced lipoxidation in cells pretreated with NAC. Cell nuclei were counterstained with DAPI. **(F)** Representative blots and semi-quantitative analysis of Gpx4, Fsp1, and HO-1 proteins of RAW264.7 cells treated with the indicated conditions. The NAC pretreatment increased Gpx4 and Fsp1 expression, but decreased Hmox1 protein in BCG-infected cells. Data obtained from three independent experiments were processed using GraphPad Prism 8.0.1 software and ImageJ 1.52.a. All values are presented as mean ± SD (**$p < 0.01$, and ***$p < 0.001$; $n = 3$).

production and ferroptosis in macrophages in response to Mtb infections. To test this hypothesis, the expression of *Hmox1* gene in RAW264.7 cells was knockdown by transfection of siRNA to *Hmox1* (Figure 6A). The three siRNA candidates to *Hmxo1* exhibited an ability to knock down the gene expression at the protein level. *siHmxo1*-193 and *siHmxo1*-172 showed more efficiency in the inhibition of HO-1 expression compared to *siHmxo1*-27, but the inhibition mediated by *siHmxo1*-193 and *siHmxo1*-172 showed no difference (Figure 6A). The mixture (*siHmxo1*) of equal molar ratio of *siHmxo1*-193 and *siHmxo1*-172 was therefore employed for further experiments in this report. In addition to the reduced expression of HO-1 protein, the siRNA-mediated knockdown of *Hmox1* amplified the inhibition of the expression of Gpx4 and Fsp1, and the induction of Ncoa4 expression in cells infected with BCG (Figures 6B–F). Functionally, the siRNA-mediated reduction of Hmox1 significantly amplified the BCG-inhibited cell viability (Figure 6G), and BCG-induced intracellular Fe^{2+}concentration (Figure 6H), intracellular ROS production (Figure 6I, Supplementary Figure S6A), and lipid peroxidation (Figures 6J, K and Supplementary Figure S6B) in RAW264.7 cells. The knockdown of *Hmox1* alone also exhibited the ability to inhibit cell viability (Figure 6G), and increase intracellular Fe^{2+} concentration (Figure 6H) and ROS production (Figure 6I and Supplementary Figure S6A) and lipid peroxidation (Figures 6J, K and Supplementary Figure S6B) to some extent in cells uninfected with BCG. In addition, morphological observation revealed worsening mitochondrial membrane ridge breaks in siRNA-transfected RAW264.7, compared to untransfected macrophages infected with BCG (Figure 6L). More importantly, the pretreatment of NAC significantly inhibited the release of BCG into the culture medium from lytic death of cells caused by necroptosis/ferroptosis during the infection (Figure 7A), while *Hmox1* knockdown induced the BCG release (Figure 7B), compared to BCG-infected untreated cells as determined by the CFU assay (Figures 7A, B). These results clearly suggest the importance of HO-1-modulated ROS in ferroptosis of macrophages against *Mtb* infections.

4 Discussion

Macrophages are the host cells and the frontline defense against Mtb infection, and the form of death of infected macrophages plays a pivotal role in the outcome of Mtb infections. Therefore, a better understanding of the mechanisms of macrophage death induced by Mtb infection will allow us to identify novel targets for HDT in TB treatments. Ferroptosis is a PCD induced by overwhelming lipid peroxidation reactions, and one of mechanisms of Mtb spread following the infection. In the present study, we found that heme oxygenase-1 (*HMOX1*) and pro-ferroptosis cytokines were upregulated, but glutathione peroxidase 4 (*GPX4*) and other key anti-lipid peroxidation factors were downregulated in TB patients and lungs of mice infected with BCG. A mechanistic study further demonstrated that HO-1 regulated the lipid peroxidation-mediated production of ROS and ferroptosis in macrophages in response to BCG infection. These findings suggest that HO-1 is an essential regulator of Mtb-induced ferroptosis, which regulates ROS production and alters macrophage death in response to Mtb infections, suggesting that HO-1 is a potential target for developing HDT in TB treatments.

Metabolic interactions between host cells (macrophages) and pathogen (Mtb) significantly affect the host immune responses and the proliferation of pathogen, and the outcome of Mtb infection (Cambier et al., 2014; Olive and Sassetti, 2016). Iron is one of the most important substances essential to the growth of both pathogen and host cells, which is required for the maintenance of macrophage functions, and the survival of intracellular Mtb (Baatjies et al., 2021). Therefore, the competition in the use of iron (Fe^{2+}) source between the macrophages and Mtb may affect the intracellular level of Fe^{2+}, and may be critical for the determination of the form of host cell death (necroptosis or apoptosis) and the fate of intracellular pathogens (eliminated or escaped) (Jones and Niederweis, 2011; Mitra et al., 2019; Zhang et al., 2020; Rodriguez et al., 2022).

Ferroptosis is mainly triggered by extra-mitochondrial lipid peroxidation (Dixon et al., 2012), which is characterized by lipid peroxidation as a consequence of iron-dependent accretion of ROS (Dixon and Stockwell, 2014; Amaral et al., 2019). This new form of cell death was also corroborated in macrophages in response to Mtb infection, and it was the main cause of lung tissue necrosis caused by Mtb (Amaral et al., 2019). This finding has gained a great interest in the field of TB research. In the present study, differential expression of genes related to ferroptosis was identified in peripheral blood of TB patients by transcriptome analysis. In particular, the ferroptosis signature gene *GPX4* was downregulated, accompanied by the upregulation of *HMOX1* gene, HO-1, and Hemin content in TB. These observations were further confirmed in RAW264.7 cells infected with BCG. The *in vitro* study demonstrated that HO-1-regulated ROS played a key role in macrophage ferroptosis induced by BCG infection. Mechanistically, scavenging ROS with NAC inhibited BCG-induced macrophage ferroptosis and the release of BCG into the culture medium caused by necroptosis/ferroptosis during the infection, while siRNA-mediated knockdown of *Hmox1* gene expression resulted in opposite effects to NAC treatments. Our results suggest that HO-1 plays a key role in Mtb-induced ferroptosis, through a mechanism by which it regulates ROS production and alters macrophage death in response to Mtb infections.

Heme is a major source of iron for Mtb growth and survival, implying that Mtb has evolved a complex heme enzymatic

10.3389/fcimb.2022.1004148

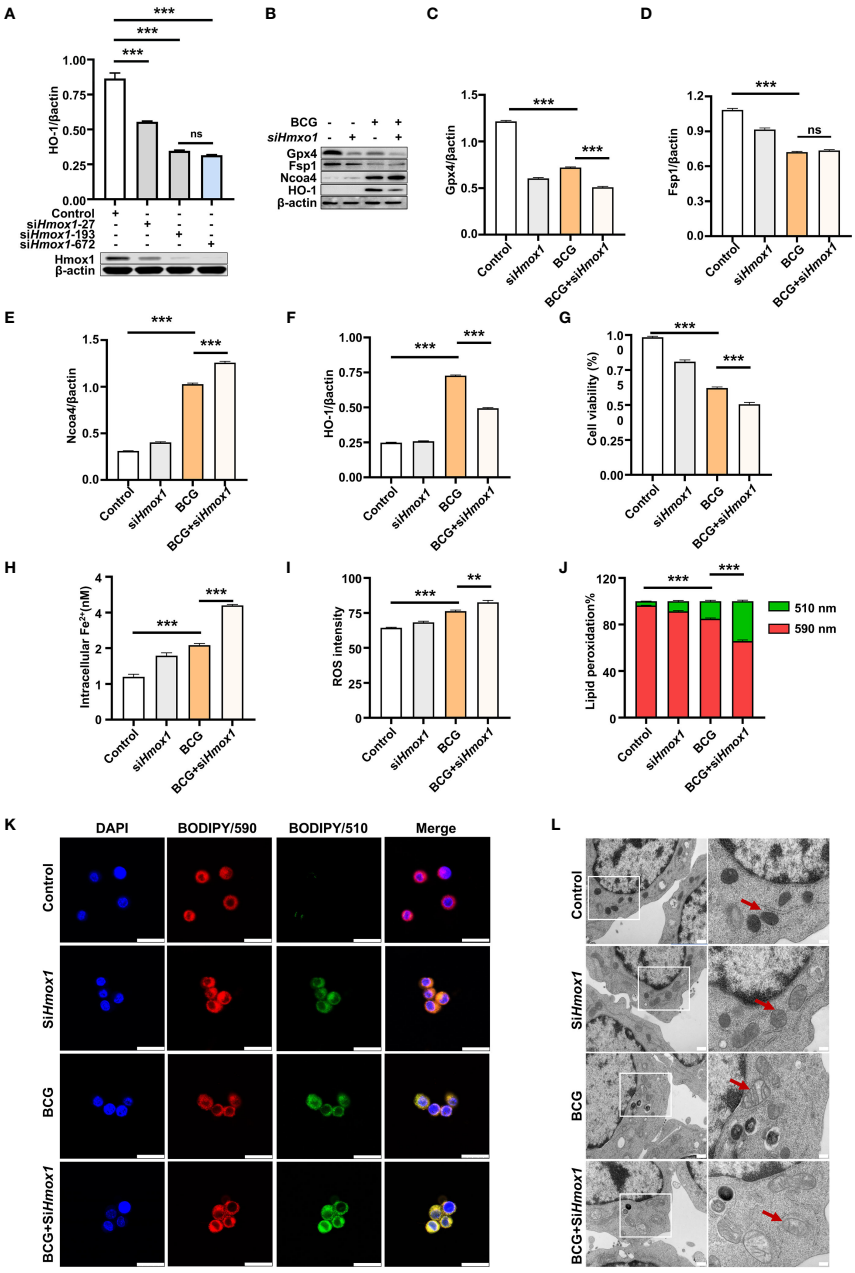

FIGURE 6
Knockdown of *Hmox1* increases BCG-induced macrophage ferroptosis. **(A)** Representative blots of Hmox1 protein in RAW264.7 cells transfected with siRNA to murine *Hmox1* gene. siRNA was transfected by Lipofectamine™ RNAiMAX, and the protein was analyzed at 24 h post-transfection. The si-*Hmox1* showed the most efficient knockdown of *Hmox1* and was used in subsequent experiments. **(B–E)** Representative blots **(B)** and semi-quantitative analysis of Gpx4 **(C)**, Fsp1 **(D)**, Ncoa4 **(E)**, and HO-1 **(F)** proteins of RAW264.7 cells treated with indicated conditions. The siRNA-mediated knockdown of *Hmox1* amplified the inhibition of Gpx4 and Fsp1 expression in cells infected with BCG. **(G–J)** The viability **(B)**, intracellular Fe^{2+} **(C)**, intracellular ROS **(D)**, and lipid peroxidation **(E)** of RAW264.7 macrophages treated with indicated conditions, as determined by Trypan Blue assay, iron ion probes, flow cytometry, and BODIPY 581/591 C11 assays, respectively. **(K)** Representative fluorescence images of BODIPY 581/591 C11-labeled lipoxidation of polyunsaturated fatty acids in RAW264.7 macrophages of the indicated conditions showed the increase of BCG-induced lipoxidation in cells transfected with siRNA to *Hmox1*. Cell nuclei were counterstained with DAPI. **(L)** Representative images of transmission electron microscopy showed mitochondrial membrane ridge breaks (arrows) in siRNA-transfected RAW264.7 and/or BCG-infected macrophages; the right panel shows the enlarged image of the boxed area in its corresponding image in the left panel. Data obtained from three independent experiments were processed using GraphPad Prism 8.0.1 software and ImageJ 1.52.a. One-way ANOVA was used to analyze the differences between groups. All values are presented as mean ± SD (**p < 0.01; ***p < 0.001; *n* = 3). Bars, 500 nm in the right panel and 200 nm in the left panel of K, and 25 μm in L. ns, no statistical difference.

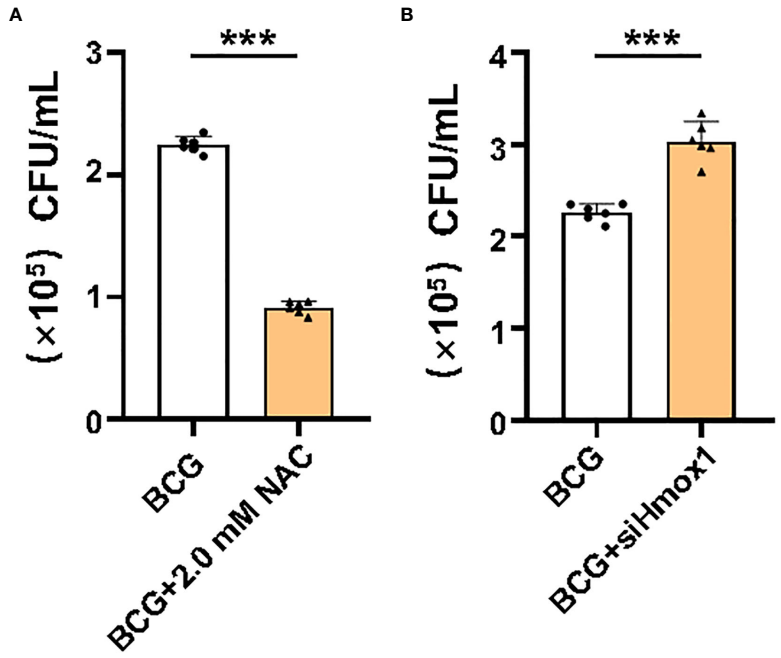

FIGURE 7
Effect of ROS and Hmox1 on intracellular bacterial loads in RAW264.7 macrophages. Intracellular ROS was scavenged by NAC treatment, and the expression of Hmox1 was inhibited by the transfection of siRNA to *Hmox1*. NAC-pretreated or si-*Hmox1*-transfected RAW264.7 macrophages were incubated with BCG at an MOI of 5 for 1 h, and cells were rinsed to remove uninfected bacteria prior to being cultured with fresh medium for an additional 24 h. The bacteria released in the culture medium was counted by CFU assay. **(A)** The count of colonies in medium of cells pretreated with NAC. **(B)** The count of colonies in medium of cells transfected with si-*Hmox1*. The NAC pretreatment significantly reduced bacteria released from cell necrosis/ferroptosis death, while si-*Hmox1*-mediated knockdown of *Hmox1* gene strikingly increased CFU count in RAW264.7 cells infected with BCG. Data obtained from three independent experiments were processed using GraphPad Prism 8.0.1 software. Unpaired *t*-test was used to analyze the differential changes of the two groups. ***$p < 0.001$; n = 3.

mechanism (Jones and Niederweis, 2011; McLean and Munro, 2017; Mitra et al., 2019; Zhang et al., 2020). During the Mtb infection, increased ROS production, oxidative mitochondrial damage, and the inducible isoform of HO-1 were observed in macrophages (Amaral et al., 2016; Amaral et al., 2019). All these lines of evidence suggest that ferroptosis may be a primary form of Mtb-induced macrophage death (Amaral et al., 2016; Amaral et al., 2019). Functionally, HO-1 catalyzes the degradation of oxidant heme into biliverdin, iron, and carbon monoxide (CO) (Szade et al., 2021). HO-1 was significantly upregulated in TB patients and in experimental animals infected with Mtb, and was a potential target for HDT for TB (Chinta et al., 2021; Uwimaana et al., 2021). In the present report, the increase of both HO-1 protein and Hemin content, a main source of iron for Mtb and host cells, was also observed in peripheral blood of TB patients, at both transcriptional and/or translational levels, which was strongly correlated with several cytokines. In particular, it was negatively associated with the level of ferroptosis inhibitors (regulators) GPX4 and FSP1 in peripheral blood of TB patients and RAW264.7 cells infected with BCG.

Of great interest, the BCG-inhibited Gpx4 was only observed in RAW264.7 cells infected with BCG at a low dose (MOI = 5). A high dose of BCG infection (MOI of 10 and 15) induced Gpx4 expression in this type of cells (Figures 2D, E). Flow cytometry assay further revealed that the low dose (MOI = 5) of BCG infection induced necrotic cell death, while the high doses (MOI = 10 and 15) of BCG promoted apoptotic cell death in RAW264.7 cells (Figure 2J). These data suggest that a low dose of Mtb infection favors macrophage ferroptosis, but an increased load of bacteria in a certain range may induce cell apoptosis. We currently do not fully understand the underlying mechanism why the dynamic changes of Gpx4 in RAW264.7 cells infected with different doses of BCG, i.e. an inhibition of Gpx4 expression at an MOI of 5, while an induction at an MOI of 10 and 15.

Biochemistry studies demonstrate that ferroptosis is mainly induced through lipid ROS generated by the iron-catalyzed Fenton reaction. Fenton reaction requires ROS and ferrous iron for initiation and space of the integrity of cells (Tang et al., 2021) (Stockwell, 2022). Indeed, scavenging ROS with NAC significantly increased Gpx4, and reduced ferroptosis and intracellular bacteria release in RAW264.7 cells in response to BCG infection. In addition, cell ferroptosis does not produce apoptotic vesicles as cell apoptosis does, and does not cause severe cell morphological changes as necrosis either; therefore, it maintains the cell integrity

and favors Fenton reaction and leads the infected RAW264.7 cells to undergo ferroptosis at an MOI of 5 in this study. In contrast, the increase of bacteria load with an MOI of 10 or 15 in RAW264.7 cells induced cell apoptosis to remove the number of intracellular bacteria (Figure 2J), which might in turn inhibit cell ferroptosis by two possible mechanisms. First, the process of formation of apoptotic vesicle has the potential to reduce intracellular ROS and block Fenton reaction. Second, divalent iron is highly oxidizing and easily converted into trivalent iron due to loss of electrons (Sukhbaatar and Weichhart, 2018; Nairz and Weiss, 2020). Trivalent iron is stored in ferritin of cells, while only cells in a viable state have an intact iron metabolism able to degrade ferritin, subsequentially release trivalent iron from ferritin, and ultimately reduce the trivalent iron to divalent iron (Li et al., 2020; Mesquita et al., 2020). However, whether the increase of apoptosis is correlated with a reduced ferroptosis needs further study.

ROS generated from lipid peroxidation is crucial in cell ferroptosis (Conrad et al., 2018), and HO-1 is an essential cytoprotective enzyme that inhibits inflammation and oxidative stress (Araujo et al., 2012; Rockwood et al., 2017; Seiwert et al., 2020; Chinta et al., 2021; de Oliveira et al., 2022), and a target for HDT of TB (McLean and Munro, 2017; Chinta et al., 2021). The expression of HO-1 is largely dependent on oxidative stress in Mtb-infected cells, where an elevated expression of HO-1 is a strategy of host cells in response to oxidative stress triggered by intracellular bacteria (Rockwood et al., 2017). HO-1 exhibits an ability to inhibit ROS formation, DNA damage, and cytotoxicity induced by heme iron in human colonocytes (Seiwert et al., 2020). Importantly, the interplay between HO-1 and iron metabolism has been demonstrated to play a critical role in modulating immune responses of macrophages, as iron is a key product of HO-1 activity for cellular biological processes in both eukaryotic cells and bacteria (Li and Stocker, 2009). Therefore, HO-1 regulates intracellular iron levels to modulate the cellular oxidation and immune responses of macrophages (de Oliveira et al., 2022). Despite the fact that HO-1 is known to play a protective role in host cells during an infectious process, the upregulated HO-1 in Mtb-infected cells increases intracellular iron level and ROS production, and subsequentially leads to lipid peroxidation and ferroptosis (Yang et al., 2022). In this report, the siRNA-mediated reduction of *Hmox1* expression increased ROS production, lipid peroxidation, and intracellular iron, and further induced ferroptosis in RAW264.7 cells infected with BCG at an MOI of 5. In addition, the siRNA silence of *Hmox1* gene also increased expression of iron autophagy protein Ncoa4, a critical cytokine in the maintenance of iron homeostasis (Bellelli et al., 2016). Together, the findings of others and this study, and the discrepancy of results from different studies imply the complicated and dynamic biological process of ferroptosis in cells in response to Mtb infections. The process of ferroptosis is tightly regulated, and may depend on the species, dose and virulence of pathogen, and host cell-type context, which requires further investigation.

Collectively, in the present report, we revealed the upregulation of *HMOX1* but a downregulation of *GPX4* in TB patients, and lungs of mice infected with BCG. An *in vitro* mechanistic study using murine macrophage-like RAW264.7 cells further demonstrated that Hmox1 regulated intracellular levels of ROS and Fe^{2+}, and subsequentially modulated cell ferroptosis induced by BCG infection. The siRNA-mediated knockdown of *Hmox1* gene increased intracellular ROS, Fe^{2+}, and Ncoa4, and promoted cell ferroptosis and the release of intracellular BCG, while scavenging ROS demonstrated opposite effects to that of siRNA-mediated knockdown of *Hmox1* gene. Our results suggest that HO-1 is an essential regulator of Mtb-induced ferroptosis, which regulates ferroptosis by modulating intracellular ROS production and Fe^{2+} to alter macrophage death against Mtb infections.

Data availability statement

The datasets presented in this study can be found in online repositories. The names of the repository/repositories and accession number(s) can be found in the article/supplementary material.

Ethics statement

This study was reviewed and approved by The Ethic Committee of Human Research at General Hospital of Ningxia Medical University. The patients/participants provided their written informed consent to participate in this study. The animal study was reviewed and approved by The Laboratory Animal Welfare Ethics Review Committee of Ningxia University.

Author contributions

CM: conception, acquisition, analysis, interpretation, writing, revision, and editing. XW: acquisition and analysis. XZ: acquisition and analysis. XL: conception, acquisition, analysis, interpretation, writing, revision, editing, and overall supervision. GD: conception, analysis, interpretation, writing, revision, editing, and overall supervision. All authors contributed to the article and approved the submitted version.

Funding

This work was supported by a grant from the National Natural Science Foundation of China (No. 32160162).

Acknowledgments

The authors thank Mr. Fuyang Song, Dr. Jing Zeng, Dr. Zhanbing Ma, and Dr. Xue Lin for their technical and bioinformatic assistances. We also thank Miss Jia Ma, Mr. Jialin Yu, and Miss Zhaoqian Gong for valuable discussions.

Conflict of interest

The authors declare that the research was conducted in the absence of any commercial or financial relationships that could be construed as a potential conflict of interest.

Publisher's note

Supplementary material

The Supplementary Material for this article can be found online at: https://www.frontiersin.org/articles/10.3389/fcimb.2022.1004148/full#supplementary-material

References

Alam, M. Z., Devalaraja, S., and Haldar, M. (2017). The heme connection: Linking erythrocytes and macrophage biology. *Front. Immunol.* 8, 33. doi: 10.3389/fimmu.2017.00033

Amaral, E. P., Conceição, E. L., Costa, D. L., Rocha, M. S., Marinho, J. M., Cordeiro-Santos, M., et al. (2016). N-acetyl-cysteine exhibits potent anti-mycobacterial activity in addition to its known anti-oxidative functions. *BMC Microbiol.* 16, 251. doi: 10.1186/s12866-016-0872-7

Amaral, E. P., Costa, D. L., Namasivayam, S., Riteau, N., Kamenyeva, O., Mittereder, L., et al. (2019). A major role for ferroptosis in mycobacterium tuberculosis-induced cell death and tissue necrosis. *J. Exp. Med.* 216, 556–570. doi: 10.1084/jem.20181776

Amaral, E. P., Vinhaes, C. L., Oliveira-De-Souza, D., Nogueira, B., Akrami, K. M., and Andrade, B. B. (2021). The interplay between systemic inflammation, oxidative stress, and tissue remodeling in tuberculosis. *Antioxid Redox Signal* 34, 471–485. doi: 10.1089/ars.2020.8124

Araujo, J. A., Zhang, M., and Yin, F. (2012). Heme oxygenase-1, oxidation, inflammation, and atherosclerosis. *Front. Pharmacol.* 3, 119. doi: 10.3389/fphar.2012.00119

Baatjies, L., Loxton, A. G., and Williams, M. J. (2021). Host and bacterial iron homeostasis, an underexplored area in tuberculosis biomarker research. *Front. Immunol.* 12, 742059. doi: 10.3389/fimmu.2021.742059

Bellelli, R., Federico, G., Matte, A., Colecchia, D., Iolascon, A., Chiariello, M., et al. (2016). NCOA4 deficiency impairs systemic iron homeostasis. *Cell Rep.* 14, 411–421. doi: 10.1016/j.celrep.2015.12.065

Cambier, C. J., Falkow, S., and Ramakrishnan, L. (2014). Host evasion and exploitation schemes of mycobacterium tuberculosis. *Cell* 159, 1497–1509. doi: 10.1016/j.cell.2014.11.024

Chinta, K. C., Pacl, H. T., Agarwal, A., and Steyn, A. J. C. (2021). Heme oxygenase-1 as a pharmacological target for host-directed therapy to limit tuberculosis associated immunopathology. *Antioxidants (Basel)* 10, 1–17. doi: 10.3390/antiox10020177

Conrad, M., Kagan, V. E., Bayir, H., Pagnussat, G. C., Head, B., Traber, M. G., et al. (2018). Regulation of lipid peroxidation and ferroptosis in diverse species. *Genes Dev.* 32, 602–619. doi: 10.1101/gad.314674.118

Crowe, A. R., and Yue, W. (2019). Semi-quantitative determination of protein expression using immunohistochemistry staining and analysis: An integrated protocol. *Bio Protoc.* 9 (24), e3465–e3465. doi: 10.21769/BioProtoc.3465

De Oliveira, J., Denadai, M. B., and Costa, D. L. (2022). Crosstalk between heme oxygenase-1 and iron metabolism in macrophages: Implications for the modulation of inflammation and immunity. *Antioxidants (Basel)* 11 (5), 1–19. doi: 10.3390/antiox11050861

Dixon, S. J., Lemberg, K. M., Lamprecht, M. R., Skouta, R., Zaitsev, E. M., Gleason, C. E., et al. (2012). Ferroptosis: An iron-dependent form of nonapoptotic cell death. *Cell* 149, 1060–1072. doi: 10.1016/j.cell.2012.03.042

Dixon, S. J., and Stockwell, B. R. (2014). The role of iron and reactive oxygen species in cell death. *Nat. Chem. Biol.* 10, 9–17. doi: 10.1038/nchembio.1416

Jones, C. M., and Niederweis, M. (2011). Mycobacterium tuberculosis can utilize heme as an iron source. *J. Bacteriol* 193, 1767–1770. doi: 10.1128/JB.01312-10

Kim, D. H., Ahn, H. S., Go, H. J., Kim, D. Y., Kim, J. H., Lee, J. B., et al. (2021). Hemin as a novel candidate for treating COVID-19 *via* heme oxygenase-1 induction. *Sci. Rep.* 11, 21462. doi: 10.1038/s41598-021-01054-3

Korb, V. C., Chuturgoon, A. A., and Moodley, D. (2016). Mycobacterium tuberculosis: Manipulator of protective immunity. *Int. J. Mol. Sci.* 17, 131. doi: 10.3390/ijms17030131

Kuang, F., Liu, J., Tang, D., and Kang, R. (2020). Oxidative damage and antioxidant defense in ferroptosis. *Front. Cell Dev. Biol.* 8, 586578. doi: 10.3389/fcell.2020.586578

Lee, J., Hartman, M., and Kornfeld, H. (2009). Macrophage apoptosis in tuberculosis. *Yonsei Med. J.* 50, 1–11. doi: 10.3349/ymj.2009.50.1.1

Li, J., Cao, F., Yin, H. L., Huang, Z. J., Lin, Z. T., Mao, N., et al. (2020). Ferroptosis: Past, present and future. *Cell Death Dis.* 11, 88. doi: 10.1038/s41419-020-2298-2

Li, C., and Stocker, R. (2009). Heme oxygenase and iron: From bacteria to humans. *Redox Rep.* 14, 95–101. doi: 10.1179/135100009X392584

Liu, C. H., Liu, H., and Ge, B. (2017). Innate immunity in tuberculosis: Host defense vs pathogen evasion. *Cell Mol. Immunol.* 14, 963–975. doi: 10.1038/cmi.2017.88

Mclean, K. J., and Munro, A. W. (2017). Drug targeting of heme proteins in mycobacterium tuberculosis. *Drug Discovery Today* 22, 566–575. doi: 10.1016/j.drudis.2016.11.004

Mesquita, G., Silva, T., Gomes, A. C., Oliveira, P. F., Alves, M. G., Fernandes, R., et al. (20203061). H-ferritin is essential for macrophages' capacity to store or detoxify exogenously added iron. *Sci. Rep.* 10 (1), 1–15. doi: 10.1038/s41598-020-59898-0

Mitra, A., Ko, Y. H., Cingolani, G., and Niederweis, M. (20194260). Heme and hemoglobin utilization by mycobacterium tuberculosis. *Nat. Commun.* 10. doi: 10.1038/s41467-019-12109-5

Nairz, M., and Weiss, G. (2020). Iron in infection and immunity. *Mol. Aspects Med.* 75, 100864. doi: 10.1016/j.mam.2020.100864

Olive, A. J., and Sassetti, C. M. (2016). Metabolic crosstalk between host and pathogen: Sensing, adapting and competing. *Nat. Rev. Microbiol.* 14, 221–234. doi: 10.1038/nrmicro.2016.12

Pajuelo, D., Gonzalez-Juarbe, N., Tak, U., Sun, J., Orihuela, C. J., and Niederweis, M. (2018). NAD(+) depletion triggers macrophage necroptosis, a cell death pathway exploited by mycobacterium tuberculosis. *Cell Rep.* 24, 429–440. doi: 10.1016/j.celrep.2018.06.042

Pillai-Kastoori, L., Schutz-Geschwender, A. R., and Harford, J. A. (2020). A systematic approach to quantitative Western blot analysis. *Anal. Biochem.* 593, 113608. doi: 10.1016/j.ab.2020.113608

Rockwood, N., Costa, D. L., Amaral, E. P., Du Bruyn, E., Kubler, A., Gil-Santana, L., et al. (2017). Mycobacterium tuberculosis induction of heme oxygenase-1

expression is dependent on oxidative stress and reflects treatment outcomes. *Front. Immunol.* 8, 542. doi: 10.3389/fimmu.2017.00542

Rodriguez, G. M., Sharma, N., Biswas, A., and Sharma, N. (2022). The iron response of mycobacterium tuberculosis and its implications for tuberculosis pathogenesis and novel therapeutics. *Front. Cell Infect. Microbiol.* 12, 876667. doi: 10.3389/fcimb.2022.876667

Seiwert, N., Wecklein, S., Demuth, P., Hasselwander, S., Kemper, T. A., Schwerdtle, T., et al. (2020). Heme oxygenase 1 protects human colonocytes against ROS formation, oxidative DNA damage and cytotoxicity induced by heme iron, but not inorganic iron. *Cell Death Dis.* 11, 787. doi: 10.1038/s41419-020-02950-8

Shastri, M. D., Shukla, S. D., Chong, W. C., Dua, K., Peterson, G. M., Patel, R. P., et al. (2018). Role of oxidative stress in the pathology and management of human tuberculosis. *Oxid. Med. Cell Longev* 2018, 7695364. doi: 10.1155/2018/7695364

Sheedy, F. J., and Divangahi, M. (2021). Targeting immunometabolism in host defence against mycobacterium tuberculosis. *Immunology* 162, 145–159. doi: 10.1111/imm.13276

Stockwell, B. R. (2022). Ferroptosis turns 10: Emerging mechanisms, physiological functions, and therapeutic applications. *Cell* 185, 2401–2421. doi: 10.1016/j.cell.2022.06.003

Sukhbaatar, N., and Weichhart, T. (2018). Iron regulation: Macrophages in control. *Pharm. (Basel)* 11 (4), 137, 1-20. doi: 10.3390/ph11040137

Szade, A., Szade, K., Mahdi, M., and Jozkowicz, A. (2021). The role of heme oxygenase-1 in hematopoietic system and its microenvironment. *Cell Mol. Life Sci.* 78, 4639–4651. doi: 10.1007/s00018-021-03803-z

Tang, D., Chen, X., Kang, R., and Kroemer, G. (2021). Ferroptosis: Molecular mechanisms and health implications. *Cell Res.* 31, 107–125. doi: 10.1038/s41422-020-00441-1

Uwimaana, E., Bagaya, B. S., Castelnuovo, B., Kateete, D. P., Godwin, A., Kiwanuka, N., et al. (2021). Heme oxygenase-1 and neopterin plasma/serum levels and their role in diagnosing active and latent TB among HIV/TB co-infected patients: A cross sectional study. *BMC Infect. Dis.* 21, 711. doi: 10.1186/s12879-021-06370-7

Visca, D., Ong, C. W. M., Tiberi, S., Centis, R., D'ambrosio, L., Chen, B., et al. (2021). Tuberculosis and COVID-19 interaction: A review of biological, clinical and public health effects. *Pulmonology* 27, 151–165. doi: 10.1016/j.pulmoe.2020.12.012

Who (2022). *Global tuberculosis report 2021* (Geneva: World Health Organization).

Xu, G., Wang, J., Gao, G. F., and Liu, C. H. (2014). Insights into battles between mycobacterium tuberculosis and macrophages. *Protein Cell* 5, 728–736. doi: 10.1007/s13238-014-0077-5

Yang, S., Ouyang, J., Lu, Y., Harypursat, V., and Chen, Y. (2022). A dual role of heme oxygenase-1 in tuberculosis. *Front. Immunol.* 13, 842858. doi: 10.3389/fimmu.2022.842858

Yong, Y. K., Tan, H. Y., Saeidi, A., Wong, W. F., Vignesh, R., Velu, V., et al. (20192789). Immune biomarkers for diagnosis and treatment monitoring of tuberculosis: Current developments and future prospects. *Front. Microbiol.* 10. doi: 10.3389/fmicb.2019.02789

Zhai, W., Wu, F., Zhang, Y., Fu, Y., and Liu, Z. (2019). The immune escape mechanisms of mycobacterium tuberculosis. *Int. J. Mol. Sci.* 20 (2), 340, 1-18. doi: 10.3390/ijms20020340

Zhang, L., Hendrickson, R. C., Meikle, V., Lefkowitz, E. J., Ioerger, T. R., and Niederweis, M. (2020). Comprehensive analysis of iron utilization by mycobacterium tuberculosis. *PloS Pathog.* 16, e1008337. doi: 10.1371/journal.ppat.1008337

frontiers | Frontiers in Cellular and Infection Microbiology

TYPE Original Research
PUBLISHED 19 January 2023
DOI 10.3389/fcimb.2023.1080100

OPEN ACCESS

EDITED BY
Adrie JC Steyn,
University of Alabama at Birmingham, United States

REVIEWED BY
Rogelio Hernandez Pando,
Instituto Nacional de Ciencias Médicas y Nutrición Salvador Zubirán (INCMNSZ), Mexico
Natalia M Araujo,
Oswaldo Cruz Foundation (FIOCRUZ), Brazil

*CORRESPONDENCE
Virginia Pasquinelli
virpasquinelli@gmail.com
vpasquinelli@unnoba.edu.ar

†These authors have contributed equally to this work and share first authorship

SPECIALTY SECTION
This article was submitted to Bacteria and Host, a section of the journal Frontiers in Cellular and Infection Microbiology

RECEIVED 25 October 2022
ACCEPTED 05 January 2023
PUBLISHED 19 January 2023

CITATION
Álvarez GI, Hernández Del Pino RE, Barbero AM, Estermann MA, Celano J, Musella RM, Palmero DJ, García VE and Pasquinelli V (2023) Association of IFN-γ +874 A/T SNP and hypermethylation of the -53 CpG site with tuberculosis susceptibility.
Front. Cell. Infect. Microbiol. 13:1080100.
doi: 10.3389/fcimb.2023.1080100

Association of IFN-γ +874 A/T SNP and hypermethylation of the -53 CpG site with tuberculosis susceptibility

Guadalupe Inés Álvarez[1,2,3†], Rodrigo Emanuel Hernández Del Pino[1,2†], Angela María Barbero[1,2], Martín Andrés Estermann[1], Josefina Celano[1], Rosa María Musella[4], Domingo Juan Palmero[4], Verónica Edith García[5,6] and Virginia Pasquinelli[1,2*]

[1]Centro de Investigaciones Básicas y Aplicadas (CIBA), Universidad Nacional del Noroeste de la Provincia de Buenos Aires (UNNOBA), Buenos Aires, Argentina, [2]Centro de Investigaciones y Transferencias del Noroeste de la Provincia de Buenos Aires (CIT NOBA), UNNOBA- Universidad Nacional de San Antonio de Areco (UNSAdA) - Consejo Nacional de Investigaciones Científicas y Técnicas (CONICET), Buenos Aires, Argentina, [3]Instituto de Inmunología, Genética y Metabolismo (INIGEM), Universidad de Buenos Aires (UBA) – CONICET, Buenos Aires, Argentina, [4]División Tisioneumonología Hospital F.J. Muñiz, Buenos Aires, Argentina, [5]CONICET-Universidad de Buenos Aires, Instituto de Química Biológica de la Facultad de Ciencias Exactas y Naturales (IQUIBICEN), Buenos Aires, Argentina, [6]Universidad de Buenos Aires, Facultad de Ciencias Exactas y Naturales, Departamento de Química Biológica, Buenos Aires, Argentina

Introduction: Tuberculosis (TB) is now the 2nd leading infectious killer after COVID-19 and the 13th leading cause of death worldwide. Moreover, TB is a lethal combination for HIV-patients. Th1 responses and particularly IFN-γ are crucial for immune protection against Mycobacterium tuberculosis infection. Many gene variants for IFNG that confer susceptibility to TB have been described in multiple ethnic populations. Likewise, some epigenetic modifications have been evaluated, being CpG methylation the major epigenetic mark that makes chromatin inaccessible to transcription factors, thus avoiding the initiation of IFNG transcription.

Methods: We evaluated both genetic and epigenetic changes involved in IFN-γ production and TB susceptibility in Argentine population. Amplification refractory mutation system-polymerase chain reaction (ARMS-PCR) was performed for the IFN-γ +874 A/T polymorphism (rs2430561) genotyping in 199 healthy donors (HD) and 173 tuberculosis (TB) patients. IFN-γ levels from M. tuberculosis-stimulated PBMCs were measured by ELISA. The methylation status at the -53 CpG site of the IFNG promoter in individuals with latent infection (LTBI), TB and HD was determine by pyrosequencing.

Results: Using a case-control study, we found that A allele and, consequently, AA genotype were overrepresented in patients with active disease. Moreover, HD carrying T allele (AT or TT genotype) evidenced an augmented IFN-γ secretion compared to TB patients. Codominance was the genetic model that best fits our results according to the Akaike information criterion (AIC). In addition, increased methylation levels at the -53 CpG site in the IFN-γ promoter were observed in whole blood of patients with active TB compared to LTBI individuals.

Discussion: IFN-γ is regulated by genetic variants and epigenetic modifications during TB. Besides, AA genotype of the rs2430561 single nucleotide polymorphism could be considered as a potential TB susceptibility genetic biomarker in Argentina and the methylation of the -53 CpG site could result in a useful predictor of TB reactivation.

KEYWORDS

tuberculosis, IFNg, SNPs, methylation, susceptibility

Introduction

Tuberculosis (TB), a chronic infectious disease caused by the pathogen *Mycobacterium tuberculosis*, remains a major cause of morbidity and mortality worldwide. Until COVID-19 pandemic, TB was the most common cause of death from a single infectious agent, surpassing HIV/AIDS (World Health Organization (WHO), 2022). The impacts generated in 2020 by the pandemic included reduced access to diagnosis and treatment with the consequent increase in the number of deaths. The WHO estimated 1.4 million TB deaths among HIV-negative patients and an additional of 187.000 among HIV-positive people (World Health Organization (WHO), 2022). In Argentina, the last report indicated 10.896 new cases and 656 deaths in 2020 with a rate of mortality of 1.4/100.000 inhabitants (Ministerio De Salud Argentina, 2022). It is estimated that about a quarter of the world's population has latent TB infection, and is therefore at risk of developing active disease during their lifetime (World Health Organization (WHO), 2022). However, only 5-10% of individuals infected with *M. tuberculosis* will progress to active TB, suggesting that both host genetic and environmental factors might influence the susceptibility to TB (Fortin et al., 2007). Moreover, it has been shown that *M. tuberculosis* sublineages evolved in different human populations showing significant differences in virulence and immunomodulatory functions (Saelens et al., 2019), demonstrating that the genetic variability of *M. tuberculosis* is also an important factor affecting the pathogenesis of the disease. Although most environmental mycobacteria are non-pathogenic species, *M. tuberculosis* has evolved from an opportunist to a professional pathogen capable of infecting and surviving within the host.

Cell-mediated immunity plays an essential role in eliciting a protective immune response against *M. tuberculosis* infection. The secretion of Th1 cytokines by antigen-specific T cells collaborates with protective granuloma formation and stimulates the antimicrobial activity of infected macrophages (Flynn and Chan, 2001). In particular, IFN-γ is a key Th1 cytokine produced primarily by natural killer cells and T cells. IFNG KO mice infected with *M. tuberculosis* fail to produce reactive nitrogen intermediates that restrict the growth of the bacilli (Cooper et al., 1993; Flynn et al., 1993). Genetic studies in families with Mendelian Susceptibility to Mycobacterial Disease (MSMD), a primary immune deficiency that results in partial or complete defects in IFN-γ secretion, production, binding, or signaling, highlighted the critical role of this cytokine in mycobacterial infections (Rosain et al., 2019).

Family-based genetic studies and population-based case-control association analyses have been used to identify candidate genes for susceptibility to tuberculosis. Besides, cytokine gene polymorphisms underlie the complexity of inter-individual differences in the susceptibility, severity and clinical outcomes of several infectious diseases (Cooke and Hill, 2001; Patarčić et al., 2015). In particular, the +874 A/T (rs2430561) single nucleotide polymorphism (SNP) is located at the 5' end of the CA repeat region in the first intron of the IFN-γ gene (Pravica et al., 2000). Pravica et al. suggested that the functional role of the +874 A/T SNP is related to its location within a putative NF-κB binding site (Pravica et al., 2000). The T allele predisposes to the binding of the transcription factor NF-κB, whereas the A allele reduces the affinity and therefore the expression of the gene in response to stimulus (Pravica et al., 2000). Thus, AA genotype or A allele have been associated with low levels of IFN-γ production, otherwise TT genotype or T allele are associated with higher production of this cytokine, and AT genotype with intermediate levels (Pravica et al., 2000). A significant association between this SNP and TB has been described in several populations around the world, as in the Sicilian, Brazilian, Chinese, Egyptian children, Spanish, Warao indigenous, South Indian and Iranian population (Lio et al., 2002; Lopez-Maderuelo et al., 2003; Tso et al., 2005; Amim et al., 2008; Mosaad et al., 2010; Bhanothu et al., 2015; Beiranvand et al., 2016; Araujo et al., 2017). Moreover, +874 A/T IFNG polymorphism has been associated with TB and extrapulmonary TB susceptibility in meta-analysis studies (Pacheco et al., 2008; Wei et al., 2017; Mandal et al., 2019; Areeshi et al., 2021). However, this SNP has not been studied in TB patients from Argentina.

On the other hand, IFN-γ gene is subject to both genetic and epigenetic modifications. This could imply a critical link between epigenetics and transcription factors in the regulation of IFN-γ and, consequently, in T cells responses elicited against *M. tuberculosis*. Host, pathogen & environment are the triad, which influences any disease, and epigenetics can bridge the gaps between them. The association between different epigenetic modifications and disease progression in *M. tuberculosis* is becoming an area of growing interest (Fatima et al., 2021; Gauba et al., 2021). Epigenetic changes, for example, histone modifications, DNA methylation, and miRNA-mediated up/downregulation of immune genes, play an important role in immunomodulation of the host at the post-TB infective phase.

The reversibility of these epigenetic modifications makes them ideal and innovative targets that can be exploited for drug development and control strategies.

In particular, methylation in the promoter region can lead to the failure of gene transcription initiation and gene silencing by hampering transcription factor binding to specific motifs. The proximal region of the IFNG promoter contains binding sites for several transcription factors, including NFAT, NF-κB, and CREB-ATF1. Interestingly, methylation at the -53 site of the IFNG promoter results in inhibition of CREB and ATF2/c-Jun binding to the proximal AP1 site and is sufficient to inhibit expression of this cytokine in a Th1 murine cell line (Jones and Chen, 2006). Moreover, hypermethylation in human Th2 cells results in chromatin condensation and exclusion of CREB proteins from the IFNG promoter (Yano et al., 2003). CREB upregulates IFN-γ production in human T cells that respond to *M. tuberculosis* (Samten et al., 2002; Samten et al., 2005). We have previously shown that costimulation through the Signal Lymphocyte Activation Molecule (SLAM) in *M. tuberculosis*-stimulated T cells induces CREB activation, leading to IFN-γ secretion (Pasquinelli et al., 2009). Thus, our hypothesis was that the methylation of the CpG -53 site of IFNG could lead to the negative regulation of this cytokine during the immune response against *M. tuberculosis*.

The aim of this study was to further characterize the genetic and epigenetic mechanisms that regulate IFN-γ responses during *M. tuberculosis* infection. To this end, we performed a study in patients with active TB and healthy donors (HD) to determine the influence of +874 A/T polymorphism on tuberculosis susceptibility. We additionally evaluated DNA methylation at the -53 CpG site of the promoter region of IFNG as a new mechanism of epigenetic regulation of IFN-γ in the immune response against *M. tuberculosis*.

Results

Demographic characteristics of the studied population

In a case-control study we genotyped the IFNG +874 A/T SNP in 199 healthy donors (HD) and 173 tuberculosis (TB) patients enrolled between 2012 and 2016. Demographic characteristics of both populations are shown in Table 1. We did not find differences

TABLE 1 Demographic Characteristics of patients with Tuberculosis (TB) and Healthy Donors (HD).

Characteristic	Groups		*P Value*
	HD	TB	HD vs TB
Age (Mean; ± SEM)	33.62 ± 1.08	32.70 ± 1.18	0.5682[a]
Sex (N; %)	**Total 199**	**Total 173**	
Male	68 (34.17)	133 (76.88)	< *0.0001*[b]
Female	126 (63.32)	26 (15.03)	
No data	5 (2.51)	14 (8.09)	
Ethnicity (N; %)	**Total 199**	**Total 173**	
Caucasian	160 (80.40)	79 (45.66)	< *0.0001*[b]
American Indian	18 (9.05)	61 (35.26)	
No data	21 (10.55)	33 (19.08)	

Categorical variables are expressed in percentages. Age value is expressed as mean ± standard error of the mean (SEM). [a] *P* values were calculated by Unpaired t test for unpaired samples, [b] *P* values were calculated by the Fisher's exact test for categorical variables.

TABLE 2 Distribution of genotype and allele frequencies of IFN-γ gene (+874 A/T) among patients with tuberculosis (TB) and Healthy Donors (HD). Categorical variables are expressed in percentages.

		Groups		Chi-square Test *P* Value	HD vs TB OR (95% IC)/*P* Value
		HD	TB	HD vs TB	
Genotypes	AA	33.67% (67/199)	63.58% (110/173)	< *0.0001*[a]	
	AT	48.24% (96/199)	30.06% (52/173)		3.031 (1.925 to 4.773)/< 0,0001[b]
	TT	18.09% (36/199)	6.36% (11/173)		5.373 (2.563 to 11.27)/< 0.0001[b]
Alleles	A	57.79% (230/398)	78.61% (272/346)	< *0.0001*[a]	
	T	42.21% (168/398)	21.39% (74/346)		

[a] *P* values were calculated by the Chi-Square ($\chi 2$) test of homogeneity. [b] *P* values were calculated by the Fisher's exact test for categorical variables.

regarding age distribution between HD and TB patients ($P>0.05$). However, we observed differences in sex distribution of recruited individuals of both populations (HD vs TB patients, $P<0.0001$). Nevertheless, we did not find differences in the genotype distributions and allele frequencies between females and males within each population (Supplementary Table S1).

Distribution of genotype and allele frequencies of IFN-γ gene (+874 A/T)

In order to investigate the association between +874 A/T SNP of IFNG and tuberculosis population in Argentina, genomic DNA extracted from whole blood and oral swabs in nucleic acid paper was genotyped by ARMS-PCR as described in Material and Methods. All populations were in Hardy-Weinberg (HW) equilibrium, with no significant Chi-square values for observed and expected genotype frequencies for this SNP.

The allelic distribution and the genotype of +874 A/T polymorphism differed significantly between TB patients and HD (Table 2 and Figure 1). In fact, the A allele was overrepresented in TB patients (TB= 78.61% and HD= 57.79%; $\times^2$ = 36.57 p<0.0001) (Figure 1 and Table 2). Accordingly, the distribution of genotype frequencies between groups was widely significant (TB vs HD $\times^2$ = 35.18; p<0.0001). The AA genotype, associated with susceptibility in other populations (Lopez-Maderuelo et al., 2003; Amim et al., 2008; Pacheco et al., 2008; Mosaad et al., 2010; Hashemi et al., 2011), was the most frequent in TB patients (TB= 63.58% and HD= 33.67%), while heterozygous AT genotype was the most frequent in HD (HD= 48.24% and TB= 30.06%) (Figure 1 and Table 2).

Odds ratios were calculated to estimate the level of association between the +874 A/T SNP and TB disease. The odds ratio (OR) AA vs AT was 3.031 (95% CI 1.925 - 4.773) and AA vs TT was 5.373 (95% CI 2.563 - 11.27) (Table 2). Taken together, these results demonstrate that individuals carrying the AA genotype are more susceptible to develop TB.

An analysis of the codominant, dominant, recessive and over dominant genetic models of inheritance was performed. We found significant differences between healthy controls and patients for the four models studied (Table 3). According to the Akaike information criterion (AIC), the codominant model (AA vs AT&TT) was the genetic model that best-fit to our data, since it showed the minimum AIC value (483.9).

Association of +874 A/T SNP with IFN-γ production and clinical parameters

The A allele and the AA genotype had been associated with low IFN-γ expression and susceptibility to TB in several populations around the world (Lio et al., 2002; Lopez-Maderuelo et al., 2003; Amim et al., 2008; Pacheco and Moraes, 2009; Mosaad et al., 2010; Prabhu Anand et al., 2010; Hashemi et al., 2011). Therefore, we evaluated the association between the IFNG +874 A/T genotypes and the levels of this cytokine produced by *M. tuberculosis*-stimulated PBMCs from HD and TB patients.

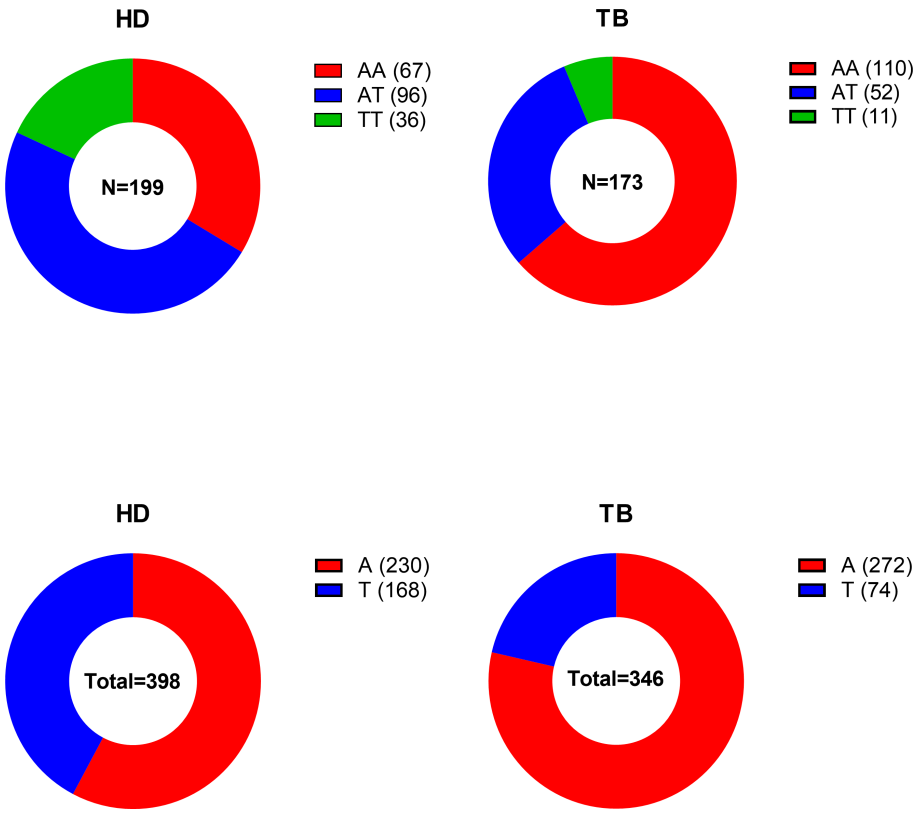

FIGURE 1
Distribution of genotype and allele frequencies of IFN-γ gene (+874 A/T) among patients with tuberculosis (TB) and Healthy Donors (HD).

10.3389/fcimb.2023.1080100

TABLE 3 Association studies of IFN-γ gene (+874 A/T) with the development of active tuberculosis.

Model	Genotype	HD	TB	OR (95% CI)	*P value*	AIC	BIC
Codominant	A/A	67 (33.7%)	110 (63.6%)	1.00	< 0.0001	483.9	495.6
	A/T	96 (48.2%)	52 (30.1%)	3.03 (1.92 – 4.77)			
	T/T	36 (18.1%)	11 (6.4%)	5.37 (2.56 – 11.27)			
Dominant	A/A	67 (33.7%)	110 (63.6%)	1.00	< 0.0001	484.2	492
	A/T - T/T	132 (66.3%)	63 (36.4%)	3.44 (2.24 – 5.27)			
Recessive	A/A - A/T	163 (81.9%)	162 (93.6%)	1.00	0.0005	505.7	513.5
	T/T	36 (18.1%)	11 (6.4%)	3.25 (1.60 - 6.61)			
Overdominant	A/A - T/T	103 (51.8%)	121 (69.9%)	1.00	0.0003	505	512.8
	A/T	96 (48.2%)	52 (30.1%)	2.17 (1.41 – 3.33)			

We found that the presence of the T allele was associated with higher IFN-γ production (Figure 2), with significant differences only in HD. We also observed that HD with the AT and TT genotypes produced higher levels of IFN-γ than TB patients with the same genotypes (Figure 2). Finally, we did not find any association between the genotypes and the clinical data, which indicates that the +874 A/T IFNG SNP is not associated with TB severity in our study population (Table 4). The increased production of IFN-γ observed in HD suggests that other genetic and epigenetic factors could be involved in the regulation of IFN-γ against *M. tuberculosis*.

Methylation status at the -53 CpG site of the promoter region of the IFN-γ gene

Methylation of the IFNG promoter could be a negative regulation mechanism during the immune response against *M. tuberculosis*. Therefore, methylation at the -53 CpG site of IFNG was evaluated by pyrosequencing of bisulfite-treated DNA from patients with active TB and HD. Individuals with latent tuberculosis (LTBI) were also included in this analysis. Although there is growing evidence of epigenetic modifications in TB (Kathirvel and Mahadevan, 2016), it is not yet fully understood how epigenetic alterations might trigger the activation from LTBI into active TB.

Interestingly, we observed a higher percentage of methylation of the CpG -53 site of the IFN-γ gene promoter region in TB patients compared to LTBI (TB = 69.30% vs. LTBI = 64.55%) (Figures 3A, B).

Moreover, we performed a ROC analysis for the methylation of IFNG, obtaining significant results for AUC analysis among TB vs LTBI individuals (Figure 4). Given that this kind of analysis plays a central role in evaluating diagnostic ability of tests to discriminate the true state of subjects (Hajian-Tilaki, 2013), our results could indicate a role for methylation at the -53 CpG site in disease reactivation.

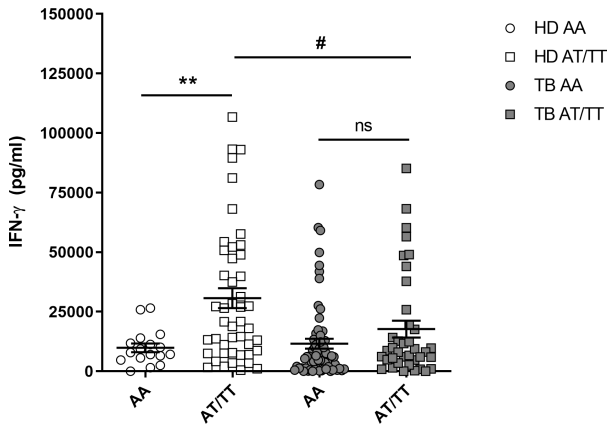

FIGURE 2
Production of IFN-γ by PBMCs from HD and TB patients carrying the genotypic variants of the IFN-γ gene (+874 A/T). PBMCs from healthy donors (HD, n = 63) and TB patients (TB, n = 102) carrying the different genotypes of the IFN-γ gene (+874 A/T) SNP were stimulated for five days with *M. tuberculosis*-Ag, and IFN-γ production was determined by ELISA. *P* values were calculated by one way ANOVA and Tukey's multiple comparison test. ** $p < 0.01$ between HD genotypes. # $p < 0.05$ between HD and TB patients AT/TT genotypes. ns, not signficant.

Discussion

Tuberculosis, an ancient disease, is still one of the biggest killers worldwide, with a high morbidity rate. It is known that only about 10% of the *M. tuberculosis*-infected population progresses to active tuberculosis which leads to the following question: Do patients with active TB have a genetic predisposition that makes them more susceptible to disease progression? Single nucleotide polymorphisms in several candidate genes, especially polymorphisms in cytokine genes are known to modulate cytokine levels, which may influence susceptibility to tuberculosis infection and disease. Given the essential role of IFN-γ to control mycobacterial replication and development of cellular immune response (Flesch and Kaufmann, 1987; Serbina et al., 2001; Salgame, 2005), our case-control study focused on determining whether rs2430561 SNP (+874 A/T) is associated with susceptibility to tuberculosis in Argentinean population.

In this study, we found a significant increase in the frequency of A allele (79%) and AA genotype (64%) in TB patients as compared with HD suggesting an association of the rs2430561 SNP A variant with susceptibility to tuberculosis disease in Argentina. Remarkably, more than 45% of individuals from the HD population (91 out of 199, QFT-GIT negative) were subjects exposed to *M. tuberculosis* (TB contacts or healthcare staff). Among them, 60.44% has a T allele, reinforcing that

10.3389/fcimb.2023.1080100

TABLE 4 Association between clinical parameters and the rs2430561 SNP genotypic variants during active tuberculosis.

TB patients	rs2430561 genotype			*P* value
	AA	AT	TT	
Hematologic Studies (n=91)				
Leukocytes (cells/ml)	10090 (± 491)	10436 (± 582)	9140 (± 1232)	>0,05[a]
Lymphocytes (cells/ml)	1525 (± 89)	1528 (± 102)	2112 (± 332)	>0,05[a]
Monocytes (cells/ml)	914 (± 48)	857 (± 53)	881 (± 156)	>0,05[a]
AFB in sputum smear (n=120)				
BAAR- or BAAR+	62 (84%)	28 (76%)	6 (67%)	0,3509[b]
BAAR++ or BAAR+++	12 (16%)	9 (24%)	3 (33%)	
Radiological Lesions (n=99)				
Mild or Moderate	26 (41%)	12 (41%)	2 (29%)	0,8033[b]
Severe	37 (59%)	17 (59%)	5 (71%)	
Days of disease evolution (n=75)	106,43 (± 13,22)	84,13 (± 10,62)	102,33 (± 22,18)	>0,05[a]

[a] *P* values were calculated by the Tukey's multiple comparisons test. [b] *P* values were calculated by the Chi-Square ($\chi 2$) test for categorical variables.

the presence of the T allele is indeed associated with resistance to *M. tuberculosis* infection. Despite Etokebe et al. did not find correlation between the +874 A/T polymorphism and tuberculosis disease in a Croatian population (Etokebe et al., 2006), our results are consistent with previous studies that have demonstrated an association of A allele and AA genotype with susceptibility to tuberculosis in Sicilian, Spanish, Hong Kong, Brazilians, South African and Egyptian populations (Lio et al., 2002; Lopez-Maderuelo et al., 2003; Rossouw et al., 2003; Tso et al., 2005; Amim et al., 2008; Mosaad et al., 2010).

A few reports have analyzed the association of rs2430561 SNP with the clinical manifestations of the disease (Lopez-Maderuelo et al., 2003; Etokebe et al., 2006; Ansari et al., 2011). Lopez-Maderuelo et al. showed an association of AA genotype with a far advanced form of radiographic extent of disease (Lopez-Maderuelo et al., 2003). Likewise, a study in a Pakistan population reported an overrepresentation of the T allele in less severe forms of pulmonary TB (Ansari et al., 2011). However, our results showed no association with clinical parameters demonstrating that IFN-γ +874 A/T polymorphism is associated with TB susceptibility but not with disease severity in our population of study.

We have previously demonstrated that low levels of IFN-γ are associated with disease severity (Pasquinelli et al., 2004; Jurado et al., 2012). Since it has been reported that +874 T to A polymorphism overlaps with a putative NF-κ B binding site which might have functional consequences for the transcription of the human IFN-γ gene (Pravica et al., 2000); we investigated the functional association of the different +874 genotypes with IFN-γ production. Our study demonstrates that *M. tuberculosis*-stimulated PBMCs from HD carrying the AA genotype produced strikingly significantly lower levels of IFN-γ than those carrying the AT and TT genotype. However, while a tendency was observed in TB patients, we did not find significant differences on the production of IFN-γ. On the other side, we did observe a significant difference in the production of IFN-γ between HD and TB patients carrying a T allele, which suggests that besides the presence of the T allele other mechanisms are regulating IFN-γ during active disease.

Indeed, genetic polymorphisms are not the only inheritable character of DNA that could influence susceptibility to disease. Epigenetic mechanisms such as DNA methylation and histone

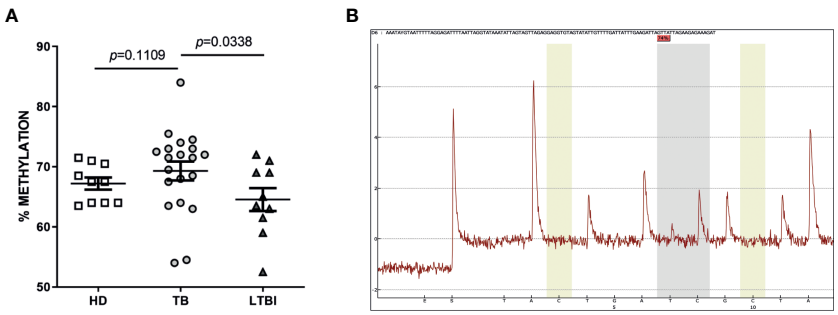

FIGURE 3
Methylation status of the -53 CpG of IFNG promoter in whole blood. Genomic DNA was obtained from whole blood from HD, TB patients and LTBI. Bisulfite converted-DNA was amplified by PCR and pyrosequencing was performed to determine the degree of methylation at the -53 CpG site of the IFNG promoter. **(A)** *P* values were calculated by one way ANOVA for non-parametric data and Dunn's multiple comparison test. **(B)** A representative pyrogram is shown.

acetylation regulate the rate of transcription and/or specific tissue expression of certain genes without altering the DNA sequence.

Recent studies suggest that *M. tuberculosis* can alter the host epigenome to modulate the transcriptional machinery and plays a major role in modulating the immune response of the host (Kathirvel and Mahadevan, 2016). However, the mechanisms involved in epigenetic alterations during *M. tuberculosis* infection have not been fully understood yet. In addition to a potential causal role in pathogenic processes, epigenetic alterations – such as *de novo* methylation of DNA – can also occur as a direct or indirect consequence of disease and might serve as biomarkers of disease activity (Esterhuyse et al., 2012).

Owing to the major role of the epigenome in the phenotypic plasticity of the immune system and its ability to link environment and cellular phenotypes, host susceptibility to TB is expected to have an epigenetic predisposition component. In addition, epigenetic analyses will probably reveal changes at the epigenome resulting either directly or indirectly from infection. Growing evidence highlights the impact of pathogens genetic variation on susceptibility and severity of infections.

In Argentina, Monteserin et al. studied the genetic diversity of *M. tuberculosis* strains circulating in the Metropolitan Area of Buenos Aires (Monteserin et al., 2018). They showed that as in the rest of South America, genotypes of the Lineage 4 Euro-American (one of the seven globally described *M. tuberculosis* strains) predominate in our country and in contrast with the neighboring country Brazil, the RD^{rio} type (associated with high rate of transmission and drug resistance) does not play a major role in the TB epidemic (Monteserin et al., 2018). Moreover, the multidrug resistant M strain which belongs to the Lineage 4 Euro-American is highly prevalent in Argentina and has been shown to induce poor immune responses (Yokobori et al., 2022). However, the *M. tuberculosis* population structure in Argentina is still not fully comprehend.

It has been demonstrated that the IFNG promoter undergoes differential methylation during *in vitro* polarization of human peripheral blood T cells (Yano et al., 2003). This promoter is hypermethylated at the -53 CpG site during Th2 differentiation whereas it becomes hypomethylated in Th1 differentiated cells, existing a correlation between the degree of promoter methylation and the production of IFN-γ (Yano et al., 2003). Janson et al. also described different methylation levels at the -53 CpG site between human naive CD4 lymphocytes which were hypermethylated and Th1 lymphocytes which showed demethylation during differentiation (Janson et al., 2008). In other work, Dong et al. demonstrated that in human T cells early Th1-cell differentiation is accompanied by dynamic demethylation of CpGs at both the promoter and the CNS-1 regions of the IFNG locus (Dong et al., 2013). Moreover, epigenetic modifications in this locus were indispensable for the establishment of stable functional Th1 cytokine memory. The authors showed considerable levels of demethylation among different CpG of the promoter and the CNS1 region, including the -53 CpG site studied in our work (Dong et al., 2013).

In mice, naive T cells show a hypomethylated state of the IFNG promoter, which is maintained as they differentiate into Th1 cells (Winders et al., 2004). On the contrary, under Th2-polarizing conditions, CD4 cells display higher levels of methylation in the IFNG promoter, including the -53 CpG site (Winders et al., 2004). Besides, it has been shown that the methylation of the -53 CpG site impairs IFNG promoter activity and ATF2/c-Jun and CREB binding *in vitro* (Jones and Chen, 2006).

Despite the presence of some differences in the regulation of IFNG transcription between mice and human T lymphocytes, these data demonstrate the epigenetic involvement in immune regulation and evidence the -53 CpG site as an evolutionarily conserved position essential for IFN-γ production. When we evaluated the methylation status of the IFNG CpG -53 site in whole blood, our results showed increased methylation levels in patients with active TB compared to LTBI people. Surprisingly, we did not find differences in the methylation status between HD and TB patients, which could be attributed to a reactive epigenome. The lowest levels of methylation were observed for LTBI, who has the ability to control the infection. Considering that patients with active TB are not able to contain the infection at the time they were studied, a hypermethylation status could be expected.

Moreover, ROC and AUC analysis demonstrated that hypermethylation of this site could be a good biomarker of disease status; which reinforce the importance of this epigenetic modification as a key mechanism during active disease.

In accordance, some reports have shown changes in human methylome during TB or in response to BCG. Lyu et al. conclude that DNA methylation might be a promising TB diagnostic biomarker, as they identified TB-related targets differentially methylated by logistic regression and elastic net regression that were validated by bisulfite conversion and PCR (Lyu et al., 2022). DNA methylation has been also associated to anti-mycobacterial

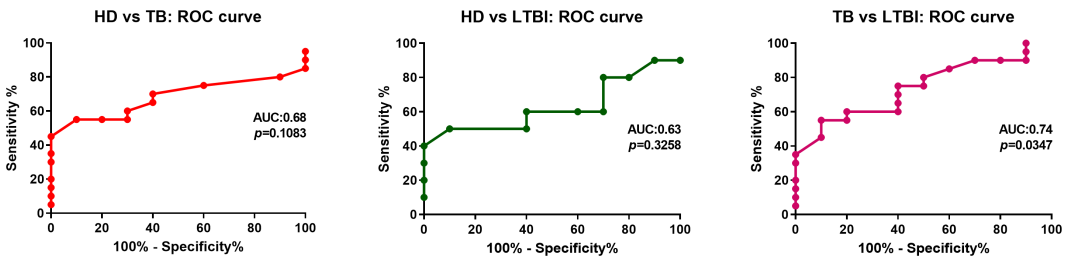

FIGURE 4
ROC curve analyses for evaluation of the predictive value of -53 CpG methylation on disease status. ROC curve analyses for evaluation of the predictive value of whole blood methylation levels at IFNG -53 CpG for differentiating HD individuals from TB, HD individual from LTBI and TB from LTBI. ROC, receiver operating characteristic; AUC, area under the ROC curve.

activity in PBMCs from BCG-vaccinated individuals (Verma et al., 2017). Recently, DiNardo et al. characterized DNA methylation of different genes that are critical to anti-mycobacterial immunity (DiNardo et al., 2020). They showed that immune cells from patients with active TB present a hypermethylated state, leading to nonspecific immune responsiveness (DiNardo et al., 2020).

These studies demonstrate the importance of evaluating the epigenome in the context of TB, however, none of them have evaluated the relevance of the -53 site in particular. Although the number of samples evaluated in the present study limits the extrapolation of our findings, since DNA methylome patterns are sensitive to environmental and seasonal factors, age, and ethnicity, it is attractive to focus on a well-defined study group as we did in our work. Another issue to highlight from our study is that we analyzed changes in the methylation of the -53 site in peripheral blood. Peripheral blood biomarkers, whether at the genomic, transcriptomic, epigenetic, or proteomic level, have received special attention in recent years. It is noteworthy that epigenetics can establish bridges between the host, *M. tuberculosis* and the environment. Therefore, epigenetic biomarkers in peripheral blood have great potential in the diagnosis and monitoring of progression to active TB. Epigenetic markers may provide a novel biosignature for discrimination between LTBI and active TB disease, for monitoring drug treatment outcome, and, in the long run, for predicting the risk of progression of LTBI to active TB disease (Esterhuyse et al., 2012).

To our knowledge, there are only three reports in South America population that study the association of the +874 A/T SNP with resistance/susceptibility to TB (Henao et al., 2006; Amim et al., 2008; Araujo et al., 2017). Recently, another IFN-γ SNP, the IFNG rs1861494, was associated with TB susceptibility in Argentinean population (Rolandelli et al., 2018). Our work, is the first to study association and functional relevance of rs1861494 SNP in Argentina. Even though we did not find correlation with the severity of the disease, we demonstrated that AA genotype and A allele are correlated with low IFN-γ production and increased susceptibility to develop active TB. Moreover, we also confirmed the methylation of -53 CpG of IFNG in TB patients. Many other polymorphic genes should be investigated in active and latent TB, but our results indicate that the AA genotype of the rs2430561 SNP could be a potential genetic biomarker for tuberculosis susceptibility in Argentina.

Methods

Healthy donors and patients

HIV-seronegative patients with active tuberculosis (TB) were evaluated at Dr. F. J. Muñiz Hospital (Buenos Aires, Argentina). Diagnosis of disease was established based on clinical and radiological data, identification of acid-fast bacilli in sputum, and isolation of *M. tuberculosis* in culture. Patients included in this study had received less than one week of anti-tuberculosis therapy. BCG-vaccinated healthy adults lacking a history of TB (household contacts and healthcare workers) were recruited at Argentinean Referral Hospitals. Among this group of individuals, diagnosis of LTBI was established using QuantiFERON-TB Gold In-Tube (QFT-GIT; Qiagen, USA; according to the manufacturer's directions). LTBI diagnosis was assigned to any subject with a positive QFT-GIT and no clinical or radiological evidence of active TB. The group of healthy donors (HD) was comprised by adult individuals who had received BCG vaccination at birth and lacked a history of TB (tested by chest X-rays and analysis of acid-fast bacilli in sputum) and with negative QFT-GIT. Peripheral blood was collected in heparinized tubes from all individuals participating in the study after receiving informed consent. All methods were carried out in accordance with relevant guidelines and regulations. All experimental protocols were approved by a licensing committee from Hospital Dr. F. J. Muñiz (Buenos Aires, Argentina).

Mycobacterium tuberculosis antigen

In vitro stimulation of cells throughout the study was performed with a cell lysate from the virulent *M. tuberculosis* H37Rv strain prepared by probe sonication (*Mtb*-Ag). The strain was obtained through BEI Resources, NIAID, NIH: *Mycobacterium tuberculosis*, Strain H37Rv, Whole cell lysate, NR-14822 (Bethesda, MD, USA).

Cell preparation and reagents

Peripheral blood mononuclear cells (PBMCs) were isolated by centrifugation over Ficoll-Hypaque (GE Healthcare) and cultured (1 X 10^6 cells/mL), with or without *Mtb*-Ag (10 μg/mL) with RPMI 1640 medium (Gibco) supplemented with L-glutamine (Sigma Aldrich), 10% Fetal Bovine Serum (Gibco), 100 U/mL of Penicillin and 100 μg/mL of Streptomycin (Gibco). After 5d, IFN-γ production was determined by ELISA (BioLegend).

DNA extraction and genotyping

Genomic DNA was extracted from whole blood samples using the Quick-gDNA™ Blood MiniPrep (Zymo Reasearch) and buccal swabs (Biodynamics) of TB patients, and HD individuals according to the manufacturer's instructions. Amplification refractory mutation system-polymerase chain reaction (ARMS-PCR) was performed for the rs2430561 SNP genotyping, as previously described (Pravica et al., 2000). The conditions included initial denaturation (95°C for 5min), 10 rounds for internal control amplification of 95°C for 30s, 62°C for 50s and 72°C for 60s; then 20 rounds of denaturation at 95°C for 20s, 56°C for 50s and 72°C for 50s with a final extension of 5min at 72°C. The amplified products were monitored by electrophoresis on a 2% agarose gel containing Syber Safe (Thermo).

Methylation analysis of -53 CpG site in the IFNG promoter

Methylation analysis was carried out by bisulfite conversion of genomic DNA from whole blood samples of TB patients, HD and LTBI individuals. After extraction of genomic DNA from whole blood, bisulfite conversion was performed using the EZ DNA Methylation-Lightning™ Kit (Zymo Research) according to the manufacturer's instructions. The IFNG promoter region was

amplified by Bisulfite PCR using Go Taq Hot Start Polymerase (Promega) and the following primers designed with Methyl Primer Express: Fw 5′-TAAGGAGTTTAA AGGAAATTTTAATTATA-3′, Rv (biotinylated) 5′-ATCTTTCTCTTCTAATAACTAATCTTCAA-3′). Following an initial denaturation of 94°C for 3min samples were subjected to 40 rounds of PCR consisting of 94°C for 30s, 48°C for 30s and 72°C for 60s with a final extension time of 10 min at 72°C. Methylation levels were determined by pyrosequencing (Service from Instituto de Genética Veterinaria (IGEVET) "Ing. Fernando Noel Dulout", UNLP-CONICET) using an internal primer Fw: 5′-TTAAAAAATTTGTGA-3′. Pyrosequencing assays were performed according to the manufacturer's instructions using the PSQ 96MA (Qiagen). The methylation levels were determined using the software PYROMARK Q96MA (Qiagen).

Statistical analysis

The genotype and allele frequencies were obtained by direct counting. Hardy–Weinberg equilibrium was tested between cases/controls separately ($\chi 2$ goodness-of-fit test). Comparisons of the distributions of the allele and genotype frequencies between cases/controls were performed using the $\chi 2$ test for homogeneity. The association between the rs2430561 genotypes and the case/control condition was estimated as an odds ratio (OR). The quantitative data were expressed as mean ± standard error of the mean (SEM), and the Mann–Whitney U test or the Kruskal-Whallis (ANOVA) test for unpaired and non-parametric samples was used to analyze differences between groups. For categorical variables, the $\chi 2$ test was performed to compare proportions of subjects between groups. All statistical analysis were performed using GraphPad Prism v8.0 (GraphPad Software). $p < 0.05$ was considered statistically significant.

Data availability statement

The original contributions presented in the study are included in the article/Supplementary Materials, further inquiries can be directed to the corresponding author/s.

Ethics statement

The studies involving human participants were reviewed and approved by Hospital Dr. F. J. Muñiz. The patients/participants provided their written informed consent to participate in this study.

Author contributions

GA, RH, AB, VG and VP contributed to the conception and design of the study. GA and RH performed the experiments and analyzed the data. AB, ME and JC contributed with some of the experiments and provided methodological support and insightful data discussion. RH, AB and VP wrote the first draft of the manuscript. All authors contributed to manuscript revision, read, and approved the submitted version. DP and RM were in charge of patients' diagnosis, obtained the blood samples and contributed with the analysis of the clinical data. All authors contributed to the article and approved the submitted version.

Funding

This work was supported by Universidad Nacional del Noroeste de la Provincia de Buenos Aires (grant number SIB 0618/2019), Agencia Nacional de Promoción Científica y Tecnológica (ANPCyT, grant number PICT A 2017-1896 to VP) and Florencio Fiorini Foundation. GA was a doctoral fellow from CONICET. RH was supported by CONICET and UNNOBA and is currently a researcher from CONICET. AB was a doctoral fellow and is currently a postdoctoral fellow from CONICET. ME and JC were fellows from Comisión de Investigaciones Científicas (CIC). VG and VP are researchers from CONICET.

Acknowledgments

We thank to Natalia Menite and Gastón Villafañe for the technical support.

Conflict of interest

The authors declare that the research was conducted in the absence of any commercial or financial relationships that could be construed as a potential conflict of interest.

Publisher's note

Supplementary material

The Supplementary Material for this article can be found online at: https://www.frontiersin.org/articles/10.3389/fcimb.2023.1080100/full#supplementary-material

References

Amim, L. H. L. V., Pacheco, A. G., Fonseca-Costa, J., Loredo, C. S., Rabahi, M. F., Melo, M. H., et al. (2008). Role of IFN-gamma +874 T/A single nucleotide polymorphism in the tuberculosis outcome among brazilians subjects. *Mol. Biol. Rep.* 35, 563–566. doi: 10.1007/s11033-007-9123-1

Ansari, A., Hasan, Z., Dawood, G., and Hussain, R. (2011). Differential combination of cytokine and interferon- gamma +874 T/A polymorphisms determines disease severity in pulmonary tuberculosis. *PloS One* 6, e27848. doi: 10.1371/journal.pone.0027848

Araujo, Z., Palacios, A., Biomon, R., Rivas-Santiago, B., Serrano, C. J., Enciso-Moreno, L., et al. (2017). Concordance between IFNgamma gene +874 A/T polymorphism and interferon-gamma expression in a TB-endemic indigenous setting. *Rev. Soc. Bras. Med. Trop.* 50, 199–207. doi: 10.1590/0037-8682-0398-2016

Areeshi, M. Y., Mandal, R. K., Dar, S. A., Jawed, A., Wahid, M., Lohani, M., et al. (2021). IFN-γ +874 A>T (rs2430561) gene polymorphism and risk of pulmonary tuberculosis: a meta-analysis. *Arch. Med. Sci.* 17, 177–188. doi: 10.5114/aoms.2019.88481

Beiranvand, E., Abediankenari, S., Valiyari, S., Rezaei, M. S., Rostamian, M., Beiranvand, B., et al. (2016). Single nucleotide polymorphisms of IFNgamma (+874 A/T) and IFNgammaR1 (-56 C/T) in Iranian patients with TB. *Trans. R Soc. Trop. Med. Hyg* 110, 604–609. doi: 10.1093/trstmh/trw074

Bhanothu, V., Lakshmi, V., Theophilus, J. P., Rozati, R., Badhini, P., and Vijayalaxmi, B. (2015). Investigation of toll-like receptor-2 (2258G/A) and interferon gamma (+874T/A) gene polymorphisms among infertile women with female genital tuberculosis. *PloS One* 10, e0130273. doi: 10.1371/journal.pone.0130273

Cooke, G. S., and Hill, A. V. (2001). Genetics of susceptibility to human infectious disease. *Nat. Rev. Genet.* 2, 967–977. doi: 10.1038/35103577

Cooper, A. M., Dalton, D. K., Stewart, T. A., Griffin, J. P., Russell, D. G., and Orme, I. M. (1993). Disseminated tuberculosis in interferon gamma gene-disrupted mice. *J. Exp. Med.* 178, 2243–2247. doi: 10.1084/jem.178.6.2243

DiNardo, A. R., Rajapakshe, K., Nishiguchi, T., Grimm, S. L., Mtetwa, G., Dlamini, Q., et al. (2020). DNA Hypermethylation during tuberculosis dampens host immune responsiveness. *J. Clin. Invest.* 130, 3113–3123. doi: 10.1172/JCI134622

Dong, J., Chang, H. D., Ivascu, C., Qian, Y., Rezai, S., Okhrimenko, A., et al. (2013). Loss of methylation at the IFNG promoter and CNS-1 is associated with the development of functional IFN-γ memory in human CD4+ T lymphocytes. *Eur. J. Immunol.* 43, 793–804. doi: 10.1002/eji.201242858

Esterhuyse, M. M., Linhart, H. G., and Kaufmann, S. H. E. (2012). Can the battle against tuberculosis gain from epigenetic research? *Trends Microbiol.* 20, 220–226. doi: 10.1016/j.tim.2012.03.002

Etokebe, G. E., Bulat-Kardum, L., Johansen, M. S., Knezevic, J., Balen, S., Matakovic-Mileusnic, N., et al. (2006). Interferon-gamma gene (T874A and G2109A) polymorphisms are associated with microscopy-positive tuberculosis. *Scand. J. Immunol.* 63, 136–141. doi: 10.1111/j.1365-3083.2005.01716.x

Fatima, S., Kumari, A., Agarwal, M., Pahuja, I., Yadav, V., Dwivedi, V. P., et al. (2021). Epigenetic code during mycobacterial infections: therapeutic implications for tuberculosis. *FEBS J.* 289, 4172–4191. doi: 10.1111/febs.16170

Flesch, I., and Kaufmann, S. H. (1987). Mycobacterial growth inhibition by interferon-gamma-activated bone marrow macrophages and differential susceptibility among strains of mycobacterium tuberculosis. *J. Immunol.* 138, 4408–4413. doi: 10.4049/jimmunol.138.12.4408

Flynn, J. L., and Chan, J. (2001). Immunology of tuberculosis. *Annu. Rev. Immunol.* 19, 93–129. doi: 10.1146/annurev.immunol.19.1.93

Flynn, J. L., Chan, J., Triebold, K. J., Dalton, D. K., Stewart, T. A., and Bloom, B. R. (1993). An essential role for interferon gamma in resistance to mycobacterium tuberculosis infection. *J. Exp. Med.* 178, 2249–2254. doi: 10.1084/jem.178.6.2249

Fortin, A., Abel, L., Casanova, J. L., and Gros, P. (2007). Host genetics of mycobacterial diseases in mice and men: forward genetic studies of BCG-osis and tuberculosis. *Annu. Rev. Genomics Hum. Genet.* 8, 163–192. doi: 10.1146/annurev.genom.8.080706.092315

Gauba, K., Gupta, S., Shekhawat, J., Sharma, P., Yadav, D., and Banerjee, M. (2021). Immunomodulation by epigenome alterations in mycobacterium tuberculosis infection. *Tuberculosis* 128, 102077. doi: 10.1016/j.tube.2021.102077

Hajian-Tilaki, K. (2013). Receiver operating characteristic (ROC) curve analysis for medical diagnostic test evaluation. *Casp J. Intern. Med.* 4, 627–635.

Hashemi, M., Sharifi-Mood, B., Nezamdoost, M., Moazeni-Roodi, A., Naderi, M., Kouhpayeh, H., et al. (2011). Functional polymorphism of interferon-gamma (IFN-gamma) gene +874T/A polymorphism is associated with pulmonary tuberculosis in zahedan, southeast Iran. *Prague Med. Rep.* 112, 38–43.

Henao, M. I., Montes, C., Paris, S. C., and García, L. F. (2006). Cytokine gene polymorphisms in Colombian patients with different clinical presentations of tuberculosis. *Tuberculosis* 86, 11–19. doi: 10.1016/j.tube.2005.03.001

Janson, P. C. J., Marits, P., Thörn, M., Ohlsson, R., and Winqvist, O. (2008). CpG methylation of the IFNG gene as a mechanism to induce immunosupression in tumor-infiltrating lymphocytes. *J. Immunol.* 181, 2878–2886. doi: 10.4049/jimmunol.181.4.2878

Jones, B., and Chen, J. (2006). Inhibition of IFN-γ transcription by site-specific methylation during T helper cell development. *EMBO J.* 25, 2443–2452. doi: 10.1038/sj.emboj.7601148

Jurado, J. O., Pasquinelli, V., Alvarez, I. B., Peña, D., Rovetta, A. I., Tateosian, N. L., et al. (2012). IL-17 and IFN-γ expression in lymphocytes from patients with active tuberculosis correlates with the severity of the disease. *J. Leukoc. Biol.* 91, 991–1002. doi: 10.1189/jlb.1211619

Kathirvel, M., and Mahadevan, S. (2016). The role of epigenetics in tuberculosis infection. *Epigenomics* 8, 537–549. doi: 10.2217/epi.16.1

Lio, D., Marino, V., Serauto, A., Gioia, V., Scola, L., Crivello, A., et al. (2002). Genotype frequencies of the +874T → a single nucleotide polymorphism in the first intron of the interferon-gamma gene in a sample of Sicilian patients affected by tuberculosis. *Eur. J. Immunogenet* 29, 371–374. doi: 10.1046/j.1365-2370.2002.00327.x

Lopez-Maderuelo, D., Arnalich, F., Serantes, R., Gonzalez, A., Codoceo, R., Madero, R., et al. (2003). Interferon-gamma and interleukin-10 gene polymorphisms in pulmonary tuberculosis. *Am. J. Respir. Crit. Care Med.* 167, 970–975. doi: 10.1164/rccm.200205-438BC

Lyu, M., Zhou, J., Jiao, L., Wang, Y., Zhou, Y., Lai, H., et al. (2022). Deciphering a TB-related DNA methylation biomarker and constructing a TB diagnostic classifier. *Mol. Ther. - Nucleic Acids* 27, 37–49. doi: 10.1016/j.omtn.2021.11.014

Mandal, R. K., Wahid, M., Jawed, A., Dar, S. A., Panda, A. K., Akhter, N., et al. (2019). A trial sequential meta-analysis of IFN-gamma +874 A>T (rs2430561) gene polymorphism and extrapulmonary tuberculosis risk. *Microb. Pathog.* 130, 1–9. doi: 10.1016/j.micpath.2018.12.050

Ministerio De Salud, Argentina (2022). Boletín N° 5. Tuberculosis y lepra en la Argentina. AÑO IV - MARZO 2022.

Monteserin, J., Paul, R., Gravina, E., Reniero, A., Hernandez, T., Mazzeo, E., et al. (2018). Genotypic diversity of mycobacterium tuberculosis in Buenos Aires, Argentina. *Infect. Genet. Evol.* 62, 1–7. doi: 10.1016/j.meegid.2018.04.006

Mosaad, Y. M., Soliman, O. E., Tawhid, Z. E., and Sherif, D. M. (2010). Interferon-gamma +874 T/A and interleukin-10 -1082 A/G single nucleotide polymorphism in Egyptian children with tuberculosis. *Scand. J. Immunol.* 72, 358–364. doi: 10.1111/j.1365-3083.2010.02426.x

Pacheco, A. G., Cardoso, C. C., and Moraes, M. O. (2008). IFNG +874T/A, IL10 -1082G/A and TNF -308G/A polymorphisms in association with tuberculosis susceptibility: a meta-analysis study. *Hum. Genet.* 123, 477–484. doi: 10.1007/s00439-008-0497-5

Pacheco, A. G., and Moraes, M. O. (2009). Genetic polymorphisms of infectious diseases in case-control studies. *Dis. Markers* 27, 173–186. doi: 10.3233/DMA-2009-0654

Pasquinelli, V., Quiroga, M. F. M. F., Martínez, G. J. G. J., Zorrilla, L. C. L. C., Musella, R. M. R. M., Bracco, M. M. M. M., et al. (2004). Expression of signaling lymphocytic activation molecule-associated protein interrupts IFN-γ/Production in human tuberculosis. *J. Immunol.* 172, 1177–1185. doi: 10.4049/jimmunol.172.2.1177

Pasquinelli, V., Townsend, J. C. J. C., Jurado, J. O. J. O., Alvarez, I. B. I. B., Quiroga, M. F. M. F., Barnes, P. F. P. F., et al. (2009). IFN-γ production during active tuberculosis is regulated by mechanisms that involve IL-17, SLAM, and CREB. *J. Infect. Dis.* 199, 661–665. doi: 10.1086/596742

Patarčić, I., Gelemanović, A., Kirin, M., Kolčić, I., Theodoratou, E., Baillie, K. J., et al. (2015). The role of host genetic factors in respiratory tract infectious diseases: systematic review, meta-analyses and field synopsis. *Sci. Rep.* 5, 16119. doi: 10.1038/srep16119

Prabhu Anand, S., Harishankar, M., and Selvaraj, P. (2010). Interferon gamma gene +874A/T polymorphism and intracellular interferon gamma expression in pulmonary tuberculosis. *Cytokine* 49, 130–133. doi: 10.1016/j.cyto.2009.11.009

Pravica, V., Perrey, C., Stevens, A., Lee, J. H., and Hutchinson, I. V. (2000). A single nucleotide polymorphism in the first intron of the human IFN-gamma gene: absolute correlation with a polymorphic CA microsatellite marker of high IFN-gamma production. *Hum. Immunol.* 61, 863–866. doi: 10.1016/S0198-8859(00)00167-1

Rolandelli, A., Pellegrini, J. M., Amiano, N. O., Santilli, M. C., Morelli, M. P., Castello, F. A., et al. (2018). The IFNG rs1861494 single nucleotide polymorphism is associated with protection against tuberculosis disease in Argentina. *Genes (Basel)* 9, 46. doi: 10.3390/genes9010046

Rosain, J., Kong, X.-F., Martinez-Barricarte, R., Oleaga-Quintas, C., Ramirez-Alejo, N., Markle, J., et al. (2019). Mendelian susceptibility to mycobacterial disease: 2014-2018 update. *Immunol. Cell Biol.* 97, 360–367. doi: 10.1111/imcb.12210

Rossouw, M., Nel, H. J., Cooke, G. S., van Helden, P. D., and Hoal, E. G. (2003). Association between tuberculosis and a polymorphic NFkappaB binding site in the interferon gamma gene. *Lancet* 361, 1871–1872. doi: 10.1016/S0140-6736(03)13491-5

Saelens, J. W., Viswanathan, G., and Tobin, D. M. (2019). Mycobacterial evolution intersects with host tolerance. *Front. Immunol.* 10. doi: 10.3389/fimmu.2019.00528

Salgame, P. (2005). Host innate and Th1 responses and the bacterial factors that control mycobacterium tuberculosis infection. *Curr. Opin. Immunol.* 17, 374–380. doi: 10.1016/j.coi.2005.06.006

Samten, B., Ghosh, P., Yi, A.-K., Weis, S. E., Lakey, D. L., Gonsky, R., et al. (2002). Reduced expression of nuclear cyclic adenosine 5'-monophosphate response element-binding proteins and IFN-gamma promoter function in disease due to an intracellular pathogen. *J. Immunol.* 168, 3520–3526. doi: 10.4049/jimmunol.168.7.3520

Samten, B., Howard, S. T., Weis, S. E., Wu, S., Shams, H., Townsend, J. C., et al. (2005). Cyclic AMP response element-binding protein positively regulates production of IFN-gamma by T cells in response to a microbial pathogen. *J. Immunol.* 174, 6357–6363. doi: 10.4049/jimmunol.174.10.6357

Serbina, N. V., Lazarevic, V., and Flynn, J. L. (2001). CD4(+) T cells are required for the development of cytotoxic CD8(+) T cells during mycobacterium tuberculosis infection. *J. Immunol.* 167, 6991–7000. doi: 10.4049/jimmunol.167.12.6991

Tso, H. W., Ip, W. K., Chong, W. P., Tam, C. M., Chiang, A. K., and Lau, Y. L. (2005). Association of interferon gamma and interleukin 10 genes with tuberculosis in Hong Kong Chinese. *Genes Immun.* 6, 358–363. doi: 10.1038/sj.gene.6364189

Verma, D., Parasa, V. R., Raffetseder, J., Martis, M., Mehta, R. B., Netea, M., et al. (2017). Anti-mycobacterial activity correlates with altered DNA methylation pattern in immune cells from BCG-vaccinated subjects. *Sci. Rep.* 7, 1–10. doi: 10.1038/s41598-017-12110-2

Wei, Z., Wenhao, S., Yuanyuan, M., Yang, L., Daming, Z., Jiangchun, X., et al. (2017). A single nucleotide polymorphism in the interferon-gamma gene (IFNG +874 T/A) is associated with susceptibility to tuberculosis. *Oncotarget* 8, 50415–50429. doi: 10.18632/oncotarget.17304

Winders, B. R., Schwartz, R. H., and Bruniquel, D. (2004). A distinct region of the murine IFN-γ promoter is hypomethylated from early T cell development through mature naive and Th1 cell differentiation, but is hypermethylated in Th2 cells. *J. Immunol.* 173, 7377–7384. doi: 10.4049/jimmunol.173.12.7377

Geneva: World Health Organization (WHO) (2022). Global tuberculosis report 2022. Licence: CC BY-NC-SA 3.0 IGO

Yano, S., Ghosh, P., Kusaba, H., Buchholz, M., and Longo, D. L. (2003). Effect of promoter methylation on the regulation of IFN- γ gene during *In vitro* differentiation of human peripheral blood T cells into a Th2 population. *J. Immunol.* 171, 2510–2516. doi: 10.4049/jimmunol.171.5.2510

Yokobori, N., López, B., and Ritacco, V. (2022). The host-pathogen-environment triad: Lessons learned through the study of the multidrug-resistant mycobacterium tuberculosis m strain. *Tuberculosis* 134, 102200. doi: 10.1016/j.tube.2022.102200

frontiers | Frontiers in Cellular and Infection Microbiology

TYPE Original Research
PUBLISHED 28 April 2023
DOI 10.3389/fcimb.2023.1067464

OPEN ACCESS

EDITED BY
Veronica Edith Garcia,
University of Buenos Aires, Argentina

REVIEWED BY
Aida Sivro,
National Laboratory for HIV Immunology, Public Health Agency of Canada, Canada
Marta C. Romano,
National Polytechnic Institute of Mexico, Mexico

*CORRESPONDENCE
María Luisa Bay
bay@idicer-conicet.gob.ar

SPECIALTY SECTION
This article was submitted to Bacteria and Host, a section of the journal Frontiers in Cellular and Infection Microbiology

RECEIVED 11 October 2022
ACCEPTED 06 April 2023
PUBLISHED 28 April 2023

CITATION
Díaz A, D'Attilio L, Penas F, Bongiovanni B, Massa E, Cevey A, Santucci N, Bottasso O, Goren N and Bay ML (2023) Studies on the contribution of PPAR Gamma to tuberculosis physiopathology. *Front. Cell. Infect. Microbiol.* 13:1067464. doi: 10.3389/fcimb.2023.1067464

Studies on the contribution of PPAR Gamma to tuberculosis physiopathology

Ariana Díaz[1], Luciano D'Attilio[1], Federico Penas[2], Bettina Bongiovanni[1,3], Estefanía Massa[1,3], Agata Cevey[2], Natalia Santucci[1], Oscar Bottasso[1], Nora Goren[2] and María Luisa Bay[1]*

[1]Facultad de Ciencias Médicas, Instituto de Inmunología Clínica y Experimental de Rosario (IDICER), CONICET - Universidad Nacional de Rosario, Rosario, Argentina, [2]Facultad de Medicina, Instituto de Investigaciones Biomédicas en Retrovirus y SIDA (INBIRS), CONICET - Universidad de Buenos Aires, Buenos Aires, Argentina, [3]Facultad de Ciencias Bioquímicas y Farmacéuticas, Universidad Nacional de Rosario, Rosario, Argentina

Introduction: Tuberculosis (TB) is a major health problem characterized by an immuno-endocrine imbalance: elevated plasma levels of cortisol and pro- and anti-inflammatory mediators, as well as reduced levels of dehydroepiandrosterone. The etiological agent, Mycobacterium tuberculosis (Mtb), is captured by pulmonary macrophages (Mf), whose activation is necessary to cope with the control of Mtb, however, excessive activation of the inflammatory response also leads to tissue damage. Glucocorticoids (GC) are critical elements to counteract the immunoinflammatory reaction, and peroxisome proliferator-activated receptors (PPARs) are also involved in this regard. The primary forms of these receptors are PPARϒ, PPARα, and PPARβ/δ, the former being the most involved in anti-inflammatory responses. In this work, we seek to gain some insight into the contribution of PPARϒ in immuno-endocrine-metabolic interactions by focusing on clinical studies in pulmonary TB patients and in vitro experiments on a Mf cell line.

Methods and results: We found that TB patients, at the time of diagnosis, showed increased expression of the PPARϒ transcript in their peripheral blood mononuclear cells, positively associated with circulating cortisol and related to disease severity. Given this background, we investigated the expression of PPARϒ (RT-qPCR) in radiation-killed Mtb-stimulated human Mf. The Mtb stimulation of Mf derived from the human line THP1 significantly increased the expression of PPARϒ, while the activation of this receptor by a specific agonist decreased the expression of pro- and anti-inflammatory cytokines (IL-1β and IL-10). As expected, the addition of GC to stimulated cultures reduced IL-1β production, while cortisol treatment together with the PPARϒ agonist lowered the levels of this proinflammatory cytokine in stimulated cultures. The addition of RU486, a

10.3389/fcimb.2023.1067464

glucocorticoid receptor antagonist, only reversed the inhibition produced by the addition of GC.

Conclusion: The current results provide a stimulating background for further analysis of the interconnection between PPARs and steroid hormones in the context of Mtb infection.

KEYWORDS

tuberculosis, cortisol, DHEA, PPARγ, infectious disease

1 Introduction

Tuberculosis (TB) is one of the top ten causes of death worldwide. Until the coronavirus (COVID-19) pandemic, TB was the leading cause of death attributed to a single infectious agent, ranking above HIV/AIDS (Global Tuberculosis Report 2022). According to WHO estimates, there were 10.6 million TB cases in 2021, reaching 1.4 million deaths, although these numbers are considered underestimates as the COVID-19 pandemic delayed global TB control services, reversing years of progress made in the fight against this disease (No Author, 2019).

TB is an ancient chronic infectious disease caused by the bacillus *Mycobacterium tuberculosis* (Mtb), which is spread when sick people expel bacteria into the air, for example, by coughing. The disease usually affects the lungs (pulmonary TB) but can also affect other body sites (extrapulmonary TB). Commonly, the host immune response (IR) controls Mtb replication, by promoting mycobacterial clearance or leading to the establishment of a latent infection, which ultimately depends on a fine balance between the pathogen and the specific IR (Ernst, 2012).

Mtb mainly infects macrophages (Mf) which need to be activated by the cellular IR for containing mycobacteria (Th1 pattern activation) (Russell, 2001; Hestvik et al., 2005; Jordao et al., 2008). Cytokines such as IFN-γ, secreted by T lymphocytes, and TNF-α are essential to achieve classical macrophage activation (M1) and intracellular pathogen elimination (Kaufmann, 2001; O'Garra et al., 2013). At the same time, an exacerbated IR and the ensuing excessive secretion of inflammatory mediators turn out to be detrimental to host tissues through immunopathological processes, which is quite pathognomonic of diseases of chronic nature like TB. In line with this, newly diagnosed TB patients (T0) show a marked consumption state together with a lower body mass index (BMI), in addition to an immune-endocrine-metabolic (IEM) imbalance (Santucci et al., 2011; Bottasso et al., 2013; Díaz et al., 2017). This mainly consists of increased circulating amounts of pro- and anti-inflammatory cytokines together with increased cortisol and lowered dehydroepiandrosterone (DHEA) values, partly associated with the degree of pulmonary involvement (Bottasso et al., 2013; Díaz et al., 2017; D'Attilio et al., 2018).

Within the broad array of regulatory processes which are likely to take place during Mtb infection, the contribution of the peroxisome proliferator-activated receptors (PPARs), which belong to the nuclear receptor superfamily, is worth exploring. PPARs are a family of 3 ligand-activated transcription factors: PPARα (NR1C1), PPARβ/δ NR1C2), and PPARγ (NR1C3). These PPARs are encoded by different genes but show similar structural features, which include an amino-terminal modulatory domain, a DNA binding domain, and a carboxyl-terminal ligand binding domain. All PPARs act as heterodimers with the retinoid X receptor (RXRs) and play important roles in the regulation of metabolic pathways, including those of lipid biosynthesis and glucose metabolism, as well as in a variety of cell functions: differentiation, proliferation, apoptosis pathways and inflammation (Blitek and Szymanska, 2017; Portius et al., 2017; Christofides et al., 2021).

PPAR ligands, in particular those of PPARα and PPARγ, inhibit the activation of inflammatory gene expression and can negatively interfere with proinflammatory transcription factor signaling pathways in vascular and inflammatory cells. Furthermore, PPAR levels are differentially regulated in a variety of inflammatory disorders in men, for which PPAR ligands may constitute promising therapies (Moraes et al., 2006). Evidence indicates that chronic metabolic diseases accompanied by immunological-endocrine disturbances, i.e., diabetes and metabolic syndrome, present a higher risk of infections together with a lower bactericidal capacity from the innate immune cells. In this regard, treatment with thiazolidinedione drugs like pioglitazone (synthetic PPARγ ligand), not only diminished the inflammation but also increased the capability of host cells to cope with pathogens, in addition to modulating hormone production and glucolipid homeostasis (Sharma et al., 2017). A study in a murine model of sepsis showed that treatment with the agonist pioglitazone improved mouse survival by enhancing the neutrophil bacterial clearance and promotion of an anti-inflammatory milieu at the site of infection (Ferreira et al., 2014). In the case of TB, some studies showed that mycobacterial infections coexist with an increased expression and activation of PPARγ at the Mf level which leads to changes in intracellular lipid homeostasis (foamy Mf) and its

activation profile, promoting an M2 pattern more favorable to Mtb survival (Almeida et al., 2012).

Given this background and considering the substantial role of IEM disturbances in TB pathophysiology, we sought to investigate the relationship of PPARγ with some IEM components in the setting of clinical pulmonary TB, at the time of diagnosis and throughout the course of specific treatment to get a better understanding on their implication in the processes dealing with disease development and resolution. We also carried out *in vitro* experiments in a macrophage cell line for a more in deep analysis of the reciprocal influences between PPARγ and glucocorticoids.

2 Materials and methods

2.1 Subjects

Thirty-nine adults who were diagnosed with lung TB based on clinical and radiological findings and identification of TB bacilli in sputum were enrolled and followed for up to nine months in a prospective cohort study of TB treatment. This observational cohort included patients with neither HIV coinfection nor multidrug-resistant TB. Patients had mild (n = 9), moderate (n = 15), or advanced (n = 15) disease according to the radiological findings, corresponding to previously described criteria (Mahuad et al., 2004).

Antituberculosis therapy consisted of six months of rifampicin and isoniazid, initially supplemented by two months of pyrazinamide and ethambutol. Among the 39 recruited patients, blood samples at all time points (see 3.1.1.1 Sample Collection) were available in 24 of them (mild = 2, moderate = 13, and severe = 9). Age-matched healthy controls (HCo, n = 24) living in the same area and without known contact with TB patients, were incorporated as controls. Exclusion criteria for all participants included pathologies affecting the hypothalamus-pituitary-thyroid or gonadal-axis, or direct compromise of the adrenal gland, pregnancy, contraceptive drugs, age under 18, or systemic or localized pathologies requiring treatment with corticosteroids or immunosuppressants. The study protocol was approved by the Ethical Committee of the Faculty of Medical Sciences, National University of Rosario (Resolution n° 6625/2018), and the Centenario Hospital of Rosario (Resolution n° 528). The study was conducted following the 1964 Helsinki declaration and its later amendments. All volunteers gave their written consent before participating in the study.

2.1.1 Sample collection

Blood samples were obtained from TB patients at the time of diagnosis (before initiation of the treatment, T0) and 2, 4, and 6 months (T2, T4, and T6) after starting the specific antituberculosis treatment (Global tuberculosis report 2021). Also, an additional sample was obtained three months after the end of treatment completion (T9). All samples were taken between 8:00 and 9:00 a.m. with and without EDTA and then centrifuged. Aprotinin (100U/mL; Aprotinin from bovine lung, Sigma) was added to the plasma shortly after collection and the samples were preserved at −80°C. One blood sample was obtained from age- and sex-matched HCo and processed in the same way (Mahuad et al., 2004; Díaz et al., 2017).

2.1.2 Mononuclear cell isolation

After blood centrifugation, the buffy coat was separated and diluted 1:1 in RPMI 1640 (Invitrogen) containing standard concentrations of L-glutamine, penicillin, and streptomycin (culture medium). The cell suspension was layered over a Ficoll-Paque (density 1.077, Amersham Biosciences) and centrifuged at 400 g for 30 min. From this column, PBMCs were obtained.

2.1.3 Flow cytometry

A sample of EDTA anticoagulated whole blood was incubated with BD Tritest CD4FITC/CD8PE/CD3PerCP reagent, another with CD3FITC/CD19PE, and the third one with CD45FITC/CD14PE (all reagents of BD Biosciences) and isotype controls, according to the manufacturer's instructions (Díaz et al., 2015). Stained cells were analyzed with a FACSAria II flow cytometer (BD Biosciences). The percentage of positive cells and the mean fluorescence intensity (arbitrary units) for a specific marker were calculated using FACSDiva software (BD Biosciences). For each sample, 30.000 events were recorded.

2.1.4 Evaluation of immunological mediators and hormones

Cytokine and hormone levels in plasma were measured by using commercial ELISA kits (BD Biosciences, IFN-γ, IL-6, detection limit -DL-: 4.7 and 2 pg/ml, respectively), or EIA assays (DRG Systems, DL: 2.5 and 0.108 ng/ml, for cortisol and DHEA, respectively).

2.1.5 RNA isolation, cDNA synthesis, and RT-qPCR

Total RNA was isolated from PBMCs using TRIzol (Invitrogen). RNA pellets were dissolved in Diethyl pyrocarbonate (DEPC) sterile water and stored at −80°C. RNA quantity and integrity were assessed as performed earlier (D'Attlio et al., 2011). cDNA was synthesized from 2 µg of total RNA by extension of oligo dT primers (Invitrogen) with M-MuLV reverse transcriptase (Thermo Fisher Scientific) in a final volume of 40 µl DEPC sterile water. cDNA was stored at −80°C until use. RT-qPCR was performed with the StepOnePlus (96-well) Real-Time PCR Systems (Applied Biosystems) using 3 µl of cDNA dilution, 0.4 µM of each primer, and 3 µl of 5x HOT FIREPol EvaGreen qPCR Mix Plus (Rox) (Solis BioDyne), the final volume of 15 µl. Thermal cycling conditions were as follows: 10 min at 95°C followed by 45 PCR cycles of denaturing at 95°C for 20 s, 30 s for annealing at 60°C, and 20 s for elongation at 72°C. Fluorescence readings were performed for 10 s at 80°C before each elongation step. To normalize the expression of every gene, the transcript of PPIA [peptidylprolyl isomerase A (Cyclophilin A)] was used as an endogenous control in each mononuclear cell sample (He et al., 2008). Serially diluted cDNA samples were used as relative external standards in each run, to make "The Relative Standard Curve Method" for the relative quantification of gene expression, as

10.3389/fcimb.2023.1067464

performed formerly (D'Attlio et al., 2011). Similarity and homogeneity of PCR products from samples were confirmed by automated melting curve analysis (StepOne Software, Applied Biosystems), which revealed the melting temperature values of the PCR products. Selected primers are detailed in Table 1. Data were expressed as fold change of the relative expression levels of the gene of interest normalized by the relative expression levels of PPIA.

2.2 Cell preparations

The characteristics of THP-1, a human monocytic leukemia cell line, have been described previously in detail (Tsuchiya et al., 1980). This cell line was grown in suspension cultures in Tissue Culture Medium RPMI-1640 supplemented with 10% of heat-inactivated fetal bovine serum and antibiotic (Penicillin-Streptomycin, Gibco, Invitrogen) at 37°C in 5% CO_2. THP-1 cells were cultured in complete RPMI-1640 containing 30 ng/ml phorbol-12-myristate-13-acetate (PMA, Sigma) and plated for differentiation to macrophages. Twenty-four hours later supernatants were removed and complete RPMI-1640 was added for 48 h before the stimulation.

2.2.1 Stimulation of macrophages with *M. tuberculosis* and treatment with cortisol and/or PPARγ agonist

Macrophages were cultured in quadruplicate in flat-bottomed 24-well dishes (4×10^5 cells/well in 0.6 mL) in RPMI 1640 (Gibco, Invitrogen) with 10% of heat-inactivated fetal bovine serum (Gibco, Invitrogen) and antibiotic (Penicillin-Streptomycin, Gibco, Invitrogen) and cultured for 24 h at 37°C in 5% CO_2, with or without the addition of *M. tuberculosis* strain H37Rv gamma irradiated (Mtbi; 8 µg/mL, Colorado University, USA), 15-Deoxy-$\Delta^{12,14}$-prostaglandin J_2 -15dPGJ$_2$- a PPARγ natural ligand (2 µM, Sigma) and/or physiological concentrations of cortisol (10^{-6} M, Sigma) (Mahuad et al., 2004). Stock 15dPGJ2 and cortisol solutions were prepared in ethanol. Thereafter, stock solutions were diluted in a culture medium to final concentrations. Treatment with 15dPGJ2 was performed 30 min before the addition of Mtbi and/or cortisol. In some cultures, RU486 (RU486 or Mifepristone 1 µM, Sigma-Aldrich), a cortisol receptor antagonist, was used 5 min before the addition of the hormone. Supernatants were collected to assess cytokine production and cells were preserved in TRIzol (Invitrogen) for mRNA extraction.

2.3 Statistical analysis

Statistical comparisons were performed by the Mann-Whitney U and Kruskal-Wallis followed by *post hoc* comparisons when applicable since some variables under analysis deviated from a normal distribution. Paired comparisons during treatment were done by the Friedman analysis of variance. Associations between variables were analyzed using the Spearman correlation test. A value of $p < 0.05$ was regarded as statistically significant.

3 Results

3.1 Features of study groups

There was no sex- or age-related differences and the frequency of Bacillus Calmette–Guerin vaccination between study groups, although the body mass index (BMI, weight/height^2) was significantly decreased in TB patients (Table 2). Newly diagnosed patients did not differ from controls in terms of erythrocyte counts (Table 3) but showed an increase in the leukocyte numbers ($p<0.05$) with a high percentage of neutrophils and low values of lymphocytes ($p<0.05$). Consequently, the ratio between the percentage of neutrophils and lymphocytes (NLR) was increased (Table 3), compatible with systemic inflammation (Song et al., 2021; Buonacera et al., 2022). From the second month of anti-TB treatment, these hematological variables reached values similar to those of the HCo. Eosinophils were found to increase during the specific treatment and remained high even after its termination (Table 3). With regards to erythrocyte sedimentation rate (ESR), TB cases displayed a significant increase at T0 and T2, further decreasing to values seen in HCo (Table 3). Levels of liver enzymes among treated patients remained within normal values (data not shown).

TABLE 1 RT-qPCR nucleotide primer sequence.

Transcript	Forward primer	Reverse primer	Size
CycA	CycA-F	CycA-R	101 bp
PPIA GeneID: 5478	5'-ggt cct ggc atc ttg tcc at-3'	5'-ttg ctg gtc ttg cca ttc ct-3'	
PPARγ	PPARγ-F	PPARγ-R	
NR1C3, GeneID: 5468	5'-ttt cag aaa tgc ctt gca gtg g-3'	5'-ctt tcc tgt caa gat cgc cct c-3'	222 bp
PPARα	PPARα-F	PPARα-R	
NR1C1, GeneID: 5465	5'-cct ttt tgt ggc tgc tat c-3'	5'-gtg gag tct gag CAC at t-3'	106 bp

TABLE 2 Main features of study groups.

	Study groups		
Parameters	HCo (n=26)	TB (n=24)	p
Age	50.5 (25.8 - 57.3)	45.0 (21.5 - 54.8)	ns
Sex (M/F)	24/2	22/2	ns
BMI	27.4 (25.1 - 30.8)	19.9 (18.3 - 23.8)	p<0.001
BCG (%)	95%	80%	ns

Data are represented as median and interquartile ranges. BMI, body mass index (weight/height^2); BCG, Bacillus Calmette–Guerin vaccination; HCo, healthy controls; TB, patients with pulmonary tuberculosis; ns, not significant.

10.3389/fcimb.2023.1067464

TABLE 3 Quantification of erythrocytes, hemoglobin, percentage of hematocrit, leukocytes, leukocyte formula, platelets, erythrocyte sedimentation rate (ESR), and the ratio between the percentage of neutrophils and lymphocytes (NLR) in patients with TB and healthy controls.

Parameters	Study groups					
	HCo (n=26)	TB (n=24)				
		T0	T2	T4	T6	T9
Red blood cells	5.1	4.9	5.1	5,0	5,0	5.1
(106/µl) [rv: 3.5-5.5]	(4.9-5.2)	(4.5-5.6)	(4.9-5.6)	(4.7-5.3)	(4.6-5.3)	(4.7-5.5)
HGB (g/dl)	14.8	13.7 *	14.6 #	14.5 #	14.7	15.1 #
[rv: 11-16]	(14.3-15.5)	(11.9-14.5)	(13.8-15.3)	(12.9-15.1)	(13.5-15.3)	(14.1-15.5)
Hematocrit (%)	44.1	41.7 *	44.0 #	43.1	43.5	44.5 #
[rv: 35-50]	(42.3-44.9)	(37.5-44.8)	(41.8-45.8)	(39.7-44.9)	(40.5-45.9)	(41.6-47.1)
White blood cells	7.2	7.9 *	5.7 #	5.6 #	7.4 #	7.2 #
(103/µl) [rv: 4-9]	(5.4-8.1)	(6.8-10.6)	(4.8-7.2)	(4.8-8.9)	(5.2-8.0)	(5.6-8.9)
Neutrophils (%)	57.8	71.1 *	57.5 #	53.0 #	58.6 #	58.7 #
[rv: 45-65]	(52.0-63.3)	(56.0-73.9)	(51.5-62.7)	(44.9-61.2)	(46.3-60.6)	(47.1-62.9)
Eosinophils (%)	2.6	2,0	3.2 #	4.0 *#	4.0 *#	4.0 *#
[rv: 0-4]	(2.0-3.5)	(0.7-3.5)	(2.3-6.5)	(2.4-5.7)	(2.2-5.4)	(2.7-6.3)
Basophils (%)	0.8	0.5	0.8	0.9	0.9	1,0
[rv: 0-1]	(0.4-1.0)	(0.0-1.0)	(0.6-1.4)	(0.4-1.3)	(0.5-1.4)	(0.7-1.3)
Lymphocytes (%)	28.1	16.5 *	25.6 #	30.1 #	27.4 #	25.6 #
[rv: 25-35]	(25.0-35.2)	(13.7-25.3)	(19.2-33.0)	(24.7-37.4)	(23.3-34.8)	(22.6-34.8)
Monocytes (%)	8.1	9.8	9.5	9.1	9.4	9.5
[rv: 0-12]	(6.8-10.0)	(7.2-13.0)	(7.4-11.6)	(8.1-12.6)	(6.9-11.2)	(8.2-10.5)
Platelets (103/µl)	236.5	323.0 *	253.0 #	220.5 #	215.0 #	248.0 #
[rv: 150-400]	(207.8-289.5)	(259.0-417.0)	(224.0-352.0)	(202.5-307.5)	(190.5-277.0)	(199.0-275.0)
ERS (mm/1°h)	5,0	44.0 *	11.0 *#	5.0 #	6.0 #	6.0 #
[rv: 1-15]	(2.0-11.0)	(17.3-75.8)	(4.5-21.5)	(4.0-18.0)	(3.0-13.0)	(2.8-10.5)
Neutrophils/lymphocytes	2.1	4.5 *	2.2 #	1.6 #	2.1 #	2.4 #
ratio (NLR)	(1.4 - 2.6)	(2.1 - 5.2)	(1.5 - 3.2)	(1.2 - 2.5)	(1.2 - 2.6)	(1.3 - 2.7)

Data are represented as median and interquartile ranges. HCo, healthy controls; TB, patients with pulmonary tuberculosis; T0, time at diagnosis; T2, T4, and T6, 2, 4, and 6 months following the initiation of anti-bacillary treatment; T9, 3 months following treatment completion. HGB, hemoglobin; ESR, erythrocyte sedimentation rate; NLR, the ratio between the percentage of neutrophils and lymphocytes; rv, reference values. *p<0.05 vs. HCo; #p<0.05 vs. T0.

In line with the decreased lymphocyte percentages, flow cytometry studies showed a decline in the percentages of CD4+ and CD8+ T lymphocytes at time 0 (Figures 1A, B, respectively), with their values starting to increase following the initiation of anti-TB treatment to the levels recorded in HCo. There were no between-group differences in B-lymphocyte numbers (Figure 1C), but the monocyte numbers did increase in TB patients either at diagnosis or during the T6 and T9 time point evaluations (Figure 1D, $p < 0.05$ vs. HCo in all cases).

3.1.1 PPARγ and PPARα expression in PBMC of TB patients

Regarding the expression levels of mRNA-PPARγ in PBMC from patients with TB, values were higher at T0 compared to those recorded in HCo (Figure 2A), in turn, these increases were found related to the degree of lung involvement (Figure 2B). After two months of specific treatment, PPARγ transcripts levels, decreased to the values found in HCo ($p < 0.05$ vs. T0, Figure 3). On the other hand, mRNA-PPARα levels did not differ between TB patients and HCo (Figure 2C).

Concerning the immune-endocrine profile, newly diagnosed TB patients had increased plasma levels of IFN-γ, IL-6, and cortisol (Figures 4A–C respectively). The latter was positively correlated with PPARγ mRNA levels (Figure 5A, $r = 0.767$, $p < 0.01$). At the same time, we also found a negative correlation between PPARγ mRNA levels and LTCD4+ (Figure 5B, $r = -0.571$, $p < 0.05$). We have formerly demonstrated that inflammatory mediators during specific anti-TB treatment reach values similar to those of HCo,

10.3389/fcimb.2023.1067464

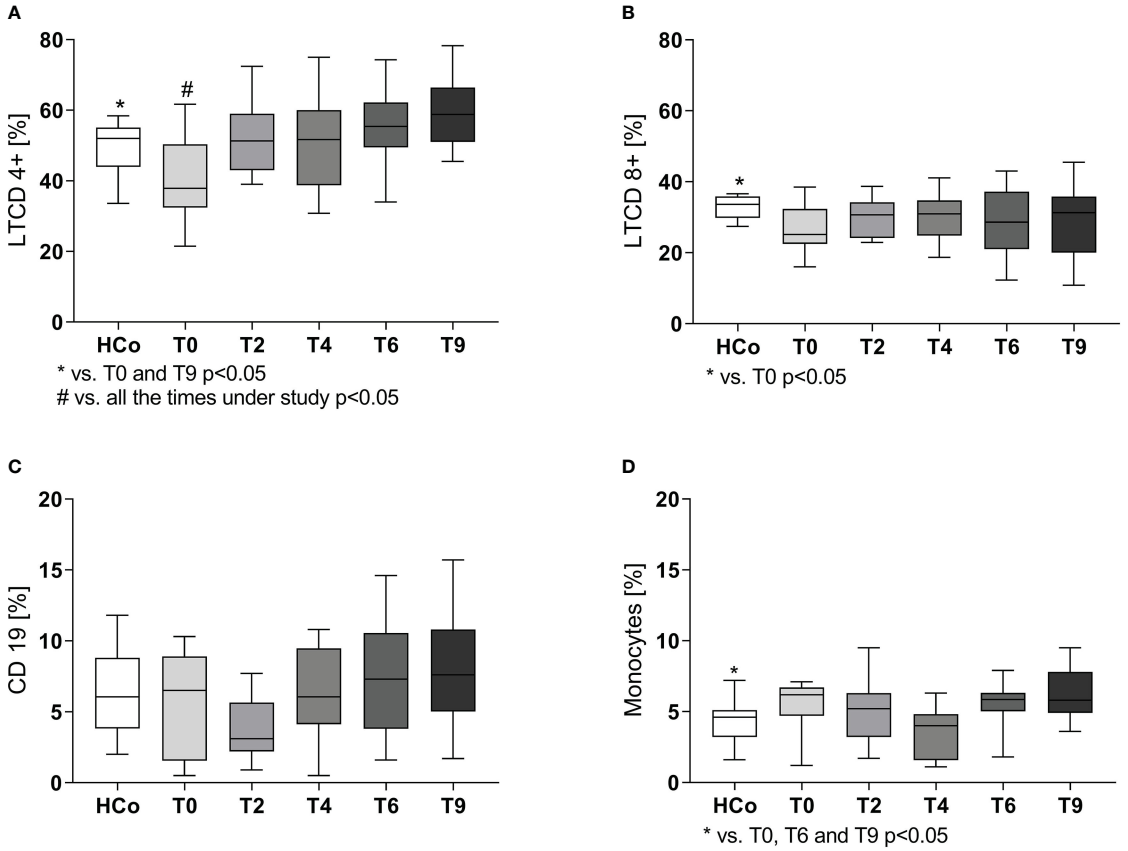

FIGURE 1
CD4+ **(A)**, CD8+ **(B)**, B **(C)** lymphocytes, and monocytes **(D)** populations in TB patients during specific treatment. Boxes represent the median (line) and interquartile range, with minimal and maximum values. HCo (n = 24): healthy controls; T0: time at diagnosis; T2, T4, and T6: 2, 4, and 6 months following the initiation of anti-bacillary treatment; T9: 3 months following treatment completion. Twenty-four TB patients were studied at all time points. Multiple comparisons were assessed through Kruskal–Wallis test with Dunn's multiple comparison testing and paired comparisons throughout treatment was done by the Friedman analysis of variance.

while Cortisol remains elevated throughout treatment (Díaz et al., 2017).

3.1.2 PPARγ transcript expression of THP1-Mf cells stimulated with Mtbi and treated with cortisol and agonist of PPARγ

Following the search for the presence of PPARγ during active TB and its relationship with compounds from the immune-endocrine response we next wished to explore the potential contribution of PPARγ to the macrophage function, in terms of cytokine production, which constitutes a relevant issue during Mtb infection. As depicted in Figure 6, stimulation of THP1-Mf cells with Mtbi increased the expression of PPARγ (panel A) as well as the production of IL-1β and IL-10 (panels B and C, respectively). Further experiments by exposing cells to a PPARγ agonist resulted in decreased levels of both cytokines (panels B and C) together with increased amounts of PPARγ transcripts (Figure 6A).

The Mtbi-driven increased synthesis of IL-1β and IL-10 was no longer seen when adding cortisol to stimulated cultures (Figures 6B, C), without significant changes in the expression levels of mRNA-PPARγ (Figure 6A). In cultures undergoing Mtbi stimulation plus cortisol treatment, the addition of PPARγ agonist increased the receptor transcript expression (Figure 6A), whereas IL-1β and IL-10 levels appeared respectively decreased and increased (Figures 6B, C). There were no differences in mRNA-PPARγ levels when comparing cultures treated with agonists alone or left untreated (data not shown).

An additional experiment by treating cells with the cortisol receptor antagonist, RU486, showed that such treatment reversed the cortisol-reduced production of IL-1β from Mtbi-stimulated cultures (Figure 7). Likewise, there were no differences in the expression of PPARγ transcripts in culture counterparts exposed to the cortisol antagonist (data not shown).

4 Discussion

The control of an infectious process depends on the type and magnitude of the defensive response that appears beneficial during the initial phase but may become harmful if prolonged due to pathogen persistence, as is the case of TB. Because of its chronic nature, TB coexists with an immuno-endocrine-metabolic imbalance and excessive inflammatory reactions accounting for the host impairment seen during the progressive disease (Bottasso

10.3389/fcimb.2023.1067464

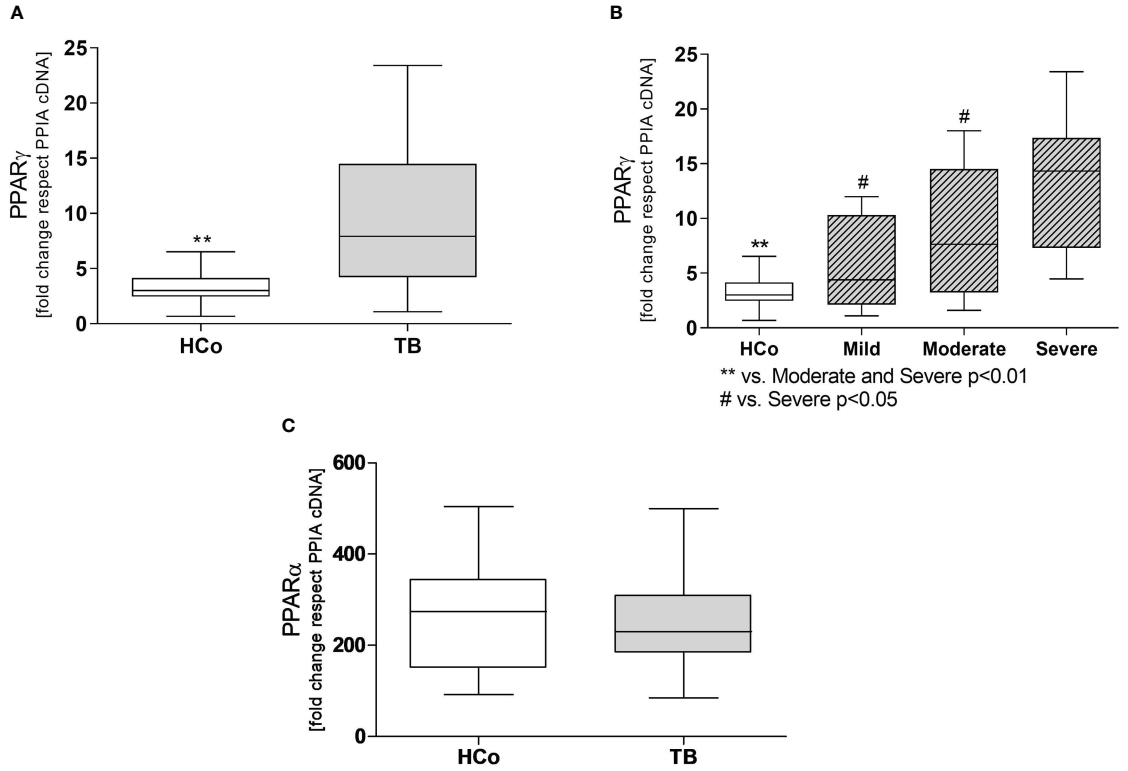

FIGURE 2
Expression levels of mRNA for PPARγ **(A)** and PPARα **(C)** in PBMC from HCo and TB patients. PPARγ mRNA expression in TB patients with different degrees of pulmonary involvement **(B)**. Boxes represent the median (line) and interquartile range, with minimal and maximum values. HCo (n = 24): healthy controls; TB (n = 39): patients with tuberculosis at the time of diagnosis. Comparisons between the two groups were made by the Mann-Whitney U test, **p<0.01. Multiple comparisons were assessed through Kruskal–Wallis test with Dunn's multiple comparison testing **(B)**.

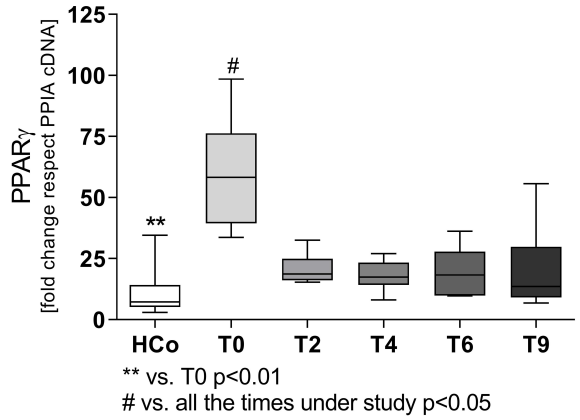

FIGURE 3
Expression levels of mRNA for PPARγ in patients with TB undergoing specific treatment. Boxes represent the median (line) and interquartile range, with minimal and maximum values. HCo (n = 24): healthy controls; T0: time at diagnosis; T2, T4, and T6: 2, 4, and 6 months following the initiation of anti-bacillary treatment; T9: 3 months following treatment completion. A total of 24 TB patients were studied at all time points. Multiple comparisons were assessed through Kruskal–Wallis test with Dunn's multiple comparison testing, and paired comparisons during treatment were done by the Friedman analysis of variance.

et al., 2013). In fact, at the time of diagnosis, TB patients showed a decrease in their BMI, an excessive pro-inflammatory response (Díaz et al., 2017), together with an increased NLR. The latter may be a surrogate reflecting the balance between two facets of the defensive reaction: acute and chronic inflammation (Song et al., 2021) coexisting at the same time. Another feature of the inflammatory response during TB was the increased percentage of eosinophils, at T0 and during the specific treatment, which may be related to the recruitment of these cells to exert a protective role against infection (Prakash Babu et al., 2019; Bohrer et al., 2021).

The control of the proinflammatory response requires not only intrinsic regulatory mechanisms from both innate and adaptive immune systems but also the ones extrinsic to the immune system, for instance, the activation of the hypothalamic-pituitary-adrenal axis leading to cortisol production (Kaufmann, 2001) as well as other regulators of inflammatory or immune responses like PPARs.

Within this setting, we here provide novel evidence that PBMC from newly diagnosed patients with pulmonary TB has an increased expression of PPARγ transcript, related to the degree of lung involvement, proinflammatory plasma mediators, and cortisol levels. The increased PPARγ expression coupled with elevated plasma cortisol concentrations may mirror a regulatory attempt for the substantial inflammatory response that patients show at the

10.3389/fcimb.2023.1067464

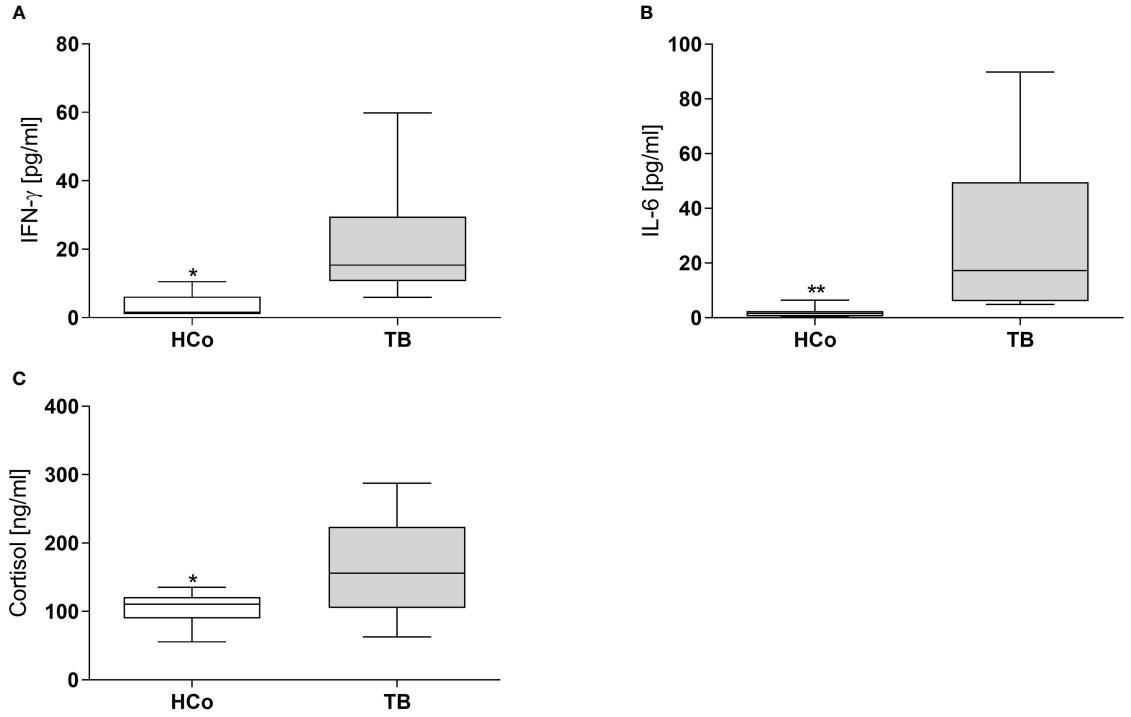

FIGURE 4
Plasma levels of IFN-γ, IL-6, and Cortisol in HCo and TB patients at the time of diagnosis. Boxes represent the median (line) and interquartile range, with minimal and maximum values. HCo (n = 24): healthy controls; TB (24): patients with tuberculosis. Comparisons between groups were made by the Mann-Whitney U test. *p<0.05; **p<0.01.

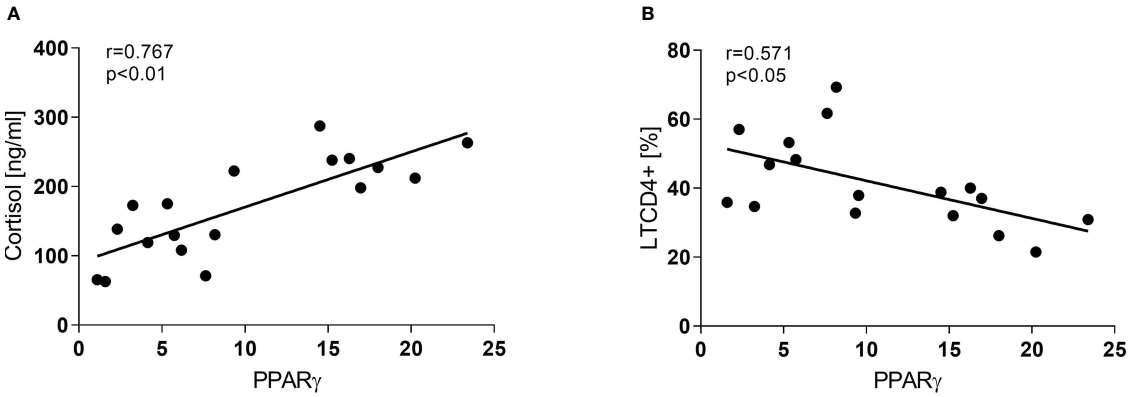

FIGURE 5
Correlation between PPARγ and Cortisol **(A)** and LTCD4+ **(B)** in TB patients at the time of diagnosis. Associations between variables were analyzed using the Spearman correlation test.

time of diagnosis, aimed to ameliorate the tissue damage and return to homeostasis. Without being mutually exclusive, the concomitant rise of plasma cortisol levels and PPARγ transcripts in relation to disease severity may also reflect the degree of immuno-endocrine-metabolic imbalance. Extending our former results that plasma levels of proinflammatory mediators started to decrease by the second month of specific treatment (Díaz et al., 2017), we now show that PPARγ transcripts also decay by the same time point. Cortisol levels remained elevated throughout treatment (Díaz et al., 2017), suggesting a higher role of cortisol immunomodulation during disease recovery (Díaz et al., 2017).

While the changes in the peripheral compartment may not be an accurate reflection of the response that takes place at the injury site (D'Attilio et al., 2013), they bear some relationship with the extent of lung compromise, as specific anti-TB treatment induced a significant drop of PPARγ transcript expression and in proinflammatory mediators, possibly related to the lower bacterial burden (Sabiiti et al., 2020; Osei-Wusu et al., 2021).

10.3389/fcimb.2023.1067464

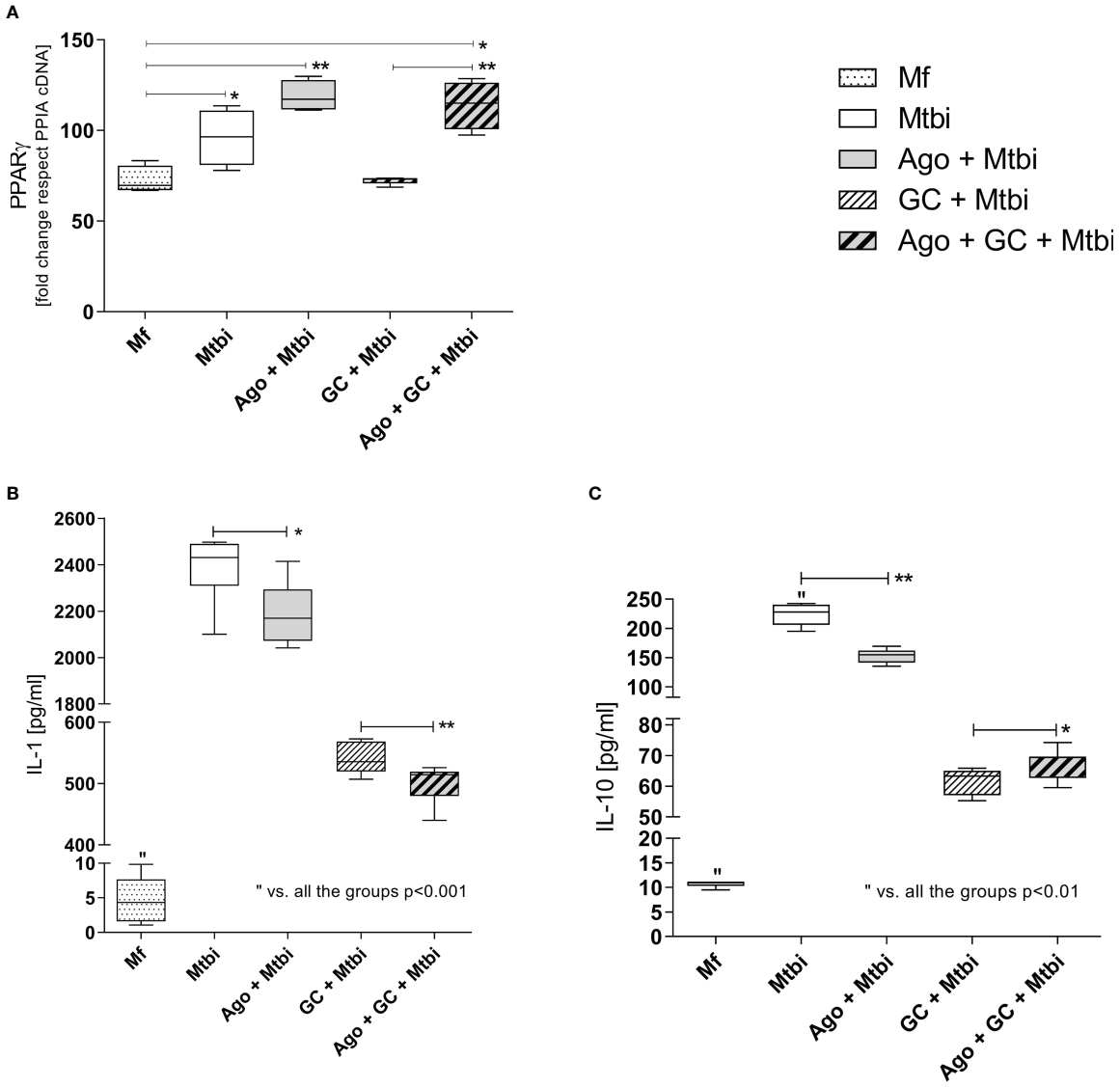

FIGURE 6
PPARγ transcript expression **(A)**, and IL-1β **(B)** and IL-10 **(C)** levels in supernatants of THP1-Mf cells stimulated with Mtbi and treated with cortisol and/or agonist of PPARγ. Boxes represent the median (line) and interquartile range, with minimal and maximum values (n=4). Mtbi: Mycobacterium tuberculosis strain H37Rv killed by γ radiation; Ago: PPARγ agonist, 15-Deoxi-Δ12,14 Prostaglandin J2 (15dPGJ2) 2μM; GC: cortisol 10-6M. Multiple comparisons were assessed through Kruskal–Wallis test with Dunn's multiple comparison testing. *p<0.05; **p<0.01.

There is evidence that PPARγ expression following TCR stimulation of T cells negatively regulates their activation by inhibiting the nuclear factor of activated T-cells (NFAT) and subsequent IL-2 production (Clark et al., 2000; Choi and Bothwell, 2012). Yang and col. also showed that the activation of this receptor in human T cells reduced IL-2 production and proliferation (Yang et al., 2000). This may help to explain our findings about the negative correlation between PPARγ and LTCD4 + cells seen in TB patients at the time of diagnosis, wherein the former was found to be significantly increased and the latter decreased. Further studies are needed to elucidate the appropriate meaning of this association. Whether PPARγ activation is also likely to promote the biased Th2 response seen in progressive TB (Stark et al., 2021) also remains to be established.

PPARs can be expressed in a variety of tissues and cell types including Mf (Chinetti et al., 1998; Rigamonti et al., 2008). These cells are among the first ones to encounter Mtb and play an important role in regulating the immune response against this pathogen. In Mf, PPARγ would act by modifying the expression of different inflammatory genes, modulating cell differentiation and activation through the trans-repression of different transcription factors such as NF-κB, AP-1, and STATs (Ricote et al., 1999), as well as diminishing the respiratory burst (von Knethen and Brune, 2002).

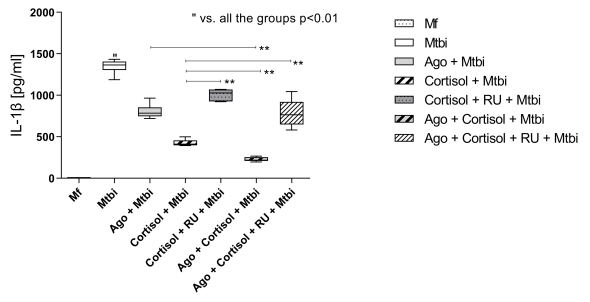

FIGURE 7
IL-1β levels in supernatants of THP1-Mf cells stimulated with Mtbi and treated with cortisol and/or agonist of PPARγ and antagonist of cortisol. Boxes represent the median (line) and interquartile range, with minimal and maximum values (n=4). Mtbi: Mycobacterium tuberculosis strain H37Rv killed by γ radiation; Ago: PPARγ agonist, 15-Deoxi-Δ12,14 Prostaglandin J2 (15dPGJ2) 2μM; RU486: glucocorticoid receptor antagonist, Mifepristone 1μM; GC: cortisol 10-6M. Multiple comparisons were assessed through Kruskal–Wallis test with Dunn's multiple comparison testing. **p<0.01.

The expression of PPARs can also be increased upon pathogen exposures (Penas et al., 2013). In this regard, up-regulation of PPARγ expression on Mf after infection by *Mycobacterium bovis* (BCG), Mtb, *Listeria monocytogenes*, and *Mycobacterium leprae* has been reported (Straub et al., 2002; Chan et al., 2010; Rajaram and Brooks, 2010; Mahajan et al., 2012). Almeida et al. demonstrated that infection with Mtb increases the expression and activation of PPARγ leading to an enhanced formation of lipid droplets (foamy Mf), in addition to modifying the activation profile of Mf (inhibition of proinflammatory cytokines) inducing an M2 profile (Almeida et al., 2012). Furthermore, Guerrini et al. showed that during Mtb infection, the development of Mf into foam cells involves the activation of signaling pathways leading to intracellular triglycerides accumulation, driven by TNF receptor signaling and the downstream activation of the caspase cascade and the mammalian target of rapamycin complex 1 (mTORC1) (Guerrini et al., 2018). Both mechanisms favor mycobacterial survival.

Regarding PPARγ, recognition of Mtb by Mf mannose receptor activates mitogen-activated protein kinase (MAPK)-p38-cytosolic phospholipase A2 (cPLA2), resulting in hydrolysis and release of arachidonic acid from the plasma membrane to generate prostaglandin E2 (PGE2) and cyclopentenone prostaglandins (15-d-PGJ2) (Rajaram and Brooks, 2010). These two compounds are natural ligands of PPARγ, for which they are likely to activate the receptor pathways in these cells. In line with this, present results showed that Mtb stimulation of THP1-Mf significantly increased pro and anti-inflammatory cytokines (IL-1β and IL-10) as well as PPARγ expression, whereas the activation of this receptor by a specific natural agonist diminished the expression of these cytokines in stimulated Mf at the early step of immune response (Ricote et al., 1999). Stimulated cultures treated with cortisol together with the PPARγ agonist showed the lowest levels of the proinflammatory cytokine IL-1β, suggestive of intercommunication between both immunomodulatory mechanisms. However, treatment with RU486 only reversed the inhibitory effect of GC without modifying the one exerted by PPARγ activation. This suggests that both effects may be mediated through different intracellular pathways, as reported by Yamamoto et al. in a mouse model of acute inflammation (Yamamoto et al., 2014). Although in studies employing colonic epithelial cells, cortisol was likely to control the expression of PPARγ (Bouguen et al., 2014).

In non-infectious chronic diseases, i.e., metabolic syndrome or diabetes, the use of PPARγ agonists, like TZDs (including rosiglitazone and pioglitazone), showed some effectiveness in parallel to side effects such as increased weight gain, fluid retention, bone loss, congestive heart failure, etc. (50), which led to its discontinuation as was the case of rosiglitazone (51). This stimulated the search for new antagonists exempted from such adverse effects. Our results along with the relevance of lipid metabolism in the pathogenesis of TB and Mtb survival, as well as the fact that PPARγ deletion in pulmonary Mfs improved the course of murine tuberculosis (52), provide no evidence to think about the potential use of a PPARγ agonist in TB.

In getting a better understanding of the role of PPARγ in the host-mycobacteria relationship, our study provides the first evaluation of the expression of PPARγ in PBMC from TB patients according to the extent of lung damage and specific treatment. Results provide a stimulating background for further analysis of the interrelation between PPARs and the immune-endocrine framework of this particular disease.

Data availability statement

The raw data supporting the conclusions of this article will be made available by the authors, without undue reservation.

Ethics statement

The studies involving human participants were reviewed and approved by the study protocol by the Ethical Committee of the Faculty of Medical Science, National University of Rosario (Resolution n° 44405/0005) and the Centenario Hospital of Rosario (Resolution n° 528). The patients/participants provided their written informed consent to participate in this study.

Author contributions

All authors have contributed to this project. All authors have read and agreed to the published version of the manuscript.

Funding

This work was supported by grants from Fund for Scientific and Technological Research–FONCyT– (PICT-2018-02375) and Facultad de Ciencias Médicas, Universidad Nacional de Rosario, Rosario, Argentina.

Acknowledgments

The authors thank Marisa Derio for her technical assistance and Asociación Cooperadora de la Facultad de Ciencias Médicas, Rosario, Argentina.

Conflict of interest

The authors declare that the research was conducted in the absence of any commercial or financial relationships that could be construed as a potential conflict of interest.

The handling editor VEG declared being in a different faculty from the affiliation they share with the author(s) ACC, NBG, FNP at the time of review.

Publisher's note

All claims expressed in this article are solely those of the authors and do not necessarily represent those of their affiliated organizations, or those of the publisher, the editors and the reviewers. Any product that may be evaluated in this article, or claim that may be made by its manufacturer, is not guaranteed or endorsed by the publisher.

References

Almeida, P. E., Carneiro, A. B., Silva, A. R., and Bozza, P. T. (2012). PPARgamma expression and function in mycobacterial infection: roles in lipid metabolism, immunity, and bacterial killing. *PPAR Res.* 2012. doi: 10.1155/2012/383829

(2019). "The paradigm shift 2018-2022," in *Global plan to end TB: 2018-2022*. Geneva, Switzerland: Global Health Campus Chemin du Pommier 40 1218 Le Grand-Saconnex Available at: https://www.stoptb.org/sites/default/files/GPR_2018-2022_Digital.pdf.

Global tuberculosis report 2022. Available at: https://www.who.int/teams/global-tuberculosis-programme/tb-reports/global-tuberculosis-report-2022.

Global tuberculosis report 2021. Available at: https://www.who.int/teams/global-tuberculosis-programme/tb-reports/global-tuberculosis-report-2021.

Blitek, A., and Szymanska, M. (2017). Peroxisome proliferator-activated receptor (PPAR) isoforms are differentially expressed in peri-implantation porcine conceptuses. *Theriogenology.* 101, 53–61. doi: 10.1016/j.theriogenology.2017.06.013

Bohrer, A. C., Castro, E., Hu, Z., Queiroz, A. T. L., Tocheny, C. E., Assmann, M., et al. (2021). Eosinophils are part of the granulocyte response in tuberculosis and promote host resistance in mice. *J. Exp. Med.* 218 (10). doi: 10.1084/jem.20210469

Bottasso, O., Bay, M. L., Besedovsky, H., and del Rey, A. (2013). Adverse neuro-immune-endocrine interactions in patients with active tuberculosis. *Mol. Cell Neurosci.* 53, 77–85. doi: 10.1016/j.mcn.2012.11.002

Bouguen, G., Langlois, A., Djouina, M., Branche, J., Koriche, D., Dewaeles, E., et al. (2014). Intestinal steroidogenesis controls PPARγ expression in the colon and is impaired during UC. *Gut* 64, 1–10. doi: 10.1136/gutjnl-2014-307618

Buonacera, A., Stancanelli, B., Colaci, M., and Malatino, L. (2022). Neutrophil to lymphocyte ratio: an emerging marker of the relationships between the immune system and diseases. *Int. J. Mol. Sci.* 23 (7). doi: 10.3390/ijms23073636

Chan, M. M., Evans, K. W., Moore, A. R., and Fong, D. (2010). Peroxisome proliferator-activated receptor (PPAR): balance for survival in parasitic infections. *J. BioMed. Biotechnol.* 2010, 828951. doi: 10.1155/2010/828951

Chinetti, G., Griglio, S., Antonucci, M., Torra, I., Delerive, P., Majd, Z., et al. (1998). Activation of proliferator-activated receptors alpha and gamma induces apoptosis of human monocyte-derived macrophages. *J. Biol. Chem.* 273 (40), 25573–25580. doi: 10.1074/jbc.273.40.25573

Choi, J. M., and Bothwell, A. L. M. (2012). The nuclear receptor PPARs as important regulators of T-cell functions and autoimmune diseases. *Molecules Cells* 33, 217–222. doi: 10.1007/s10059-012-2297-y

Christofides, A., Konstantinidou, E., Jani, C., and Boussiotis, V. A. (2021). The role of peroxisome proliferator-activated receptors (PPAR) in immune responses. *Metabolism* 114:154338. doi: 10.1016/j.metabol.2020.154338

Clark, R. B., Bishop-Bailey, D., Estrada-Hernandez, T., Hla, T., Puddington, L., and Padula, S. J. (2000). The nuclear receptor PPARγ and immunoregulation: PPARγ mediates inhibition of helper T cell responses. *J. Immunol.* 164 (3), 1364–1371. doi: 10.4049/jimmunol.164.3.1364

D'Attilio, L., Díaz, A., Santucci, N., Bongiovanni, B., Gardeñez, W., Marchesini, M., et al. (2013). Levels of inflammatory cytokines, adrenal steroids, and mRNA for GRα, GRβ and 11βHSD1 in TB pleurisy. *Tuberculosis.* 93 (6), 635–641. doi: 10.1016/j.tube.2013.07.008

D'Attilio, L., Santucci, N., Bongiovanni, B., Bay, M. L., and Bottasso, O. (2018). Tuberculosis, the disrupted immune-endocrine response and the potential thymic repercussion as a contributing factor to disease physiopathology. *Front. Endocrinol. (Lausanne).* 9, 214. doi: 10.3389/fendo.2018.00214

D'Attlio, L., Trini, E., Bongiovanni, B., Dídoli, G., Gardeñez, W., Nannini, L. J., et al. (2011). mRNA expression of alpha and beta isoforms of glucocorticoid receptor in peripheral blood mononuclear cells of patients with tuberculosis and its relation with components of the immunoendocrine response. *Brain Behav. Immun.* 25 (3), 461–467. doi: 10.1016/j.bbi.2010.11.006

Díaz, A., Bongiovanni, B., D'Attilio, L., Santucci, N., Dídoli, G., Fernández R del, V., et al. (2017). The clinical recovery of tuberculosis patients undergoing specific treatment is associated with changes in the immune and neuroendocrine responses. *Pathog. Dis.* 75 (7). doi: 10.1093/femspd/ftx087

Díaz, A., Santucci, N., Bongiovanni, B., Attilio, L. D., Massoni, C., Lioi, S., et al. (2015). Increased frequency of CD4+ CD25+ FoxP3+ T regulatory cells in pulmonary tuberculosis patients undergoing specific treatment and its relationship with their immune-endocrine profile. *J. Immunol. Res.* 2015, 985302. doi: 10.1155/2015/985302

Ernst, J. D. (2012). The immunological life cycle of tuberculosis. *Nat. Rev. Immunol.* 12 (8), 581–591. doi: 10.1038/nri3259

Ferreira, A. E., Sisti, F., Sônego, F., Wang, S., Filgueiras, L. R., Brandt, S., et al. (2014). PPAR-γ/IL-10 axis inhibits MyD88 expression and ameliorates murine polymicrobial sepsis. *J. Immunol.* 192 (5), 2357–2365. doi: 10.4049/jimmunol.1302375

Guerrini, V., Prideaux, B., Blanc, L., Bruiners, N., Arrigucci, R., Singh, S., et al. (2018). Storage lipid studies in tuberculosis reveal that foam cell biogenesis is disease-specific. *PloS Pathog.* 14 (8). doi: 10.1371/journal.ppat.1007223

He, J., Sandford, A., Wang, I., Stepaniants, S., Knight, D., Kicic, A., et al. (2008). Selection of housekeeping genes for real-time PCR in atopic human bronchial epithelial cells. *Eur. Respir. J.* 32 (3), 755–762. doi: 10.1183/09031936.00129107

Hestvik, A. L. K., Hmama, Z., and Av-Gay, Y. (2005). Mycobacterial manipulation of the host cell. *FEMS Microbiol. Rev.* 29 (5), 1041–1050. doi: 10.1016/j.femsre.2005.04.013

Jordao, L., Bleck, C. K. E., Mayorga, L., Griffiths, G., and Anes, E. (2008). On the killing of mycobacteria by macrophages. *Cell Microbiol.* 10 (2), 529–548. doi: 10.1111/j.1462-5822.2007.01067.x

Kaufmann, S. H. (2001). How can immunology contribute to the control of tuberculosis? *Nat. Rev. Immunol.* 1 (1), 20–30. doi: 10.1038/35095558

Mahajan, S., Dkhar, H. K., Chandra, V., Dave, S., Nanduri, R., Janmeja, A. K., et al. (2012). Mycobacterium tuberculosis modulates macrophage lipid-sensing nuclear receptors PPARγ and TR4 for survival. *J. Immunol.* 188 (11), 5593–5603. doi: 10.4049/jimmunol.1103038

Mahuad, C., Bay, M. L., Farroni, M. A., Bozza, V., Del Rey, A., Besedovsky, H., et al. (2004). Cortisol and dehydroepiandrosterone affect the response of peripheral blood mononuclear cells to mycobacterial antigens during tuberculosis. *Scand. J. Immunol.* 60 (6), 639–646. doi: 10.1111/j.0300-9475.2004.01514.x

Moraes, L. A., Piqueras, L., and Bishop-Bailey, D. (2006). Peroxisome proliferator-activated receptors and inflammation. *Pharmacol. Ther.* 110 (3), 371–385. doi: 10.1016/j.pharmthera.2005.08.007

O'Garra, A., Redford, P. S., McNab, F. W., Bloom, C. I., Wilkinson, R. J., and Berry, M. P. R. (2013). The immune response in tuberculosis. *Annu. Rev. Immunol.* 31 (1), 475–527. doi: 10.1146/annurev-immunol-032712-095939

Osei-Wusu, S., Morgan, P., Asare, P., Adams, G., Musah, A. B., Siam, I. M., et al. (2021). Bacterial load comparison of the three main lineages of mycobacterium tuberculosis complex in West Africa. *Front. Microbiol.* 12, 3176. doi: 10.3389/fmicb.2021.719531

Penas, F., Mirkin, G. A., Hovsepian, E., Cevey, Á, Caccuri, R., Sales, M. E., et al. (2013). PPARγ ligand treatment inhibits cardiac inflammatory mediators induced by infection with different lethality strains of trypanosoma cruzi. *Biochim. Biophys. Acta* 1832 (1), 239–248. doi: 10.1016/j.bbadis.2012.08.007

Portius, D., Sobolewski, C., and Foti, M. (2017). MicroRNAs-dependent regulation of PPARs in metabolic diseases and cancers. *PPAR Res.* 2017, 1–19. doi: 10.1155/2017/7058424

Prakash Babu, S., Narasimhan, P. B., and Babu, S. (2019). Eosinophil polymorphonuclear leukocytes in TB: what we know so far. *Front. Immunol.* 10, 2639. doi: 10.3389/fimmu.2019.02639

Rajaram, M., and Brooks, M. (2010). Mycobacterium tuberculosis activates human macrophage peroxisome proliferator-activated receptor γ linking mannose receptor recognition to regulation of immune. *J. Immunol.* 185 (2), 929–942. doi: 10.4049/jimmunol.1000866

Ricote, M., Huang, J., Welch, J., and Glass, C. (1999). The peroxisome proliferator-activated receptor(PPARgamma) as a regulator of monocyte/macrophage function. *J. Leukoc. Biol.* 66 (5), 733–739. doi: 10.1002/jlb.66.5.733

Rigamonti, E., Fontaine, C., Lefebvre, B., Duhem, C., Lefebvre, P., Marx, N., et al. (2008). Induction of CXCR2 receptor by peroxisome proliferator-activated receptor gamma in human macrophages. *Arterioscler. Thromb. Vasc. Biol.* 28 (5), 932–939. doi: 10.1161/ATVBAHA.107.161679

Russell, D. G. (2001). Mycobacterium tuberculosis: here today, and here tomorrow. *Nat. Rev. Mol. Cell Biol.* 2 (8), 569–577. doi: 10.1038/35085034

Sabiiti, W., Azam, K., Charles, E., Farmer, W., Kuchaka, D., Mtafya, B., et al. (2020). Tuberculosis bacillary load, an early marker of disease severity: the utility of tuberculosis molecular bacterial load assay. *Thorax.* 75 (7), 606–608. doi: 10.1136/thoraxjnl-2019-214238

Santucci, N., D'Attilio, L., Kovalevski, L., Bozza, V., Besedovsky, H., del Rey, A., et al. (2011). A multifaceted analysis of immune-endocrine-metabolic alterations in patients with pulmonary tuberculosis. *PloS One* 6 (10), 1–8. doi: 10.1371/journal.pone.0026363

Sharma, M., Mohapatra, J., Malik, U., Nagar, J., Chatterjee, A., Ramachandran, B., et al. (2017). Effect of pioglitazone on metabolic features in endotoxemia model in obese diabetic db/db mice. *J. Diabetes.* 9 (6), 613–621. doi: 10.1111/1753-0407.12450

Song, M., Graubard, B. I., Rabkin, C. S., and Engels, E. A. (2021). Neutrophil-to-lymphocyte ratio and mortality in the united states general population. *Sci. Rep.* 11 (1), 1–9. doi: 10.1038/s41598-020-79431-7

Stark, J. M., Coquet, J. M., and Tibbitt, C. A. (2021). The role of PPAR-γ in allergic disease. *Curr. Allergy Asthma Rep.* 21 (11), 3. doi: 10.1007/s11882-021-01022-x

Straub, R. H., Schuld, A., Mullington, J., Haack, M., Schölmerich, J., and Pollmächer, T. (2002). The endotoxin-induced increase of cytokines is followed by an increase of cortisol relative to dehydroepiandrosterone (DHEA) in healthy male subjects. *J. Endocrinol.* 175 (2), 467–474. doi: 10.1677/joe.0.1750467

Tsuchiya, S., Yamabe, M., Yamaguchi, Y., Kobayashi, Y., Konno, T., and Tada, K. (1980). Establishment and characterization of a human acute monocytic leukemia cell line (THP-1). *Int. J. cancer.* 26 (2), 171–176. doi: 10.1002/ijc.2910260208

von Knethen, A., and Brune, B. (2002). Activation of peroxisome proliferator-activated receptor gamma by nitric oxide in monocytes/macrophages down-regulates p47phox and attenuates the respiratory burst. *J. Immunol.* 169, 2619–2626. doi: 10.4049/jimmunol.169.5.2619

Yamamoto, A., Kakuta, H., and Sugimoto, Y. (2014). Involvement of glucocorticoid receptor activation on anti-inflammatory effect induced by peroxisome proliferator-activated receptor?? agonist in mice. *Int. Immunopharmacol.* 22 (1), 204–208. doi: 10.1016/j.intimp.2014.06.028

Yang, X. Y., Wang, L. H., Chen, T., Hodge, D. R., Resau, J. H., DaSilva, L., et al. (2000). Activation of human T lymphocytes is inhibited by peroxisome proliferator-activated receptor γ (PPARγ) agonists. PPARγ co-association with transcription factor NFAT. *J. Biol. Chem.* 275 (7), 4541–4544. doi: 10.1074/jbc.275.7.4541

frontiers | Frontiers in Cellular and Infection Microbiology

TYPE Original Research
PUBLISHED 15 May 2023
DOI 10.3389/fcimb.2023.1120570

OPEN ACCESS

EDITED BY
Veronica Edith Garcia,
Universidad De Buenos Aires, Argentina

REVIEWED BY
Cristina Lourdes Vazquez,
Instituto Nacional de Tecnología Agropecuaria (INTA), Oliveros, Argentina
Luciana Balboa,
Academia Nacional de Medicina, Argentina

*CORRESPONDENCE
Zhaohui Ge
myovid@126.com
Guangxian Xu
xuguangxian@gdmu.edu.cn

†These authors have contributed equally to this work and share first authorship

RECEIVED 10 December 2022
ACCEPTED 27 April 2023
PUBLISHED 15 May 2023

CITATION
Yuan W, Zhan X, Liu W, Ma R, Zhou Y, Xu G and Ge Z (2023) Mmu-miR-25-3p promotes macrophage autophagy by targeting DUSP10 to reduce mycobacteria survival.
Front. Cell. Infect. Microbiol. 13:1120570.
doi: 10.3389/fcimb.2023.1120570

Mmu-miR-25-3p promotes macrophage autophagy by targeting DUSP10 to reduce mycobacteria survival

Wenqi Yuan[1†], Xuehua Zhan[1†], Wei Liu[2], Rong Ma[1], Yueyong Zhou[2], Guangxian Xu[3*] and Zhaohui Ge[1*]

[1]Department of Orthopedics, General Hospital of Ningxia Medical University, Yinchuan, China, [2]Clinical Medicine School, Ningxia Medical University, Yinchuan, China, [3]The First Dongguan Affiliated Hospital, Guangdong Provincial Key Laboratory of Medical Molecular Diagnostics, School of Medical Technology, Guangdong Medical University, Dongguan, China

Background: The present study aimed to investigate the regulation of miR-25-3p on macrophage autophagy and its effect on macrophage clearance of intracellular Mycobacterium bovis Bacillus Calmette-Guerin (BCG) retention based on the previous findings on the differential expression of exosomal miRNA in macrophages infected with BCG.

Methods: Through enrichment analysis and Hub gene analysis, key differentially expressed miRNA and its target genes were selected. The targeted binding ability of the screened mmu-miR-25-3p and its predicted target gene DUSP10 was determined through the TargetScan database, and this was further verified by dual luciferase reporter gene assay. mmu-miR-25-3p mimics, mmu-miR-25-3p inhibitor, si-DUSP10, miR-NC,si-NC and PD98059 (ERK Inhibitor) were used to intervene macrophages Raw264.7. Rt-qPCR was used to detect the expression levels of mmu-miR-25-3p and DUSP10 mRNA. Western blot was used to detect the expression levels of DUSP10, LC3-II, p-ERK1/2, beclin1, Atg5 and Atg7. The autophagy flux of macrophage Raw264.7 in each group was observed by confocal laser microscopy, and the expression distribution of DUSP10 and the structure of autophagosomes were observed by transmission electron microscopy. Finally, the intracellular BCG load of macrophage Raw264.7 was evaluated by colony-forming unit (CFU) assay.

Results: Bioinformatics analysis filtered and identified the differentially expressed exosomal miRNAs. As a result, mmu-miR-25-3p expression was significantly increased, and dual specificity phosphatase 10 (DUSP10) was predicted as its target gene that was predominantly involved in autophagy regulation. The dual luciferase reporter gene activity assay showed that mmu-miR-25-3p was targeted to the 3'-untranslated region (UTR) of DUSP10. The infection of BCG induced the upregulation of mmu-miR-25-3p and downregulation of DUSP10 in RAW264.7 cells, which further increased the expression of LC3-II and promoted autophagy. Upregulated mmu-miR-25-3p expression decreased the level of DUSP10 and enhanced the phosphorylation of ERK1/2, which in turn upregulated the expression of LC3-II, Atg5, Atg7, and Beclin1. Immuno-electron microscopy, transmission electron microscopy, and autophagic flux analysis further confirmed that the upregulation of mmu-miR-25-3p promotes the autophagy of macrophages after BCG infection. The CFU number indicated

that upregulated mmu-miR-25-3p expression decreased the mycobacterial load and accelerated residual mycobacteria clearance.

Conclusion: mmu-miR-25-3p promotes the phosphorylation of ERK1/2 by inhibiting the expression of DUSP10, thus enhancing the BCG-induced autophagy of macrophages. These phenomena reduce the bacterial load of intracellular Mycobacterium and facilitate the clearance of residual mycobacteria. mmu-miR-25-3p has great potential as a target for anti-tuberculosis immunotherapy and can be the optimal miRNA loaded into exosomal drug delivery system in future studies.

KEYWORDS

mmu-miR-25-3p, tuberculosis, autophagy, DUSP10, macrophage

1 Introduction

Spinal tuberculosis is one of the major infectious diseases that seriously endanger human health. Hitherto, there has been no satisfactory treatment method. The bone marrow-blood barrier is altered in the sclerotic region surrounding tuberculous granulomas of spinal tuberculosis, characterized by structural and quantitative changes, trabecular dysplasia, partial closure of the medullary cavity, and the inclusion of the microscopic satellite tuberculosis lesions. Conventional formulations of first-line anti-tuberculosis drugs, such as isoniazid (INH), rifampicin (RFP), and pyrazinamide (PZA) cannot effectively penetrate the above tissue barrier and maintain effective bactericidal or bacteriostatic concentration in the lesion area due to their structural and pharmacokinetic characteristics. This in turn leads to residual chronic bacteria in tuberculosis granuloma in the diseased area and the drug resistance of tuberculosis bacteria, which is the primary reason for the ineffectiveness of conventional chemotherapy for spinal tuberculosis and the persistence and recurrence of the disease (Wang et al., 2007).

Exosomes consist of a class of nanovesicles that contain various substances derived from parental cells and transport them to recipient cells (Kalluri and LeBleu, 2020). Currently, exosomes are receiving increasing attention from various fields because they can be used as efficient shuttle vehicles to transport traditional medicines and also as genetic medicines (such as miRNA and proteins) with immunomodulatory functions (Salvi et al., 2018; Wu and Liu, 2018; Peng et al., 2020; Sharma and Johnson, 2020; Tang et al., 2020). Some studies on exosomes have focused on tissue repair and regenerative medicine, immune regulation, and nervous system diseases (Haney et al., 2015; Kalani et al., 2016; Lee et al., 2017; Izco et al., 2019). Nonetheless, the treatment of spinal tuberculosis with exosome-loaded anti-tuberculosis drugs and microRNAs (miRNAs) has not yet been studied. Therefore, we proposed to construct a novel anti-tuberculosis drug delivery system using exosomes as vectors loaded with RFP and specific miRNAs that have anti-tuberculosis and immunoregulatory functions. Based on the nanosized and low immunogenicity of exosomes, we suggested that conventional anti-tuberculosis drugs can cross multiple biological barriers *via* exosomes to effectively increase the effective drug concentration of spinal tuberculosis lesions. miRNA loaded with exosomes can exert an anti-tuberculosis immunomodulatory role and accelerate the clearance of macrophages to *Mycobacterium*. Therefore, identifying functional miRNAs is crucial for subsequent studies.

When *Mycobacterium tuberculosis* (MTB) infects the body, macrophages play a role in the first line of defense against infection (Cohen et al., 2018) and initiate multiple mechanisms, such as intracellular autophagy, to inhibit or eliminate MTB. Several studies have shown that miRNAs are involved in the regulation of autophagy and induce autophagy in macrophages to clear the intracellular MTB by regulating autophagy-related genes, the formation of autophagosomes in macrophages, and the maturation of autophagosomes (Deretic et al., 2006; Wang et al., 2013; Kim et al., 2015; Guo et al., 2017). In previous studies, we completed the extraction and identification of exosomes of the macrophages infected by *Mycobacterium bovis* Bacillus Calmette-Guerin (BCG). The miRNA was analyzed by high-throughput sequencing analysis of the differences in the exosomes of the macrophages after a 72-h BCG infection (Zhan et al., 2022). A total of 1853 miRNAs were detected, of which 506 overlapped between the BCG-infected and uninfected groups. The data showed that compared to the uninfected group, the expression of 20 miRNAs was upregulated, and that of 7 miRNAs was downregulated in the infected group (Table 1).

The mitogen-activated protein kinase (MAPK) signal transduction pathway is one of the major regulatory mechanisms in eukaryotic cells. Its signal transduction occurs through sequential phosphorylation of MAPKKK (mitogen-activated protein 3 kinase), MAPKK (mitogen-activated protein 2 kinase), and MAPK. MAPK is a highly conserved serine/threonine protein kinase that is part of a key signaling transduction system (Krishna and Narang, 2008). After activation by upstream kinases, different subfamilies regulate various physiological processes in cells, including autophagy, inflammation, stress, and cell growth, development, differentiation, and death (Bogoyevitch and Kobe, 2006; Park

TABLE 1 Differentially expressed miRNAs and their expression levels (Zhan et al., 2022).

miRNAs	Fold Change	log2 FC	p-value	Exp level	Up/down
mmu-miR-27b-3p	1.17	0.22	2.22E-02	high	up
mmu-miR-93-5p	1.19	0.26	2.84E-02	high	up
mmu-miR-25-3p	1.33	0.41	3.98E-02	high	up
mmu-miR-1198-5p	1.16	0.21	4.19E-02	high	up
mmu-let-7c-5p	1.28	0.36	4.36E-02	high	up
mmu-let-7a-5p	1.28	0.36	4.36E-02	high	up
mmu-miR-7658-5p	inf	inf	1.44E-02	low	up
mmu-miR-7069-5p	inf	inf	2.85E-02	low	up
mmu-miR-8092	inf	inf	3.35E-02	low	up
mmu-miR-98-5p	1.18	0.24	1.10E-02	middle	up
mmu-miR-212-3p	1.38	0.47	1.36E-02	middle	up
mmu-miR-181b-5p	1.25	0.32	1.78E-02	middle	up
mmu-miR-3057-5p	1.40	0.49	2.00E-02	middle	up
mmu-miR-203-3p	2.55	1.35	2.23E-02	middle	up
mmu-miR-6516-5p	3.40	1.77	2.62E-02	middle	up
mmu-miR-181d-5p	1.97	0.97	3.38E-02	middle	up
mmu-miR-30a-3p	1.30	0.37	3.56E-02	middle	up
mmu-miR-1933-3p	2.03	1.02	3.77E-02	middle	up
mmu-miR-148b-5p	1.70	0.76	3.80E-02	middle	up
mmu-miR-99b-3p	1.34	0.42	4.88E-02	middle	up
mmu-mir-7018-p5	0.28	-1.85	2.38E-02	middle	down
mmu-miR-194-5p	0.69	-0.54	2.67E-02	middle	down
mmu-miR-301b-3p	0.82	-0.28	3.30E-02	middle	down
mmu-miR-5110	0.25	-2.02	3.61E-02	middle	down
mmu-miR-144-3p	0.28	-1.83	3.74E-02	middle	down
mmu-miR-874-3p	0.66	-0.59	4.05E-02	middle	down
mmu-miR-363-3p	0.34	-1.54	4.92E-02	middle	down

et al., 2014; Zhou et al., 2015). Since phosphorylation is required to activate the MAPK signaling pathway, dephosphorylation of the members of the DUSP (dual-specificity protein phosphatase) family plays a key role in controlling MAPK signaling. However, the function of DUSPs in autophagy is yet to be explored. Nomura et al. (Nomura et al., 2012) observed that DUSP10 suppresses the activation of ERK. Lu et al. (Lu et al., 2020) used Raw264.7 cells and confirmed that DUSP10 (namely MKP-5) promotes the transformation of macrophages from M1 phenotype to M2 phenotype, and as an inflammatory inhibitor, it participates in obesity-induced adipose tissue inflammation and PA-induced macrophage inflammation through ERK, P38, and JNK.

In the present study, we conducted a bioinformatics analysis and screened out mmu-miR-25-3p and its target gene *DUSP10*; these participated in the autophagy of macrophages. Therefore, we hypothesized that miR-25-3p regulates autophagy of macrophages after BCG infection through DUSP10/ERK pathway and further affects their ability to clear BCG retention in the cells.

2 Materials and methods

2.1 Tissue culture medium and reagents

Dulbecco's modified Eagle's medium (DMEM) and fetal bovine serum (FBS) were produced by Gibco and purchased from Thermo Fisher Scientific (Waltham, MA, USA). Complete *Mycobacterium*

medium was purchased from Shanghai Gene-Optimal Science & Technology Co., Ltd (Shanghai, China).

Opti-MEM I reduced serum medium was produced by Gibco and purchased from Thermo Fisher Scientific. FuGENE® HD Transfection Reagent was obtained from Promega (Beijing) Biotech Co., Ltd (Beijing, China). Antibodies against DUSP10 (# ab228987) and LC3-I/II (# ab128025) were purchased from Abcam (Cambridge, UK). Antibodies against Beclin1 (# D160120) and Atg5 (# D121650) were procured from Sangon Biotech (Shanghai) Co., Ltd (Shanghai, China). Antibodies against Atg7 (# AA820) and p-Erk1/2 (# AF5818) were purchased from Beyotime Biotech Inc. (Shanghai, China). Antibody against β-actin (# P60710) was purchased from Servicebio (Wuhan, China). Horseradish peroxidase (HRP)-labeled goat anti-rabbit IgG (# SSA004) was purchased from SinoBiological (Beijing, China). Anti-Rabbit IgG (whole molecule)-Gold (# G7402) was purchased from Sigma–Aldrich (Shanghai) Trading Co. Ltd (Shanghai, China). ERK1/2 signaling inhibitor PD98059 (# HY-12028) was procured from MCE (MedChem Express, Monmouth Junction, NJ, USA).

2.2 Cell and BCG cultures

ATCC® SC6003™ standard was strictly observed. Raw264.7 cells (Gene-Optimal, Shanghai, China) were cultured with DMEM containing 10% FBS and 1% penicillin-streptomycin (Solarbio, China) at a low passage number at 37°C in a 5% CO_2 atmosphere. The *Mycobacterium bovis* strain Bacillus Calmette-Guérin (BCG, St. Pasteur 1173P2 strain) was purchased from Shanghai Gene-Optimal Science & Technology Co., Ltd. Complete mycobacterium medium (Gene-Optimal) was used to culture the BCG bacilli at 37°C. A turbidimetric assay was used to detect the optical density (OD) of the bacteria in the logarithmic phase of growth on a microplate reader (Multiskan FC, Thermoe) at a wavelength of 600 nm. BCG bacilli were harvested at OD_{600} = 0.6–0.8 by centrifugation for 10 min at 4500 rpm; the cell pellets were resuspended in DMEM without antibiotics for subsequent use.

2.3 Infection assay

Mycobacteria in suspension and the logarithmic growth phase were counted with an electronic McFarland turbidity meter, and the number of mycobacteria was estimated by measuring the McFarland (McF). The mycobacteria count corresponding to 1 MCF was approximately 3×10^8 colony-forming units (CFU)/mL. According to the standards set for infection steps (Singh et al., 2015; Bettencourt et al., 2017), RAW264.7 cells were seeded into the plates overnight 1 day prior to infection. On the day of infection, the cells were rinsed with (BI, Israel) three times at room temperature. DMEM supplemented with 10% FBS but without antibiotics replaced the original culture medium, following which the cells were infected with BCG at a multiplicity of 10 (MOI = 10) and incubated at 37°C under a 5% CO_2 atmosphere for 4 h. Subsequently, the medium was discarded, and phosphate-buffered saline (PBS) (37°C) was selected to gently wash the cells three times to the remove extracellular mycobacteria. DMEM supplemented with 10% FBS containing antibiotics was used for the culture. All the BCG culture and infection experiments were accomplished at Ningxia Key Laboratory of Pathogenic Microorganisms (biosafety level-3) in the General Hospital of Ningxia Medical University, China.

2.4 Bioinformatics analysis

In previous studies, we extracted and identified the exosomes of the macrophages infected by BCG. The miRNAs were analyzed by high-throughput sequencing analysis of the differences expressed in the exosomes of the macrophages after 72-h BCG infection (Zhan et al., 2022). The high-throughput sequencing data were deposited in the Genome Sequence Archive at the National Genomics Data Center, China National Center for Bioinformation/Beijing Institute of Genomics, Chinese Academy of Sciences (GSA: CRA006010). In present study, based on the differentially expressed miRNAs of the sequencing, enrichment analyses of their targeted genes were subsequently performed using GO and KEGG. Further visual analysis of the target genes related to cell growth and death was carried out using the Metascape database and the CytoHubba plug-in available in Cytoscape (v3.9.1).

2.5 Cell transfection

miR-25-3p mimics, miR-25-3p inhibitor, miR-NC (nontarget control oligonucleotide chain), three small interfering RNAs sequences against DUSP10 (Table 2), and their corresponding nontarget control siRNA (si-NC) were designed and generated by Shanghai Gene-Optimal Science & Technology Co., Ltd (Table 2). The confluency of RAW264.7 cells was 80% at the time of transfection. After cell digestion, the plates were prepared based on group classification. miR-25-3p mimics, miR-25-3p inhibitor, miR-NC, and all siRNAs were transfected into the cells using FuGENE® HD transfection reagent as per the manufacturer's instructions. 24 h after transfection, q-PCR was performed.

2.6 Dual luciferase reporter gene assay

The wild-type (WT) 3' UTR and a mutant type (MUT) sequence of DUSP10 were synthesized and cloned into a pmirGLO reporter vector. 293T cells were grown to 80% confluence, and the mixture containing the reporter vector and mmu-miR-25-3p mimics or inhibitors was cotransfected into different groups. A dual luciferase reporter gene assay kit (Beyotime, China, # RG089S) was selected to detect the relative luciferase activity.

2.7 Quantitative real-time PCR

RNA was extracted using an RNAeasy™ Animal RNA isolation kit with a spin column (Beyotime, #R0026), and

TABLE 2 Sequences of mimics and inhibitor of mmu-miR-25-3p and small interfering RNAs to *DUSP10* genes.

Gene name	Sequences (5′→3′)
miRNA nontarget control (miR-NC)	UUCUCCGAACGUGUCACGUTT
miR-25-3p-mimics	CAUUGCACUUGUCUCGGUCUGA AGACCGAGACAAGUGCAAUGUU
miR-25-3p-inhibitor	UCAGACCGAGACAAGUGCAAUG
siRNA nontarget control (si-NC)	UUCUCCGAACGUGUCACGUTT ACGUGACACGUUCGGAGAATT
si-DUSP10#1	GCUGCGAAUCUGACGUAUA UAUACGUCAGAUUCGCAGC
si-DUSP10#2	GGCCUUUCAUGGAGUACAA UUGUACUCCAUGAAAGGCC
si-DUSP10#3	CUAACCAGAUGGUCAACAA UUGUUGACCAUCUGGUUAG

miRNA was extracted using a SanPrep column miRNA extraction kit (Sangon Biotech, #B518811), according to the manufacturer's instructions. RNA reverse transcription, cDNA verification, preparation of a real-time PCR system, and determination of the reaction conditions were carried out as described previously. *β-actin* and *U6* were the reference genes. The primers are listed in Table 3.

2.8 Western blotting assay

A membrane and Cytosol Protein Extraction Kit (Beyotime, #P0033) and Enhanced BCA Protein Assay Kit (Beyotime, # P0010S) were used for the extraction and concentration determination of total protein. Subsequently, the proteins were separated by SDS-PAGE and transferred to PVDF membrane (Aspen, China, #AS1021). Subsequently, the membranes were probed overnight at 4°C with primary antibodies to β-actin (1:1000), DUSP10 (1:1000), LC3-I/II (1:500), Atg5 (1:2000), Atg7 (1:1000), Beclin1 (1:2000), and p-Erk1/2 (1:1000). Then, the membranes were incubated with secondary antibody (HRP-labeled goat anti-rabbit IgG, 1:2000) for 30 min after washing with 1X TBST. Finally, the immunoreactive bands were visualized by chemiluminescence detection.

2.9 Immunoelectron microscopy

1×10^7 Raw264.7 cells fixed with 2.5% glutaraldehyde at room temperature in the dark for 30 min, followed by three centrifugation washes at 3000 rpm, 4 °C for 10 min. The supernatant was discarded, and the pellet was resuspended in 0.1 M PBS (pH 7.4) and mixed with 2% molten agarose in the EP tube. Dehydration was performed with gradient ethanol at −20°C prior to embedding in LR white resin. Ultrathin sections (70–80 nm) were sliced, followed by immunolabeling. Then, the sections were blocked with 1% BSA/TBS blocking solution at room temperature for 30 min and incubated with the primary antibody (DUSP10, 1:1000) overnight at 4°C and secondary antibody (anti-Rabbit IgG (whole molecule)-Gold, 1:50) at room temperature for 20 min and then at 37°C for 1 h. Finally, the sections were stained with 2% uranyl acetate-saturated alcohol in the dark for 8 min and washed three times with 70% alcohol and ultrapure water. The images were captured using a Hitachi HT7800/HT7700 transmission electron microscope (Tokyo, Japan). Gold particles with a size of 10 nm in black indicate positive expression.

TABLE 3 Primer information.

Gene name	Primer Sequences (5′→3′)
U6	Forward primer: CTCGCTTCGGCAGCACA Reverse primer: AACGCTTCACGAATTTGCGT
mmu-miR-25-3p	Forward primer: GCGCATTGCACTTGTCTCG Reverse primer: AGTGCAGGGTCCGAGGTATT
β-actin	Forward primer: GCTTCTTTGCAGCTCCTTCG Reverse primer: GGCCTCGTCACCCACATAG
DUSP10	Forward primer: AGTAAATAGTCTGTGCGGGCT Reverse primer: GTTGTGCAGTCAGTTCCAGG

2.10 Autophagy flux analysis

RAW264.7 cells were seeded on 12-well plates and cultured overnight. The pAAV-mCherry-GFP-LC3B (Gene-Optimal, China) adenovirus was used to infect Raw 264.7 cells at an MOI of 100 for 24 h. Autophagic flux was determined by assessing the number of mCherry and GFP puncta under a NIKON Eclipse Ti confocal microscope.

2.11 Transmission electron microscopy

The cells were fixed, and sections were prepared, stained with uranyl acetate, and examined as described in 5.8 above, except that they were not stained with any antibodies. The autophagosomes were identified based on the morphological criteria described previously (Mizushima et al., 2010).

2.12 Colony-forming unit determination

Macrophages infected with BCG were used as controls. The other cells were transfected with mmu-miR-25-3p mimics, mmu-miR-25-3p inhibitor, and si-DUSP10 before BCG stimulation. The infection process was as described previously. DMEM-containing antibiotics were used to replace the medium, and the cells were cultured for 8 h. Subsequently, the lysed cells were serially diluted, coated with *Mycobacterium* solid culture medium (Gene-Optimal, China, #GOMY0020), and cultured at 37°C for 2-3 weeks; then, the number of colonies in each culture dish was counted.

2.13 Statistical analysis

SPSS Statistics 26 software (IBM Corporation, NY, USA) was utilized for data analysis. The measurement data were presented as mean ± standard error of the mean (SEM). Group comparison was tested using one-way analysis of variance (ANOVA). Significant results of ANOVA were further analyzed using the LSD (Least Significant Difference) test and Dunnett T3 test. Statistical comparison between the two groups was tested using Student's t-test. $p < 0.05$ indicated a statistically significant difference.

3 Results

3.1 Enrichment analysis and hub genes

In a previous study, we extracted and identified the exosomes of the macrophages after BCG infection and analyzed the differentially expressed miRNAs in macrophage exosomes after 72-h infection by high-throughput sequencing (Zhan et al., 2022). The data showed that compared to the uninfected group, the expression of 20 miRNAs was upregulated and that of 7 miRNAs was downregulated in the infected group (Table 1). Next, we performed bioinformatics analysis on these 27 miRNAs.

TargetScan (v5.0) and miRanda (v3.3a) were used to complete the Gene Ontology (GO) and genome pathway annotation. A total of 10667 target genes underwent enrichment analyses with OmicStudio, which is an online tool for bioinformatics. GO analysis indicated that these genes participated in multiple biological processes (Figures 1A, B). The bar chart analysis results of Kyoto Encyclopedia of Genes and Genomes (KEGG) enrichment analysis show that according to the number of enriched target genes, the top ten items are signal transduction, infectious disease: viral, cancer: overview, endocrine system, immune system, cell growth and death, cancer: specific types, cellular community – eukaryotes, endocrine and metabolic disease, and transport and catabolism (Figure 2A). It shows that these target genes play an important role in the regulation of cell growth, death, signal transduction, infection and immunity. The scatter plot analysis results of KEGG enrichment analysis show that according to the number of enriched target genes with significant differences, the top ten are pathways in cancer, MAPK signaling pathway, Ras signaling pathway, PI3K-Akt signaling pathway, Rap1 signaling pathway, mTOR signaling pathway, human cytomegalovirus infection, autophagy – animal, human T-cell leukemia virus 1 infection and AMPK signaling pathway (Figure 2B). Among them, Pathways in cancer has the largest number of target genes, but its rich factor is low, so it is not considered. The number of target genes enriched by MAPK signaling pathway ranks second, and its rich factor is greater than 0.8, while the rich factors of "autophagy-animal" and "mTOR signaling pathway" were the highest among the above 10 items (Figure 2B). Therefore, our subsequent analysis will focus on these three items. Next, we used Metascape to conduct in-depth data mining and online analysis of the functional visualization of these target genes. The results showed that autophagy, PI3K-Akt, mTOR, Ras, MAPK, and JAK-STAT were the top-ranked related signaling pathways (Figure 3A). Although the ranking of autophagy is not the top (Figure 3A), but some studies have proved that autophagy is closely related to the survival of MTB retained in macrophages (Gutierrez et al., 2004; Amano et al., 2006). Considering the above results comprehensively, we finally chose MAPK signaling pathway and autophagy as the direction of further analysis. Among these 27 miRNAs, 6 were highly expressed. Of these, mmu-miR-25-3p showed the highest fold-change (1.33) (Table 1), and hence was selected for further analysis of the Hubs gene of mmu-miR-25-3p. Current studies have confirmed that MAPK signaling pathway is closely related to autophagy regulation (Zhou et al., 2015; Wang et al., 2016). Therefore, we analyzed the target genes of mmu-miR-25-3p related to MAPK signaling pathway and autophagy through CytoHubba. Finally, *Dusp10*, *Akt1*, *Mapk8*, *Rps6ka4*, *Elk4*, *Map2k4*, *Tsc1*, *Pik3ca*, *Prkaa2*, *Pik3r3*, and *Pik3cb* were identified as Hub genes (Figure 3B). Since the function of DUSPs in autophagy has not been explored extensively, we chose to study the role of mmu-miR-25-3p and its target gene *DUSP10* in autophagy.

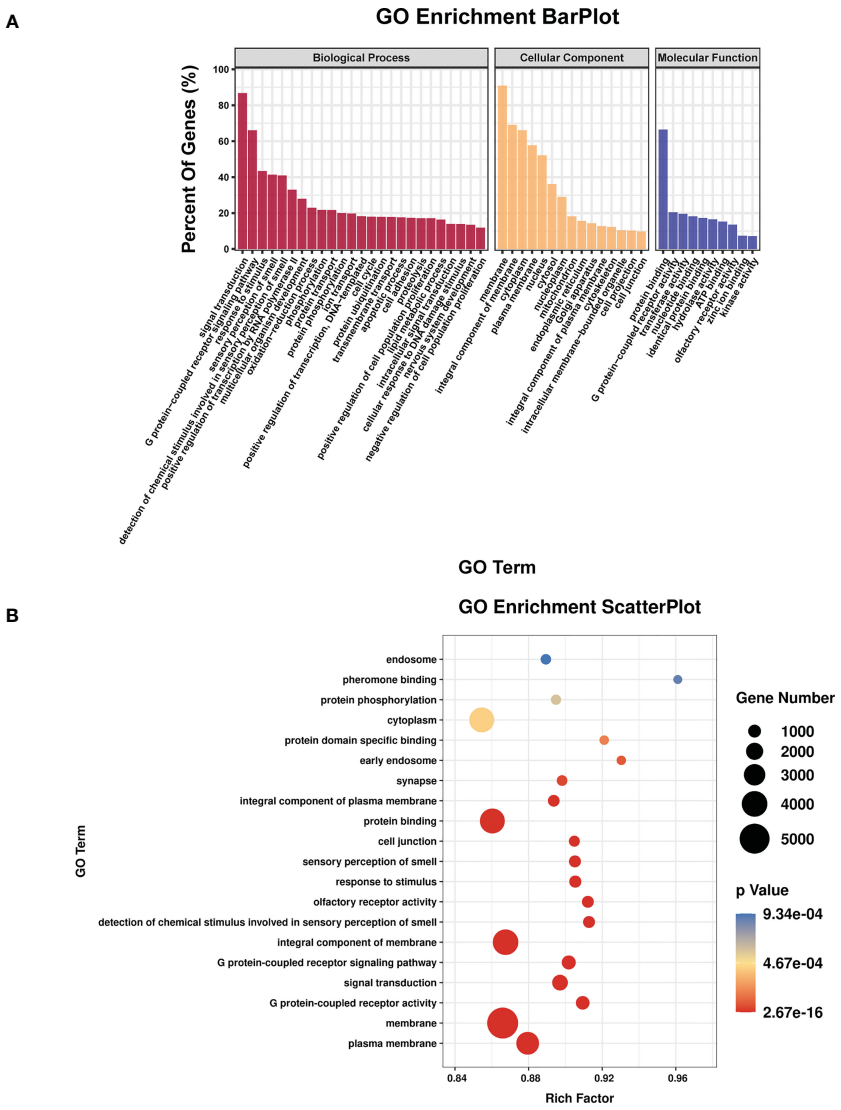

FIGURE 1
The results of GO enrichment analysis. **(A)** Bar plot shows GO terms of the biological process (BP), cellular component (CC), and molecular function (MF) categories. **(B)** Scatterplot shows the enrichment factors, indicates the ratio of the number of differentially expressed genes divided by the total number of genes annotated with a specific term. The smaller the value of p, the higher the degree of enrichment. The larger the diameter of a point, the greater the number of enriched genes.

3.2 mmu-miR-25-3p targets the 3′-UTR of DUSP10

Bioinformatics analysis results predicted that *DUSP10* might be the target gene of mmu-miR-25-3p and that the seed sequence in mmu-miR-25-3p is complementary to the 754–761 oligomer in the 3′-UTR of DUSP10, as determined with TargetScan (v8.0) (Figure 4A). The base pairing type was an 8-mer, the Context++ score was -0.23, the Context++ score percentage was 92%, and the PCT value was 0.95. The fluorescence intensity of the miR-25-3p mimics + DUSP10 wild type (WT) 3′-UTR was obviously weakened compared to that of the NC mimics + DUSP10 WT 3′-UTR, and the difference between the groups was statistically significant ($p < 0.05$) (Figure 4B). The dual luciferase reporter gene activity assay confirmed that mmu-miR-25-3p targeted the 3′-UTR of DUSP10 and that DUSP10 was one of the target genes of mmu-miR-25-3p.

3.3 BCG infection induces alters mmu-miR-25-3p and DUSP10 expression in RAW264.7 cells

In innate immune cells, protein phosphorylation cascades regulate the activation of signaling pathways that are crucial for defense against bacterial infection (Zhang and Dong, 2005). Herein, we infected Raw264.7 macrophages with BCG at MOI 10 and detected the expression levels of mmu-miR-25-3p, *DUSP10* mRNA, and DUSP10 protein by qRT-PCR and Western blotting at 0, 1, 4, 8, 12, 24, 48, and 72 h post-infection. Compared to the blank group, the expression trend of mmu-miR-25-3p showed a peak expression at 4 h after BCG infection ($p < 0.05$), while the expression trend of *DUSP10* mRNA was significantly downregulated between 1 and 12 h post-infection ($p < 0.05$)

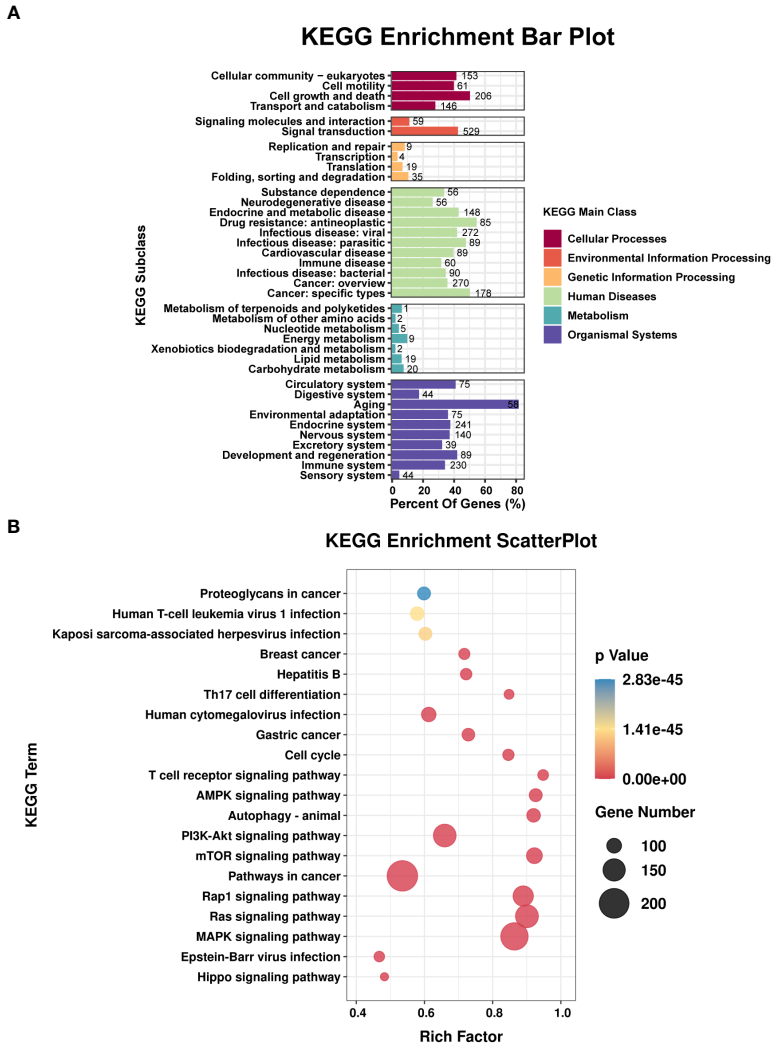

FIGURE 2
Results of the KEGG enrichment analysis. **(A)** Bar plot shows the KEGG subclasses of the target genes enriched in the six main KEGG classes. **(B)** Scatterplot shows the enrichment factors. The smaller the value of p, the higher the degree of enrichment. The larger the diameter of a point, the greater the number of enriched genes.

(Figure 5A). Compared to the blank group, the expression level of DUSP10 protein was continuously downregulated after infection ($p < 0.05$) (Figure 5B). Immunoelectron microscopy detected a decreased abundance of DUSP10 in cells infected with BCG and DUSP10 proteins that were mainly localized in cell nucleus (Figure 5C). These results indicated an increased expression of mmu-miR-25-3p and a decreased expression of DUSP10 in RAW264.7 cells in response to BCG infection.

3.4 BCG infection alters the autophagy in RAW264.7 cells

Autophagy plays a critical role in the process of macrophage resistance against tuberculosis (Gutierrez et al., 2004; Amano et al., 2006). In the current study, Raw264.7 macrophages were infected with BCG at MOI 10, and the expression levels of LC3-II were detected at 0, 1, 4, 8, 12, 24, 48, and 72 h after infection. Compared to the blank group, the expression level of LC3-II increased after infection and peaked at 8 h post-infection ($p < 0.05$) (Figure 6A). Therefore, we further detected the expression levels of Beclin1, Atg5, and Atg7 at 8 h after infection, and found that the levels of these three autophagy-related proteins in BCG-infected macrophages were higher than those in the blank group ($p < 0.05$) (Figure 6B). The BCG-induced autophagy was further corroborated by ascertaining autophagy flux in cells expressing pAAV-mCherry-GFP-LC3B transduced by adenovirus. Indeed, accumulated autophagosomes (yellow puncta in Merge) and autolysosomes (mCherry-LC3B puncta), indicatives of the occurrence of autophagy were observed in the cytoplasm of BCG-infected Raw264.7 macrophages relative to the uninfected Raw264.7 macrophages ($p < 0.05$) (Figure 6C). Transmission electron microscopy (TEM) further confirmed that the number of autophagosomes in Raw264.7 cells at 8 h after BCG infection was significantly higher than that in the blank group (Figure 6D).

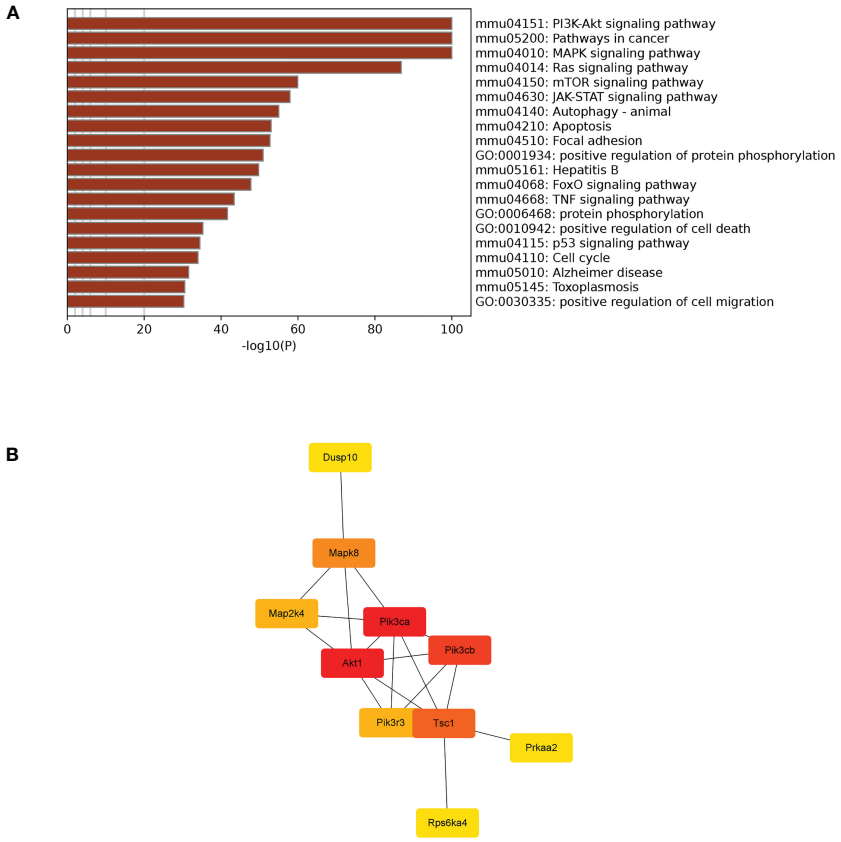

FIGURE 3
Visual analysis and hub genes. **(A)** Visualization of the 20 terms enriched with target genes related to cell growth and death as determined by Metascape. **(B)** Hub genes participating in apoptosis were identified by CytoHubba in Cytoscape (v3.9.1).

3.5 mmu-miR-25-3p/DUSP10 mediates autophagy upon BCG infection by regulating ERK1/2 phosphorylation

Since phosphorylation activates the MAPK signaling pathway, dephosphorylation of the members of the DUSP family plays a key role in controlling MAPK signaling (Huang et al., 2019; Ye et al., 2019). Also, DUSP10 suppresses the activation of ERK (Nomura et al., 2012). Next, we investigated whether the ERK1/2 signaling was regulated by mmu-miR-25-3p/DUSP10 in BCG-infected RAW264.7 macrophages. qRT-PCR showed that the overexpression of mmu-miR-25-3p and knockout of DUSP10 by siRNA significantly downregulated the expression level of *DUSP10* mRNA ($p < 0.05$) (Figure 7A). Western blotting assay confirmed that both the overexpression of miR-25-3p and knockdown of DUSP10 downregulate the level of DUSP10 ($p < 0.05$) and upregulate the level of p-ERK1/2 ($p < 0.05$); this trend was reversed by inhibiting the expression of miR-25-3p, the expression trend was reversed, that is, the expression level of DUSP10 was upregulated ($p < 0.05$) and the expression level of p-ERK1/2 was down-regulated ($p < 0.05$) (Figure 7B). Immunoelectron microscopy assay further demonstrated a decreased abundance of DUSP10 in BCG-infected cells with overexpression of miR-25-3p and knockdown of DUSP10 and an increased abundance of DUSP10 in BCG-infected cells by inhibiting miR-25-3p (Figure 7C). Next, we further the expression levels of LC3-II, beclin1, Atg5, and Atg7, and found that overexpressing mmu-miR-25-3p and knocking down the expression of DUSP10 significantly upregulates the levels of the above four autophagy-related proteins ($p < 0.05$) (Figure 7D). After inhibiting mmu-miR-25-3p and using ERK1/2 inhibitor PD98059, the expression levels of the above four proteins were significantly downregulated ($p < 0.05$) (Figure 7D). The mmu-miR-25-3p/DUSP10-mediated autophagy was further corroborated by ascertaining autophagy flux in cells expressing pAAV-mCherry-GFP-LC3B transduced by adenovirus. The autophagosome-lysosome fusion, as determined by quantity of red puncta in BCG-infected cells. Obviously, the autophagy activities were enhanced significantly (more quantity of yellow and red puncta) in BCG-infected cells with overexpressing mmu-miR-25-3p or knocked down the level of DUSP10 ($p < 0.05$), while the autophagy activities were significantly reduced (less quantity of red puncta) in BCG-infected cells by inhibiting mmu-miR-25-3p or using ERK1/2 inhibitor PD98059 ($p < 0.05$) (Figure 8). TEM further confirmed that the number of autophagosomes in BCG-infected cells with overexpressing mmu-miR-25-3p or knocked down DUSP10 was significantly higher than that in BCG-infected cells *via* miR-NC and si-NC (Figure 9).

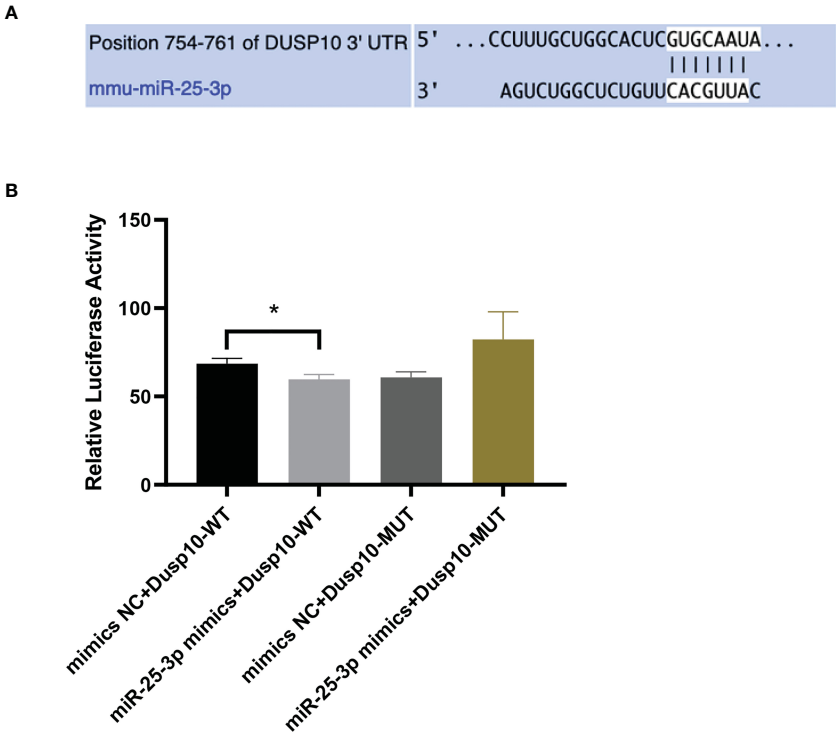

FIGURE 4
mmu-miR-25-3p targets the 3′-UTR of DUSP10. **(A)** Predicted sequential pairing of *DUSP10* seed and mmu-miR-25-3p 3′-UTR as determined by TargetScan (v8.0). **(B)** The dual luciferase gene reporter assay test results (This part of the experiment was repeated 5 times independently). *p < 0.05.

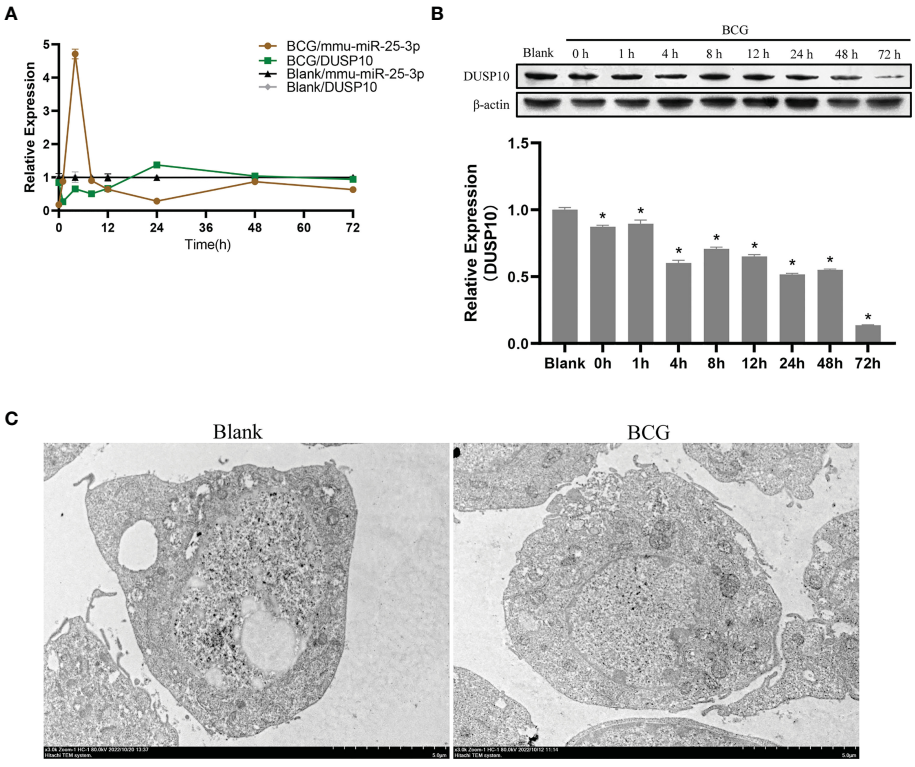

FIGURE 5
Infection of BCG alters the mmu-miR-25-3p and DUSP10 expression in RAW264.7 cells. **(A)** Expression trends of mmu-miR-25-3p and *DUSP10* mRNA in RAW264.7 cells. **(B)** Expression trends of DUSP10 in RAW264.7 cells. **(C)** After 8 h post-BCG infection at MOI 10, the localization of DUSP10 was observed by immunoelectron microscopy. All the experiments were repeated 3 times independently. Gold particles with a size of 10 nm in black indicate DUSP10 expression. Bars in D: 5 μm. *p < 0.05.

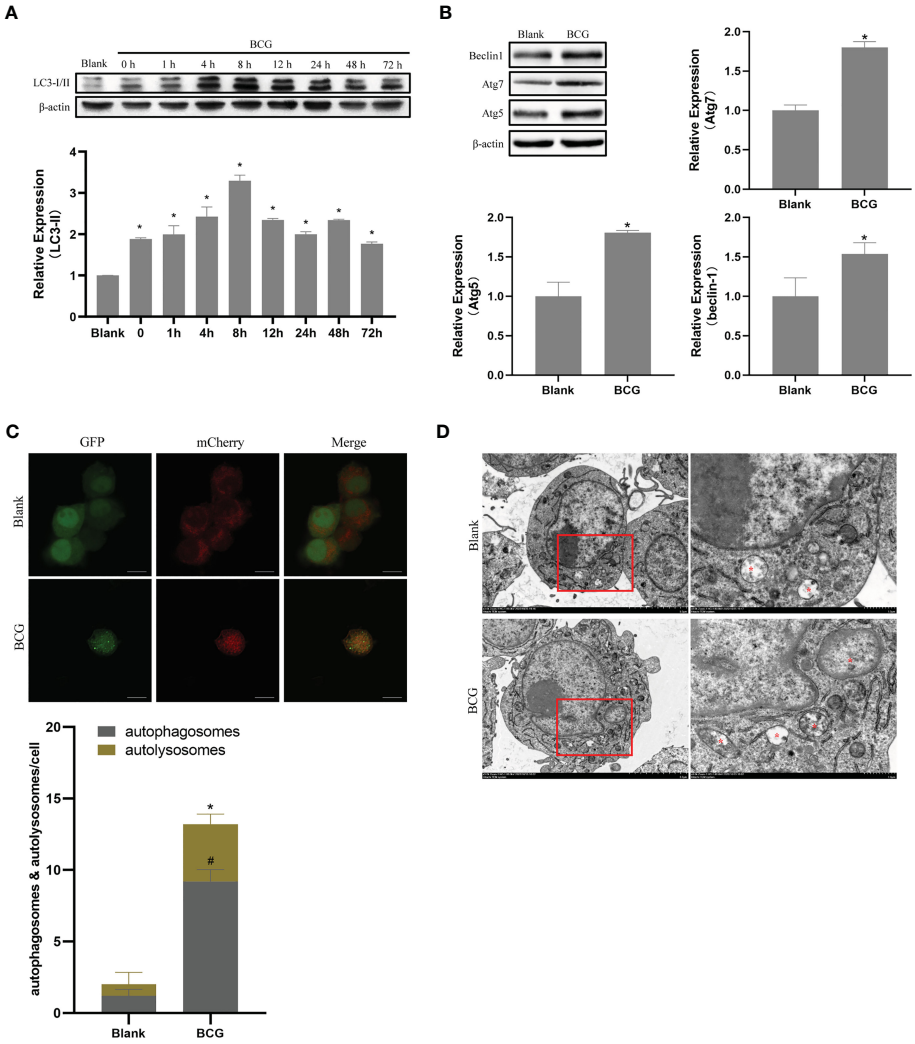

FIGURE 6
BCG infection alters autophagy in RAW264.7 cells. **(A)** Expression trends of LC-3I/II in RAW264.7 cells, *p < 0.05. **(B)** Levels of Atg5, Atg7, and Beclin1 at 8 h post-BCG infection, *p < 0.05. **(C)** RAW264.7 cells were infected with pAAV-mCherry-GFP-LC3B adenovirus (MOI = 100) for 24 h prior to 8 h of BCG infection (MOI = 10); mCherry-LC3B and GFP-LC3B puncta were observed by confocal microscopy, #p < 0.05 (compared with autophagosomes of Blank), *p < 0.05 (compared with autolysosomes of Blank). **(D)** After 8 h of infection at MOI 10, autophagic vesicles (marked with red *) were observed by transmission electron microscopy. All the experiments were repeated 3 times independently. Bars in C: 10 μm. Bars in D: 5 μm (×3.0k), 1μm (×8.0k).

3.6 mmu-miR-25-3p/DUSP10/ERK1/2 regulates BCG survival in Raw264.7 macrophages

The CFU assay results showed that compared to the control group (BCG-infected cells alone) the number of CFUs decreased significantly in the mmu- miR-25-3p mimics and si-DUSP10 groups ($p < 0.05$) and increased markedly in the mmu-miR-25-3p inhibitor group ($p < 0.05$) (Figures 10A, B).

4 Discussion

In the present study, enrichment analysis of 27 differentially expressed miRNAs (Table 1) screened from exosomes of Raw264.7 macrophages infected with BCG in our previous study (Zhan et al., 2022) revealed that their target genes were closely related to autophagy regulation. The results of GO enrichment analysis showed that most of the target gene products were located in the cell membrane, cytoplasm, plasma membrane, nucleus, and mitochondria. Their molecular functions are mainly concentrated in protein binding with metal ions, G protein-coupled receptor activity, and transferase activity. KEGG enrichment analysis showed that these target genes were widely involved in autophagy and PI3K-Akt, mTOR, Rap1, Ras, and MAPK signaling pathways. Similar findings were previously reported by Aplipoor et al. (Alipoor et al., 2017), who identified a panel of exosomal miRNAs after stimulation of human monocyte-derived macrophages, which are involved in host metabolic processes and cell signal transduction, using BCG. As mentioned in the results section, considering the number of target genes enriched by each item and their rich factors, we selected MAPK signaling pathway, autophagy-animal, and mTOR signaling pathway as the focus of further analysis. Herein, we

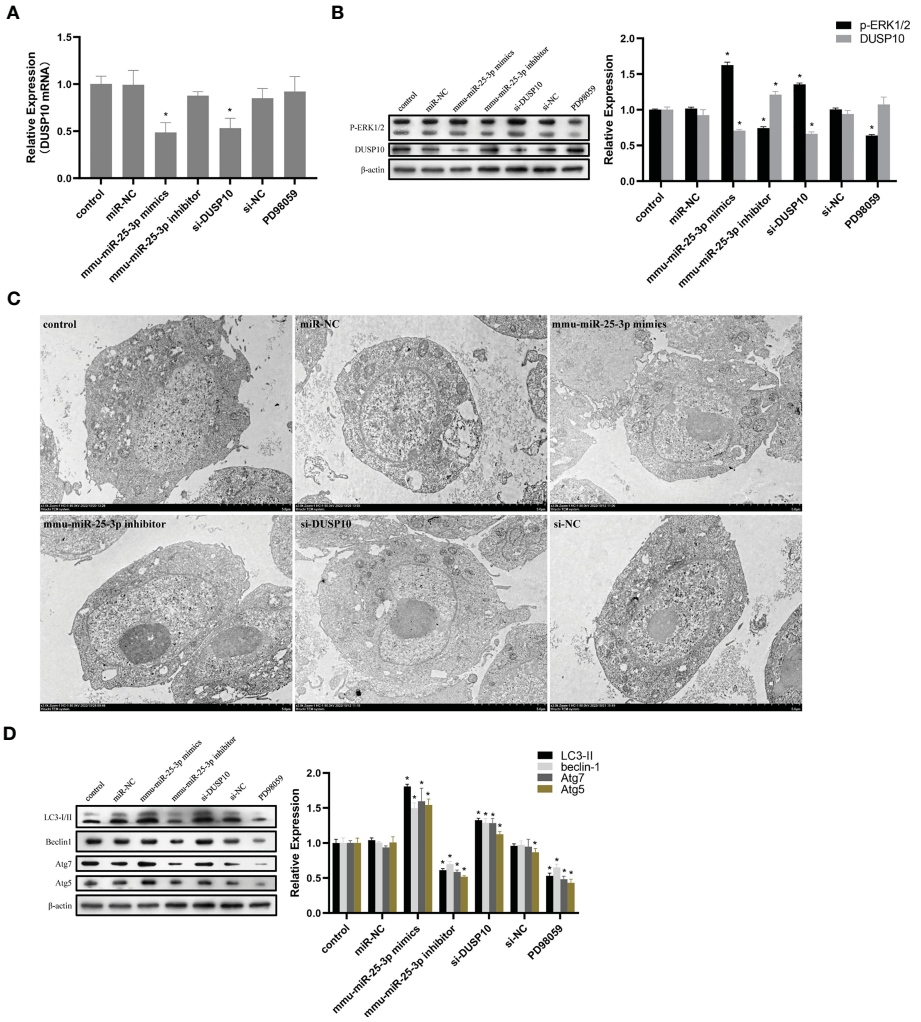

FIGURE 7
mmu-miR-25-3p/DUSP10 mediates autophagy upon BCG infection by regulating ERK1/2 phosphorylation. **(A)** 8 h post-BCG infection, the expression of *DUSP10* mRNA in the control group (only infected with BCG, no other interventions) and each intervention group (miR-NC, mmu-miR-25-3p mimics, mmu-miR-25-3p inhibitor, si-DUSP10, si-NC, and PD98059). **(B)** 8 h post-BCG infection, DUSP10 and p-ERK1/2 levels in the control group and each intervention group (miR-NC, mmu-miR-25-3p mimics, mmu-miR-25-3p inhibitor, si-DUSP10, si-NC, and PD98059) were analyzed by Western blotting. **(C)** After 8 h post-BCG infection at MOI 10, the localization of DUSP10 was observed using immunoelectron microscopy in the control group and each intervention group (miR-NC, mmu-miR-25-3p mimics, mmu-miR-25-3p inhibitor, si-DUSP10, and si-NC). 10-nm gold particles in black indicate DUSP10 expression. **(D)** 8-h post-BCG infection, levels of Atg5, Atg7, Beclin1, and LC3-I/II proteins were analyzed by Western blot in the control group and each intervention group (miR-NC, mmu-miR-25-3p mimics, mmu-miR-25-3p inhibitor, si-DUSP10, si-NC, and PD98059). All the experiments were repeated 3 times independently. Bars in C: 5 μm. *p < 0.05.

used Metascape to conduct an in-depth data mining and online analysis of functional visualization of these target genes, and the results showed that autophagy and PI3K-Akt, mTOR, Ras, MAPK, and JAK-STAT signaling pathways are top-ranked related signaling pathways. Although the ranking of autophagy is not the top, but it has been proved that autophagy is closely related to the survival of MTB retained in macrophages (Gutierrez et al., 2004; Amano et al., 2006). Considering the above results comprehensively, we finally chose MAPK signaling pathway and autophagy as the direction of further analysis. 6/27 miRNAs are highly expressed, and among them, mmu-miR-25-3p has the highest fold change (1.33) (Table 1); hence, it was selected to further analyze the Hub genes of mmu-miR-25-3p.

Autophagy is a cellular "self-feeding" process that is the innate and adaptive immune defense of host cells against intracellular pathogens (Bah and Vergne, 2017). Based on the concept of autophagy-mediated bacterial clearance, signal transduction pathways involved in the autophagy process may be potential new targets for anti-tuberculosis therapy (Dara et al., 2019). It has also been confirmed that MAPK signaling pathway is involved in the regulation of autophagy (Moruno-Manchon et al., 2013; Zhou et al., 2015). Therefore, we analyzed target genes of mmu-miR-25-3p related to MAPK signaling pathway and autophagy through CytoHubba. Finally, *Dusp10*, *Akt1*, *Mapk8*, *Rps6ka4*, *Elk4*, *Map2k4*, *Tsc1*, *Pik3ca*, *Prkaa2*, *Pik3r3*, and *Pik3cb* were identified as hub genes. Since phosphorylation is required to activate MAPK signal transduction pathways, dephosphorylation of DUSP (bispecial protein phosphatase) family members plays a key role in controlling MAPK signaling. Wang et al. (Wang et al., 2016)

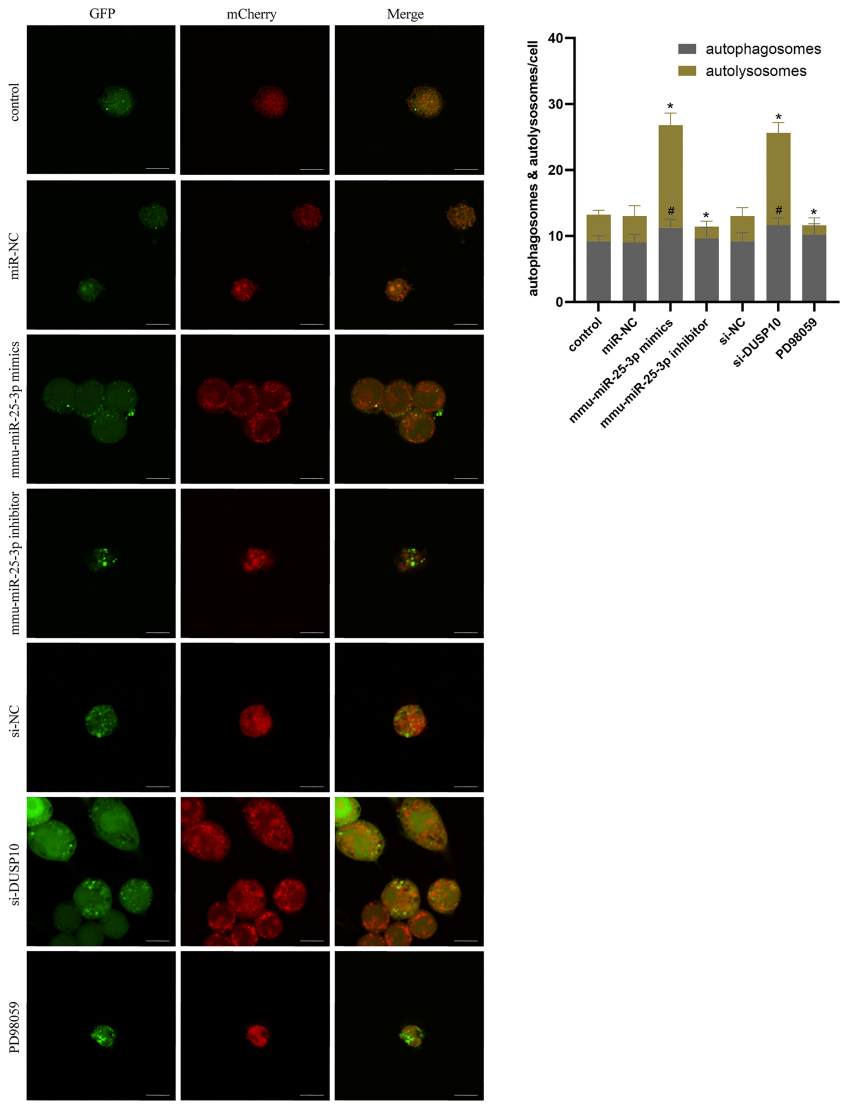

FIGURE 8
Autophagy flux analysis in each group. RAW264.7 cells were infected with pAAV-mCherry-GFP-LC3B adenovirus (MOI = 100) for 24 h prior to 8 h of BCG infection (MOI = 10). mCherry-LC3B and GFP-LC3B puncta were observed by confocal microscopy in the control group (only infected with BCG, no other interventions) and each intervention group (miR-NC, mmu-miR-25-3p mimics, mmu-miR-25-3p inhibitor, si-DUSP10, si-NC, and PD98059). All the experiments were repeated 3 times independently. Scale bars: 10 μm. #$p < 0.05$ (compared with autophagosomes of control), *$p < 0.05$ (compared with autolysosomes of control).

found that DUSP1 inhibited autophagy of ovarian cancer cells by negatively regulating MAPK/ERK pathway, and inhibition of DUSP1 could enhance rapamycin-induced autophagy. Zhou et al. (Zhao et al., 2020) confirmed that DUSP10 (also known as MKP-5) alleviates lipid toxin-induced islet cell dysfunction and apoptosis by inhibiting autophagy. Nomura et al. (Nomura et al., 2012) observed that DUSP10 suppresses the activation of ERK.

Therefore, we hypothesized that mmu-miR-25-3p regulates macrophage autophagy by targeting DUSP10, and that this regulation affects the outcome of MTB infection. Mmu-miR-25-3p is seems to be a novel immunoregulatory target for effective control of *Mycobacterium* infection, and may be crucial in guiding the development of exosome drug delivery systems loaded with specific regulators simultaneously. The prediction of TargetScan (Mouse v8.0) and the validation of the dual luciferase reporter gene assay results demonstrated that the seed sequence of mmu-miR-25-3p targeted binds with the 3'-UTR of DUSP10, and that *DUSP10* is a target gene of mmu-miR-25-3p. Finally, the regulatory mechanism of mmu-miR-25-3p in BCG-induced macrophage autophagy *via* DUSP10 expression and its effect on the survival of intracellular BCG was verified *in vitro*.

Another study confirmed that DUSP10 promotes the transformation of macrophages from M1 to M2 (Lu et al., 2020). The M1-type macrophages participate in the positive immune response and carry out immune surveillance by secreting pro-inflammatory cytokines and chemokines and presenting antigens exclusively. Using murine RAW264.7 macrophage cells *in vitro*, the current results demonstrated that the expression of *DUSP10* mRNA

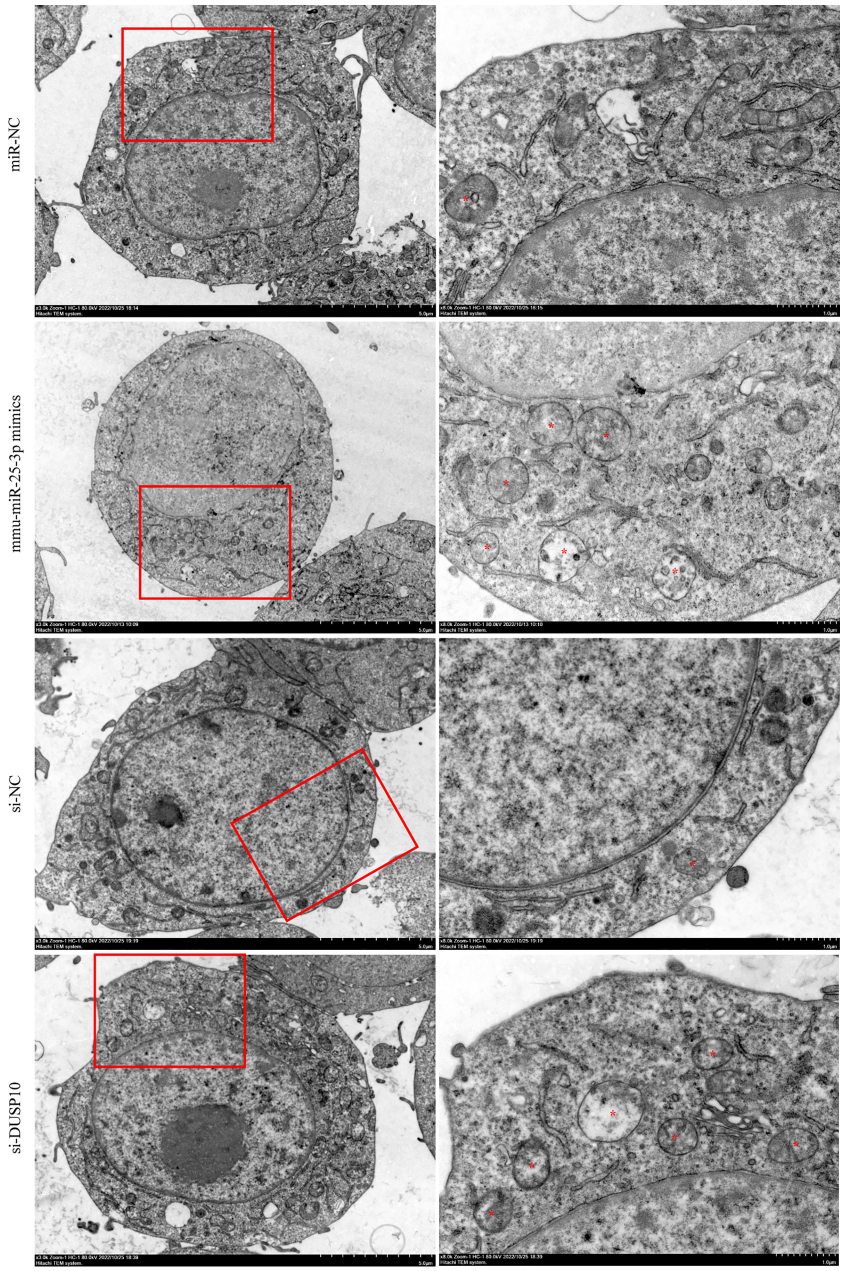

FIGURE 9
Observation of autophagic vesicles. After 8 h of BCG infection at MOI 10, autophagic vesicles (marked with red *) were observed by TEM in miR-NC, mmu-miR-25-3p mimics, si-NC, and si-DUSP10 groups. All the experiments were repeated 3 times independently. Scale bars: 5 μm (×3.0k), 1μm (×8.0k).

was dynamically decreased within 0–12 h after BCG infection, while the protein level was continuously and dynamically decreased after BCG infection. Contrary to the expression trend of *DUSP10* mRNA, the expression level of mmu-miR-25-3p increased dynamically within 0–8 h after BCG infection, i.e., reached a peak at 4 h and returned to the baseline level at 8 h post-BCG infection. miRNAs downregulate the expression of their target genes through two post-transcriptional mechanisms: mRNA cleavage or translation inhibition (Bartel, 2004). Therefore, the downregulated expression of *DUSP10* mRNA in this study may be related to the regulatory effect of mmu-miR-25-3p through mRNA cleavage. In addition, we found that the expression level of LC3-II in macrophages increased dynamically after BCG infection and reached a peak at 8 h after infection. Considering that after BCG infection, cell viability decreases significantly with the passage of culture time, we considered that 8 h after BCG infection is the best time point to observe autophagy and conduct a further experimental intervention. To better understand the effect of mmu-miR-25-3p/DUSP10 on autophagy of macrophages after BCG infection, autophagic markers, Beclin1 (Liang et al., 1999), Atg5, and Atg7 (Romanov et al., 2012) were further examined for autophagosome membrane formation and extension, respectively. At 8 h after BCG infection, the levels of Beclin-1, Atg7, and Atg5 were significantly higher than those of uninfected macrophages, indicating that BCG

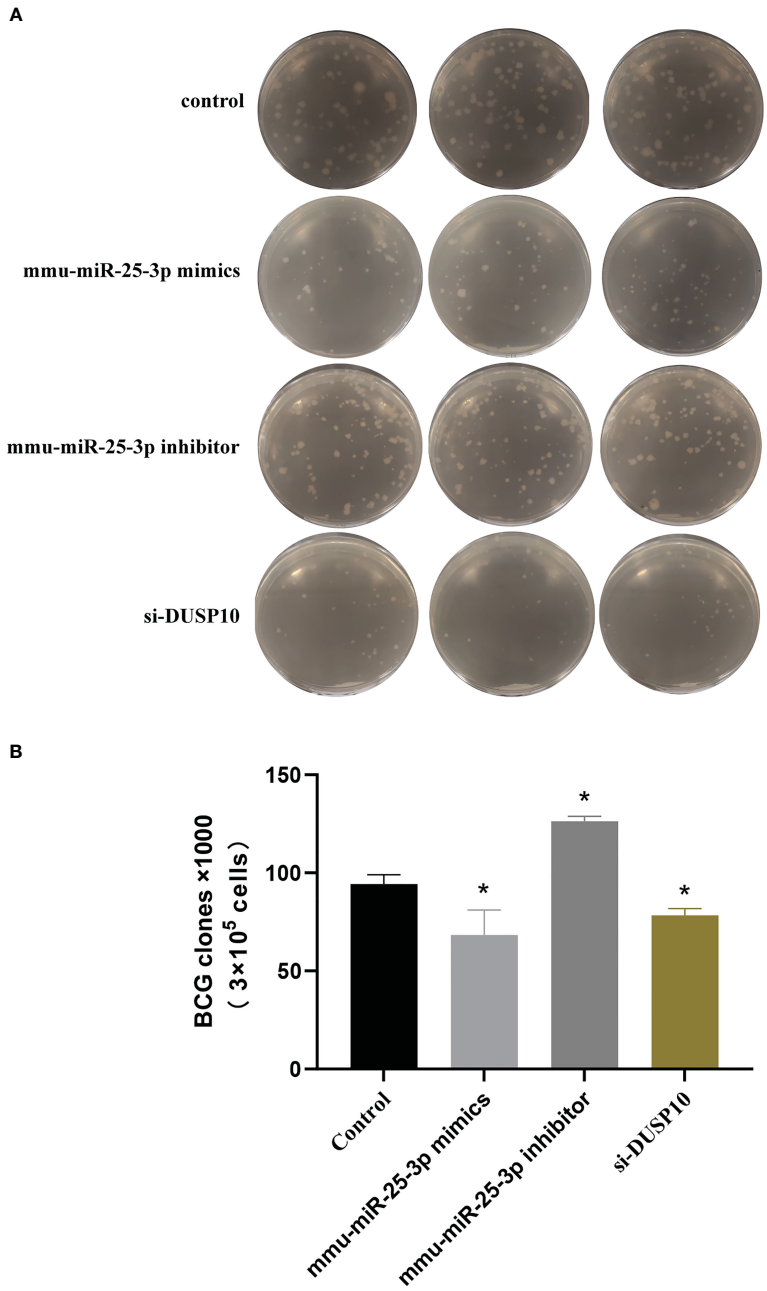

FIGURE 10
Results of mycobacteria CFU determination. **(A)** Number of mycobacteria CFUs in different groups after $\times 10^6$ dilution. **(B)** CFU comparison in control, mmu-miR-25-3p mimics group, mmu-miR-25-3p inhibitor, and si-DUSP10 groups. All the experiments were repeated 3 times independently. *p < 0.05.

induces autophagy in macrophages. Both autophagy flux (pAAV-mCherry-GFP-LC3B adenovirus) and transmission electron microscopy assays further confirmed that BCG infection induces autophagy in macrophages. This finding is consistent with the study of Luo et al. (Luo et al., 2020), which demonstrated that the autophagy of macrophages was enhanced after BCG infection.

Since phosphorylation is required to activate the MAPK signaling pathway, dephosphorylation of the members of the DUSP family plays a key role in controlling MAPK signaling (Huang et al., 2019; Ye et al., 2019). DUSP10 is shown to suppress the activation of ERK (Nomura et al., 2012; Ng et al., 2017). Next, we investigated whether ERK1/2 signaling was regulated by mmu-miR-25-3p/DUSP10 in BCG-infected RAW264.7 macrophages. Interestingly, a decreased expression of DUSP10 was detected in BCG-infected RAW264.7 cells with mmu-miR-25-3p mimics and DUSP10 knockdown (si-DUSP10). However, using mmu-miR-25-3p inhibitor exhibited the opposite effect in BCG-infected RAW264.7 cells. Conversely, an enhanced

expression of p-ERK1/2, Beclin1, Atg5, and Atg7 was detected in BCG-infected RAW264.7 cells with mmu-miR-25-3p mimics and DUSP10 knockdown (si-DUSP10) and a decreased expression of p-ERK1/2, Beclin1, Atg5, and Atg7 was detected in BCG-infected RAW264.7 cells with mmu-miR-25-3p inhibitor. Park et al. (Park et al., 2014) confirmed the activation of ERK pathway in bare −FeNPs−induced autophagy in RAW264.7 and observed upregulated levels of Beclin1, Atg5 and LC3B. This finding is consistent with that of our study. Therefore, we concluded that mmu-miR-25-3p promotes the phosphorylation of ERK1/2 by inhibiting DUSP10, thus promoting the initiation of autophagy to enhance BCG-induced autophagy in RAW264.7 cells. Further autophagy flux assay confirmed that overexpression of mmu-miR-25-3p and downregulation of DUSP10 expression by si-DUSP10 can increase the number of autophagosome and autolysosomes in macrophages, which indicated that overexpression of mmu-miR-25-3p or DUSP10 knockdown can enhance the autophagy activity of macrophages. And TEM confirmed that overexpression of mmu-miR-25-3p or DUSP10 knockdown promotes the formation of autophagosomes in Raw264.7 cells infected with BCG.

Current studies have demonstrated that autophagy is closely related to the survival of mycobacteria in macrophages, and induction of autophagy can effectively eliminate the intracellular residual mycobacteria (Gutierrez et al., 2004; Amano et al., 2006; Singh et al., 2006; Biswas et al., 2008). Finally, the CFU was determined to estimate the intracellular bacterial load and mycobacteria clearance rate. The results showed that mmu-miR-25-3p and DUSP10 are closely related to the bacterial load in Raw264.7 cells. By inhibiting the expression of DUSP10, mmu-miR-25-3p reduces the bacterial load and survival rate of Raw264.7 cells.

In conclusion, mmu-miR-25-3p promotes the phosphorylation of ERK1/2 by inhibiting the expression of DUSP10. This enhances the BCG-induced autophagy of macrophages, which in turn reduces the bacterial load of intracellular *Mycobacterium* and facilitates the clearance of residual mycobacteria. mmu-miR-25-3p has significant potential as a target for anti-tuberculosis immunotherapy and can be the optimal miRNA loaded into exosomal drug delivery system in our future studies.

Data availability statement

The datasets presented in this study can be found in online repositories. The names of the repository/repositories and accession number(s) can be found below: https://ngdc.cncb.ac.cn/gsa/, CRA006010.

Author contributions

ZG: conceptualization and writing - review & editing. RM: methodology and resources. WY: investigation, formal analysis, writing - original draft. XZ: investigation, software, visualization. WL: data curation. YZ: data curation. GX: supervision.

Funding

This study was supported by the National Natural Science Foundation of China (Grant number 8196090244), Key Research and Development Program of Ningxia (Project number 2020BEG03034) and the Natural Science Foundation of Ningxia Province (2021AAC03333).

Acknowledgments

We wish to gratefully acknowledge Professor Li Gang, the director of the Ningxia Key Laboratory of Pathogenic Microorganisms at the General Hospital of Ningxia Medical University, for providing the experimental site, equipment and invaluable technical suggestions.

Conflict of interest

The authors declare that the research was conducted in the absence of any commercial or financial relationships that could be construed as a potential conflict of interest.

Publisher's note

References

Alipoor, S. D., Mortaz, E., Tabarsi, P., Farnia, P., Mirsaeidi, M., Garssen, J., et al. (2017). Bovis bacillus calmette-guerin (BCG) infection induces exosomal miRNA release by human macrophages. *J. Transl. Med.* 15 (1), 105. doi: 10.1186/s12967-017-1205-9

Amano, A., Nakagawa, I., and Yoshimori, T. (2006). Autophagy in innate immunity against intracellular bacteria. *J. Biochem.* 140 (2), 161–166. doi: 10.1093/jb/mvj162

Bah, A., and Vergne, I. (2017). Macrophage autophagy and bacterial infections. *Front. Immunol.* 8. doi: 10.3389/fimmu.2017.01483

Bartel, D. P. (2004). MicroRNAs: genomics, biogenesis, mechanism, and function. *Cell* 116 (2), 281–297. doi: 10.1016/s0092-8674(04)00045-5

Bettencourt, P., Carmo, N., Pires, D., Timóteo, P., and Anes, E. (2017). "Mycobacterial infection of macrophages: the effect of the multiplicity of infection". in *Antimicrobial research: novel bioknowledge and educational programs*. Eds. A. Méndez-Vilas (Formatex Research Center), 651–664. Available at: https://www.researchgate.net/publication/318960339_Mycobacterial_infection_of_macrophages_the_effect_of_the_multiplicity_of_infection.

Biswas, D., Qureshi, O. S., Lee, W. Y., Croudace, J. E., Mura, M., and Lammas, D. A. (2008). ATP-induced autophagy is associated with rapid killing of intracellular mycobacteria within human monocytes/macrophages. *BMC Immunol.* 9, 35. doi: 10.1186/1471-2172-9-35

Bogoyevitch, M. A., and Kobe, B. (2006). Uses for JNK: the many and varied substrates of the c-jun n-terminal kinases. *Microbiol. Mol. Biol. Rev.* 70 (4), 1061–1095. doi: 10.1128/MMBR.00025-06

Cohen, S. B., Gern, B. H., Delahaye, J. L., Adams, K. N., Plumlee, C. R., Winkler, J. K., et al. (2018). Alveolar macrophages provide an early mycobacterium tuberculosis niche and initiate dissemination. *Cell Host Microbe* 24 (3), 439–446.e434. doi: 10.1016/j.chom.2018.08.001

Dara, Y., Volcani, D., Shah, K., Shin, K., and Venketaraman, V. (2019). Potentials of host-directed therapies in tuberculosis management. *J. Clin. Med.* 8 (8), 1166. doi: 10.3390/jcm8081166

Deretic, V., Singh, S., Master, S., Harris, J., Roberts, E., Kyei, G., et al. (2006). Mycobacterium tuberculosis inhibition of phagolysosome biogenesis and autophagy as a host defence mechanism. *Cell Microbiol.* 8 (5), 719–727. doi: 10.1111/j.1462-5822.2006.00705.x

Guo, L., Zhou, L., Gao, Q., Zhang, A., Wei, J., Hong, D., et al. (2017). MicroRNA-144-3p inhibits autophagy activation and enhances bacillus calmette-guerin infection by targeting ATG4a in RAW264.7 macrophage cells. *PloS One* 12 (6), e0179772. doi: 10.1371/journal.pone.0179772

Gutierrez, M. G., Master, S. S., Singh, S. B., Taylor, G. A., Colombo, M. I., and Deretic, V. (2004). Autophagy is a defense mechanism inhibiting BCG and mycobacterium tuberculosis survival in infected macrophages. *Cell* 119 (6), 753–766. doi: 10.1016/j.cell.2004.11.038

Haney, M. J., Klyachko, N. L., Zhao, Y., Gupta, R., Plotnikova, E. G., He, Z., et al. (2015). Exosomes as drug delivery vehicles for parkinson's disease therapy. *J. Control Release* 207, 18–30. doi: 10.1016/j.jconrel.2015.03.033

Huang, Z., Wu, L. M., Zhang, J. L., Sabri, A., Wang, S. J., Qin, G. J., et al. (2019). Dual specificity phosphatase 12 regulates hepatic lipid metabolism through inhibition of the lipogenesis and apoptosis signal-regulating kinase 1 pathways. *Hepatology* 70 (4), 1099–1118. doi: 10.1002/hep.30597

Izco, M., Blesa, J., Schleef, M., Schmeer, M., Porcari, R., Al-Shawi, R., et al. (2019). Systemic exosomal delivery of shRNA minicircles prevents parkinsonian pathology. *Mol. Ther.* 27 (12), 2111–2122. doi: 10.1016/j.ymthe.2019.08.010

Kalani, A., Chaturvedi, P., Kamat, P. K., Maldonado, C., Bauer, P., Joshua, I. G., et al. (2016). Curcumin-loaded embryonic stem cell exosomes restored neurovascular unit following ischemia-reperfusion injury. *Int. J. Biochem. Cell Biol.* 79, 360–369. doi: 10.1016/j.biocel.2016.09.002

Kalluri, R., and LeBleu, V. S. (2020). The biology, function, and biomedical applications of exosomes. *Science* 367 (6478), eaau6997. doi: 10.1126/science.aau6977

Kim, J. K., Yuk, J. M., Kim, S. Y., Kim, T. S., Jin, H. S., Yang, C. S., et al. (2015). MicroRNA-125a inhibits autophagy activation and antimicrobial responses during mycobacterial infection. *J. Immunol.* 194 (11), 5355–5365. doi: 10.4049/jimmunol.1402557

Krishna, M., and Narang, H. (2008). The complexity of mitogen-activated protein kinases (MAPKs) made simple. *Cell Mol. Life Sci.* 65 (22), 3525–3544. doi: 10.1007/s00018-008-8170-7

Lee, S. T., Im, W., Ban, J. J., Lee, M., Jung, K. H., Lee, S. K., et al. (2017). Exosome-based delivery of miR-124 in a huntington's disease model. *J. Mov Disord.* 10 (1), 45–52. doi: 10.14802/jmd.16054

Liang, X. H., Jackson, S., Seaman, M., Brown, K., Kempkes, B., Hibshoosh, H., et al. (1999). Induction of autophagy and inhibition of tumorigenesis by beclin 1. *Nature* 402 (6762), 672–676. doi: 10.1038/45257

Lu, Y., Ma, J., Zhao, J., Song, Z., Zhou, C., Liu, X., et al. (2020). The role of MKP-5 in adipocyte-macrophage interactions during obesity. *Obes. Facts* 13 (1), 86–101. doi: 10.1159/000505343

Luo, J., Xue, D., Song, F., Liu, X., Li, W., and Wang, Y. (2020). DUSP5 (dual-specificity protein phosphatase 5) suppresses BCG-induced autophagy *via* ERK 1/2 signaling pathway. *Mol. Immunol.* 126, 101–109. doi: 10.1016/j.molimm.2020.07.019

Mizushima, N., Yoshimori, T., and Levine, B. (2010). Methods in mammalian autophagy research. *Cell* 140 (3), 313–326. doi: 10.1016/j.cell.2010.01.028

Moruno-Manchon, J. F., Perez-Jimenez, E., and Knecht, E. (2013). Glucose induces autophagy under starvation conditions by a p38 MAPK-dependent pathway. *Biochem. J.* 449 (2), 497–506. doi: 10.1042/BJ20121122

Ng, K. Y., Chan, L. H., Chai, S., Tong, M., Guan, X. Y., Lee, N. P., et al. (2017). TP53INP1 downregulation activates a p73-dependent DUSP10/ERK signaling pathway to promote metastasis of hepatocellular carcinoma. *Cancer Res.* 77 (17), 4602–4612. doi: 10.1158/0008-5472.CAN-16-3456

Nomura, M., Shiiba, K., Katagiri, C., Kasugai, I., Masuda, K., Sato, I., et al. (2012). Novel function of MKP-5/DUSP10, a phosphatase of stress-activated kinases, on ERK-dependent gene expression, and upregulation of its gene expression in colon carcinomas. *Oncol. Rep.* 28 (3), 931–936. doi: 10.3892/or.2012.1862

Park, E. J., Umh, H. N., Kim, S. W., Cho, M. H., Kim, J. H., and Kim, Y. (2014). ERK pathway is activated in bare-FeNPs-induced autophagy. *Arch. Toxicol.* 88 (2), 323–336. doi: 10.1007/s00204-013-1134-1

Peng, H., Ji, W., Zhao, R., Yang, J., Lu, Z., Li, Y., et al. (2020). Exosome: a significant nano-scale drug delivery carrier. *J. Mater Chem. B* 8 (34), 7591–7608. doi: 10.1039/d0tb01499k

Romanov, J., Walczak, M., Ibiricu, I., Schuchner, S., Ogris, E., Kraft, C., et al. (2012). Mechanism and functions of membrane binding by the Atg5-Atg12/Atg16 complex during autophagosome formation. *EMBO J.* 31 (22), 4304–4317. doi: 10.1038/emboj.2012.278

Salvi, V., Gianello, V., Busatto, S., Bergese, P., Andreoli, L., D'Oro, U., et al. (2018). Exosome-delivered microRNAs promote IFN-alpha secretion by human plasmacytoid DCs *via* TLR7. *JCI Insight* 3 (10), e98204. doi: 10.1172/jci.insight.98204

Sharma, A., and Johnson, A. (2020). Exosome DNA: critical regulator of tumor immunity and a diagnostic biomarker. *J. Cell Physiol.* 235 (3), 1921–1932. doi: 10.1002/jcp.29153

Singh, S. B., Davis, A. S., Taylor, G. A., and Deretic, V. (2006). Human IRGM induces autophagy to eliminate intracellular mycobacteria. *Science* 313 (5792), 1438–1441. doi: 10.1126/science.1129577

Singh, P. P., Li, L., and Schorey, J. S. (2015). Exosomal RNA from mycobacterium tuberculosis-infected cells is functional in recipient macrophages. *Traffic* 16 (6), 555–571. doi: 10.1111/tra.12278

Tang, T. T., Wang, B., Lv, L. L., and Liu, B. C. (2020). Extracellular vesicle-based nanotherapeutics: emerging frontiers in anti-inflammatory therapy. *Theranostics* 10 (18), 8111–8129. doi: 10.7150/thno.47865

Wang, Z., Ge, Z., Jin, W., Qiao, Y., Ding, H., Zhao, H., et al. (2007). Treatment of spinal tuberculosis with ultrashort-course chemotherapy in conjunction with partial excision of pathologic vertebrae. *Spine J.* 7 (6), 671–681. doi: 10.1016/j.spinee.2006.07.016

Wang, J., Yang, K., Zhou, L., Minhaowu,, Wu, Y., Zhu, M., et al. (2013). MicroRNA-155 promotes autophagy to eliminate intracellular mycobacteria by targeting rheb. *PloS Pathog.* 9 (10), e1003697. doi: 10.1371/journal.ppat.1003697

Wang, J., Zhou, J. Y., Kho, D., Reiners, J. J.Jr., and Wu, G. S. (2016). Role for DUSP1 (dual-specificity protein phosphatase 1) in the regulation of autophagy. *Autophagy* 12 (10), 1791–1803. doi: 10.1080/15548627.2016.1203483

Wu, C. X., and Liu, Z. F. (2018). Proteomic profiling of sweat exosome suggests its involvement in skin immunity. *J. Invest. Dermatol.* 138 (1), 89–97. doi: 10.1016/j.jid.2017.05.040

Ye, P., Xiang, M., Liao, H., Liu, J., Luo, H., Wang, Y., et al. (2019). Dual-specificity phosphatase 9 protects against nonalcoholic fatty liver disease in mice through ASK1 suppression. *Hepatology* 69 (1), 76–93. doi: 10.1002/hep.30198

Zhan, X., Yuan, W., Zhou, Y., Ma, R., and Ge, Z. (2022). Small RNA sequencing and bioinformatics analysis of RAW264.7-derived exosomes after mycobacterium bovis bacillus calmette-guerin infection. *BMC Genomics* 23 (1), 355. doi: 10.1186/s12864-022-08590-w

Zhang, Y. L., and Dong, C. (2005). MAP kinases in immune responses. *Cell Mol. Immunol.* 2 (1), 20–27.

Zhao, T., Ma, J., Li, L., Teng, W., Tian, Y., Ma, Y., et al. (2020). MKP-5 relieves lipotoxicity-induced islet beta-cell dysfunction and apoptosis *via* regulation of autophagy. *Int. J. Mol. Sci.* 21 (19), 7161. doi: 10.3390/ijms21197161

Zhou, Y. Y., Li, Y., Jiang, W. Q., and Zhou, L. F. (2015). MAPK/JNK signalling: a potential autophagy regulation pathway. *Biosci. Rep.* 35 (3), e00199. doi: 10.1042/BSR20140141

frontiers | Frontiers in Cellular and Infection Microbiology

TYPE Original Research
PUBLISHED 22 May 2023
DOI 10.3389/fcimb.2023.1105872

OPEN ACCESS

EDITED BY
Veronica Edith Garcia,
Universidad de Buenos Aires, Argentina

REVIEWED BY
Silvia De La Barrera,
National Scientific and Technical Research Council (CONICET), Argentina
Virginia Pasquinelli,
CITNOBA (CONICET-UNNOBA), Argentina

*CORRESPONDENCE
Rogelio Hernandez-Pando
rhdezpando@hotmail.com

RECEIVED 23 November 2022
ACCEPTED 02 May 2023
PUBLISHED 22 May 2023

CITATION
Lozano-Ordaz V, Rodriguez-Miguez Y, Ortiz-Cabrera AE, Hernandez-Bazan S, Mata-Espinosa D, Barrios-Payan J, Saavedra R and Hernandez-Pando R (2023) Beneficial or detrimental activity of regulatory T cells, indoleamine 2,3-dioxygenase, and heme oxygenase-1 in the lungs is influenced by the level of virulence of *Mycobacterium tuberculosis* strain infection. *Front. Cell. Infect. Microbiol.* 13:1105872. doi: 10.3389/fcimb.2023.1105872

Beneficial or detrimental activity of regulatory T cells, indoleamine 2,3-dioxygenase, and heme oxygenase-1 in the lungs is influenced by the level of virulence of *Mycobacterium tuberculosis* strain infection

Vasti Lozano-Ordaz[1], Yadira Rodriguez-Miguez[1], Angel E. Ortiz-Cabrera[1], Sujhey Hernandez-Bazan[1], Dulce Mata-Espinosa[1], Jorge Barrios-Payan[1], Rafael Saavedra[2] and Rogelio Hernandez-Pando[1]*

[1]Experimental Pathology Section, Department of Pathology, National Institute of Medical Sciences Nutrition Salvador Zubiran, Mexico City, Mexico, [2]Immunology Deparment, Biomedical Research Insitute, National Autonomous University of Mexico (UNAM), Mexico City, Mexico

Tuberculosis (TB) caused by the complex Mycobacterium tuberculosis (Mtb) is the main cause of death by a single bacterial agent. Last year, TB was the second leading infectious killer after SARS-CoV-2. Nevertheless, many biological and immunological aspects of TB are not completely elucidated, such as the complex process of immunoregulation mediated by regulatory T cells (Treg cells) and the enzymes indoleamine 2,3-dioxygenase (IDO) and heme oxygenase 1 (HO-1). In this study, the contribution of these immunoregulatory factors was compared in mice infected with Mtb strains with different levels of virulence. First Balb/c mice were infected by intratracheal route, with a high dose of mild virulence reference strain H37Rv or with a highly virulent clinical isolate (strain 5186). In the lungs of infected mice, the kinetics of Treg cells during the infection were determined by cytofluorometry and the expression of IDO and HO-1 by RT-PCR and immunohistochemistry. Then, the contribution of immune-regulation mediated by Treg cells, IDO and HO-1, was evaluated by treating infected animals with specific cytotoxic monoclonal antibodies for Treg cells depletion anti-CD25 (PC61 clone) or by blocking IDO and HO-1 activity using specific inhibitors (1-methyl-D,L-tryptophan or zinc protoporphyrin-IX, respectively). Mice infected with the mild virulent strain showed a progressive increment of Treg cells, showing this highest number at the beginning of the late phase of the infection (28 days), the same trend was observed in the expression of both enzymes being macrophages the cells that showed the highest immunostaining. Animals infected with the highly virulent strain showed lower survival (34 days) and higher amounts of Treg cells, as well as higher expression of IDO and HO-1 one week before. In comparison with non-treated animals, mice infected with strain H37Rv with depletion of Treg cells or treated with the enzymes blockers during late infection showed a significant decrease of bacilli loads, higher

expression of IFN-g and lower IL-4 but with a similar extension of inflammatory lung consolidation determined by automated morphometry. In contrast, the depletion of Treg cells in infected mice with the highly virulent strain 5186 produced diffuse alveolar damage that was similar to severe acute viral pneumonia, lesser survival and increase of bacillary loads, while blocking of both IDO and HO-1 produced high bacillary loads and extensive pneumonia with necrosis. Thus, it seems that Treg cells, IDO and HO-1 activities are detrimental during late pulmonary TB induced by mild virulence Mtb, probably because these factors decrease immune protection mediated by the Th1 response. In contrast, Treg cells, IDO and HO-1 are beneficial when the infection is produced by a highly virulent strain, by regulation of excessive inflammation that produced alveolar damage, pulmonary necrosis, acute respiratory insufficiency, and rapid death.

KEYWORDS

tuberculosis, immunoregulation, T regulatory cells, IDO, HO-1

1 Introduction

Mycobacterium tuberculosis (MTB), the etiological agent of human tuberculosis (TB) has latently infected one-fourth of the world's population; however, only 10% of this population will develop the active disease at some point in their lives. In 2021, there were 10.6 million new cases and 1.6 million deaths due to TB; it is the 13th leading cause of death and the second leading infectious killer after COVID-19 (above HIV/AIDS) (Global Tuberculosis reporT 2022, 2022). In an efficient encounter, macrophages engulf MTB in a phagosome and later destroy them by enzymatic lysis (Collins and Kaufmann, 2001). MTB antigens are processed and presented to CD4+ and CD8+ T cells, triggering a protective Th1 response with the production of pro-inflammatory cytokines, such as IL-2, IFN-γ, IL-12, IL-8, and TNF-α (Ladel et al., 1995). Several mechanisms of immune evasion by mycobacteria can impair this Th1 response and cytokines such as IL-4, IL-5, IL-6, IL-10, IL-13, and TGF-β increase their production during progressive disease with a detriment to the protective response (Ladel et al., 1995; Behar et al., 2010). Virulent strains of MTB evade apoptosis and cause necrosis of infected alveolar macrophages (AM), favoring bacilli survival and dissemination to other macrophages (Meena and Rajni, 2010). MTB can also induce immune regulatory responses by activating Treg cells (CD4+CD25+FoxP3+) and their functions (Scott-Browne et al., 2007).

Treg cells are CD4+ lymphocytes that constitutively express the CD25 marker (α-chain of the IL-2 receptor) and FoxP3 transcription factor (Hori and Sakaguchi, 2004). These cells suppress effector immune cells by decreasing their proliferative capacity, antibody production, and cytokine secretion, for instance, FoxP3 downregulates IFN-γ, IL-4, and IL-2 (Hori and Sakaguchi, 2004; Bettelli et al., 2005). Studies in humans with active and latent TB infection show a higher number of Treg cells than non-infected controls, and patients infected with drug-resistant MTB strains show an increase of Treg cells in peripheral blood, compared with healthy subjects (Scott-Browne et al., 2007; Wergeland et al., 2011; Arram et al., 2014). After treatment of patients with TB, the Treg cell number fall, but naïve Treg cell recovery was similar to healthy controls (Zewdie et al., 2016). The number of Treg cells is increased in the infection sites and local lymph node and spleen; during active TB, this increase is more pronounced in mice infected with H37Rv MTB for prolonged periods of infection (Churina et al., 2012). Treg cells can delay the priming of effector CD4+ cells and their recruitment at the lung, prolonging the initial phase of bacterial expansion (Shafiani et al., 2010).

Another system for the immune response regulation is mediated by the enzymes indoleamine 2,3-dioxygenase (IDO) and heme oxygenase 1 (HO-1). IDO catalyzes the degradation of the essential amino acid tryptophan to N-formylkynerunine produced by dendritic cells (DCs) and macrophages, mainly induced by IFN-γ, TGF-α and β, CTLA4, and lipopolysaccharide (Divanovic et al., 2012). IDO activity decreases the production of IL-2 and therefore diminishes the proliferation of T lymphocytes; also, its metabolites can lead effector cells to apoptosis and polarize naïve cells to Treg cells (Filippini et al., 2012). In addition, TB patients with a higher amount of IDO had a worse prognosis and lower survival (Suzuki et al., 2012). Regarding HO, three isoforms of this enzyme, HO-1, HO-2, and HO-3 catalyze the degradation of heme, and their expression varies in different cell types and tissues (Wagener et al., 2003). HO-1 is the most relevant isoform for immune-regulation due to its high anti-inflammatory action that is mediated through the degradation products, such as carbon monoxide (CO), biliverdin/bilirubin, and ferritin induced by iron. CO promotes vasodilation, inhibits platelet aggregation, and suppresses cytokine production, while the other two by-products have also potent immunological properties (Fei et al., 2012). HO-1 is a determining factor in the maturation of DC; its presence promotes the production of anti-inflammatory cytokines such as

IL-10 and TGF-β while decreasing the production of IL-2 (Schumacher et al., 2012). People with latent MTB infection have an increased expression of HO-1 compared with uninfected subjects, although not much is known about its role in TB (Andrade et al., 2014).

When BALB/c mice are infected with the reference mild virulence strain H37Rv, there is an initial cell-mediated immune response with a high number of activated macrophages and expression of Th1 cytokines such as IFN-γ and IL-12, which peak at 21-day post-infection that efficiently control bacterial growth (Hernandez-Pando et al., 1996). Then, 1 month after infection, there is a progressive immune-regulation mediated by Th-2 cells and high production of anti-inflammatory cytokines, such as IL-10 and TGF-β, that in coexistence with a decrease in the production of Th1 cytokines, progressive pneumonia, and high bacillary load, produce animal's death (Hernández-Pando et al., 2008). In this model, there is also a biphasic increase in the expression of HO-1 and FoxP3 the distinctive transcription factor of Treg cells (Hernández-Pando et al., 2008). In contrast, strain 9005186, which was isolated from an epidemic burst in the South of Mexico, induced in BALB/c mice rapid death (Hernández-Pando et al., 2012). Infected animals with this strain started to die after 3 weeks and by the 5th week, all the animals died, in coexistence with high bacterial growth that peak at day 21 and significantly more pneumonia than H37Rv infection. Mice infected with a high dose of strain 9005186-showed IFNγ delayed expression and high but transient TNFα expression (Marquina-Castillo et al., 2009). Thus, this strain is more virulent than H37Rv and does not induce a protective immune response in this animal model. With the aim to study immune regulation during the infection with mild and highly virulent MTB, we compared the kinetics of Treg cells, IDO, and HO-1 during the infection in BALB/c mice with H37Rv or 5186 strain. Then, we studied the evolution of the disease after Treg cell elimination by the administration of cytolytic monoclonal antibodies and blocking IDO or HO-1 activity with the administration of specific antagonist drugs.

2 Materials and methods

2.1 Mycobacterium tuberculosis growth

All procedures were performed in a laminar flow cabinet in a biosafety level III laboratory. Mild virulent strains H37Rv and highly virulent clinical isolate 9005186 (5186) were grown in Middlebrook 7H9 broth (Difco, Detroit, MI, USA) supplemented with 10% ADC (albumin/dextrose/catalase) (Difco, Detroit, MI, USA), 0.05% Tween 80 and 0.5% glycerol to mid-exponential phase before freezing at −70°C. Frozen stocks were freshly thawed and reconstituted at room temperature at the time of infection. A vial of stock bacilli was diluted in PBS to a final concentration of 2.5×10^5 colony-forming units (CFUs) in 100 µl of PBS. Before infection, each stock vial was plated for CFU enumeration to reconfirm the standard concentration of the inoculum. The CFU concentration of stock vials was calculated by serial dilution and plating in multiple replicates on Middlebrook 7H11 agar (Difco, Detroit, MI, USA) containing 0.5% glycerol and 10% OADC (Oleic albumin/dextrose/catalase) growth enrichment. Plates were incubated for 21 days at 37°C before the determination of CFU.

2.2 Experimental model of progressive pulmonary tuberculosis

Pathogen-free male BALB/c mice, 6–8 weeks of age, were anesthetized (Sevoflurane; Abbott Laboratories, IL, USA) and infected by intratracheal (i.t.) cannulation, administering 2.5×10^5 viable bacteria suspended in 100 µl of PBS. Infected mice were maintained in groups of five in cages fitted with microisolators connected to negative pressure. Animals were randomly selected in groups of five and euthanized by exsanguination on days 7, 14, 21, 28, 60, or 90 post-infection with the H37Rv strain. Mice infected with 5186 were euthanized at days 1, 3, 7, 14, 21 and 28 post-infection, there were no survivor animals after 37 days of infection. Lungs were either immediately frozen in liquid nitrogen, fixed by perfusion with absolute ethanol for histological studies or collected in RPMI to be processed immediately for flow cytometry. Two independent experiments were performed. All procedures were done in a biological security cabinet at a Biosafety level III facility. All the animal work was carried out according to the guidelines and approval of the Ethical Committee for Experimentation on Animals of the National Institute of Medical Sciences and Nutrition (INCMNSZ) in Mexico City, permit number CINVA 224.

2.3 Assessment of colony-forming units

Lungs were frozen for at least 24h at −70°C. Frozen lungs were disrupted in a Polytron homogenizer (Kinematica; Lucerne, Switzerland) in sterile tubes containing 1 ml of PBS-Tween 80 0.05%. Four dilutions of each homogenate were spread onto duplicate plates containing Bacto Middlebrook 7H10 agar (Difco BD, Sparks, MD, USA) enriched with OADC (Oleic albumin/dextrose/catalase. Difco). The incubation time of the plates was 21 days, and data points are the means of four animals.

2.4 Flow cytometry

The right lungs from three mice were processed immediately after euthanizing. Lungs were immersed in 2 ml of RPMI (Gibco Life Technologies, Grand Island, NY, USA) with 1 mg/ml of collagenase II (Gibco Life Technologies, Grand Island, NY, USA) and incubated for 1h at 37°C. After that, lungs were disaggregated by passing through needles of different caliber (18G and 21G), and the obtained cells were washed with PBS/albumin 2% and filtered in a 70-µm strainer (Beckton Dikinson, USA). 5×10^6 cells from each mouse were stimulated for 6h with Cell Stimulation Cocktail (Tonbo Bioscience, San Diego, CA, USA). Later 1×10^6 cells were harvested and washed with PBS and blocked with 1 µl of purified anti-mouse CD16/CD32 (Fc Shield) (Tonbo Bioscience, San Diego, CA, USA). After that, cells were stained with Ghost Dye 450 (Tonbo) to separate dead/living cells and then were stained with

anti-CD3 AF, anti-CD4/BV450 and anti-CD25/BB515, all diluted 1:100 in PBS. Finally, intracellular labeling to detect FoxP3/PE was performed with specific antibodies and diluted 1:100 in FixPerm (eBioscience, USA). Samples were analyzed in BD LSRFortessa™ (BD LSRTFortessa, USA). Data were analyzed by FlowJo™ v.10 (FlowJo v.10, USA). First, the lymphocytes zone was selected from FSC *vs.* SSC gate, and then alive cells were selected for gated CD3 *vs.* CD4. Finally, the percentage of CD25+FoxP3+ cells was obtained from CD3+CD4+ lymphocytes (Supplementary Figure S1).

2.5 Immunohistochemistry and morphometry

The left lungs from four mice in two independent experiments were immersed in absolute ethanol for 2 days, and parasagittal sections were taken through the hilum. Tissue samples were dehydrated, cleared, and embedded in paraffin. Lung paraffin blocks were sectioned at 4 μm and stained with hematoxylin and eosin (H&E) or phosphotungstic acid/hematoxylin stain for histological analysis. The percentage of lung area affected by pneumonia was measured using a Leica Q500/W Image Analysis System (Milton Keynes, UK).

The same paraffin blocks were used for immunohistochemistry. Lung sections 5 μm were mounted on silane-covered slides. After deparaffination and rehydration, peroxidase activity was blocked by incubation with 0.3% H_2O_2 in absolute methanol. Lung sections were incubated overnight at room temperature with polyclonal rabbit antibody against HO-1 (Aviva System Biology, USA) or polyclonal goat antibody against IDO-1 (LS Bio, USA) both diluted 1:200, monoclonal rabbit anti FoxP3 (R&D System, USA) diluted 1:20 in PBS, monoclonal rat anti–IL-17 (Santa Cruz, CA, USA) diluted 1:100, polyclonal mouse anti–PECAM-1(CD31), polyclonal mouse anti-GPIV (CD36), polyclonal mouse anti–P-selectin (CD62P), polyclonal anti–VCAM-1 (CD106) all diluted 1:200, polyclonal mouse anti–IL-1 (Santa Cruz, CA, USA) 1:100, polyclonal anti–TGF-β (Santa Cruz, CA, USA) diluted 1:100, polyclonal anti–IL-4 (Santa Cruz, CA, USA), polyclonal anti–TNF-α (Santa Cruz, CA, USA), and polyclonal Ly6G (Santa Cruz, CA, USA) diluted 1:250. Followed by incubation with Goat-on-Rodent HRP-polymer (BioCare, USA), anti-rabbit IgG (Vectastain, Vector Laboratories, USA) or biotinylated antimouse IgG. Bound antibodies were detected with diamino-bencidin (ImmPACT DAB, Vector Laboratories). For semi-quantification, five random fields of each sample were analysed, and the total number of cells and percentage of immunostained cells were determined using an automated image analyzer (QWin Leica, Milton Keynes, UK) to acquire images and ImageJ 1.52a software (National Institute of Health) for positive cell counting.

2.6 Real-time polymerase chain reaction analysis of enzymes and cytokines expression

Three lungs from each of the groups were used to isolate mRNA using the RNAeasy minikit (Qiagen, Valencia, CA, USA). The quality and quantity of RNA were evaluated through spectrophotometry (260/280) and on agarose gels. Reverse transcription of the mRNA was performed using 100 ng RNA, oligo (dT), and the Omniscript kit (Qiagen, Valencia, CA, USA). Real-time polymerase chain reaction (PCR) was carried out using the 7500 real-time PCR system (Applied Biosystems) and Quantitect SYBR green Mastermix kit (Qiagen, Valencia, CA, USA). Standard curves of quantified and diluted PCR products, as well as negative controls, were included in each PCR run. Specific primers for genes encoding the ribosomal protein, large P0 (RPLP0) as house-keeping gene, IL-4, IFN-ϒ, TGF-β, TNF-α, IDO, HO-1, IL-22, or IL-17 were designed using the program Primer Express (Applied Biosystem, San Francisco, CA, USA) (Table 1). Data are shown as copies of cytokine-specific mRNA/10^6 copies of RLP0 mRNA.

2.7 Inhibition of immunoregulation

In order to evaluate the contribution of immune regulatory response, Treg cells were deleted using 200 μg of anti-CD25 mAb (PC61 clone), and as a negative control, isotype IgG antibody was administrated by intraperitoneal (i.p.) route, 1 day before infection in H37Rv or 5186 infected mice or on day 17 after infection with strain 5186 (Supplementary Figure S2), as previously described (Tenorio et al., 2010).

TABLE 1 Primers sequences.

Gen	Forward primer	Reverse primer
Rplp0	5′-CTCTCGCTTTCTGGAGGGTG-3′	5′-ACGCGCTTGTACCCATTGAT-3′
IFN-γ	5′-CCTCAAACTTGGCAATACTCATGA-3′	5′-GGTGACATGAAAATCCTGCAG-3′
TNF-α	5′-AAATGGGCTCCCTCTCATCAGT-3′	5′-GATCTGAGTGTGAGGGTCTGGG-3′
IL-4	5′-ATGCCTGGATTCATCGATAAGC-3′	5′-GAGTAATCCATTTGCATGATGCTCT-3′
TGF-β	5′-GCTGATCCCGTTGATTTCCA-3′	5′-GTGGCTGAACCAAGGAGACG-3′
IDO	5′-CAGGCCAGAGCAGCATCTTC-3′	5′-GCCAGCCTCGTGTTTTATTCC-3′
HO-1	5′-GCCGAGAATGCTGAGTTCATG-3′	5′-TGGTACAAGGAAGCCATCACC-3′
IL-17	5′-TGACCCCTAAGAAACCCCCA-3′	5′-GTGGAGGGCAGACAATTCTGA-3′
IL-22	5′-TCAACTTCACCCTGGAAGACG-3′	5′-TGAGTTTGGTCAGGAAAGGCA-3′

The activity of the regulatory enzymes was inhibited using specific blocker drugs. 1-methyl-D, L-tryptophan (1-MT) 8 mg/kg was administrated by oral route, dissolved in 100 µl of 0.5% Tween 80/ 0.5% Methylcellulose, v/v in distilled water was administrated to block IDO, and 50 µmol/kg of zinc protoporphyrin-IX(ZnPp) administered by intraperitoneal route, diluted in 0.05% DMSO v/v in PBS, to suppress HO-1. Control groups received the respective vehicle. Inhibitors were administrated daily in separate groups of H37Rv-infected mice to evaluate during the acute or progressive phase. In 5186-infected mice, both inhibitors were administered daily for 1 week, starting 17 days after infection. (Supplementary Figure S2).

2.8 Statistical analysis

All data were analyzed with GraphPad Prism 6 (GraphPad Software, Inc., La Jolla, CA). Statistical significance was defined using two-way analysis of variance (ANOVA) or one-way ANOVA test according to data characteristics, for comparing experimental groups at a 95% confidence interval ($p < 0.05$).

3 Results

3.1 Kinetics of Treg cells, indoleamine 2,3-dioxygenase, and heme oxygenase 1 during pulmonary tuberculosis produced by mild and highly virulent strains

Mice infected with mild virulent H37Rv strain showed a progressive increase of bacillary loads from day 14 post-infection, raising its peak at day 60, which correlated with progressive and extensive pneumonia that affects more than 50% of lung surface area at this time of infection (Figure 1). Mice infected with strain 5186 showed similar bacillary loads than infected mice with strain H37Rv until day 21, and then a striking sudden increase of bacillary burdens and pneumonia was seen in mice infected with the highly virulent strain at day 28 after infection (Figure 1).

The immune regulatory response was evaluated by the percentage of Treg cells (CD3+CD4+CD25+FoxP3+) from a total of CD3+CD4+ live cells (Supplementary Figure S1). Animals infected with strain H37Rv showed a stable low percentage of regulatory T cells, except at day 28 when a non-significant increase was seen (Figure 2A). Similar kinetics was observed in mice infected with the highly virulent strain 5186, but at day 28 of infection was also the peak of the percentage of Treg cells being twofold higher compared with the previous days and the same day of infection with H37Rv (Figure 2A). By immunohistochemistry in lung sections of 28 days of infection, Treg cells were found in the inflammatory infiltrate around blood vessels and airways, as well as in granulomas and pneumonic areas, being more abundant in mice infected with the highly virulent strain (Figure 2B).

IDO and HO-1 exhibited similar gene expression kinetics, showing an increase since day 1 post-infection and raising its peak at day 28 post-infection in mice infected with the H37Rv strain. Animals infected with hypervirulent strain 5186 showed maximal expression on days 14 and 21 for IDO and on day 21 for HO-1 (Figure 2C). According to these results, IDO and HO-1 expression in the lungs were studied by immunohistochemistry at 28 days post-infection with either strain. Both IDO and HO-1 were

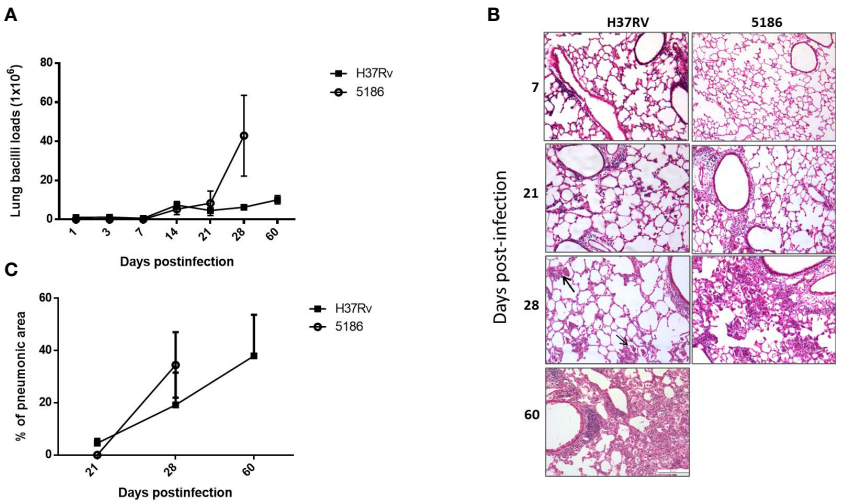

FIGURE 1
Comparison of pulmonary bacillary loads and tissue damage in BALB/c mice infected with mild or hypervirulent M. tuberculosis strains. **(A)** Male mice infected by intratracheal route with high dose of mild virulent H37Rv strain or highly virulent 5186 strain were euthanized in the indicated days, and the right lungs of three mice were used to determine bacillary loads by colony forming units count. **(B)** Left lungs were perfused with absolute ethylic alcohol and used to get tissue sections to determine the percentage of area affected by pneumonia with automated morphometry. Asterisks represent statistical significance ($p < 0.5$). **(C)** Representative micrographs of the lungs after the indicated days of infection, similar inflammatory infiltrate around blood vessels and airways was produced by either mycobacterial strains after 1 and 3 weeks of infection, small and focal areas of pneumonia were observed after 1 month of infection with mild virulent H37Rv strain (arrows), while extensive pneumonia at the same time point was seen in animals infected with highly virulent 5186 strain that was similar after two months of infection with strain H37Rv (all micrographs 200× magnification, stain with haematoxylin/eosin).

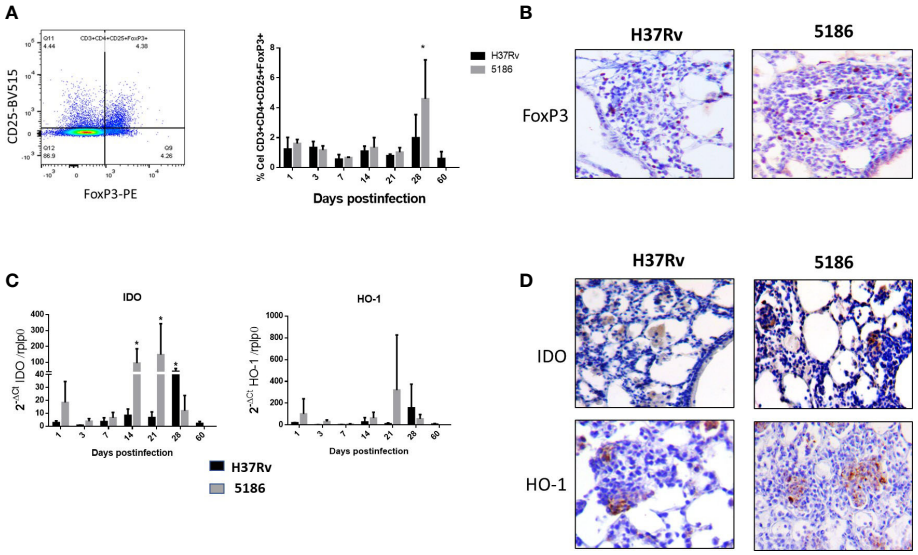

FIGURE 2
Comparative kinetics of Treg cells during pulmonary infection with mild or highly virulent M. tuberculosis strains. **(A)** Left panel shows the cytofluorometry dot distribution for the selection of CD-4/CD-25/FoxP3 cells. Right panel shows the comparative percentage of Treg cells determined by cytofluorometry in lung homogenates after the infection with mild virulent strain H37Rv (black bars) and hyper-virulent strain 5186 (gray bars). **(B)** Representative micrographs of perivascular inflammation after 28 of infection with the indicated strain, positive immunostaining of FoxP3 is observed in some lymphocytes, being more numerous in the mouse infected with the 5186 highly virulent strain. **(C)** Groups of three mice infected with mild virulent strain H37Rv (black bars) or highly virulent strain 5186 (gray bars) were euthanized at the indicated days of infection, their lungs were homogenized and the gene expression of IDO and HO-1 was determined by RT-PCR. Asterisks represent statistical significance ($p < 0.5$). **(D)** Representative micrographs of IDO and HO-1 detection by immunohistochemistry after 28 days of infection with the indicated strain, immunostained cells are macrophages located in pneumonia areas, being more numerous in the infection with 5186 strain (40× magnification).

essentially detected in pneumonic areas, particularly strong staining was detected in macrophages (Figure 2D).

3.2 The effect of depletion of regulatory T cells during H37Rv and 5186 *Mycobacterium tuberculosis* strains infection

To study the participation of Treg cells during the course of the disease, these cells were depleted by the administration of monoclonal antibody anti-CD25 (PC61 clone). To confirm the antibody effect, percentages of T cells were determined at days 7 and 21 after antibody administration in mice infected with H37Rv. Treated mice showed a significant fivefold lesser Treg cells percentage compared with controls on day 7, while on day 21, similar percentages between control and treated mice were observed. No significant differences in the percentages of Th1/Th2 cells were found in treated mice (Supplementary Figure S3).

Considering that Treg cells are constantly present during the course of H37Rv strain infection with minimal fluctuations, anti-CD25 antibodies were administrated 1 day before infection; the control group received an irrelevant isotype IgG antibody. In comparison with control mice, a significant decrease in bacillary load was seen in animals treated with the antibodies at day 60 post-infection (Figure 3A). The expression of significant cytokines in the immune response during pulmonary TB (IFN-γ, IL-4, TNF- α, and TGF-β) was determined. Treated animals showed an increase of IFN-γ that was significant on days 21 and 28, while IL-4 shows a significant decrease on day 28 post-infection. Due to the large SD, treated mice showed a non-significant increase in TNF-α at days 21 and 28. No differences were observed in TGF-β expression, while the extension of pneumonic areas was similar between treated and control animals (Figures 3B, C).

Mice infected with the highly virulent strain 5186 also showed a constant percentage of pulmonary Treg cells during the course of the infection, except at day 28 when the significantly higher increase was determined in coexistence with extensive pneumonia and high bacillary loads. Thus, mice infected with this highly virulent strain received the anti-CD25 1 day before infection or at day 17 post-infection in order to get efficient Treg depletion at day 28 of infection. When Treg cells were depleted since day 1 of infection, a decrease in bacilli load was seen at day 21 postinfection when compared with control mice (Figure 4A). In comparison with control mice, histopathology analysis showed in treated mice more inflammatory infiltrate constituted by macrophages, lymphocytes, and numerous neutrophils around blood vessels and airways, as well as more well-formed granulomas after 2 weeks of infection. At day 21 of infection, treated mice showed groups of macrophages with lymphocytes congregated in the center of some alveoli that correspond to areas of alveolitis, while control mice showed extensive pneumonia (Figure 4B). Neutrophil recruitment was confirmed by immunohistochemistry, showing a higher number of Ly6G positive cells in treated mice compared with control (Figure 4C). Because the inflammatory response in treated mice was different than in control animals, the production of

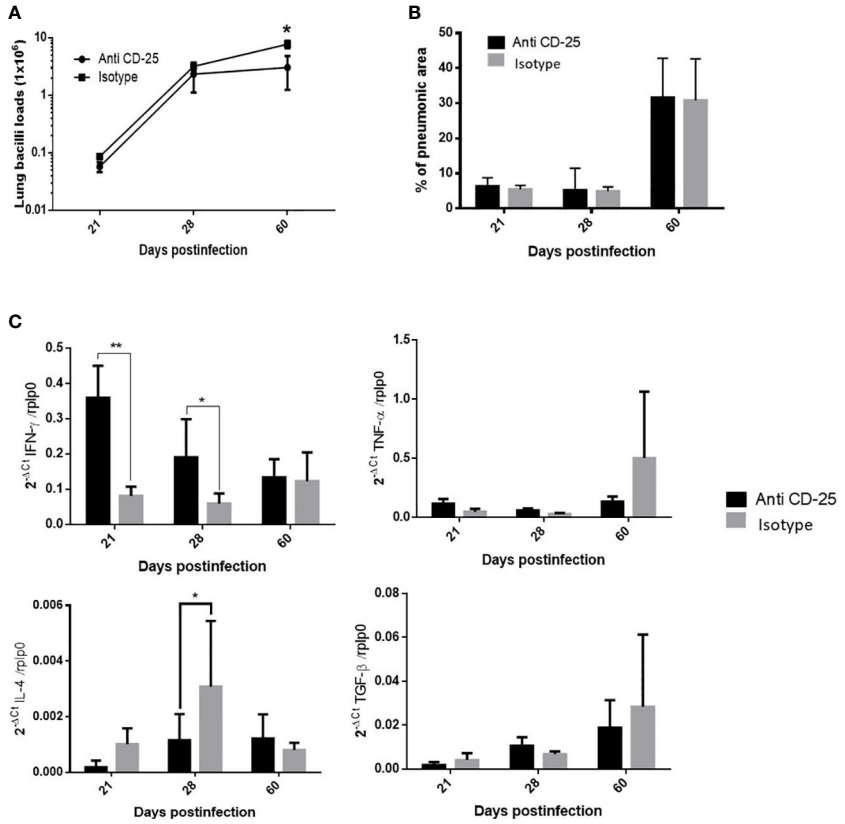

FIGURE 3
The effect of Treg cells depletion in BALB/c mice infected with mild virulent M. tuberculosis strain H37Rv. **(A)** Treg cells were depleted by the intraperitoneal administration of 200 µg of monoclonal antibodies anti-CD25 mAb (PC61 clone), 1 day before infection with mild virulent strain H37Rv in BALB/c mice, while control infected mice received the same amount of irrelevant isotype antibodies by the same route, groups of three mice were euthanized at the indicated days and their right lungs were used to determine bacillary loads by colony forming units quantification. **(B)** Left lungs were perfused with ethylic alcohol to obtain histological sections that were used to determine the percentage area affected by pneumonia by automated morphometry. **(C)** Frozen lungs from three mice per group in the indicated days of infection were used to isolate total RNA, which was used to determine the expression of pro-inflammatory (IFN-γ and TNF-α) and anti-inflammatory (IL-4 and TGF-β) cytokines by RT-PCR. Asterisks represent statistical significance ($p < 0.5$).

cytokines was evaluated by immunohistochemistry and automated morphometry, which showed more immune stained cells to IFN-γ, TNF-α, and IL-17 in the perivascular inflammatory infiltrate and granulomas of treated mice than in control animals (Figure 4C).

Infected mice with highly virulent TB strain and treated with anti-CD25 antibodies at day 17 of infection showed similar bacillary loads and pneumonia to the control group after 1 week of Treg cell depletion (24 days postinfection) (Figure 5A). However, survival decreased considerably in anti-CD25–treated mice before day 28 post-infection and survivor animals were very sick; so, for humane reasons, all the animals were euthanized on day 28 after infection. At this time point, animals with Treg cell depletion showed fivefold more CFU than control mice (Figure 5A). The lungs of control mice showed extensive pneumonia, while animals treated with monoclonal antibodies against CD-25 exhibited diffuse alveolar damage that affect 46 ± 8% of the lung surface. Diffuse alveolar damage was characterized by the deposition of thick eosinophilic hyaline membranes on the surface of alveolar walls, in coexistence with mononuclear inflammatory cells infiltrate in the alveolar-capillary interstitium (Figure 5B). These histological abnormalities are quite similar to the common tissue damage induced by severe acute viral infection. Diffuse alveolar damage was confirmed by the presence of fibrin in these hyaline membranes demonstrated by histochemistry (phosphotungstic acid/hematoxylin staining) (Figure 5C). An imbalance of Th17/Treg cells can induce acute lung injury with elevated expression of IL-17 and IL-22, as well as pro-inflammatory cytokines such as TNF-α and IL-1-β (Zhang et al., 2016; Stephen et al., 2018; Wang et al., 2019). In agreement with this, areas with hyaline membranes exhibited numerous lymphocytes with intense IL-17 immunostaining and macrophages showing strong reactivity to TNF-α and IL-1-β, while in non-treated mice, these cytokines were expressed in pneumonic areas. Automated morphometry confirmed the higher percentage of positive cells to IL-17 and TNF-α in treated mice compared with the control group (Figure 5D), but no differences were observed in the expression of IL-17 and TNF-α determined by RT-PCR in whole lungs homogenates; only IL-22 showed higher but no significant expression in treated mice compared with controls (Figure 6A). To evaluate changes in endothelium in areas of diffuse alveolar damage, PECAM-1, GPIV, P selectin, and VCAM-1 showed strong immunostaining in endothelial cells, alveolar epithelium and leukocytes that was confirmed by

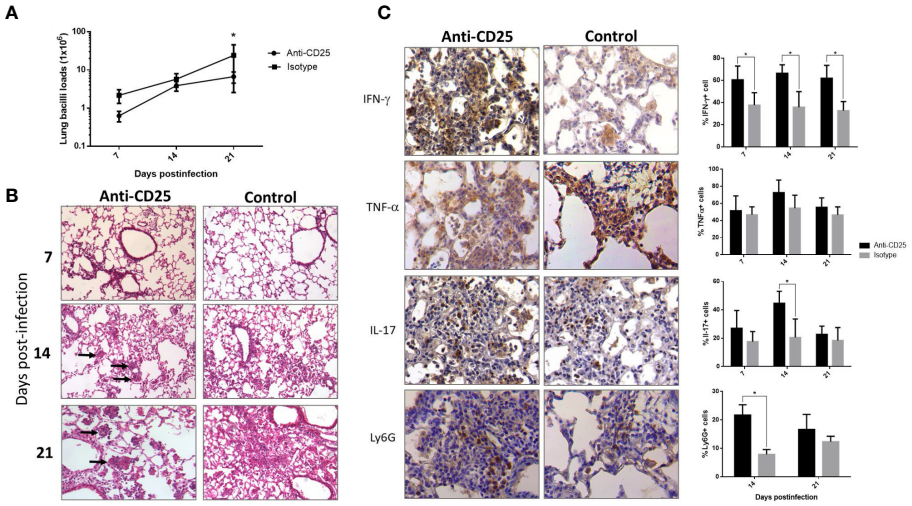

FIGURE 4
The effect of Treg cells depletion during early phase, in BALB/c mice infected with highly virulent M. tuberculosis strain. **(A)** Treg cells were depleted by the intraperitoneal administration of 200 μg of monoclonal antibodies anti-CD25 mAb (PC61 clone) 1 day before infection with highly virulent strain 5186 in BALB/c mice, while control infected mice received the same amount of irrelevant isotype antibodies by the same route, groups of three mice were euthanized at 7, 14, and 21 days of infection and their right lungs were used to determine bacillary loads by colony forming units quantification. **(B)** Representative comparative micrographs of the lungs from anti CD-25 mAb-treated and control-infected mice; at day 7 of infection, there is slight higher perivascular inflammation in mouse treated with the CD-25 antibodies. After 2 weeks of infection, treated mouse show more well-formed granulomas (arrows). After 3 weeks of infection, treated animal show in the center of many alveoli conglomerates of inflammatory cells (arrows) that correspond to alveolitis, while control mouse shows extensive pneumonia. **(C)** Representative comparative immunohistochemistry micrographs of the lungs from anti CD-25 mAb treated and control; after 21 days of infection, there are more immunostained cells of the indicated cytokine in granulomas from treated than control animals, perivascular inflammation also shows more neutrophils positive to the marker Ly6G in treated mice. This was confirmed by semi-quantitative automated morphometry (right panel). Asterisks represent statistical significance ($p < 0.5$).

automated morphometry, which showed higher percentages of positive cells for these adherence molecules in anti-CD25–treated mice than in control animals (Figure 6B).

3.3 The effect of blocking indoleamine 2,3-dioxygenase, and heme oxygenase 1 during infection with mild virulent H37Rv or highly virulent 5186 strain

Considering that gene expression of IDO and HO-1 was detected since the beginning of the H37Rv strain infection and showed their peak at 28 days of infection, the inhibitor 1MT of IDO activity and ZnPp that block HO-1 was administrated during the second and third week of infection, and mice were euthanized at 2 months of infection. In comparison with non-treated control mice, treated animals with IDO blocker showed a non-significant decrease of pulmonary bacillary counts and lesser expression of IFN-γ, IL-4, TNF-α, and TGF-β, as well as lesser pneumonia, but these were non-significant (Supplementary Figure S4A). Infected animals with the H37Rv strain and treated with the HO-1 inhibitor ZnPp administered during the second and third week of the infection, and euthanizing mice after 60 days of infection showed lower bacillary loads and pneumonia, as well as higher expression of IFN-γ and lower transcription of IL-4 and TGF-β, but only the transcription of TGF-β was significant (Supplementary Figure S5A).

Because macrophages from pneumonic areas in late disease were the principal IDO and HO-1 immunostained cells, another experiment was performed administrating the inhibitors of these enzymes from the first month after infection and for 2 months, euthanizing mice at 60 and 90 days after infection. In comparison with control, non-treated mice, blocking IDO produced a decrease of bacilli burdens at day 60 post-infection, without significant difference in IFN-γ, TNF-α, and IL-4 expression. No changes in the pneumonic area were observed either (Supplementary Figure S4B**).** Blocking HO-1 administrating ZnPp during late TB induced non-significant lesser bacterial loads, while cytokines expression and pneumonic area were similar in both groups (Supplementary Figure S5B).

To evaluate the role of regulatory response mediated by IDO and HO-1 during hypervirulent strain infection and due to the low number of survivor mice, animals infected with strain 5186 were treated with both 1MT and ZnPp to block IDO and HO-1 since day 17 post-infection, and control non-treated and treated mice were euthanized at day 28 post-infection. In comparison with control animals, mice treated with both 1MT and ZnPp showed higher bacillary loads at day 28 of infection (Figure 7A). There was a lower percentage of lung surface area affected by pneumonia in treated animals, and some of these pneumonic areas show extensive necrosis manifested by numerous cells with a condensed or fragmented nucleus and cytoplasmic disruption (Figure 7B). To study the inflammatory response related to necrosis in TB infection, the expression of IL-4, IL-17, TGF-β, and TNF-α was evaluated.

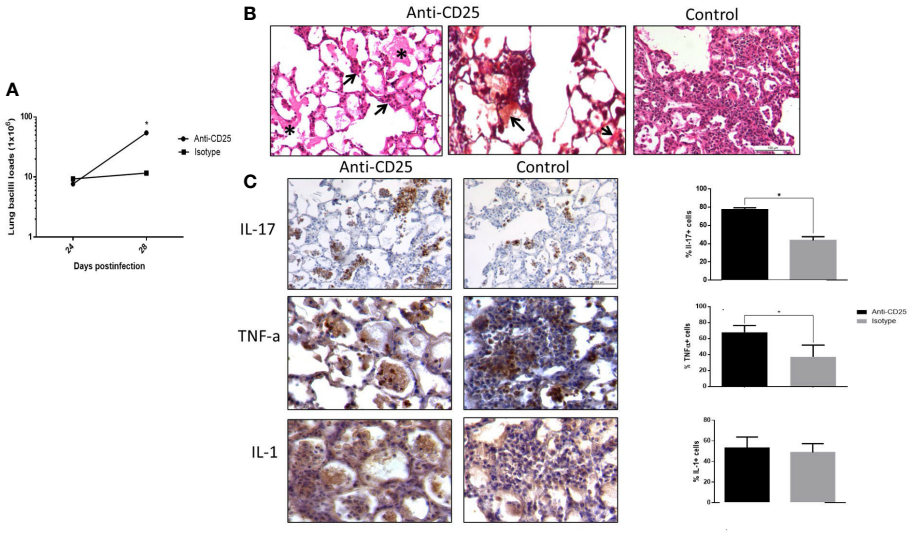

FIGURE 5
The effect of Treg cells depletion in BALB/c mice infected with highly virulent M. tuberculosis strain. **(A)** Treg cells were depleted by the intraperitoneal administration of 200 µg of monoclonal antibodies anti-CD25 mAb (PC61 clone) at day 17 of infection with highly virulent strain 5186 in BALB/c mice, while control-infected mice received the same amount of irrelevant isotype antibodies by the same route, groups of three mice were euthanized at 24 and 28 days of infection and their right lungs were used to determine bacillary loads by colony forming units quantification. There is a significant increase of bacillary burdens at 28 days of infection in treated animals. **(B)** Representative comparative micrographs of treated and control animals after 28 days of infection, left figure correspond to treated mouse that shows eosinophilic hyaline membranes on the surface of alveolar walls (asterisk) and chronic inflammatory infiltrate in the alveolar capillary interstitium (arrows), which characterize diffuse alveolar damage. Centre figure show a section from the same treated mouse stained with Phosphotungstic acid haematoxylin that show positivity, red staining (arrows) of the hyaline membranes confirming that they are constituted by fibrin, while control non-treated infected mice show extensive pneumonia (right figure). **(C)** Representative micrographs of cytokines detection by immunohistochemistry in the lungs of mice after 28 days of infection with highly virulent M. tuberculosis strain and treated or not with anti-CD25 monoclonal antibodies, treated mouse shows more immunostained cells of the indicated cytokines in areas of alveolar damage than in pneumonic areas of control animal, which is confirmed by automated semiquantitative morphometry (right panel). Asterisks represent statistical significance ($p < 0.5$).

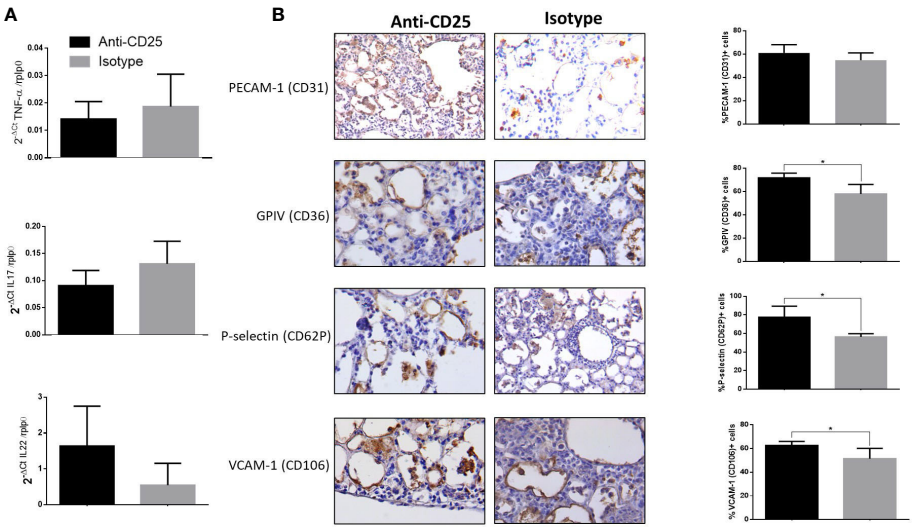

FIGURE 6
Detection of adherence molecules by immunohistochemistry and expression of cytokines in mice infected with hyper virulent M. tuberculosis strain. **(A)** Groups of mice infected with highly virulent strain 5186 and treated or not with monoclonal antibodies anti-CD25 mAb (PC61 clone) were euthanized after 28 days of infection, and their right lungs were used to determine the expression of IL-22, IL-17, and TNF-α by RT-PCR. **(B)** Representative immunohistochemistry micrographs of the indicated molecules detected after 28 days of infection, in areas of diffuse alveolar damage from treated animals with anti-CD25 monoclonal antibodies and pneumonic areas from control non-treated animals. All the determined adhesion molecules are more expressed in treated mice than in control animals, which is confirmed by automated semiquantitative morphometry (right panel) determining in five fields for each sample the number and percentage of positive cells. Asterisks represent statistical significance ($p < 0.5$).

The expression of cytokines determined at day 28 of infection showed similar expression between control and treated groups; only significantly lower gene expression of TGF-β in treated animals than control mice was observed, and these treated mice showed lesser but no significative percentage of TGF-β–stained cells in the pneumonic areas than control mice (Figures 7C, D).

4 Discussion

A successful host immune response is generally the result of pro- and anti-inflammatory factors that are carefully tuned with the aim to eliminate the pathogen and limiting tissue damage. The tune and balance of pro and anti-inflammatory factors is a dynamic process that requires a constant relation between the pathogen and the immune cells and their cytokines production. This interaction is not always quantitative, with equal concentrations of pro- and anti-inflammatory cytokines and a similar number of immune cells, but it is more a qualitative harmonization in downstream activation and inhibition in which the pathogen is also a significant participant (Cicchese et al., 2018). Regarding TB, the participation of Treg cells in this regulatory activity and whether they are beneficial or detrimental is a recurring debate (Cardona and Cardona, 2019).

Many reports revealed that there is an increase in Treg cells, IDO, and HO-1 in patients with active or latent TB (Churina et al., 2012; Suzuki et al., 2012; Andrade et al., 2015). These high levels of immune-regulatory factors should be a consequence of intense inflammation, but it is not completely clear if these immune-regulatory factors are beneficial or deleterious for the development or severity of TB. Previously in our murine TB model using the H37Rv strain was observed a biphasic increase in the gene expression of Fox-p3, IDO, and HO-1 (Hernández-Pando et al., 2008), with high expression of these molecules after one week, followed by a decrease and an increase again after one month of infection (Hernández-Pando et al., 2008), which is the time point when in our model start pneumonia formation and there is high production of IFN-γ (Hernandez-Pando et al., 1996). It is known that Treg cells, IDO, and HO-1 increase in stress conditions and pro-inflammatory environments, mainly with high IFN-γ levels (Quinn et al., 2006; Sun et al., 2011; Schumacher et al., 2012). Treg cells, IDO, and HO-1 enzymes lead to a decrease of effector cell proliferation and induce apoptosis by diverse mechanisms, resulting in a decrease in pro-inflammatory cytokines production (Hori and Sakaguchi, 2004; Bettelli et al., 2005; Fontenot and Rudensky, 2005), which is the type of immune response produced during late infection in our murine model (Hernandez-Pando et al., 1996). Treg cells were depleted or the activity of IDO and HO-1 was inhibited since the beginning of infection with mild virulence strain H37Rv, the administration of anti-CD25 antibodies or enzyme blockers was initiated at this time because these regulatory factors started their increase since day 1 and it was relatively stable during the infection, an increase of IFN-γ expression was observed, but this was only significant with Treg cell depletion. This result is in concordance with the results of other groups that also observed an increment in pro-inflammatory cytokines and a decrease in anti-inflammatory activity when they used inhibitors of these immune

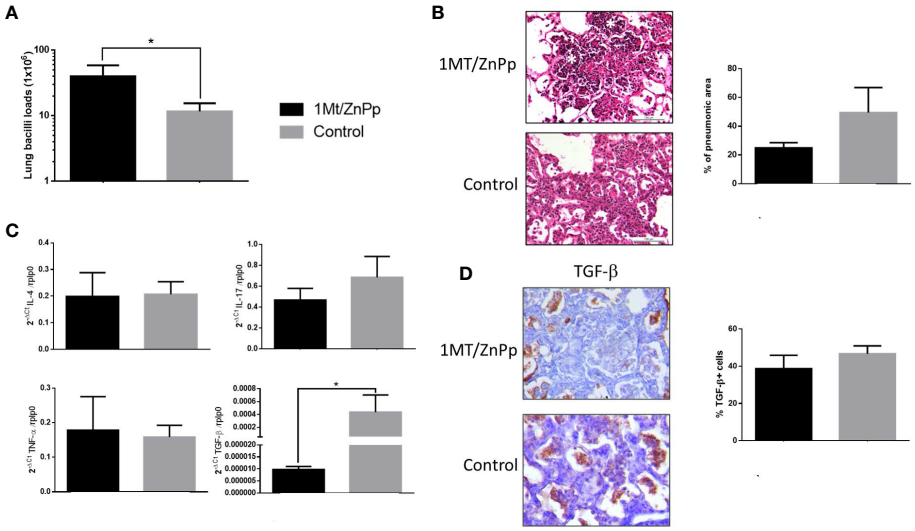

FIGURE 7
The effect of suppress IDO and HO-1 during pulmonary infection with hyper virulent mycobacteria. **(A)** Mice infected with highly virulent strain 5186 were treated or not with 1MT and ZnPp to block both IDO and HO-1 since day 17 post-infection, and groups of mice were euthanized at days 24 and 28 post-infection, right lungs were used to determine bacillary burdens. Treated mice showed significant higher bacillary loads. **(B)** Representative micrographs of control non-treated mice after 28 days of infection showed extensive pneumonia, treated mice showed also extensive pneumonia but with focal areas of necrosis manifested by cells with condensed (picnotic) or fragmented (cariorrexis) nucleus (white asterisks). In the same section was determined the percentage of pneumonic areas by automated morphometry. **(C)** The lungs of other group of mice after 28 days of infection from treated and control groups were used to isolate total RNA, and the expression of the indicated cytokines was determined by RT-PCR. Treated mice only showed significant lower expression of TGF-β. **(D)** Representative micrographs of the immunohistochemistry detection of TGF-β. Semi-quantitative analysis was performed to identified percentage of positive cells, from five fields random chosen. Asterisks represent statistical significance ($p < 0.5$).

regulator factors (Belkaid et al., 2002; Kohm et al., 2006; Jaron et al., 2008). Our determination of pulmonary bacilli burdens showed a significant decrease in mice infected with mild virulence H37Rv strain and depletion of Treg cells or late inhibition of IDO activity, which correlated with an increase of IFN-γ and a decrease of IL-4 that favored the protective Th1 response. Thus, the experimental decrease of Treg cells and IDO in BALB/c mice infected with mild virulence reference strain H37Rv is beneficial, which is in agreement with the previous observations that show delayed recruitment of effector cells by Treg cells in the lung during early TB (Shafiani et al., 2010), when Tregs were depleted in the early phase of infection, effector T cells migrated correctly and limit the expansion of bacilli load in progressive phase but is not enough to change the course of infection. One limitation of our work was the missed experiment of Treg cells depletion since day 28 of infection with strain H37Rv, when the peak of these cells was seen and pneumonia started its formation, we suppose that the beneficial effect of Treg cells deletion should be more evident starting at this time, because there is in the pneumonic areas Treg cells in co-existence with macrophages that exhibited IDO and HO-1 strong immunostaining. Other groups reported previously that when they depleted Treg or inhibited IDO enzyme, bacilli loads were not affected, although there was an increase in pro-inflammatory cytokines (Quinn et al., 2006; Mulley and Nikolic-Paterson, 2008; Divanovic et al., 2012), and a similar response was observed in mice that received ZnPP to inhibit HO-1 (Hou et al., 2007). In this regard, it is important to consider the complexity of these immune regulatory mechanisms; actually, they mutually modulate directly or indirectly. This is the case of nitric oxide (NO), which is produced by the enzyme inducible nitric oxidase synthase (iNOS) and is a significant mycobactericidal agent, particularly in mice (Hernández-Pando et al.,). HO-1 expression reduced iNOS activity and therefore NO production, while NO diminished IDO activity. Hence, a decrease in NO production by HO-1 activity indirectly increased IDO activity (Srisook and Cha, 2005). Another example is the close relationship between IDO expression and Treg polarization from Th0 cells and their maintenance (Sun et al., 2011); also, Treg cells induce IDO expression through CTLA-4 in DCs and macrophages (Sun et al., 2011; Efimov et al., 2012). Nevertheless, the pro-inflammatory environment is the principal inductor of the regulatory response, so that the experimental depletion of Treg or the specific inhibition of IDO or HO-1 can induce diverse mechanisms that compensate for the intervened regulatory response.

When Treg cells were depleted 1 day before infection with highly virulent strain 5186, recruitment of leukocyte cells was higher than in control mice after 1 week of infection, which correlated with a previous report that observed Treg cells delay migrations cells to the lung (Shafiani et al., 2010). Also, a higher IFN-γ production was observed at all analyzed days postinfection, as was previously described (Quinn et al., 2006; Singh et al., 2012). This was manifested in the more organized and effective inflammatory response, with well-organized granulomas and lower bacilli load, with alveolitis instead of pneumonia at day 21 postinfection in treated mice, that contrasted with control animals, that showed extensive pneumonia. A previous report has characterized the TB granuloma microenvironment and observed an important regulatory activity that includes Treg cells and IDO expression, which can decrease the efficiency of granuloma to contain mycobacteria growth (McCaffrey et al., 2022). Mice that received anti-CD25 at the beginning of infection to deplete Treg cells showed well-formed granulomas than in control mice at day 21 post-infection. Moreover, there was higher neutrophil recruitment in treated mice compared with control, associated with higher production of IL-17 that correlated with the well-known imbalance of Th17/Treg (Fletcher et al., 2009; Da Silva et al., 2015; Agrawal et al., 2018; Safar et al., 2020). All these observations may influence the decrease of lung bacilli load and inflammation in our treated mice.

Interestingly, when Treg cells were depleted after 2 weeks of infection in mice infected with a highly virulent strain 5186, extensive diffuse alveolar damage was observed, which was quite similar to sepsis or severe acute viral pneumonia, such as the fatal cases of COVID-19 (Sadegh Beigee et al., 2020) or in HIV/AIDS immune deficient patients with bacterial infections (de Matos Soeiro et al., 2008). Alveolar diffuse damage is occasionally reported in miliary TB, which is a condition similar to sepsis (Kim et al., 2003).

It is known that an imbalance of Th17/Tregs is associated with poor prognosis in acute pulmonary inflammation (Cheung et al., 2011), and it has been demonstrated that Treg cells constrain pathogenic Th17 cells (Fletcher et al., 2009). We observed numerous IL-17 cells, particularly in the inflammatory infiltrate associated with areas of alveolar diffuse damage, which suggest an imbalance of Th17/Treg cells in these areas. This focal circumscribed location of a high number of IL-17 cells could explain the similar expression of IL-17 between Treg cells depleted and control animals that showed extensive pneumonia with numerous Treg cells, determined by RT-PCR in whole lung homogenates. A similar pattern was seen in the expression of the pro-inflammatory cytokine TNF-α and IL-22 which are significant participants in this kind of pulmonary lesion (Eyerich et al., 2017). Diffuse alveolar damage is characterized by hyaline eosinophilic membranes deposited on the surface of the alveolar epithelium. These membranes are essentially constituted by fibrin, which was clearly evidenced by its positive staining with the phosphotungstic acid hematoxylin technique. Capillary endothelium in areas of diffuse alveolar damage suffers changes that permit leukocyte recruitment and activation, as well as plasma proteins exudation. Among the most important changes is the overexpression of adhesion molecules, such as PECAM-1, GPIV, P-selectin, and VCAM-1. In areas of diffuse alveolar damage, all these molecules were demonstrated by strong immunohistochemistry positivity in capillary endothelium and some inflammatory cells. PECAM-1 is highly expressed in activated endothelial cells and in platelets, monocytes, neutrophils, T cells, and B cells; it has a crucial role in capillary morphogenesis, migration, and junctional development (Privratsky and Newman, 2014). PECAM-1 has anti-inflammatory and pro-inflammatory functions (Carrithers et al., 2005; Sugimoto et al., 2008; Privratsky and Newman, 2014). Here, we observed more expression of PECAM-1, particularly in endothelial cells and recruited leucocytes in the areas of alveolar damage, so this molecule may contribute to this type of lesion through cell

recruitment and fluid exudate production. Major glycoprotein of platelets (CD36) is a scavenger receptor expressed by platelets, macrophages, endothelial cells, and smooth muscle cells. CD36 participates in tumor maintenance through its expression in intratumoral Treg cells by CD36-dependent metabolic adaptation (Wang et al., 2020) and also participates in inflammation and sterile inflammation *via* TLR 4 and 6 activations (Stewart et al., 2010; Xu et al., 2018). We observed an increase of CD36 positive cells in mice with 5186 strain infection treated with anti-CD25; the high expression of CD-36 can enhance a pro-inflammatory environment favoring alveolar acute damage. Another adhesion molecule that we observed increased in mice infected with hypervirulent strain and treated with anti-CD25, was P-selectin. This molecule is expressed on activated endothelium and platelets, and its ligands PSGL1 and PSL2 are expressed in leucocytes, participating in T-cell recruitment during antigen stimulation (Carlow et al., 2018). We observed P-selectin expression in endothelial cells and interestingly in macrophages, which indicates endothelium activation that enhances inflammatory cells recruitment. Recently there was reported the importance of homeostasis of Treg cells and platelets *via* CD40L-CD40 and PSGL1-P-Sel interaction, the interruption of these pathways leads to hyperinflammation (Rupp et al., 2021), which partially can explain the excessive inflammatory response when Tregs cells were depleted during infection with hypervirulent MTB strain. Finally, we evaluated VCAM-1, which is an Ig-like adhesion molecule expressed on endothelial cells induced by inflammatory cytokines that play a critical role in leucocyte recruitment during acute or chronic inflammation (Chen and Massagué, 2012). VCAM-1 overexpression was associated with lung inflammation (Park et al., 2021), and it is highly expressed on endothelial cells located in the areas of alveolar damage developed in mice treated with anti-CD25. Thus, the high expression of all these adhesion molecules in lungs from mice infected with strain 5186 and treated with anti-CD25 should contribute to the observed diffuse alveolar damage; however, more studies are necessary to elucidate their real contribution in this type of tissue damage, which should also be related with devitalization of the lung tissue and the immune response considering the very high bacillary loads that were found in these mice.

Small and occasional areas of alveolar damage were seen in mice infected with highly virulent strain 5186 treated with both drugs to block the activity of IDO and HO-1; the percentage of pneumonic areas was lesser in treated mice than in control animals, but in contrast with control animals, treated mice showed in the pneumonic areas extensive areas of necrosis. On the other hand, HO-1 metabolites also have cytoprotective proprieties, for example, which protect against free radical-mediated immunopathology, limiting the damage during TB infection (Chinta et al., 2018), there is evidence of the importance of HO-1 to protect from necrosis during TB infection that was observed in mice infected with hypervirulent strain and blocking HO-1 and IDO activity. The lungs of these treated animals showed significantly lower expression of TGF-β than control mice, suggesting that one of the factors related to necrosis was the suppression of TGF-β, which is a significant anti-inflammatory factor that participates in the control of excessive inflammation during late infection in this experimental model (Hernández-Pando et al., 2006) and human TB (Toossi and Ellner, 1998).

In conclusion, our results suggest that Treg cells delay the recruitment of effector cells and balance the inflammatory response during early infection with mild virulence or hypervirulent MTB strain, their depletion increases some proinflammatory cytokines and neutrophil recruitment that reduce the bacillary load but is not enough to change the final course of the disease. IDO and HO-1 activities facilitate bacterial growth during late pulmonary TB when the infection is produced by mild virulence MTB. It seems that Treg cells and the enzymes IDO and HO-1 are crucial to suppress excessive inflammation, preventing diffuse alveolar damage or necrosis when the infection is produced by a highly virulent strain. Thus, one important factor that contributes to the protective or detrimental immune regulation activity is the infection phase and mycobacterial level of virulence.

Data availability statement

The original contributions presented in the study are included in the article/Supplementary Material. Further inquiries can be directed to the corresponding author.

Ethics statement

The animal study was reviewed and approved by Ethical Committee for Experimentation on Animals of the National Institute of Medical Sciences and Nutrition (INCMNSZ).

Author contributions

VL-O and RH-P contributed to the background work. VL-O and RH-P conceived experiments. VL-O performed, organized, and analyzed the results. YR-M, AO-C and SH-B performed the experiments. DM-E and JB-P contributed to mice infection procedures. RS contributed to the production of anti-CD25 and flow cytometry design. All authors contributed to the article and approved the submitted version.

Funding

VL-O is a PhD student from Programa de Doctorado en Ciencias Bioquimicas, Universidad Nacional Autónoma de México (UNAM) and received fellowship 385125 from Consejo Nacional de Ciencia y Tecnología (CONACyT). This study was supported by the CONACyT project Fon Inst./58/2016.

Conflict of interest

The authors declare that the research was conducted in the absence of any commercial or financial relationships that could be construed as a potential conflict of interest.

Publisher's note

All claims expressed in this article are solely those of the authors and do not necessarily represent those of their affiliated organizations, or those of the publisher, the editors and the reviewers. Any product that may be evaluated in this article, or claim that may be made by its manufacturer, is not guaranteed or endorsed by the publisher.

Supplementary material

The Supplementary Material for this article can be found online at: https://www.frontiersin.org/articles/10.3389/fcimb.2023.1105872/full#supplementary-material

References

Agrawal, S., Parkash, O., Palaniappan, A. N., Bhatia, A. K., Kumar, S., Chauhan, D. S., et al. (2018). Efficacy of T regulatory cells, Th17 cells and the associated markers in monitoring tuberculosis treatment response. *Front. Immunol.* 9. doi: 10.3389/fimmu.2018.00157

Andrade, B. B., Pavan Kumar, N., Amaral, E. P., Riteau, N., Mayer-Barber, K. D., Tosh, K. W., et al. (2015). Heme oxygenase-1 regulation of matrix metalloproteinase-1 expression underlies distinct disease profiles in tuberculosis. *J. Immunol.* 195, 2763–2773. doi: 10.4049/jimmunol.1500942

Andrade, B. B., Pavan Kumar, N., Sridhar, R., Banurekha, V., Jawahar, M. S., Nutman, T. B., et al. (2014). Heightened plasma levels of heme oxygenase-1 and tissue inhibitor of metalloproteinase-4 as well as elevated peripheral neutrophil counts are associated with TB-diabetes comorbidity. *Chest* 145, 1244–1254. doi: 10.1378/chest.13-1799

Arram, E. O., Hassan, R., and Saleh, M. (2014). Increased frequency of CD4+CD25+FoxP3+ circulating regulatory T cells (Treg) in tuberculous patients. *Egyptian. J. Chest. Dis. Tuberculosis.* 63, 167–172. doi: 10.1016/j.ejcdt.2013.10.013

Behar, S. M., Divangahi, M., and Remold, H. G. (2010). Evasion of innate immunity by mycobacterium tuberculosis: is death an exit strategy? *Nat. Rev. Microbiol.* 8, 668–674. doi: 10.1038/nrmicro2387

Belkaid, Y., Piccirillo, C. A., Mendez, S., Shevach, E. M., and Sacks, D. L. (2002). CD4+CD25+ regulatory T cells control leishmania major persistence and immunity. *Nature* 420, 502–507. doi: 10.1038/nature01152

Bettelli, E., Dastrange, M., and Oukka, M. (2005). Foxp3 interacts with nuclear factor of activated T cells and NF-b to repress cytokine gene expression and effector functions of T helper cells. *Proc Natl Acad Sci USA* 102 (14), 5138–5143. doi: 10.1073/pnas.0501675102

Cardona, P., and Cardona, P.-J. (2019). Regulatory T cells in mycobacterium tuberculosis infection. *Front. Immunol.* 10. doi: 10.3389/fimmu.2019.02139

Carlow, D. A., Tra, M. C., and Ziltener, H. J. (2018). A cell-extrinsic ligand acquired by activated T cells in lymph node can bridge l-selectin and p-selectin. *PloS One* 13, e0205685. doi: 10.1371/journal.pone.0205685

Carrithers, M., Tandon, S., Canosa, S., Michaud, M., Graesser, D., and Madri, J. A. (2005). Enhanced susceptibility to endotoxic shock and impaired STAT3 signaling in CD31-deficient mice. *Am. J. Pathol.* 166, 185–196. doi: 10.1016/S0002-9440(10)62243-2

Chen, Q., and Massagué, J. (2012). Molecular pathways: VCAM-1 as a potential therapeutic target in metastasis. *Clin. Cancer Res.* 18, 5520–5525. doi: 10.1158/1078-0432.CCR-11-2904

Cheung, O.-Y., Graziano, P., and Leslie, K. O. (2011). "Acute lung injury," in *Practical pulmonary pathology: a diagnostic approach*. Eds. K. O. Leslie and M. R. Wick (United States: Elsevier), 117–136. doi: 10.1016/B978-1-4160-5770-3.00005-5

Chinta, K. C., Rahman, M. A., Saini, V., Glasgow, J. N., Reddy, V. P., Lever, J. M., et al. (2018). Microanatomic distribution of myeloid heme oxygenase-1 protects against free radical-mediated immunopathology in human tuberculosis. *Cell Rep.* 25, 1938–1952.e5. doi: 10.1016/j.celrep.2018.10.073

Churina, E. G., Urazova, O. I., and Novitskiy, V. v. (2012). The role of Foxp3-expressing regulatory T cells and T helpers in immunopathogenesis of multidrug resistant pulmonary tuberculosis. *Tuberc. Res. Treat* 2012, 1–9. doi: 10.1155/2012/931291

Cicchese, J. M., Evans, S., Hult, C., Joslyn, L. R., Wessler, T., Millar, J. A., et al. (2018). Dynamic balance of pro- and anti-inflammatory signals controls disease and limits pathology. *Immunol. Rev.* 285, 147–167. doi: 10.1111/imr.12671

Collins, H. L., and Kaufmann, S. H. E. (2001). The many faces of host responses to tuberculosis. *Immunology* 103, 1–9. doi: 10.1046/j.1365-2567.2001.01236.x

Da Silva, M. V., Massaro Junior, V. J., Machado, J. R., Silva, D. A. A., Castellano, L. R., Alexandre, P. B. D., et al. (2015). Expression pattern of transcription factors and intracellular cytokines reveals that clinically cured tuberculosis is accompanied by an increase in mycobacterium-specific Th1, Th2, and Th17 cells. *BioMed. Res. Int.* 2015. doi: 10.1155/2015/591237

de Matos Soeiro, A., Hovnanian, A. L. D., Parra, E. R., Canzian, M., and Capelozzi, V. L. (2008). Post-mortem histological pulmonary analysis in patients with HIV/AIDS. *Clinics* 63, 497–502. doi: 10.1590/S1807-59322008000400014

Divanovic, S., Sawtell, N. M., Trompette, A., Warning, J. I., Dias, A., Cooper, A. M., et al. (2012). Opposing biological functions of tryptophan catabolizing enzymes during intracellular infection. *J. Infect. Dis.* 205, 152–161. doi: 10.1093/infdis/jir621

Efimov, I., Basran, J., Sun, X., Chauhan, N., Chapman, S. K., Mowat, C. G., et al. (2012). The mechanism of substrate inhibition in human indoleamine 2,3-dioxygenase. *J. Am. Chem. Soc.* 134, 3034–3041. doi: 10.1021/ja208694g

Eyerich, K., Dimartino, V., and Cavani, A. (2017). IL-17 and IL-22 in immunity: driving protection and pathology. *Eur. J. Immunol.* 47, 607–614. doi: 10.1002/eji.201646723

Fei, D., Meng, X., Zhao, M., Kang, K., Tan, G., Pan, S., et al. (2012). Enhanced induction of heme oxygenase-1 suppresses thrombus formation and affects the protein c system in sepsis. *Trans. Res.* 159, 99–109. doi: 10.1016/j.trsl.2011.10.009

Filippini, P., del Papa, N., Sambataro, D., del Bufalo, A., Locatelli, F., and Rutella, S. (2012). Emerging concepts on inhibitors of indoleamine 2,3-dioxygenase in rheumatic diseases. *Curr. Med. Chem.* 19, 5381–5393. doi: 10.2174/092986712803833353

Fletcher, J. M., Lonergan, R., Costelloe, L., Kinsella, K., Moran, B., O'Farrelly, C., et al. (2009). CD39 $^{+}$ Foxp3 $^{+}$ regulatory T cells suppress pathogenic Th17 cells and are impaired in multiple sclerosis. *J. Immunol.* 183, 7602–7610. doi: 10.4049/jimmunol.0901881

Fontenot, J. D., and Rudensky, A. Y. (2005). A well adapted regulatory contrivance: regulatory T cell development and the forkhead family transcription factor Foxp3. *Nat. Immunol.* 6, 331–337. doi: 10.1038/ni1179

Global Tuberculosis reporT 2022 (2022). Available at: http://apps.who.int/bookorders.

Hernández-Pando, R., Aguilar, D., Orozco, H., Cortez, Y., Brunet, L. R., and Rook, G. A. (2008). Orally administered mycobacterium vaccae modulates expression of immunoregulatory molecules in BALB/c mice with pulmonary tuberculosis. *Clin. Vaccine Immunol.* 15, 1730–1736. doi: 10.1128/CVI.00286-08

Hernández-Pando, R., Marquina-Castillo, B., Barrios-Payán, J., and Mata-Espinosa, D. (2012). Use of mouse models to study the variability in virulence associated with specific genotypic lineages of mycobacterium tuberculosis. *Infection. Genet. Evol.* 12, 725–731. doi: 10.1016/j.meegid.2012.02.013

Hernandez-Pando, R., Orozcoe, H., Sampieri, A., Pavon, L., Velasquillo, C., Larriva-Sahd, J., et al. (1996). Correlation between the kinetics of Thl/Th2 cells and pathology in a murine model of experimental pulmonary tuberculosis.

Hernández-Pando, R., Orozco-Esteves, H., Maldonado, H. A., Aguilar-León, D., Vilchis-Landeros, M. M., Mata-Espinosa, D. A., et al. (2006). A combination of a transforming growth factor-β antagonist and an inhibitor of cyclooxygenase is an effective treatment for murine pulmonary tuberculosis. *Clin. Exp. Immunol.* 144, 264–272. doi: 10.1111/j.1365-2249.2006.03049.x

Hernández-Pando, R., Schön, T., Orozco, E. H., Serafin, J., Estrada-García, I., and Hernandez Pando, R. *Expression of inducible nitric oxide synthase and nitrotyrosine during the evolution of experimental pulmonary tuberculosis*. Available at: http://www.urbanfischer.de/journals/exptoxpath.

Hori, S., and Sakaguchi, S. (2004). Foxp3: a critical regulator of the development and function of regulatory T cells. *Microbes Infect.* 6, 745–751. doi: 10.1016/j.micinf.2004.02.020

Hou, D. Y., Muller, A. J., Sharma, M. D., DuHadaway, J., Banerjee, T., Johnson, M., et al. (2007). Inhibition of indoleamine 2,3-dioxygenase in dendritic cells by

stereoisomers of 1-methyl-tryptophan correlates with antitumor responses. *Cancer Res.* 67, 792–801. doi: 10.1158/0008-5472.CAN-06-2925

Jaron, B., Maranghi, E., Leclerc, C., and Majlessi, L. (2008). Effect of attenuation of treg during BCG immunization on anti-mycobacterial Th1 responses and protection against mycobacterium tuberculosis. *PloS One* 3, e2833. doi: 10.1371/journal.pone.0002833

Kim, J. Y., Park, Y. B., Kim, Y. S., Kang, S. B., Shin, J. W., Park, I. W., et al. (2003). Miliary tuberculosis and acute respiratory distress syndrome. *Int. J. Tuberc. Lung Dis.* 7, 359–364.

Kohm, A. P., McMahon, J. S., Podojil, J. R., Begolka, W. S., DeGutes, M., Kasprowicz, D. J., et al. (2006). Cutting edge: anti-CD25 monoclonal antibody injection results in the functional inactivation, not depletion, of CD4 + CD25 + T regulatory cells. *J. Immunol.* 176, 3301–3305. doi: 10.4049/jimmunol.176.6.3301

Ladel, C. H., Daugelat, S., and Kaufmann, S. H. E. (1995). Immune response toMycobacterium bovis bacille calmette guérin infection in major histocompatibility complex class I- and II-deficient knock-out mice: contribution of CD4 and CD8 T cells to acquired resistance. *Eur. J. Immunol.* 25, 377–384. doi: 10.1002/eji.1830250211

Marquina-Castillo, B., García-García, L., Ponce-De-León, A., Jimenez-Corona, M. E., Bobadilla-Del Valle, M., Cano-Arellano, B., et al. (2009). Virulence, immunopathology and transmissibility of selected strains of mycobacterium tuberculosis in a murine model. *Immunology* 128, 123–133. doi: 10.1111/j.1365-2567.2008.03004.x

McCaffrey, E. F., Donato, M., Keren, L., Chen, Z., Delmastro, A., Fitzpatrick, M. B., et al. (2022). The immunoregulatory landscape of human tuberculosis granulomas. *Nat. Immunol.* 23, 318–329. doi: 10.1038/s41590-021-01121-x

Meena, L. S., and Rajni, T. (2010). Survival mechanisms of pathogenic mycobacterium tuberculosis h 37Rv. *FEBS J.* 277, 2416–2427. doi: 10.1111/j.1742-4658.2010.07666.x

Mulley, W. R., and Nikolic-Paterson, D. J. (2008). Indoleamine 2,3-dioxygenase in transplantation. *Nephrology* 13, 204–211. doi: 10.1111/j.1440-1797.2007.00921.x

Park, J. H., Jiang, Y., Zhou, J., Gong, H., Mohapatra, A., Heo, J., et al. (2021). Genetically engineered cell membrane–coated nanoparticles for targeted delivery of dexamethasone to inflamed lungs. *Sci. Adv.* 7. doi: 10.1126/sciadv.abf7820

Privratsky, J. R., and Newman, P. J. (2014). PECAM-1: regulator of endothelial junctional integrity. *Cell Tissue Res.* 355, 607–619. doi: 10.1007/s00441-013-1779-3

Quinn, K. M., McHugh, R. S., Rich, F. J., Goldsack, L. M., Lisle, G. W., Buddle, B. M., et al. (2006). Inactivation of CD4 $^{+}$ CD25 $^{+}$ regulatory T cells during early mycobacterial infection increases cytokine production but does not affect pathogen load. *Immunol. Cell Biol.* 84, 467–474. doi: 10.1111/j.1440-1711.2006.01460.x

Rupp, M. C., Bergmann, C. B., Jung, S., Bock, M., Biberthaler, P., Heimann, L., et al. (2021). The posttraumatic response of CD4+ regulatory T cells is modulated by direct cell-cell contact *via* CD40L- and p-selectin-dependent pathways. *Cent. Eur. J. Immunol.* 46, 283–294. doi: 10.5114/ceji.2021.109171

Sadegh Beigee, F., Pourabdollah Toutkaboni, M., Khalili, N., Nadji, S. A., Dorudinia, A., Rezaei, M., et al. (2020). Diffuse alveolar damage and thrombotic microangiopathy are the main histopathological findings in lung tissue biopsy samples of COVID-19 patients. *Pathol. Res. Pract.* 216, 153228. doi: 10.1016/j.prp.2020.153228

Safar, H. A., Mustafa, A. S., Amoudy, H. A., and El-Hashim, A. (2020). The effect of adjuvants and delivery systems on Th1, Th2, Th17 and treg cytokine responses in mice immunized with mycobacterium tuberculosis-specific proteins. *PloS One* 15. doi: 10.1371/journal.pone.0228381

Schumacher, A., Wafula, P. O., Teles, A., El-Mousleh, T., Linzke, N., Zenclussen, M. L., et al. (2012). Blockage of heme oxygenase-1 abrogates the protective effect of regulatory T cells on murine pregnancy and promotes the maturation of dendritic cells. *PloS One* 7. doi: 10.1371/journal.pone.0042301

Scott-Browne, J. P., Shafiani, S., Tucker-Heard, G., Ishida-Tsubota, K., Fontenot, J. D., Rudensky, A. Y., et al. (2007). Expansion and function of Foxp3-expressing T regulatory cells during tuberculosis. *J. Exp. Med.* 204, 2159–2169. doi: 10.1084/jem.20062105

Shafiani, S., Tucker-Heard, G., Kariyone, A., Takatsu, K., and Urdahl, K. B. (2010). Pathogen-specific regulatory T cells delay the arrival of effector T cells in the lung during early tuberculosis. *J. Exp. Med.* 207, 1409–1420. doi: 10.1084/jem.20091885

Singh, A., Dey, A. B., Mohan, A., Sharma, P. K., and Mitra, D. K. (2012). Foxp3+ regulatory T cells among tuberculosis patients: impact on prognosis and restoration of antigen specific IFN-γ producing T cells. *PloS One* 7. doi: 10.1371/journal.pone.0044728

Srisook, K., and Cha, Y.-N. (2005). Super-induction of HO-1 in macrophages stimulated with lipopolysaccharide by prior depletion of glutathione decreases iNOS expression and NO production. *Nitric. Oxide* 12, 70–79. doi: 10.1016/j.niox.2004.12.002

Stephen, X., Gurczynski, J., and Moore, B. B. (2018). IL-17 in the lung: the good, the bad, and the ugly. *Am. J. Physiol. Lung Cell Mol. Physiol.* 314, 6–16. doi: 10.1152/ajplung.00344.2017.-The

Stewart, C. R., Stuart, L. M., Wilkinson, K., van Gils, J. M., Deng, J., Halle, A., et al. (2010). CD36 ligands promote sterile inflammation through assembly of a toll-like receptor 4 and 6 heterodimer. *Nat. Immunol.* 11, 155–161. doi: 10.1038/ni.1836

Sugimoto, N., Rui, T., Yang, M., Bharwani, S., Handa, O., Yoshida, N., et al. (2008). Points of control exerted along the macrophage-endothelial cell-polymorphonuclear neutrophil axis by PECAM-1 in the innate immune response of acute colonic inflammation. *J. Immunol.* 181, 2145–2154. doi: 10.4049/jimmunol.181.3.2145

Sun, J., Yu, J., Li, H., Yang, L., Wei, F., Yu, W., et al. (2011). Upregulated expression of indoleamine 2, 3-dioxygenase in CHO cells induces apoptosis of competent T cells and increases proportion of treg cells. *J. Exp. Clin. Cancer Res.* 30. doi: 10.1186/1756-9966-30-82

Suzuki, Y., Suda, T., Asada, K., Miwa, S., Suzuki, M., Fujie, M., et al. (2012). Serum indoleamine 2,3-dioxygenase activity predicts prognosis of pulmonary tuberculosis. *Clin. Vaccine Immunol.* 19, 436–442. doi: 10.1128/CVI.05402-11

Tenorio, E. P., Olguín, J. E., Fernández, J., Vieyra, P., and Saavedra, R. (2010). Reduction of foxp 3+ cells by depletion with the PC61 mAb induces mortality in resistant BALB/c mice infected with toxoplasma gondii. *J. BioMed. Biotechnol.* 2010. doi: 10.1155/2010/786078

Toossi, Z., and Ellner, J. J. (1998). The role of TGFβ in the pathogenesis of human tuberculosis. *Clin. Immunol. Immunopathol.* 87, 107–114. doi: 10.1006/clin.1998.4528

Wagener, F. A. D. T. G., Volk, H.-D., Willis, D., Abraham, N. G., Soares, M. P., Adema, G. J., et al. (2003). Different faces of the heme-heme oxygenase system in inflammation. *Pharmacol. Rev.* 55, 551–571. doi: 10.1124/pr.55.3.5

Wang, H., Franco, F., Tsui, Y. C., Xie, X., Trefny, M. P., Zappasodi, R., et al. (2020). CD36-mediated metabolic adaptation supports regulatory T cell survival and function in tumors. *Nat. Immunol.* 21, 298–308. doi: 10.1038/s41590-019-0589-5

Wang, L., Shi, M., Tong, L., Wang, J., Ji, S., Bi, J., et al. (2019). Lung-resident mesenchymal stem cells promote repair of LPS-induced acute lung injury *via* regulating the balance of regulatory T cells and Th17 cells. *Inflammation* 42, 199–210. doi: 10.1007/s10753-018-0884-6

Wergeland, I., Amus, J., and Dyrhol-Riise, A. M. (2011). T Regulatory cells and immune activation in mycobacterium tuberculosis infection and the effect of preventive therapy. *Scand. J. Immunol.* 73, 234–242. doi: 10.1111/j.1365-3083.2010.02496.x

Xu, C., Zhang, C., Ji, J., Wang, C., Yang, J., Geng, B., et al. (2018). CD36 deficiency attenuates immune-mediated hepatitis in mice by modulating the proapoptotic effects of CXC chemokine ligand 10. *Hepatology* 67, 1943–1955. doi: 10.1002/hep.29716

Zewdie, M., Howe, R., Hoff, S. T., Doherty, T. M., Getachew, N., Tarekegne, A., et al. (2016). Ex-vivo characterization of regulatory T cells in pulmonary tuberculosis patients, latently infected persons, and healthy endemic controls. *Tuberculosis* 100, 61–68. doi: 10.1016/j.tube.2016.06.007

Zhang, F., Li, M. Y., Lan, Y. T., and Wang, C.B. (2016). Imbalance of Th17/Tregs in rats with smoke inhalation-induced acute lung injury. *Sci. Rep.* 6. doi: 10.1038/srep21348

frontiers | Frontiers in Cellular and Infection Microbiology

TYPE Original Research
PUBLISHED 22 June 2023
DOI 10.3389/fcimb.2023.1095060

OPEN ACCESS

EDITED BY
Veronica Edith Garcia,
Universidad de Buenos Aires, Argentina

REVIEWED BY
Hernan Terenzi,
Federal University of Santa Catarina, Brazil
Daniela Albanesi,
National Scientific and Technical Research Council (CONICET), Argentina

*CORRESPONDENCE
Andrea Villarino
avillarino@fcien.edu.uy
Fernando E. Herrera
herrerafer@fbcb.unl.edu.ar

RECEIVED 10 November 2022
ACCEPTED 29 May 2023
PUBLISHED 22 June 2023

CITATION
Margenat M, Betancour G, Irving V, Costábile A, García-Cedrés T, Portela MM, Carrión F, Herrera FE and Villarino A (2023) Characteristics of *Mycobacterium tuberculosis* PtpA interaction and activity on the alpha subunit of human mitochondrial trifunctional protein, a key enzyme of lipid metabolism. *Front. Cell. Infect. Microbiol.* 13:1095060. doi: 10.3389/fcimb.2023.1095060

Characteristics of *Mycobacterium tuberculosis* PtpA interaction and activity on the alpha subunit of human mitochondrial trifunctional protein, a key enzyme of lipid metabolism

Mariana Margenat[1], Gabriela Betancour[1], Vivian Irving[1], Alicia Costábile[1], Tania García-Cedrés[1], María Magdalena Portela[2,3], Federico Carrión[4], Fernando E. Herrera[5]* and Andrea Villarino[1]*

[1]Instituto de Biología, Sección Bioquímica, Facultad de Ciencias-Universidad de la República, Montevideo, Uruguay, [2]Instituto de Biología, Facultad de Ciencias-Universidad de la República, Montevideo, Uruguay, [3]Unidad de Bioquímica y Proteómica Analíticas, Institut Pasteur de Montevideo and Instituto de Investigaciones Biológicas Clemente Estable, Montevideo, Uruguay, [4]Laboratorio de Inmunovirología, Institut Pasteur de Montevideo, Montevideo, Uruguay, [5]Departamento de Física, Facultad de Bioquímica y Ciencias Biológicas-Universidad Nacional del Litoral – CONICET, Santa Fe, Argentina

During *Mycobacterium tuberculosis (Mtb)* infection, the virulence factor PtpA belonging to the protein tyrosine phosphatase family is delivered into the cytosol of the macrophage. PtpA interacts with numerous eukaryotic proteins modulating phagosome maturation, innate immune response, apoptosis, and potentially host-lipid metabolism, as previously reported by our group. *In vitro*, the human trifunctional protein enzyme (*h*TFP) is a *bona fide* PtpA substrate, a key enzyme of mitochondrial β-oxidation of long-chain fatty acids, containing two alpha and two beta subunits arranged in a tetramer structure. Interestingly, it has been described that the alpha subunit of *h*TFP (ECHA, *h*TFPα) is no longer detected in mitochondria during macrophage infection with the virulent *Mtb* H37Rv. To better understand if PtpA could be the bacterial factor responsible for this effect, in the present work, we studied in-depth the PtpA activity and interaction with *h*TFP$_\alpha$. With this aim, we performed docking and *in vitro* dephosphorylation assays defining the P-Tyr-271 as the potential target of mycobacterial PtpA, a residue located in the helix-10 of *h*TFP$_\alpha$, previously described as relevant for its mitochondrial membrane localization and activity. Phylogenetic analysis showed that Tyr-271 is absent in TFP$_\alpha$ of bacteria and is present in more complex eukaryotic organisms. These results suggest that this residue is a specific PtpA target, and its phosphorylation state is a way of regulating its subcellular localization. We also showed that phosphorylation of Tyr-271 can be catalyzed by Jak kinase. In addition, we found by molecular dynamics that PtpA and *h*TFP$_\alpha$ form a stable protein complex through the PtpA active site, and we determined the dissociation equilibrium constant. Finally, a

detailed study of PtpA interaction with ubiquitin, a reported PtpA activator, showed that additional factors are required to explain a ubiquitin-mediated activation of PtpA. Altogether, our results provide further evidence supporting that PtpA could be the bacterial factor that dephosphorylates *h*TFP$_\alpha$ during infection, potentially affecting its mitochondrial localization or β-oxidation activity.

KEYWORDS

***Mycobacterium tuberculosis*, tyrosine phosphatase, PtpA, human mitochondrial trifunctional protein, TFP, ECHA, lipid metabolism, Jak**

Introduction

Phosphatases and kinases are essential players in signal transduction, modulating enzyme activities, protein-protein interactions, and subcellular localization, among other processes. Our group is interested in contributing to a deeper understanding of the eukaryotic pathways modulated by the *Mycobacterium tuberculosis (Mtb)* phosphatase PtpA (Chiaradia et al., 2008; Mascarello et al., 2010; Margenat et al., 2015). This enzyme, which belongs to the Protein Tyrosine Phosphatase (PTP) family, is delivered into the macrophage during infection, acting as a critical virulence factor (Bach et al., 2008; Mascarello et al., 2010). PtpA was detected in the cytoplasm and the nucleus of mycobacteria-infected macrophages, despite lacking an export signal sequence. It has been suggested that the bacterial SecA2 and ESX/type VII export systems are the candidates responsible for PtpA export (Sullivan et al., 2012; Wong et al., 2013; Wang et al., 2016; Wang et al., 2017). The *Mtb* PtpA-deletion mutant strain showed reduced survival in infected human THP-1 derived macrophages and in mouse SPF C57BL/6, and expression of PtpA neutralizing antibodies and inhibitors simulated this effect (Bach et al., 2008; Mascarello et al., 2010; Wang et al., 2015). In addition, a *Mtb* mutant (*Mtb*Dmms) lacking the genes encoding PtpA, PtpB, and the acid phosphatase, SapM12, displayed a significantly reduced ability to infect and grow inside human THP-1 macrophages. Moreover, no bacilli were recovered in the spleens and lungs of guinea pigs ten weeks following infection with this mutant, suggesting an important role of these phosphatases in the colonization of these organs (Chauhan et al., 2013).

PtpA is a member of the Low-Molecular-Weight PTP (LMW-PTP) family (Denu et al., 1996) and shows 37% of sequence identity and high structural similarity with the *h*ACP1 (UniProt code P24666 isoforms 1 and 2) (Alonso et al., 2004; Madhurantakam et al., 2005). PtpA is a secreted protein during infection; thus, it constitutes an ideal target for drug design (Bach et al., 2008; Sullivan et al., 2012; Wong et al., 2013; Wang et al., 2017) as the drugs would not need to cross the mycobacterial envelope, a barrier that explains much of the resistance of *Mtb* to antibiotics (Chiaradia et al., 2017; Abrahams and Besra, 2020). Numerous groups, including ours, have identified PtpA inhibitors (Mascarello et al., 2010; Silva and Tabernero, 2010; Wong et al., 2013; Mascarello et al., 2016). However, the candidates targeted the PtpA active site, which is highly conserved within PTPs including human ones (Denu et al., 1996; Madhurantakam et al., 2005). Thus, identifying less conserved secondary sites continues to be a challenge. During infection, the action of PtpA seems to depend in part of its phosphatase activity (Wang et al., 2017, 2016; 2020). PtpA interacts with numerous eukaryotic proteins modulating several cell signaling pathways such as phagosome maturation, innate immune response, apoptosis, and host lipid metabolism. Dephosphorylation of VPS33B (Vacuolar Protein Sorting 33B) by PtpA seems to exclude host vacuolar-H1-ATPase from phagosomes, leading to inhibition of phagosome acidification and maturation (Bach et al., 2008; Wong et al., 2011). Also, the presence of PtpA correlates with a decrease in the production of pro-inflammatory cytokines (TNFα, IL-1β, and IL-12) during macrophage infection (Wang et al., 2015). In addition, GSK3α (Glycogen Synthase Kinase 3, alpha subunit) dephosphorylation by PtpA avoids kinase activation promoting an anti-apoptotic pathway, supporting pathogen survival within host macrophage (Poirier et al., 2014). On the other hand, some reports connect PtpA with the degradation pathways induced by ubiquitin (Wang et al., 2017, 2015; 2016; 2020) showing that it acts as an activator of PtpA (using the artificial substrate pNPP or other reported substrates as VPS33B, Jnk and p38) (Wang et al., 2015). Finally, our group identified the human trifunctional enzyme *h*TFP, a key enzyme in the β-oxidation of long-chain fatty acids, as a bona fide PtpA substrate (Eaton et al., 2000; Margenat et al., 2015). Like most proteins with a role in the mitochondria, TFP is synthesized in the cytosol and then translocated to this organelle (Bykov et al., 2020). In the mitochondria, TFP plays a central role in the β-oxidation of long-chain fatty acids, catalyzing three of the four stages of this pathway (Eaton et al., 2000). Recently, the crystallographic structure of *h*TFP has been resolved, showing that it is a $\alpha_2\beta_2$-heterotetramer in which helix-10 of the alpha subunit (*h*TFP$_\alpha$) appears to be important for anchoring to the inner mitochondrial membrane and for its activity (Xia et al., 2019). Our group has a particular interest in the alpha subunit *h*TFP$_\alpha$ because during five independent assays of substrate trapping it was the only PtpA-substrate candidate isolated in the five replicates and identified with the best Mascot score (Margenat et al., 2015). In addition, *h*TFP$_\alpha$ was no longer detected in the mitochondria of macrophages infected with the virulent *Mtb* H37Rv, where its

expression was strongly modulated (more than a 10-fold mRNA decrease) (Jamwal et al., 2013). To better understand if PtpA could be the bacterial factor responsible for this effect, in the present work, we identified by *in vitro* and *in silico* approaches the characteristics of the PtpA-*h*TFP$_\alpha$ interaction, the *h*TFP$_\alpha$ Tyr phosphorylation/dephosphorylation and evaluated the potential regulation of PtpA phosphatase activity by ubiquitin.

Results and discussion

The p-Tyr271 of *h*TFP$_\alpha$ is the potential target of mycobacterial PtpA

We have previously reported that recombinant PtpA (rPtpA) interacts and dephosphorylates *h*TFP$_\alpha$ immunopurified from macrophages and that its dephosphorylation is dependent on the PtpA dose (Margenat et al., 2015). To identify the phosphotyrosine potentially dephosphorylated by PtpA, we performed *in silico* docking studies, using the crystal structure of *h*TFP$_\alpha$ (extracted from PDB 6DV2) and of *Mtb* PtpA (PDB 1U2P) (Madhurantakam et al., 2005; Xia et al., 2019). The reported structure of the *h*TFP (Xia et al., 2019) showed that, as its bacterial homolog (*P. fragi*, PDB 1WDK) (Ishikawa et al., 2004), the biological unit was a $\alpha_2\beta_2$-heterotetramer. Nevertheless, *h*TFP presents significant primary and secondary structure differences compared to its bacterial counterparts, some of them in the α subunit, described as relevant for its association with the inner mitochondrial membrane (Fould et al., 2010; Xia et al., 2019). To drive the docking process, we selected the PtpA active site as we previously showed by SPR assays that the PtpA-*h*TFP interaction involves the active site of PtpA (Margenat et al., 2015). For *h*TFP$_\alpha$, we selected all tyrosine residues located at the surface (Tyr43, Tyr239, Tyr271, Tyr435, Tyr637, Tyr639, Tyr724, and Tyr762), and we phosphorylated them *in silico*. The inset table (Figure 1A) shows the different numbers of complexes (PtpA/*h*TFP$_\alpha$) and clusters obtained for each p-Tyr evaluated in the docking assays. The first four best representative complexes from each cluster were selected, counting 256 possible solutions. It is worth observing that a p-Tyr, with a lower number of clusters, indicates that the binding mode is well-defined and better than another with a greater number of clusters. Additionally, the clusters with lower electrostatic interaction energies (represented by HADDOCK scores) or with a higher number of members are preferable. Considering this, the interaction through the p-Tyr271 or p-Tyr639 of *h*TFP$_\alpha$ and the active site of PtpA results in at least one complex with negative electrostatic interaction energy. However, only the cluster of *h*TFP$_\alpha$ phosphorylated at the Tyr271 residue has a negative average electrostatic interaction energy. In this case, all complexes within this cluster have negative electrostatic interaction energy, and this cluster represents the one with the least energy and the most populated. The situation is different for the results of *h*TFP$_\alpha$

A

Phosphotyrosine	Total number of clusters	Number of members for:		Electrostatic binding energy (Kcal/mol) for:		
		MPC	CLHS	MPC (average)	CLHS (average)	CLEBE
p-Tyr 43	10	67	42	122.4±20.1	193.1±18.1	11.527
p-Tyr 239	7	92		163.9±48.9		34.467
p-Tyr 271	3	173		**-17.3±8.2**		**-56.526**
p-Tyr 435	7	49		121.7±22.7		44.186
p-Tyr 637	8	64	8	99.9±20.4	151.1±21.0	7.88
p-Tyr 639	8	75	7	124.2±11.6	**14.7±35.1**	**-32.129**
p-Tyr 724	11	34	16	133.6±45.1	88.2±32.7	30.632
p-Tyr 762	10	42		52.5±41.9		2.229

B

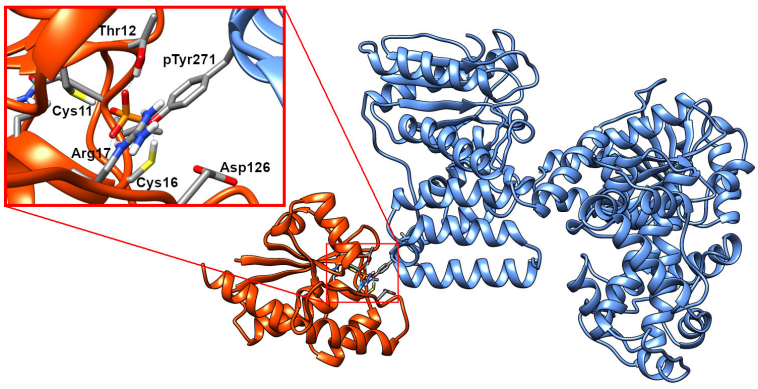

FIGURE 1
The P-Tyr271 of *h*TFP$_\alpha$ is the potential target of mycobacterial PtpA. **(A)** Table showing the results of the docking assays between mycobacterial PtpA and *h*TFP$_\alpha$. The total number of clusters obtained for each p-Tyr evaluated, the number of members, and the electrostatic binding energy are indicated. MPC: Most Populated Cluster; CLHS: Cluster with the Lowest Haddock Score, CLEBE: Complex with the Lowest Electrostatic Binding Energy. In the case where the MPC is the same as the CLHS, both columns are merged into one. **(B)** Molecular structure of the best model of the PtpA/*h*TFP$_\alpha$ complex obtained after docking assays. In the enlarged inset, the most critical residues of the PtpA (orange) binding region and *h*TFP$_\alpha$ (blue) are represented as sticks. These include the catalytic residues of PtpA (Cys11, Thr12, Cys16, Arg17, Asp126) and the p-Tyr 271 of *h*TFP$_\alpha$.

interaction through p-Tyr639. In this case, we found that the cluster with a higher number of members differs from the one with lower energy. Only one complex in the last has negative electrostatic interaction energy. The best PtpA-*h*TFP$_\alpha$ complex, involving Tyr271, is shown in Figure 1B. In this protein complex, it is possible to observe that the p-Tyr-271 fits in the PtpA active site, and there are no steric clashes between both proteins. The p-Tyr271 of *h*TFP$_\alpha$ is directly interacting with the catalytic Asp126 and the Cys11 and Cys16 of PtpA, as it should be for the enzymatic reaction to occur (Madhurantakam et al., 2008).

In addition, we evaluated if there exists a common sequence or structure pattern among the reported PtpA targets. For the mycobacterial substrate of PtpA, the ATP synthase subunit alpha (ATPA), the p-Tyr targeted by PtpA still needs to be elucidated (Chatterjee et al., 2019). For the eukaryotic substrates, GSK3α and VPS33B, only indirect evidence of which Tyr could be dephosphorylated by PtpA has been reported (Bach et al., 2008; Poirier et al., 2014). When considering these residues (Tyr279 of GSK3α, Tyr133 or Tyr382 of VPS33B) and the available alphafold structures models of these substrates, we did not find any sequence pattern around those residues (Figure S1A) or a conserved structural motif of interaction between PtpA and the reported substrates. One reason that could explain this result is that the p-Tyr of GSK3α and VPS33B were not identified using the same approach as our study, where an unbiased *in silico* analysis was applied to determine the p-Tyr candidates dephosphorylated by PtpA. Therefore, we cannot rule out that other Tyr of GSK3α and VPS33B could be the target of PtpA. Another reason is that alphafold models of GSK3α, VPS33B, and ATPA did not consider the phosphorylated state of the residues. Therefore, the orientation of the side chain of these residues might not be the correct one in the alphafold-modeled structure. Overall, we think that an unbiased *in silico* study, as carried out for PtpA with the *h*TFP$_\alpha$ as substrate, is needed for the other reported substrates to be sure of which Tyr is potentially dephosphorylated by PtpA and to evaluate correctly if a conserved recognition motif exists.

The Tyr271 of *h*TFP$_\alpha$ is absent in bacteria and is conserved in mammals and located in a helix described as relevant to its localization and activity

As it has been proved that mycobacterial PtpA introduced into the cytosol of the infected cells acts principally on eukaryotic proteins, this enzyme is expected to dephosphorylate a specific tyrosine residue of *h*TFP$_\alpha$, absent or not phosphorylated in the bacterial homologs. Thus, we evaluate the conservation of the Tyr271 and Tyr639 in bacterial TFP$_\alpha$ and eukaryotic homologs (Figure 2A, see Figures S1–S3 for the complete alignments). While Tyr639 is in the HACD catalytic domain and is conserved in mammals and bacteria, Tyr271 seems specific to the mammal's group, and it is part of the helix-10 of *h*TFP$_\alpha$ which is absent in bacterial TFP homologs (Figures 2A, B). Interestingly, this helix-10 was described as one of the helices relevant for the activity and mitochondrial localization of the *h*TFP (Xia et al., 2019). Then, we analyzed in detail the conservation of Tyr271 in eukaryotes employing blastp searches of the *h*TFP against the NCBI RefSeq protein database and a maximum likelihood phylogenetic analysis (Figure 2B). In chordates, Tyr271 is mainly conserved in mammals, birds, reptiles, and amphibians (Figures 2B, S3). In fish, there are two major clades; one contains 146 genes with a high degree of Tyr271 conservation, and the other with 57 genes without conservation of Tyr271. A closer look at this non-conserved clade indicates that these genes are, in most cases (53/57), different isoforms of a gene containing a conserved Tyr271. Fishes are generally polyploid (Rajkov et al., 2014), and additional copies of duplicated genes are free to change regarding one of the copies remaining functional. On the contrary, there is no conservation of Tyr271 in non-chordates (like arthropods, mollusks, or cnidaria), suggesting that the preservation of the Tyr271 is a characteristic of more complex organisms. These results allowed us to hypothesize a potential role of the Tyr271 residue in the regulation of *h*TFP$_\alpha$ subcellular localization/activity, supported by the fact that the subcellular localization of *h*TFP$_\alpha$ was modulated during TB infection, where this subunit was no longer detected in the mitochondria of macrophages infected with the virulent *Mtb* H37Rv (Jamwal et al., 2013).

p-Tyr271 of *h*TFP$_\alpha$ is detected after phosphorylation by Jak kinase

The next step was to show if Tyr271 of *h*TFP$_\alpha$ could exist in its phosphorylated state. The *h*TFP$_\alpha$ contains several post-translational modifications (PTMs) identified after large-scale MS studies and noted in the PhosphoSitePlus (Hornbeck et al., 2012). Among them, nine Tyr residues of *h*TFP$_\alpha$ were reported as phosphorylated, but the Tyr271 is not included (Figure S7). The functional significance of p-Tyr and the kinase involved has not been elucidated yet. In this context, to improve the identification of the p-residues of *h*TFP$_\alpha$, we prepared a batch of immunopurified *h*TFP from a macrophage phosphoprotein-enriched extract, as previously described (Margenat et al., 2015). We verified in this sample the presence of *h*TFP$_\alpha$ by MS (Figure S4A). However, the amounts of immunopurified *h*TFP were insufficient to detect the p-Tyr by MS and evaluate PtpA-mediated p-Tyr271 dephosphorylation. Phosphorylation generally represents a lower percentage of the total protein and could be lost during MS fragmentation (Mann et al., 2002; Dephoure et al., 2013) or by the action of endogenous phosphatases during the protein extract preparation, despite the precautions taken to inhibit them. This explanation is supported by the fact that Tyr271 is exposed to the solvent, as seen in its crystallographic structure (Figure 1B). Thus, to obtain enough material, we decided to produce and purify the recombinant *h*TFP$_\alpha$ based on previous evidence of its successful production in a soluble form in *E. coli* (Fould et al., 2010). After IMAC, SEC, and removal of the His-tag, 2.5 mg of soluble *h*TFP$_\alpha$/gr of *E. coli* pellet was obtained. As illustrated on the SEC chromatogram, we observed the main peak with a shoulder aspect (Figure 3A). A pool of the eluting fractions corresponding to this peak was analyzed by SDS-PAGE and MS, showing that the principal band is the *h*TFP$_\alpha$, and the less intense

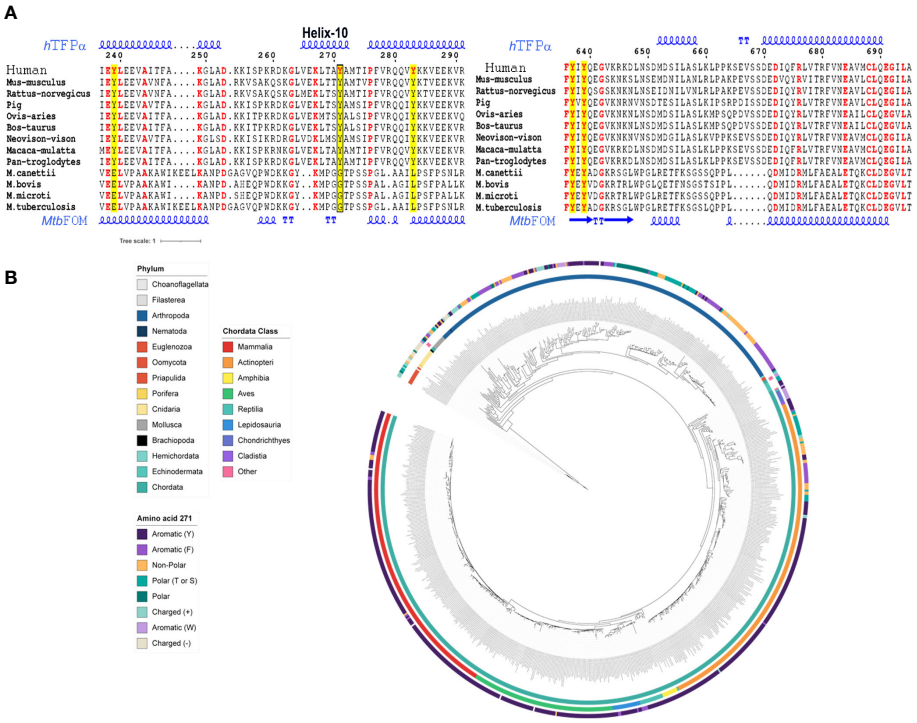

FIGURE 2
The Tyr271 of hTFP$_\alpha$ is conserved in several eukaryotic protein homologs and part of the helix-10, absent in bacterial homologs. **(A)** Multiple sequence alignment of hTFP$_\alpha$ homologous, representative of mammals and bacterial TB complex. The Tyr271 (left alignment) and Tyr639 (right alignment) conservation are shown. The complete alignments are shown in Figures S1–S3. The tyrosines of hTFP$_\alpha$ are in red and highlighted in yellow. The box indicates the Y271 residue placed in the helix-10 of the hTFP$_\alpha$. The alignment was obtained using the MUSCLE server (Edgar, 2004), and the figure was done using the ESPrit 3.0 server (Robert and Gouet, 2014). The secondary protein structure of hTFP$_\alpha$ and the *Mtb* FOM are also shown, based on the pdb structures 6DV2 (Xia et al., 2019) and 4B3H (Venkatesan and Wierenga, 2013), respectively. **(B)** Eukaryotic TFP$_\alpha$ phylogenetic analysis. Circular representation of a maximum likelihood tree of TFP$_\alpha$ of eukaryotes ranging from euglenozoos to vertebrates. The tree is midpoint rooted. Inner circle: phylum colored according to the legend. Middle circle: Chordata class colored according to the legend. Outer circle: amino acid present in each gene at the position aligned to human Tyr-271, colored according to the legend. For details, see Figure S3.

band corresponds to an *E. coli* chaperone contaminant (Figure S4B). Then, taking into account that it is not known which eukaryotic kinase is involved in its phosphorylation, we decided to evaluate the Tyr phosphorylation by Janus kinase (Jak). This enzyme is an intracellular kinase involved in cytokine-mediated signaling, for which inhibitors of its activity were proposed for host-directed therapy of TB as an adjunct to standard TB chemotherapy (Dorhoi, 2015; Schwartz et al., 2017). Thus, we incubated the recombinant hTFP$_\alpha$ with catalytic amounts of the Jak kinase domain, using an E:S molar ratio of 1:3000 to avoid non-specific phosphorylation. For the recombinant hTFP$_\alpha$ non-treated with Jak, after SDS-PAGE and WB using an anti-p-Tyr antibody, we detected a signal of Tyr phosphorylation of hTFP$_\alpha$, and by MS, we identified Tyr499 as phosphorylated (Figure S6, already reported in PhosphoSitePlus). This result is explained because the recombinant hTFP$_\alpha$ was expressed in an *E. coli* strain with a tyrosine kinase/phosphatase system (Vincent et al., 1999). Then, for the recombinant hTFP$_\alpha$ pre-treated with Jak and ATP, we observed additional phosphorylation, detected by the electrophoretic shift of the protein in the SDS-PAGE (Villarino et al., 2005) as well as by WB and MS analysis (Figures S5, S6). Using this strategy, we identified two new sites of phosphorylation of hTFP$_\alpha$, the p-Tyr271 of helix-10 (Figure 3B) and the p-Tyr43 of the predicted signal peptide; and the p-Tyr435 of HACD already reported in the PhosphoSitePlus. This result is relevant because until now, the phosphorylation sites Tyr43 and Tyr271 and the potential kinase involved in hTFP$_\alpha$ phosphorylation were not described. Figure S7 summarizes all the PTMs of hTFP$_\alpha$ reported up to now.

PtpA specifically dephosphorylates the recombinant hTFP$_\alpha$

First, we characterized the recombinant protein hTFP$_\alpha$ by SEC. We determined its apparent protein molecular weight noting that hTFP$_\alpha$ eluted as a protein dimer (179 kDa) of two alpha subunits (Figure 3A). We suggest that this dimer is stabilized by hydrophobic regions of the alpha subunits, which in the biological unit of hTFP ($\alpha_2\beta_2$-heterotetramer) interact with the beta subunits (Xia et al., 2019). We also produced with a high degree of purity and yield, the recombinant hTFP$_\alpha$-Y271F mutant, which, as the hTFP$_\alpha$-wt protein, is a dimer in solution (Figure S8). For the PtpA activity assay both hTFP$_\alpha$ and hTFP$_\alpha$-Y271F were previously phosphorylated by Jak. The recombinant PtpA-wt and the inactive mutant PtpA-C11S were also produced as described previously (Margenat et al., 2015), and characterized by SEC as

10.3389/fcimb.2023.1095060

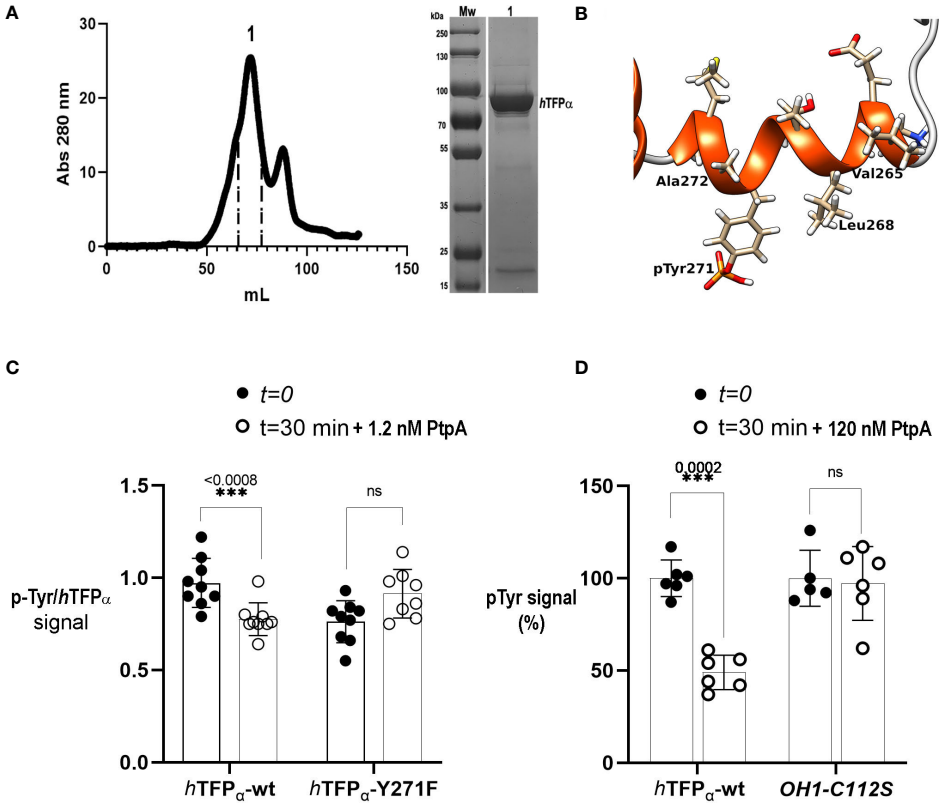

FIGURE 3
Mycobacterial PtpA activity and interaction with recombinant *hTFP*$_\alpha$. **(A)** SEC profiles of recombinant *h*TFP$_\alpha$ purification on Superdex 200 column. SEC was performed in an AKTA Basic system (GE Healthcare), injecting a sample volume of 5 mL in a Superdex 200 16/60 preparative grade column (GE Healthcare). Elution was carried out with two-bed column volumes of the equilibration buffer, and fractions containing the recombinant protein were pooled (fractions indicated in peak 1, elution volume 72 mL). The apparent molecular weight was calculated using the following equation K_{av}= −0.3872 (log*M*w) + 2.2662 corresponding to the previous calibration curve of the column using SEC molecular weight (SIGMA). **(B)** Cartoon representation of the helix-10 of the *h*TFP$_\alpha$ containing the p-Tyr 271 phosphorylated by Jak. The residues of the helix are represented as sticks. The figure was generated with UCSF Chimera [Pettersen EF, 2004 et al.]. **(C)** Evaluation of dephosphorylation of *h*TFP$_\alpha$-wt and *h*TFP$_\alpha$-Y271F by PtpA. The graph shows the mean of p-Tyr/*h*TFP$_\alpha$ ratios ± SD of three independent experiments including three technical replicates. The asterisks indicate the p-value obtained after an unpaired t-test. Equal amounts of the recombinant *h*TFP$_\alpha$ and *h*TFP$_\alpha$ -Y271F previously phosphorylated by Jak were incubated with 1.2 nM of PtpA for 30 min at 37°C in solution. After this time, spots of 5 µL of the reaction were applied in a nitrocellulose membrane by triplicates. Dephosphorylation was evaluated by a Dot Blot assay with an anti-p-Tyr antibody and anti *h*TFP$_\alpha$ antibody to determine the ratio between p-Tyr and *h*TFP$_\alpha$ chemiluminescent signals, quantified using ImageJ (Schneider et al., 2012). Figure S11 shows a representative dot blot used in the analysis. **(D)** Evaluation of PtpA specificity using *h*TFP$_\alpha$-wt and rOH1-C112S as substrates. The graph shows the obtained p-Tyr signal (expressed as %) after incubation with PtpA. Equal amounts of *h*TFP$_\alpha$ or rOH1-C112S previously phosphorylated by Jak were incubated with 120 nM of PtpA (corresponding to a E:S molar ratio of 1:50) for 30 min at 37°C. Then, spots of 5 µL of the reaction were applied in a nitrocellulose membrane by triplicates to perform a Dot Blot assay using an anti-p-Tyr antibody. Chemiluminescent signals were quantified using ImageJ (Schneider et al., 2012). The average p-Tyr signal at t=0 was considered as 100%. After a two-way ANOVA a significant difference (***) was detected between both groups (*h*TFP$_\alpha$ or rOH1-C112S). The asterisks represent the p-value obtained after an unpaired t-test between t=0 and t=30 minutes, and ns: not statistically significant. Figure S12 shows a representative dot blot used in the analysis.

monomeric proteins (Figure S9). Then, we evaluated PtpA activity using a method previously reported (Najarro et al., 2001), based on the incubation of the phosphatase with the protein substrate previously separated by SDS-PAGE, transferred and immobilized to a membrane in a non-covalent way. After immobilization, the *h*TFP$_\alpha$ substrate was expected to recover part of its secondary structure, because the denaturing agent was removed. Using this method we verified the p-Tyr phosphatase activity of PtpA (Figure S10A-D). However, this strategy was not appropriate to evaluate the substrate specificity of PtpA, because the substrate did not preserve its global structure needed to a correct enzyme-substrate recognition. In this context, we observed that PtpA dephosphorylated p-Tyr residues no matter which immobilized protein was used (TFP or the viral protein OH1-C112S) (Figure S10E). On the other hand, carrying out the activity assay in solution presents difficulties, as a detergent is needed to maintain the recombinant *h*TFP$_\alpha$ protein in solution, since this protein is described as associated to the mitochondrial membrane (Fould et al., 2010; Liang et al., 2018; Xia et al., 2019). High concentrations of detergent inhibit PtpA and interfere with the commonly used Malachite Green reagent in the Pi detection. Thus, it was necessary to define the optimal conditions of the reaction to preserve the *h*TFP and PtpA stability during the incubation at 37°C (see methodology). In this assay we used catalytic amounts of PtpA (1.2 nM) corresponding to an E:S molar ratio of 1:5000, and observed a significant PtpA dephosphorylation of *h*TFP$_\alpha$-wt but

not of hTFP$_\alpha$-Y271F (Figure 3C). This result can be explained by the absence of p-Y271 in the mutant, suggesting that this residue is the preferred target of PtpA *in vitro*. When the assay was performed with a higher concentration of PtpA (12 nM, E:S molar ratio of 1:500) the dephosphorylation of hTFP$_\alpha$-Y271F started to be detected (Figure S11). In this condition, it is not possible to avoid dephosphorylation of other p-Tyr residues that probably do not represent specific targets of PtpA. Then, to confirm the dephosphorylation site/s of the recombinant hTFP$_\alpha$ we performed nanoLC-MS/MS analyses. Nevertheless, despite the addition of phosphopeptide enrichment steps, we could not confidently detect phosphorylation sites in hTFP$_\alpha$ to perform a quantitative analysis of dephosphorylation by PtpA. More long-term research efforts to improve and optimize the detection of phosphosites in this protein are needed. Finally, to evaluate PtpA specificity, we used the recombinant hTFP$_\alpha$ and the inactive mutant of the viral protein OH1 (OH1-C112S) as a substrate (Segovia et al., 2017), previously phosphorylated by Jak kinase. As shown in Figure 3D we observed a significant decrease of the p-Tyr signal when hTFP$_\alpha$ was used as a substrate but not using OH1-C112S (120 nM of PtpA, E:S molar ratio of 1:50), demonstrating the specificity of PtpA for hTFP$_\alpha$.

In silico mycobacterial PtpA and hTFP$_\alpha$ form a stable complex that involves PtpA active site

We have already observed by SPR studies that PtpA interacts through the active site with hTFP immunopurified from macrophage (Margenat et al., 2015). In the present study, we performed additional SPR studies to determine the affinity constant of the interaction of the complex, whose value was 0.31 µM (Figure S13), a value similar to that reported for other phosphatases and their substrates (Czikora et al., 2011). Previously to this assay, we verified that 21% of the immunopurified hTFP is phosphorylated on Tyr, using an anti-p-Tyr-Ab (Figure S10A). In addition, we performed molecular dynamics simulations (MD) to determine features of the interaction between PtpA and hTFP$_\alpha$, using the best complex obtained by docking described above. Three systems were considered for MD simulations in solution: PtpA, hTFP$_\alpha$, and the PtpA-hTFP$_\alpha$ complex. For the last, three sets of independent simulations (with different initial random Maxwell-Boltzmann velocities) were performed. According to the Root Mean Square Distance (RMSD) of the backbone atoms along the nanoseconds of simulation, both proteins in the complex maintained their structure stable, as they are alone in solution (Figure 4A). This result suggests that the complex is stable and remains formed over the time analyzed. Concerning the Root Mean Square Fluctuation (RMSF) values, we observed that hTFP$_\alpha$ fluctuation in the complex is similar (on average) to the protein alone. In contrast, PtpA fluctuations in the complex are reduced compared to when the protein alone is evaluated (Figure 4B). The last suggests a change in PtpA behavior when the complex is formed. Interestingly, the regions corresponding to the active site of PtpA have a more considerable relative decrease in their fluctuation when the complex is formed. For instance, the region that corresponds to the D-loop (Asp126) of PtpA is stabilized upon the PtpA-hTFP$_\alpha$ complex formation, probably reflecting the conformational change that allows the catalytic Asp to adopt the correct position during catalysis (Madhurantakam et al., 2008; Hobiger and Friedrich, 2015).

Additional factors are required to explain an ubiquitin-mediated activation of PtpA

As described in the introduction, some reports connect PtpA with the degradation pathways induced by ubiquitin. It has been reported that PtpA binds non-covalently host ubiquitin *via* a previously unknown ubiquitin-interacting motif-like (UIML) and that this interaction activates PtpA to dephosphorylate the kinase Jnk and the p38 MAPK, which leads to the suppression of innate

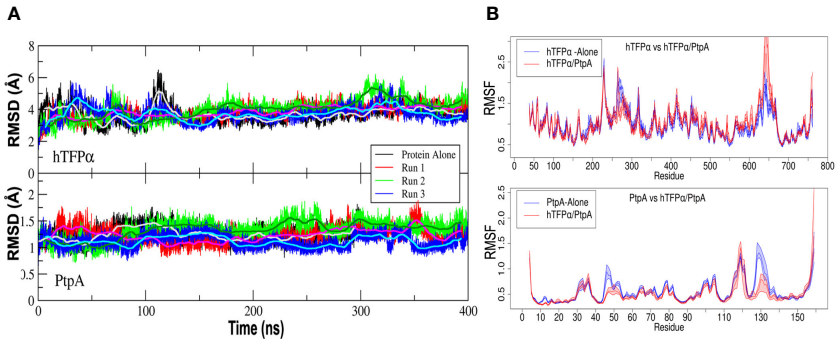

FIGURE 4
Mycobacterial PtpA and hTFP$_\alpha$ form a stable complex that involves PtpA active site. **(A)** Graphical representation of the Root Mean Square Deviation (RMSD) along time (nanoseconds) for three parallel molecular dynamics simulations of hTFP$_\alpha$ (up) and PtpA (down) proteins alone in solution, and forming part of the interacting complex (run1, run 2 and 3). **(B)** Graphical representation of the Root Mean Square Fluctuation (RMSF) of the backbone atoms along the trajectory (average over each residue) for hTFP$_\alpha$ (up) and PtpA (down) proteins alone in solution (blue curve) and the three simulations together (red curve). The RMSF values were calculated over a moving window of 10 ns with a step of 2 ns during the last 200 ns of simulation. Each curve is plotted from the percentile 25 to the percentile 75 of the obtained values, with the median at the center. For the calculation of the statistical values, only one trajectory was taken into account for the proteins alone, while for the complex, three trajectories were taken into account.

immunity (Wang et al., 2015). In this context, we decided to characterize the ubiquitin:PtpA interaction by molecular docking and MD and perform kinetic studies to evaluate the proposed modulation of PtpA activity. The interacting configuration between ubiquitin and PtpA was determined using the HADDOCK web server (Van Zundert et al., 2016). For that, the residues from the UIML region of PtpA and the residues of ubiquitin proposed as relevant for the interaction (His 68, Ile 44, and Leu 8) were selected (Wang et al., 2015). The best result was obtained from the cluster with the lowest HADDOCK score and also the most populated one. The interacting region has a hydrophobic core (HC) composed of residues from the UIML region of PtpA (Ala 140 and Val 141) and ubiquitin residues (Leu 8 and Val 70) (indicated in Figure 5A), flanked by hydrogen bond interacting residues, Glu 143 (PtpA) with Arg 42 (ubiquitin), Glu 137 (PtpA) with His 68 (ubiquitin), and Arg 111 (PtpA) interacting with the backbone oxygen of Leu 8 (ubiquitin). To test the stability of the complex, we performed three parallel MD simulations using as a starting point the interacting complex described above. The MD results show that the HC is stable and remains conserved in all three simulations while the surrounding hydrogen bonds form, break down, and change over time. In particular, the final configuration of the complex is different in the simulations, as shown in Figure 5B. In the first MD, the ubiquitin rotates around the HC and forms different H-bonds in comparison with the starting point during the MD simulation. In the second case, the interactions between both proteins are stable and the same as at the beginning of the MD. Finally, in the third MD the ubiquitin moves and rotates over the HC, changing all H-bonds interaction in comparison with the initial configuration and the relative position of the Val 70 residue;

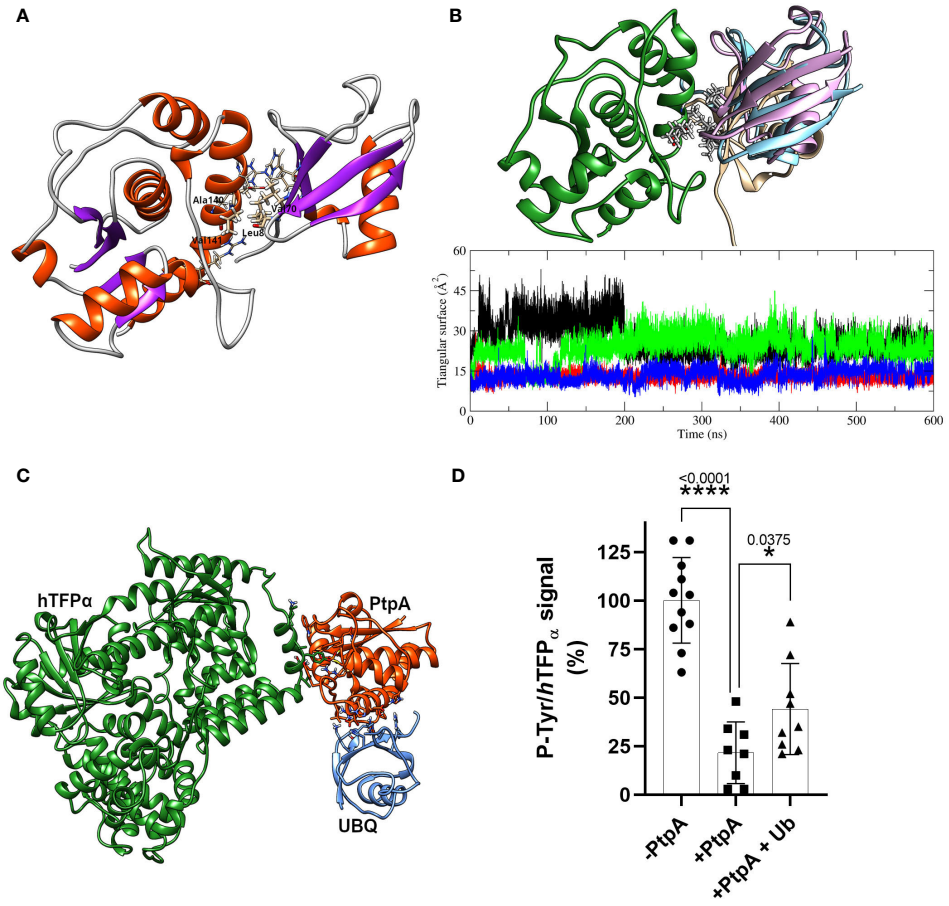

FIGURE 5
PtpA-ubiquitin interaction assays and evaluation of the ubiquitin effect on phosphatase activity. **(A)** Best PtpA/Ub complex structure obtained after the protein/protein docking protocol. The residues involved in the hydrophobic core are labeled and plotted with thicker bonds, while the residues involved in the h-bonds interactions are plotted with thinner bonds. **(B)** The upper structure represents the final configuration of the three MD runs for ubiquitin molecules (1-pink, 2- brown, and 3-light blue) with respect to PtpA (green). For the PtpA MD, only one conformation is shown since the changes in its conformation were negligible between the three runs. The graphical inset represents the triangular area of the PtpA binding site (defined in the text) along the trajectory of the simulation of PtpA in solution (black curve) and in the three simulations of the complex PtpA/Ub (1-red, 2-green, and 3-blue). **(C)** Hypothetical complex of the *h*TFP$_\alpha$/PtpA/Ub. The image shows that there are no steric interferences between proteins suggesting that the complex could form. **(D)** Dephosphorylation of recombinant *h*TFP$_\alpha$ in the presence or absence of ubiquitin. Equal amounts of the recombinant *h*TFP$_\alpha$ were resolved by SDS-PAGE, transferred to PVDF membrane and blocked, and treated at 37°C for 30 min with a buffer containing 0 µM PtpA-wt (-PtpA), 1.5 µM PtpA (+PtpA), and 1.5 µM PtpA preincubated with ubiquitin for 15 min (+PtpA and Ub). Dephosphorylation was evaluated with the anti-p-Tyr antibody. The same membranes were re-probed with anti *h*TFP$_\alpha$ antibody to determine the ratio between p-Tyr and *h*TFP$_\alpha$ chemiluminescent signals (expressed as %). Error bars represent experimental variability detected between three independent experiments, and the asterisks are the p-value obtained after an unpaired t-test.

nevertheless, the HC is still formed. This result suggests that ubiquitin can interact with PtpA during the simulation, albeit with nonspecific interactions and with the HC anchoring the interaction. Furthermore, the RMSD along the trajectory for both proteins of the complex shows values of less than 3 Å (Figure S14A), similar to the values for the proteins alone in solution, implying that both keep their respective internal conformation along the trajectory, without additional stabilization.

To check whether ubiquitin could affect PtpA activity, we evaluated putative changes in the PtpA active site during the interaction. To this end, we performed a simple geometric approach, in which the surface of the triangle formed by three relevant heavy atoms of the PtpA active site was followed along the trajectory (S atom of Cys 11 and Cys 16 together with a C atom of the Asp 126 lateral chain) when PtpA is alone or interacting with ubiquitin (Figure 5B). This figure shows two possible and stable values for the calculated triangular surface, meaning two possible conformations of the PtpA active site: one with a higher area reflecting an open conformation and the other with a lower area indicating a closed conformation. In the case of the MD simulation of PtpA alone, and only one trajectory of the complex, we found an open conformation, while in two other MDs of the complex, a close conformation was found (Figure S14B). However, no correlation between the final position of ubiquitin in the complex and the conformation of the PtpA active site was found, explaining the reported PtpA activating effect of the ubiquitin. In addition, we experimentally tested the impact of ubiquitin on PtpA activity using good-quality recombinant ubiquitin and active PtpA proteins (Figure S15A). Contrary to what was previously reported (Wang et al., 2015), we did not detect activation of PtpA acting on the artificial substrate pNPP. We observed the same result, even varying the PtpA:ubiquitin molar ratio from 1:0 to 1:10 (Figure S15B). Considering that the authors used the PtpA linked to the GST-tag and we used PtpA linked to a His-tag, we evaluated whether the discrepancy could be due to the His-tag used. Even after removing the tag, no activating effect of ubiquitin on PtpA phosphatase activity was observed (Figure S15C). Thus, our discrepancy with the data reported by Wang et al., 2015 could be due to the distinct fusion protein used. Overall, our *in silico* and experimental results suggest that the interaction of ubiquitin with PtpA cannot explain the reported PtpA activation. However, we cannot discard that additional factors may be required to achieve this effect. In parallel, we also analyzed whether the interaction of PtpA with ubiquitin can occur in the context of the PtpA-*h*TFP$_\alpha$ complex. This analysis could be interesting because *h*TFP$_\alpha$ has several ubiquitylation sites noted in the database Phosphosite (Hornbeck et al., 2015), and we demonstrated that it co-purifies with the E3 ubiquitin ligase (TRIM21, Figure S4A), which could connect *h*TFP$_\alpha$ with the Ub-mediated proteasomal degradation. Figure 5C shows that PtpA could form the protein complex with ubiquitin without steric clashes. However, our study did not detect activation of PtpA by ubiquitin acting on *h*TFP$_\alpha$, after three independent assays (Figure 5D). As shown in the graph, we observed a significant decrease in P-Tyr/*h*TFP$_\alpha$ signal level after incubation with PtpA in the absence or presence of Ub. However, in the case of the assay with PtpA+Ub, this decrease was lower than without Ub. This suggests an inhibitory effect of ubiquitin on the phosphatase activity of PtpA acting on *h*TFP$_\alpha$ as a substrate, consistently with the detection of an alternation of the active site between an open (active) and closed (inactive) conformation during PtpA/ubiquitin MD simulation (Figure S14B). Further studies using the recombinant TFP$_{\alpha/\beta}$ heterotetramer as a substrate will be interesting to determine if the inhibitory effect of the ubiquitin is maintained.

Conclusion

Our results allow advancement in the characterization of *Mtb* PtpA interaction and activity on the alpha subunit of *h*TFP, a key enzyme of lipid metabolism. These lead us to suggest that the p-Tyr271 of *h*TFP$_\alpha$ is the potential target of mycobacterial PtpA, located in a conserved helix relevant to its localization and activity. Our working hypothesis, integrating our results with those already published, was included in Figure 6.

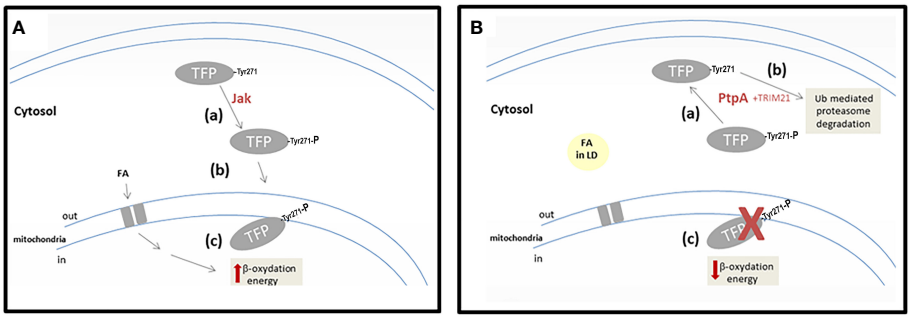

FIGURE 6
Scheme showing our working hypothesis. **(A)** A hypothetical scenario in the cells without *Mtb* infection. Step-a corresponds to the phosphorylation of *h*TFP$_\alpha$ by a cellular kinase (maybe Jak). Step-b corresponds to the correct localization of *h*TFP$_\alpha$, in the mitochondrial inner membrane. Step-c represents the activity of *h*TFP$_\alpha$, in the *β*-oxidation of the long-chain fatty acids transported to the mitochondria. **(B)** A hypothetical scenario in the cells infected with *Mtb*. Step-a corresponds to the dephosphorylation of TFP by mycobacterial PtpA. Step-b corresponds to the Ub-mediated proteasomal degradation stimulated by *h*TFP-TRIM21 interaction. Step-c represents *h*TFP$_\alpha$ decrease in mitochondria, with a concomitant accumulation of long-chain fatty acids into LD in the cytosol of the cells.

In cells, *h*TFP$_\alpha$ is synthesized by cytosolic ribosomes, like most mitochondrial proteins, and then it is translocated to the inner mitochondrial membrane (Bykov et al., 2020). Despite *h*TFP$_\alpha$ being a central protein of the metabolism and having several PTMs, including phosphorylation (Figure S7), its role is unknown. Considering that PTMs have an important role in regulating cell functions (Ribet and Cossart, 2010), it is appropriate to think that specific phosphorylation of *h*TFP can modulate its cellular localization. In the present work, we demonstrated *in vitro* that *h*TFP$_\alpha$ could be phosphorylated by Jak in three residues, two of them (p-Tyr271 of helix-10 and p-Tyr43 of the predicted signal peptide) located in important sites of the protein that could define its cellular localization. The p-Tyr271 of helix-10 from the alpha subunit was described as relevant for *h*TFP$_{\alpha,}$ anchor to the mitochondrial membrane, and for its activity since it contributes to the formation of the channels that connect the different active sites of the enzyme (Xia et al., 2019). In this context, we suggest that the tyrosine phosphorylation of *h*TFP$_\alpha$ by a cellular kinase (possibly Jak) defines its correct localization in the mitochondrial membrane (Figure 6A, steps a and b). Once located in the mitochondria *h*TFP$_{\alpha/\beta}$ plays a central role in the β-oxidation of long-chain fatty acids, catalyzing three of the four stages of this pathway (Eaton et al., 2000). Indeed, oxidation of the long-chain fatty acids, transported from the cytosol to the mitochondria, contributes directly (by the generated NADH and $FADH_2$) and indirectly (by the acetyl-CoA) to the mitochondrial ATP synthesis (Figure 6A, step c).

On the other hand, during *Mtb* infection, the phosphatase PtpA is introduced to the cytosol of the macrophages, as previously demonstrated (Bach et al., 2008). In this location, PtpA could dephosphorylate *h*TFP$_\alpha$, as demonstrated *in vitro* by our group. As a consequence, we suggest that the dephosphorylated *h*TFP$_\alpha$ will not be able to reach the mitochondria (Figure 6B, step a). This would explain why *h*TFP$_\alpha$ is no longer detected in the mitochondria of macrophages infected specifically with the virulent *Mtb* H37Rv (Jamwal et al., 2013). In this experiment the authors did not describe changes in the mitochondria levels of *h*TFP$_\beta$ after infection with the virulent *Mtb* H37Rv, and in the levels of both *h*TFP subunits after infection with the avirulent *Mtb* strain. Despite these observations, in an *in vitro* PtpA activity assay, using immunoprecipitated TFP from macrophages, we observed a reduction in the phosphorylation levels of both subunits (Margenat et al., 2015). In addition, there is evidence that during *Mtb* infection PtpA also reaches the nucleus of host cells and regulates the expression of genes involved in host innate immunity or in cell proliferation and migration (Wang et al., 2017). The PtpA nuclear localization, could contribute to explain the observed 10-fold decrease in the *h*TFP$_\alpha$ mRNA observed during the infection with the virulent *Mtb* H37Rv (Jamwal et al., 2013). The relevance of this result needs to be evaluated in future studies of infected macrophages with *Mtb*.

Furthermore, *h*TFP$_\alpha$ has several ubiquitylation sites noted in the database Phosphosite (Hornbeck et al., 2015), and we demonstrated by MS that *h*TFP$_\alpha$ from macrophages co-purify with the E3 ubiquitin ligase TRIM21 (Figure S4). This enzyme could be responsible for *h*TFP$_\alpha$ ubiquitylation, connecting TFP with the Ub-mediated proteasomal degradation (Figure 6B, step b) and the metabolic modulation. Similarly, it has been observed that TRIM21 is involved in the downregulation of glycolysis, *via* proteasomal degradation of the rate-limiting metabolic enzyme phosphofructokinase (PFK) (Chen et al., 2021). This is an enzyme that catalyzes a key regulatory step of glycolytic metabolism, which was also identified by our group as another of the potential substrates of PtpA (Margenat et al., 2015). A drop in mitochondrial *h*TFP$_\alpha$ level (Figure 6B, step c) could contribute to explaining some of the metabolic changes described during mycobacterial infection (Cumming et al., 2018; Genoula et al., 2018) such as decreased mitochondrial activity and changes in lipid metabolism as a cytoplasmic accumulation of lipid droplets (Figure 6B, step d). The storage of lipids during infection can act as a mechanism that allows reestablishing a cellular balance, avoiding the death of the macrophage, and in turn, favoring the persistence of the pathogen (Laval et al., 2021). With respect to how PtpA activity is regulated during infection, we think that in view of our results and our hypothesis, more studies must be carried out to understand the potential regulatory role of ubiquitin and other relevant molecules as fatty acids.

Altogether, we suggest that the role of this virulence factor is to promote the survival of mycobacteria in infected cells, affecting not only the innate immunity (Bach et al., 2008; Wang et al., 2017, 2015; 2020) and apoptosis (Poirier et al., 2014), but also macrophage pathways involved in lipid metabolism. Future studies will be performed using cellular models to evaluate whether potential changes in macrophage metabolism can be correlated with PtpA activity on TFP.

Materials and methods

Molecular docking: PtpA/*h*TFP$_\alpha$

The following protocol was used to select which tyrosine may be phosphorylated in the *h*TFP$_\alpha$ protein, in addition to those reported in the PhosphoSitePlus® (Hornbeck et al., 2015), and acts as putative interacting residue with mPtpA when *h*TFP$_\alpha$ is its substrate. The protocol was performed for each tyrosine in *h*TFP$_\alpha$ located at the surface of the protein, and it consists of three steps involving (i) Selection of the putative phosphotyrosine on the *h*TFP$_\alpha$, (ii) docking simulations, and (iii) electrostatics calculations. (i) Selection of putative phosphotyrosine on *h*TFP$_\alpha$. The selected pdb structure for *h*TFP$_\alpha$ was the only X-ray structure available in the PDB databank (Berman et al., 2000), pdb code 6DV2, with a resolution of 3.6 Å (Xia et al., 2019). The putative tyrosines from this structure that could be phosphorylated were selected based on their exposure to the protein's surface. The selected tyrosines, with at least 40% of their surface exposed to solvent in the pdb structure, were Y43, Y239, Y271, Y435, Y637, Y639, Y724, and Y762. Each of these residues was phosphorylated *in silico* by hand one by one, adding the necessary atoms to the tyrosine residue. Energy minimization of the complete protein structure was then performed in implicit solvent using the Amber package of programs (Pearlman et al., 1995) with the amber ff14sb

force field (Maier et al., 2015). The force field parameters for the phosphotyrosine were taken from the publication by Homeyer (Homeyer et al., 2006). The implicit solvent was taken into account using the modified Generalized Born model developed by A. Onufriev et al. (Onufriev et al., 2004, 2000) as implemented in the amber program (Case et al., 2005). Finally, 8 different *h*TFP$_\alpha$ structures were obtained, each with one phosphotyrosine. (ii) *Docking simulations:* The HADDOCK program (Dominguez et al., 2003; Van Zundert et al., 2016) was used for the molecular docking simulations between PtpA and *h*TFP$_\alpha$ with one phosphotyrosine. The conformation of the PtpA protein was taken from the X-ray structure with a resolution of 1.9 Å with the pdb code 1U2P (Madhurantakam et al., 2005). The active residues at the protein interface for docking simulation were defined as the catalytic residues Cys 11, Cys 16, and Asp 126. For *h*TFP$_\alpha$, each phosphorylated tyrosine was treated as an active residue. The passive residues for both proteins were defined as all surface residues within 6.5 Å from the active residues on each protein. Different numbers of clusters were obtained for each docking simulation. Results, around 200 different complexes for each docking simulation were clustered according to the HADDOCK protocol (Dominguez et al., 2003; Van Zundert et al., 2016). (iii) *Electrostatic calculations*: Since the HADDOCK score cannot be used to compare the results of the *h*TFP$_\alpha$ protein with different phosphorylated tyrosines, but only to compare different solutions with the same phosphorylated tyrosines for a given complex (Kastritis and Bonvin, 2010), the electrostatic contribution to the free energy of binding of the interaction between PtpA and *h*TFP$_\alpha$ was used as a criterion for selecting the best representative complex. Therefore, the complex with the lowest electrostatic energy of binding was selected as the best representative. The electrostatic energy was calculated by solving the nonlinear Poisson-Boltzmann equation for the complex and each protein using APBS 3.2.0 software (Jurrus et al., 2018), using a dielectric constant for points within and outside the protein of 2.0 and 78.5 D respectively. The electrostatic energy of binding (E) was then calculated as the difference between the electrostatic energy of the complex, composed of the *h*TFP$_\alpha$ and PtpA proteins, and the electrostatic energy calculated for both *h*TFP$_\alpha$ and PtpA proteins individually, E=E*h*TFP$_\alpha$+PtpA-(EPtpA+E*h*TFP$_\alpha$). We consider a negative value of E as an indicator that the complex is formed and may be stable.

Molecular dynamics simulations

All MD simulations were performed using the Amber package version 2018 (Case et al., 2005). Parameters from the Amber ff14SB force field were used for all protein residues (Maier et al., 2015); while the parameters for the phosphotyrosine were taken from the literature (Homeyer et al., 2006). Periodic boundary conditions were taken into account in all simulations. A weak-coupling algorithm (Berendsen et al., 1984) was used to couple the simulation boxes with an isotropic pressure of 1 atm and a reference temperature of 300 K. Relaxation times were chosen to be 5 ps and 2 ps for pressure and temperature coupling, respectively. All bonds involving hydrogen were constrained using the SHAKE algorithm (Hess et al., 1997). The time step for all simulations was set to 2 fs. All systems were immersed into a truncated octahedron of TIP3P water molecules (Price and Brooks, 2004) with a minimum distance between the edges of the simulation box and the protein surface atom of 11 Å. The bonds of the water molecules were constrained using the SETTLE algorithm (Miyamoto and Kollman, 1992). The complete systems were neutralized with counter-ions. A direct cutoff for nonbonded interactions of 10 Å and the particle mesh Ewald for long-range electrostatics were applied (Essmann et al., 1995). A standard protocol was used for all MD simulations, and it begins with two initial energy minimizations: the first one only for the solvent molecules, constraining the position of all non-solvent atoms, and a second minimization for the entire system. In order to equilibrate the systems at 300 K, each of them was slowly heated from 100 K to 300 K over a period of 1 ns under NVT conditions, followed by MD simulations at 300 K up to 100 ns. Subsequently, a production run of 400 ns or 500 ns was performed for each complex under NPT conditions. For each simulated system, different numbers of parallel runs were performed with different random initial velocities in order to have more statistics.

Phylogenetic analyses

The human trifunctional enzyme (NCBI accession: NP_000173.2) was used as a query for a blastp search against the NCBI RefSeq database (e-value: 1e-5, number of hits: 5000). Hits were manually filtered to those containing "trifunctional" in their descriptions. When more than one isoform was available, the longest one was maintained. Hits were further filtered to those with a query coverage greater than 50%. Sequences were submitted to NGPhylogeny.fr (Lemoine et al., 2019) for alignment with MAFFT (Katoh and Standley, 2013), alignment curation with BMGE (Criscuolo and Gribaldo, 2010), evolutionary model selection, and phylogenetic analysis with SMS (Lefort et al., 2017) and PhyML (Guindon et al., 2010), respectively. Trees were visualized and annotated using ITOL (Letunic and Bork, 2021).

Production of recombinant PtpA-wt and PtpA-C11S

The plasmid pET28 containing the sequence of PtpA was obtained as described previously (Margenat et al., 2015). The construct expressing the single PtpA mutant C11S was obtained by site-directed mutagenesis (Quikchange Site-Directed Mutagenesis kit, Stratagene) using the following primers forward and reverse, respectively: 5′ -TTC GTT TCT ACG GGC AAC ATC TG-3, -5′- CA GAT GTT GCC CGT AGA AAC GAA - 3′. The sequence was verified by DNA sequencing (Macrogen). Expression was done as described previously (Margenat et al., 2015). Briefly, Transformed *E. coli* BL21 (DE3) cells were grown at 15°C in LB medium with 50 μg ml^{-1} kanamycin, and protein synthesis induced with 0.5 mM isopropyl β-D-thiogalactoside (IPTG). The recombinant proteins were purified to homogeneity by metal-affinity (Cu-column) and size exclusion chromatography (SEC).

Immunoprecipitation of *h*TFP from macrophages

The $hTFP_{\alpha/\beta}$ was obtained from macrophage extracts by immunoprecipitation with an anti-TFP monoclonal antibody. Briefly, the anti-TFP MAb (8μg, ab110302, MitoSciences) was first covalently cross-linked to anti-mouse IgG Ab on the beads (100 μl, 11201D, Life technologies) using BS3 (Sigma). Then, beads were washed and incubated with 500 μg of macrophage extract, prepared as previously described (Margenat et al., 2015). Beads were washed, and bound proteins were eluted with 50 mM citrate pH 2.6 (2x100 μl), and neutralized immediately. Samples were resolved by SDS-PAGE, stained with colloidal Coomassie, or transferred to PVDF membranes for 1 h at 100 V. Membranes were blocked for 16 hs at 4°C, washed twice with TBS-T, and subsequently incubated with anti-$h\text{TFP}_{\alpha}$ MAb (ab200652) at 1/1000 dilution in TBS-T, 1.5h at RT. After washing, membranes were incubated (1 h at RT) with an anti-rabbit antibody conjugated with horseradish peroxidase (HRP) (1/50000, Sigma-Aldrich 0545). After four washes with TBS-T and one wash with TBS, the reaction was developed with Pierce ECL western blotting substrate (Thermo Scientific). Immunoreactive bands were visualized using the GBOX ChemiSystem tool (SynGene). The presence of the TFP was confirmed by mass spectrometry (MS).

Production of recombinant $h\text{TFP}_{\alpha}$ and the mutant $h\text{TFP}_{\alpha}$ -Y271F

The $h\text{TFP}_{\alpha}$-wt (ECHA sequence) was sub-cloned by RF-cloning (Unger et al., 2010), in a modified pET32a vector (named pT7), carrying an ampicillin-resistance cassette, an N-terminus His-tag sequence, and the tobacco etch virus (TEV) protease recognition site between this tag and the target gene insertion site (Correa et al., 2014). As a template the ECHA sequence already cloned in the pMyr-plasmid was used. The following forward and reverse primers were used, respectively: 5'-GGATCGGAAAAC CTGTA TTTTCAGGGATCCACCAGAACCCATATTAACTATGGAG-3' and 5'-GAACTGCGGGTGGCTCCAGCTGCCGGATC CTCACTGGTAGAACTTCTTGTTAGG-3'. PCR were done using Phusion Polymerase (Thermo), and the PCR conditions were: a denaturing step at 98°C for 30 s and 35 amplification cycles of 98°C for 10 s, 65°C for 30 sec and 72°C for 1 min 20 sec, with a final extension step at 72°C for 10 min. The obtained products (megaprimer) were analyzed by agarose gel electrophoresis, purified with GeneJET Extraction Kit (Thermo) and quantified in a nanodrop spectrophotometer. The generated megaprimers contained 30 bp in both ends that overlaps with the insertion site in the destination vector T7. The integration into the vector was done by performing a second PCR reaction using 200 ng megaprimer, 30 ng pT7 vector, and the PCR conditions as follows: a denaturing step at 98°C for 30 s, 30 amplification cycles of 98°C for 10 s, 60°C for 1 min and 72°C for 5 min, with a final extension step at 72°C for 7 min. 20 µl of the PCR product was the treated with 20 U of DpnI (Thermo) for 2 hours at 37°C to selectively degrade the methylated parental vector, and 20 min at 80°C to inactivate the enzyme. Then, 1µl was used to transform 50 µl of electrocompetent XL-1 *E. coli* cells or *E. coli* BL21 (DE3). Plasmids were purified using the GeneJET Plasmid Miniprep (Thermo) and the sequence verified by DNA sequencing (Macrogen).

Transformed *E. coli* BL21 (DE3) were grown overnight in 10 ml of Lysogeny broth (LB) containing 100 μg ml^{-1} ampicillin at 37°C. For protein expression, 4 ml of overnight culture was transferred into 800 ml of LB with ampicillin and grown at 37°C to an OD_{600} of 0.6-0.7. Protein synthesis was induced by adding 0.5 mM IPTG at 19°C for 24 h. Cells were then harvested by centrifugation and lysed by sonication on ice in the lysis buffer (100 mM Tris, pH 8.0, 200 mM NaCl, 10% glycerol, containing EDTA-free protease inhibitor cocktail (Amersham Biosciences). The suspension was supplemented with 1.5% Tween 20 and incubated for 90 min at 4°C with gentle agitation. Cell debris was removed by centrifugation at 15000 xg for 40 min, and the supernatant was diluted with 100 mM Tris, pH 8.0, 200 mM NaCl, and 10% glycerol to obtain a final concentration of 0.5% Tween 20. Then, imidazole was added to the supernatant to a final concentration of 10 mM and incubated with the Ni-NTA resin (GE Healthcare) equilibrated in binding buffer (100 mM Tris pH 8, 200 mM NaCl, 10% glycerol, 10 mM imidazole, and 0,5% Tween 20), for 1 hour with gentle shaking. The mixture was then packed into a column, washed with binding buffer, and the recombinant protein was eluted with elution buffer (100 mM Tris pH 8, 200 mM NaCl, 10% glycerol, 300 mM imidazole, and 0.5% Tween 20). Imidazole was rapidly extracted by using a PD-10 column equilibrated in 50 mM Tris pH 8, 100 mM NaCl, 5% glycerol, and 0.5% Tween 20. The protein was further purified by SEC using a Superdex 200 16/60 preparative grade column (GE Healthcare) previously equilibrated in SEC-buffer (50 mM Tris-HCl pH 8.0, 100 mM NaCl, 5% glycerol, 0.1% Tween 20). Fractions containing purified $h\text{TFP}_{\alpha}$ were pooled and concentrated using an *Amicon Ultra-15 Millipore* concentrator to 1 mg/mL. The 6xHis-tag was removed with TEV protease in a 1:20 ratio overnight at 18°C, and then the TEV was removed using a Ni-NTA resin. The identity of the recombinant $h\text{TFP}_{\alpha}$ was confirmed by MS. Two batches of recombinant protein were produced and used in the present study.

For the production of the $h\text{TFP}_{\alpha}$-Y271F mutant, we used as a template the plasmid containing the sequence of the $h\text{TFP}_{\alpha}$-wt, and the mutation introduced by PCR site-directed mutagenesis using the following forward and reverse primers, respectively: 5' - GAA AAA TTG ACA GCG TTT GCC ATG ACT ATT C -3', and 5' - G AAT AGT CAT GGC AAA CGC TGT CAA TTT TTC -3'. The presence of the mutation was verified by DNA sequencing (Macrogen). Recombinant $h\text{TFP}_{\alpha}$-Y271F was expressed in *E. coli* BL21 (DE3), following the same procedure described for the wt protein. The only difference was that the 6xHis-tag was removed with TEV protease before SEC purification, and not after this chromatography as described for the WT.

Phosphorylation of *h*TFP$_\alpha$ and OH1-C112S by Jak

The recombinant *h*TFP$_\alpha$-wt, *h*TFP$_\alpha$-Y271F, and OH1-C112S produced as reported previously (Segovia et al., 2017), were phosphorylated with commercial Jak-1 kinase (Thermo Fisher Scientific) in the SEC-buffer supplemented with 2.5 mM $MnCl_2$, 7.5 mM $MgCl_2$, 1 mM DTT, and 1 mM ATP as substrate for 2 hours at 30°C. An enzyme:substrate (E:S) molar ratio of 1:3000 was used. Then, Jak-1 was removed by purification with glutathione agarose (LifeTech) and ATP was removed by SEC (PD-10, GE). The phosphorylated proteins were then used in PtpA activity and MS assays.

PtpA activity assays on the recombinant *h*TFP$_\alpha$

To evaluate PtpA activity in solution using the recombinant proteins (*h*TFP$_\alpha$-wt or *h*TFP$_\alpha$-Y271F, OH1-C112S) we first phosphorylated them with Jak-1 as described above. The buffer of the proteins was changed by SEC to the activity buffer (50 mM Tris-HCl pH 8.0, 50 mM NaCl, 5% glycerol, 3 mM EDTA, 1 mM DTT and 0.1% Tween 20). To avoid PtpA inactivation and interference of the detergent during MS identification of the phospho-peptides (Feist & Hummon, 2015) it was not possible to increase the concentration of detergent more than 0.1% Tween 20. To preserve both proteins in solution the maximal incubation time at 37°C was 30 min. The E:S molar ratios used were 1:5000, 1:500 and 1:50. After 30 min, spots of 5 µL of the reaction were applied in a nitrocellulose membrane by triplicates and then the membrane was dried and blocked with membrane blocking solution (Invitrogen #00-0105). Afterward, membranes were washed in TBS-T and probed for p-Tyr levels with anti-p-Tyr antibody (Cell Signalling #9411) at 1/2000 dilution in TBS-T, ON at 4°C. Blots were then incubated with horseradish peroxidase (HRP)-linked anti-mouse (Sigma-Aldrich A4416, 1/10000) secondary antibody for 1 h at RT. After four washes with TBS-T, and one wash with TBS, the reaction was developed with Pierce ECL western blotting substrate (Thermo Scientific). The chemiluminescent signals of the bands were visualized using the GBOX ChemiSystem tool (SynGene). For the assays using *h*TFP$_\alpha$-wt or *h*TFP$_\alpha$-Y271F as substrate, the membrane was reprobed with anti *h*TFP$_\alpha$ antibody (Abcam ab200652) to determine the ratio between p-Tyr and *h*TFP$_\alpha$ chemiluminescent signals, quantified using ImageJ (Schneider et al., 2012).

Mass spectrometry identification

The samples were separated 1.5 cm by SDS-PAGE and stained with colloidal Coomassie Brilliant Blue G-250. Each lane was excised into 4 slices that were destained by incubation with 0.2 M ammonium bicarbonate/ACN (1:1) for 1 h at room temperature with agitation. After this, proteins were reduced with 10 mM DTT at 56°C for 60 min and then alkylated with 55 mM iodoacetamide at room temperature for 45 min and in darkness. Then, in-gel proteolytic digestion and peptide extraction were performed as described earlier (Gil et al., 2019). To verify the identity of the *h*TFP$_\alpha$ immunopurified or produced as recombinant protein and for p-Tyr identification, online MS detection/analysis was carried out in a nano-HPLC (UltiMate 3000, Thermo) coupled to a hybrid quadrupole-orbitrap mass spectrometer (QExactive Plus, Thermo). Peptide mixtures were loaded on C18 columns and separated using a two-solvent system (solvent A: 0.1% formic acid in water and solvent B: 0.1% formic acid in acetonitrile) with a gradient from 0% to 90% of B) and a flow rate of 0.2 mL/min over 100 min. Peptide analysis was performed in a Q-exactive Plus (Q-Orbitrap, Thermo) associated with a Nano HPLC. Xcalibur 2.1 was used for data acquisition of a full MS scan in the positive ion mode with m/z between 200 and 2000 m/z. Sequential fragmentation of the ten most intense ions with a normalized collision energy of 35, an isolation width of 2 m/z. The activation Q was set at 0.25, the activation time at 15 ms, and a dynamic exclusion time of 30 s. MS source parameters were set as follows: 2.3 kV electrospray voltage and 260°C capillary temperature. PatternLab V (Version 5.0.0.109) (Santos et al., 2022) was employed to generate a target-decoy database using sequences from *E. coli* and *h*TFP$_\alpha$, PtpA, Jak, downloaded from the UniProt. In addition, 127 common mass spectrometry contaminants were included (Carvalho et al., 2016). The Comet search engine was operated using the following parameters: trypsin as a proteolytic enzyme with full specificity; oxidation of Met and phosphorylation on Tyr as variable modifications, carbamidomethylation of Cys as fixed modification; and 35 ppm of tolerance from the measured precursor m/z. XCorr and Z-Score were used as the primary and secondary search engine scores, respectively. Peptide spectrum matches were filtered using the Search Engine Processor (SEPro), and acceptable false discovery rate (FDR) criteria were set at ≤1% at the protein level and ≤2% at the peptide level.

To improve the identification of the phospho-peptides by MS, the phosphoproteins contained in one mg of recombinant *h*TFP$_\alpha$ were purified using the Pierce Phosphoprotein Enrichment kit (Thermo). This sample was used in the phosphatase assay (1 h at 37°C) without or with PtpA. Then the proteins were treated with sequencing-grade trypsin (0.25 µg, 3h or ON at 25°C), and the detergent was removed using a specific resin (Pirce#87780). Prior to MS analysis samples were desalted using C18 reverse phase micro-columns (Omix®Tips, Varian), dried by vacuum, and resuspended at 1 µg/ul in 0.1% formic acid (v/v) in water. Samples were injected into a nano-HPLC (UltiMate 3000, Thermo) coupled to a hybrid quadrupole-orbitrap mass spectrometer (QExactive Plus, Thermo), and separated and analyzed as described above.

Data availability statement

The data presented in this study are deposited in the ProteomeXChange and accession number PXD038119.

Author contributions

AV participated in the conception and supervision of the work. AV and. FH contributed to the experimental design and analyzed the data. MM, and GB, performed the main *in vitro* experiments of PtpA activity on *h*TFPα protein substrate; TG-C and VI produced the recombinant PtpA proteins and performed the PtpA activity assay using the artificial substrate pNPP, and evaluating the effect of ubiquitin. MM and MP prepared samples and analyzed the data of MS. MM and FC performed and analyzed the SPR experiments. AC performed the phylogenetic sequences analysis. FH performed all in silico studies, with the participation of V. Irving. AV and FH wrote the paper, and MM participated in manuscript writing and revision. All authors contributed to the article and approved the submitted version.

Funding

This work was supported by Agencia Nacional de Investigación e Innovación (ANII, grants FCE_1_2017_1_136458 and FCE_1_2021_1_166706) and Programa para el Desarrollo de las Ciencias Básicas (PEDECIBA, Uruguay). TG-C and VI were funded by national postgraduate fellowships from Comisión Académica de Posgrado (CAP-UdelaR) and ANII, respectively. AV, AC, and MM were funded by Universidad de la República and Sistema Nacional de Investigadores (SNI-ANII) from Uruguay. FH was funded by the Argentinian National Scientific and Technological Research Council (CONICET) and the National University of the Litoral (UNL) in Argentina.

Acknowledgments

We thank R. Durán and A. Leiva from the Institut Pasteur of Montevideo (UByPA) for their help with some mass spectrometry experiments. We acknowledge F.M. Rossi and C. Rossi for their critical reading of the manuscript.

Conflict of interest

The authors declare that the research was conducted in the absence of any commercial or financial relationships that could be construed as a potential conflict of interest.

Publisher's note

Supplementary material

The Supplementary Material for this article can be found online at: https://www.frontiersin.org/articles/10.3389/fcimb.2023.1095060/full#supplementary-material

References

Abrahams, K. A., and Besra, G. S. (2020). Mycobacterial drug discovery. *RSC. Med. Chem.* 11, 1354–1365. doi: 10.1039/d0md00261e

Alonso, A., Sasin, J., Bottini, N., Friedberg, I., Friedberg, I., Osterman, A., et al. (2004). Protein tyrosine phosphatases in the human genome. *Cell* 117, 699–711. doi: 10.1016/j.cell.2004.05.018

Bach, H., Papavinasasundaram, K. G., Wong, D., Hmama, Z., and Av-Gay, Y. (2008). Mycobacterium tuberculosis virulence is mediated by PtpA dephosphorylation of human vacuolar protein sorting 33B. *Cell Host Microbe* 3, 316–322. doi: 10.1016/j.chom.2008.03.008

Berendsen, H. J. C., Postma, J. P. M., Van Gunsteren, W. F., Dinola, A., and Haak, J. R. (1984). Molecular dynamics with coupling to an external bath. *J. Chem. Phys.* 81, 3684–3690. doi: 10.1063/1.448118

Berman, H. M., Westbrook, J., Feng, Z., Gilliland, G., Bhat, T. N., Weissig, H., et al. (2000). The protein data bank. *Nucleic Acids Res.* 28, 235–242. doi: 10.1093/nar/28.1.235

Bykov, Y. S., Rapaport, D., Herrmann, J. M., and Schuldiner, M. (2020). Cytosolic events in the biogenesis of mitochondrial proteins. *Trends Biochem. Sci.* 45, 650–667. doi: 10.1016/j.tibs.2020.04.001

Carvalho, P. C., Lima, D. B., Leprevost, F. V., Santos, M. D. M., Fischer, J. S. G., Aquino, P. F., et al. (2016). Integrated analysis of shotgun proteomic data with PatternLab for proteomics 4.0. *Nat. Protoc.* 11, 102–117. doi: 10.1038/nprot.2015.133

Case, D. A., Cheatham, T. E., Darden, T., Gohlke, H., Luo, R., Merz, K. M., et al. (2005). The amber biomolecular simulation programs. *J. Comput. Chem.* 26, 1668–1688. doi: 10.1002/jcc.20290

Chatterjee, A., Pandey., S., Dhamija, E., Jaiswal, S., Yabaji, S. M., and Srivastava, K. K. (2019). ATP synthase, an essential enzyme in growth and multiplication is modulated by protein tyrosine phosphatase in mycobacterium tuberculosis H37Ra. *Biochimie* 165, 156–160. doi: 10.1016/j.biochi.2019.07.023

Chauhan, P., Reddy, P. V., Singh, R., Jaisinghani, N., Gandotra, S., and Tyagi, A. K. (2013). Secretory phosphatases deficient mutant of mycobacterium tuberculosis imparts protection at the primary site of infection in Guinea pigs. *PloS One* 8. doi: 10.1371/JOURNAL.PONE.0077930

Chen, X., Li, Z., Yong, H., Wang, W., Wang, D., Chu, S., et al. (2021). Trim21-mediated HIF-1α degradation attenuates aerobic glycolysis to inhibit renal cancer tumorigenesis and metastasis. *Cancer Lett.* 508, 115–126. doi: 10.1016/j.canlet.2021.03.023

Chiaradia, L., Lefebvre, C., Parra, J., Marcoux, J., Burlet-Schiltz, O., Etienne, G., et al. (2017). Dissecting the mycobacterial cell envelope and defining the composition of the native mycomembrane. *Sci. Rep.* 7, 1. doi: 10.1038/S41598-017-12718-4

Chiaradia, L. D., Mascarello, A., Purificação, M., Vernal, J., Cordeiro, M. N. S., Zenteno, M. E., et al. (2008). Synthetic chalcones as efficient inhibitors of mycobacterium tuberculosis protein tyrosine phosphatase PtpA. *Bioorg. Med. Chem. Lett.* 18, 6227–6230. doi: 10.1016/j.bmcl.2008.09.105

Correa, A., Ortega, C., Obal, G., Alzari, P., Vincentelli, R., and Oppezzo, P. (2014). Generation of a vector suite for protein solubility screening. *Front. Microbiol.* 5. doi: 10.3389/fmicb.2014.00067

Criscuolo, A., and Gribaldo, S. (2010). BMGE (Block mapping and gathering with entropy): a new software for selection of phylogenetic informative regions from multiple sequence alignments. *BMC Evol. Biol.* 10. doi: 10.1186/1471-2148-10-210

Cumming, B. M., Addicott, K. W., Adamson, J. H., and Steyn, A. J. C. (2018). Mycobacterium tuberculosis induces decelerated bioenergetic metabolism in human macrophages. *Elife* 7. doi: 10.7554/eLife.39169

Czikora, I., Kim, K., Kása, A., Bécsi, B., Verin, A. D., Gergely, P., et al. (2011). Characterization of the effect of TIMAP phosphorylation on its interaction with protein phosphatase 1. *Biochimie* 93, 1139–1145. doi: 10.1016/j.biochi.2011.03.011

Denu, J. M., Stuckey, J. A., Saper, M. A., and Dixon, J. E. (1996). Form and function in protein dephosphorylation. *Cell* 87, 361–364. doi: 10.1016/S0092-8674(00)81356-2

Dephoure, N., Gould, K. L., Gygi, S. P., and Kellogg, D. R. (2013). Mapping and analysis of phosphorylation sites: a quick guide for cell biologists. *Mol. Biol. Cell* 24, 535–542. doi: 10.1091/mbc.E12-09-0677

Dominguez, C., Boelens, R., and Bonvin, A. M. J. J. (2003). HADDOCK: a protein-protein docking approach based on biochemical or biophysical information. *J. Am. Chem. Soc* 125, 1731–1737. doi: 10.1021/ja026939x

Dorhoi, A. (2015). Suppress for Success: a JAK inhibitor for adjunct therapy of tuberculosis. *EBIOM* 2, 786–787. doi: 10.1016/j.ebiom.2015.08.010

Eaton, S., Bursby, T., Middleton, B., Pourfarzam, M., Mills, K., Johnson, A. W., et al. (2000). The mitochondrial trifunctional protein: centre of a beta-oxidation metabolon? *Biochem. Soc. Trans.* 28, 177–182. doi: 10.1042/bst0280177

Edgar, R. C. (2004). MUSCLE: multiple sequence alignment with high accuracy and high throughput. *Nucleic Acids Res.* 32, 1792–1797. doi: 10.1093/nar/gkh

Essmann, U., Perera, L., Berkowitz, M. L., Darden, T., Lee, H., and Pedersen, L. G. (1995). A smooth particle mesh ewald method. *J. Chem. Phys.* 103, 8577–8593. doi: 10.1063/1.470117

Feist, P., and Hummon, A. B. (2015). Proteomic challenges: sample preparation techniques for microgram-quantity protein analysis from biological samples. *Int. J. Mol. Sci.* 16 (2), 3537–3563. doi: 10.3390/ijms16023537

Fould, B., Garlatti, V., Neumann, E., Fenel, D., Gaboriaud, C., and Arlaud, G. J. (2010). Structural and functional characterization of the recombinant human mitochondrial trifunctional protein. *Biochemistry* 49, 8608–8617. doi: 10.1021/bi100742w

Genoula, M., Franco, J. L. M., Dupont, M., Kviatcovsky, D., Milillo, A., Schierloh, P., et al. (2018). Formation of foamy macrophages by tuberculous pleural effusions is triggered by the interleukin-10/signal transducer and activator of transcription 3 axis through ACAT upregulation. *Front. Immunol.* 9. doi: 10.3389/fimmu.2018.00459

Gil, M., Lima, A., Rivera, B., Rossello, J., Urdániz, E., Cascioferro, A., et al. (2019). New substrates and interactors of the mycobacterial Serine/Threonine protein kinase PknG identified by a tailored interactomic approach. *J. Proteomics* 192, 321–333. doi: 10.1016/j.jprot.2018.09.013

Guindon, S., Dufayard, J. F., Lefort, V., Anisimova, M., Hordijk, W., and Gascuel, O. (2010). New algorithms and methods to estimate maximum-likelihood phylogenies: assessing the performance of PhyML 3.0. *Syst. Biol.* 59, 307–321. doi: 10.1093/sysbio/syq010

Hess, B., Bekker, H., Berendsen, H. J. C., and Fraaije, J. G. E. M. (1997). LINCS: a linear constraint solver for molecular simulations. *J. Comput. Chem.* 18, 1463–1472. doi: 10.1002/(SICI)1096-987X(199709)18:12<1463::AID-JCC4>3.0.CO;2-H

Hobiger, K., and Friedrich, T. (2015). Voltage sensitive phosphatases: emerging kinship to protein tyrosine phosphatases from structure-function research. *Front. Pharmacol.* 6. doi: 10.3389/fphar.2015.00020

Homeyer, N., Horn, A. H. C., Lanig, H., and Sticht, H. (2006). AMBER force-field parameters for phosphorylated amino acids in different protonation states: phosphoserine, phosphothreonine, phosphotyrosine, and phosphohistidine. *J. Mol. Model.* 12, 281–289. doi: 10.1007/s00894-005-0028-4

Hornbeck, P. V., Kornhauser, J. M., Tkachev, S., Zhang, B., Skrzypek, E., Murray, B., et al. (2012). PhosphoSitePlus: a comprehensive resource for investigating the structure and function of experimentally determined post-translational modifications in man and mouse. *Nucleic Acids Res.* 40, D261–D270. doi: 10.1093/nar/gkr1122

Hornbeck, P. V., Zhang, B., Murray, B., Kornhauser, J. M., Latham, V., and Skrzypek, E. (2015). PhosphoSitePlus 2014: mutations, PTMs and recalibrations. *Nucleic Acids Res.* 43, D512–D520. doi: 10.1093/nar/gku1267

Ishikawa, M., Tsuchiya, D., and Morikawa, K. (2004). Structural basis for channelling mechanism of a fatty acid beta-oxidation multienzyme complex. *EMBO J.* 23, 2745–2754. doi: 10.1038/sj.emboj.7600298

Jamwal, S., Midha, M. K., Verma, H. N., Basu, A., Rao, K. V. S., and Manivel, V. (2013). Characterizing virulence-specific perturbations in the mitochondrial function of macrophages infected with mycobacterium tuberculosis. *Sci. Rep.* 3, 1328. doi: 10.1038/srep01328

Jurrus, E., Engel, D., Star, K., Monson, K., Brandi, J., Felberg, L. E., et al. (2018). Improvements to the APBS biomolecular solvation software suite. *Protein Sci.* 27, 112–128. doi: 10.1002/PRO.3280

Kastritis, P. L., and Bonvin, A. M. J. J. (2010). Are scoring functions in protein-protein docking ready to predict interactomes? clues from a novel binding affinity benchmark. *J. Proteome Res.* 9, 2216–2225. doi: 10.1021/pr9009854

Katoh, K., and Standley, D. M. (2013). MAFFT multiple sequence alignment software version 7: improvements in performance and usability. *Mol. Biol. Evol.* 30, 772–780. doi: 10.1093/molbev/mst010

Laval, T., Chaumont, L., and Demangel, C. (2021). Not too fat to fight: the emerging role of macrophage fatty acid metabolism in immunity to mycobacterium tuberculosis. *Immunol. Rev.* 301, 84–97. doi: 10.1111/imr.12952

Lefort, V., Longueville, J. E., and Gascuel, O. (2017). SMS: Smart model selection in PhyML. *Mol. Biol. Evol.* 34, 2422–2424. doi: 10.1093/MOLBEV/MSX149

Lemoine, F., Correia, D., Lefort, V., Doppelt-Azeroual, O., Mareuil, F., Cohen-Boulakia, S., et al. (2019). NGPhylogeny.fr: new generation phylogenetic services for non-specialists. *Nucleic Acids Res.* 47, W260–W265. doi: 10.1093/nar/gkz303

Letunic, I., and Bork, P. (2021). Interactive tree of life (iTOL) v5: an online tool for phylogenetic tree display and annotation. *Nucleic Acids Res.* 49, W293–W296. doi: 10.1093/NAR/GKAB301

Liang, K., Li, N., Wang, X., Dai, J., Liu, P., Wang, C., et al. (2018). Cryo-EM structure of human mitochondrial trifunctional protein. *Proc. Natl. Acad. Sci. U. S. A.* 115 (27), 7039–7044. doi: 10.1073/pnas.1801252115

Madhurantakam, C., Chavali, V. R. M., and Das, A. K. (2008). Analyzing the catalytic mechanism of MPtpA: a low molecular weight protein tyrosine phosphatase from mycobacterium tuberculosis through site-directed mutagenesis. *Proteins* 71, 706–714. doi: 10.1002/prot.21816

Madhurantakam, C., Rajakumara, E., Mazumdar, A., Saha, B., Mitra, D., Harald, G., et al. (2005). Crystal structure of low-Molecular-Weight protein tyrosine phosphatase from mycobacterium tuberculosis at 1. 9-Å resolution. *J. Bacteriol.* 187, 2175–2181. doi: 10.1128/JB.187.6.2175

Maier, J. A., Martinez, C., Kasavajhala, K., Wickstrom, L., Hauser, K. E., and Simmerling, C. (2015). ff14SB: improving the accuracy of protein side chain and backbone parameters from ff99SB. *J. Chem. Theory Comput.* 11, 3696–3713. doi: 10.1021/acs.jctc.5b00255

Mann, M., Ong, S., Gr, M., Steen, H., Jensen, O. N., and Pandey, A. (2002). Analysis of protein phosphorylation using mass spectrometry: deciphering the phosphoproteome. *Trends Biotechnol.* 20, 261–268. doi: 10.1016/S0167-7799(02)01944-3

Margenat, M., Labandera, A.-M., Gil, M., Carrion, F., Purificação, M., Razzera, G., et al. (2015). New potential eukaryotic substrates of the mycobacterial protein tyrosine phosphatase PtpA: hints of a bacterial modulation of macrophage bioenergetics state. *Sci. Rep.* 5, 8819. doi: 10.1038/srep08819

Mascarello, A., Chiaradia, L. D., Vernal, J., Villarino, A., Guido, R. V. C., Perizzolo, P., et al. (2010). Inhibition of mycobacterium tuberculosis tyrosine phosphatase PtpA by synthetic chalcones: kinetics, molecular modeling, toxicity and effect on growth. *Bioorg. Med. Chem.* 18, 3783–3789. doi: 10.1016/j.bmc.2010.04.051

Mascarello, A., Domeneghini Chiaradia-Delatorre, L., Mori, M., Terenzi, H., and Botta, B. (2016). Mycobacterium tuberculosis-secreted tyrosine phosphatases as targets against tuberculosis: exploring natural sources in searching for new drugs. *Curr. Pharm. Des.* 22, 1561–1569. doi: 10.2174/1381612822666160112130539

Miyamoto, S., and Kollman, P. A. (1992). Settle: an analytical version of the SHAKE and RATTLE algorithm for rigid water models. *J. Comput. Chem.* 13, 952–962. doi: 10.1002/jcc.540130805

Najarro, P., Traktman, P., and Lewis, J. A. (2001). Vaccinia virus blocks gamma interferon signal transduction: viral VH1 phosphatase reverses Stat1 activation. *J. Virol.* 75, 3185–3196. doi: 10.1128/jvi.75.7.3185-3196.2001

Onufriev, A., Bashford, D., and Case, D. A. (2000). Modification of the generalized born model suitable for macromolecules. *J. Phys. Chem. B.* 104, 3712–3720. doi: 10.1021/jp994072s

Onufriev, A., Bashford, D., and Case, D. A. (2004). Exploring protein native states and Large-scale conformational changes with a modified generalized born model. *Proteins Struct. Funct. Genet.* 55, 383–394. doi: 10.1002/prot.20033

Pearlman, D. A., Case, D. A., Caldwell, J. W., Ross, W. S., Cheatham, T. E., DeBolt, S., et al. (1995). AMBER, a package of computer programs for applying molecular mechanics, normal mode analysis, molecular dynamics and free energy calculations to simulate the structural and energetic properties of molecules. *Comput. Phys. Commun.* 91, 1–41. doi: 10.1016/0010-4655(95)00041-D

Pettersen, E. F., Goddard, T. D., Huang, C. C., Couch, G. S., Greenblatt, D. M., Meng, E. C., et al. (2004). UCSF Chimera - A visualization system for exploratory research and analysis. *J. Comput. Chem.* 25, 1605–1612. doi: 10.1002/jcc.20084

Poirier, V., Bach, H., and Av-Gay, Y. (2014). Mycobacterium tuberculosis promotes anti-apoptotic activity of the macrophage by PtpA protein-dependent dephosphorylation of host GSK3α. *J. Biol. Chem.* 289, 29376–29385. doi: 10.1074/jbc.M114.582502

Price, D. J., and Brooks, C. L. (2004). A modified TIP3P water potential for simulation with ewald summation. *J. Chem. Phys.* 121, 10096–10103. doi: 10.1063/1.1808117

Rajkov, J., Shao, Z., and Berrebi, P. (2014). Erratum: evolution of polyploidy and functional diploidization in sturgeons: microsatellite analysis in 10 sturgeon species. *J. Hered.* 105 (4), 521–531. doi: 10.1093/jhered/esu058

Ribet, D., and Cossart, P. (2010). Post-translational modifications in host cells during bacterial infection. *FEBS Lett.* 584, 2748–2758. doi: 10.1016/j.febslet.2010.05.012

Robert, X., and Gouet, P. (2014). "Deciphering key features in protein structures with the new ENDscript server". *Nucl. Acids Res.* 42 (W1), W320–W324. doi: 10.1093/nar/gku316

Santos, M. D. M., Lima, D. B., Fischer, J. S. G., Clasen, M. A., Kurt, L. U., Camillo-Andrade, A. C., et al. (2022). Simple, efficient and thorough shotgun proteomic analysis with PatternLab V. *Nat. Protoc.* 17, 1553–1578. doi: 10.1038/s41596-022-00690-x

Schneider, C. A., Rasband, W. S., and Eliceiri, K. W. (2012). NIH Image to ImageJ: 25 years of image analysis. *Nat. Methods* 9, 671–675. doi: 10.1038/nmeth.2089

Schwartz, D. M., Kanno, Y., Villarino, A., and Ward, M. (2017). JAK inhibition as a therapeutic. *Nat. Publ. Gr.* 17, 843–862. doi: 10.1038/nrd.2017.201

Segovia, D., Haouz, A., Porley, D., Olivero, N., Martínez, M., Mariadassou, M., et al. (2017). OH1 from orf virus: a new tyrosine phosphatase that displays distinct structural

features and triple substrate specificity. *J. Mol. Biol.* 429, 2816–2824. doi: 10.1016/j.jmb.2017.07.017

Silva, A. P. G., and Tabernero, L. (2010). New strategies in fighting TB: targeting mycobacterium tuberculosis-secreted phosphatases MptpA & MptpB. *Future Med. Chem.* 2, 1325–1337. doi: 10.4155/fmc.10.214

Sullivan, J. T., Young, E. F., McCann, J. R., and Braunstein, M. (2012). The mycobacterium tuberculosis SecA2 system subverts phagosome maturation to promote growth in macrophages. *Infect. Immun.* 80, 996–1006. doi: 10.1128/IAI.05987-11

Unger, T., Jacobovitch, Y., Dantes, A., Bernheim, R., and Peleg, Y. (2010). Applications of the restriction free (RF) cloning procedure for molecular manipulations and protein expression. *J. Struct. Biol.* 172, 34–44. doi: 10.1016/j.jsb.2010.06.016

Van Zundert, G. C. P., Rodrigues, J.P.G.L.M., Trellet, M., Schmitz, C., Kastritis, P. L., Karaca, E., et al. (2016). The HADDOCK2.2 web server: user-friendly integrative modeling of biomolecular complexes. *J. Mol. Biol.* 428, 720–725. doi: 10.1016/j.jmb.2015.09.014

Venkatesan, R., and Wierenga, R. K. (2013). Structure of mycobacterial β-oxidation trifunctional enzyme reveals its altered assembly and putative substrate channeling pathway. *ACS Chem Biol.* 8, 1063–1073. doi: 10.1021/cb400007k

Villarino, A., Duran, R., Wehenkel, A., Fernandez, P., England, P., and Alzari, P. M. (2005). Proteomic identification of m. tuberculosis protein kinase Substrates: PknB recruits GarA, a FHA domain-containing protein, through activation loop-mediated interactions. *J. Mol. Biol.* 350, 953–963. doi: 10.1016/j.jmb.2005.05.049

Vincent, C., Doublet, P., Grangeasse, C., Vaganay, E., Cozzone, A. J., and Duclos, B. (1999). Cells of escherichia coli contain a protein-tyrosine kinase, wzc, and a phosphotyrosine-protein phosphatase, wzb. *J. Bacteriol.* 181, 3472–3477. doi: 10.1128/JB.181.11.3472-3477.1999

Wang, J., Ge, P., Qiang, L., Tian, F., Zhao, D., Chai, Q., et al. (2017). The mycobacterial phosphatase PtpA regulates the expression of host genes and promotes cell proliferation. *Nat. Commun.* 8, (1). doi: 10.1038/s41467-017-00279-z

Wang, J., Li, B.-X., Ge, P.-P., Li, J., Wang, Q., Gao, G. F., et al. (2015). Mycobacterium tuberculosis suppresses innate immunity by coopting the host ubiquitin system. *Nat. Immunol.* 16, 237–245. doi: 10.1038/ni.3096

Wang, J., Teng, J. L. L., Zhao, D., Ge, P., Li, B., Woo, P. C. Y., et al. (2016). The ubiquitin ligase TRIM27 functions as a host restriction factor antagonized by mycobacterium tuberculosis PtpA during mycobacterial infection. *Sci. Rep.* 6, 1–13. doi: 10.1038/srep34827

Wang, L., Wu, J., Li, J., Yang, H., Tang, T., Liang, H., et al. (2020). Host-mediated ubiquitination of a mycobacterial protein suppresses immunity. *Nature* 577, 682–688. doi: 10.1038/s41586-019-1915-7

Wong, D., Bach, H., Sun, J., Hmama, Z., and Av-Gay, Y. (2011). Mycobacterium tuberculosis protein tyrosine phosphatase (PtpA) excludes host vacuolar-H+-ATPase to inhibit phagosome acidification. *Proc. Natl. Acad. Sci.* 108, 19371–19376. doi: 10.1073/pnas.1109201108

Wong, D., Chao, J. D., and Av-Gay, Y. (2013). Mycobacterium tuberculosis-secreted phosphatases: from pathogenesis to targets for TB drug development. *Trends Microbiol.* 21, 100–109. doi: 10.1016/j.tim.2012.09.002

Xia, C., Fu, Z., Battaile, K. P., and Kim, J. J. P. (2019). Crystal structure of human mitochondrial trifunctional protein, a fatty acid β-oxidation metabolon. *Proc. Natl. Acad. Sci. U. S. A.* 116, 6069–6074. doi: 10.1073/pnas.1816317116

frontiers | Frontiers in Cellular and Infection Microbiology

TYPE Original Research
PUBLISHED 05 July 2023
DOI 10.3389/fcimb.2023.1113744

OPEN ACCESS

EDITED BY
Joaquin Pellegrini,
INSERM U1104 Centre d'immunologie de Marseille-Luminy (CIML), France

REVIEWED BY
Luciana Balboa,
Academia Nacional de Medicina, Argentina
Chinnaswamy Jagannath,
Cornell University, United States
Paulina A. García-González,
Aix Marseille Université, France

*CORRESPONDENCE
Mary P. O'Sullivan
mary.osullivan@tcd.ie

RECEIVED 01 December 2022
ACCEPTED 02 June 2023
PUBLISHED 05 July 2023

CITATION
Triglia D, Gogan KM, Keane J and O'Sullivan MP (2023) Glucose metabolism and its role in the maturation and migration of human CD1c$^+$ dendritic cells following exposure to BCG.
Front. Cell. Infect. Microbiol. 13:1113744.
doi: 10.3389/fcimb.2023.1113744

Glucose metabolism and its role in the maturation and migration of human CD1c$^+$ dendritic cells following exposure to BCG

Denise Triglia[1], Karl M. Gogan[2], Joseph Keane[1,2] and Mary P. O'Sullivan[1]*

[1]TB Immunology Laboratory, Department of Clinical Medicine, Trinity Translational Medicine Institute, Trinity College Dublin, The University of Dublin, Dublin, Ireland, [2]Department of Respiratory Medicine, St James Hospital, Dublin, Ireland

Introduction: Tuberculosis (TB) still kills over 1 million people annually. The only approved vaccine, BCG, prevents disseminated disease in children but shows low efficacy at preventing pulmonary TB. Myeloid dendritic cells (mDCs) are promising targets for vaccines and immunotherapies to combat infectious diseases due to their essential role in linking innate and adaptive immune responses. DCs undergo metabolic reprogramming following exposure to TLR agonists, which is thought to be a prerequisite for a successful host response to infection. We hypothesized that metabolic rewiring also plays a vital role in the maturation and migration of DCs stimulated with BCG. Consequently, we investigated the role of glycolysis in the activation of primary human myeloid CD1c$^+$ DCs in response to BCG.

Methods/results: We show that CD1c$^+$ mDC mature and acquire a more energetic phenotype upon challenge with BCG. Pharmacological inhibition of glycolysis with 2-deoxy-D-glucose (2-DG) decreased cytokine secretion and altered cell surface expression of both CD40 and CCR7 on BCG-challenged, compared to untreated, mDCs. Furthermore, inhibition of glycolysis had differential effects on infected and uninfected bystander mDCs in BCG-challenged cultures. For example, CCR7 expression was increased by 2-DG treatment following challenge with BCG and this increase in expression was seen only in BCG-infected mDCs. Moreover, although 2-DG treatment inhibited CCR7-mediated migration of bystander CD1C$^+$ DCs in a transwell assay, migration of BCG-infected cells proceeded independently of glycolysis.

Discussion: Our results provide the first evidence that glycolysis plays divergent roles in the maturation and migration of human CD1c$^+$ mDC exposed to BCG, segregating with infection status. Further investigation of cellular metabolism in DC subsets will be required to determine whether glycolysis can be targeted to elicit better protective immunity against Mtb.

KEYWORDS

dendritic cell, immunometabolism, tuberculosis, glycolysis, *Mycobacterium tuberculosis*, *Mycobacterium bovis*, vaccines, Bacille Calmette-Guérin vaccine (BCG)

1 Introduction

Infection with *Mycobacterium tuberculosis* (Mtb), the causative agent of tuberculosis (TB), was the second leading cause of death by a single infectious agent in 2021 - killing 1.6 million people (WHO, 2021). New cases of multi-drug resistant and extensively-drug resistant TB are emerging every year. Consequently, the need for an effective vaccine is clear. Bacille Calmette-Guérin (BCG), a live attenuated strain of *M. bovis*, is the only vaccine licensed to prevent TB disease. Although BCG vaccination does not prevent primary infection with Mtb (Moliva et al., 2017), it is effective at preventing TB meningitis and extra pulmonary disseminated TB in children (Rodrigues et al., 1993; Trunz et al., 2006). BCG also affords limited protection against non-tuberculous mycobacterial infections such as Buruli ulcer and leprosy (Setia et al., 2006; Zimmermann et al., 2018). However, its efficacy at protecting against adult pulmonary TB varies from zero to 80% in different populations (Rodrigues et al., 1993).

Despite its shortcomings, BCG vaccination of high-risk individuals is still a key component of the WHO's End TB Strategy (WHO, 2021) and BCG remains the benchmark against which candidate vaccines are measured. BCG is one of the most widely used vaccines globally and is administered *via* the intradermal route to neonates in countries with a high burden of TB – with approximately 100 million babies vaccinated each year (WHO, 2008). BCG is also an integral part of several new vaccination strategies tested in clinical trials, including recombinant strains with improved immunogenicity (Loxton et al., 2017; Nieuwenhuizen and Kaufmann, 2018), subunit vaccines designed to boost the immune response elicited by BCG (Nemes et al., 2018; Van Der Meeren et al., 2018) and revaccination of adolescents (Nemes et al., 2018). BCG is also used as a first line immunotherapy for early stage bladder cancer (Lamm, 1985). Vaccination with BCG also confers heterologous protection against a variety of infectious diseases unrelated to TB (Kleinnijenhuis et al., 2014; Higgins et al., 2016) (Giamarellos-Bourboulis et al., 2020) as well as showing therapeutic potential in protection against certain autoimmune diseases (Ristori et al., 2014; Kuhtreiber et al., 2018).

Trafficking of DCs infected with live bacilli to the draining lymph node (LN) is essential for the generation of an antigen-specific immune response following infection with mycobacteria (Marino et al., 2004; Reiley et al., 2008; Wolf et al., 2008; Samstein et al., 2013; Bollampalli et al., 2015) although virulent strains of mycobacteria can also impair the ability of infected DCs to migrate (Rajashree et al., 2008; Roberts and Robinson, 2014; Lai et al., 2018). Pulmonary delivery of Mtb antigen-primed DCs into naïve (Gonzalez-Juarrero et al., 2002; McShane et al., 2002) and vaccinated mice (Griffiths et al., 2016) has been shown to accelerate T-cell responses to Mtb infection. In addition, $CD11c^+$ DCs have been successfully targeted with mycobacterial antigens conjugated to a DC-Sign antibody to produce protective T cell responses (Velasquez et al., 2018). Myeloid or conventional (m/cDCs) are one of the major cell populations infected with Mtb in the lung and draining lymph nodes (LN) in mouse models of TB (Wolf et al., 2007) and in humans comprise of three subsets: cDC1, $CD1c^+$ cDC2 and the recently identified inflammatory cDC3 which also express CD1c in addition to CD163 and CD14 (Segura, 2022). The murine counterpart of human $CD1c^+$ mDCs - $CD11b^+$ cDCs - initiate Th1 T cell immunity during pulmonary Mtb infection (Lai et al., 2018). Moreover, migratory epidermal $CD11b^{hi}$ cDCs transport BCG from the skin to draining LN to prime $CD4^+$ T cells following BCG inoculation (Bollampalli et al., 2015; Krmeska et al., 2022). Human blood-derived $CD1c^+$ mDCs are susceptible to infection with BCG, up-regulating CD40, CCR7, HLA-DR, CD86 and other maturation markers, as well as producing TNF-α and IL-6 (Lozza et al., 2014). However, the intracellular processes that enable primary human $CD1c^+$ mDCs to perform these immune functions in response to bacterial infection are unknown.

Interactions between innate immune cells and microorganisms can result in changes in host cell metabolism that shape the subsequent immune response. A shift from oxidative phosphorylation (OXPHOS) to aerobic glycolysis is required for maturation of murine bone marrow derived DCs (BMDCs) stimulated with LPS and eventually results in an almost complete abrogation of mitochondrial metabolism (Krawczyk et al., 2010; Everts et al., 2014). Human $CD1c^+$ mDCs stimulated with single-stranded RNA, a TLR7/8 agonist, also undergo similar metabolic reprogramming to support their maturation (Basit et al., 2018). Our group previously showed that a metabolic switch to aerobic glycolysis plays an important role in the control of Mtb infection by macrophages (Gleeson et al., 2016). Here, we investigated the metabolic requirements of human $CD1c^+$ mDCs in response to the BCG vaccine. Upon challenge with BCG, $CD1c^+$ mDCs exhibited increased rates of OXPHOS and glycolysis. Inhibition of glycolysis with 2-Deoxy-D-Glucose (2-DG) decreased cytokine secretion and decreased the cell surface expression of CD40 in BCG-challenged cells. Unexpectedly, we found that inhibition of glycolysis had distinct effects on bystander and directly infected DCs, being required for optimal cell surface expression of CD40 and for CCR7-mediated migration of bystander cells, while both these functions were independent of glycolysis in BCG-infected cells. Our results suggest that the glycolytic pathway plays an important but nuanced role in the function of $CD1c^+$ mDCs in the response to mycobacterial infection. A better understanding of the metabolic response of DCs to BCG vaccination may aid the development of a vaccine that stimulates more effective protection against Mtb.

2 Materials and methods

2.1 Mycobacteria

Bacillus Calmette-Guerin (BCG) expressing GFP (green fluorescent protein) was a gift from V. Deretic (University of New Mexico, Albuquerque, NM). Stocks were propagated in Middlebrook 7H9 (Difco; Becton Dickinson) containing 10μg/ml Kanamycin (Sigma-Aldrich). Aliquots were stored at -80°C, thawed and grown to log phase in Middlebrook 7H9 medium before use.

2.2 $CD1c^+$ mDC isolation

Human $CD1c^+$ myeloid DCs (mDCs) were isolated from blood samples obtained from patients with no known infections attending

the Haemochromatosis Clinic in St. James's Hospital after informed consent, as approved by the St. James's Hospital and Tallaght University Hospital Joint Research Ethics Committee. First, PBMCs were separated by density gradient centrifugation on Lymphoprep™ (Axis-Shield). Cells were re-suspended in DC isolation buffer (2mM EDTA, 0.05% BSA in PBS) and DCs were enriched from PBMCs by negative magnetic separation using the EasySep™ Human Pan-DC Pre-Enrichment Kit following the manufacturer's instructions (STEMCELL Technologies). The negative fraction containing DCs was then stained in DC isolation buffer with antibodies against lineage markers (Lin) (CD3, CD14, CD16, CD19, CD20, CD56), HLA-DR, CD1c and CD304 for 20min on ice in the dark. $CD1c^+$ mDCs were further purified by cell sorting according to the following staining: Lin^- $HLA\text{-}DR^+CD304^-CD1c^+$.

2.3 CD1c+ mDC culture and infection

$CD1c^+$ mDCs were cultured in RPMI 1640 Medium (Lonza) containing 5% Human Serum (Sigma-Aldrich) without antibiotics and challenged with BCG on the same day of isolation. Unless otherwise stated, cells were seeded at a density of 7.5×10^5 cells/well in 200µl and infected for 20h with BCG at a ratio of 10 bacilli:cell. Alternatively, mDCs were stimulated with a combination of the TLR ligands Resiquimod (R-848, 5µg/ml, Enzo Life Sciences) and Polyinosinic-Polycytidylic acid (poly(I:C), 20µg/ml, Sigma-Aldrich) for the same period. Where indicated $CD1c^+$ mDCs were treated for 1h prior to, and for the duration of infection with 1mM 2-Deoxyglucose (2-DG, Sigma-Aldrich).

For analysis by confocal microscopy $CD1c^+$ mDCs were challenged with GFP-BCG as outlined above, washed and fixed with 2% paraformaldehyde and then mounted onto Polysine slides (ThermoFisher Scientific). Cells were imaged with a 63X magnification oil immersion objective on a Leica SP8 confocal microscope using LAS X software (Leica).

2.4 Flow cytometry

Flow cytometry analysis (CyAn ADP, Beckman Coulter) and cell sorting (MoFlo XDP, Beckman Coulter) were performed with the following antibodies (anti-human): Lineage Cocktail-FITC (CD3, CD14, CD16, CD19, CD20, CD56), HLA-DR-BrilliantViolet 421 (L243), CD304-PE (12C2), CD1c-APC (V T-CD01.18), CD40-APC/Cy7 (5C3), CCR7- PerCP/Cy5.5 (G043H7), Zombie Red (or Zombie Aqua) Fixable Viability Dye and anti-mouse IgG1-PE (RMG1-1) (all from Biolegend); CD83-APC and CD86-PE (BD Pharmingen). $CD1c^+$ mDCs were harvested following BCG infection or TLR stimulation and stained for 20 minutes on ice in the dark in DC isolation buffer. Cells were then washed and fixed in 2% paraformaldehyde when necessary. $CD1c^+$ mDCs were gated on forward scatter and side scatter to exclude cell clumps and debris. Dead cells were excluded from analysis according to Zombie Red staining (or with Zombie Aqua when cells were stained with Texas red conjugated to Dextran). Unstained $CD1c^+$ mDCs, BCG-GFP and FMO controls were used to determine negative populations and to adjust gates appropriately. GLUT1 (Metafora Biosystems) staining was performed according to the manufacturer's instructions. Mean fluorescence intensity (MFI) and the percentage of positive cells was determined for CD83, CD86, CD40 and CCR7. Analysis was performed using FlowJo® (Tree Star, Inc).

2.5 Dextran uptake assay

Peripheral venous blood samples were obtained from healthy adult donors following informed consent. PBMCs were separated by density gradient centrifugation on Lymphoprep™ and cells were washed twice with Ca/Mg-free PBS. PBMCs were resuspended in RPMI supplemented with 2% human serum and 1mg/ml dextran conjugated to Texas red (ThermoFisher) (Wang et al., 2009). Cells were incubated for 24 h at 4°C (as a negative control) or 37°C, washed, stained with cell surface markers, and analysed by flow cytometry. Dextran uptake was measured in live $CDC1^+$ mDCs which were defined as Zombie $Aqua^-$ Lin^- $HLA\text{-}DR^+$ $CD11c^+CD1c^+$ and $CD304^-$ cells.

2.6 Cytokine measurements

Cytokine concentration was assessed in cell-free supernatants at 20h post-infection using Meso Scale Discovery Proinflammatory Panel 1 (human) (MSD, Gaithersburg, MD) for the detection of IFN-γ, IL-1β, IL-2, IL-4, IL-5, IL-8, IL-10, IL-12p70, IL-13, and tumor necrosis factor (TNF)-α. Assay was performed according to the manufacturer's instructions and data analyzed using Discovery Workbench 3.0 software (MSD).

2.7 Migration assay

$CD1c^+$ mDCs migration assay towards CCL19 was performed using 24-well Transwell plates containing 5µm pore polycarbonate membrane inserts (Corning Life Sciences). A total of $1x10^5$ $CD1c^+$ mDCs were challenged with BCG, with or without 2-DG (1mM), for 20h. Following infection, the cells were harvested, counted and suspended in 200µl of culture medium and placed on the upper side of the membrane. A portion of the cells ("input") was kept aside for analysis as detailed below. The remaining mDCs were allowed to migrate to the lower chamber containing 750µl of complete RMPI medium containing CCL19 (50ng/ml, Bio-Techne) for 3h at 37°C. Input and transmigrated cells were stained with 10µg/ml cell-permeable Hoechst 33342 (Thermo Scientific) and counted using the Cytell Cell Imaging System (GE Life Sciences). Results were expressed as the percentage of cells migrating to the lower chamber in relation to the initial cell number added to the upper chamber (input). Input and migrating cells, challenged with BCG with or without 2-DG treatment, were recovered, fixed with 2% paraformaldehyde and then mounted onto Polysine slides (ThermoFisher Scientific). 200 cells in each sample were counted

using an Olympus IX51 fluorescent microscope with a 100X oil objective. Infected cells were detected using the FITC filter to visualize GFP and nuclei were visualized using the DAPI filter to count all of the cells. Changes in migration of bystander (GFP^-) and directly infected (GFP^+) cells were calculated as the ratio of the number of migrated cells (GFP^- or GFP^+) to the original numbers of GFP^- or GFP^+ cells added to the top of the transwell.

2.8 Metabolic assays

Real-time analysis of extracellular acidification rate (ECAR) and oxygen consumption rate (OCR) was determined in mDCs using an XFe24 Extracellular Flux Analyzer (Seahorse Biosciences). Briefly, $2x10^5$ $CD1c^+$ mDCs were seeded onto Seahorse XF24 Cell Culture Microplates pre-coated with CellTak™ (1µg/well, Corning) and challenged with rifampacin-killed BCG-GFP at a ratio of 50 bacilli: cell for 20h in complete RPMI. $CD1c^+$ mDCs were then carefully washed with Seahorse Media supplemented with 2mM L-glutamine and 10mM glucose. The Agilent Seahorse XF Cell Mito Stress Test Kit was used to assess mitochondrial function. The optimal concentrations of oligomycin and FCCP were determined in an initial pilot study. Measurement of baseline ECAR and OCR was carried out followed by successive injections of the following reagents to obtain the indicated concentrations: oligomycin (1 µM), FCCP (2 µM) and finally rotenone (0.5 µM) + antimycin A (0.5 µM). Glycolytic function was assessed in the cells using the Seahorse XF Glycolysis Stress Test Kit according to the manufacturer's instructions. Cells were challenged with BCG-GFP as above and $CD1c^+$ mDCs were then carefully washed with Seahorse Media supplemented with 2mM L-glutamine and incubated in a non-CO_2 incubator for 1 hour prior to the run. Baseline ECAR and OCR were measured before and after injection of glucose (10mM) to determine basal rates of ECAR and OCR followed by injections of oligomycin (1 µM) and finally 2-DG (50mM). Results were normalized by cell number in each well which was determined by staining the cells with 10µg/ml Hoechst 33342 followed by analysis using the Cytell Cell Imager as described above.

L-Lactate concentration was measured in the cell supernatants at 20h p.i. with BCG by colorimetric assay in 96-well plates according to the manufacturer's instructions (Sigma-Aldrich). The absorbance of samples and standards was read at 570 nm using an Epoch Microplate Spectrophotometer with Gen5 Data Analysis software (BioTek Instruments).

2.9 Statistical analysis

Statistical analysis was performed using Graph Pad Prism 9 Software (San Diego, CA, USA). Results are expressed as mean ± SEM. Data was considered non-parametric as per normality test performed on the data sets. Tests used were unpaired/paired two-tailed t test or Wilcoxon-ranked sum test as appropriate to compare two groups and Repeated Measures One-Way Analysis of Variance (ANOVA) to compare more than two sets of data followed by the recommended post tests. Repeated Measures or mixed model Two-Way ANOVA was used to compare more than two sets of paired grouped data followed by the recommended post tests. A p value < 0.05 was considered statistically significant.

3 Results

3.1 Challenge of $CD1c^+$ mDCs with BCG results in up-regulation of surface markers and cytokine secretion

Myeloid dendritic cells are very scarce, comprising of between 0.3% - 0.9% of all peripheral blood mononuclear cells. These cells have a short lifespan *in vitro* (Nopora and Brocker, 2002; Hou and Van Parijs, 2004) and can become activated upon culturing (Dzionek et al., 2000), facts that restrict the use of these cells *in vitro*. We first attempted to isolate $CD1c^+$ mDCs from the buffy coats provided by the Irish Blood Transfusion Service facility in St James Hospital Dublin, Ireland. Following isolation of PBMCs from blood and enrichment of the DC population by magnetic beads, $CD1c^+$ mDCs were sorted according to expression of the surface markers $Lineage^-$, $HLA\text{-}DR^+$, $CD1c^+$ and $CD304^-$ (Figure 1A). However, buffy coats are available for processing only 48 hours after they are drawn, which could explain the low yield of DCs isolated from these buffy coats: the number of $CD1c^+$ mDCs obtained by this methodology ranged from $4.2x10^3$ to $0.7x10^6$ cells (mean = $0.30x10^6$, SD ± $0.28x10^6$) per buffy coat. For this reason, we isolated $CD1c^+$ mDCs from fresh blood collected from patients with Hereditary Hemochromatosis (HH). The number of $CD1c^+$ mDCs obtained from one unit (approximately 500ml) of freshly drawn blood was significantly higher and ranged from $4x10^5$ to $1x10^6$ cells with purity of 94.03% (SD ± 4.15%, n= 62). Our preliminary analysis showed no significant differences regarding expression of surface markers and endocytic capacity (assessed by Dextran-internalization assay) between mDCs from HH patients and healthy controls (Supplementary Figure 1).

In keeping with a previously published report (Dzionek et al., 2000) confocal microscopy of the sorted $CD1c^+$ mDCs revealed that they were medium-sized cells with hyperlobulated nuclei (Supplementary Figure 2A). Purified $CD1c^+$ mDCs were challenged with a GFP-tagged strain of BCG, at a ratio of 10:1 mycobacteria:cell or stimulated with a mixture of the TLR ligands poly(I:C) and R-848 for 20h. Analysis by flow cytometry showed that an average of 22.7% (SD ± 7.8) of the mDCs had successfully phagocytosed bacilli (Figure 1B). Z-stack imaging of BCG-challenged mDCs (n=5 individual donors) indicated that the bacteria were located within the infected cells rather than adhering to the surface (Supplementary Figure 2B).

The maturation status of the $CD1c^+$ mDCs following infection was performed by assessing expression of maturation markers on the cell surface and cytokine secretion on the cell supernatants. Challenge with BCG or stimulation with poly(I:C)/R-848 resulted in up-regulation of the surface markers CD83, CD40 and CCR7. Expression of CD86 trended towards an increase but did not reach statistical significance with either stimulus (Figure 1C, D).

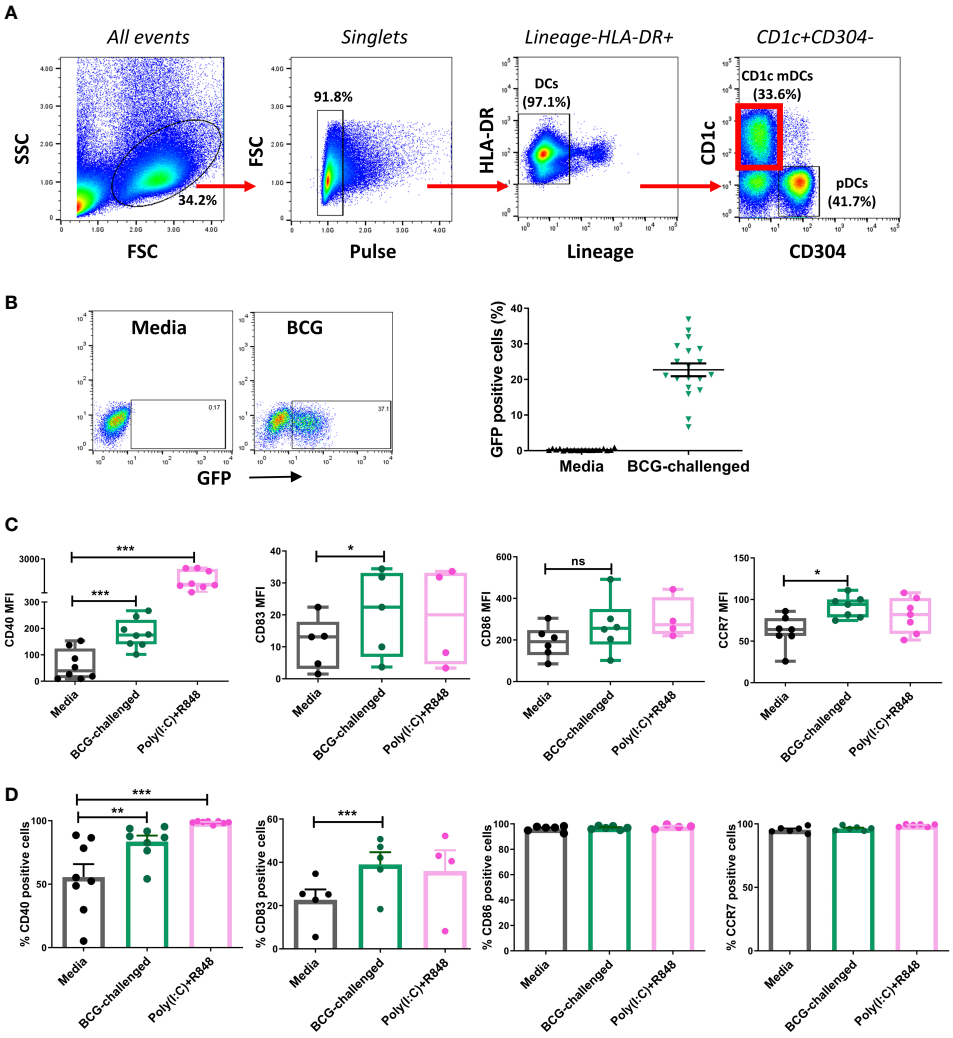

FIGURE 1
CD1c$^+$ myeloid DCs respond to challenge with BCG through phagocytosis and up-regulation of maturation markers. **(A)** Gating strategy used for sorting CD1c$^+$ mDCs. Dendritic cells were enriched from PBMCs by application of Pan-DC Pre-Enrichment Kit and purified by cell sorting. Lineage marker consisted of a cocktail of antibodies against CD3, CD14, CD16, CD19, CD20 and CD56 surface markers. Dot plots show one representative donor. **(B)** Percentage of infected (BCG-GFP$^+$) CD1c$^+$ mDCs at 20h post infection with MOI 10. Dot plots show one representative donor and graph shows individual and mean value ($\pm$ SEM) from 19 different donors. **(C)** Surface marker levels for CD40 (n=8), CD83 (n=4-5) CD86 (n=4-5), CCR7 (n=7) shown as mean fluorescence intensity (MFI) in CD1c$^+$ mDCs challenged with BCG (MOI 10) or combination of the TLR ligands poly(I:C) (20µg/ml) + R-848 (5µg/ml) compared to control (media). Box plots extend from the 25-75% interquartile range, the horizontal bar depicts the median and whiskers indicate the minimum to maximum values. Each dot represents the result from an individual donor. **(D)** Surface marker levels shown as percentage of positive cells. Each dot represents the result from an individual donor, bars show mean and SEM. Statistical significance was determined using a repeated measures one way analysis of variance (or mixed effects model where appropriate) with Dunnett's multiple comparisons test comparing BCG and poly(I:C)+R-848 to the media control. * p< 0.05, **p<0.01 and ***p<0.001, ns, not significant.

3.2 Challenge with BCG induces changes in the cell metabolism of humans CD1c$^+$ mDCs

Increasing evidence has reinforced the importance of metabolic reprogramming in licensing immune cells to perform their effector functions. TLR stimulation of murine DCs boosts their rate of aerobic glycolysis, which is necessary to meet increased biosynthetic demand during maturation (Krawczyk et al., 2010; Everts et al., 2014; Thwe and Amiel, 2018). A shift towards glycolysis is also necessary for human macrophages to control infection with Mtb (Gleeson et al., 2016). Therefore, we hypothesized that human CD1c$^+$ mDCs would also undergo metabolic reprogramming upon challenge with BCG and decided to characterize the energetic profile of these cells. We first analyzed the baseline extracellular acidification rate (ECAR) and oxygen consumption rate (OCR) of immature and BCG-challenged CD1c$^+$ mDCs at 20h p.i using a Seahorse metabolic analyzer in the presence of glucose (Figure 2A). We observed that BCG and poly(I:C)/R848 modestly increased the rates of glycolysis (ECAR measurement) and mitochondrial respiration (OCR measurement) in CD1c$^+$ mDCs, resulting in a more energetic phenotype (Figure 2B). An examination of mitochondrial function using the Mito Stress Test (Supplementary Figure 3) revealed a trend towards increased basal

OCR in BCG-challenged cells and maximal respiration was significantly higher with BCG challenge compared to the control, indicating that they have an increased capacity to oxidise mitochondrial fuels when stressed. In addition, non-mitochondrial OCR was significantly decreased in BCG-challenged mDCs compared to control cells. The increase in baseline OCR observed in poly(I:C)/R848-treated cells was primarily due to an increase in non-mitochondrial OCR, possibly due to increased cytosolic ROS production.

Lactate is an end product of glycolysis, and its production is increased as a result of LPS-mediated enhancement of glycolytic flux in dendritic cells (Jantsch et al., 2008; Everts et al., 2012). To confirm an increase in glycolysis in our model, in parallel we measured the levels of lactate secreted in the cell supernatants. Lactate production was significantly increased in BCG-challenged CD1c$^+$ mDCs in comparison to uninfected control cells in response to both BCG and the TLR ligands poly(I:C)/R-848 (Figure 2C). Increased glycolytic flux can also be accompanied by increases in the expression of glucose transporters on the cell surface. We measured the expression of Glucose Transporter 1 (GLUT1) on CD1c$^+$ mDCs by flow cytometry but no significant differences were observed between the different groups (Supplementary Figure 4). Taken together, these results suggest that challenge with BCG results in changes in cell metabolism of CD1c$^+$ mDCs, inducing a more energetic phenotype and increased lactate production but without a concomitant increase in GLUT1 cell surface expression.

3.3 Challenge with BCG boosts the glycolytic function of CD1c$^+$ mDCs

As the glycolytic pathway has been shown to have an important role in survival and function of DCs and basal rates of glycolysis were significantly increased following exposure to BCG, we examined glycolytic function of CD1c$^+$ mDCs in response to BCG infection in more detail. To specifically interrogate extracellular glucose-driven metabolism we performed a glycolysis stress test of BCG-challenged CD1c$^+$ mDCs in comparison to naive cells. Cells were exposed to BCG as described before and the culture medium was replaced with glucose-free medium for 1 hour prior to the assay. Then, ECAR was measured at baseline levels and again after re-introduction of glucose to determine the basal glycolytic rate. Next, oligomycin was added to the cells to block mitochondrial respiration and promote maximal levels of glycolysis and, finally, glycolysis was blocked by addition of 2-DG to the cells (Figure 3A). With this methodology it was possible to determine the basal glycolytic rate (difference between ECAR before and after glucose addition), glycolytic capacity (difference between ECAR following injection with oligomycin and basal readings) and glycolytic reserve (difference in ECAR between addition of glucose and oligomycin) of the cells. Both uninfected and BCG-infected CD1c$^+$ mDCs increased ECAR following addition of glucose to the cells (Figure 3A) but the basal glycolytic rate was significantly higher for BCG-infected cells (Figure 3B). In addition, OCR was increased in BCG-challenged cultures following the addition of glucose. (Figures 3B, C). BCG-infected cells also showed enhanced glycolytic capacity when compared to uninfected cells. However, we observed that infection with BCG did not alter the glycolytic reserve of the CD1c$^+$ mDCs. These data indicate that BCG challenge increases the glycolytic rate and boosts the capacity of CD1c$^+$ mDCs to use glucose to produce ATP *via* glycolysis when stressed. Non-glycolytic acidification was also significantly increased in BCG-challenged cultures compared to control (Figure 3C).

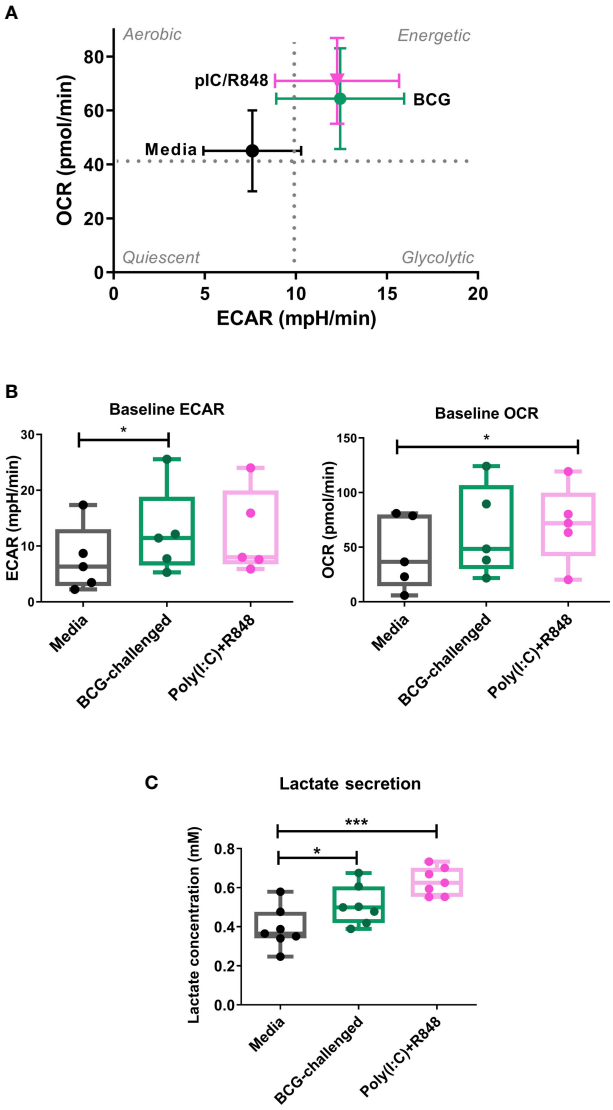

FIGURE 2
Metabolic profile of CD1c$^+$ mDCs in response to BCG. **(A)** XF Cell Energy Phenotype of uninfected and BCG-challenged CD1c$^+$ mDCs at 20h p.i. Plot shows average of baseline readings ($\pm$ SEM) for 5 donors of oxygen consumption rates (OCR) and extracellular acidification rates (ECAR) obtained with the Seahorse Extracellular Flux Analyzer. Box plots extend from the 25-75% interquartile range, the horizontal bar depicts the median and whiskers indicate the minimum to maximum values. Superimposed dots represent the results from five individual donors. **(B)** Lactate secreted in the cell supernatants measured at 20h p.i with BCG challenge or stimulation with TLR ligands. Box plots extend from the 25-75% interquartile range, the horizontal bar depicts the median and whiskers indicate the minimum to maximum values. Superimposed dots represent the results from seven different donors. Statistical significance was determined using a repeated measures one way analysis of variance with Dunnet's multiple comparisons test. * $p< 0.05$, ***$p<0.001$.

10.3389/fcimb.2023.1113744

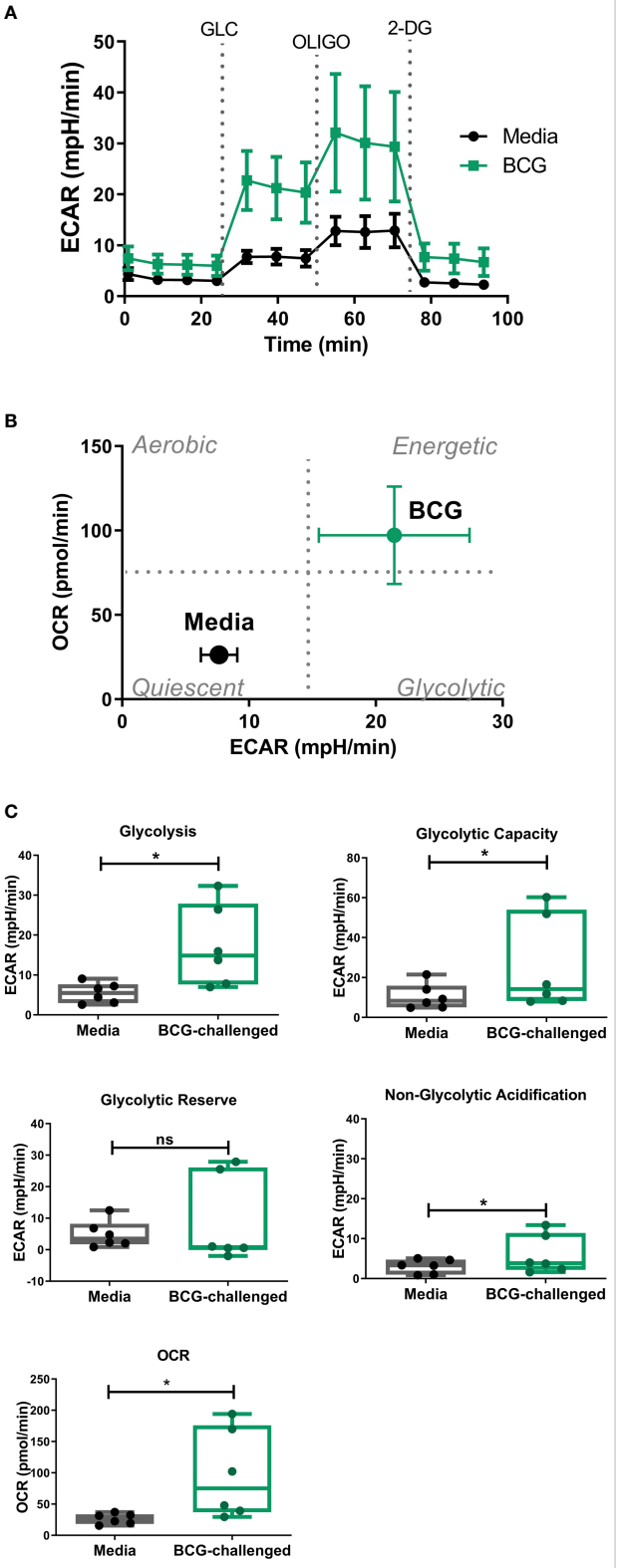

FIGURE 3 (Continued)

FIGURE 3 (Continued)
Analysis of glycolytic function in CD1c$^+$ mDCs following challenge with BCG. **(A)** ECAR readings (mean ± SEM) for six independent donors) of CD1c$^+$ mDCs subjected to the Glycolysis Stress test which were initially cultured in glucose-free medium and ECAR was measured following glucose (Glu), oligomycin (Oligo), and 2-Deoxy-D-glucose (2-DG) injections in control and BCG-challenged CD1c$^+$ mDCs at 20h p.i. **(B)** XF Cell Energy Phenotype of uninfected and BCG-challenged CD1c$^+$ mDCs (n=6) at 20h p.i. ECAR changes as determined by Seahorse metabolic profiling. Plot shows average of basal readings (± SEM) for oxygen consumption rates (OCR) and extracellular acidification rates (ECAR) after the addition of 10mM glucose obtained with the Seahorse Extracellular Flux Analyzer. **(C)** Box plots depict Glycolysis rates (ECAR after glucose addition subtracted from baseline ECAR before the first injection), Glycolytic Capacity (ECAR after oligomycin infection subtracted from basal ECAR) and Glycolytic Reserve (glycolytic capacity minus basal glycolysis) calculated from the ECAR curve. Box plots extend from the 25-75% interquartile range, the horizontal bar depicts the median and whiskers indicate the minimum to maximum values. Superimposed dots represent the results from six independent donors. Statistical significance was determined using paired t-tests. * $p< 0.05$, ns, not significant.

3.4 Inhibition of glycolysis decreases cytokine secretion of BCG-challenged CD1c$^+$ mDCs

To understand the role of the glycolytic pathway in CD1c$^+$ mDC function in response to BCG, we pretreated the cells with the glycolysis inhibitor 2-DG prior to infection. We first investigated if inhibition of glycolysis affected the phagocytic capacity of the CD1c$^+$ mDCs. However, pre-treatment with 2-DG had no impact on the level of BCG infection when compared to untreated control cells (Figures 4A, B) although it had a small but significant effect on viability of BCG challenged DCs (Figure 4C). We then assessed the effect of 2-DG on cytokine production by the CD1c$^+$ mDCs following challenge with mycobacteria. Exposure to BCG induced secretion of the cytokines IL-1β, IL-6, TNF-α and IL-10 (Figure 4D). Production of IL-12p70, IFN-γ and low levels of IL-4 was only detected after TLR stimulation but not in BCG-challenged cells (data not shown). These results are consistent with previous findings (Lozza et al., 2014) and suggest no functional abnormalities in response to infection with BCG in the CD1c$^+$ mDCs used in this study.

Inhibition of glycolysis significantly decreased the secretion of IL-1β, TNF-α and IL-10 by BCG-infected cells (Figure 5). Production of IL-6 was not altered by 2-DG. These results suggest that the glycolytic pathway is involved not only in the secretion of pro-inflammatory cytokines but also is necessary for optimal IL-10 production by CD1c$^+$ mDCs.

3.5 Expression of the maturation markers CD40 and CCR7 in BCG-challenged CD1c$^+$ mDCs is altered by inhibition of the glycolytic pathway

To further investigate the role of glycolysis in the effector function of CD1c$^+$ mDCs in response to infection with BCG, we analyzed the cell surface expression levels of the costimulatory

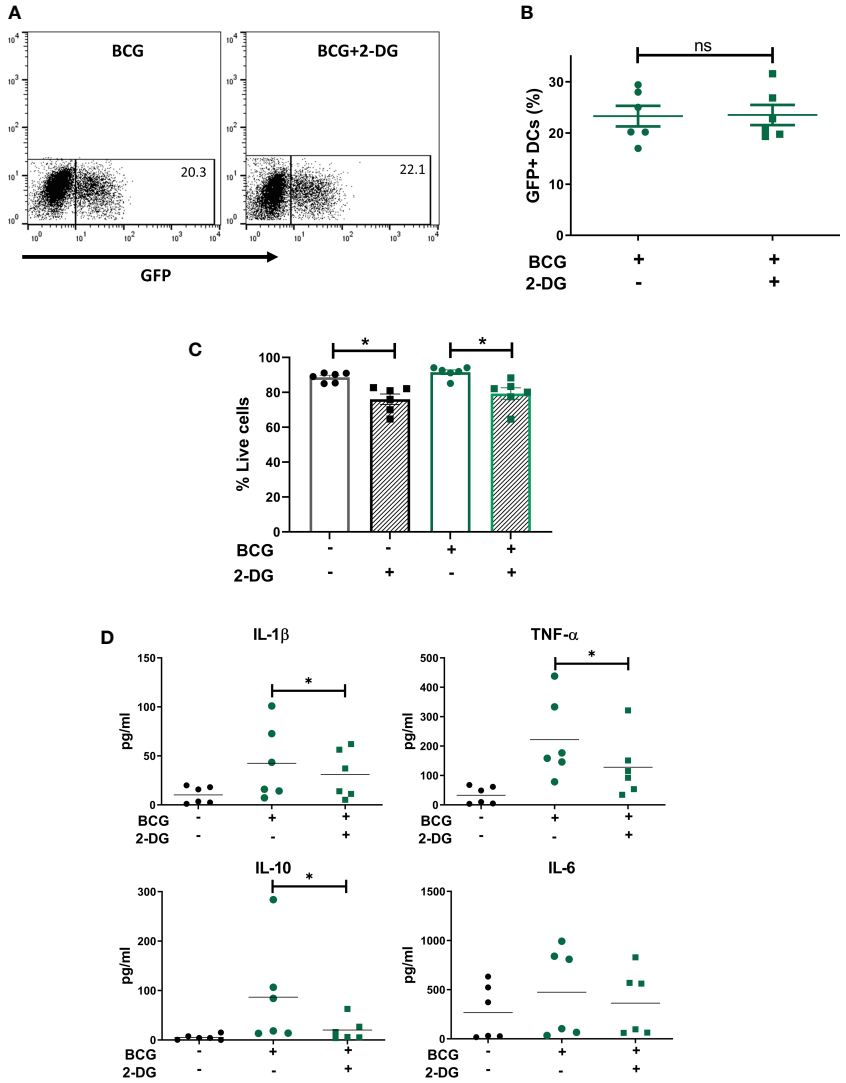

FIGURE 4
Inhibition of glycolysis decreases secretion of cytokines but does not affect phagocytosis of BCG by CD1c$^+$ mDCs. **(A)** Representative dot plots from one donor showing percentage of GFP$^+$ untreated or 2-DG treated CD1c$^+$ mDCs and graph **(B)** showing percentage of BCG$^+$ cells (mean value ± SEM) of six independent donors at 20h upon infection with BCG in cells pre-treated or not with 2-DG (1mM). **(C)** CD1c$^+$ mDCs were treated or not with 1mM 2-DG and then challenged with BCG for 20h. Viability (% live cells) was then determined by staining the cells with Zombie red dye followed by analysis by flow cytometry. Cells that were negative for Zombie red were considered viable. Bar charts show mean (± SEM) and superimposed dots represent the results from six independent donors. Statistical significance was determined by two-way repeated measures analysis of variance followed by Šídák's multiple comparison test. **(D)** Cytokine production was measured in the cell supernatants at 20h p.i. Graphs show values (± SEM) from six independent donors. Statistical significance was determined using a Wilcoxon signed-rank test, * $p< 0.05$, ns, not significant.

molecule CD40 and the chemokine receptor CCR7. The cells were once more pre-treated or not with 2-DG and challenged with BCG. Cell surface staining of the markers CD40 and CCR7 was analyzed by flow cytometry at 20h p.i. First, the analysis was performed considering all live cells in the cell population. As before, the percentage of CD40 positive cells and CD40 expression levels (measured as mean fluorescence intensity) were significantly increased in response to challenge with BCG. Inhibition of glycolysis with 2-DG significantly decreased the expression of CD40 (both percent positive cells and MFI) on BCG-challenged CD1c$^+$ mDCs. Increased expression of CD40 was also observed with poly(I:C)/R848 stimulation compared to unstimulated cells and there was a trend towards decreased CD40 expression with 2-DG treatment, but this was not statistically significant (Figures 5A, B).

Most cells expressed CCR7 at baseline and the percentage of cells positive for CCR7 did not change significantly following challenge with BCG or treatment with 2-DG (Figure 5E). Surprisingly, surface expression of CCR7 was significantly increased after blocking glycolysis with 2-DG in infected cells. Expression levels of CCR7 were also significantly increased in poly(I:C)/R848 treated CD1c$^+$ DCs with inhibition of glycolysis (Figure 5F).

As we used GFP-tagged BCG in our assays, we analyzed the surface levels of both CD40 and CCR7 maturation markers separately in the population of cells that successfully

10.3389/fcimb.2023.1113744

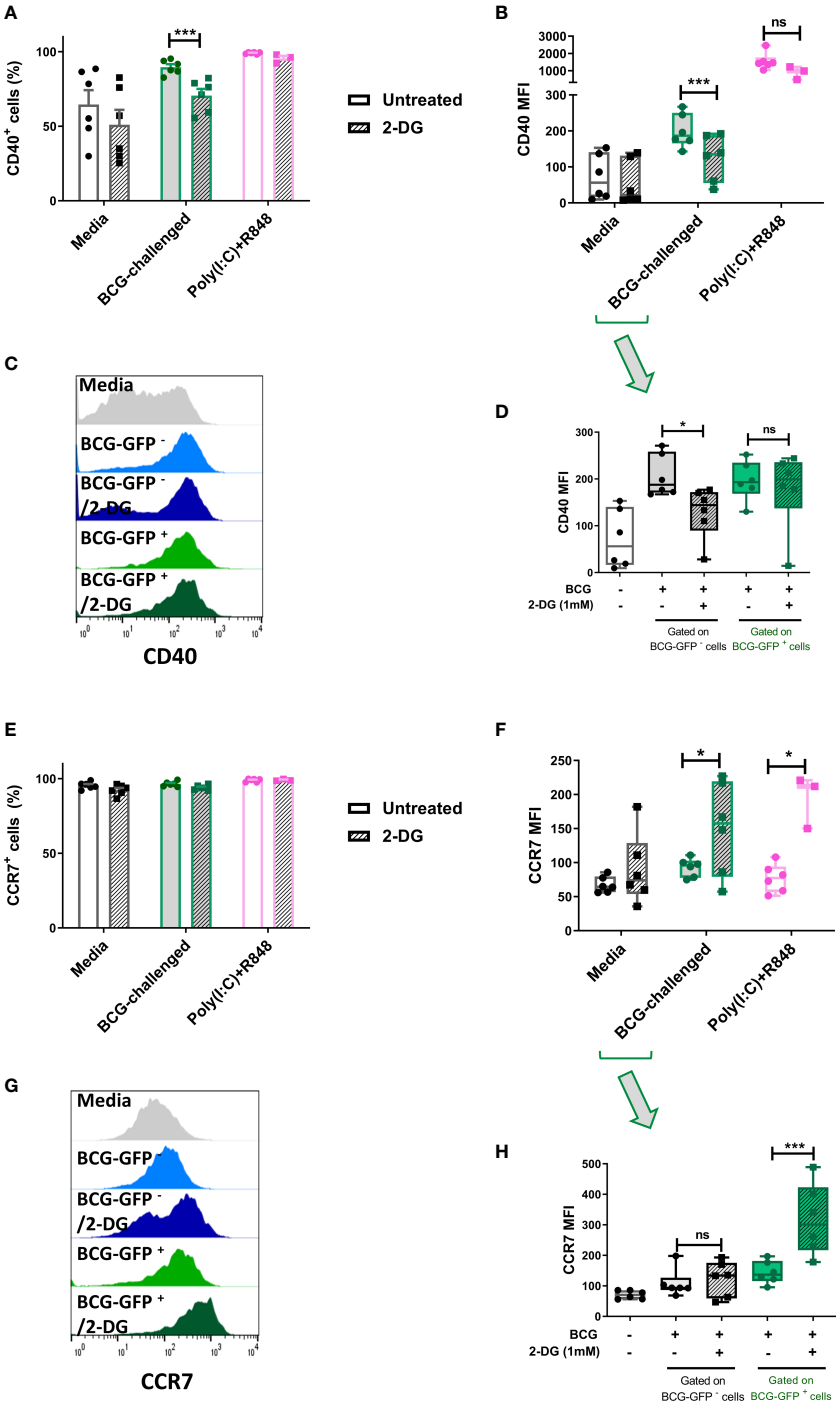

FIGURE 5
Inhibition of glycolysis has differential effects on cell surface expression of CD40 and CCR7 of bystander and BCG-infected CD1c$^+$ mDCs. Surface levels of CD40 and CCR7 were analyzed by flow cytometry at 20h p.i. with BCG in CD1c$^+$ mDCs pre-treated or not with 2-DG (1mM). **(A)** Percentage of CD40 positive and **(E)** CCR7 positive and **(B)** MFI of CD40 and **(F)** CCR7 positive live CD1c$^+$ mDCs with and without preincubation with 2DG when gating strategy comprised all live cells. Graphs show mean fluorescence intensity (MFI). **(D)** CD40 and **(H)** CCR7 levels resulting from analysis in which the BCG-challenged CD1c$^+$ mDCs that had phagocytosed BCG (BCG-GFP$^+$) were gated and analyzed separately from cells that had not taken up mycobacteria (BCG-GFP$^-$). Bar charts show mean and SEM and superimposed dots represent the results from three - six individual donors. Box graphs show mean - whiskers min to max values, and superimposed dots represent the results from three - six individual donors. Histogram overlays plots **(C, G)** are representative. Statistical significance was determined by two-way mixed model analysis of variance with Šídák's multiple comparison tests. *p<0.05 and ***p<0.001, ns, not significant.

phagocytosed the mycobacteria, named here BCG-GFP$^+$ cells, and those bystander cells which had been exposed to but had not engulfed any bacilli (BCG-GFP$^-$ cells). The results for CD40 showed that for the bystander BCG-GFP$^-$ CD1c$^+$ mDCs, the surface levels of this marker were increased following challenge with BCG whereas inhibition of glycolysis for this cell population resulted in failure to up-regulate CD40. In contrast, in BCG-GFP$^+$ CD1c$^+$ mDCs, the expression levels of CD40 were up-regulated in response to challenge with BCG in both untreated and 2-DG treated cells indicative of differential effects of glycolysis on CD40 expression depending on whether or not the cells had phagocytosed the bacteria (Figures 5C, D).

Regarding the expression of CCR7 on the cell surface of CD1c$^+$ mDCs following challenge with BCG, we observed that for the BCG-GFP$^-$ cells, the levels of CCR7 were similar for both untreated and 2-DG-treated cells. However, for the BCG-GFP$^+$ population, inhibition of glycolysis significantly increased CCR7 expression levels compared to untreated BCG-GFP$^+$ CD1c$^+$ mDCs (Figures 5G, H).

3.6 The migratory capacity of CD1c$^+$ mDCs infected with BCG is not dependent on glycolysis

Migration of infected mDCs to draining LNs is required to initiate an adaptive immune response to BCG (Bollampalli et al., 2015). Following our observation that treatment with 2-DG increased levels of CCR7 on the cell surface of BCG-infected CD1c$^+$ mDCs, we set up a transwell migration assay to determine if inhibition of glycolysis influenced CCR7-dependent cell migration. CD1c$^+$ mDCs, either unchallenged or challenged with BCG in the presence or not of 2-DG for 20h, were allowed to migrate for 3 hours through a membrane towards a gradient of CCL19, a ligand for CCR7 (Figure 6A). The numbers of transmigrated cells were counted by automated microscopy and then further analyzed by fluorescence microscopy to determine the proportion of GFP$^-$ and GFP$^+$ cells. Few DCs migrated through the membrane in both uninfected and BCG-challenged control samples where culture medium alone was added to the lower chamber of the transwell plate. The number of migrated cells was significantly higher when medium containing CCL19 was present in the lower chamber (Supplementary Figure 5A). Analysis of the total CD1c$^+$ mDCs that migrated through the membrane showed that treatment with 2-DG significantly decreased the overall migration of immature CD1c$^+$ mDCs towards CCR7 from 57.50% (+/-13.60%) to 28.45% (+/- 8.52%) of the original number of DCs added to the upper chamber (input), in line with previously published results obtained with murine BMDC migrating to a CCR7 ligand (CCL21) (Guak et al., 2018). Blocking glycolysis with 2-DG decreased the overall migration of BCG-challenged CD1c DCs from 68.09% (+/-16.34%) to 48.78% (+/-6.82%) of the input (Figure 6B).

As before, based on the presence of GFP-expressing BCG, it was possible to differentiate between uninfected bystander (GFP$^-$) and BCG-infected (GFP$^{+)}$ CD1c$^+$ mDCs in the BCG-challenged cultures. Aliquots of the input and the transmigrated BCG-challenged cells from each donor - untreated (media) or treated with 2-DG - were mounted on slides and 200 mDCs per sample were visualised at 1000X magnification by fluorescent microscopy. We counted the numbers of input and migrated cells that were infected with BCG-GFP versus those bystander cells that were uninfected. The numbers of migrated BCG-infected and uninfected mDCs were normalised to the numbers of BCG-infected and uninfected mDCs respectively in the input. A significantly higher proportion of 2-DG-treated BCG-GFP$^+$ mDCs migrated towards the chemokine stimulus relative to untreated BCG-GFP$^+$ mDCs. Conversely, the proportion of BCG-GFP$^-$ bystander cells in the same samples was significantly reduced in the presence of 2-DG (Figure 6D). The percentages of transmigrated GFP$^+$ and GFP$^-$ mDCs without normalisation are shown in Supplementary Figure 5B. Taken together, these data suggest that, although glycolysis potentiates the migration of immature and of mature bystander BCG-challenged CD1c DCs, glycolytic flux is not required for CCR7-mediated trafficking of BCG-infected CD1c$^+$ mDCs.

4 Discussion

In this study, we characterized the metabolic profile and investigated the role of the glycolytic pathway in the response of CD1c$^+$ mDCs the BCG vaccine. We found that CD1c$^+$ mDC mature and acquire a more energetic phenotype upon challenge with BCG. Pharmacological inhibition of glycolysis with 2-DG decreased cytokine secretion and regulated the expression of both CD40 and CCR7 on BCG-challenged, compared to untreated, mDCs. In addition, inhibition of glycolysis had differential effects on infected and uninfected bystander mDCs in BCG-challenged cultures. To our knowledge, this is the first study investigating immunometabolism in human CD1c$^+$ mDCs infected with mycobacteria.

A significant barrier to studying natural human DCs is their low frequency in blood and tissues which severely limits the number of assays that can be carried out on cells from any one donor. To optimize the purification procedure and assays and carry out the experiments presented here we processed blood from over 60 donors. Due to the low yield of viable DCs from buffy coats we isolated CD1c$^+$ mDCs from freshly drawn blood collected from patients with Hereditary Hemochromatosis (HH). Our preliminary analysis showed no differences regarding expression of surface markers and endocytic capacity (assessed by Dextran-internalization assay) between mDCs from HH patients and healthy controls. We cannot rule out the possibility that there are differences between the response of HH and healthy control mDCs to BCG. However, a report investigating the characteristics of monocyte-derived DCs from HH patients showed no phenotype and functional differences at both the immature and mature stages in these cells (Phothirath et al., 2002). Despite the considerable challenges of working with these cells we believe it is important to carry out these studies using natural human DCs given that most of our knowledge of DC metabolism to date is based on *in vitro* studies of murine BMDCs or human monocyte-derived DCs which are

10.3389/fcimb.2023.1113744

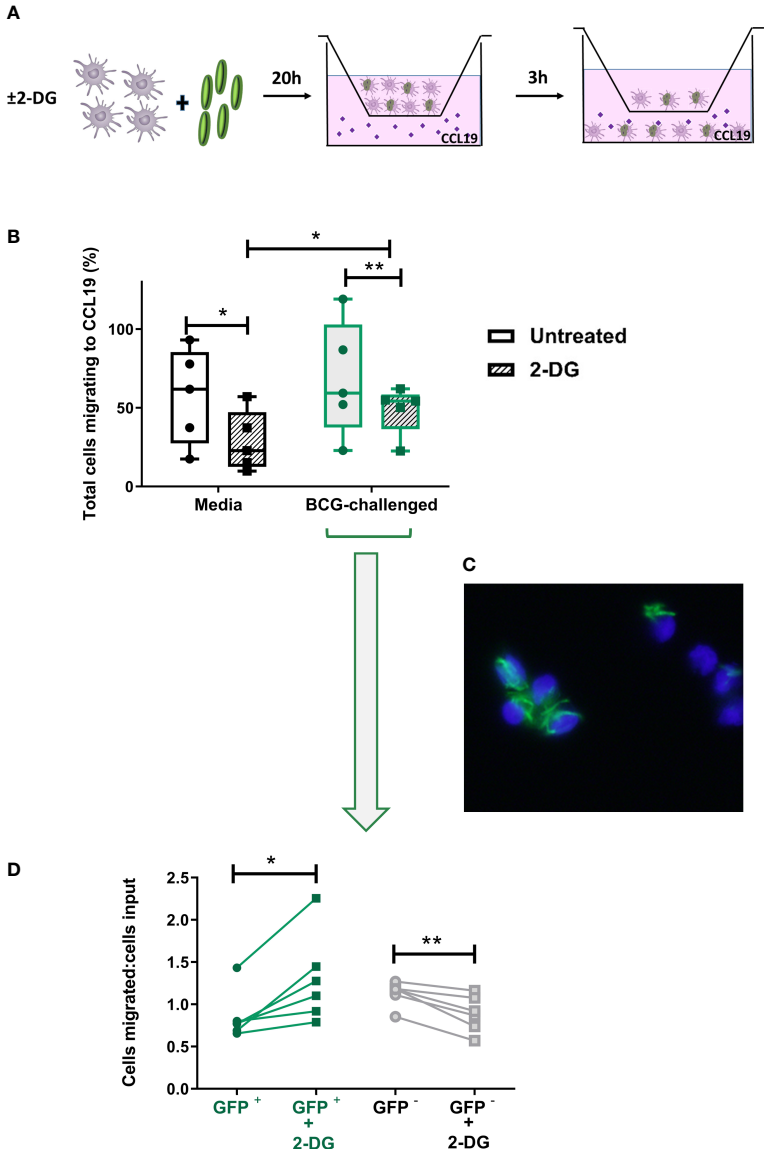

FIGURE 6
Inhibition of glycolysis has differential effects on CCR7-mediated migration of bystander and BCG-infected CD1c$^+$ mDCs. **(A)** *In vitro* cell migration assay outline: CD1c$^+$ mDCs were pre-treated or not with 1mM of 2-DG and challenged with BCG-GFP for 20h. They were then resuspended in fresh medium and allowed to migrate for 3h in a transwell system through a 5µm pore membrane toward a gradient of CCL19 chemokine (50ng/ml). The total number of cells migrating into the lower chamber after 3h was enumerated using a Cytell Imager. Results were calculated as the percentage of cells migrating to CCL19. **(B)** Graph shows data from five different donors as a percentage of initial number of cells added to the chamber (input). Box plots extend from the 25-75% interquartile range, the horizontal bar depicts the median and whiskers indicate the minimum to maximum values. Each dot represents the result from an individual donor. Data were analyzed using Two-Way mixed model ANOVA with Šídák's multiple comparisons test. **(C)** Representative image of transmigrated CD1c$^+$ mDCs obtained using an epifluorescent microscope, showing intracellular GFP$^+$ bacilli. Cell nuclei were counterstained with Hoechst 33342. **(D)** Aliquots of the cells added to the top chamber, and transmigrating cells collected from the lower chamber after 3 hours, were placed on slides and fixed. For each condition 200 cells were counted using the 100X objective of an epifluorescent microscope and the numbers of BCG-infected (GFP $^+$) and uninfected cells (GFP $^-$) was calculated. Results are plotted as a ratio of the number of infected or uninfected cells added to the top chamber (input) divided by the number of infected or uninfected transmigrated cells with and without 2DG treatment. Graph shows data from six different donors. Statistical significance was determined using paired t-tests. *p<0.05 and **p<0.01.

ontologically and phenotypically distinct (Collin and Bigley, 2018) (Minarrieta et al., 2021).

Enhanced glycolysis is considered essential for the effector function and survival of activated immune cells, including DCs (Krawczyk et al., 2010; Everts et al., 2012). This increase in flux through glycolysis is associated with the high levels of protein and lipid synthesis that are necessary for DC functions such as cytokine secretion and increased cell surface expression of co-stimulatory molecules (Amiel et al., 2014). In line, we found that exposure of CD1c$^+$ mDCs to BCG stimulated increased production of lactate and increased both the basal rate of glycolysis and the glycolytic capacity of human CD1c$^+$ mDCs compared to immature mDCs. In contrast, the glycolytic reserve of BCG-challenged CD1c$^+$ mDCs was similar to that of immature mDCs, suggesting that the highly

glycolytic state induced in CD1c$^+$ mDCs by BCG infection may exhaust their ability to further boost their rate of glycolysis. Although generally considered to play a pro-inflammatory role in DCs, a high glycolytic rate is also observed in tolerogenic mo-DCs, which are resistant to maturation and can inhibit T cell proliferation and cytokine production (Ferreira et al., 2015; Malinarich et al., 2015). BCG vaccination has been shown to induce both protective Th1/Th17 (Boer et al., 2015) and Treg responses in humans (Boer et al., 2015; Keefe et al., 2021). In agreement with a pro-inflammatory role for glycolysis in BCG-challenged DCs, we observed that treatment with 2-DG significantly decreased secretion of IL-1β and TNF-α by CD1c$^+$ mDCs in response to BCG infection. Nonetheless, secretion of the anti-inflammatory cytokine IL-10 was also reduced after inhibition of glycolysis in human CD1c$^+$ mDCs upon infection with BCG, like murine BMDCs stimulated with LPS (Krawczyk et al., 2010). Trafficking of BCG-infected CD11c$^+$ DCs to draining LN is partially dependent on IL-1R signaling (Bollampalli et al., 2015) and both TNFα and IL-1β are crucial to host defence against Mtb infection (Mayer-Barber et al., 2010). IL-10 production, on the other hand, impairs the development of protective Th1/Th17 immune responses following BCG vaccination (Pitt et al., 2012).

Aerobic glycolysis is required to maintain the viability of iNOS-expressing murine DC subsets stimulated with LPS by providing ATP and metabolic intermediates in the face of sustained inhibition of mitochondrial respiration (Krawczyk et al., 2010; Everts et al., 2012; Everts et al., 2014; Thwe and Amiel, 2018). Our data, in contrast, show that the human CD1c$^+$ mDCs population utilizes both pathways 20 hours after stimulation with BCG. This may reflect differences in the response to the stimulus used (LPS *versus* BCG), analogous to murine BMDCs stimulated with "weak" stimuli e.g. house dust mite - where an early increase in the rate of glycolysis is not sustained and does not lead to a concomitant decrease in OXPHOS - compared to "strong" stimuli (LPS, zymosan) which skew metabolism almost exclusively towards aerobic glycolysis (Guak et al., 2018). Basit and colleagues observed that TLR7/8 stimulation of human CD1c$^+$ DCs with single-stranded RNA induces metabolic reprogramming by down-regulating OXPHOS *via* BNIP3-mediated mitophagy and inducing glycolysis to support maturation (Basit et al., 2018), indicating that this DC subset is capable of undergoing a Warburg-like switch to aerobic glycolysis under certain circumstances. Therefore, the more balanced response to BCG may be stimulus-dependent rather than a DC subset-specific response. Interestingly, TLR stimulation with poly(I:C)/R848 did not seem to inhibit OXPHOS either. Maintaining metabolic flexibility *in vivo* where maturing mDCs are competing with other immune cells for finite levels of nutrients could be an advantage (Amiel et al., 2012; Lawless et al., 2017). The bioenergetic requirements of mDCs responding to bacteria may also vary at different stages of maturation, in which case maintaining mitochondrial function could also be necessary to mount an effective immune response. Whether the changes we observed in ECAR and oxygen consumption are a true reflection of metabolic flexibility - whereby individual BCG-challenged cells increase their use of both pathways - or are the net result of heterogeneous metabolic responses of different mDCs is unclear and requires further investigation (discussed below).

BCG-challenged CD1c$^+$ mDCs had increased expression of CD40 compared to unchallenged cells, which was significantly reduced by treatment with 2-DG. CD40 on antigen-presenting cells interacts with CD40L on CD4$^+$ T cells to enhance IL-12 and IFN-γ production (Stuber et al., 1996), although Mtb impairs CD40-mediated induction of protective Th17 responses by DCs both *in vitro* and *in vitro* in mice (Sia et al., 2017). CD40 stimulation of BCG-infected murine BMDCs enhanced their capacity to produce IL-12 and activate a Th1 response (Demangel et al., 2001). In addition, treatment of antigen loaded murine BMDCs with a CD40 agonist before tracheal instillation increased protection against subsequent aerosol challenge with Mtb (Sia et al., 2017), highlighting the important protective role of this co-stimulatory molecule in immunity to Mtb.

Our data also indicated that CD40 expression is regulated differently in CD1c$^+$ mDCs that successfully phagocytosed BCG-GFP (directly infected cells) compared to bystander cells which had been exposed to but had not taken up any bacilli. Both populations of cells upregulated CD40 levels on their cell surface after exposure to BCG but, whereas inhibition of glycolytic flux in the CD1c$^+$ mDCs that had phagocytosed BCG resulted in sustained up-regulation of CD40, it was significantly decreased in GFP$^-$ DCs treated with 2-DG. Bystander cells may have received signals from mycobacterial components released by infected cells (Beatty et al., 2000), through cell surface interaction with extracellular mycobacteria that were not subsequently phagocytosed and/or *via* cytokines or other inflammatory mediators released by infected cells. This may enable bystander cells to bypass pathogen-mediated inhibition of innate immune signaling in the directly infected cell (Holmgren et al., 2017). Indeed, BCG retains immunomodulatory factors like Hip1 that negatively impact DC responses, including CD40 expression, leading to impaired control of Mtb after challenge (Bizzell et al., 2018). Bystander effects have been observed previously in murine DCs infected with BCG: secretion of IL-12p40 was impaired in directly infected splenic CD11c$^+$ DCs from mice expressing a YFP-tagged IL-12p40 gene and bystander DCs were responsible for IL-12p40 secretion (Rothfuchs et al., 2009). Moreover, migratory lung DCs infected with Mtb transfer antigen to bystander DCs in the mediastinal LN to stimulate CD4$^+$ T cell proliferation (Samstein et al., 2013; Srivastava and Ernst, 2014) (Srivastava et al., 2016).

Migration of CD11b$^+$ cDCs from the skin to draining LN is required for induction of adaptive immunity after intradermal injection of BCG in the mouse footpad model (Bollampalli et al., 2015). DC migration from sites of Mtb infection in the lung to the mediastinal LN is also required to initiate an adaptive immune response in murine models of TB (Khader et al., 2006; Wolf et al., 2007; Wolf et al., 2008) and is highly dependent on CCR7 signaling (Olmos et al., 2010). Inhibition of glycolysis by glucose starvation or treatment with 2-DG has previously been shown to constrain the migration of murine BM and splenic DCs *in vitro* to the CCR7 ligand CCL21 by inhibiting oligomerization of CCR7 without altering expression levels of CCR7 (Guak et al., 2018). Guak and

colleagues also found that inhibition of glycolysis impaired LPS- or house dust mite-stimulated DCs migrating to draining LN *in vivo* in sensitized mice (Guak et al., 2018). CCR7 signaling alone can also trigger metabolic reprogramming by increasing HIF1-α-mediated expression of glycolytic genes in murine BMDCs (Liu et al., 2019). In line, we found that expression of CCR7 on immature human CD1c$^+$ mDCs was unchanged by treatment with 2-DG although their migration towards CCL19 was inhibited. Consequently, it was surprising that glycolysis blockade significantly increased cell surface expression of CCR7 on BCG-challenged and poly(I:C)/R848-treated CD1c$^+$ mDCs although it did significantly inhibit migration of BCG-challenged CD1c$^+$ mDCs.

Analogous to CD40 expression, we observed divergent effects of glycolysis inhibition on CCR7-mediated migration of bystander and BCG-infected cells. While CCR7-mediated migration of bystander cells was reduced by 2-DG treatment, BCG-infected cells in the same population displayed higher migratory capacity toward the chemokine stimulus. Since a fixed number of cells were counted and the data was proportional, an increase in infected cells was inevitably accompanied by a decrease in uninfected cells. Therefore 2-DG may have inhibited the migration of bystander cells and/or enhanced the migration of infected cells. Nevertheless, our data clearly show that migration of BCG-infected DCs does not depend on glycolysis - in contrast to that of bystander DCs - and that CCR7 levels are increased on infected cells when glycolytic flux is inhibited. Although immune cell migration is generally thought to be dependent on aerobic glycolysis, there are several reports showing that cell motility can be inhibited by glycolysis or improved by inhibition of glycolytic flux. For example, reduced cell migration has been observed in migratory DCs from UV-irradiated mice, despite higher lactate production and increased glycolytic rates compared to DCs from non-irradiated mice (McGonigle et al., 2017). In addition, murine CD8$^+$ T cells treated with 2-DG *in vitro* also upregulate CCR7 mRNA. Adoptive transfer of these 2-DG-treated CD8$^+$ T cells resulted in their preferential migration to the LN where they adopted a memory phenotype (Sukumar et al., 2013). Treatment with 2-DG is likely to have skewed mDC metabolism towards OXPHOS therefore it is tempting to speculate that BCG-infected DCs require OXPHOS for efficient migration, in contrast to bystander DCs and, at the very least, can migrate when glycolysis is inhibited. In fact, BMDCs infected with influenza virus require mitochondrial respiration for optimal motility despite being predominantly dependent on glycolysis for ATP production (Rezinciuc et al., 2020). Changes in mitochondrial dynamics have also been observed to influence CCR7 expression and migration of immature murine BMDCs (Ryu et al., 2015). Since delayed migration of Mtb-infected migratory DCs impairs the development of adaptive immunity (Wolf et al., 2007; Lai et al., 2018), identifying the mechanisms that regulate CCR7-dependent migration in infectious disease may help to inform the design of new therapeutics and improved vaccines and requires further investigation.

The increase in basal OCR we observed following the addition of glucose to BCG-infected mDCs suggests an increased ability of BCG-challenged cultures to utilize glucose for mitochondrial respiration compared to control mDCs (Pike Winer and Wu, 2014). Conversely, it should also be acknowledged that 2-DG treatment may have inhibited glucose-dependent OXPHOS by reducing pyruvate availability for the TCA cycle. In addition to generating lactate as an end product, engagement of the glycolytic pathway by activated DCs can also channel glucose through both the TCA cycle and the ETC (Pike Winer and Wu, 2014) or *via* a truncated TCA cycle to generate citrate for fatty acid synthesis (FAS) (Moller et al., 2022) enabling expansion of the Golgi and ER membranes required for cytokine secretion and the formation of lipid mediators (Everts et al., 2014) as well as fueling fatty acid oxidation. Increased FAS has been observed in murine DCs infected with BCG and, while not required to control the growth of mycobacteria *in vitro* (Stuve et al., 2018), it may impact other aspects of DC function important for protective immunity. The observed increase in non-glycolytic ECAR in BCG-challenged cultures might also reflect increased oxygen consumption, as CO_2 produced by the TCA cycle can be a source of extracellular acidification *via* the formation of carbonic acid (Mookerjee et al., 2015). However, glycogenolysis can also contribute to ECAR and DCs are known to have intracellular stores of glycogen which can be utilized to fuel glycolysis (Thwe et al., 2017) and which could have contributed to ECAR in the absence of glucose in the medium. In the present study we focused primarily on the role of glycolysis in mDC maturation, but it will be important in the future to assess the contribution of OXPHOS to the ability of these cells to stimulate an effective immune response to mycobacteria.

Taken together, our data indicate that maturation and migration of CD1c$^+$ mDCs in response to BCG does not rely solely on the glycolytic pathway once the cells have phagocytosed the mycobacteria. Importantly, our data indicate that significant differences can occur between BCG-infected versus uninfected bystander DCs in terms of activation marker expression and cell migration, as well as in the regulation of these processes by glycolysis. Most of the limitations of this study arise from the logistical difficulties of performing functional assays with a rare population of primary cells. The Seahorse metabolic flux assays carried out to measure the bioenergetic profile of the DCs were performed, by necessity, on the entire BCG-challenged population of DCs. Therefore, it is possible that the differences we observed in expression of maturation markers and migratory capacity could also reflect metabolic heterogeneity of infected and uninfected populations of DCs, as alluded to above. Due to restricted cell numbers, it was not possible to sort sufficient BCG$^+$ and BCG$^-$ cells to perform separate metabolic flux measurements in our study. Additionally, it has recently become clear that CD1c $^+$ mDC comprise a rather heterogeneous population of cells and that the recently characterized cDC3 subset also expresses CD1c. Based on our sorting strategy which excludes Lin$^+$ cells, and therefore CD14$^+$ DCs, it is likely that our population of CD1c$^+$ mDCs are representative of cDC2 (Segura, 2022) but this will require additional investigation. Further analysis - perhaps using flow cytometry based single cell methods such as SCENITH (Arguello et al., 2020) and/or ssRNAseq to compare metabolism/metabolic gene expression and cell surface markers in the uninfected and infected cell populations - will be required to determine if CD1c$^+$ mDCs metabolism differs between bystander and BCG-infected

cells. Such methods might also allow for comparison of the metabolism of healthy control and HH mDCs in PBMCs, thus avoiding the necessity to isolate pure subset populations from large volumes of blood using stringent sorting protocols. This is important given the association of iron with cellular metabolism (Zhang et al., 2022). Another limitation is that we were unable to carry out extracellular flux analysis of DCs infected with live BCG due to biosafety restrictions in our institution. However, the observed increased in lactate secretion by $CD1c^+$ mDCs infected with live BCG indicate that glycolysis is indeed increased by live as well as killed BCG infection. Similar to our results in DCs with killed BCG, live BCG was shown to increase both OCR and ECAR of human monocytes (Arts et al., 2016) and monocyte-derived macrophages (Cumming et al., 2018). However, it will be important going forward to determine whether there are differences between the effects of live and killed BCG on DC metabolism.

In conclusion, our results identify metabolic pathways in $CD1c^+$ mDCs as potential targets to promote the protective immunity given by the BCG vaccine in tuberculosis infection. However, the disparate effects of glycolysis on bystander and infected $CD1c^+$ mDCs function following exposure to mycobacteria highlight the complexity of this host response. Our data also suggest that there may be differences in the immunometabolic response of host cells to vaccines consisting of whole bacteria versus those composed of bacterial-derived antigens. In addition, this work raises several important questions outside the scope of the current study: i) what is the role of mitochondrial metabolism in DC maturation and migration? ii) what is the basis of the differences in metabolic requirements between bystander and BCG-infected DCs? iii) Is DC glycolysis required to stimulate optimal T cell responses to BCG and thus adaptive immunity against Mtb? Further investigation, including testing of these pathways in animal models of infection, will be needed to evaluate the feasibility of manipulating mDC metabolism to aid rational vaccine design.

Data availability statement

The raw data supporting the conclusions of this article will be made available by the authors, without undue reservation.

Ethics statement

The studies involving human participants were reviewed and approved by St James Hospital and Tallaght University Hospital Joint Research Ethics Committee. The patients/participants provided their written informed consent to participate in this study.

Author contributions

DT and MO'S designed and planned the study. DT, MO'S and KG performed experiments, DT and MO'S analysed the data. MO'S and JK obtained funding. DT wrote the first draft of the manuscript, MO'S and DT wrote sections of the manuscript. All authors contributed to manuscript revision, read, and approved the submitted version.

Funding

This work was supported by the Health Research Board, Ireland (HRA-POR-2013-387) (to MO'S), the Faculty of Health Science, Trinity College Dublin, Dean's Research Initiative Fund (to MO'S), and The Royal City of Dublin Hospital Trust (to JK).

Acknowledgments

We thank Dr Suzanne Norris, Ms Jona Yusingco and patients from the Hemochromatosis Clinic in St James's Hospital, Dublin for providing access to blood samples, Dr Eamon Breen from the Flow Cytometry Facility in the Trinity Translational Medicine Institute for sorting the cells and for assistance with flow cytometry and Dr Gavin McManus of the School of Biochemistry and Immunology Microscopy Facility for assistance with confocal microscopy. Parts of this manuscript were presented as a poster at the American Thoracic Society 2019 International Conference (O'Sullivan et al., 2019).

Conflict of interest

The authors declare that the research was conducted in the absence of any commercial or financial relationships that could be construed as a potential conflict of interest.

Publisher's note

Supplementary material

The Supplementary Material for this article can be found online at: https://www.frontiersin.org/articles/10.3389/fcimb.2023.1113744/full#supplementary-material

References

Amiel, E., Everts, B., Freitas, T. C., King, I. L., Curtis, J. D., Pearce, E. L., et al. (2012). Inhibition of mechanistic target of rapamycin promotes dendritic cell activation and enhances therapeutic autologous vaccination in mice. *J. Immunol.* 189, 2151–2158. doi: 10.4049/jimmunol.1103741

Amiel, E., Everts, B., Fritz, D., Beauchamp, S., Ge, B., Pearce, E. L., et al. (2014). Mechanistic target of rapamycin inhibition extends cellular lifespan in dendritic cells by preserving mitochondrial function. *J. Immunol.* 193, 2821–2830. doi: 10.4049/jimmunol.1302498

Arguello, R. J., Combes, A. J., Char, R., Gigan, J. P., Baaziz, A. I. , Bousiquot, E., et al. (2020). SCENITH: a flow cytometry-based method to functionally profile energy metabolism with single-cell resolution. *Cell Metab.* 32, 1063-1075 e1067. doi: 10.1016/j.cmet.2020.11.007

Arts, R. J. W., Carvalho, A., La Rocca, C., Palma, C., Rodrigues, F., Silvestre, R., et al. (2016). Immunometabolic pathways in BCG-induced trained immunity. *Cell Rep.* 17, 2562–2571. doi: 10.1016/j.celrep.2016.11.011

Basit, F., Mathan, T., Sancho, D., and De Vries, I. J. M. (2018). Human dendritic cell subsets undergo distinct metabolic reprogramming for immune response. *Front. Immunol.* 9, 2489. doi: 10.3389/fimmu.2018.02489

Beatty, W. L., Rhoades, E. R., Ullrich, H. J., Chatterjee, D., Heuser, J. E., and Russell, D. G. (2000). Trafficking and release of mycobacterial lipids from infected macrophages. *Traffic* 1, 235–247. doi: 10.1034/j.1600-0854.2000.010306.x

Bizzell, E., Sia, J. K., Quezada, M., Enriquez, A., Georgieva, M., and Rengarajan, J. (2018). Deletion of BCG Hip1 protease enhances dendritic cell and CD4 T cell responses. *J. Leukoc. Biol.* 103, 739–748. doi: 10.1002/JLB.4A0917-363RR

Boer, M. C., Prins, C., Van Meijgaarden, K. E., Van Dissel, J. T., Ottenhoff, T. H., and Joosten, S. A. (2015). Mycobacterium bovis BCG vaccination induces divergent proinflammatory or regulatory T cell responses in adults. *Clin. Vaccine Immunol.* 22, 778–788. doi: 10.1128/CVI.00162-15

Bollampalli, V. P., Harumi Yamashiro, L., Feng, X., Bierschenk, D., Gao, Y., Blom, H., et al. (2015). BCG Skin infection triggers IL-1R-MyD88-Dependent migration of EpCAMlow CD11bhigh skin dendritic cells to draining lymph node during CD4+ T-cell priming. *PloS Pathog.* 11, e1005206. doi: 10.1371/journal.ppat.1005206

Collin, M., and Bigley, V. (2018). Human dendritic cell subsets: an update. *Immunology* 154, 3–20. doi: 10.1111/imm.12888

Cumming, B. M., Addicott, K. W., Adamson, J. H., and Steyn, A. J. (2018). Mycobacterium tuberculosis induces decelerated bioenergetic metabolism in human macrophages. *Elife* 7, e39169. doi: 10.7554/eLife.39169.018

Demangel, C., Palendira, U., Feng, C. G., Bean, A. G., and Britton, W. J. (2001). Stimulation of dendritic cells via CD40 enhances immune responses to Mycobacterium tuberculosis infection. *Infect Immun* 69, 2456–2461.

Dzionek, A., Fuchs, A., Schmidt, P., Cremer, S., Zysk, M., Miltenyi, S., et al. (2000). BDCA-2, BDCA-3, and BDCA-4: three markers for distinct subsets of dendritic cells in human peripheral blood. *J. Immunol.* 165, 6037–6046. doi: 10.4049/jimmunol.165.11.6037

Everts, B., Amiel, E., Huang, S. C., Smith, A. M., Chang, C. H., Lam, W. Y., et al. (2014). TLR-driven early glycolytic reprogramming *via* the kinases TBK1-IKKvarepsilon supports the anabolic demands of dendritic cell activation. *Nat. Immunol.* 15, 323–332. doi: 10.1038/ni.2833

Everts, B., Amiel, E., van der Windt, G. J., Freitas, T. C., Chott, R., Yarasheski, K. E., et al. (2012). Commitment to glycolysis sustains survival of NO-producing inflammatory dendritic cells. *Blood* 120, 1422–1431. doi: 10.1182/blood-2012-03-419747

Ferreira, G. B., Vanherwegen, A. S., Eelen, G., Gutierrez, A. C. F., Van Lommel, L., Marchal, K., et al. (2015). Vitamin D3 induces tolerance in human dendritic cells by activation of intracellular metabolic pathways. *Cell Rep.* 10, 711–725. doi: 10.1016/j.celrep.2015.01.013

Giamarellos-Bourboulis, E. J., Tsilika, M., Moorlag, S., Antonakos, N., Kotsaki, A., Dominguez-Andres, J., et al. (2020). Activate: randomized clinical trial of BCG vaccination against infection in the elderly. *Cell* 183, 315-323. doi: 10.1016/j.cell.2020.08.051

Gleeson, L. E., Sheedy, F. J., Palsson-Mcdermott, E. M., Triglia, D., O'leary, S. M., O'sullivan, M. P., et al. (2016). Cutting edge: mycobacterium tuberculosis induces aerobic glycolysis in human alveolar macrophages that is required for control of intracellular bacillary replication. *J. Immunol.* 196, 2444–2449. doi: 10.4049/jimmunol.1501612

Gonzalez-Juarrero, M., Turner, J., Basaraba, R. J., Belisle, J. T., and Orme, I. M. (2002). Florid pulmonary inflammatory responses in mice vaccinated with antigen-85 pulsed dendritic cells and challenged by aerosol with mycobacterium tuberculosis. *Cell Immunol.* 220, 13–19. doi: 10.1016/S0008-8749(03)00010-8

Griffiths, K. L., Ahmed, M., Das, S., Gopal, R., Horne, W., Connell, T. D., et al. (2016). Targeting dendritic cells to accelerate T-cell activation overcomes a bottleneck in tuberculosis vaccine efficacy. *Nat. Commun.* 7, 13894. doi: 10.1038/ncomms13894

Guak, H., Al Habyan, S., Ma, E. H., Aldossary, H., Al-Masri, M., Won, S. Y., et al. (2018). Glycolytic metabolism is essential for CCR7 oligomerization and dendritic cell migration. *Nat. Commun.* 9, 2463. doi: 10.1038/s41467-018-04804-6

Higgins, J. P., Soares-Weiser, K., Lopez-Lopez, J. A., Kakourou, A., Chaplin, K., Christensen, H., et al. (2016). Association of BCG, DTP, and measles containing vaccines with childhood mortality: systematic review. *BMJ* 355, i5170. doi: 10.1136/bmj.i5170

Holmgren, A. M., Mcconkey, C. A., and Shin, S. (2017). Outrunning the red queen: bystander activation as a means of outpacing innate immune subversion by intracellular pathogens. *Cell Mol. Immunol.* 14, 14–21. doi: 10.1038/cmi.2016.36

Hou, W. S., and Van Parijs, L. (2004). A bcl-2-dependent molecular timer regulates the lifespan and immunogenicity of dendritic cells. *Nat. Immunol.* 5, 583–589. doi: 10.1038/ni1071

Jantsch, J., Chakravortty, D., Turza, N., Prechtel, A. T., Buchholz, B., Gerlach, R. G., et al. (2008). Hypoxia and hypoxia-inducible factor-1 alpha modulate lipopolysaccharide-induced dendritic cell activation and function. *J. Immunol.* 180, 4697–4705. doi: 10.4049/jimmunol.180.7.4697

Keefe, R. C., Takahashi, H., Tran, L., Nelson, K., Ng, N., Kuhtreiber, W. M., et al. (2021). BCG Therapy is associated with long-term, durable induction of treg signature genes by epigenetic modulation. *Sci. Rep.* 11, 14933. doi: 10.1038/s41598-021-94529-2

Khader, S. A., Partida-Sanchez, S., Bell, G., Jelley-Gibbs, D. M., Swain, S., Pearl, J. E., et al. (2006). Interleukin 12p40 is required for dendritic cell migration and T cell priming after mycobacterium tuberculosis infection. *J. Exp. Med.* 203, 1805–1815. doi: 10.1084/jem.20052545

Kleinnijenhuis, J., Quintin, J., Preijers, F., Benn, C. S., Joosten, L., Jacobs, C., et al. (2014). Long-lasting effects of BCG vaccination on both heterologous Th1/Th17 responses and innate trained immunity. *J. Innate Immun.* 6, 152–158. doi: 10.1159/000355628

Krawczyk, C. M., Holowka, T., Sun, J., Blagih, J., Amiel, E., Deberardinis, R. J., et al. (2010). Toll-like receptor-induced changes in glycolytic metabolism regulate dendritic cell activation. *Blood* 115, 4742–4749. doi: 10.1182/blood-2009-10-249540

Krmeska, V., Aggio, J. B., Nylen, S., Wowk, P. F., and Rothfuchs, A. G. (2022). Cyclooxygenase-derived prostaglandin E(2) drives IL-1-Independent mycobacterium bovis bacille calmette-Guerin-Triggered skin dendritic cell migration to draining lymph node. *J. Immunol.* 208, 2549–2557. doi: 10.4049/jimmunol.2100981

Kuhtreiber, W. M., Tran, L., Kim, T., Dybala, M., Nguyen, B., Plager, S., et al. (2018). Long-term reduction in hyperglycemia in advanced type 1 diabetes: the value of induced aerobic glycolysis with BCG vaccinations. *NPJ Vaccines* 3, 23. doi: 10.1038/s41541-018-0062-8

Lai, R., Jeyanathan, M., Afkhami, S., Zganiacz, A., Hammill, J. A., Yao, Y., et al. (2018). CD11b(+) dendritic cell-mediated anti-mycobacterium tuberculosis Th1 activation is counterregulated by CD103(+) dendritic cells *via* IL-10. *J. Immunol.* 200, 1746–1760. doi: 10.4049/jimmunol.1701109

Lamm, D. L. (1985). Bacillus calmette-guerin immunotherapy for bladder cancer. *J. Urol* 134, 40–47. doi: 10.1016/S0022-5347(17)46972-2

Lawless, S. J., Kedia-Mehta, N., Walls, J. F., Mcgarrigle, R., Convery, O., Sinclair, L. V., et al. (2017). Glucose represses dendritic cell-induced T cell responses. *Nat. Commun.* 8, 15620. doi: 10.1038/ncomms15620

Liu, J., Zhang, X., Chen, K., Cheng, Y., Liu, S., Xia, M., et al. (2019). CCR7 chemokine receptor-inducible lnc-Dpf3 restrains dendritic cell migration by inhibiting HIF-1alpha-Mediated glycolysis. *Immunity* 50, 600–615 e615. doi: 10.1016/j.immuni.2019.01.021

Loxton, A. G., Knaul, J. K., Grode, L., Gutschmidt, A., Meller, C., Eisele, B., et al. (2017). Safety and immunogenicity of the recombinant mycobacterium bovis BCG vaccine VPM1002 in HIV-unexposed newborn infants in south Africa. *Clin. Vaccine Immunol.* 24, e00439-16. doi: 10.1128/CVI.00439-16

Lozza, L., Farinacci, M., Fae, K., Bechtle, M., Staber, M., Dorhoi, A., et al. (2014). Crosstalk between human DC subsets promotes antibacterial activity and CD8(+) T-cell stimulation in response to bacille calmette-guerin. *Eur. J. Immunol.* 44, 80–92. doi: 10.1002/eji.201343797

Malinarich, F., Duan, K., Hamid, R. A., Bijin, A., Lin, W. X., Poidinger, M., et al. (2015). High mitochondrial respiration and glycolytic capacity represent a metabolic phenotype of human tolerogenic dendritic cells. *J. Immunol.* 194, 5174–5186. doi: 10.4049/jimmunol.1303316

Marino, S., Pawar, S., Fuller, C. L., Reinhart, T. A., Flynn, J. L., and Kirschner, D. E. (2004). Dendritic cell trafficking and antigen presentation in the human immune response to mycobacterium tuberculosis. *J. Immunol.* 173, 494–506. doi: 10.4049/jimmunol.173.1.494

Mayer-Barber, K. D., Barber, D. L., Shenderov, K., White, S. D., Wilson, M. S., Cheever, A., et al. (2010). Caspase-1 independent IL-1beta production is critical for host resistance to mycobacterium tuberculosis and does not require TLR signaling *in vivo*. *J. Immunol.* 184, 3326–3330. doi: 10.4049/jimmunol.0904189

McGonigle, T. A., Keane, K. N., Ghaly, S., Carter, K. W., Anderson, D., Scott, N. M., et al. (2017). UV Irradiation of skin enhances glycolytic flux and reduces migration capabilities in bone marrow-differentiated dendritic cells. *Am. J. Pathol.* 187, 2046–2059. doi: 10.1016/j.ajpath.2017.06.003

McShane, H., Behboudi, S., Goonetilleke, N., Brookes, R., and Hill, A. V. (2002). Protective immunity against mycobacterium tuberculosis induced by dendritic cells

pulsed with both CD8(+)- and CD4(+)-t-cell epitopes from antigen 85A. *Infect. Immun.* 70, 1623–1626. doi: 10.1128/IAI.70.3.1623-1626.2002

Minarrieta, L., Velasquez, L. N., Sparwasser, T., and Berod, L. (2021). Dendritic cell metabolism: moving beyond *in vitro*-culture-generated paradigms. *Curr. Opin. Biotechnol.* 68, 202–212. doi: 10.1016/j.copbio.2020.12.010

Moliva, J. I., Turner, J., and Torrelles, J. B. (2017). Immune responses to bacillus calmette–guérin vaccination: why do they fail to protect against mycobacterium tuberculosis? *Front. Immunol.* 8. doi: 10.3389/fimmu.2017.00407

Moller, S. H., Wang, L., and Ho, P. C. (2022). Metabolic programming in dendritic cells tailors immune responses and homeostasis. *Cell Mol. Immunol.* 19, 370–383. doi: 10.1038/s41423-021-00753-1

Mookerjee, S. A., Goncalves, R. L. S., Gerencser, A. A., Nicholls, D. G., and Brand, M. D. (2015). The contributions of respiration and glycolysis to extracellular acid production. *Biochim. Biophys. Acta* 1847, 171–181. doi: 10.1016/j.bbabio.2014.10.005

Nemes, E., Geldenhuys, H., Rozot, V., Rutkowski, K. T., Ratangee, F., Bilek, N., et al. (2018). Prevention of m. tuberculosis infection with H4:IC31 vaccine or BCG revaccination. *N Engl. J. Med.* 379, 138–149. doi: 10.1056/NEJMoa1714021

Nieuwenhuizen, N. E., and Kaufmann, S. H. E. (2018). Next-generation vaccines based on bacille calmette-guerin. *Front. Immunol.* 9, 121. doi: 10.3389/fimmu.2018.00121

Nopora, A., and Brocker, T. (2002). Bcl-2 controls dendritic cell longevity *in vivo*. *J. Immunol.* 169, 3006–3014. doi: 10.4049/jimmunol.169.6.3006

Olmos, S., Stukes, S., and Ernst, J. D. (2010). Ectopic activation of mycobacterium tuberculosis-specific CD4+ T cells in lungs of CCR7-/- mice. *J. Immunol.* 184, 895–901. doi: 10.4049/jimmunol.0901230

O'Sullivan, M., Triglia Van Nierop, D., Gogan, K., and Keane, J. (2019). Immunometabolism directs human CD1c-positive myeloid dendritic cell responses to BCG infection. *Am. J. Respir. Crit. Care Med.* 199, A4237–A4237. doi: 10.1164/ajrccm-conference.2019.199.1_MeetingAbstracts.A4237

Phothirath, P., Duperrier, K., Bernaud, J., Durieu, D., Picollet, J., Bienvenu, J., et al. (2002). Generation of monocyte-derived dendritic cells in patients with hereditary hemochromatosis. *Clin. Immunol.* 105, 93–103. doi: 10.1006/clim.2002.5276

Pike Winer, L. S., and Wu, M. (2014). Rapid analysis of glycolytic and oxidative substrate flux of cancer cells in a microplate. *PloS One* 9, e109916. doi: 10.1371/journal.pone.0109916

Pitt, J. M., Stavropoulos, E., Redford, P. S., Beebe, A. M., Bancroft, G. J., Young, D. B., et al. (2012). Blockade of IL-10 signaling during bacillus calmette-guerin vaccination enhances and sustains Th1, Th17, and innate lymphoid IFN-gamma and IL-17 responses and increases protection to mycobacterium tuberculosis infection. *J. Immunol.* 189, 4079–4087. doi: 10.4049/jimmunol.1201061

Rajashree, P., Supriya, P., and Das, S. D. (2008). Differential migration of human monocyte-derived dendritic cells after infection with prevalent clinical strains of mycobacterium tuberculosis. *Immunobiology* 213, 567–575. doi: 10.1016/j.imbio.2008.01.007

Reiley, W. W., Calayag, M. D., Wittmer, S. T., Huntington, J. L., Pearl, J. E., Fountain, J. J., et al. (2008). ESAT-6-specific CD4 T cell responses to aerosol mycobacterium tuberculosis infection are initiated in the mediastinal lymph nodes. *Proc. Natl. Acad. Sci. U.S.A.* 105, 10961–10966. doi: 10.1073/pnas.0801496105

Rezinciuc, S., Bezavada, L., Bahadoran, A., Duan, S., Wang, R., Lopez-Ferrer, D., et al. (2020). Dynamic metabolic reprogramming in dendritic cells: an early response to influenza infection that is essential for effector function. *PloS Pathog.* 16, e1008957. doi: 10.1371/journal.ppat.1008957

Ristori, G., Romano, S., Cannoni, S., Visconti, A., Tinelli, E., Mendozzi, L., et al. (2014). Effects of bacille calmette-guerin after the first demyelinating event in the CNS. *Neurology* 82, 41–48. doi: 10.1212/01.wnl.0000438216.93319.ab

Roberts, L. L., and Robinson, C. M. (2014). Mycobacterium tuberculosis infection of human dendritic cells decreases integrin expression, adhesion and migration to chemokines. *Immunology* 141, 39–51. doi: 10.1111/imm.12164

Rodrigues, L. C., Diwan, V. K., and Wheeler, J. G. (1993). Protective effect of BCG against tuberculous meningitis and miliary tuberculosis: a meta-analysis. *Int. J. Epidemiol.* 22, 1154–1158. doi: 10.1093/ije/22.6.1154

Rothfuchs, A. G., Egen, J. G., Feng, C. G., Antonelli, L. R., Bafica, A., Winter, N., et al. (2009). *In situ* IL-12/23p40 production during mycobacterial infection is sustained by CD11bhigh dendritic cells localized in tissue sites distinct from those harboring bacilli. *J. Immunol.* 182, 6915–6925. doi: 10.4049/jimmunol.0900074

Ryu, S. W., Han, E. C., Yoon, J., and Choi, C. (2015). The mitochondrial fusion-related proteins Mfn2 and OPA1 are transcriptionally induced during differentiation of bone marrow progenitors to immature dendritic cells. *Mol. Cells* 38, 89–94. doi: 10.14348/molcells.2015.2285

Samstein, M., Schreiber, H. A., Leiner, I. M., Susac, B., Glickman, M. S., and Pamer, E. G. (2013). Essential yet limited role for CCR2(+) inflammatory monocytes during mycobacterium tuberculosis-specific T cell priming. *Elife* 2, e01086. doi: 10.7554/eLife.01086.013

Segura, E. (2022). Human dendritic cell subsets: an updated view of their ontogeny and functional specialization. *Eur. J. Immunol.* 52, 1759–1767. doi: 10.1002/eji.202149632

Setia, M. S., Steinmaus, C., Ho, C. S., and Rutherford, G. W. (2006). The role of BCG in prevention of leprosy: a meta-analysis. *Lancet Infect. Dis.* 6, 162–170. doi: 10.1016/S1473-3099(06)70412-1

Sia, J. K., Bizzell, E., Madan-Lala, R., and Rengarajan, J. (2017). Engaging the CD40-CD40L pathway augments T-helper cell responses and improves control of mycobacterium tuberculosis infection. *PloS Pathog.* 13, e1006530. doi: 10.1371/journal.ppat.1006530

Srivastava, S., and Ernst, J. D. (2014). Cell-to-cell transfer of m. tuberculosis antigens optimizes CD4 T cell priming. *Cell Host Microbe* 15, 741–752. doi: 10.1016/j.chom.2014.05.007

Srivastava, S., Grace, P. S., and Ernst, J. D. (2016). Antigen export reduces antigen presentation and limits T cell control of m. tuberculosis. *Cell Host Microbe* 19, 44–54. doi: 10.1016/j.chom.2015.12.003

Stuber, E., Strober, W., and Neurath, M. (1996). Blocking the CD40L-CD40 interaction *in vivo* specifically prevents the priming of T helper 1 cells through the inhibition of interleukin 12 secretion. *J. Exp. Med.* 183, 693–698. doi: 10.1084/jem.183.2.693

Stuve, P., Minarrieta, L., Erdmann, H., Arnold-Schrauf, C., Swallow, M., Guderian, M., et al. (2018). *De novo* fatty acid synthesis during mycobacterial infection is a prerequisite for the function of highly proliferative T cells, but not for dendritic cells or macrophages. *Front. Immunol.* 9, 495. doi: 10.3389/fimmu.2018.00495

Sukumar, M., Liu, J., Ji, Y., Subramanian, M., Crompton, J. G., Yu, Z., et al. (2013). Inhibiting glycolytic metabolism enhances CD8+ T cell memory and antitumor function. *J. Clin. Invest.* 123, 4479–4488. doi: 10.1172/JCI69589

Thwe, P. M., and Amiel, E. (2018). The role of nitric oxide in metabolic regulation of dendritic cell immune function. *Cancer Lett.* 412, 236–242. doi: 10.1016/j.canlet.2017.10.032

Thwe, P. M., Pelgrom, L. R., Cooper, R., Beauchamp, S., Reisz, J. A., D'alessandro, A., et al. (2017). Cell-intrinsic glycogen metabolism supports early glycolytic reprogramming required for dendritic cell immune responses. *Cell Metab.* 26, 558–567 e555. doi: 10.1016/j.cmet.2017.08.012

Trunz, B. B., Fine, P., and Dye, C. (2006). Effect of BCG vaccination on childhood tuberculous meningitis and miliary tuberculosis worldwide: a meta-analysis and assessment of cost-effectiveness. *Lancet* 367, 1173–1180. doi: 10.1016/S0140-6736(06)68507-3

Van Der Meeren, O., Hatherill, M., Nduba, V., Wilkinson, R. J., Muyoyeta, M., Van Brakel, E., et al. (2018). Phase 2b controlled trial of M72/AS01E vaccine to prevent tuberculosis. *N Engl. J. Med.* 379, 1621–1634. doi: 10.1056/NEJMoa1803484

Velasquez, L. N., Stuve, P., Gentilini, M. V., Swallow, M., Bartel, J., Lycke, N. Y., et al. (2018). Targeting mycobacterium tuberculosis antigens to dendritic cells *via* the DC-Specific-ICAM3-Grabbing-Nonintegrin receptor induces strong T-helper 1 immune responses. *Front. Immunol.* 9, 471. doi: 10.3389/fimmu.2018.00471

Wang, J. C., Kobie, J. J., Zhang, L., Cochran, M., Mosmann, T. R., Ritchlin, C. T., et al. (2009). An 11-color flow cytometric assay for identifying, phenotyping, and assessing endocytic ability of peripheral blood dendritic cell subsets in a single platform. *J. Immunol. Methods* 341, 106–116. doi: 10.1016/j.jim.2008.11.002

WHO (2008). *Implementing the WHO stop TB strategy: a handbook for national tuberculosis control programmes* (Geneva: World Health Organization).

WHO (2021). *Global tuberculosis report* (Geneva: World Health Organization).

Wolf, A. J., Desvignes, L., Linas, B., Banaiee, N., Tamura, T., Takatsu, K., et al. (2008). Initiation of the adaptive immune response to mycobacterium tuberculosis depends on antigen production in the local lymph node, not the lungs. *J. Exp. Med.* 205, 105–115. doi: 10.1084/jem.20071367

Wolf, A. J., Linas, B., Trevejo-Nunez, G. J., Kincaid, E., Tamura, T., Takatsu, K., et al. (2007). Mycobacterium tuberculosis infects dendritic cells with high frequency and impairs their function *in vivo*. *J. Immunol.* 179, 2509–2519. doi: 10.4049/jimmunol.179.4.2509

Zhang, S., Xin, W., Anderson, G. J., Li, R., Gao, L., Chen, S., et al. (2022). Double-edge sword roles of iron in driving energy production versus instigating ferroptosis. *Cell Death Dis.* 13, 40. doi: 10.1038/s41419-021-04490-1

Zimmermann, P., Finn, A., and Curtis, N. (2018). Does BCG vaccination protect against nontuberculous mycobacterial infection? a systematic review and meta-analysis. *J. Infect. Dis.* 218, 679–687. doi: 10.1093/infdis/jiy207

frontiers | Frontiers in Cellular and Infection Microbiology

TYPE Original Research
PUBLISHED 14 August 2023
DOI 10.3389/fcimb.2023.1163993

OPEN ACCESS

EDITED BY
Veronica Edith Garcia,
Universidad de Buenos Aires, Argentina

REVIEWED BY
Suzie Hingley-Wilson,
University of Surrey, United Kingdom
Margarida Saraiva,
Universidade do Porto, Portugal

*CORRESPONDENCE
Dorothy Yeboah-Manu
dyeboah-manu@noguchi.ug.edu.gh

†These authors have contributed equally to this work

RECEIVED 11 February 2023
ACCEPTED 24 July 2023
PUBLISHED 14 August 2023

CITATION
Osei-Wusu S, Tetteh JKA, Musah AB, Ntiamoah DO, Arthur N, Adjei A, Arbues A, Ofori EA, Mensah KA, Galevo SEA, Frempong AF, Asare P, Asante-Poku A, Otchere ID, Kusi KA, Lenz TL, Gagneux S, Portevin D and Yeboah-Manu D (2023) Macrophage susceptibility to infection by Ghanaian *Mycobacterium tuberculosis* complex lineages 4 and 5 varies with self-reported ethnicity. *Front. Cell. Infect. Microbiol.* 13:1163993. doi: 10.3389/fcimb.2023.1163993

Macrophage susceptibility to infection by Ghanaian *Mycobacterium tuberculosis* complex lineages 4 and 5 varies with self-reported ethnicity

Stephen Osei-Wusu[1,2], John K. A. Tetteh[1], Abdul Basit Musah[1], Desmond Opoku Ntiamoah[1], Nelly Arthur[3], Abraham Adjei[3], Ainhoa Arbues[4,5], Ebenezer Addo Ofori[1], Kwadwo Akyea Mensah[1], Sutaya Elsie Afua Galevo[1], Abena Frema Frempong[1], Prince Asare[1], Adwoa Asante-Poku[1], Isaac Darko Otchere[1], Kwadwo Asamoah Kusi[1], Tobias L. Lenz[6], Sebastien Gagneux[4,5], Damien Portevin[4,5†] and Dorothy Yeboah-Manu[1*†]

[1]Noguchi Memorial Institute for Medical Research, University of Ghana, Legon, Ghana, [2]West African Centre for Cell Biology of Infectious Pathogens (WACCBIP), University of Ghana, Legon, Ghana, [3]Department of Chest Diseases, Korle-Bu Teaching Hospital, Accra, Ghana, [4]Swiss Tropical and Public Health Institute, Allschwil, Switzerland, [5]University of Basel, Basel, Switzerland, [6]Research Group for Evolutionary Immunogenomics, Department of Biology, University of Hamburg, Hamburg, Germany

Background: The epidemiology of *Mycobacterium tuberculosis* complex (MTBC) lineage 5 (L5) infections in Ghana revealed a significantly increased prevalence in Ewes compared to other self-reported ethnic groups. In that context, we sought to investigate the early phase of tuberculosis (TB) infection using *ex vivo* infection of macrophages derived from the blood of Ewe and Akan ethnic group volunteers with MTBC L4 and L5 strains.

Methods: The study participants consisted of 16 controls, among which self-reported Akan and Ewe ethnicity was equally represented, as well as 20 cured TB cases consisting of 11 Akans and 9 Ewes. Peripheral blood mononuclear cells were isolated from both healthy controls and cured TB cases. $CD14^+$ monocytes were isolated and differentiated into monocyte-derived macrophages (MDMs) before infection with L4 or L5 endemic strains. The bacterial load was assessed after 2 hours (uptake) as well as 3 and 7 days post-infection.

Results: We observed a higher capacity of MDMs from Ewes to phagocytose L4 strains ($p < 0.001$), translating into a higher bacillary load on day 7 ($p < 0.001$) compared to L5, despite the higher replication rate of L5 in Ewe MDMs (fold change: 1.4 *vs.* 1.2, $p = 0.03$) among the controls. On the contrary, within macrophages from Akans, we observed a significantly higher phagocytic uptake of L5 ($p < 0.001$) compared to L4, also translating into a higher load on day 7 ($p = 0.04$). However, the replication rate of L4 in Akan MDMs was higher than that of L5 (fold change: L4 = 1.2, L4 = 1.1, $p = 0.04$). Although there was no

significant difference in the uptake of L4 and L5 among cured TB cases, there was a higher bacterial load of both L4 (p = 0.02) and L5 (p = 0.02) on day 7 in Ewe MDMs.

Conclusion: Our results suggest that host ethnicity (driven by host genetic diversity), MTBC genetic diversity, and individual TB infection history are all acting together to modulate the outcome of macrophage infections by MTBC.

KEYWORDS

macrophage infection, Ghana, West Africa, tuberculosis, Ewe, Akan, ethnicity, *Mycobacterium tuberculosis* complex

1 Introduction

Tuberculosis (TB) remains a global health challenge irrespective of the control measures and the advances made since the World Health Organization (WHO) declared TB a global health emergency in 1993 (WHO, 2021). TB has been the leading cause of death from a single infectious agent worldwide until the recent mortality associated with the SARS-CoV-2 pandemic in 2019 (WHO, 1994; WHO, 2021). It is estimated that approximately 10.6 million people fell ill with TB and 1.6 million died from the disease in 2021. The TB epidemic in Ghana reported an incidence of 136 per 100,000 in 2021 (WHO, 2022).

TB is caused by *Mycobacterium tuberculosis* complex (MTBC), which comprises 11 closely related species, some of which transmit preferentially within specific host genetic groups, while others have spread globally (Gagneux and Small, 2007; Stucki et al., 2016). Phylogenetic analysis of the major human-adapted MTBC (hMTBC) species classifies them into seven lineages (L1–7). Nonetheless, two additional lineages, L8 and L9, were recently discovered and mostly sporadically isolated in East Africa (NGabonziza et al., 2020; Coscolla et al., 2021). Phylogeographic distribution analysis revealed that lineage 4 in particular is globally distributed whereas other hMTBC lineages are mostly restricted to specific geographic areas (Comas et al., 2013; Stucki et al., 2016). TB epidemiology in Ghana is relatively unique for hosting six out of the nine known hMTBC lineages (de Jong et al., 2010b; Asante-Poku et al., 2016; Yeboah-Manu et al., 2016). Nevertheless, hMTBC lineages 5 and 6 remained restricted to West Africa for reasons not well understood. L5 and L6 MTBC strains constitute important human pathogens in West Africa, causing approximately 40% of TB cases in the region and approximately 20% of all TB cases in Ghana (de Jong et al., 2010b; Yeboah-Manu et al., 2016). Studies have reported a specific association of L5 infections with the Ewe ethnic group and L6 with HIV patients (de Jong et al., 2005; Asante-Poku et al., 2015; Asante-Poku et al., 2016). While a lower virulence of L6 isolates could support the reported association with HIV infection, the underlying reasons behind the association of L5 infection with specific ethnic groups remain puzzling and unresolved (de Jong et al., 2010a; Brites and Gagneux, 2015). A better understanding of this phenomenon would enlighten us on the underlying reasons driving the specific phylogeographic distribution of MTBC lineages in West Africa and may also support improved control strategies of L5 infections in particular.

MTBC is a successful pathogen due to its ability to invade and replicate within host cells in the lungs. It is transmitted following inhalation of infectious droplets from an infected person by an uninfected person (Sia and Rengarajan, 2019). Transmission may therefore occur through coughing, sneezing, or even talking and singing (Sia and Rengarajan, 2019). Upon inhalation, MTBC bacilli might interact with throat epithelial cells that aid their migration through the trachea to the alveoli (Fernández Tena and Casan Clarà, 2012; Torrelles and Schlesinger, 2017). Within the lung alveoli, bacilli are phagocytosed by alveolar macrophages that migrate to the parenchyma and generate an inflammatory response, leading to the chemotactic attraction of other immune cells and the generation of granulomas, multicellular structures encapsulating the infectious bacilli (Scriba et al., 2017).

The presence of MTBC in the alveoli leads to different outcomes: 1) bacilli may be directly eliminated by innate immune responses before the onset of adaptive immunity and memory of exposure, 2) MTBC infections are controlled and walled off within granulomatous responses potentially leading to latent infections, or 3) immunity is unable to control MTBC replication, and active TB disease ensues (Scriba et al., 2017; Sia and Rengarajan, 2019). These different outcomes depend on intricate host–pathogen interactions. While MTBC's genetic background may influence its pathogenicity, the host-specific immune response also plays an important role in the outcome of the disease (Gagneux et al., 2006; Coscolla and Gagneux, 2010; Gagneux, 2012). Macrophages are at the forefront of the battle against MTBC bacilli invading the lung (Scriba et al., 2017). Macrophages are not only phagocytic cells, but they can also regulate important cellular processes such as tissue homeostasis, repair, and wound healing (Wynn and Vannella, 2016; Sreejit et al., 2020). Hence, the role of macrophages is central to the pathogenesis of a variety of infectious and non-infectious inflammatory diseases.

Previous research has shown the impact of ethnicity, gender, and nutrition on innate immune cell function including macrophages (Nahid et al., 2018). In conjunction with MTBC genetic factors associated with inflammatory responses of macrophages (Portevin et al., 2011), heterogeneity in macrophage

functions that are genetically encoded may have been evolutionarily selected to influence TB disease outcome (Fan et al., 2023). We hypothesized that the association of L5 infections with the Ewe ethnic group and L4 with the Akan ethnic group may be supported by inherent variation in macrophage responses to different MTBC lineages. Therefore, the study was designed to characterize the early phase of L4 and L5 infections of macrophages derived from the blood of volunteers belonging to the self-reported Ewe or Akan ethnic group.

2 Materials and methods

2.1 Ethical consideration

Ethical clearance was obtained from the Institutional Review Boards (IRB) of Korle-Bu Teaching Hospital (KBTH) and Noguchi Memorial Institute for Medical Research (NMIMR), University of Ghana (Federal wide assurance number: FWA00001824). The study protocol was explained to all participants, and written informed consent was obtained from participants voluntarily. A questionnaire was then administered to the participants to obtain their demographic data.

2.2 Study design

This case–control study resulted from the prospective collection of blood samples between January 2020 and September 2020 and a retrospective inclusion of MTBC isolates characterized previously (Yeboah-Manu et al., 2016; Asare et al., 2018). The study was conducted at the Department of Chest Diseases of the Korle-Bu Teaching Hospital, and the Departments of Bacteriology and Immunology of NMIMR, University of Ghana.

2.3 Inclusion and exclusion criteria

Participants belonging to either the Akan or Ewe ethnic group who had successfully completed treatment of TB caused by MTBC L4 or L5 and confirmed to be without an active TB infection were recruited as cured TB case participants. The control group was composed of healthy individuals without a history of TB and above the age of 15 years. Since host genetic analysis was not carried out to confirm the ethnicity of the participants, only individuals with both parents belonging to a specific ethnic group were included in the study. Only individuals with hemoglobin levels above 10 g/dL, systolic blood pressure between 100 and 130 mm Hg, and diastolic pressure between 70 and 90 mm Hg were recruited. Individuals with TB co-morbidities (such as HIV, diabetes, and cancer), pregnant women, and persons on anti-depressant drugs were excluded from the study.

2.4 Blood sample collection

Before phlebotomy, blood pressure was monitored using an OMRON monitor (OMRON Healthcare Co., Ltd., Kyoto, Japan), hemoglobin levels were assessed using HemoCue Hb 201+ (HEMOCUE AB, Ängelholm, Sweden), and random blood sugar levels were measured using OneTouch Select Plus Simple glucometer (LifeScan, Malvern, PA, USA). For women, a pregnancy test was carried out using the One-Step Pregnancy Test (Hubei Meibao Biotechnology Co., Ltd., Hubei, China). Venous blood samples ranging between 30 and 50 mL were collected with 10-mL Vacutainer blood collection tubes containing sodium heparin (BD Biosciences, San Jose, CA, USA) and inverted multiple times to prevent blood clotting. The tubes were transported at room temperature within 4 hours of blood sample collection to the laboratory for peripheral blood mononuclear cell (PBMC) isolation.

2.5 Isolation of peripheral blood mononuclear cells

Blood diluted twofold in Roswell Park Memorial Institute (RPMI) 1640 (with L-glutamine and penicillin–streptomycin) was gently overlayed on Ficoll-Paque™ under sterile conditions and centrifuged at room temperature for 10 minutes at 400×*g* without breaks. The top plasma layer was carefully pipetted away, and mononuclear cells were collected and washed twice with RPMI–5% fetal bovine serum (FBS). PBMCs were counted using the Countess II automated cell counter and cryopreserved in liquid nitrogen at 20 million cells per mL in a cryo-vial until further analyses.

2.6 CD14 monocyte isolation, macrophage differentiation, and harvest

Cryopreserved PBMCs were briefly thawed in a 37°C water bath and washed twice with 10 mL of pre-warmed RPMI–10% FBS and benzonase at 0.0125 U/μL final. PBMCs were rested for 2 hours at 37°C/5% CO_2. Monocyte isolation was performed using CD14 magnetic beads following the manufacturer's recommendations (Miltenyi Biotec Swiss AG, Solothurn, Switzerland). CD14 monocytes were counted and differentiated into macrophages for 6 days at 37°C and 5% CO_2 into tissue culture-treated dishes (Verreck et al., 2004) in the presence of human granulocyte–macrophage colony-stimulating factor (Thermo Fisher Scientific Inc., Waltham, MA, USA) at a final concentration of 10 ng/mL and a cell density of 8×10^5 monocytes/cm^2. The monocyte-derived macrophage (MDM) monolayer was treated with 9 volumes of a trypsin solution at 37°C for 20 minutes before neutralization with one volume of undiluted FBS and MDMs scraped off the dish. MDMs were seeded in 200 μL of RPMI–10% FBS at 1×10^5 cells per well in 96-well tissue culture plates and incubated for 2 hours for attachment before infection.

2.7 MTBC single-cell suspension

Previously described drug-susceptible hMTBC isolates (Otchere et al., 2018) including three independent L4 and three independent

L5 strains selected from the hMTBC maximum likelihood phylogeny below (Figure 1) generated with RAxML as previously described (Otchere et al., 2018) were cultivated in 10% albumin dextrose catalase (ADC)-supplemented 7H9 Middlebrook media containing 0.5% sodium pyruvate (Table S1). Single-cell suspensions were prepared using sonication and differential centrifugation as previously reported (Arbués et al., 2020) and stored at −80°C. The colony-forming unit (CFU) content of each mycobacterial isolate preparation was determined following serial dilution and plating on an oleic acid albumin dextrose catalase (OADC)-supplemented 7H11 solid medium.

2.8 Macrophage infections and bacterial load assessment

The volume of cryopreserved single-cell suspension required to reach a multiplicity of infection (MOI) of 2 was added onto MDMs (MTBCs L4 and L5 against MDMs from the Akan and Ewe ethnic groups: Table S2) and incubated at 37°C in 5% CO_2 for 2 hours. MDMs from the cured TB cases were infected with MTBC lineages they were previously diagnosed with to establish a sympatric infection assay. MDMs were washed twice with pre-warmed RPMI 1640 to remove non-phagocytosed bacteria. A complete medium was then added for later time points. To assess intracellular bacterial load at indicated time points, MDMs were lysed with 100 µL of 0.1% Triton X-100 in water for 20 minutes, and lysates were serially diluted before plating onto 7H11 agar plates supplemented with 10% OADC and 0.2% glycerol. CFU was assessed after 3–4 weeks of incubation at 37°C.

2.9 Fluorescence staining and flow cytometric analyses

Cell surface staining was performed by incubating the investigated cellular fractions with fluorochrome-conjugated antibodies in the dark on ice for 30 minutes before washing with cold phosphate-buffered saline (PBS) and fixing with 10% Cell Fix (250 µL) (BD Biosciences, USA). A cocktail of fluorescently labeled antibodies (BioLegend, San Diego, CA, USA) containing anti-human CD3-FITC (clone HIT3a) and CD4-PE (clone RPA-T4); CD14-FITC (clone: 63D3), CD16-PE (clone: B73.1), and HLA-DR-APC (clone L243); or CD40-FITC (clone 5C3), CD206-PE (clone 15-2) and CD14-APC (clone M5E2) was used for staining. A minimum of 10,000 events were acquired on gated lymphocytes and monocytes on a BD FACSCalibur flow cytometer (BD Biosciences, USA), and data were analyzed using FlowJo software following the gating strategy presented in Figure 2.

2.10 Data analysis

Figures were constructed and statistical tests including the Mann–Whitney test and two-way analysis of variance (ANOVA) were computed using GraphPad Prism Software, Inc.

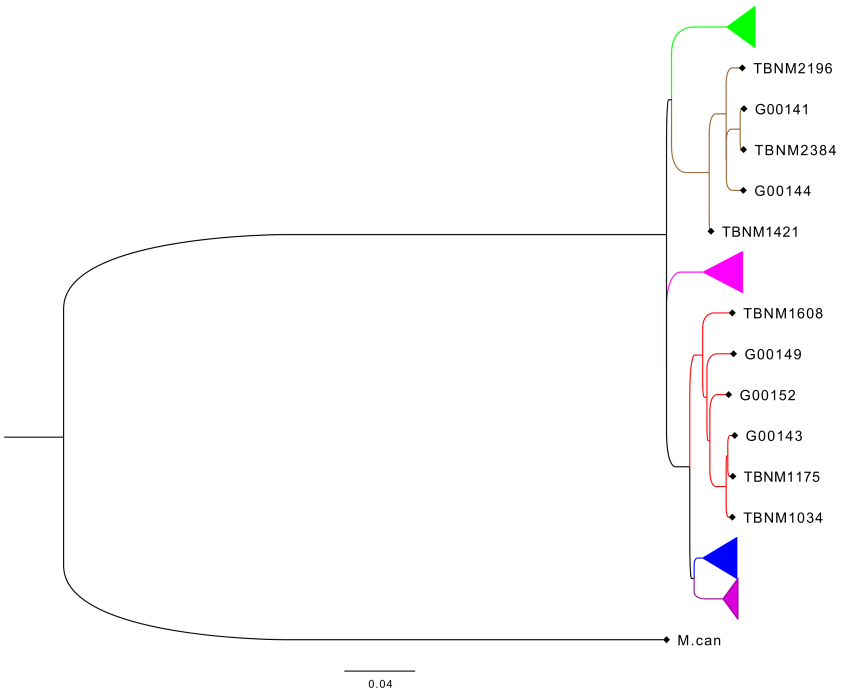

FIGURE 1
Phylogenetic analysis of mycobacterial isolates used for the study. Phylogenetic tree based on whole-genome sequencing data from L4 (red) and L5 (brown) mycobacterial isolates (TBNM) used for the infection assays as well as other West African sequence data (Genome IDs) and all four other major MTBC lineages (L6 in green, L1 in pink, L2 in blue, and L3 in purple). MTBC, *Mycobacterium tuberculosis* complex.

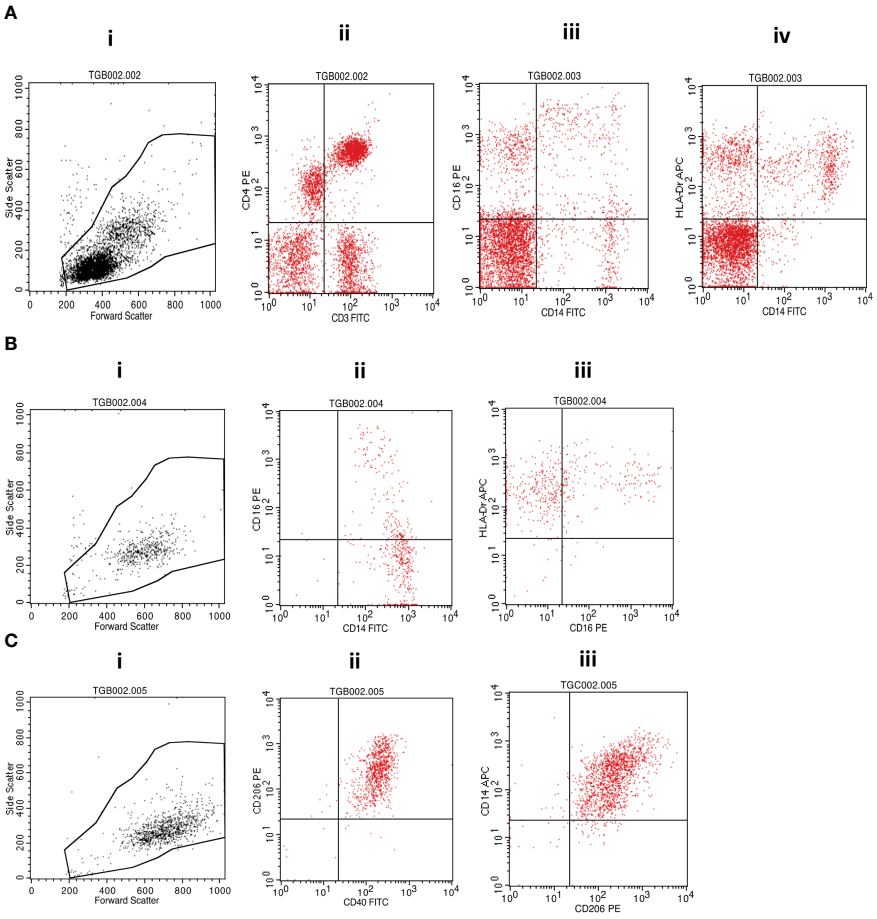

FIGURE 2
Flow cytometry gating strategy. **(A)** (i) Morphological cell gating on lymphocyte and monocyte based on forward versus side scatter signals was used to determine the representation of (ii) $CD3^+CD4^+$ T cells or (iii) $CD14^+CD16^+$ monocytic cells and (iv) $CD14^+HLA\text{-}DR^+$ monocytes within PBMCs. **(B)** Isolated monocytes were analyzed first following morphological gating (i) and then based on their propensity to express (ii) CD14 and/or CD16 and (iii) CD16 and/or HLA-DR. **(C)** Monocyte-derived macrophages were also first analyzed based on their morphology (i) and subsequent fluorescence propensity to express (ii) CD206 and CD40 or (iii) CD14 and CD206. MTBC, *Mycobacterium tuberculosis* complex; PBMCs, peripheral blood mononuclear cells.

3 Results

3.1 Study participants

A total of 53 participants comprising 20 healthy controls and 33 cured TB patients consented to be enrolled in the study and provided blood for PBMC isolation and phenotyping by flow cytometry (Table S2). Out of the total recruited participants, PBMCs from 16 controls and 20 cured TB patients were used for the macrophage infection assay. The median age for the controls was 24.5 years (95% confidence interval: 23–30), and that of the cured TB cases was 32 years (95% confidence interval: 30–43). The controls consisted of eight Akans (female = 4, male = 4) and eight Ewes (female = 3, male = 5), whereas the cured TB cases comprised 11 Akans (female = 1, male = 10) and nine Ewes (female = 4, male = 5) (Table S3).

3.2 Phenotypic profiling of T cells and isolated PBMCs from controls or cured cases across Ewe and Akan ethnic groups

Median CD4 T-cell frequencies for the two self-reported ethnic groups fell within normal physiological values of 30%–60% for PBMCs (Kleiveland, 2015). However, PBMCs from Akan participants showed significantly higher frequencies and absolute counts of CD4 T cells when compared to Ewe participants with a median frequency of 41.75 and 34.42, respectively (Figure 3A.i, $p = 0.02$). Moreover, the Akan participants showed higher median absolute counts of 3.17×10^7 cells/mL when compared to Ewes with 2.25×10^7 cells/mL (Figure 3A.ii, $p = 0.02$). We observed no significant difference in the proportion of $CD3^+/CD4^-$ T-cell compartment (median: Akan = 20.35, Ewe = 23.33) (Figure 3A.iii, $p = 0.51$). In contrast, the median CD4 T-cell frequencies and

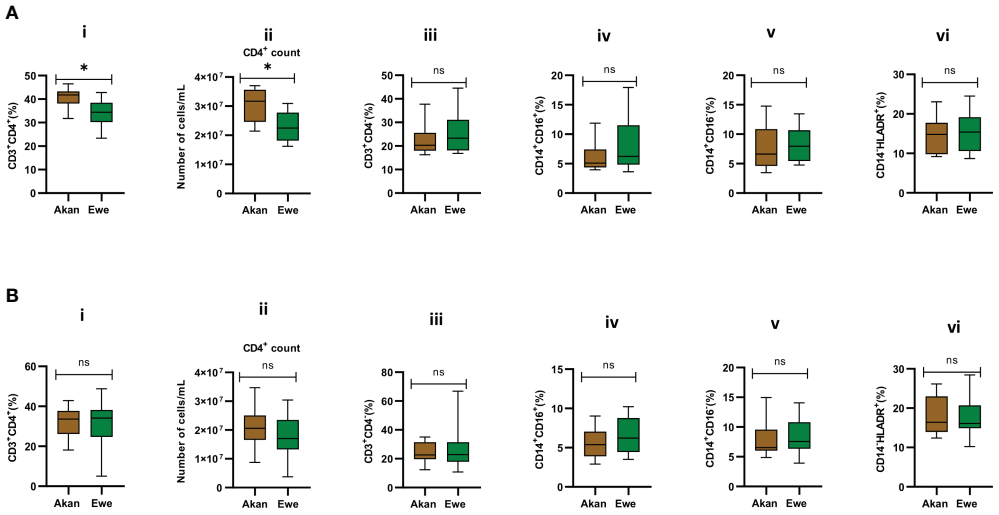

FIGURE 3
Comparison of the cellular composition of PBMCs from participants. Phenotypic and quantitative characterization of cells in PBMCs of **(A)** healthy controls [Akan, n = 10; Ewe, n = 10] and **(B)** cured TB cases [Akan, n = 18; Ewe, n = 15] of the two ethnic groups. Significant difference was observed only in the proportions (p = 0.02) and counts of $CD3^+CD4^+$ cells (p = 0.02) among the two ethnic groups using Mann–Whitney test. PBMCs, peripheral blood mononuclear cells; TB, tuberculosis. *p-value ≤ 0.05; ns, not significant (statistically), that is, p-value > 0.05.

absolute counts for the cured TB cases did not differ statistically between self-reported Akan and Ewe ethnic groups (Figure 3B.i, p = 0.76; Figure 3B,ii, p = 0.23). Also, the $CD3^+/CD4^-$ cell compartment did not show any significant difference between the two ethnic groups (median: Akan = 22.63, Ewe = 22.88) (Figure 3B.iii, p = 0.90).

The representation of inflammatory monocytes, $CD14^+/CD16^+$ (Figures 3A.iv, B.iv), within the isolated PBMC fractions, showed no significant difference between the ethnic groups for both controls (median: Akan = 5.09, Ewe = 6.23, p = 0.39) and cured TB cases (median: Akan = 5.38, Ewe = 6.22, p = 0.32), nor did the classical monocyte compartment, $CD14^+/CD16^-$ (Figures 3A.v, B.v), for both controls (median: Akan = 6.63, Ewe = 7.96, p = 0.53) and cured TB cases (median: Akan = 6.54, Ewe = 7.58, p = 0.47). Since increasing proportions of $CD14^+/HLA\text{-}DR^+$ cells have been associated with increased disease severity (McGill et al., 2022), we sought to also compare their proportions in PBMCs from both controls and cured TB cases for the ethnic groups to eliminate the possible effect of any underlining disease on the study participants (Figures 3A.vi, B.vi). We observed no statistically significant difference in their frequency for both cohorts, controls (median: Akan = 10.32, Ewe = 12.93, p = 0.11) and cases (median: Akan = 10.66, Ewe = 12.71, p = 0.34).

3.3 Phenotypic profiling of sorted monocytes and derived macrophages

Sorted monocytes were analyzed by flow cytometry to assess their purity and composition before differentiation into macrophages (Figures 4A.i, B.i). $CD14^+$ fractions' purity was systematically above 90% and composed of equal representation across study groups by classical $CD14^+/CD16^-$ (controls: Akan = 65.02%, Ewe = 65.96%, p = 0.91; cases: Akan = 76.05%, Ewe = 73.77%, p = 0.85) and $CD14^+/CD16^+$ inflammatory monocytes (controls: Akan = 30.28, Ewe = 28.46, p = 0.85; cases: Akan = 20.92, Ewe = 23.27, p = 0.42). The proportion of HLA-DR-expressing monocytes was also found constant (controls: Akan = 92.69, Ewe = 90.68, p = 0.45; cases: Akan = 91.64, Ewe = 92.67, p = 0.53) across the ethnic groups for both controls and cured TB cases.

Consequently, the phenotype of MDMs expressing CD40, which are responsible for the production of pro-inflammatory cytokines and nitric oxide upon stimulation (Danese et al., 2004), and CD206, which function in phagocytosis and immune homeostasis (Azad et al., 2014), were also found homogenous across ethnic groups for controls (median: Akan = 97.58; Ewe = 97.30, p = 0.66) (Figure 4A.ii) and cases (median: Akan 96.88; Ewe = 97.18, p = 0.32) (Figure 4B.ii).

As reflected by an increased mean fluorescence intensity (MFI) of the HLA-DR staining, the expression of MHC-II molecules by monocytes from Akan control blood donors (median = 288.3) was significantly higher than that of Ewes (median = 195.9) (p = 0.03) (Figure 4A.i). However, this observation was no longer found among cured TB cases (median: Akan = 318.5, Ewe = 304.9, p = 0.76) (Figure 4B.i). Analysis of CD40 and CD206 MFI revealed no significant difference across ethnicity for both controls (CD40: Akan = 243.6, Ewe = 287.8, p = 0.18; CD206: Akan = 429.4, Ewe = 523.3, p = 0.73) and cases (CD40: Akan = 276.3, Ewe = 287.7, p = 0.91; CD206: Akan = 552.3, Ewe = 450.0, p = 0.43).

3.4 Growth assessment of L4 and L5 in macrophages of the same ethnic group

The first analysis was carried out to assess the growth of either L4 or L5 MTBC strains in macrophages derived from monocytes

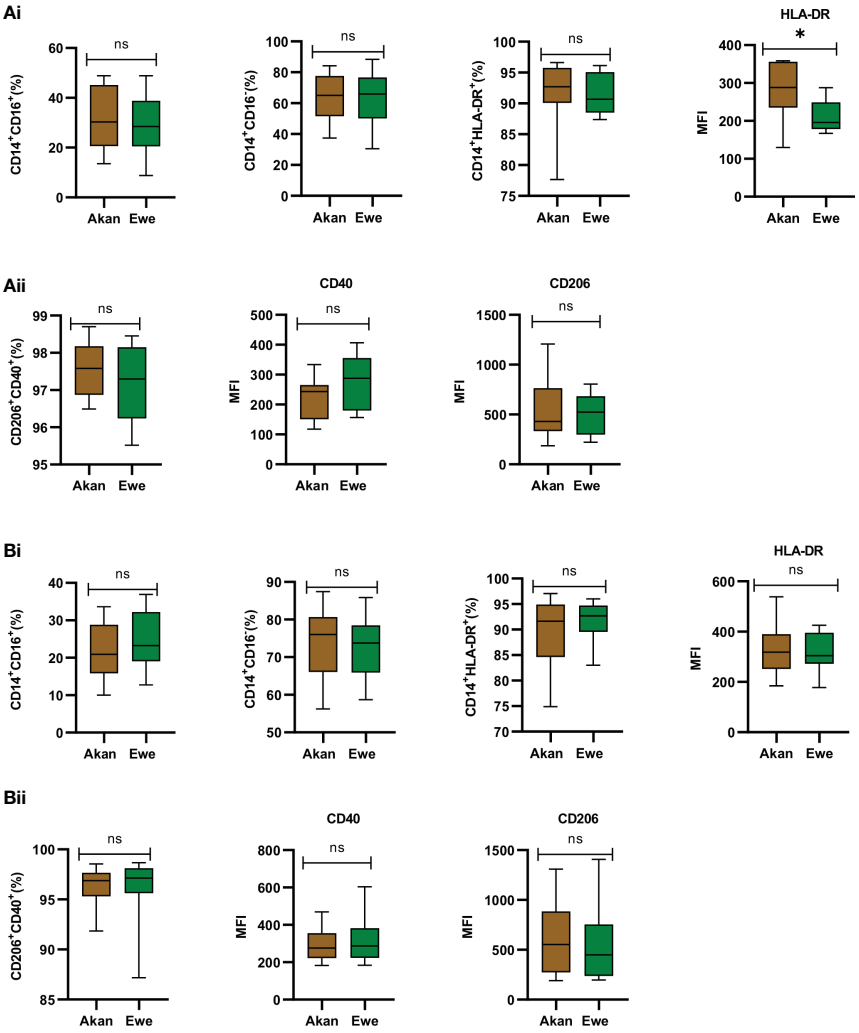

FIGURE 4
Phenotypic profiling of sorted monocytes and derived macrophages. **(A.i)** Comparison of the proportions of sorted monocytes ($CD14^+CD16^+$, $CD14^+CD16^-$, $CD14^+HLA\text{-}DR^+$, and median fluorescent intensity (MFI) of HLA-DR) for controls [Akan, n = 8; Ewe, n = 8]. **(A.ii)** Comparison of derived macrophages ($CD206^+CD40^+$ and MFI of CD40 and CD206) for controls. **(B.i)** Comparison of the proportions of sorted monocytes ($CD14^+CD16^+$, $CD14^+CD16^-$, $CD14^+HLA\text{-}DR^+$, and MFI of HLA-DR) for cured TB cases [Akan, n = 11; Ewe, n = 9] across ethnicity. **(B.ii)** Comparison of the proportions of macrophages ($CD206^+CD40^+$ and MFI of CD40 and CD206) among the ethnic groups for cured TB cases. A significant difference was seen for MFI of HLA-DR of the controls (p = 0.03) using Mann–Whitney test. TB, tuberculosis. *p-value ≤ 0.05; ns, not significant (statistically), that is, p-value > 0.05.

from the same ethnic group. Compared to L4 strains, L5 strains resulted in higher bacillary loads 7 days post-infection in Akan macrophages of control participants ($p < 0.0001$, Figure 5A.i). This difference seems to reflect an increased capacity of Akan macrophages to phagocytose L5 strains, as the intracellular bacterial load was already statistically superior at uptake ($p < 0.001$) and was still higher at D7 ($p = 0.04$) (Figure 5A.ii). However, the replication of L4 strains compared to L5 in Akan macrophages was 1.2 versus 1.1, respectively ($p = 0.04$).

In contrast, Ewe macrophages from healthy controls (Figure 3A.iii) showed a higher growth for L4 ($p < 0.0001$) linked to a statistically significant difference at uptake ($p < 0.001$) (Figure 5A.iv). Nevertheless, the replication of L5 strains in Ewe macrophages was higher than that of L4 strains (fold change: L5 = 1.4, L4 = 1.2, $p = 0.03$).

Further analysis of the growth of L4 and L5 in Akan macrophages of the cured TB cases showed no significant difference ($p = 0.49$) (Figure 5B.i). Moreover, there was no difference in the $\log_{10}$CFU/mL at uptake ($p = 0.71$) and D7 ($p = 0.27$) (Figure 5B.ii), and the replication of L4 and L5 strains was 1.3 and 1.2, respectively ($p = 0.50$). We observed similar patterns with the growth comparison of the two lineages in Ewe macrophages of the cured TB cases where there was no significant difference in bacillary load (Figure 5B.iii) ($p = 0.99$). There was no difference in the uptake of L4 and L5 ($p = 0.48$), but there was a significant difference in the growth of L4 at D7 ($p = 0.02$) (Figure 5B.iv) with a fold change of 1.4 for L4 and 1.3 for L5 ($p = 0.08$).

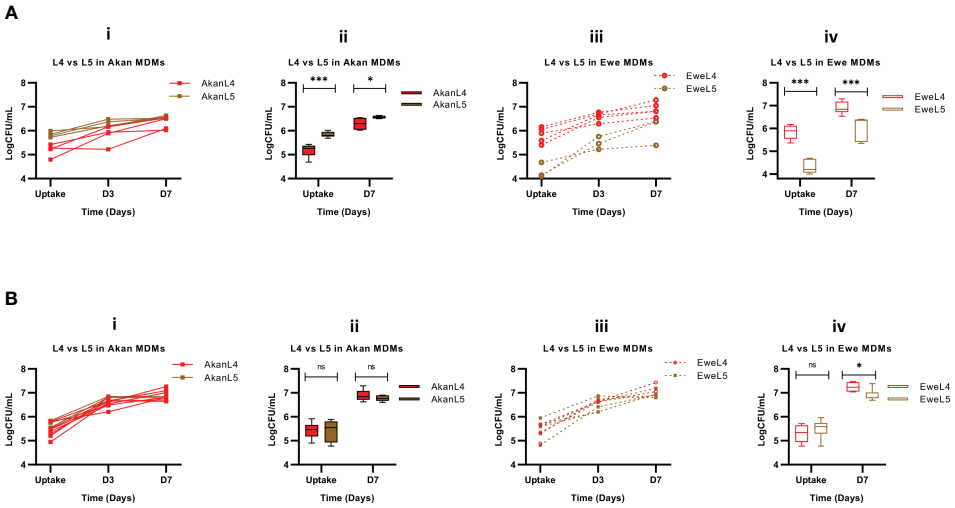

FIGURE 5
Growth assessment of L4 and L5 in control macrophages **(A)** [Akan, n = 8; Ewe, n = 8] and cured TB cases **(B)** [Akan, n = 11; Ewe, n = 9]. (i) Comparison of growth of L4 and L5 at uptake, day 3 (D3), and day 7 (D7) in Akan macrophages. (ii) Comparison of the growth rate of L4 and L5 in Akan macrophages between uptake and D7. (iii) Comparison of the growth of L4 and L5 in Ewe macrophages (iv) using multiple Mann–Whitney test. TB, tuberculosis. *p-value ≤ 0.05; ***p-value ≤ 0.001; ns, not significant (statistically), that is, p-value > 0.05.

3.5 Growth assessment in macrophages from Akans and Ewes

We then sought to stratify our analysis by comparing the influence of macrophage donors' ethnicity on the uptake and subsequent growth of L4 and L5 strains. This analysis revealed that L4 strains achieved higher bacterial load in macrophages derived from Ewe control donors in comparison to Akans ($p < 0.0001$, Figure 6A.i), reflecting a significantly higher bacterial uptake 2 hours post-infection ($p < 0.0001$) and higher bacterial growth 7 days ($p < 0.001$) post-infection (Figure 6A.ii). However, the replication of L4 in Akan versus Ewe macrophages was comparable (fold change: 1.2, $p = 0.85$). In contrast, L5 strains in macrophages derived from Ewes displayed significantly lower uptake ($p < 0.001$, Figure 6A.iv) that also translated into reduced intracellular bacterial load 7 days post-infection ($p < 0.0001$). Hence, Akan macrophages obtained from healthy controls supported the uptake of L5 and consequently higher bacterial load at day 7 than Ewe macrophages. On the contrary, the bacterial replication of L5 in Ewe macrophages was higher than that of Akans (fold change: L5 in Ewe MDMs = 1.4, L5 in Akan MDMs = 1.1, $p = 0.004$).

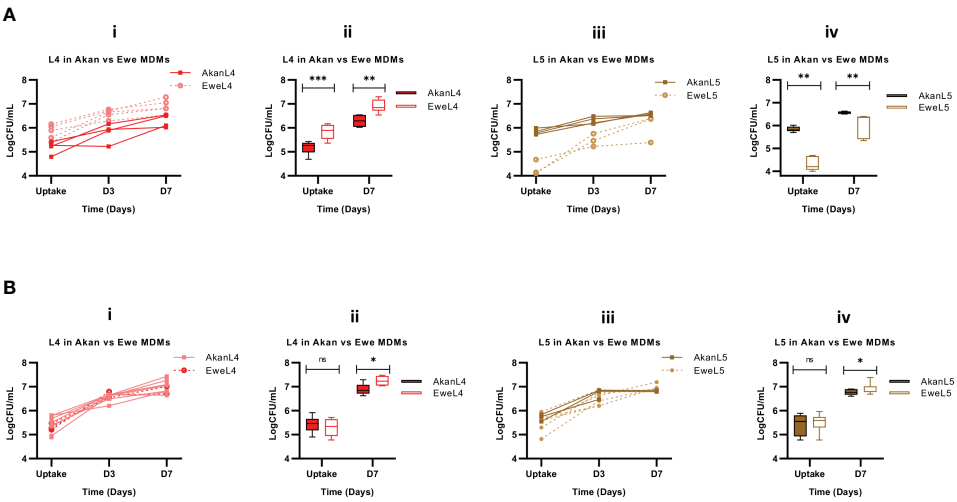

FIGURE 6
Comparison of Akan and Ewe macrophages from control **(A)** [Akan, n = 8; Ewe, n = 8] and cured TB cases **(B)** [Akan, n = 11; Ewe, n = 9] in support of MTBC growth. (i) Comparison of the growth of L4 at uptake, D3, and D7 in Akan and Ewe macrophages. (ii) Comparison of the growth rate of L4 in Akan and Ewe macrophages between uptake and D7. (iii) Comparison of the growth of L5 in Akan and Ewe macrophages. (iv) Growth rate comparison of L5 in Akan and Ewe macrophage between uptake and D7 using multiple Mann–Whitney test. TB, tuberculosis; MTBC, *Mycobacterium tuberculosis* complex. *p-value ≤ 0.05; **p-value ≤ 0.01; ***p-value ≤ 0.001; ns, not significant (statistically), that is, p-value > 0.05.

Further analysis among the cured TB cases showed that L4 strains displayed similar uptake in both macrophages after 2 hours of infection ($p = 0.48$); however, there was a higher bacterial load in Ewe macrophages compared to that of the Akans at day 7 ($p = 0.02$) (Figure 6B.ii) with a fold change of 1.3 in Akan macrophages and 1.4 in Ewe macrophages ($p = 0.03$). Similarly, we observed a significantly higher bacterial load of L5 strains in Ewes macrophages at day 7 post-infection ($p = 0.02$) and no significant difference at uptake ($p = 0.67$) (Figure 6B.iv). The fold change of L5 in Ewe macrophages was 1.3, whereas that of Akans' was 1.2 ($p = 0.55$). Ewe macrophages from the cured TB cases supported the replication of L4 strains better than Akan macrophages.

4 Discussion

We aimed to investigate the early phase of the pathogenesis of representative MTBC strains endemic in Ghana that could sustain our previously observed epidemiological findings. Akans, the largest ethnic group in Ghana, are mostly affected by MTBC-L4 infections and to a lesser extent by L5 and L6 MTBC strains. In return, individuals that self-reported to belong to the Ewe ethnic group were described to be ~3 times more likely to be affected by MTBC-L5 infections (Asante-Poku et al., 2015; Asante-Poku et al., 2016). We hypothesized that such epidemiological linkage may translate into the differential capacity of macrophages from these two ethnic groups to endure intracellular infections *in vitro*. To test our hypothesis, we performed *ex vivo* infections of monocyte-derived macrophages from the blood of donors belonging to the above-mentioned ethnic groups that were found to be epidemiologically linked with specific MTBC lineages isolated in Ghana.

Considering data obtained from the blood of healthy controls, Ewe macrophages displayed a superior propensity to phagocytose L4 bacilli when compared to Akan MDMs. However, the replication of L4 was higher in Akan MDMs, which is consistent with the previous epidemiological observation that L4 is associated with the Akan ethnic group. In contrast, we observed increased uptake of L5 by Akan MDMs. Despite the lower uptake of L5 by Ewe MDMs, the bacterial load measured 1 week post-infection resulted in a substantially higher replication rate of L5 in macrophages derived from Ewe compared to Akan blood donors. This observation also corroborates findings from epidemiological studies where L5 infections were associated with the Ewe ethnic group. However, the uptake observed was the reverse of the mycobacterial growth in the macrophages. This shows a possible co-evolution of phagocytosis of MTBC by macrophages of different ethnicity. Several pathogens have evolved subtle strategies to evade phagocytosis or induce reduced phagocytosis as a virulence mechanism (Uribe-Querol and Rosales, 2017). MTBC L4 might have co-evolved with Akan macrophages where they have both mechanisms to reduce phagocytosis and increase intracellular growth, whereas L5 has also developed mechanisms to reduce phagocytosis and increase its growth within Ewe macrophages.

The analysis of data generated with blood from cured TB patients did not reveal the same differential uptake between the two ethnic groups. However, MDMs from Ewes displayed a mild but significant tendency to allow higher multiplication rates for both L4 and L5 strains. These results suggest that host ethnicity, MTBC genetic diversity, and trained innate immunity mediated by recent infection would all be acting in concert to modulate the outcome of macrophage infections.

Indeed, recent studies have reported the ability of trained innate immunity to impact MTBC infection outcomes (Zhou et al., 2021). Some individuals who are highly exposed to TB do not develop the disease nor latent infection due to early clearance attributed to *Mycobacterium bovis* BCG exposure. BCG vaccination boosts innate immune responses through epigenetic remodeling. Similarly, previous TB infections also promote innate immunity training (Koeken et al., 2019; Ferluga et al., 2020). Taken together, we propose that trained innate immunity due to recent TB eliminates the effect of self-reported ethnicity observed in healthy controls and induces similar outcomes in the phagocytosis capacity of MDMs independently of self-reported ethnicity. As a limitation of this study, information on the BCG vaccination of the participants was not obtained for further analysis of its impact on trained immunity. However, the role of pathogen virulence and possibly host genetic background could reduce the effect of trained immunity. This was observed in the higher growth of L4 even among the cured TB cases and the general higher growth of MTBC in Ewe macrophages. Thus, diversity in macrophage infection with MTBC could be multifactorial.

The higher replication rate of L5 in Ewe macrophages but lower phagocytosis of L5 in Ewe macrophages supports our hypothesis of a possible host–pathogen co-evolution. We propose that L5 strains have co-evolved with the Ewe ethnic group, resulting in the sympatric association observed nowadays, which translates experimentally into an increased intracellular replication propensity. Nonetheless, a lower bacillary load can be associated with the fact that recovery may be suboptimal due to differentially cultivable mycobacteria associated with non-replicative dormant states. MTBC is able to adapt to environmental conditions such as hypoxia and reduced nutrients presented in macrophages and progress to a non-replicative dormant state (Gengenbacher and Kaufmann, 2012). L5 and L6 strains have been associated with a higher tendency to progress into a dormant state when compared to L4 (Ofori-Anyinam et al., 2017).

Macrophages have been reported to respond to hypoxia and other environmental conditions differentially, which is very relevant to the understanding of disease mechanisms. Low oxygen tension has been associated with changes in macrophage morphology, phagocytosis, release of cytokines, and metabolic activities (Lewis et al., 1999). Macrophages from the different ethnic groups might be responding differently to comparable environmental conditions, hence resulting in the diversity in phagocytic abilities of the macrophages obtained from donors of the two ethnic groups.

Phenotypic studies on *in vitro* growth assessment revealed slower growth of L5 strains compared to L4 isolates (Gehre et al., 2013; Ates et al., 2018; Osei-Wusu et al., 2021). The slow growth of L5 has been attributed to its attenuated virulence. Due to the unique phenotypic characteristics of L5, it was expected to be outcompeted by more virulent lineages such as L4. However, it has remained a relevant causative agent for TB in West Africa over the years

(Yeboah-Manu et al., 2016). The *ex vivo* infection data presented here suggest that L5 strains may replicate as well as L4 isolates once inside their natural host cell and so particularly when cells originated from the self-reported Ewe ethnic group. This observation could explain the unexplained prevalence of L5 infections in West Africa over the years. Host genetics is beginning to provide answers in TB host–pathogen interplays. For instance, it was reported that 5-lipoxygenase (*ALOX5*) variants are associated with ethnicity and susceptibility to TB in Ghana (Herb et al., 2008). Another recent study in Ghana on host susceptibility to TB has suggested two potentially protective genes, SLC11A1 and SORBS2 (Asante-Poku et al., 2022). Further investigations looking into the distribution of genetic variants in Ewes compared to other Ghanaian ethnic groups are needed to further our mechanistic understanding of the macrophage phenotypes presented in this study.

5 Limitation

The MTBC lineage diversity observed could have been a result of the individual strain effect, which is very prominent among MTBC. Different strains of MTBC may differ in virulence and immunogenicity. However, we have carefully selected strains representative of the two most prevalent L4 sub-lineages (Cameroon and Ghana sub-lineages) and the most prevalent L5 sub-lineages to attempt to circumvent this limitation. However, gender distribution was a challenge since we could recruit equal numbers for the cured TB cases.

Although our study may not provide a very conclusive explanation of the epidemiological association of specific MTBC lineages with ethnicity in Ghana, it provides insight into this relationship and serves as the platform for future studies.

6 Conclusion

We observed that Ewe MDMs demonstrated a higher propensity to phagocytose L4 strains compared to Akan MDMs; nevertheless, the replication rate of L4 was higher in Akan MDMs. In contrast, we observed an increased uptake of L5 by Akan MDMs, despite the substantially higher replication rate of L5 in Ewe MDMs compared to that of Akans. Interestingly, the impact of self-reported ethnicity disappeared when using cells derived from the blood of cured TB cases. In return, Ewe MDMs appeared more susceptible to both L4 and L5 strains. These results suggest that host ethnicity and, by extension, host genetic diversity together with MTBC genetic diversity and previous exposure to MTBC are all acting together to modulate macrophage invasion and intracellular replication. Further studies are required to explain the mechanism underlying the observation while considering host genetic, social, and nutritional factors. Also, with the observed diversity in CD4 T cells of the controls, we would like to study their activation, maturation, and exhaustion in a detailed study in the future. Moreover, it is important to study the interaction of surface markers of the macrophages with the different lineages of MTBC to further understand the mechanism of the higher phagocytic properties of the Akan macrophages for L5 and Ewe macrophages for L4. Studies on the cytokine profiles of the infection assay are recommended.

Data availability statement

The original contributions presented in the study are included in the article/Supplementary Material, further inquiries can be directed to the corresponding author/s.

Ethics statement

The studies involving human participants were reviewed and approved by Institutional Review Boards (IRB) of Korle-Bu Teaching Hospital (KBTH) and Noguchi Memorial Institute for Medical Research (NMIMR), University of Ghana (Federal wide assurance number: FWA00001824). Written informed consent to participate in this study was provided by the participants' legal guardian/next of kin.

Author contributions

All authors contributed to the article and approved the submitted version.

Funding

This study was funded by a grant from the Deutsche Forschungsgemeinschaft (DFG) awarded to Dorothy Yeboah-Manu and Tobias L. Lenz (grant no 444810852). The study was supported by funding from The Royal Society Africa Prize 2018 awarded to Dorothy Yeboah-Manu who is also a GSK-EDCTP Senior Fellow (TMA.2017.GSF.1942-TB-DM).

Acknowledgments

We would like to acknowledge the contributions of Miriam Reinhard and Anna Doetsch of Swiss Tropical and Public Health Institute, Switzerland, and Amanda Yaa Tetteh, Ishaque Siam Mintah, and Eric Kyei-Baafour of Noguchi Memorial Institute for Medical Research, Ghana.

Conflict of interest

The authors declare that the research was conducted in the absence of any commercial or financial relationships that could be construed as a potential conflict of interest.

The reviewer VF declared a past collaboration with the author SG to the handling editor.

Publisher's note

All claims expressed in this article are solely those of the authors and do not necessarily represent those of their affiliated organizations, or those of the publisher, the editors and the reviewers. Any product that may be evaluated in this article, or claim that may be made by its manufacturer, is not guaranteed or endorsed by the publisher.

Supplementary material

The Supplementary Material for this article can be found online at: https://www.frontiersin.org/articles/10.3389/fcimb.2023.1163993/full#supplementary-material

References

Arbués, A., Brees, D., Chibout, S.-D., Fox, T., Kammüller, M., and Portevin, D. (2020). TNF-α antagonists differentially induce TGF-β1-dependent resuscitation of dormant-like Mycobacterium tuberculosis. *PloS pathogens* 16 (2), e1008312. doi: 10.1371/journal.ppat.1008312

Asante-Poku, A., Morgan, P., Osei-Wusu, S., Aboagye, S. Y., Asare, P., Otchere, I. D., et al. (2022). Genetic analysis of TB susceptibility variants in Ghana reveals candidate protective loci in SORBS2 and SCL11A1 genes. *Front. Genet.* 12, 729737. doi: 10.3389/fgene.2021.729737

Asante-Poku, A., Otchere, I. D., Osei-Wusu, S., Sarpong, E., Baddoo, A., Forson, A., et al. (2016). Molecular epidemiology of Mycobacterium africanum in Ghana. *BMC Infect. diseases* 16 (1), 385. doi: 10.1186/s12879-016-1725-6

Asante-Poku, A., Yeboah-Manu, D., Otchere, I. D., Aboagye, S. Y., Stucki, D., Hattendorf, J., et al. (2015). Mycobacterium africanum is associated with patient ethnicity in Ghana. *PloS Negl. Trop. Dis.* 9 (1), e3370. doi: 10.1371/journal.pntd.0003370

Asare, P., Asante-Poku, A., Prah, D. A., Borrell, S., Osei-Wusu, S., Otchere, I. D., et al. (2018). Reduced transmission of Mycobacterium africanum compared to Mycobacterium tuberculosis in urban West Africa. *Int. J. Infect. Dis.* 73, 30–42. doi: 10.1016/j.ijid.2018.05.014

Ates, L. S., Dippenaar, A., Sayes, F., Pawlik, A., Bouchier, C., Ma, L., et al. (2018). Unexpected genomic and phenotypic diversity of Mycobacterium africanum lineage 5 affects drug resistance, protein secretion, and immunogenicity. *Genome Biol. Evol.* 10 (8), 1858–1874. doi: 10.1093/gbe/evy145

Azad, A. K., Rajaram, M. V., and Schlesinger, L. S. (2014). Exploitation of the macrophage mannose receptor (CD206) in infectious disease diagnostics and therapeutics. *J. Cytol. Mol. Biol.* 1 (1), 1000003. doi: 10.13188/2325-4653.1000003

Brites, D., and Gagneux, S. (2015). Co-evolution of Mycobacterium tuberculosis and Homo sapiens. *Immunol. Rev.* 264 (1), 6–24. doi: 10.1111/imr.12264

Comas, I., Coscolla, M., Luo, T., Borrell, S., Holt, K. E., Kato-Maeda, M., et al. (2013). Out-of-Africa migration and Neolithic coexpansion of Mycobacterium tuberculosis with modern humans. *Nat. Genet.* 45 (10), 1176–1182. doi: 10.1038/ng.2744

Coscolla, M., and Gagneux, S. (2010). Does M. tuberculosis genomic diversity explain disease diversity? *Drug Discov. Today Dis. mechanisms* 7 (1), e43–e59. doi: 10.1016/j.ddmec.2010.09.004

Coscolla, M., Gagneux, S., Menardo, F., Loiseau, C., Ruiz-Rodriguez, P., Borrell, S., et al. (2021). Phylogenomics of Mycobacterium africanum reveals a new lineage and a complex evolutionary history. *Microb. Genom.* 7 (2), 000477. doi: 10.1099/mgen.0.000477

Danese, S., Sans, M., and Fiocchi, C. (2004). The CD40/CD40L costimulatory pathway in inflammatory bowel disease. *Gut* 53 (7), 1035–1043. doi: 10.1136/gut.2003.026278

de Jong, B. C., Adetifa, I., Walther, B., Hill, P. C., Antonio, M., Ota, M., et al. (2010a). Differences between tuberculosis cases infected with Mycobacterium africanum, West African type 2, relative to Euro-American Mycobacterium tuberculosis: an update. *FEMS Immunol. Med. Microbiol.* 58 (1), 102–105. doi: 10.1111/j.1574-695X.2009.00628.x

de Jong, B. C., Antonio, M., and Gagneux, S. (2010b). Mycobacterium africanum—review of an important cause of human tuberculosis in West Africa. *PloS Negl. Trop. Dis.* 4 (9), e744. doi: 10.1371/journal.pntd.0000744

de Jong, B. C., Hill, P. C., Brookes, R. H., Otu, J. K., Peterson, K. L., Small, P. M., et al. (2005). Mycobacterium africanum: a new opportunistic pathogen in HIV infection? *Aids* 19 (15), 1714–1715. doi: 10.1097/01.aids.0000185991.54595.41

Fan, J., Hale, V. L., Lelieveld, L. T., Whitworth, L. J., Busch-Nentwich, E. M., Troll, M., et al. (2023). Gaucher disease protects against tuberculosis. *Proc Natl Acad Sci U.S.A.* 120 (7), e2217673120. doi: 10.1073/pnas.2217673120

Ferluga, J., Yasmin, H., Al-Ahdal, M. N., Bhakta, S., and Kishore, U. (2020). Natural and trained innate immunity against Mycobacterium tuberculosis. *Immunobiology* 225 (3), 151951. doi: 10.1016/j.imbio.2020.151951

Fernández Tena, A., and Casan Clarà, P. (2012). Deposition of inhaled particles in the lungs. *Archivos bronconeumologia* 48 (7), 240–246. doi: 10.1016/j.arbr.2012.02.006

Gagneux, S. (2012). Host–pathogen coevolution in human tuberculosis. *Phil. Trans. R Soc. B.* 367 (1590), 850–859. doi: 10.1098/rstb.2011.0316

Gagneux, S., DeRiemer, K., Van, T., Kato-Maeda, M., de Jong, B. C., Narayanan, S., et al. (2006). Variable host–pathogen compatibility in Mycobacterium tuberculosis. *Proc. Natl. Acad. Sci. U.S.A.* 103 (8), 2869–2873. doi: 10.1073/pnas.0511240103

Gagneux, S., and Small, P. M. (2007). Global phylogeography of Mycobacterium tuberculosis and implications for tuberculosis product development. *Lancet Infect. Dis.* 7 (5), 328–337. doi: 10.1016/S1473-3099(07)70108-1

Gehre, F., Otu, J., DeRiemer, K., de Sessions, P. F., Hibberd, M. L., Mulders, W., et al. (2013). Deciphering the growth behaviour of Mycobacterium africanum. *PloS Negl. Trop. diseases* 7 (5), e2220. doi: 10.1371/annotation/fb002e1b-e345-4832-a793-d2f4988de308

Gengenbacher, M., and Kaufmann, S. H. E. (2012). Mycobacterium tuberculosis: success through dormancy. *FEMS Microbiol. Rev. J.* 36 (3), 514–532. doi: 10.1111/j.1574-6976.2012.00331.x

Herb, F., Thye, T., Niemann, S., Browne, E. N. L., Chinbuah, M. A., Gyapong, J., et al. (2008). ALOX5 variants associated with susceptibility to human pulmonary tuberculosis. *Hum. Mol. Genet.* 17 (7), 1052–1060. doi: 10.1093/hmg/ddm378

Kleiveland, C. R. (2015). "Peripheral Blood Mononuclear Cells," in *The Impact of Food Bioactives on Health: in vitro and ex vivo models*. Eds. K. Verhoeckx, P. Cotter, I. López-Expósito, C. Kleiveland, T. Lea, A. Mackie, et al. (Cham (CH: Springer), 161–167.

Koeken, V. A. C. M., Verrall, A. J., Netea, M. G., Hill, P. C., and van Crevel, R. (2019). Trained innate immunity and resistance to Mycobacterium tuberculosis infection. *Clin. Microbiol. Infect.* 25 (12), 1468–1472. doi: 10.1016/j.cmi.2019.02.015

Lewis, J. S., Lee, J. A., Underwood, J. C., Harris, A. L., and Lewis, C. E. (1999). Macrophage responses to hypoxia: relevance to disease mechanisms. *J. leukocyte Biol.* 66 (6), 889–900. doi: 10.1002/jlb.66.6.889

McGill, R. B., Steyn, F. J., Ngo, S. T., Thorpe, K. A., Heggie, S., Henderson, R. D., et al. (2022). Monocyte CD14 and HLA-DR expression increases with disease duration and severity in amyotrophic lateral sclerosis. *Amyotrophic Lateral Sclerosis Frontotemporal Degeneration* 23 (5-6), 430–437. doi: 10.1080/21678421.2021.1964531

Nahid, P., Jarlsberg, L. G., Kato-Maeda, M., Segal, M. R., Osmond, D. H., Gagneux, S., et al. (2018). Interplay of strain and race/ethnicity in the innate immune response to M. tuberculosis. *PloS One* 13 (5), e0195392–e. doi: 10.1371/journal.pone.0195392

NGabonziza, J. C. S., Loiseau, C., Marceau, M., Jouet, A., Menardo, F., Tzfadia, O., et al. (2020). A sister lineage of the Mycobacterium tuberculosis complex discovered in the African Great Lakes region. *Nat. Commun.* 11 (1), 1–11. doi: 10.1038/s41467-020-16626-6

Ofori-Anyinam, B., Dolganov, G., Van, T., Davis, J. L., Walter, N. D., Garcia, B. J., et al. (2017). Significant under expression of the DosR regulon in M. tuberculosis complex lineage 6 in sputum. *Tubercul. (Edinb).* 104, 58–64. doi: 10.1016/j.tube.2017.03.001

Osei-Wusu, S., Otchere, I. D., Morgan, P., Musah, A. B., Siam, I. M., Asandem, D., et al. (2021). Genotypic and phenotypic diversity of Mycobacterium tuberculosis complex genotypes prevalent in West Africa. *PloS One* 16 (8), e0255433. doi: 10.1371/journal.pone.0255433

Otchere, I. D., Coscollá, M., Sánchez-Busó, L., Asante-Poku, A., Brites, D., Loiseau, C., et al. (2018). Comparative genomics of Mycobacterium africanum Lineage 5 and Lineage 6 from Ghana suggests distinct ecological niches. *Sci. Rep.* 8 (1), 1–11. doi: 10.1038/s41598-018-29620-2

Portevin, D., Gagneux, S., Comas, I., and Young, D. (2011). Human macrophage responses to clinical isolates from the Mycobacterium tuberculosis complex discriminate between ancient and modern lineages. *PloS pathogens* 7 (3), e1001307. doi: 10.1371/journal.ppat.1001307

Scriba, T. J., Coussens, A. K., and Fletcher, H. A. (2017). Human immunology of tuberculosis. *Microbiol. Spectr.* 5 (1). doi: 10.1128/microbiolspec.tbtb2-0016-2016

Sia, J. K., and Rengarajan, J. (2019). Immunology of mycobacterium tuberculosis infections. *Microbiol. Spectr. J.* 7 (4), 10. doi: 10.1128/microbiolspec.GPP3-0022-2018

Sreejit, G., Fleetwood, A. J., Murphy, A. J., and Nagareddy, P. R. (2020). Origins and diversity of macrophages in health and disease. *J. Clin. Trans. Immunol.* 9 (12), e1222–e122e. doi: 10.1002/cti2.1222

Stucki, D., Brites, D., Jeljeli, L., Coscolla, M., Liu, Q., Trauner, A., et al. (2016). Mycobacterium tuberculosis lineage 4 comprises globally distributed and geographically restricted sublineages. *Nat. Genet.* 48 (12), 1535–1543. doi: 10.1038/ng.3704

Torrelles, J. B., and Schlesinger, L. S. (2017). Integrating lung physiology, immunology, and tuberculosis. *Trends Microbiol.* 25 (8), 688–697. doi: 10.1016/j.tim.2017.03.007

Uribe-Querol, E., and Rosales, C. (2017). Control of phagocytosis by microbial pathogens. *Front. Immunol.* 8, 1368. doi: 10.3389/fimmu.2017.01368

Verreck, F. A., de Boer, T., Langenberg, D. M., Hoeve, M. A., Kramer, M., Vaisberg, E., et al. (2004). Human IL-23-producing type 1 macrophages promote but IL-10-producing type 2 macrophages subvert immunity to (myco) bacteria. *Proc. Natl. Acad. Sci. U.S.A.* 101 (13), 4560–4565. doi: 10.1073/pnas.0400983101

WHO (1994). "47th World Health Assembly: provisional agenda item 19," in *Tuberculosis programme—Progress report by the Director-General*. (Geneva: WHO).

WHO (2021). *Global Tuberculosis Report*. (Geneva: WHO).

WHO (2022). *Global Tuberculosis Report*. (Geneva: WHO), Vol. 2022.

Wynn, T. A., and Vannella, K. M. (2016). Macrophages in tissue repair, regeneration, and fibrosis. *Immunity* 44 (3), 450–462. doi: 10.1016/j.immuni.2016.02.015

Yeboah-Manu, D., Asare, P., Asante-Poku, A., Otchere, I. D., Osei-Wusu, S., Danso, E., et al. (2016). Spatio-temporal distribution of mycobacterium tuberculosis complex strains in Ghana. *PloS One* 11 (8), e0161892. doi: 10.1371/journal.pone.0161892

Zhou, J., Lv, J., Carlson, C., Liu, H., Wang, H., Xu, T., et al. (2021). Trained immunity contributes to the prevention of Mycobacterium tuberculosis infection, a novel role of autophagy. *Emerg. Microbes Infect.* 10 (1), 578–588. doi: 10.1080/22221751.2021.1899771

Frontiers in
Cellular and Infection Microbiology

Investigates how microorganisms interact with their hosts

Explores bacteria, fungi, parasites, viruses, endosymbionts, prions and all microbial pathogens as well as the microbiota and its effect on health and disease in various hosts.

Discover the latest Research Topics

See more →

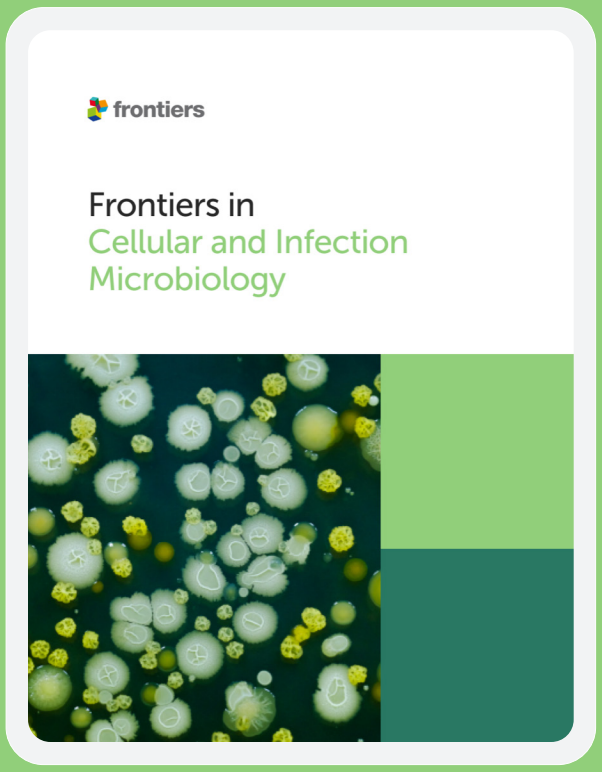

Frontiers

Avenue du Tribunal-Fédéral 34
1005 Lausanne, Switzerland
frontiersin.org

Contact us

+41 (0)21 510 17 00
frontiersin.org/about/contact